HEINRICH HEINE
UNIVERSITÄT DÜSSELDORF

Catalytic applications and shaping of metal-organic frameworks

Dissertation

zur Erlangung des Doktorgrades
Dr. rer. nat.
der Mathematisch-Naturwissenschaftlichen Fakultät
der Heinrich-Heine-Universität Düsseldorf

vorgelegt von

Annika Herbst
aus Düsseldorf

Düsseldorf, Juni 2016

aus dem Institut für Anorganische Chemie und Strukturchemie I
der Heinrich-Heine-Universität Düsseldorf

Gedruckt mit der Genehmigung der
Mathematisch-Naturwissenschaftlichen Fakultät der
Heinrich-Heine-Universität Düsseldorf

Referent: Prof. Dr. Christoph Janiak
Korreferent: Prof. Dr. Christian Ganter

Tag der mündlichen Prüfung:

Die vorliegende Arbeit wurde in der Zeit von November 2012 bis Juni 2016 an der Heinrich-Heine-Universität-Düsseldorf im Institut für Anorganische Chemie und Strukturchemie I im Arbeitskreis von Prof. Dr. Christoph Janiak angefertigt. Im November 2014 wurde ein Teil der praktischen Arbeiten an der Wuhan University of Technology (China) in der Arbeitsgruppe von Prof. Dr. Xiao-Yu Yang im Rahmen eines Austauschprogramms durchgeführt.

Eidesstattliche Erklärung

Ich versichere an Eides statt, dass die Dissertation von mir selbstständig und ohne unzulässige fremde Hilfe unter der Beachtung der □Grundsätze zur Sicherung guter wissenschaftlicher Praxis□an der Heinrich-Heine-Universität Düsseldorf erstellt worden ist. Die aus fremden Quellen direkt oder indirekt übernommenen Gedanken sind als solche kenntlich gemacht. Die Arbeit wurde bisher weder im Inland noch im Ausland in gleicher oder ähnlicher Form einer anderen Prüfungsbehörde vorgelegt. Es wurden keine früheren erfolglosen Promotionsversuche unternommen.

□ □ □ □ □ □ □ □ □ □ □ □ □ .   □ □ □ □ □ □ □ □ □ □ □ □ □ .

Ort, Datum   Unterschrift

"Everybody is a genius. But if you judge a fish by its ability to climb a tree,
it will live its whole life believing that it is stupid."
Albert Einstein

Danksagung

Ich danke Herrn Prof. Dr. Christoph Janiak für die Möglichkeit, meine Dissertation in seinem Arbeitskreis anzufertigen. Vielen Dank für das interessante Promotionsthema und für die Freiheit, die Sie mir in der thematischen Gestaltung meiner Projekte gewährt haben. Besonders bedanke ich mich bei Herrn Prof. Janiak für die konstruktiven Diskussionen und die Korrektur von Manuskripten.

Herrn Prof. Dr. Christian Ganter danke ich herzlich für die Übernahme der Zweitkorrektur.

Ich danke meinen Master bzw. Diplom Studenten/innen Irina Gruber, Sandra Niessing und Felix Klaus, sowie meinem „halben“ Bachelorstudenten Serkan Gökpinar für die gute Zusammenarbeit im Labor und die tolle Arbeitsatmosphäre.

Ein großer Dank geht an meine jetzigen und vergangen Bürokollegen für das angenehme Büroklima, für konstruktive Diskussionen und für Eure Hilfsbereitschaft. Ein besonderer Dank geht an Vera Vasylyeva für die vielen hilfreichen Gespräche und an Ilka Simon für die angenehme Gesellschaft an langen Arbeitstagen.

Ein ganz großes Dankeschön geht an die Mitarbeiter des Arbeitskreises. Vielen lieben Dank, dass ihr mich vom ersten Tag an so herzlich aufgenommen habt. Von Anfang an hat mich die Hilfsbereitschaft, die hier im Arbeitskreis gelebt wird beeindruckt. Ich werde die MOF-Treffen, Grillabende, die „Void Droids“ und unsere gemeinsame Zeit, immer in guter Erinnerung behalten.

Natürlich möchte ich mich auch bei allen, die mir bei Messungen und anderen Aufbauten geholfen haben, bedanken. Hier gilt mein Dank besonders Annette Ricken, Dietmar Frunzke und Birgit Tommes, sowie Frau Schäfer für die Unterstützung bei allen organisatorischen Fragen. Außerdem bedanke ich mich bei Marion Nissen für die TEM Messungen und bei Steffen Köhler für die REM Messungen und den schönen CAI Kalender.

Ich danke Sandra, Irina, Carsten, Martin, Sebastian, Dennis und Sophie für das Korrekturlesen meiner Arbeit. Außerdem bedanke ich mich bei Miriam und Julia für den „Literatursendeservice“.

Danke an Dennis Dietrich und Sandra Niessing für die tolle Zusammenarbeit bei der Betreuung unseres REMs. Martin Wickenheisser danke ich für die erfolgreiche Zusammenarbeit und die angenehme gemeinsame Zeit in China. Bedanken möchte ich mich auch bei Sebastian Glomb für die guten Gespräche, ich hoffe, wir bleiben doch auch noch nach meiner Promotion in Kontakt ;).

Ganz herzlich Bedanken möchte ich mich bei Christina Rutz, Anna Kautz, Janina Dechnik, Raquel Marcos Esteban, Sandra Niessing, Ilka Simon und Irina Gruber. Danke für die tolle Zeit, für die Umarmungen, die Notfall-Schokolade, die Mädelsabende und für Eure Geduld mit dem (liebenswerten) Wieselchen ;).

Meinen Eltern und meinen beiden Schwestern danke ich für die bedingungslose Unterstützung. Danke, dass ihr so viel Vertrauen in mich habt und immer für mich da seid!

Am allermeisten danke ich meinem Freund Maik. Danke fürs Zuhören, für deine ehrliche Meinung, für die Unterstützung und für deine Geduld. Danke, dass Du immer für mich da bist. Danke für alles!

Kurze Zusammenfassung

Metallorganische Gerüstverbindungen (MOFs) sind eine neue Klasse hochporöser Materialien. Sie bestehen aus Knotenpunkten (Metalleinheiten), die durch organische Bausteine (Linker) zu 1□, 2□ oder 3□dimensionalen Netzwerken verbunden werden. MOFs mit hohen Oberflächen (über 7000 m^2/g) und Poren größer als 2 nm im Durchmesser wurden bereits synthetisiert. Durch diese Eigenschaften sind MOFs anderen porösen Materialien wie Zeolithen und Aktivkohlen überlegen und bieten Raum für Anwendungen im Bereich Gasreinigung, Trennung, Sensorik und Katalyse. Zum aktuellen Stand der Forschung und Anwendung wurde von der DECHEMA ein empfehlenswertes Positionspapier veröffentlicht.[I]
Als Katalysatoren sind MOFs vor allem aufgrund ihrer Anpassungsmöglichkeit von hohem Interesse (Abb. Ia). Durch Linker Design oder post-synthetische Modifizierungen können elektronische Eigenschaften, Hydrophilie und Porengröße verändert werden. Die anwendungsnahe Entwicklung von heterogenen MOF-Katalysatoren setzt ein tiefergehendes Verständnis der zahlreichen Faktoren, die Einfluss auf die Aktivität des Katalysators haben können, voraus. In dieser Arbeit wurden MIL-101Cr und Derivate dieses MOFs als Katalysatoren eingesetzt. MIL-101Cr besteht aus oktaedrischen Chrom(III) Clustern, die über Terephthalsäure-linker zu einem dreidimensionalen Netzwerk verbrückt werden. 1 g dieses Material weißt eine innere Oberfläche von über 3000 m^2 auf, sowie zusätzlich freie Koordinationsstellen am Metall. Zusammen mit seiner außerordentlichen chemischen Stabilität, insbesondere Wasserstabilität, ist es geeignet für die Anwendung als Katalysator. Die Diacetalisierung von Benzaldehyd mit verschiedenen Alkoholen, sowie die Umwandlung von Glucose zur Plattformchemikalie 5-Hydroxymethylfurfural (5-HMF) wurde mit verschiedenen MIL-101Cr Derivaten als Katalysatoren untersucht (Abb. Ib,c).

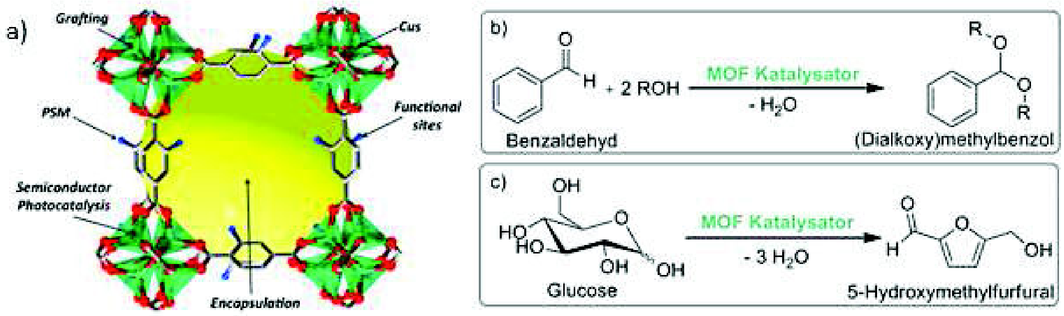

Abbildung I: a) Strategien um katalytische Eigenschaften in MOFs zu modifizieren; b) Diacetalisierung von Benzaldehyd mit MIL-101Cr Derivaten; c) Umsetzung von Glucose zu der Plattformchemikalie 5-Hydroxymethylfurfural mit MIL-101Cr Derivaten. Gedruckt mit der Erlaubnis von Referenz [1], Copyright 2014 American Chemical Society.

[I] *Roadmap Metallorganische Gerüstverbindungen,* DECHEMA Positionspapier **2014**, ISBN 978-3-89746-263-5.

Es wurden MIL-101Cr Derivate mit Nitro□ und Amino□Funktionalität hergestellt. Anhand der Modellreaktion der Diacetalisierung von Benzaldehyd mit Methanol wurde der Einfluss von elektronenziehenden gegenüber donierenden Effekten, als auch der Einfluss der Partikelgröße auf die Katalysatoraktivität untersucht. Hier zeigte sich die höchste Aktivität für das Nitro□funktionalisierte MOF mit einem Umsatz von 99 % nach 90 min. Außerdem wurden verschiedene langkettige Alkohole von Ethanol bis Pentanol eingesetzt, wobei ein Trend zu abnehmender Aktivität mit der Länge des Alkohols gemessen wurde. Es konnte gezeigt werden, dass die Katalysatoraktivität auf einen Brønsted sauren Mechanismus zurückgeführt werden kann. Hierbei ist die Deprotonierung von polarisierten Aqua-Liganden durch den Nitro□Substituenten stark begünstigt.

In einem Folgeprojekt wurde untersucht ob die Selektivität der Produktbildung durch MIL-101Cr Derivate beeinflusst werden kann. Hierzu wurde die Kaskadenreaktion von Glucose zu 5-Hydroxymethylfurfural (5-HMF) (Abb. 1c) gewählt. 5-HMF gilt als Plattformchemikalie, da viele wertvolle Folgeprodukte wie zum Beispiel Polymer Precursoren (2, 5-Furandicarbon-säure, Adipinsäure) und auch Kraftstoffadditive daraus hergestellt werden können. Als Nebenprodukte können verschiedene Zucker (Fruktose, Mannose, Sorbitol) sowie Lävulinsäure, Ameisensäure und Furfural entstehen, so wie auch lösliche und nichtlösliche Polymere, die allgemein als Humins bezeichnet werden. Es konnte gezeigt werden, dass die eingesetzten MOFs die Reaktion zu 5-HMF bei relativ niedriger Temperatur (130 °C), in einem Gemisch aus THF/H_2O im Vergleich mit Schwefelsäure und Amberlyst in hoher Selektivität katalysieren. Die beste Ausbeute von 29% nach 24 h wurde mit MIL-101Cr-SO_3H erhalten. Der Fokus des Projektes lag auf der Aufklärung der Faktoren, die die Aktivität und Selektivität des MOF Katalysators beeinflussen.

Ein wichtiger technischer Aspekt für die Anwendung von MOFs ist deren Formgebung, da diese meist als mikrokristalline ultraleichte Pulver vorliegen, die für viele Anwendungen ungeeignet sind. Im Rahmen dieser Arbeit wurden verschiedene Methoden zur Formgebung untersucht, mit dem Ziel die Eigenschaften der MOFs (Porosität und Kristallinität) zu erhalten. Mit dem Ziel kombinierte CO_2/H_2O Sorptions-Messungen in einem Festbettreaktor durchzuführen wurde die mechanische Stabilität von MIL-101Cr Derivaten getestet, da diese für die Messung als Pellets vorliegen sollten. Es konnte gezeigt werden, dass mit steigendem Druck die Porosität und Kristallinität abnimmt. Bei einem Druck von 0.5 kPa konnten Pellets geformt werden (Erhalt der Oberfläche 90% für MIL-101Cr-NH_2). In einer Kooperation mit dem *Deutschen Institut für Luft und Raumfahrt (DLR)* wurden die Einbettung von MOFs in Resorcinol-Formaldehyde Xerogele untersucht. Es wurde u.a. für MIL-101Cr eine Methode entwickelt, die die Herstellung von formstabilen Monolithen unter vollständigem Erhalt der Oberfläche ermöglichte.

Short summary

Metal-organic frameworks (MOFs) are a new class of highly porous materials. They are composed of metal nodes, which are connected through organic linkers to 1, 2 or 3 dimensional networks. MOFs display a uniform and modular structure, with a huge variety of possible metals and linkers. Very high surface areas above 7000 m^2/g have already been obtained. They are promising materials for application in gas purification and separation, as sensors and in catalysis. Summarizing industry relevant state-of-the-art research a recommendable position paper was published by DECHEMA (2014).[II]

As catalysts, metal-organic frameworks are of high interest because of their high tuneability (Figure I a). Modifications affecting electronic properties, hydrophilicity and pore sizes are possible. Mesopores (larger than 2 nm) are accessible. Due to these properties, MOFs can be superior to other porous materials as zeolites or active carbon.

Application development of heterogeneous MOF catalysts requires a thorough understanding of how catalyst performance is influenced by the numerous parameters affecting the activity of MOFs. In this work, MIL-101Cr and functionlized MIL-101Cr derivates have been applied as catalysts (MIL = Matériaux de l'Institut Lavoisier). MIL-101Cr is composed of trimeric Chrom(III) octahedral clusters, connected through terephthalic acid linker to a 3D network. 1 g of MIL-101Cr exhibits a Brunauer-Emmett-Teller (BET) surface area of about 3100 m^2/g (determined experimentally) and two open metal sites (OMS) per secondary building unit are available. In combination with its high water stability, MIL-101Cr is a promising candidate as catalyst. In the present work, the diacetalization of benzaldehyde with different alcohols and the conversion of glucose to 5-hydroxymethylfurfural (5-HMF) was investigated (Figure I b,c)

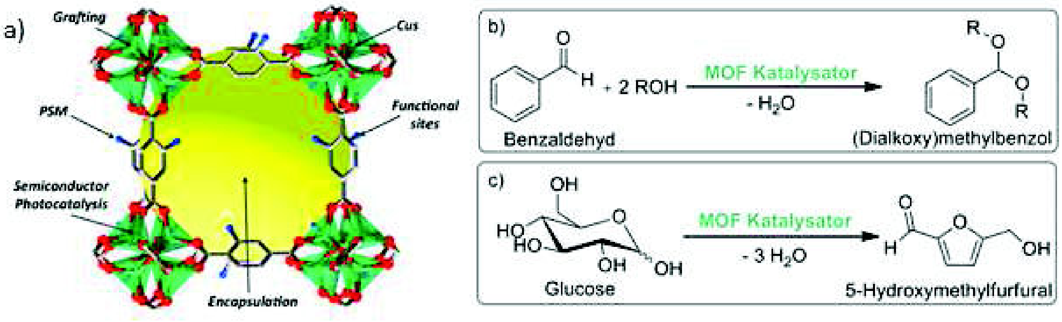

Figure II: a) Strategies to modify catalytic properties in MOFs; b) diacetalization of benzaldehyde with alcohols catalyzed by ML-101Cr derivatives; c) conversion of glucose to the platformchemical 5-hydroxymethylfurfural with MIL-101Cr derivates. Reprinted with permission from ref. [1]. Copyright (2014) American Chemical Society.

MIL-101Cr derivates with nitro- and amino functionality have been synthesized. Based on the model reaction of diacetalization of benzaldehyde with methanol, the influences of

---

[II] *Roadmap Metallorganische Gerüstverbindungen,* DECHEMA Positionspapier **2014**, ISBN 978-3-89746-263-5.

electron-withdrawing versus donating effects and the influence of particle size on catalyst activity was investigated. The nitro-functionalized MIL-101Cr exhibited the highest activity with a conversion of 99 % after 90 min. Using longer chain alcohols from ethanol to pentanol a decrease in activity was observed. Lewis- and Brønsted acid catalyzed mechanisms were examined. From experimental data is was concluded that catalyst activity derived from Brønsted acid conversion by polarized aqua-ligands, which was significantly enhanced by the electron-withdrawing effect of nitro-moiety.

The follow-up project expanded the scope of acid catalysis with MIL-101Cr derivates by selectivity of product distributions. The cascade reaction of glucose to 5-HMF was selected (Figure I c). 5-HMF was rated as platform chemical, because it can be converted to numerous valuable products as polymer precursors (2, 5-furandicaboxylic acid, adipic acid) and fuel additives. As byproducts different sugars (fructose, mannose, sorbitol), levulinic acid, formic acid and furfural can be formed. Furthermore, undesired soluble and insoluble polymers, called humins usually are generated. This diminishes the yield and selectivity of the reaction. In the present work, for the first time, MIL-101Cr-SO_3H, MIL-101Cr-NO_2 and mixed materials were applied as catalysts for the conversion of glucose to 5-HMF in a THF/H_2O system at 130°C. MIL-101Cr-SO_3H performed best with a 5-HMF yield of 29% after 24 h with a high selectivity towards 5-HMF. Only small amounts of Levulinic acid were produced (7%), in contrast to reference experiments using acidic resin Amberlyst-15 and sulfuric acid which formed levulinic acid as major product. The focus of the project was on investigation of parameters influencing activity and selectivity of the MOF catalysts.

An important technical aspect concerning application of MOFs is shaping. Usually, MOFs are obtained as microcrystalline fine powders, which are unsuitable in handling. Within the scope of this work different methods for shaping of MOFs were investigated, all pursuing the retention of MOF properties (porosity and crystallinity). The mechanical stability of MIL-101Cr and MIL-101Cr-NH_2 was tested by forming pellets using different pressures. Both MOFs were found to be unstable to mechanical pressure. When raising the pressure from 0.5 kPa (retention of surface area for MIL-101Cr-NH_2: 90%) to higher pressure a continuous loss in surface area and crystallinity until collapse was observed. In cooperation with national german aeronautics and space research centre the embedding of MOFs in resorcinol-formaldehyde xerogels was investigated. Using MIL-101Cr as model compound a method for the formation of stable MOF@polymer composites was developed. After thorough characterization, the retention of surface area, crystallinity and pore accessibility was confirmed. Up to 77wt% MIL-101Cr could be loaded to the polymer matrix.

List of abbreviations and symbols

bar	Unit of pressure (1 bar $\triangleq$ 100000 Pa $\triangleq$ 100 kPa)
BDC	1,4-Benzenedicarboxylate
BET	Brunauer-Emmett-Teller
BJH	Barrett-Joyner-Halenda Method
CCR	Carbonization and carbothermal reduction
CTAB	Cetyltrimethylammoniumbromid
d	Day(s)
DEF	*N,N*-Diethylformamide
DMF	*N,N*-Dimethylformamide
DMSO	Dimethylsulfoxide
EtOH	Ethanol
h	Hour(s)
IR	Infrared spectroscopy
IUPAC	International Union of Pure and Applied Chemistry
K	Degree Kelvin
MC	mesoporous compound
mg	(Milli)gram
MIL	Matériaux de l’Institut Lavoisier
min	Minute(s)
mL	Milliliter(s)
(m)mol	(Milli)mol, unit of amount of substance (1 mol $\triangleq 6.022 \cdot 10^{23}$ particles)
MO	Metal oxide
MOF	Metal-organic framework
NL(DFT)	(Nonlocal) density functional theory
nm	Nanometer(s)
NMR	Nuclear Magnetic resonance
p	Pressure
(P)XRD	(Powder) X-ray diffraction
r.t.	Room temperature
R,F-xerogel	Resorcinol-formaldehyde based xerogel
SBU	Secondary building unit
SEM	Scanning electron microscopy
TGA	Thermogravimetric analysis
TMAOH	Tetramethylammonium hydroxide
wt%	Weight percentage (weight%)
δ	Delta (stands for chemical shift)

Table of contents

1. Introduction

Globalization, climate change, increasing expectations on quality of life, consumption, resources, renewable energy, CO_2, energy storage and distribution … are interrelated challenges we have to face in the present and in the future.

“*Pollution is nothing but resources we’re not harvesting. We allow them to disperse because we’ve been ignorant of their value. But if we got onto a planning basis, the government could trap pollutants in the stacks and spillages and get back more money than this would cost out of the stockpiled chemistries they’d be collecting.*” (quote of Richard Buckminster Fuller, cited by Geoffrey A. Ozin in his perspective[2]).

This problem has been redefined in the last years, resulting in powerful transformations of modes of thoughts. These involve the infinite use of materials in cycles, following the cradle to cradle principle[3], treatment of CO_2 as resource for chemical industry[4] as well as the development of new materials from waste streams, including non-food biomass waste.[5],[6]

Accepting these challenges gives rise to radical innovations in terms of materials and technology. Within this context catalysis is a key technology for material innovation since about 90% of chemical processes involve catalysts in at least one of their steps.[7] Porous heterogeneous catalysts are auspicious candidates as reviewed by I. Fechete *et al*.[7]

Powerful heterogeneous catalysts currently used in industry are zeolites. Zeolites are porous materials, which have been first applied as catalysts in industry in 1959 as isomerization catalyst (zeolite-Y, by Carbide) and 1962 as hydrocarbon cracking catalyst (zeolite X by Mobile Oil).[8]
Zeolites can be chemically described by the empirical formula $M_{2/n}O \cdot Al_2O_3 \cdot ySiO_2 \cdot wH_2O$ ($y = 2\text{-}200$, n = cation valence, w = water in the voids of zeolites). In general, they are build up from infinitely extending 3D framework of AlO_4 and SiO_4 tetrahedra, which are connected through oxygen bonds.[8]

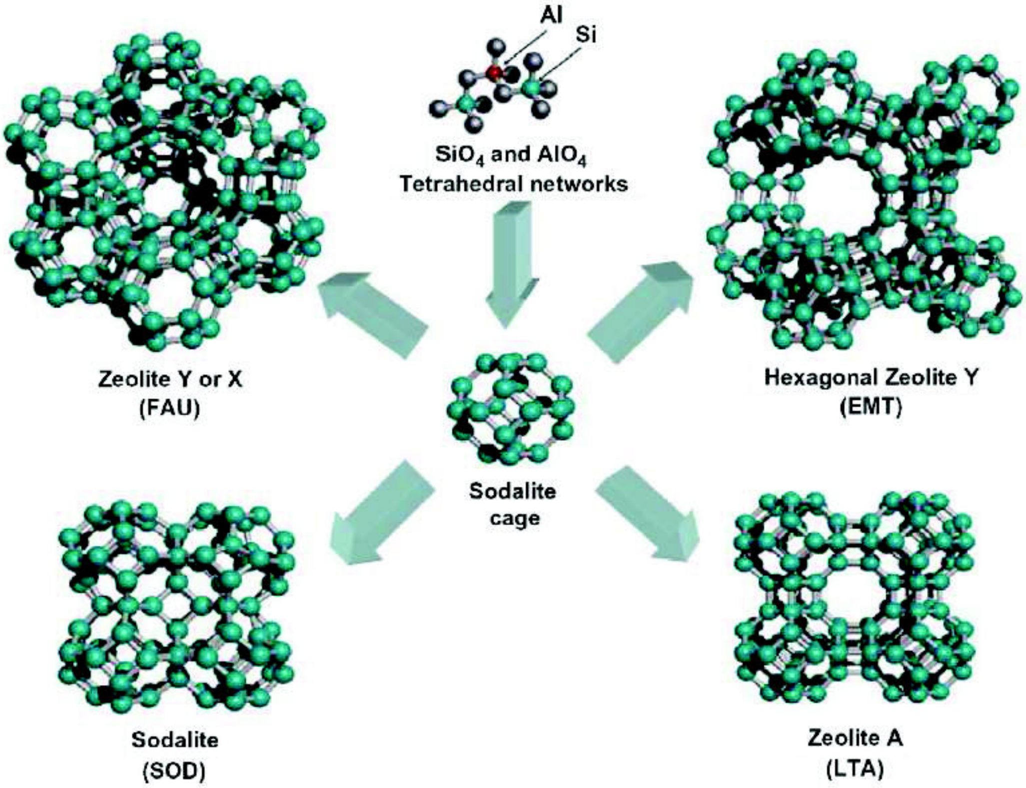

Figure 1: Sodalite based zeolite structures, consisting of SiO_4 and AlO_4 tetrahedral networks. Reprinted from ref.[9], Copyright 2008, with permission from Elsevier.

However, zeolites have certain weaknesses, such as pore sizes limited to micropores (usually only up to 1 nm)[8], which maybe overcome if other catalysts were used. During the last 25 years a new class of porous materials called metal-organic frameworks (MOFs) or coordination polymers emerged which display fascinating properties and may help to meet future challenges, especially in the area of catalysis.[10],[11],[12],[13]

1.1 Metal-organic frameworks (MOFs)

Metal-organic frameworks (MOFs) □also named coordination polymers □generally belong to the class of organic-inorganic hybrid materials. They consist of metal nodes and bridging organic linkers.[10],[14] The term □coordination polymer□ only describes the extended connection of metal and ligand monomers through coordination bonds.[15] Coordination polymers exhibit infinite connectivity at least in one dimension, but can also be 2- or 3 dimensional. The term □metal-organic framework□was introduced for the first time by Yaghi *et al* in 1995.[16] The International Union of Pure and Applied Chemistry (IUPAC) provided a set of definitions for use in the classification of coordination polymers and metal□organic frameworks (MOFs).[17],[18] According to IUPAC, MOFs are defined as □*a coordination network with organic ligands containing potential voids.*□[17]

In this work, the term MOF is extended following the terminology of Rowsell and Yaghi.[15] MOFs are materials displaying the following properties: i) strong bonding, ii) geometrical well-defined structure, iii) crystallinity and iv) permanent porosity. The latter describes that the material was proven porous by gas sorption measurements. The framework retains its integrity upon removing of solvent and guest molecules.[10,15]

Another difference between coordination polymers and MOFs is the nature of metal nodes: In coordination polymers the metal node often is mono-atomic, while in MOFs the meal node consists of polyatomic clusters. These clusters increase the stability of MOFs and are termed secondary building unit (SBU).[19] They can be used as concept to organize the variety of MOF structures.[19] The SBUs serve as connectors for the organic ligands and predetermine fixed linking geometries. Both SBU and linker orientation determine the final framework topology. Three examples of MOF framework topologies are depicted in Figure 2.[20]

Anionic linkers, such as sulfonates, phosphonates, heterocyclic compounds and carboxylates are used as organic bridging units between the metal nodes. The most prominent of these organic bridging units are carboxylates as they are easily accessible and form MOFs with a variety of SBUs.[20]

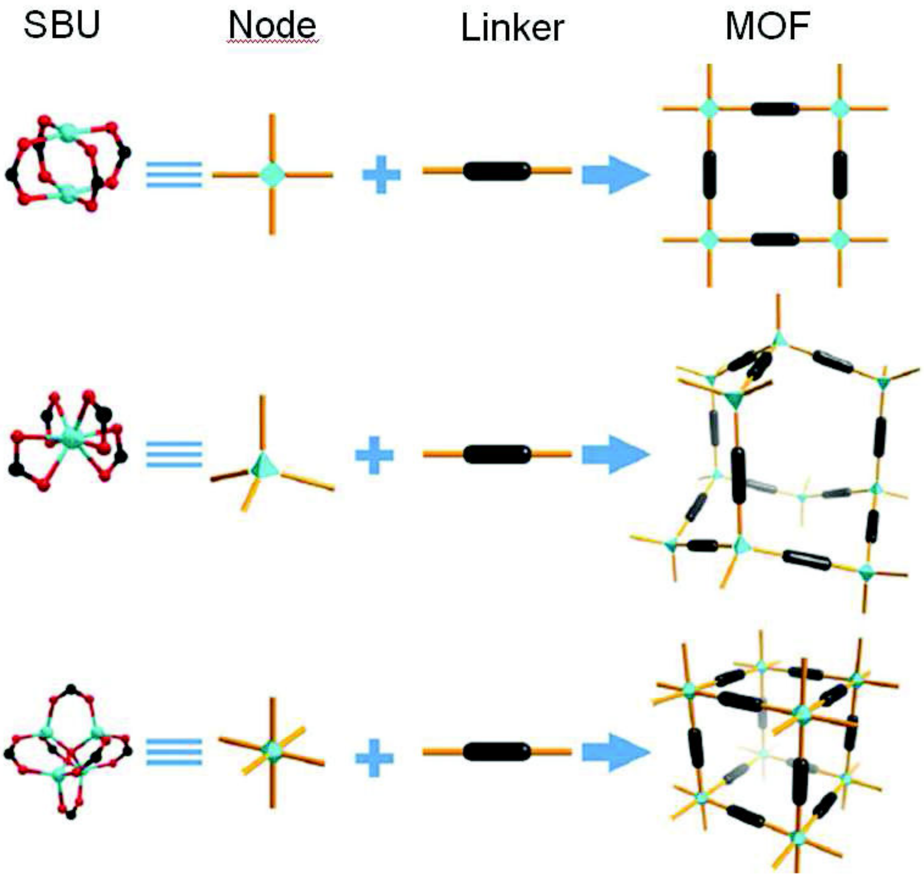

Figure 2: Graphical illustration of the construction of some representative coordination polymers/MOFs from SBUs and rigid linkers. Reprinted from ref. [20], Copyright 2014, with permission from the Royal Society of Chemistry.

1.2 MOFs versus zeolites

One of the first examples of metal-organic framework used as a catalyst was reported in 1994 by Fujita *et al*..[21] A Cd-based framework was investigated as catalyst for the cyanosilylation of aldehydes.[21] However, in-depth research on MOFs as catalysts started around 2009 (Figure 3). Comparing the development of the two classes of porous materials, zeolites and MOFs, it becomes obvious that the application of MOFs as catalysts still is in its infancy. In 2015 only 22% of publications about MOF research addressed catalytic reactions compared to 43% of the publications in zeolite research (Figure 3).

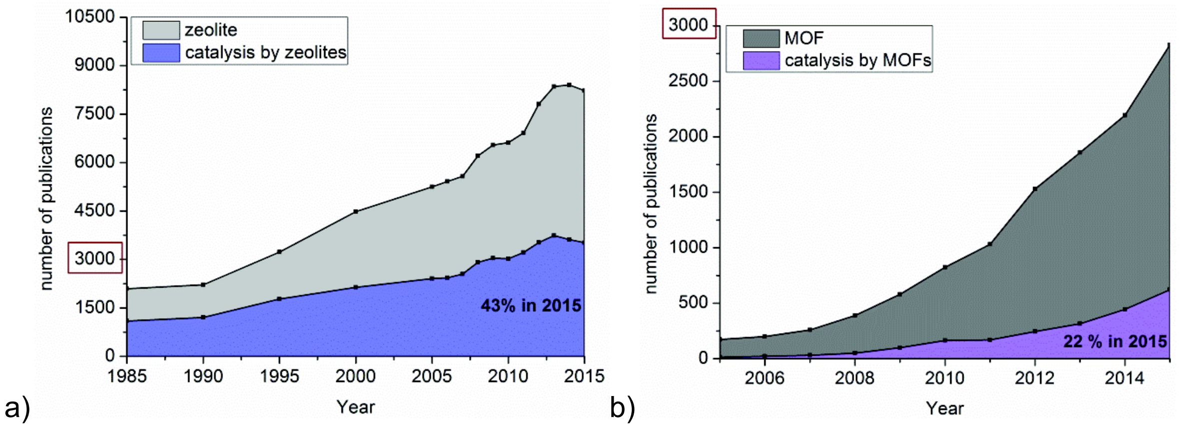

Figure 3: Comparison of the total number of publications for a) zeolites and b) MOFs, respectively, related to general research activity and in special to the area of catalysis. Source: Scifinder, (search carried out in May 2016), Search term “catalysis by MOFs”, “catalysis by zeolites” compared to “MOF” and “zeolite”.

Despite the minor fraction of publications on MOFs as catalysts, a rapid development in the field of MOF catalysis is obvious, as the topic has been reviewed extensively in the last 5 years.[12],[22],[23],[11],[24],[13] Apart from the work presenting a general overview about the progress, also reviews about specific fields of catalytic reactions with MOFs can be recommended: condensation reactions of carbonyl groups[25], synthesis of nitrogen-containing heterocycles[26], for the production of fine chemicals[27] oxidation reactions[28], photocatalysis[29] or embedding of metal nanoparticles in MOFs in order to obtain cage isolated catalysts.[30]

To extend the scope of catalysis with MOFs, a comparison of the properties of zeolites and MOFs can help to determine areas of catalysis in which MOFs can be superior to state-of-the-art heterogeneous catalyst.

Currently, zeolites are successfully used as heterogeneous porous catalysts in variety of reactions and industrial processes.[7],[8] Comparing the properties of zeolites and MOFs significant differences can be determined (Figure 4).[31],[32]

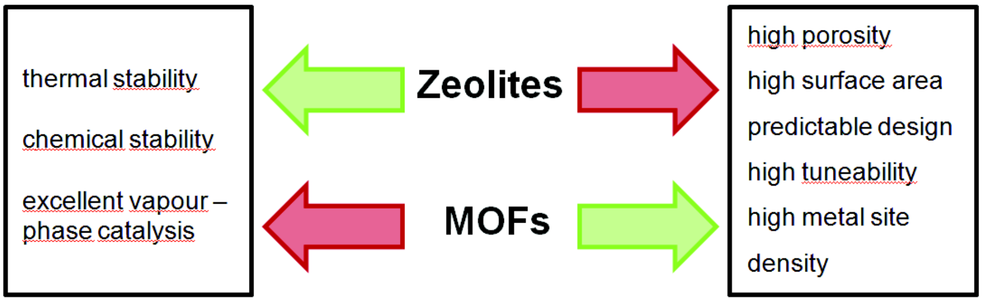

Figure 4: Strengths (green) and weaknesses (red) of zeolites and MOFs, modified from ref. [31].

In general, zeolites outperform MOFs in terms of thermal and chemical stability, whereas MOFs are superior in terms of tuneability due to the variety of organic linkers and metal building units they can be composed of. MOFs possess a large variety of different pore sizes and geometries, reaching until 9.8 nm in diameter[33], thus circumventing diffusion limitations that exist for microporous zeolites (Figure 5).[32],[34] Taking the properties together MOFs are most suitable for liquid phase catalysis, instead of gas phase reactions where zeolites are dominant.[31]

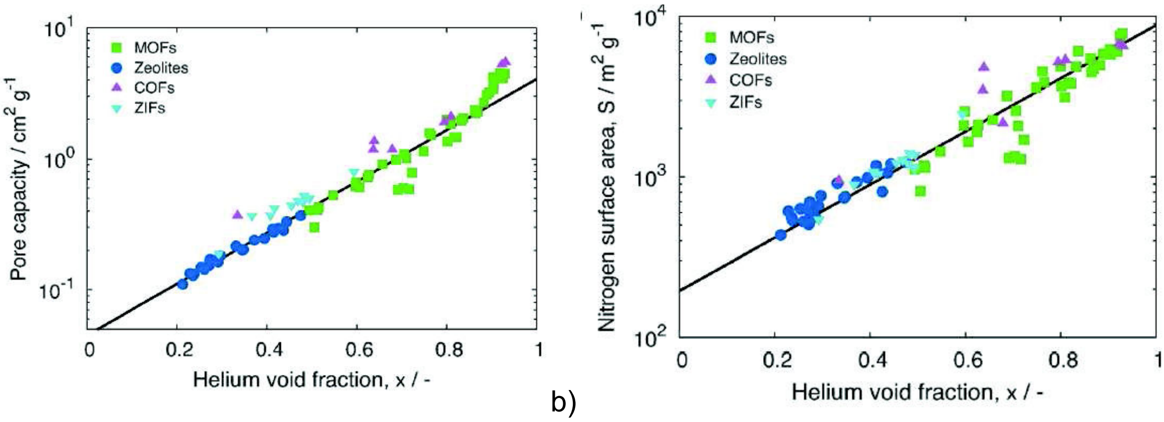

a) b)

Figure 5: Plot of surface areas and pore capacities as a function of the porosity of a wide range of MOFs, zeolites, COFs, and ZIFs. Note that the y axes are in the log scale. Reprinted from ref. [34], Copyright 2015, with permission from John Wiley and Sons.

Furthermore, ligand design and post-synthetic modifications (PSM) allow for tailoring the pore environment of MOFs, enabling high shape-selectivity in catalysis. Shape-selectivity means the MOF being restrictive to a certain kind of molecule or molecule size which is an important tool in reaction engineering. Larger pores can facilitate the diffusion and mass transfer of reagents and products. Smaller pores lead to a higher control of substrate orientation. Functionalization of the organic linker or metal nodes allow for a better control of the chemical pore environment.[35]

Moreover, MOFs have a high metal site density compared to zeolites (Table 1). The SBUs serve as active metal sites, if coordinated unsaturated sites are available based on the framework topology.[35] Figure 4 displays relevant properties of MOFs and zeolites in terms of catalysis.

Table 1: Comparison of relevant properties for catalysis, modified from reference [31].

Properties	Zeolites	MOFs
Thermal stability	stable above 450 °C	Not stable above 300 °C
Chemical stability	Stable to solvents, acids, oxidizing and reducing agents	Limited chemical stability especially towards water for most cases
BET Surface area	around 200-500 m^2/g	around 1000-10 000m^2/g
Pore volume	0.1-0.5 cm^3	over 1 cm^3
Metal site density	low	high
Lewis acidity	accessible framework metal ions	accessible framework metal ions
Brønsted acidity	bridging Si(OH)/Al hydroxyl groups	introducible through organic linker (e.g. SO_3H)
Basicity	From framework oxygens	introducible through organic linker (e.g. NH_2)
Active site environment	Mostly hydrophilic but can be made hydrophobic	Considerably hydrophobic, but linker dependent
Additional features		chiral functionalities, flexible and stimuli responsive behavior
Reactivation	By thermal treatment	Washing procedures, thermal treatment not possible

The reviews of P. García-García and J. Gascon are recommended, which not only evaluate recent work, but also provide a guideline for catalytic testing practice and interpretations.[35],[1] Especially, the catalyst stability under the applied reaction conditions has to be proven carefully, which is sometimes disregarded in literature. Specifically, when reactions are performed in the presence of water problems can occur, as not many water stable MOFs have been described so far.[36]

Although the interest and research activity in catalysis with MOFs increases (Figure 3), the development of MOF catalysts is still in its infancy and breakthroughs in practice remain to be done. In the following, the focus will be on acid catalysis, which is one of the most promising application of MOFs, because i) many reactions, also related to fine chemistry, proceed via acid catalysis, ii) catalytic activity originates from the MOF itself (not from an incorporated guest molecule) and iii) acid catalysis can be combined with various other mechanism resulting in multifunctional catalysis.[37]

1.3 Stability of MOFs

Acid catalyzed reactions involve mechanisms such as hydrolysis, condensation, dehydration and esterification.[25],[27] All these acid catalyzed reactions have in common that they either take place in the presence of or generate H_2O.[25],[27] Although there are more than 20 000 MOFs reported in literature, for such reactions, only water stable MOFs, which also display a certain degree of thermal and chemical stability are suitable. This requirement reduces the number of applicable MOFs dramatically.

J. J. Low and coworkers described first the hydrothermal steam stability of prototypical MOFs.[38] F. Jeremias and coworkers investigated the water vapor stability of several MOFs of the MIL family (abbreviation for Materials Institute Lavoisier) for sorption-based heat transformation and storage appliances.[39],[40],[41],[42],[43] Especially, MIL-101Cr-NH_2 showed a very promising performance over 40 cycles of water ad- and desorption.[42]

N. C. Burtch *et al.* categorize the factors governing water stability of MOFs into i) thermodynamic stability, including metal-ligand bond strength and lability with water and ii) kinetic stability with the subcategories hydrophobicity and steric factors.[44] After defining minimum testing conditions and a understanding of water stability the review provides a comprehensive overview about stability of MOFs in terms of water stability.[44]

Very recently, K. Leus and coworkers carried out a systematic study about the stability of some selected prototypical frameworks. Here, not only water stability, but also stability towards acids and bases, as well as peroxides were tested (Figure 6).[45] All cited studies determined the following materials as the most stable MOFs under water vapor and aqueous conditions: MIL-101Cr, MIL-53Al, MIL-53-NH_2, UiO-66, UiO-66-NH_2 and UiO-67.[45],[44],[38],[42]

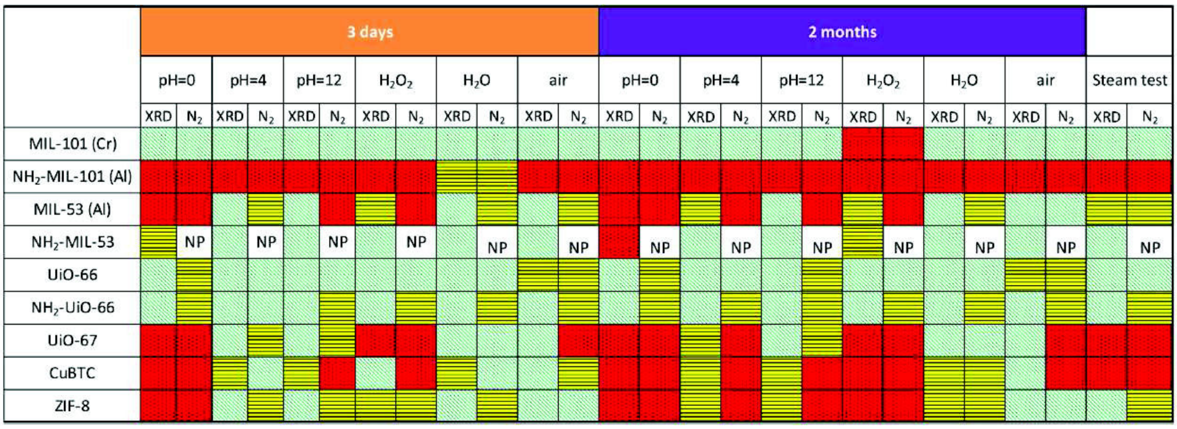

	3 days												2 months													
	pH=0		pH=4		pH=12		H_2O_2		H_2O		air		pH=0		pH=4		pH=12		H_2O_2		H_2O		air		Steam test	
	XRD	N_2	XRD	N_2	XRD	N_2	XRD	N_2	XRD	N_2	XRD	N_2	XRD	N_2	XRD	N_2	XRD	N_2	XRD	N_2	XRD	N_2	XRD	N_2	XRD	N_2
MIL-101 (Cr)	🟩	🟩	🟩	🟩	🟩	🟩	🟩	🟩	🟩	🟩	🟩	🟩	🟩	🟩	🟩	🟩	🟩	🟩	🟥	🟥	🟩	🟩	🟩	🟩	🟩	🟩
NH_2-MIL-101 (Al)	🟥	🟥	🟥	🟥	🟥	🟥	🟥	🟥	🟨	🟨	🟥	🟥	🟥	🟥	🟥	🟥	🟥	🟥	🟥	🟥	🟥	🟥	🟥	🟥	🟥	🟥
MIL-53 (Al)	🟥	🟥	🟩	🟨	🟩	🟥	🟨	🟥	🟩	🟨	🟩	🟨	🟥	🟥	🟨	🟥	🟩	🟥	🟨	🟥	🟩	🟨	🟩	🟩	🟨	🟨
NH_2-MIL-53	🟨	NP	🟩	NP	🟩	NP	🟩	NP	🟩	NP	🟩	NP	🟥	NP	🟩	NP	🟩	NP	🟨	NP	🟩	NP	🟩	NP	🟩	NP
UiO-66	🟩	🟨	🟩	🟩	🟩	🟩	🟩	🟩	🟩	🟩	🟨	🟨	🟩	🟨	🟩	🟩	🟩	🟨	🟩	🟩	🟩	🟩	🟨	🟨	🟩	🟩
NH_2-UiO-66	🟩	🟨	🟩	🟩	🟩	🟨	🟩	🟨	🟩	🟨	🟩	🟨	🟩	🟨	🟩	🟨	🟩	🟨	🟩	🟨	🟩	🟨	🟩	🟨	🟩	🟨
UiO-67	🟥	🟥	🟩	🟨	🟩	🟨	🟥	🟥	🟩	🟩	🟩	🟥	🟥	🟥	🟨	🟥	🟩	🟨	🟥	🟥	🟩	🟩	🟩	🟥	🟥	🟥
CuBTC	🟥	🟥	🟨	🟩	🟨	🟥	🟩	🟥	🟨	🟩	🟩	🟨	🟥	🟥	🟨	🟥	🟨	🟥	🟥	🟥	🟨	🟨	🟩	🟥	🟥	🟥
ZIF-8	🟥	🟥	🟩	🟨	🟩	🟨	🟨	🟨	🟩	🟨	🟩	🟩	🟥	🟥	🟨	🟥	🟨	🟥	🟥	🟥	🟨	🟨	🟩	🟩	🟩	🟨

Figure 6: Overview of the stability of the examined MOFs in various media (blue: the XRPD pattern and surface area is largely preserved, red: the XRPD pattern and surface area is completely destroyed, yellow: the XRPD pattern and surface area is partially decreased/degraded or transformed). Reprinted from ref. [45], Copyright 2016, with permission from Elsevier.

One of the most stable, most popular and most widely applied MOFs is MIL-101Cr. In this work, MIL-101Cr was mainly used and therefore is introduced in the following.

1.4 MIL-101Cr

G. Férey discovered the class of porous polycarboxylates of MIL type as for instance MIL-53, ML-100, MIL-88 and MIL-101Cr. [46],[47],[48],[49],[50],[51] MIL frameworks mostly contain trivalent metal cations as Cr^{3+}, Fe^{3+}, Al^{3+} and carboxylate connecting linkers.

The Chromium terephthalate MOF MIL-101Cr was first synthesized in 2005.[51] The secondary building units are composed of trimeric chromium(III) octrahedral clusters, which are interconnected by benzene-1,4-dicarboxylate linker (Figure 7). MIL-101Cr, 3D-$[Cr_3(O)(bdc)_3(F)(H_2O)_2]$-$25H_2O$, is a highly porous material, exhibiting a Brunauer-Emmett-Teller (BET) surface area up to 4000 m^2/g. Although the material is crystalline, only crystalline powder instead of larger single crystals could be obtained so far. The structure was analyzed by synchrotron powder data and computer simulation in combination with a series of sorption, TGA and XRD experiments.[51]

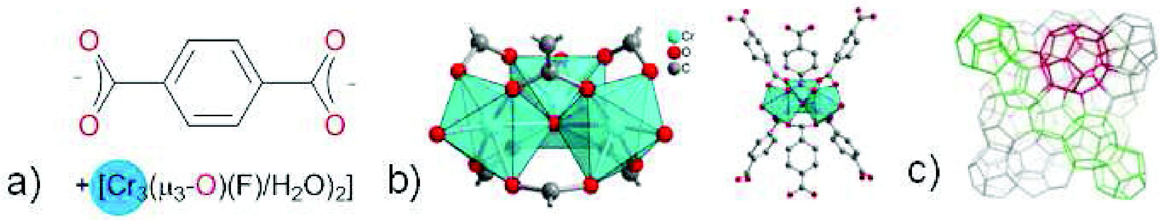

Figure 7: (a) Building blocks for MIL-101, 3D-$[Cr_3(O)(bdc)_3(F)(H_2O)_2]\cdot 25H_2O$, (b) ball-and-stick and polyhedral presentations of the trigonalprismatic $\{Cr_3(O)(F)(H_2O)_2\}$ secondary building unit with the carboxylate groups that bridge between the Cr octahedra (transparent lines) (Note: fluorine atoms could not be distinguished from aqua ligand). Copyright belongs to Prof. C. Janiak. c) zeotype architecture of MIL-101Cr. Reprinted from ref. [51], Copyright 2005, with permission of American Association for the Advancement of Science.

From these experiments it was concluded that MIL-101Cr possesses two types of mesoporous cages with diameters of 29 Å and 34 Å, which are accessible through two types of microporous windows. The smaller cages have pentagonal windows with a free opening of 12 Å, while the larger cages have both pentagonal and hexagonal windows with a free opening diameter of 14.7 Å to 16 Å) (Figure 8).[51] Additionally, MIL-101Cr displays two water molecules and one fluorine ion which are coordinated to chromium (III). The water molecules can be removed through heating in vacuum and enable the accessibility of open metal sites (OMS). A thermal stability up to 350 °C was measured using TGA.[51] On SEM and TEM pictures the typical octahedral shape of the crystalline particles can be observed (Figure 9).

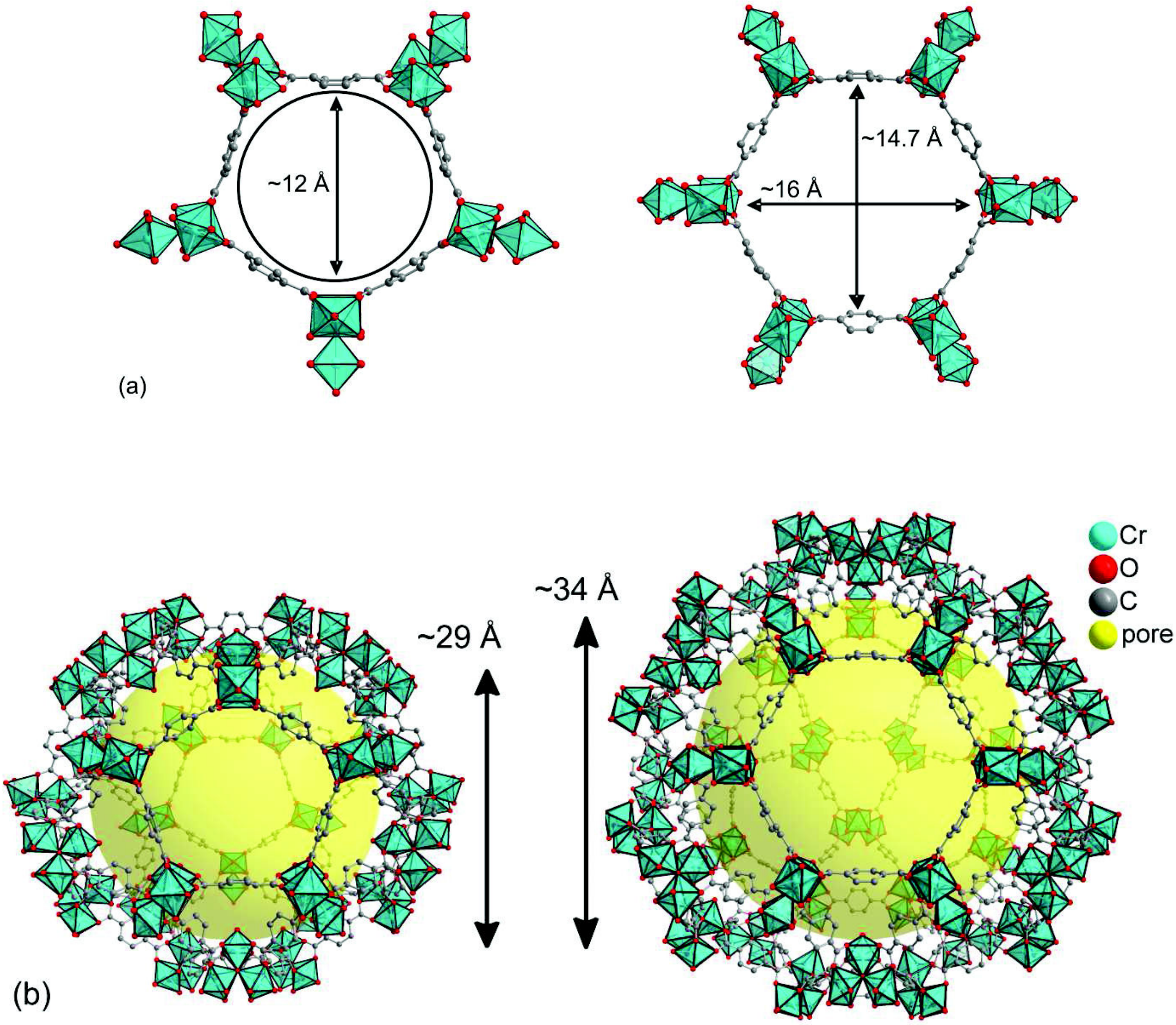

Figure 8: Building blocks for MIL-101, $[Cr_3(\mu_3\text{-}O)(F,OH)(BDC)_3(H_2O)_2]$, generated from the deposited X-ray data file at the Cambridge Structure Database (CSD-Refcode OCUNAK) using the program DIAMOND. Trinuclear $\{Cr_3(\mu_3\text{-}O)(F,OH)(H_2O)_2(O_2C\text{-})_6\}$ building units and bridging benzene-1,4-dicarboxylate ligands a) form pentagonal and hexagonal rings (b) which are assembled into mesoporous cages. The different objects in this figure are not drawn to scale. Copyright belongs to Prof. C. Janiak.

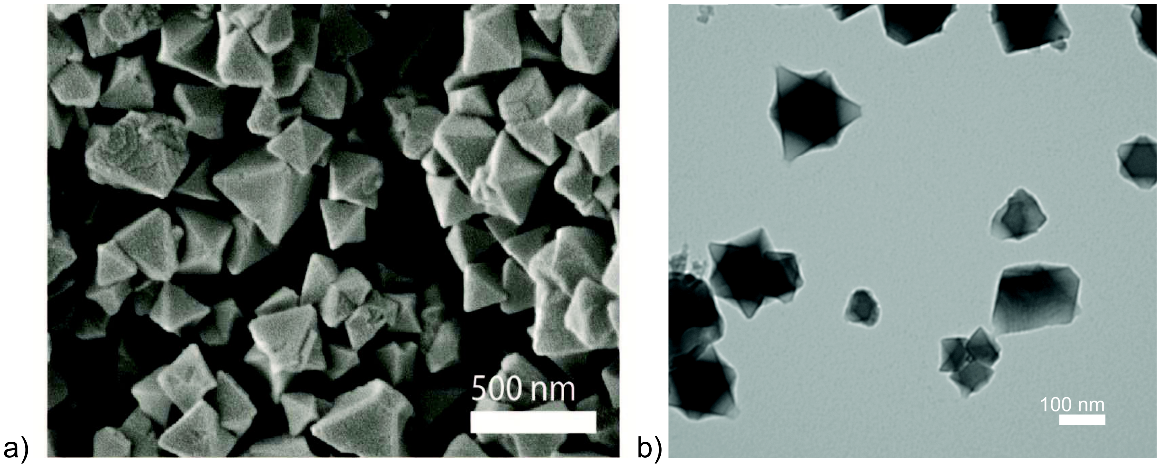

Figure 9: a) SEM and b) TEM images of MIL-101Cr.

Originally, MIL-101Cr was synthesized hydrothermally with the addition of hydrofluoric acid as mineralizing agent.[51] However, due to the enormous interest in this material in the last years many studies have been conducted in order to improve the synthesis of MIL-101Cr.[52],[53] The effect of acetic and nitric acid modifiers was found to increase the yield of MIL-101Cr from 50% (average from literature) to over 80% while maintaining porosity and crystallinity.[53]

Because of the remarkable chemical and solvent stability of MIL-101Cr[45], the MOF was studied for numerous applications ranging from gas sorption and guest encapsulation to separation and catalysis. Two excellent reviews about MIL-101Cr were published by D. Hong in 2009 and S. Bhattacharjee in 2014, providing a thorough overview about MIL-101Cr based research.[54],[52] Caused by the industrially relevant properties of MIL-101Cr, the MOF was and still is the object of intense research.

1.5 Post-synthetic modification of metal-organic frameworks

The limited amount of water stable MOFs is critical since possible application as catalyst is reduced to basically 3 framework structures: MIL-101Cr, MIL-53, UiO-66.

Fortunately, during the last years a toolbox of post-synthetic modification (PSM) methods was developed. PSM refers to a chemical modification of the MOF lattice in a heterogeneous manner. The structure of the MOF itself has to be preserved upon functionalization, which is usually shown by XRD and sorption experiments after the reaction.[55],[56] General strategies for post-synthetic modifications are shown in Figure 10.

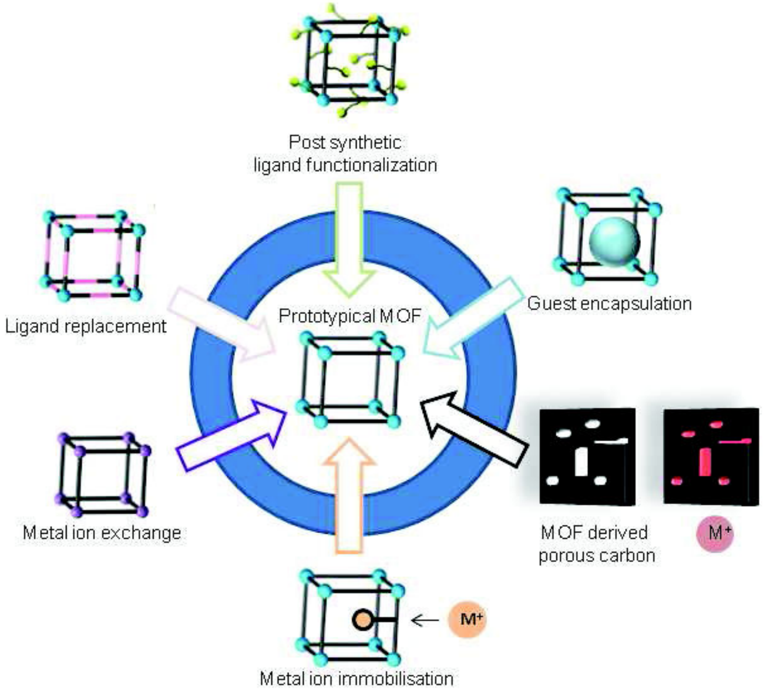

Figure 10: Post synthetic modifications of prototypical MOFs. Modified from ref. [57], Copyright 2016, with permission from the Royal Society of Chemistry.

PSM can be subdivided into non-covalent and covalent PSM.[56] Among the non-covalent PSM guest exchange, formation of metal nanoparticles insides the pores of a MOF and even activation procedures can be numbered.[58] Post-synthetic ligand functionalization and metal ion coordination through linkers belong to the covalent PSM methods.[56]

During the last few years a □second generation□ of PSMs emerged. These include i) *solvent assisted linker exchange* (SALE)[59], ii) non-bridging ligand replacement[60] and iii) transmetalation of metal nodes or within linkers.[58],[61] These methods have been merged by P. Deria and co workers under the hyponym *building block replacement* (BBR).[62] Even decomposition of MOFs into metal nanoparticles or porous metal oxides as well as metal supported nanoporous carbon can be regarded as post-synthetic modification. Based on the properties of the parent MOF material the resulting products still display high porosity and attracted much attention during the last years.[63]

1.6 Solid acid catalysis

Industrial processes for the formation of fine chemicals often use mineralic acids and corrosive substances. These processes are often not very efficient, since homogenous acid catalysts are used in over-stoichiometric amounts and have to be destroyed/neutralized after each batch in order to separate the products. In this case the usage of heterogeneous solid acid catalysts, as for instance MOFs, can contribute to the case of recovery, reactivation and reuse.[64] Therefore, the industry of bulk chemistry replaced homogenous to solid acids during the last years, but there is still a great demand for the same regarding liquid phase reactions in fine chemical production.[25],[27],[64]

MOF based solid acid catalysis attracted much attention, since some MOFs possess open metal sites, which can be active in Lewis acid catalysis.[25],[65] In addition, the size and shape selectivity generated by MOFs is interesting for acid catalyzed reactions, since by this the formation of undesired byproducts can be prevented.[35] Due to these properties, MOFs have been employed intensively, for example, in C □C bond forming condensation reactions, and were shown to outperform zeolites and aluminosilicates in some cases, such as in the Friedländer reaction. The Friedländer reaction occurs between an aromatic 2-amino-substituted carbonyl compound and a carbonyl derivative containing a α-methylene group, followed by cyclodehydration. The reaction is catalyzed by a base- or acid (Bronsted or Lewis acid).[66] Cu(btc)$_2$ (HKUST-1) showed high activity for the reaction and resulted in quinoline derivatives under solvent-free conditions at 80 °C. 3-Acetyl-2-methyl-4-phenylquinoline was obtained within 1 h in 80% yield and quantitative after 2 h using 8.3 mol% HKUST-1. In comparison under the same conditions HBEA and Al-SBA-15 gave only 38 and 36% product after 1h.[67]

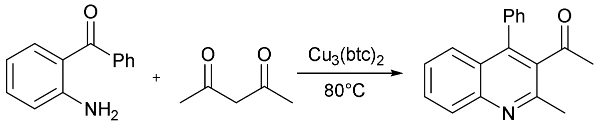

Figure 11: Friedländer reaction catalyzed by Cu$_3$(btc)$_2$ (HKUST-1). Redrawn from ref.[67].

The authors concluded that the reaction was catalyzed by Lewis acid sites present in HKUST-1, whereas contribution from Brønsted acid sites was minor. Catalyst stability under the applied conditions was proven.[67] Further work revealed that the better performance of HKUST-1 could be attributed to the lowering of energy barriers, especially for the annulation reaction step. Also the favorable geometry of the reaction precursor formed by adsorption of reactants on two adjacent Cu^{2+} sites in HKUST-1 contributed to this increase in performance.[68] The effect of the adjacent (dual) active sites in HKUST-1 was confirmed by a theoretical study of M. Polo□ij and coworkers.[69] The higher concentration of active sites in

HKUST-1 compared with H-BEA or Cu-BEA was found to play a key role due to the concerted effect of two adjacent active sites.

Regarding other organic reactions MOF-based Lewis acid catalysts were similar or less active in direct comparison with their homogeneous equivalents or inorganic catalysts.[35]

Therefore, efforts were made to increase the number of accessible Lewis acid sites. The group around D. de Vos introduced the concept of active site engineering.[65] They showed that more active sites can be generated by adding trifluoroacetic acid and hydrochloric acid to the one-pot synthesis of carboxylate based UiO-66(Zr). The resulting MOF is more active in the conversion of citronellal than the parent UiO-66 (Figure 12)[70].

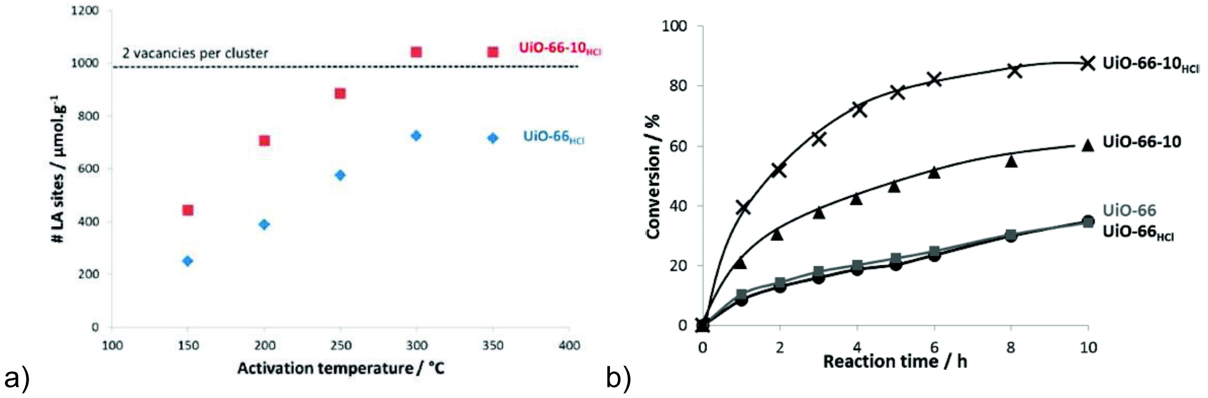

Figure 12: a) Number of Lewis acid sites as a function of activation temperature; b) conversion of citronellal with UiO-66-X synthesized with and without HCl vs. time (toluene, 110 °C, citronellal: Zr^{4+} = 15). Reprinted with permission from ref. [70]. Copyright 2013 American Chemical Society.

Those studies mainly concentrated on how to generate the most accessible groups. However, one great advantage of MOFs is the tuneability of the organic linker. In terms of popularization of PSM, the rational question of what effect the functional groups can potentially have on the linker, in terms of catalytic activity on metal open sites, emerged.

Therefore, we investigated systematically the effect of electron withdrawing (NO_2-) or donating (NH_2-) linker-functionalization of MIL-101Cr on the catalytic activity in diacetalization reaction of benzaldehyde with methanol.[71] A comprehensive study including investigation of leaching effect, cycling experiments, different reagents and a comparison with homogenous $Cr(NO_3)_3 \cdot 9H_2O$ was performed (chapter 3.2).[71] Furthermore the potential role of Brønsted acidity generated through polarized water molecules was addressed (Figure 14).[71]

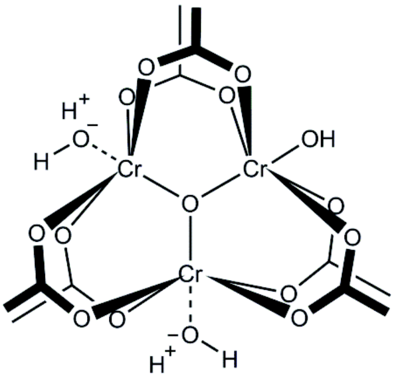

Figure 13: Polarized water at metal sites (OMS) of MIL-101Cr SBU.

In 2015 a review by J. Jiang and O. M. Yaghi highlighted the importance of MOF based Brønsted acid catalysis which lags behind the work already done in other field of catalysis.[72] There are several possibilities to introduce Brønsted acidity into MOFs (Figure 14). Acidic molecules, for example polytungstic acid, can be encapsulated through the MOFs pores. The organic linker can be functionalized with acidic moieties as SO_3H-groups. Alternatively, acidic molecules can be ligated on available metal sites.[72]

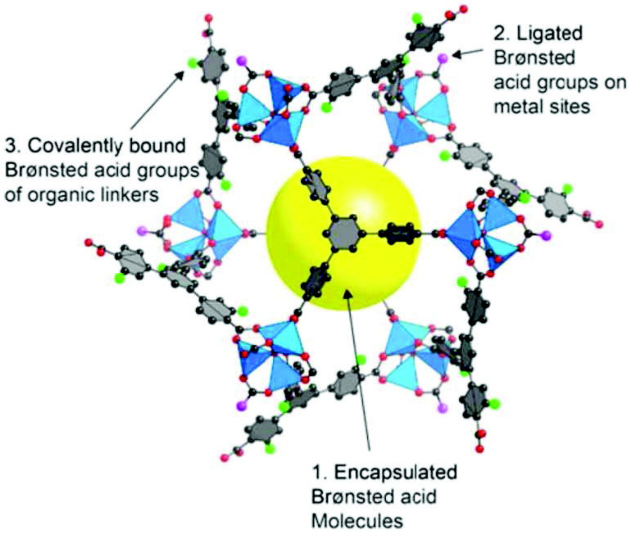

Figure 14: Various Brønsted acid sites in MOFs. Reprinted with permission from ref. [72]. Copyright 2015 American Chemical Society.

The coordinating group in the latter case can also be water. This water can be the solvent, generated during the reaction (for instance in condensation reactions) or be part of the framework structure, if not all solvent molecules of the metal sites (OMS) have been removed. Apart from difficulties in the synthesis of MOFs, which can withstand the acidic environment that is intended to be introduced to the framework, the characterization of the different types of acidity is another challenge that needs to be overcome when working with MOFs.[72]

Previous examples introduced solid acid catalysis with MOFs. The investigated reactions are mostly based on common organic reactions using model compounds targeting a general understanding of MOF catalysis.

Valorization of non-food related biomass was identified as an emerging future challenge. In the following chapter we intend to summarize and evaluate the developments in this area with respect to MOFs.

1.7 MOF catalysts in biomass upgrading towards value added fine chemicals

Valorization of waste biomass attracted tremendous research interests during the last years because it is a sustainable feedstock for a number of valuable chemical and materials. Upgrading biomass into fuel and fine chemicals can reduce the dependency on fossil fuels.

The research efforts to turn biomass into useful chemicals are summarized and evaluated in a number of excellent reviews, which are so numerous that only a small selection can be mentioned here: □Redefining biorefinery□ (2015)[5], □valorization of industrial waste and byproduct streams□ (2014)[6], □recent advancement in catalytic materials for biodiesel production□(2015)[73], □catalytic routes towards acrylic acid, adipic acid and ε-caprolactam starting from biorenewables□(2015)[74], □chemical conversion pathways for carbohydrates□ (2015)[75], □cellulose and lignocellulosic biomass to chemicals and fuels, combined solvent-nanocatalysis approach□(2014)[76], □environmental performance of biomass refining into high-added value compounds□(2016)[77], □recent progress in the development of solid catalysts for biomass conversion into high value-added chemicals□(2016)[78], □catalysis for biomass and CO_2 use through solar energy□ (2014)[79], □targeted chemical upgrading of lignocellulosic biomass to platform molecules□ (2014)[80], □Green chemistry, catalysis and valorization of waste biomass□(2016).[81]

It has to be the aim to use non-food biomass waste that is, for example, generated in agricultural production, such as sugar cane bagasse, corn stover, wheat straw, rice husks and orange peel to ensure that there is no competition with food production.[81] Also waste and by-product streams from other existing industrial sectors (e.g., food industry, pulp and paper industry, biodiesel and bioethanol production) as well as marine biomass as algae could be used as renewable resources for both biorefinery development and production of fine chemicals.[6]

Most of the biomass is composed of three major feedstocks: cellulose (45%), hemicelluloses (29%) and lignin (25%) (Figure 15).

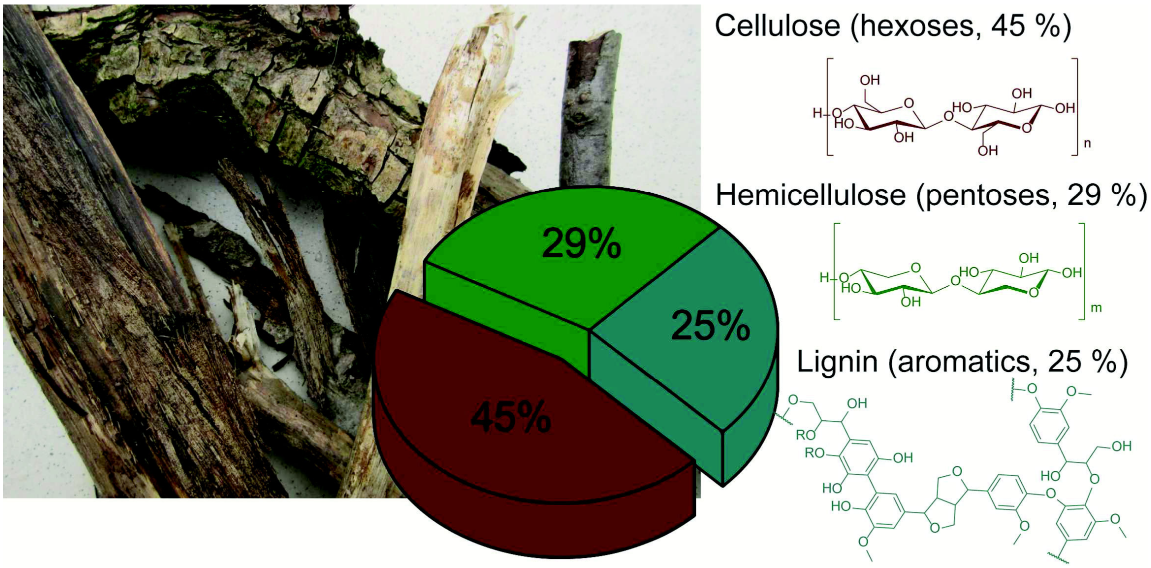

Figure 15: Schematic representation of woody biomass composition. Modified from ref. [5], Copyright 2015, with permission from the Royal Society of Chemistry.

The first step of biomass valorization is the hydrolysis of cellulose and hemicelluloses for an efficient production of hexoses and pentoses.[82] It is also possible to directly convert cellulose into various fine-chemical products (Figure 16). Different reactions as pyrolysis, hydrolysis, condensation, isomerization, deoxygenation, hydrogenation and oxidation have to be performed to obtain high valuable chemicals ranging from C1 until C6 based compounds (Figure 16). A great challenge is the controlled removal of oxygen-containing functional groups without reduction of carbon atoms and production of CO_2.[83]

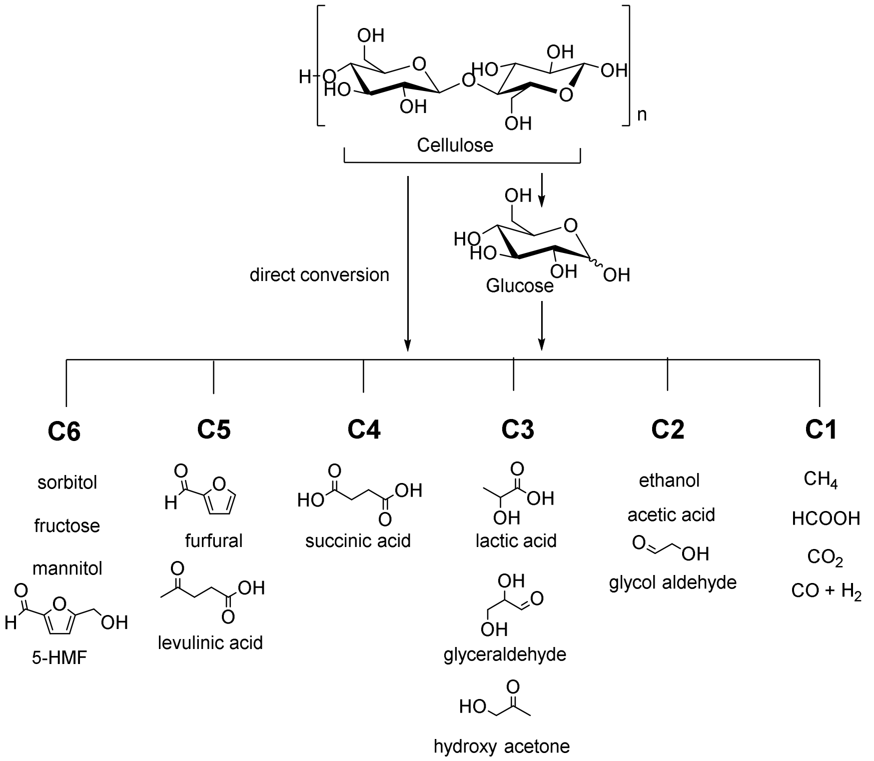

Figure 16: Possible valuable chemicals based on carbohydrate feedstock. Figure was modified from ref. [84], Copyright 2011, with permission from the Royal Society of Chemistry.

Especially, 5-hydroxymethylfurfural (5-HMF), levulinic acid as well as lactic acid are discussed as so called platform chemicals, since they can be converted into important chemicals (Figure 17). 5-HMF can be oxidized to yield 2,5-furan dicarboxylic acid (Figure 17) which might replace terephthalic acid in PET production in future. γ-Valerolactone (Figure 17) is a sustainable solvent and fuel additive. From both 5-HMF and γ-valerolactone adipic acid can be obtained, which is the mainly used for the production of nylon 6.6.[74]

γ-Valerolactone and derivates of levulinic acid, for instance alkyl levulinates are valuable products because they are suitable additives for gasoline and diesel fuels. Especially, ethyl levulinate is a suitable gasoline blendstock due to its high octane rating and lubricity, solubility and volatility. Apart from fuel additives levulinate esters can be used as flavoring compounds and plasticizers.[85]

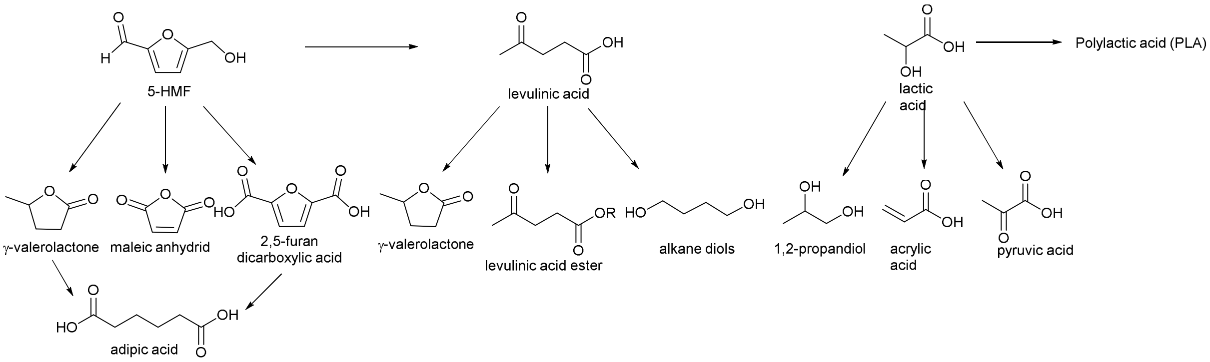

Figure 17: Examples for high value chemicals obtained from conversion of platform chemicals (5-HMF, levulinic acid and lactic acid).[5],[84]

The third important platform molecule adressed in this review is lactic acid. Lactic acid is applied in cosmetics and pharmaceuticals, but most importantly in polymer industry for the formation of biodegradable polylactic acid (PLA).[86] Besides 1,2-propandiol and acrylic acid can also be generated from lactic acid (Figure 15). Acrylic acid derived polymers are used for superabsorbents, plastics and synthetic rubbers.[74] The formation of lactic acid from carbohydrates involves multiple reactions as retro-aldol reaction, isomerization and 1,2-hydride shift. Lewis and Brønsted acids are necessary for hydrolysis and dehydration of lactic acid and intermediate products. Therefore, up to now over 90% of commercial lactic acid is produced by a biotechnological route[87] - the fermentation of aqueous glucose. However, this process has some drawbacks such as long reaction times due to its low reaction rates, high energy consumption and an increased waste production in the neutralization and purification steps.[88] The third major feedstock of biomass is lignin. Lignin was recognized as a potential source of aromatic compounds because it is mainly composed of aliphatic and phenolic alcohols, which are connected through aryl ether and carbon-carbon bonds. In Figure 18 the framework of softwood lignin as well as common linkages found in lignin are presented.[89]

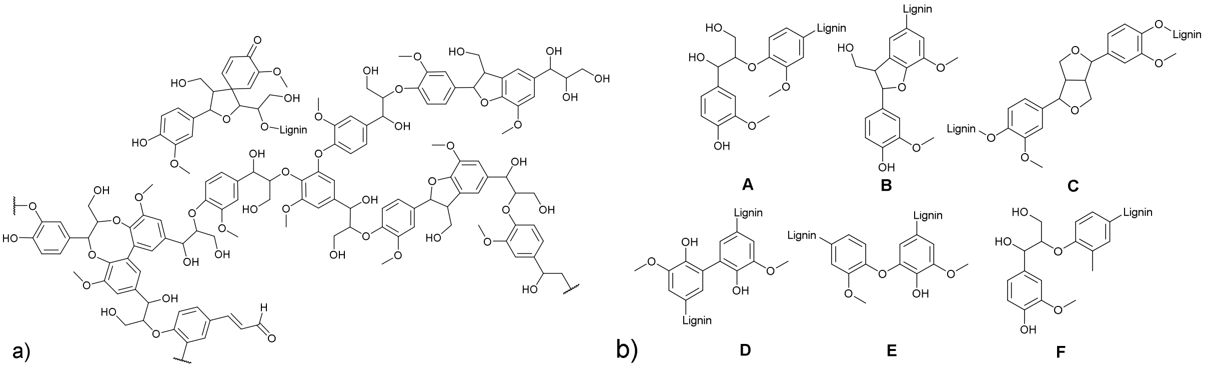

Figure 18: a) Structural motifs of softwood lignin; b) six common linkages found in lignin: A = β-O-4, B = β-5, C = β-β′, D = 5-5′, E = 4-O-5, F = β-1´. Redrawn with permission from. [89]. Copyright 2016 American Chemical Society.

As of 2007, only three products are commercially produced from lignin: vanillin, dimethyl sulfide, and dimethyl sulfoxide.[90] Vanillin is often regarded as a lignin model compound for further reactions. In their recent review, B. M. Upton and A. M. Kasko described possible strategies to convert lignin (regarded as macromonomer) into polymeric materials, such as polyurethanes, polyester and phenol-formaldehyde resins.[89]

One target is the development of new synthetic routes ending up in already existing molecules, which are then so called bio-based. An even greater impact on chemical technology landscape is the potential of biomass valorization into new buildings blocks and new materials.[5]

MOFs entered the stage of catalysts for biomass valorization about 5 years ago, when G. Akiyama and coworkers investigated the potential of MIL-101Cr-SO_3H for cellulose hydrolysis.[91] A recent review of X. Liu and coworkers on the □catalytic transformations of organic compounds and biomass derivatives with functionalized metal-organic frameworks□ touched this field and should be mentioned at this point.[92]

This research field bears a huge unexplored potential in the field of MOF catalysis which simultaneously raise the question if there is a true benefit for product formation?

Therefore, we aim to critically compare available studies applying MOF catalysts for the formation of platform chemicals (Figure 16). Synthesis conditions, product yields and selectivity of products are given in tables at the end of each chapter.

Regarding the above mentioned reagents and products, a reasonable question arises in terms of adsorption capability: Can MOFs adsorb glucose, 5-HMF and others molecules? This question was already answered in theory by J. S. Kruger *et al.*, who summarized the diameter of platform molecules in comparison to catalyst pore sizes (Figure 19).[83]

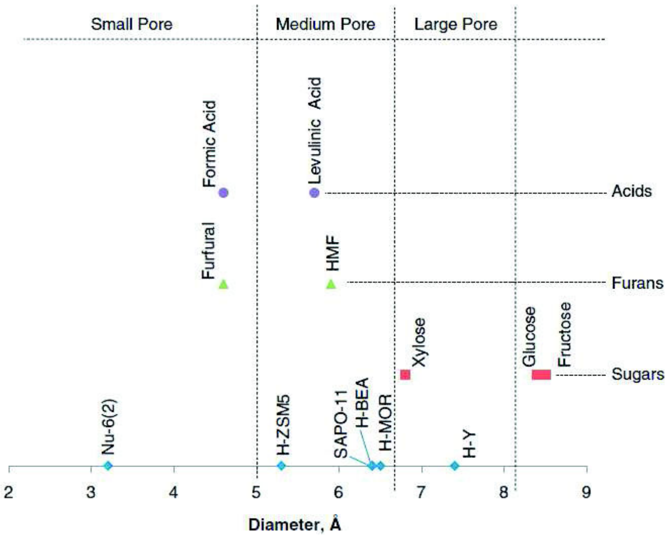

Figure 19: Comparison of catalyst pore dimensions and molecular dimensions. Reprinted from ref. [83], Copyright 2012 with permisson of Elsevier.

Within the named catalysts (Nu-6(2), H-ZSM5, SAPO-11, H-BEA, H-MOR and H-Y) H-Y displays the largest pore size with 7.5 Å.[83] However, the MOFs covered in the following work all display larger pore diameters. For instance, MIL-101Cr possesses pore diameters of 29 Å and 34 Å, although the pore windows are smaller with 12 Å and 15 Å.[51] The porosity of UiO-66 consists of octahedral cavities with a diameter of 11 Å, and tetrahedral cavities with a diameter of 8 Å. But its triangular windows are narrow with a free diameter close to 6 Å.[93] K. M. Gupta *et al.* suggested that MIL-101Cr can be suitable for glucose recovery, based on the results of their molecular simulation study.[94] For some cases also adsorption studies of reagents and products were performed in the analyzed literature, which will be mentioned.

1.7.1 Sugars as feedstock

Cellulose to glucose and fructose

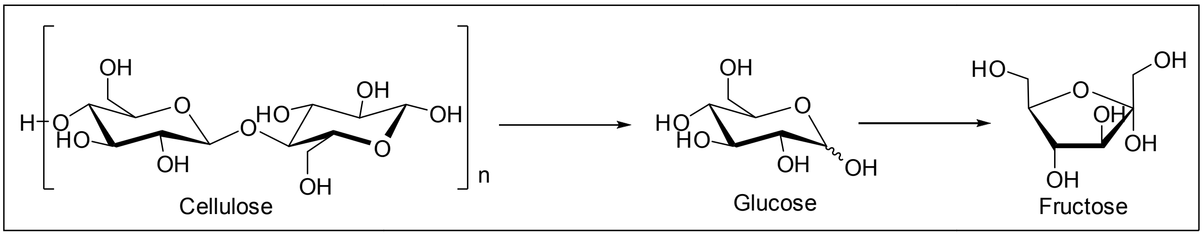

Scheme 1: Cellulose hydrolysis to glucose and isomerization to fructose.

In 2011 G. Akiyama *et al.* tested the reactivity of MIL-101Cr-SO_3H in cellulose hydrolysis.[91] The Brønsted acid functionalized MIL-101Cr derivate MIL-101Cr-SO_3H was obtained based on a one-pot synthesis using 2-sulfoterephthalate monosodium salt (Figure 20). The difficulty to retain strong Brønsted acid sites in a MOF results from the need of strong acidic solutions to avoid formation of the Brønsted base form. Most of the known MOFs cannot withstand strong acidic conditions which explains the rare amount of strong Brønsted acid MOFs.[91]

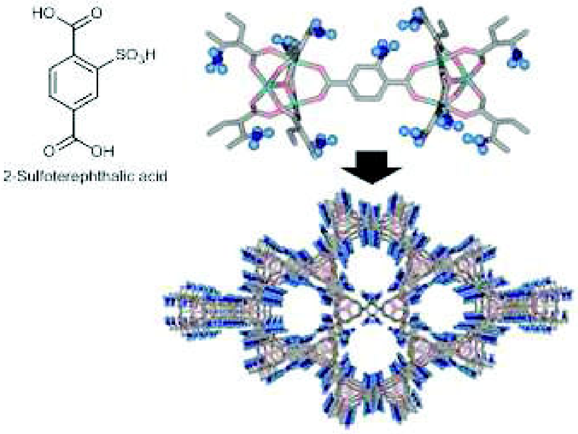

Figure 20: linker 2-sulfoterephthalic acid, MIL-101Cr-SO_3H SBU and network, adopted from ref [91], Copyright 2011, with permisson from John Wiley and Sons.

MIL-101Cr-SO_3H gave only a very poor yield of 5.4% for mono-and disaccharides (total amount). Multiple run reactions over 13 cycles revealed robustness of the catalyst. The overall low yield was explained by the poor solubility of crystalline cellulose in water.[91]

Consequently, the same research group around S. Kitagawa investigated water soluble amylose and glucose as feedstock for isomerization to fructose and other monosaccharides. For the first time for this reaction MIL-101Cr-SO_3H as well as other functionalized MIL-101Cr derivatives were used as catalysts.[95]

MIL-101Cr-SO_3H gave the best glucose-to-fructose yield with 21.6% (0.2 g catalyst, 25 mg glucose, water, 373 K, 24 h). NH_2- and NO_2-functionalized MIL-101Cr resulted in lower fructose yield (10.9% and 18.4%, respectively).

The observed catalytic activity was ascribed to open metal sites (OMS) of the framework (Figure 21). Coordination to the chromium metal center in *cis*-position was described as it is reported for homogenous metal complexes catalyzing the isomerization of glucose to fructose.[96] It is reasonable that the electron withdrawing effect of NO_2- and SO_3H- groups enhances the acidity of chromium centers, which explains the higher activity for glucose isomerization in comparison to MIL-101Cr-NH_2. Otherwise, MIL-101Cr does not possess any *cis* metal coordination sites, apparent from the structure of the secondary building unit (Figure 21). To enable the hydride shift for Lewis catalyzed isomerization of glucose to fructose, linkers have to be partly detached from the SBU or otherwise defects have to be present in the structure, leading to *cis* OMS. Both phenomenons have already been observed for MOFs,[70] but are not reported for MIL-101Cr. This together with the reaction conditions, where a larger amount of catalyst in comparison to substrate was used (0.2 g catalyst vs. 25 mg glucose), we think that other mechanisms than Lewis acid catalyzed reaction, have to be taken into account.

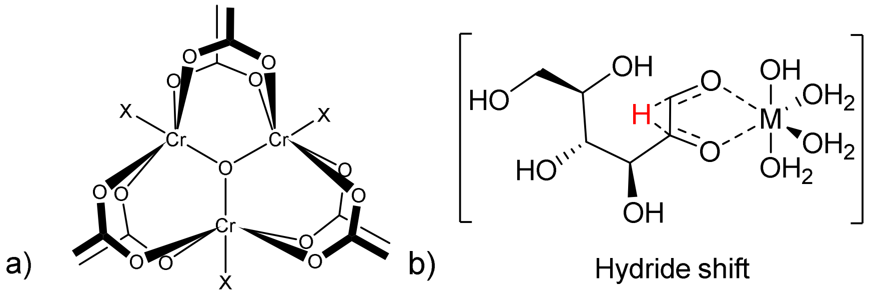

Figure 21: a) MIL-101Cr SBU, X = F, OH, solvent; b) homogeneous metal catalyzed hydride shift in glucose to fructose isomerization. Figure was redrawn from ref. [96].

For the conversion of amylose, it was shown that fructose can only be obtained when hydrochloric acid served as a co-catalyst for the conversion to glucose. The authors reported good stability of the catalyst in acidic environment, nevertheless, no sorption or PXRD data was given to prove that the catalyst is intact after the reaction. After long reaction times (48-120 h) 5-HMF and levulinic acid have been detected but conversion rates were not reported.

Cellulose to sorbitol and ethylene glycol

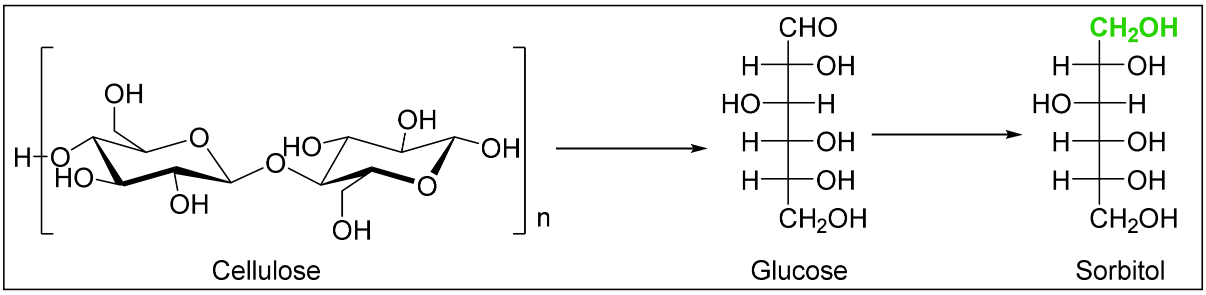

Scheme 2: Cellulose and cellobiose into sorbitol and ethylene glycol.

Sorbitol is used as sweetener and was chosen as a model compound for the combined hydrolysis and hydrogenation of cellulose and cellobiose with a multifunctional MOF based catalyst.[97] The MOF serves as host for two different catalysts. As shown in Figure 22, the multifunctional catalyst combines the acid catalyzed hydrolysis of cellulose to glucose with the subsequent metal catalyzed hydrogenation resulting in sorbitol as the desired product. Furthermore mannitol, ethylene glycol, glycerol, 1,2-propanediol, and other low molecular weight polyols are possible byproducts of the reaction.

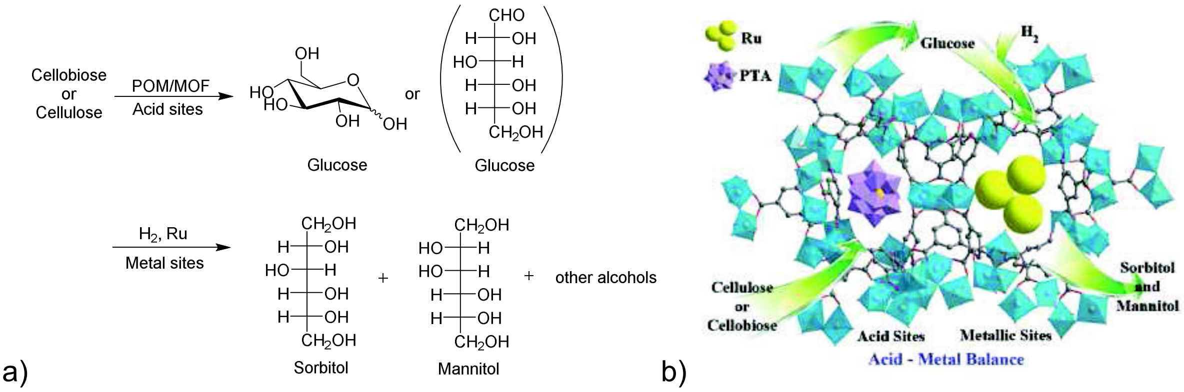

Figure 22: a) Reaction scheme of cellulose conversion to sorbitol with Ru/PTA@MIL-100Cr; b) proposed function of MOF composite catalyst. Redrawn and reprinted from ref. [97], Copyright 2013, with permisson of John Wiley and Sons.

A MOF was chosen as support because using the □ship in a bottle□ approach the phosphotungstic acid, (PTA = $H_3PW_{12}O_{40}$) loading could be controlled effectively. A sorbitol yield of 57.9% was achieved by adjusting the ratio of amount of acid (PTA) to metal catalyst (Ru NP). The MOF alone shows no significant catalytic activity. Only very low amounts of glucose ethylene glycol and glycerol (0.5% and 4.1%) were measured. For cellobiose an even higher sorbitol yield of 95.1% was achieved, using Ru-PTA/MIL-100Cr.[97] Reference experiments using only MIL-100Cr or PTA@MIL-100Cr gave as single product low amounts of glucose and ethylene glycol/glycerol, 13.5% 7.2% and 11.3% 5.6%, respectively. Ru@MIL-100Cr resulted in a sorbitol yield of 56%, which illustrates the need of careful balance of acidity.[97] This example shows the advantages of MOFs as host matrix. It would be very interesting to investigate this reaction using a strong Brønsted acid MOF as previously presented MIL-101Cr-SO_3H. By adjusting parameters as amount of PTA, ruthenium and temperature, the group around J. Chen showed that the selectivity of products can be significantly changed for the production of ethylene glycol (44.6%) using the same catalysts. HKUST-1 was used as MOF support instead of MIL-100Cr.[98]

Competitive heterogeneous catalysts applied in the conversion of biomass derived compounds are sulfonated resins as Amberlyst, EBD resins and Nafion, nanoporous metal oxides (sulfated protonated metal oxides as $SO_4^{2-/}ZrO_2$), hydrotalcites, activated carbon and ordered mesoporous carbon as well as silica (MCM, SBA) and zeolites.[99]

In case of cellulose hydrolysis and glucose isomerization, MOF based catalysts cannot compete with other heterogeneous catalysts. Zeolites and sulfonated carbon display significantly higher activity than MIL-101Cr-SO_3H (Table 2).[100],[101] By contrast the PTA@MIL-100Cr catalyst can compete with comparable heterogeneous catalysts for the conversion of cellulose into sorbitol and especially exhibits higher selectivity than 1% Rh 5%Ni/mesoporous carbon and $H_4SiW_{12}O_{40}$□Ru/C.[102],[103]

Table 2: Comparison of synthesis conditions based on carbohydrate feedstock.

Catalyst	**Substrate**	**Conditions (solvent, time, temperature, pressure)**	**Product (%)^a**	**Byproducts**	**Ref.**
MIL-101Cr-SO_3H (0.2 g)	Cellulose (25 mg)	H_2O (2.0 g), 3 h,. 393 K.	glucose (1%) mono+disaccharides (5%)		[91]
MIL-101Cr-SO_3H (0.2 g)	glucose (25mg)	H_2O (2.0 g), 24 h, 373 K.	conversion (22 %) fructose (22%)	glucose was recovered (78%)	[95]
HCl	amylose (25 mg)	HCl aq, (2.0 g), 24 h, 373 K	conversion (99%) glucose (99%) fructose(0%)		[95]
MIL-101Cr-SO_3H (0.2g)	amylose (25 mg)	water, 2.0 g, 373 K, 24 h;	conversion (n.s) glucose (5%) fructose(1%)	Cellobiose (10%)	[95]
aqueous solution of HCl (pH 1) + MIL-101Cr-SO_3H (0.2g)	amylose (25 mg)	HCl aq, 2.0 g, 373 K, 24 h;	conversion (100%) glucose (83%) fructose(17%)		[95]
Ru-PTA/MIL-100Cr (30 mg; Ru (3.2wt%)); PTA (16.7 wt%)	cellulose (50 mg)	H_2O (8.0 mL), 10 h, 190 °C, H_2 (2.0 MPa)	conversion (100%) sorbitol (58%)	mannitol (5%) glycerol +ethylene glycol (1.%)	[97]
Ru-PTA/MIL-100Cr (30 mg; Ru (3.2wt%)); PTA (16.7 wt%)	cellobiose (50 mg),	H_2O (5.0 mL), 10 h, 150 °C, H_2 (2.0 MPa),	conversion (100%) sorbitol (95%)	mannitol (2%) glycerol +ethylene glycol (1%)	[97]
Ru/NENU-3 (30 mg; 2.4 wt% Ru, 34.8 wt% PTA	cellulose (50 mg)	H_2O (8.0 mL), 4 h, 245 °C, H_2 (4.0 MPa)	conversion (80%) ethylene glycol (45%)	1,2-propylene glycol (5%) glycerol (6%), glucose (2%),sorbitol +mannitol (2%)	[98]
other heterogeneous catalysts					
Sn-Beta 1:50 metal:glucose	glucose (10 wt%))	H_2O, 30 min, 383 K	conversion (55%) fructose(32%)	mannose (9%)	[100]
Sn-Beta 1:225 metal:glucose	glucose (45 wt%))	H_2O, 1 h, 383 K	conversion (54%) fructose(29%)	mannose (8%)	[100]
sulfonated activated carbon (50 mg)	cellulose (45 mg)	H_2O (5 mL), 24 h, 423 K	glucose (41%)	water soluble byproducts	[101]
1%Rh-5%Ni/Mesoporous carbon (0.15 g)	cellulose (0.5 g)	H_2O (50 mL), 30 min, 245 °C, 6 MPa H2	conversion (100%) sorbitol (52%)	various hexitols	[102]
$H_4SiW_{12}O_{40}$□Ru/C (0.25 g)	cellulose (1 g)	H_2O (50 mL), 1 h, 463 K**,** 5 MPa H_2	conversion (99%) sorbitol + mannitol (68%)	sorbitan (19%), glucose (1%)	[103]

a) If no conversion is stated, the data was not found in the literature

Fructose to 5-HMF

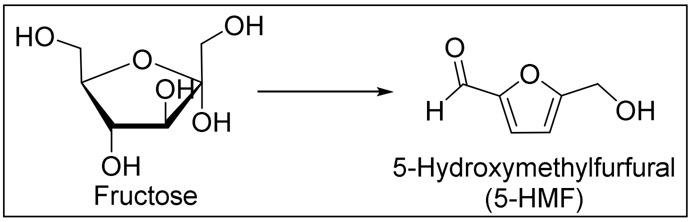

Scheme 3: Conversion of fructose to 5.HMF.

Y. Zhang *et al.* applied PTA@MOF composites for the first time for the dehydration of fructose into 5-hydroxymethylfurfural (5-HMF). The final catalyst was composed of phosphotungstic acid (PTA) encapsulated in MIL-101Cr. The average number of PTA cluster loaded per cages was measured and calculated using inductively coupled plasma (ICP) analysis. A maximal loading of three PTA molecules per cage was achieved (PTA3.0@MIL-101Cr).[104] Pore accessibility was shown by nitrogen sorption analysis, the BET surface area of PTA3.0@MIL-101Cr was determined to be 1353 m^2/g. This is lower compared to the parent MIL-101Cr (S_{BET} = 2772 m^2/g). MIL-101Cr was activated at 200 °C *in vacuo* for 6 h to uncover the open metal sites and was subsequently tested in fructose dehydration in the ionic liquid1-ethyl-3-methylimidazolium chloride [EMIM][Cl]. Conversions below 10% were measured and no 5-HMF could be detected. Based on these results, the authors concluded that MIL-101Cr is inactive for fructose dehydration. PTA@MIL-101Cr showed good conversion rates and 5-HMF yields. The yields increased the higher the PTA loading from 45% conversion and 20% 5-HMF yield for PTA0.5@MIL-101Cr to 84% conversion and 63% 5-HMF after 1h and 79% after 2.5h for PTA3.0@MIL-101Cr.[104] This increase enables the reaction system to compete with $CrCl_2$ in [EMIM][Cl] (fructose (50 mg), [EMIM][Cl] (0.5 g), 80 °C, 1 h 78% conversion, 60% 5-HMF). However, the activity of PTA3.0@MIL-101Cr is lower than the activity of pure PTA (2 mg PTA, fructose (50 mg), [EMIM][Cl] (0.5 g), 80 °C, 1h; 87% conversion, 80 °C 5-HMF yield).[104],[105]

In addition, PTA3.0@MIL-101Cr was also tested in DMSO instead of [EMIM][Cl]. In this solvent 63% conversion was achieved after 30 min at 130 °C. Albeit, it was observed that also DMSO alone has also a significant activity for fructose dehydration. The blank experiment in DMSO alone gave 59% conversion and 18% 5-HMF yield.

MIL-101Cr and PTA3.0@MIL-101Cr were also tested for glucose dehydration in [EMIM][Cl] (catalyst 20 mg, glucose 50 mg,100 °C, 3 h). No 5-HMF was obtained in case of MIL-101Cr and PTA3.0@MIL-101Cr showed only a negligible yield of 2%.[104]

L. Bromberg and coworkers investigated the conversion of fructose into 5-hydroxy-methylfurfural using MIL-101Cr embedded in a cross-linked poly(N-bromomaleimide) polymer (PMAi-Br) (Figure 23).[106]

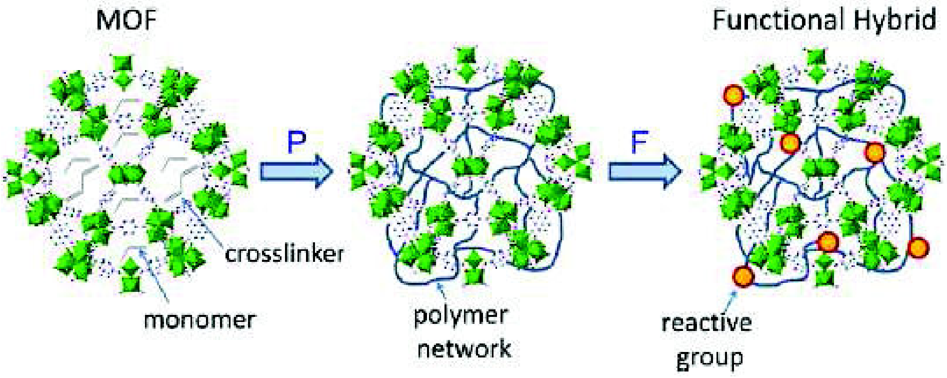

Figure 23: Schematic representation of polymer@MIL-101Cr composite. Reprinted with permission from ref. [106]. Copyright 2014 American Chemical Society.

The amorphous polymer network fills the MOF pores to some extent, but BET surface area of the hybrids is still between 1100-1600 m^2/g. This showed a certain accessibility of the pores. PMAi-Br is a polymeric, water-, and solvent-insoluble analogue of N-bromosuccinimide (NBS). Homogeneous NBS catalyst is active in dehydration of fructose and other monosaccharides, because it is a source of electrophilic bromine. Figure 24 shows the proposed mechanism of fructose dehydration involving a nucleophilic attack of a Br$^-$ ion.

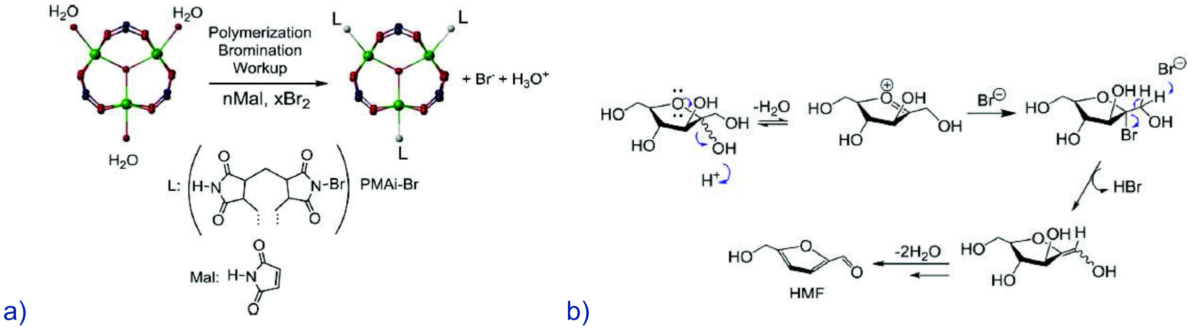

Figure 24: a) Presentation of the MIL-101Cr trimeric building block sharing an oxygen center and chelated by six carboxylates, with OMS sites coordinated with water molecules. Note: graphic part a) was taken from reference 105 but we have to note that three water molecules on the $\{Cr_3(\mu_3\text{-}O)(O_2C\text{-})_6\}$ SBU cannot be correct as charge neutrality requires a hydroxido (OH$^-$) or a fluorido (F$^-$) ligand, depending on the synthesis. Upon polymerization of N-maleimide (Mal), workup of the resulting hybrid polymer/MOF network, and subsequent bromination, the OMS sites become coordinated with Mal units of the PMAi-Br network as ligands (L), while bromide evolves; b) proposed mechanism of the fructose dehydration via nucleophilic attack by bromide. Reprinted with permission from ref. [106]. Copyright 2014 American Chemical Society.

PMAi-Br alone already gives a 5-HMF of 50% after 1 h, but the MOF-PMAi-Br composite achieves significant higher 5-HMF with 86% after 1 h (Figure 25). The authors explain the increased activity with the higher surface area of MOF-PMAi-Br in comparison to the non-porous polymer and with synergism in which the polymer Ligand (L) is coordinated to the unsaturated sites of MIL-101Cr and thereby release a Br$^-$ ion (Figure 24).

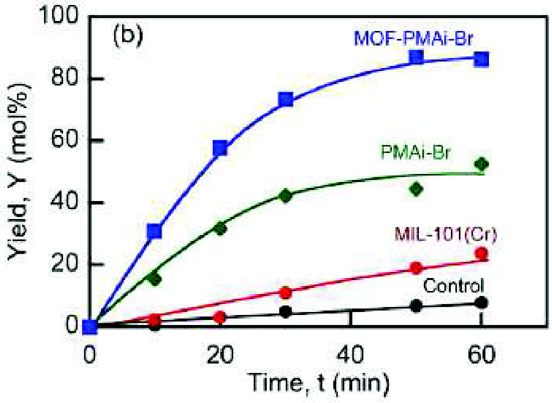

Figure 25: 5-HMF (%) yield at 100 °C. Conditions: DMSO, 5 mL; D-fructose concentration (C_{fo}), 0.555 mol/mL; catalyst loading, 50 mg/mL. Control: no catalysts added. Reprinted with permission from ref.[106]. Copyright 2014 American Chemical Society.

5-HMF formation is also observed without catalyst in DMSO solvent which is in agreement with the previous study of Y. Zhang et al..[104] MIL-101Cr in DMSO under the standard conditions (Figure 25) gave a 5-HMF yield of 24% after 1 h. For the dehydration of glucose a 5-HMF yield of 7% and 16% after 2 and 6 h, respectively, was reported and used as an argument against the leaching of chromium species from MIL-101Cr, because chromium salts are known to catalyze the isomerization of glucose to fructose.[106]

J. Chen *et al.* reported the conversion of fructose into 5-hydroxymethylfurfural by different sulfonic acid functionalized MOFs, using DMSO as a solvent at 120 °C for 1 h.[107] The water stable MOFs MIL-101Cr, UiO-66 and MIL-53Al were functionalized by post-synthetic reaction with chlorosulfonic acid.[107]

The three SO_3H-functionalized MOFs were active in fructose dehydration. For MIL-101Cr-SO_3H different degrees of sulfonic acid functionalization from 3 mol% to 15 mol% revealed an increase in 5-HMF yield with the SO_3H content. At 120 °C and after 1 h, 5-HMF was obtained in 90% yield with MIL-101Cr-SO_3H-15% as catalyst (Figure 26). Adsorption experiments indicated that MIL-101Cr-SO_3H-15% shows the highest adsorption of fructose (0.006 mmol/g), whereas MIL-53Al-SO_3H-8.2% adsorbed the most 5-HMF (0.09 mmol/g) (changes were measured with HPLC). For the SO_3H-functionalized MOFs the 5-HMF adsorption is significantly higher than the fructose uptake.[107]

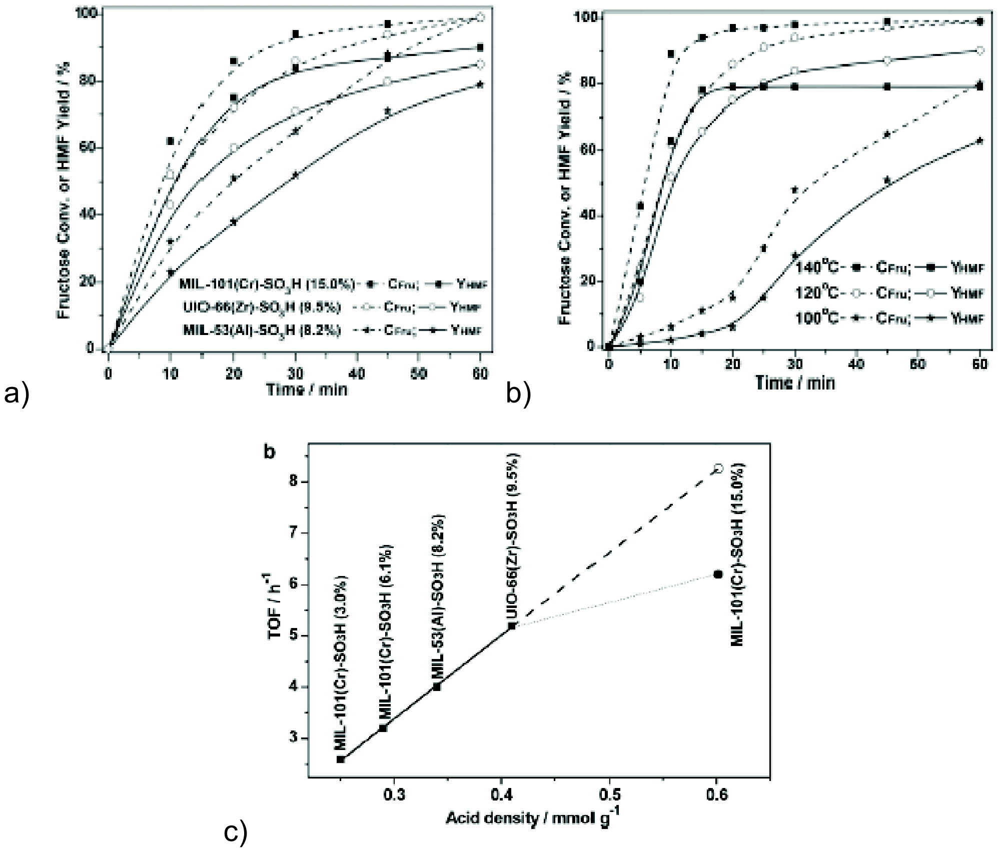

Figure 26: a) Comparison of catalytic performance of different MOF-SO_3H on fructose to 5-HMF transformation. Fructose conversion also includes the formation of by-products (polymeric humins) to 5-HMF Conditions: fructose (500 mg), MOF-SO_3H (300 mg), DMSO (5 mL), 120 °C; b) effect of temperature and reaction time for MIL-101Cr-SO_3H-15% on fructose to 5-HMF transformation; c) TOFs versus molar sulfonic acid-site density of MOF-SO_3H. (TOFs for the fructose-to-HMF transformation were measured at t = 10 min, given as amount of consumed fructose per amount of MOF-SO_3H per hour. Conditions: fructose (500 mg), MOF-SO_3H (300 mg), DMSO (5 mL), 120 °C, 10 min). Reprinted from ref. [107], Copyright 2014, with permisson of the Royal Society of Chemistry.

The turnover frequency (TOF) of fructose transformation showed a linear relation with the sulfonic acid-site content of MOF-SO_3H from 3% to 9.5% SO_3H-derivatization irrespective of the actual MOF (MIL-101Cr, MIL-53Al or UiO-66Zr). Hence, the catalytic activity of MOF-SO_3H was ascribed to the Brønsted acid SO_3H groups, and suggested to be independent from the parent MOF. Only for MIL-101Cr-SO_3H-15% the TOF is lower than expected from the extrapolation (6.2 h^{-1} instead of 8.3 h^{-1}) (Figure 26c). For MIL-101Cr-SO_3H-15% the authors ascribed this discrepancy to the lower accessible pore volume. We suggest, however, that the leveling-off of the TOF increase with SO_3H content stems from diffusion control of the reaction rate. The pore volume of MIL-53Al-8.2% is already lower than that of MIL-101Cr-6.2%. Above a certain number of active sites a further increase will not lead to an increase in reaction rate if the diffusion rate limit has already been reached or is being approached.

Kinetic studies of MIL-101Cr-SO_3H-15% (k_{obs} 2.01 h^{-1} activation energy 55 kJ/mol) and MIL-101Cr-PMAi-Br (k_{obs} 2.97 h^{-1}, activation energy 53 kJ/mol) revealed a slightly better performance of MIL-101Cr-PMAi-Br.[106,107]

The carbohydrate feedstocks inulin, sucrose and cellobiose gave moderate 5-HMF yields of 46, 44, 24%, respectively, with MIL-101Cr-SO_3H-15% as the catalyst. Glucose conversion using MIL-101Cr-SO_3H-15% in DMSO or the ionic liquid [Bmim]Cl resulted in very low 5-HMF yields of 7-8%.[107]

Z. Hu and coworkers reported the superior performance of a hafnium based MOF named NUS-6(Hf) for the dehydration of fructose to 5-HMF. [108] Together with NUS-6(Hf) also NUS-6(Zr) framework was synthesized. Both are largely isostructural to the UiO-66 structure, although they contained 2-sulfoterephthalate instead of the terephthalate linker and additionally showed partially missing linkers (Figure 27). Defect formation led to the formation of additional mesopores. The mesopores had a diameter of approximately 4 nm according to Barrett-Joyner-Halenda method (BJH). NUS-6(Hf) and NUS-6(Zr) exhibited BET surface areas of 550 m^2/g and 530 m^2/g, respectively. NUS-6(Hf) and NUS-6(Zr) were hydrothermally synthesized at (only) 80 °C in water with acetic acid as a modulator. The linker 2-sulfotherephthalic acid monosodium salt that was used in the synthesis, was previously reported to give instable UiO-type frameworks. The use of a modified synthesis procedure for NUS-6(Zr) and NUS-6(Hf) allowed an activation of the two MOFs and the retention of their structure.[108]

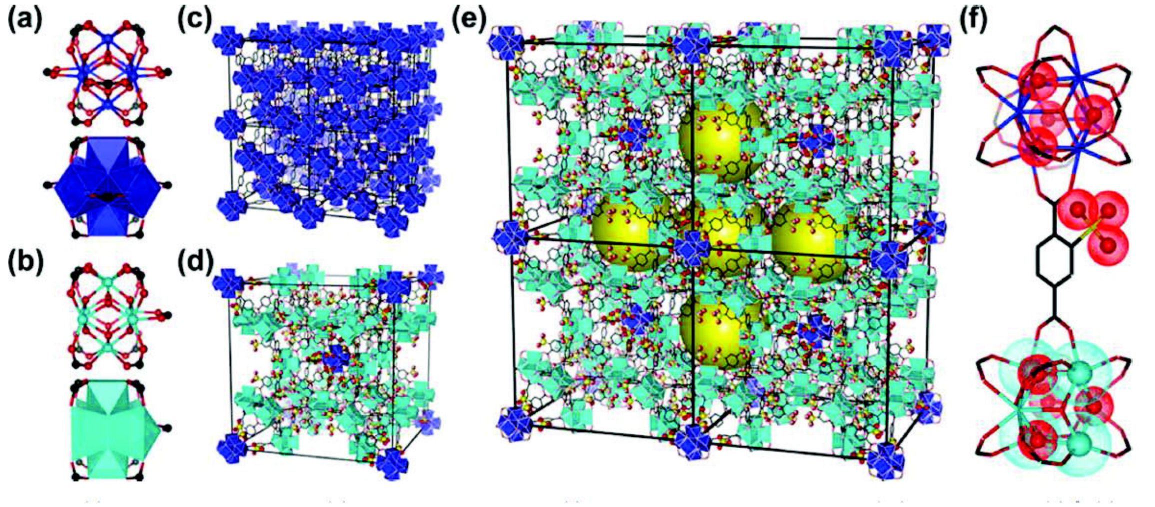

Figure 27: (a) 12-connected Hf_6 cluster. (b) 9-connected Hf_6 cluster. (c) 2 × 2 × 2 unit cells of UiO-66(Hf) with a = 20.7006(3) Å. (d) Single unit cell of NUS-6(Hf) with a = 41.4718(2) Å. (e) 1 × 2 × 2 super unit cell of NUS-6(Hf) with mesopores indicated by yellow spheres. (f) A fragment of NUS-6(Hf) with potential Brønsted acid sites labeled by red spheres and Lewis acid sites labeled by cyan spheres. Reprinted with permission from ref [108]. Copyright 2016 American Chemical Society.

The first attempts of fructose dehydration with NUS-6 were performed in water as solvent, but resulted only in negligible amounts of 5% 5-HMF. Therefore, the authors adjusted their solvent to DMSO following the work of J. Chen *et al.*.[107] Subsequently, NUS-6(Zr) (3.5 mol%) gave quantitative conversion of fructose (50 mg) with a yield of 5-HMF of 84 % after 1 h. NUS-6(Hf) outperformed all presently known other MOF or common heterogeneous catalysts[99] with a 5-HMF yield of 98 % after 1 h using the same reaction conditions (Figure 28).

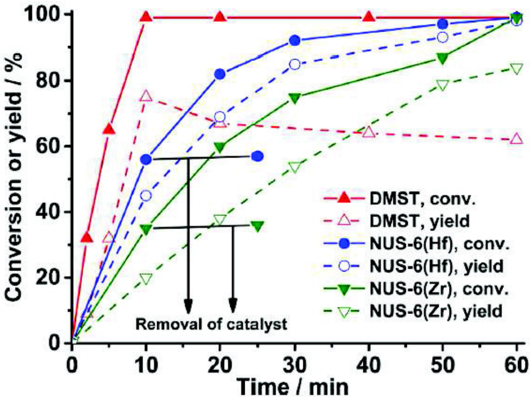

Figure 28: Kinetic study of frucose dehydration to 5-HMF with NUS-6 and DMST catalysts (DMST = dimethyl-2-sulfoterephthalate). Conditions: fructose (50mg), 3.5 mol% catalyst (2.7 mg for DMST, 35 mg for NUS-6(Zr), 50 mg for NUS-6(Hf)), DMSO (1 mL), 100 °C, 1 h. Reprinted with permission from ref. [108]. Copyright 2016 American Chemical Society.

Catalysis with the homogeneous linker dimethyl-2-sulfoterephthalate (DMST) resulted in a faster conversion of fructose than with the heterogeneous MOF NUS-6 catalysts, but gave a lower yield (and selectivity) of 5-HMF (Figure 28).

As indicated by the studies mentioned above, MOF Brønsted acidic catalysts can compete with other heterogeneous catalysts, such as Amberlyst[109] and Nafion[110] in the dehydration of fructose to 5-HMF. In water or biphasic (aqueous-organic) solvent mixtures, MOFs have not been tested yet for the conversion of fructose, although numerous other catalysts were shown to be active in the presence of water.[111]

To ensure a fair comparison only fructose-to-5-HMF reactions in DMSO have, thus, been considered. DMSO is apparently inhibiting humin formation to a large extent. Humins are insoluble polymers, complex carbonaceous materials which usually form as undesired byproducts in acid catalyzed conversion of biomass.[112] With this constraint, MIL-101Cr-SO_3H-15% and NUS-6(Hf) are among the best heterogeneous catalysts, reported so far, for the conversion of fructose into 5-HMF (Table 3).[111]

Although high 5-HMF yields are reported from fructose dehydration in dimethyl sulfoxide (DMSO), product separation is problematic due to the formation of toxic sulfur compounds during high temperature DMSO distillation. Therefore, low boiling solvents or water would be required if a technical process is envisioned.[113]

More sustainable than using fructose as feedstock are the so called “second generation biomass feedstocks”. These are obtained from non-food components of crops (stems, leaves and husks) or agricultural and forestry waste. These resources are mainly composed of cellulose (45%) (Figure 15).Therefore, processes must be optimized to yield 5-HMF from glucose or even cellulose (Figure 16).[81]

Table 3: Comparison of fructose to 5-HMFsynthesis conditions.

Catalyst	Conditions (fructose amount, solvent, time, temperature, pressure)	Product (yield) (Byproduct[a], yield)	Ref.
PTA (3.0)/MIL-101 (20 mg)	fructose (50mg), 1-ethyl-3-methylimidazolium chloride (0.5 g), 1 h, 80 °C	conversion (84%) 5-HMF (63%)	[104]
PTA (3.0)/MIL-101 (200 mg),	fructose (0.5 g), DMSO (5 mL), 30 min, 130 °C	conversion (82%) 5-HMF (63%)	[104]
MIL-101Cr	fructose (0.555 mol/L), DMSO (5mL), 1 h, 100 °C	conversion (>99%) 5-HMF (24%)	[106]
MIL-101Cr-PMAi-Br (250mg)	fructose (0.555 mol/L), DMSO (5mL), 1 h, 100 °C	conversion (>99%) 5-HMF (86%)	[106]
MIL-101Cr-SO_3H-15% (0.3 g)	fructose (0.5g) DMSO (5mL), 1 h, 120 °C	conversion (>99%) 5-HMF (90%)	[107]
MIL-101Cr-SO_3H-3% (0.3 g)	fructose (0.5g), DMSO (5mL), 1 h, 120 °C	conversion (83%) 5-HMF (63%)	[107]
MIL-53Al-SO_3H-8.2% (0.3 g)	fructose (0.5g), DMSO (5mL), 1 h, 120 °C	conversion (>99%) 5-HMF (79%)	[107]
UiO-66Zr-SO_3H-9.5% (0.3 g)	fructose (0.5g), DMSO (5mL), 1 h, 120 °C	conversion (>99%%) 5-HMF (85%)	[107]
NUS-6Zr (3.5 mol%, 35 mg)	fructose (50 mg) ,DMSO (1 mL), 1 h, 100 °C	conversion (>99%) 5-HMF (84%)	.[108]
NUS-6Hf (3.5 mol%, 50 mg)	fructose (50 mg), DMSO (1 mL), 1 h, 100 °C	conversion (>99%) 5-HMF (98%)	.[108]
other heterogeneous catalysts			
Amberlyst 15 (20 mg)	fructose (1.7 mmol), DMSO (10 g), 2 h, 120 °C, $1.01 \cdot 10^5$ Pa N_2	conversion (100%) 5-HMF (76%) Levulinic acid (2%)	[109]
Nafion(15)/MCF (0.1 mmol/L H^+)	fructose (3wt%), DMSO, 2 h, 90 °C	5-HMF (83%)	[110]
Amberlyst-15 (175 g L^{-1})	fructose (0.5 M), 5:3 (v/v) [BMIM]BF_4–DMSO, 32 h, 80 °C	conversion n.s. 5-HMF (87%)	[114]

MCF: mesocellular silica foam; n.s.= not stated.

a) If no additional byproducts are given, the difference is attributed to the formation of humins.

Glucose to 5-HMF

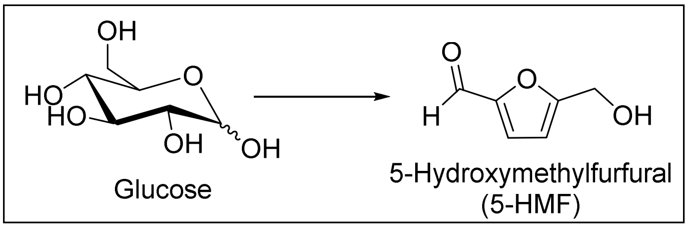

Scheme 4: Conversion of glucose to 5-HMF.

In 2015 experimental and theoretical work was done showing the possibility for Brønsted acid catalyzed glucose-to-5-HMF conversion (Scheme 4).[115],[116] As emphasized by previous studies, MIL-101Cr and functionalized MIL-101Cr seemed unable to catalyze the isomerization of glucose to fructose. This limitation results from the missing *cis* metal coordination sites and low Lewis acidity, which is required for the isomerization mechanism as described for homogenous metal complexes and zeolites.[96],[117]

For the conversion of glucose involving MOFs the highest reported yield is low, reported with 16% after 6 h using MIL-101Cr-PMAi-Br and the activity was mainly ascribed to PMAi-Br instead to the MOF MIL-101Cr (Figure 25).[106]

A. Herbst *et al.* investigated the potential of MIL-101Cr, its nitro, sulfonic acid and mixed nitro/sulfonic acid derivatives, MIL-101Cr, MIL-101Cr-NO_2, MIL-101Cr-NO_2/SO_3H, MIL-101Cr-SO_3H(33%) and MIL-101Cr-SO_3H(100%) for glucose conversion into 5-HMF. The activity of different MIL-101Cr derivatives and their selectivity towards 5-HMF and levulinic acid was compared.[118]

For the first time a MOF was applied in biphasic water based solvent mixture, THF:H_2O (v:v 39:1) to achieve a glucose-to-5-HMF conversion. Application of MIL-101Cr-SO_3H as catalyst resulted in 29% conversion of glucose to 5-HMF after 24 h.[118]

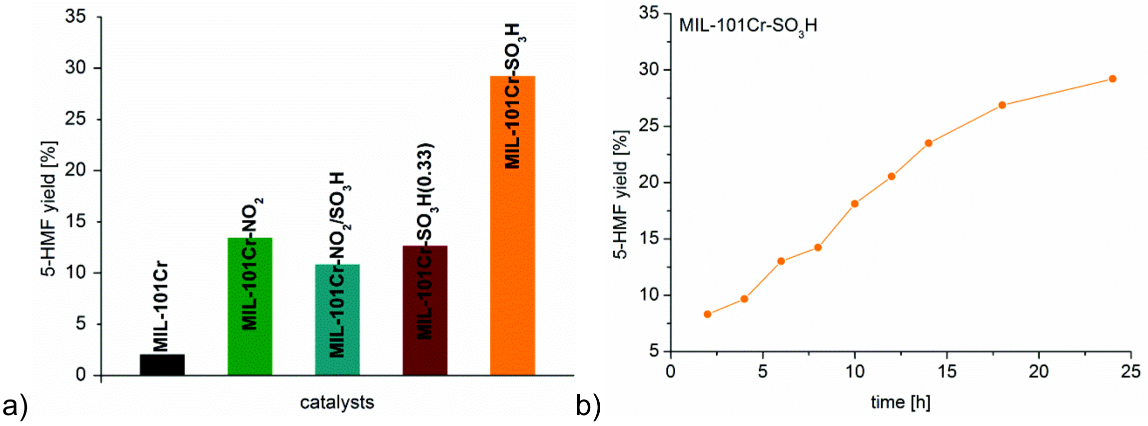

Figure 29: a) 5-HMF yield with different MIL-101Cr catalysts; b) time dependent conversion for MIL-101Cr-SO_3H (glucose 223 mg, catalyst ($5.22 \cdot 10^{-5}$ mol), THF/H_2O (v:v 39:1) 5 mL, 130 °C, 24 h). Reprinted from ref. [118], Copyright 2016, with permission of the Royal Society of Chemistry.

In contrast, when the reaction with the MIL-101Cr-X catalysts was carried out in pure THF, no product was formed. This further supports the indispensability of water for the glucose to

5-HMF conversion. MIL101Cr-NO_2 is the most selective of all MIL-101Cr catalysts tested, yielding only 5-HMF. The use of 5-HMF as substrate with MIL-101Cr-SO_3H as catalyst, did not result in any conversion. Hence, the catalytic formation of levulinic acid occurring from 5-HMF can be excluded. Other reaction pathways to levulinic acid, as conversion of intermediates formed within the cascade reactions have to be taken into account.[118]

Conversion of glucose with MIL-101Cr-SO_3H preferentially led to 5-HMF over levulinic acid (molar ratio 1:0.3) while other catalysts, such as Amberlyst-15 and sulfuric acid, formed mostly levulinic acid with 5-HMF to levulinic acid ratios of 1:3 and 1:10, respectively (Figure 30).[118]

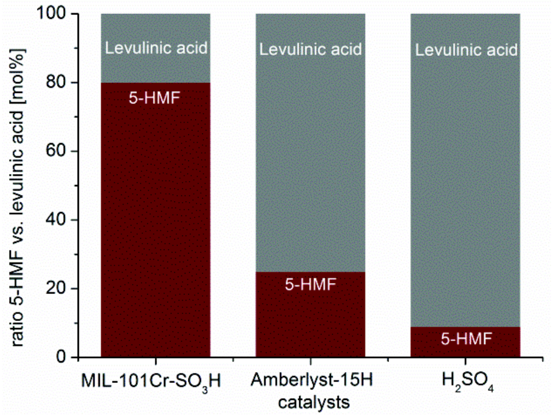

Figure 30: Comparison between MIL-101Cr-SO_3H, Amberlyst-15H and H_2SO_4 for the ratio between 5-HMF and levulinic acid from ^{1}H-NMR.. Conditions: catalyst MIL-101Cr-SO_3H 5.22 • 10^{-5} mol, glucose 223 mg, 5 mL THF:H_2O (v:v) 39:1, 130 °C. For Amberlyst-15 and H_2SO_4 the reaction was conducted with 1.57 • 10^{-4} mol of the catalyst under the same conditions. Reprinted from ref. [118], Copyright 2016, with permission of the Royal Society of Chemistry.

Conversion of maltose resulted in 50 % 5-HMF yield (saccharide solutions were 5 wt%) with MIL-101Cr-SO_3H catalyst (Figure 31).[118] The higher yield with respect to glucose conversion might be explained by the slower decomposition of glucose to humins, since first the disaccharide bond of maltose had to be cleaved.

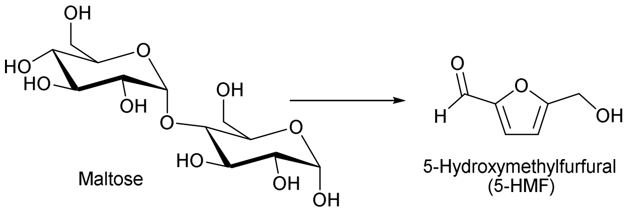

Figure 31: Conversion of maltose to 5-HMF.

Catalyst recycle experiments showed that MIL-101Cr-SO_3H stays porous and crystalline, but becomes deactivated through fouling by humin formation. With the use of ethanol as an alternative reaction medium, the formation of insoluble humins could be prevented. The yield of 5-HMF and 5-ethyl-HMF, however, decreased to 5% and 11% respectively, after 24 h (Figure 32).[118]

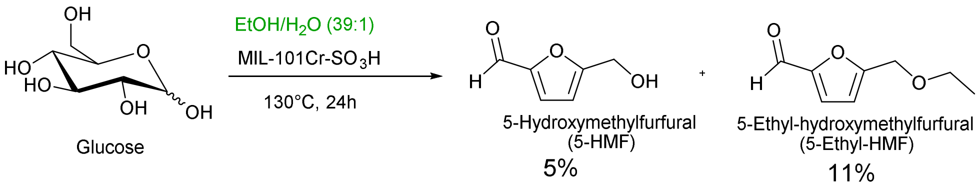

Figure 32: Ethanol as alternative reaction medium for the formation of 5-Ethyl-HMF.

In conclusion, it is more difficult to obtain 5-HMF from glucose with high selectively and high yield using heterogeneous catalysts than when homogenous metal salts as $AlCl_3 \cdot H_2O$.[111]

In contrast to fructose conversion, for the glucose-to-5-HMF transformation MIL-101Cr-SO_3H is only a low-to-medium active catalyst with moderate yields below 30% for 5-HMF.[119] For instance mesoporous tantalum phosphate as well as Sn montmorillonite (Sn-Mont) displayed significant higher 5-HMF yield under similar conditions and after shorter time.[120],[121] Taking reaction temperature and biphasic solvent mixture into account, MIL-101Cr-SO_3H showed similar activity as zirconium phosphate (ZrPO, 24% H_2O/methyl isobutyl ketone (MIBK), 165 °C,6 h).[122]

Sucrose into methyl lactate

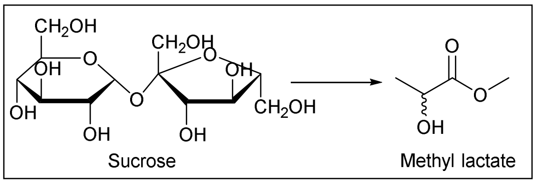

Scheme 5: Conversion of sucrose to methyl lactate.

B. Murillo et al. reported for the first time about the conversion of sugars to lactic acid derivatives in the presence of zeolitic imidazolate frameworks (ZIFs) (Scheme 5).[88] Other MOFs, such as HKUST-1, MIL-53Al und MIL-101Cr were also tested, but gave methyl lactate yields below 5% and, for this reason, have not been followed up further.[88]

ZIF-8 and ZIF-67 are both composed of 2-methylimidazole and display the same sodalite type structure.[123],[124] They differ in the metal, which is Zn for ZIF-8 and Co for ZIF-67. ZIF-8 achieved a methyl lactate yield of 35% (24 h, 160 °C, 225 mg sucrose, 160 mg catalyst, methanol) (Figure 33). Low amounts (<2%) of pyruvaldehyde dimethyl acetal (PADA), 1,1,2,2-tetramethoxypropane (TMP) and other non-identified products (<4%) were also observed. When the amount of catalyst was changed from 160 mg to 500 mg, a slight increase of the methyl lactate yield to 42% was measured. In direct comparison with $Zn(NO_3)_2$, ZIF-8 outperformed the metal salt since the Zn nitrate gave only 22% yield of methyl lactate. In contrast ZIF-67 is less active than $Co(NO_3)_2$, with 19% versus 26% yield. The higher activity of ZIF-8 over ZIF-67 is ascribed to the smaller particle size (150 nm vs. 1 µm) and stronger Lewis-acidity of Zn over Co sites.[88]

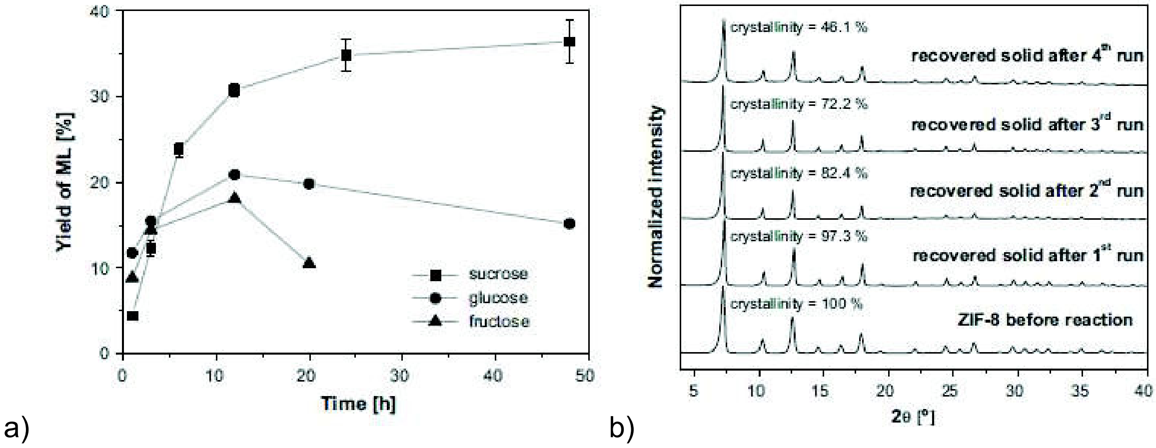

Figure 33: a) Yield of methyl lactate (ML) obtained over ZIF-8 using different sugars as reactants. Error bars in the case of sucrose derived from at least 4 different experiments (Reaction conditions: 160 °C, 160 mg of catalyst and 225 mg of sugar, methanol; b) XRD patterns of ZIF-8 before the reaction (fresh catalyst) and recovered solids after the various catalytic cycles. Including percentage of crystallinity, referred to catalyst before reaction. Reprinted from ref. [88], Copyright 2016, with permission of Elsevier.

After reuse of the ZIF-8 catalyst over four cycles the methyl lactate yield decreased from 35% in the first cycle to 27% in the fourth cycle. However, PXRD measurements after each cycle showed that the bulk ZIF-8 material stayed crystalline and its structure was retained (Figure 33). In contrast, BET surface decreased from 1391 m^2/g to 757 m^2/g. This indicated deactivation of the catalyst through fouling processes. It is known that in carbohydrate conversion various products including insoluble humins can be formed.[112]

Different activation processes for ZIF-8, such as methanol washing, calcination at different temperatures and vacuum drying were investigated. The latter method gave the best results. Yet, the discrepancy of sugar conversion (for ZIF-8 around 98%) and total identified product yield of (only) 12-40% depending on reagent (sucrose or glucose) shows the significance of unwanted and unidentified side reactions. The higher yield for sucrose in comparison with glucose and fructose in the conversion to methyl lactate was ascribed to the slower hydrolysis of sucrose in water to 1 eq. glucose and 1 eq. fructose resulting in less side reactions.

Sucrose is a disaccharide and too large to diffuse into the MOF´s pores (11.6 Å in diameter, pore windows of 3.4 Å) in case of ZIF-8, hence, the hydrolysis occurred at the pore mouth. The molecular diameter of the monosaccharides glucose and fructose was given with 8.5 Å, which is much smaller than the pore window. Even though, adsorption of carbohydrates was suggested to be possible because of the gate effect of ZIF-8[125] and its adsorption ability of caffeine (6.1 x 7.6 Å).[126] However, based on the given molecule and pore diameter data, we think it remains questionable if catalysis really occurs inside the MOF pores.

The group of E. Taarning *et al.* investigated the activity of the tin containing heterogeneous catalysts Sn-Beta, Sn-MCM-41 and Sn-MFI for the conversion of sucrose to methyl lactate.[127],[128] For this reaction similar conditions as for the previous presented study were used. The performance of ZIF-8 (35% methyl lactate yield) is better than the one of Sn-MCM-41 (28%) and Sn-MFI (24%) but Sn-Beta gave a higher yield of 57% methyl lactate (Table 4).[127],[128]

Table 4: Comparison of synthesis conditions based on sugar feedstock.

Catalyst	**Substrate**	**Conditions (solvent, time, temperature, pressure)**	**Product (%)[a]**	**Byproducts [b]**	**Ref.**
MIL-101Cr-PMAi-Br(250mg)	glucose (0.555 mol/L)	DMSO (5mL), 2 h/6 h,100 °C	5-HMF (7%/ 16%)		[106]
MIL-101Cr-SO_3H-15%, (0.06 g)	glucose (0.1g)	DMSO (2mL), 2 h, 120 °C	5-HMF (7%)		[107]
4 mol% (50 mg) MIL-101Cr-SO_3H	glucose (223 mg)	THF:H_2O (v:v 39:1) 5mL, 24 h, 130 °C	5-HMF (29%%)	Levulinic acid (7%)	[118]
ZIF-8 (160 mg)	sucrose (225 mg)	methanol (8 g), 24 h, 160 °C	conversion (>99%) methyl lactate (35%)	PADA (2%), TMP (0.4%)	[88]
ZIF-67 (160 mg)	sucrose (225 mg)	methanol (8 g), 24 h, 160 °C	conversion (66%) methyl lactate (19%)	PADA (0.1%), TMP (0.2%)	[88]
ZIF-8 (160 mg)	glucose (225 mg)	methanol (8 g), 20 h, 160 °C	conversion (98%) methyl lactate (20%)	PADA (1%), TMP (0.1%)	[88]
ZIF-8 (160 mg)	fructose (225 mg)	methanol (8 g), 20 h, 160 °C	conversion (98%) methyl lactate (11%)	-	[88]
other heterogeneous catalysts					
ZrPO (20 wt%)	glucose (6.5 wt%)	H_2O: MIBK 1 : 3 (v/v), 6 h,165 °C	conversion (60%) 5-HMF (24%)		[122]
Sn-Mont (0.2 g)	glucose (5 wt%)	THF–DMSO (70 : 30 (v/v), 6 mL), 3 h, 160 °C	conversion (98%) 5-HMF (54%)		[121]
mesoporous $TaOPO_4$ (50 mg) Catalyst:glucose 1:3 (weight ratio)	glucose (150 mg)	H_2O: MIBK 1 h, 170 °C	conversion (56%) 5-HMF (33%)		[120]
Sn-MCM-41 (150 mg)	sucrose (0.45 g)	methanol (15 g), 16 h, 160 °C	methyl lactate (28%)		[128]
Sn-MFI(150 mg)	sucrose (0.45 g)	methanol (15 g), 16 h, 160 °C	methyl lactate (24%)		[128]
Sn-Beta (100 mg)	sucrose (0.3 g)	methanol (10 g), 16 h, 160 °C	conversion (98%) methyl lactate (57%)	MVG (5%)	[127]

a) If no conversion is stated, the data was not found in the literature. b) PADA: pyruvaldehyde dimethyl acetal; TMP: 1,1,2,2-tetramethoxypropane; n.i.p.: non-identified products, MVG: methyl vinylglycolate, MIBK: methyl isobutylketone; n.s.: not stated.

1.7.2 Furans as feedstock

Furfural to furfuryl alcohol and 5-HMF to 2,5-dihydroxymethyl-tetrahydrofuran

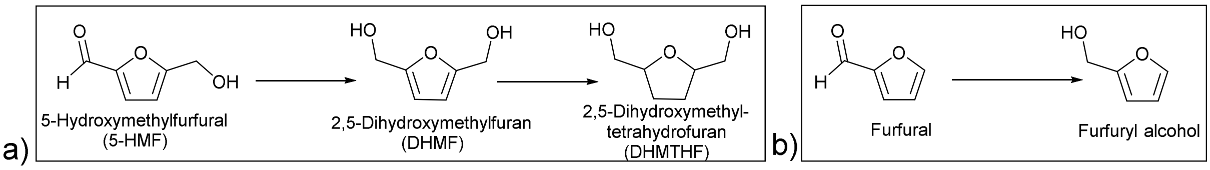

Scheme 6: a) Conversion of 5-HMF to 2,5-dihydroxymethyl-tetrahydrofuran (DHMTHF) and b) conversion of furfural to furfuryl alcohol.

Palladium nanoparticles in MIL-101Al-NH_2 were described for the selective hydrogenation of 5□hydroxymethylfurfural to 2,5-dihydroxymethyl-tetrahydrofuran (DHMTHF) (Scheme 6a).[129] Further, ruthenium nanoparticles encapsulated in different Zr-MOFs were described for the hydrogenation of furfural to furfuryl alcohol (Scheme 6b).[130] The Ru/UiO-66Zr catalyst resulted in the highest yield of furfuryl alcohol (95%). Additionally, the catalyst system could maintain its activity over 5 cycles. The activity of Ru/UiO-66Zr catalyst was assigned to the encapsulated Ru or RuO_x NPs, whereas the MOF served as suitable support, but not as catalyst itself.[130]

Alternatively, J. Chen *et al.* described the presence of amine moieties in different MOFs (MIL-101Cr, MIL-53Al, MIL-101Al-NH_2, and MIL-53Al-NH_2) as a key feature for the formation of uniform and well dispersed Pd NP. The amine functionalization also was suggested to be responsible for the preferential adsorption of 2,5-dihydroxymethylfuran (DHMF) over 5-HMF. In turn, this was supposed to enable a further hydrogenation to 2, 5-dihydroxymethyl-tetrahydrofuran (DHMTHF). The higher adsorption of DHMF is ascribed to its more hydrophilic nature as well as the improved hydrogen bonding interactions of DHMF compared to 5-HMF. The stronger H-bonding interactions through two hydroxyl groups of DHMF may hamper the dissociation of DHMF from coordinating metal sites of the MOF and can lead to further hydrogenation to DHMTHF.[129]

The procedure for Pd NP encapsulation has to be regarded critically, because the reaction involved the treatment of activated MIL-101Al-NH_2 in H_2O with hydrochloric acid followed by reduction of the Pd precursor H_2PdCl_4 with $NaBH_4$ at 0 °C.[129] The detailed study of K. Leus *et al.* showed that MIL-101Al-NH_2 is not stable under aqueous and acidic conditions.[45] In addition, surface areas of the parent MOFs were unusually low compared with the literature. Nevertheless, the supposed material Pd@MIL-101Al-NH_2 was probed in a 5-recycle run experiment in the hydrogenation of 5-HMF to DHMTHF (Scheme 6). After the 5th cycle product selectivity decreased from 96% (1th cycle) to 80% and Pd leaching was determined to only 0.03% by ICP-AES analysis. The other tested catalysts (Pd@MIL-101Cr, Pd@MIL-53Al and Pd@MIL-53Al-NH_2) showed lower activity than Pd@MIL-101Al-NH_2, but still moderate to good selectivity for DHMTHF. Generally, the amino modified MILs displayed a better product selectivity than comparable non-amino supports. This underlined the above stated key role of amine groups for the hydrogenation to DHMTHF.

5-Hydroxymethylfurfural to 2,5-diformylfuran

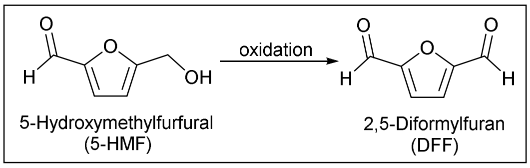

Scheme 7: Conversion of 5-HMF to 2,5-diformylfuran (DFF).

R. Fang *et al.* investigated the selective aerobic oxidation of 5-HMF to 2,5-diformylfuran (DFF) using a MOF–derived magnetic hollow Fe–Co nanocatalyst.[131] MOF–derived metal/metal oxides/metal-carbon composites emerged as highly interesting materials, not only for application as catalysts, but also as electrode materials and supercapacitors.[63] In terms of catalysis, MOF derived metal-carbon composites combine advantages of MOFs, such as comparable high porosity and uniformly distributed metal centers, with those of active carbons, such as high thermal and chemical stability.

The work of R. Fang presented the first application of MOF–derived metal-carbonaceous material for biomass transformation.[131] The MOF parent material, the mixed metal MOF MIL-45b, was formed by $CoCl_2 \cdot 4H_2O$, fine Fe powder and trimesic acid in H_2O at 180 °C. The characterized MOF was pyrolized by heating in argon atmosphere at different temperatures from 500 °C to 800 °C.[131]

The resulting FeCo/C catalysts were characterized by XRD, TEM, XPS and EDX. EDX analysis revealed homogeneous distribution of Fe and Co within the particle. Different metal and metal oxide species were detected by XRD and XPS. The real composition of the catalyst remained inconclusive, but was described by R. Fang as Fe/Co alloy. The lowest calcination temperature was 500 °C and seemed to yield hollow nanoparticles of approximately 60 nm (Figure 34). FeCo/C(500) exhibited a BET surface area of 243 m^2/g. The BET surface area decreased with higher calcination temperature and along with this also the catalytic 5-HMF conversion.

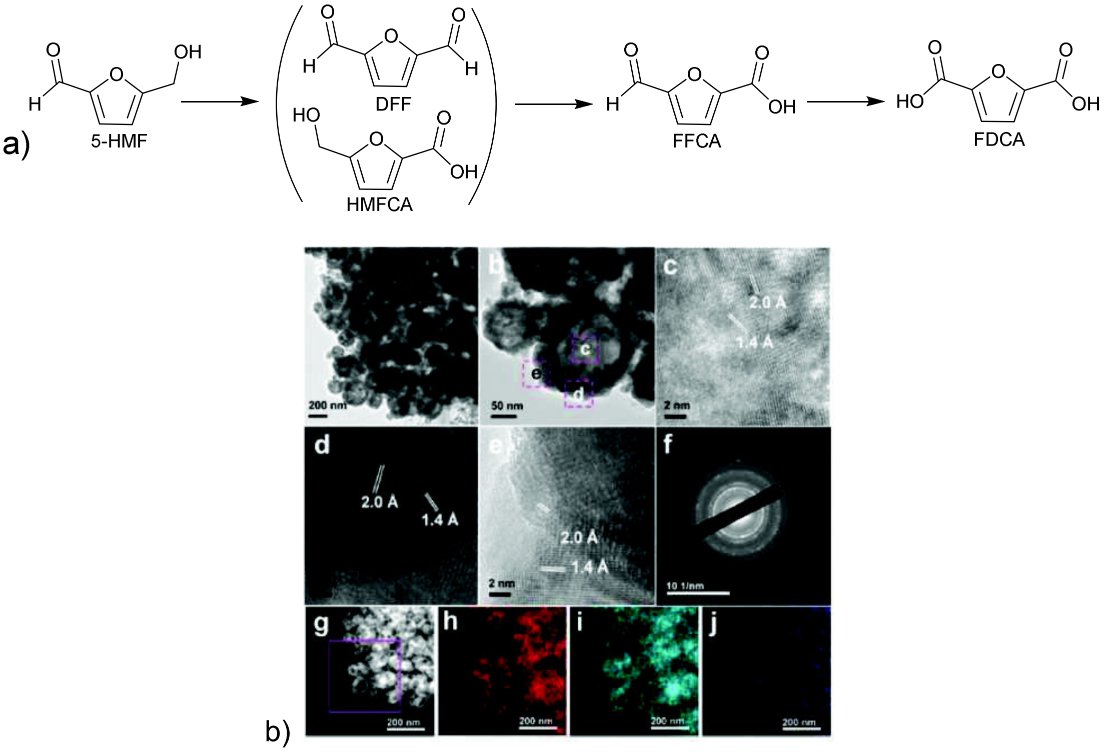

Figure 34: a) Products of HMF oxidation; b) (a–e) HRTEM images of FeCo/C(500), (f) SAED pattern, (g) HAADF-STEM images of FeCo/C(500), and the corresponding elemental mappings of (h) Fe, (i) Co and (j) C. Redrawn and reprinted from ref. [131], Copyright 2016, with permisson of the Royal Society of Chemistry.

The effect of several parameters such as temperature, O_2 pressure, solvent and calcination temperature of the catalyst on the 5-HMF oxidation was investigated. After optimizing the reactions conditions (to 100 °C, 1 MPa O_2, 6 h, toluene, Na_2CO_3) a yield >99% 2,5-diformylfuran (DFF) was obtained. FeCo/C(500) was easily recovered by magnetic separation and reused up to six runs without any significant loss in reactivity.[131]

With the non-noble Fe-Co based MOF–derived catalysts the authors presented a sustainable, cost-effective, and highly efficient system for the conversion of 5-HMF to DFF.[131] The activity of FeCo/C(500) was compared to several noble metal catalysts and was found to have a comparable high activity, while using similar or even milder reaction conditions (Table 7).[132],[133]

γ-Valerolactone to levulinic acid

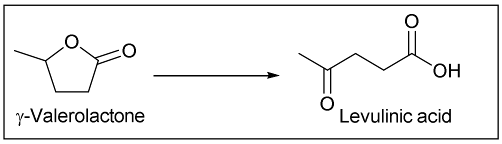

Scheme 8: Conversion of γ-valerolactone to levulinic acid.

J. Kim and coworkers reported highly porous composites of metal nanoparticles supported on nanoporous carbon (M/NC) synthesized by carbonization and carbothermal reduction (CCR) of metal-coordinated IRMOF-3 (giving M/NC3). CCR was carried out using the following conditions: 30 mL min^{-1} of Ar flow, heated at a ramp rate of 10 °C min^{-1} to 1000 °C, for 6 h. The M/NC3 materials were cooled down to room temperature under Ar flow and passivated using 10 mL min^{-1} of 1% O_2 in He for 1.5 h.

The resulting composites were composed of metal nanoparticles supported on nanoporous carbon. The materials exhibited mesoporosity and BET surface areas of 900 m^2/g up to 2300 m^2/g. The embedded nanoparticles have sizes between 3 – 8 nm (derived from IRMOF-3) and 10 – 18 nm (derived from IRMOF-1). Metal loadings differed significantly from 1 up to 10 wt% depending on the incorporated metal. The Zn ions, derived from the parent framework (IRMOF-1+3), were completely removed, which was proven by X-ray fluorescence analysis. IRMOF-3 is isoreticular to MOF-5 with a 2-aminoterephthalate linker. Due to the amine moiety of IRMOF-3 a post synthetic metal coordination (Ru, W, V, Ti) to the MOF framework was possible (before calcination). For M/NC3 materials, smaller sized metal nanoparticles were obtained in comparison to materials prepared with metal impregnated IRMOF-1 (= MOF-5) (M/NC1). The smaller size of the nanoparticles was traced to the ability of amine containing IRMOF-3 to coordinate metal precursors via PSM. This was proposed to result in site isolation and minimization of aggregation of metal nanoparticles during CCR. The synthesis procedure of J. Kim *et al.* and R. Fang *et al.* differed in the calcination temperature (500 – 800 °C vs. 1000 °C) and an additional passivation in O_2 flow (J. Kim *et al.*). Nevertheless, the most significant difference was the MOF material, since for MIL-45b no experimental surface area was described, whereas the IRMOF materials exhibited BET surface areas between 1500 m^2/g – 320 m^2/g (IRMOF-3, before and after metal impregnation) and 800 m^2/g – 330 m^2/g (IRMOF-1, before and after metal impregnation).[134]
M/NC3 materials were found to be highly active catalysts for the conversion of model compounds and derivates of lignocellulosic biomass in the liquid phase. [135]
Benzyl alcohol as a model compound for aromatic groups in lignin was oxidized into benzaldehyde. Levulinic acid, as raw material obtainable from lignocellulosic biomass, was hydrogenated into γ-valerolactone and esterificated to methyl levulinate using different M/NC materials. In all cases materials derived from aminoterephthalate IRMOF3 showed better performance than terephthalate IRMOF-1 which correlates with the observed smaller sized

NP.[135] The best results were obtained for hydrogenation of levulinic acid using Ru/NC3. γ-Valerolactone was obtained with 97 % yield and 100 % selectivity under the following conditions: levulinic acid (1.36 mmol), H_2O (20 mL), 2 MPa N_2, 130 °C, 6 h, Ru/NC3 (Ru 8.64 μmol), catalyst:reactant 1:160.

γ-Valerolactone to ethyl valerate

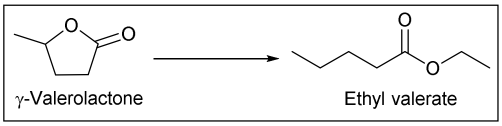

Scheme 9: Conversion of γ-Valerolactone to ethyl valerate.

D. Zhang and coworkers applied Pd nanoparticles supported on sulfonic acid substituted MIL-101Cr for the hydrogenation of γ-valerolactone (GVL) to ethyl valerate.[136] MIL-101Cr-SO_3H(X) was synthesized by direct one-pot method using monosodium 2-sulfoterephthalic acid in combination with terephthalic acid resulting in varying acid site density.[136] The Pd-MIL material was synthesized by a deposition-reduction method. H_2PdCl_4 was added to MIL-101Cr-SO_3H(X) and the Pd precursor was reduced with N_2H_4. TEM pictures showed that the Pd NPs became larger and more agglomerated with an increased amount of SO_3H groups in the framework. The particle sizes ranged from 2-5 nm for 25% SO_3H modified MIL-101Cr up to agglomerated 20 nm Pd NP for MIL-101Cr-SO_3H(100).[136]

MIL-101Cr-SO_3H(X) not only acted as support for Pd NPs, but had an influence on the selectivity. Hydrogenation of γ-valerolactone can yield different products. In the presented study ethyl valerate **4** was the desired product. D. Zhang *et al.* detected products 1-3 (Figure 35), but more (by)products are possible, which have been omitted in this figure for clarity.

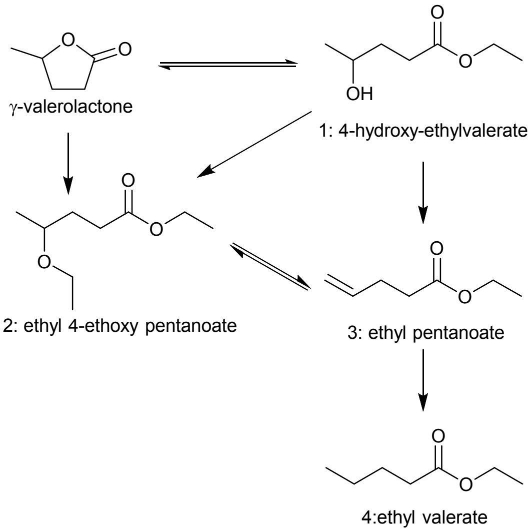

Figure 35: Reaction pathways of GVL hydrogenation in ethanol under H_2, obtainable products(1-4) with MIL-101Cr-SO_3H or Pd@MIL-101Cr-SO_3H are depicted. Additional byproducts were omitted for clarity. Modified from ref.[136].

The authors carefully compared the activity and selectivity of MOF catalysts MIL-101Cr-SO_3H(X) with the Pd NP supported Pd@MIL-101Cr-SO_3H(X) catalysts. Different product distributions were obtained; hence, first the results for solely MIL-101Cr-SO_3H(X) are described and are subsequently compared to the Pd@MIL-101Cr-SO_3H(X) catalysts.

Significant conversions of 39% to 44% were obtained for MIL-101Cr-SO_3H(50) and for MIL-101Cr-SO_3H(100), respectively (Table 5). The reaction temperature was about 200 °C. When raising the temperature to 250 °C (entry 7) a conversion of 86% for GVL to three different products was achieved. A trend concerning product formation could be observed: the higher the SO_3H content, the more ethyl pentanoate (3) was obtained. In contrast, using MIL-101Cr-SO_3H(50, 80, 100) the main product is ethyl 4-ethoxy pentanoate (2) with a selectivity of 66 % to 70 % (Table 5).[136]

Table 5: Product distributions for GVL ring-opening on MIL-101Cr and MIL-101-SO_3H(X) materials. Redrawn from ref. [136], Copyright 2014, with permisson of the Royal Society of Chemistry.

				Selectivity (%)		
Entry	**Catalyst**	**S/Cr[a]**	**Conv. (%)**	**1**	**2**	**3**
1	Blank	—	0	0	0	0
2	MIL-101Cr	0	3	100	0	0
3	MIL-101Cr-SO_3H(25)	0.20	8	94	6	0
4	MIL-101Cr-SO_3H(50)	0.40	39	20	66	14
5	MIL-101Cr-SO_3H(80)	0.45	45	11	69	20
6	MIL-101Cr-SO_3H(100)	0.80	44	14	70	16
7	MIL-101Cr-SO_3H(100)[b]	—	86	0	3	90

a) catalysts 100 mg, GVL 10 mmol, ethanol 5.8 mL, 200 °C, 10 h, 3 MPa N_2; b) 250 °C).1: 4-hydroxy-ethylvalerate, 2:ethyl 4-ethoxy pentanoate, 3: ethyl pentanoate.

When raising the temperature to 250 °C, 90% selectivity for ethyl pentanoate **3** could be achieved using MI-101Cr-SO_3H(100). This result was traced to the endothermic, only entropically favored formation of ethyl pentanoate (3). The latter one is a promising candidate for a biobased solvent with a vapor pressure higher than GVL, but lower than common octane boosters. Hence, ethyl pentanoate is also a valuable product obtainable with MIL-101Cr-SO_3H.[136]

Comparing conversions and product selectivity of MIL-101Cr-SO_3H(X) to Pd@MIL-101Cr-SO_3H(X) substantial differences were observed. Firstly, Pd@MIL101Cr-SO_3H(50) gave the desired product **4** ethyl valerate with 26% selectivity (35% conversion), whereas product **3** was absent. Pd@MIL-101Cr-SO_3H(100) gave the highest conversion (51%) at 200 °C, distributed to **2** (ethyl 4-ethoxy pentanoate, 66%) and **4** (ethyl valerate, 26%) (Figure 36). A physical mixture MIL-101Cr-SO_3H(100) and Pd@C gave a higher selectivity towards ethyl valerate (44%), but lower conversion (42%). Here, the authors concluded that Pd nanoparticles in close proximity to SO_3H groups show lower C=C and C=O bond hydrogenation activity. To increase the yield of desired ethyl valerate **4** using Pd@MIL-101Cr-SO_3H(100) the temperature was increased up to 250 °C. A conversion of 98% with a selectivity towards ethyl valerate **4** of 83% was achieved. Reusability experiments of Pd@MIL-101Cr-SO_3H(80) revealed a dramatic change in product selectivity after the first run from ethyl valerate **4** to ethyl pentanoate **3** (Figure 36).

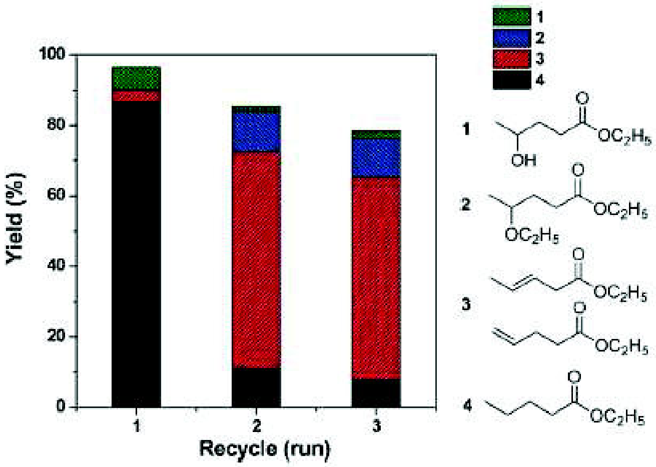

Figure 36: The reusability of Pd@MIL-101-SO_3H(80) catalyst in GVL ringopening reaction. Reaction conditions: 10 mmol GVL, 5820 mL ethanol, 250 °C, 10 h, 3 MPa H_2. Reprinted from ref.[136], Copyright 2014, with permisson of the Royal Society of Chemistry.

The authors explained this by further aggregation of the Pd NP resulting in deactivation and framework collapse. Leaching of Pd species was excluded by a hot filtration test and ICP-AES analysis. However, initial TEM analysis before the catalytic reaction also showed agglomeration of Pd NP (20 nm) for MIL-101Cr-SO_3H(80 and 100). No data was given which confirmed the integrity of the MIL-101Cr-SO_3H framework after the reaction at 250 °C.[136] Therefore, although the results are promising for valorization of biomass, final catalyst stability remained inconclusive.

Levulinic acid to ethyl levulinate

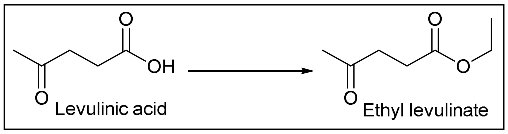

Scheme 10: Esterification of levulinic acid to ethyl levulinate.

Generally, esterification of levulinic acid (LA) is carried out using mineralic acids such as sulfuric acid. Additionally, a wide range of solid acid catalysts as for instance Amberlyst resin, zeolites and sulfated metal oxides have been successfully applied.[137],[138]

Recently, F.G. Cirujano and coworkers investigated the activity of UiO-66Zr as well as UiO-66Zr-NH_2 for the esterification of levulinic acid with ethanol, butanol and long chain alcohols (C12, C16, C18).[138]

Under the applied conditions (levulinic acid, LA 1 mmol, EtOH:LA 15:1, 8 h, 78 °C, catalyst 1.8 mol%Zr with respect to LA), both UiO-66Zr as well as UiO-66Zr-NH_2 converted levulinic acid quantitatively into ethyl levulinate after 8 h. Both MOFs displayed very similar activities of 94 and 95 % yield, respectively. The ratio of ethanol:LA was reduced to 5:1 to allow for comparison to literature results (T = 78 °C). UiO-66Zr gave activities of 49 % (4 h/78 °C) and 73 % (4 h/100 °C), respectively. In comparison, Amberlyst-15[139] (5 h/70 °C) gave 55% conversion and sulfated TiO_2[139] (5 h/70 °C) 40%. UiO-66Zr displayed higher conversions than sulfated ZrO_2, or the zeolites and mesoporous silica H-ZSM-5 and H-MCM-22. Otherwise, desilicated zeolite loaded with dodecatungstophosphoric acid (DTPA/DHZSM-5) (82% at 4 h/78 °C)[140] and sulfated TiO_2 nanorods (83% at 4 h/105 °C)[141] performed better than UiO-66Zr even when the temperature was increased to 100 °C. This was ascribed to the lower excess of alcohol in the reaction using DTPA/DHZSM-5 or sulfated TiO_2 nanorods as catalysts.[138] Nevertheless, the above stated comparison pointed out, that UiO-66Zr catalysts can compete with current state-of-the-art catalysts for the levulinic esterification reaction to ethyl levulinate.

The authors further characterized the material in-depth and investigated the influence of linker deficiency[70] on the catalytic activity of UiO-66Zr MOFs in levulinic acid esterification. Different batches of the same material were found to have strongly different activities leading to a 9-fold increase from the less active to the most active material (Figure 37).[138]

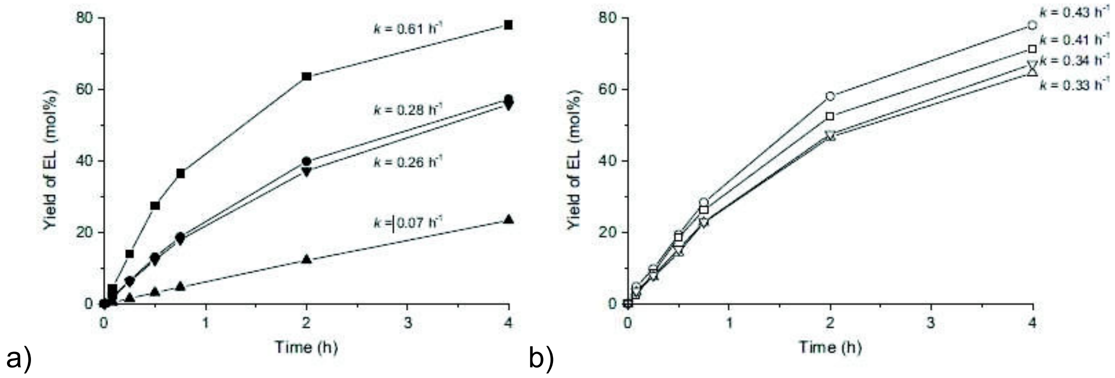

Figure 37: a) Yield of ethyl levulinate (EL) obtained over (a) UiO-66, batches B1 to B4 (from top to bottom); b) UiO-66–NH_2, batches A1 to A4 (from top to bottom). For each curve, the calculated pseudo-first order kinetic rate constant is indicated. Reprinted from ref.[138], Copyright 2015, with permission of Elsevier.

Linker deficiencies were calculated by a method of Valenzano *et al.*[142], where thermogravimetric analysis was used to determine the relative weight loss of the organic ligand (above 300 ºC) with respect to the expected amount based on the stoichiometry of the ideal structure (solid residue calculated as ZrO_2). The derived linker deficiencies (%) correlated with the corresponding rate constants (*k*, h^{-1}) (Figure 37, Table 6). These linker deficiencies have been calculated from the linker to cluster ratios (coordination number, c.n.,Table 6), revealing in all cases a lower ratio than expected (c.n. 12) for the ideal UiO-66 structure. The higher the amount of missing linkers, the higher the activity of the MOF catalyst, demonstrating the importance of OMS for the reaction.

Table 6: Kinetic rate constant (*k*) for the esterification of levulinic acid to ethyl levulinate, linker deficiencies (%def), average coordination number ($\overline{c.n.}$, calculated from TGA) and the mean particle size (d_c, calculated from TEM) for different batches of UiO-66 materials. Redrawn from ref. [138], Copyright 2015, with permission of Elsevier.

Material	**Sample batch**	***k*** **(h^{-1})**	$\%def$	$\overline{c.n.}$	$d_c\ (nm)$
UiO-66	B1	0.61	13.2	10.42	120±5
	B2	0.28	7.2	11.14	65±5
	B3	0.26	4.8	11.42	200±10
	B4	**0.07**	**2.5**	**11.70**	**95±5**
UiO-66-NH_2	A1	0.43	6.3	11.24	45±10
	A2	0.41	8	11.04	65±5
	A3	**0.34**	**2.5**	**11.70**	**110±5**
	A4	0.33	2.1	11.75	103±9
UiO-66-NO_2	N1	0.07	0.4	11.95	95±5

UiO-66Zr-NO_2 was obtained with a linker to cluster ratio very close to 12 (Table 6). As expected, its catalytic activity was low. By comparing UiO-66Zr with UiO-66Zr-NH_2, it is evident that not only defect formation but also the amino group influences the catalyst performance. Batches B4 of Ui-66Zr and A3 of UiO-66Zr-NH_2 displayed the same degree of linker deficiency (2.5%) and have similar particle sizes, but the rate constant of A3 is almost 5 fold higher than for B4 (Table 6). This indicates a supporting effect of the amino group of UiO-66Zr-NH_2. A possible reaction pathway proposed by the authors is depicted in Figure 38.

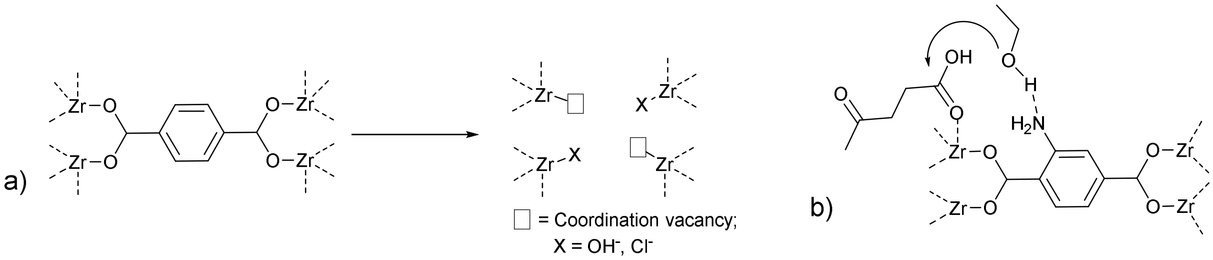

Figure 38: a) Defect formation through a missing linker. Two Zr atoms have a vacancy and. two Zr ions from different Zr_6 clusters are coordinated by hydroxido or chlorido anions in order to retain framework neutrality. b) Proposed reactivation pathway over UiO-66-NH_2. Redrawn from ref.[138], Copyright 2015, with permission of Elsevier.

The authors attributed the different grades of linker deficiency to small differences in nucleation and crystal growth rates as well as stochastic variations in temperature, time or reagent concentrations. Accordingly, recalculation of activities based on the experimentally determined Zr content gave higher values, comparable to the homogeneous p-toluene-sulfonic acid.[138]

Esterification products using longer chain alcohols (C12-OH – C18-OH) are much larger in size. Therefore, it can be expected that conversion takes place at the MOF surface, instead of inside the pores. This correlates with a much slower reaction rate (For C16-OH, 66%/8 h, 82%/20 h).[138]

Triglycerides to esters and glycerol

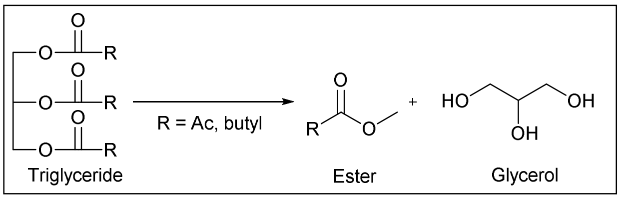

Scheme 11: Transesterification of triglycerides to the corresponding ester and glycerol.

Bio-diesel consists of fatty acid alkyl ester (FAAE) molecules that differ by the length of the carbon chains, and the nature and position of double bonds in these chains. The type of carbon chains in FAAE determines the bio-diesel quality, such as oxidation resistance and viscosity. The most common way to produce bio-diesel is transesterification of triglycerides of vegetable oil with alcohol by a acid or base catalyst. The resulting products are fatty acid alkyl esters and glycerol.[143],[144] Glycerol is a valuable resource for industrial relevant C3 chemicals as for instance lactic acid, acrolein and 1,3-propanediol.[145] Recent developments are reviewed by D. Sun and coworkers.[145]

The transesterification of vegetable oil by a metal-organic framework was investigated first by C. Chizallet in 2010 using unfunctionalized ZIF-8.[146] After detailed experimental and theoretical studies they concluded that the acid- and basic sites are located at the external surface of the material or at defects, but not in the microporosity of ZIF-8. Surface N-moieties and OH groups as basic sites, were shown to be particularly interesting for the combined activation of alcohols and esters. Hence, they were proposed as the active sites.[146]

J. Chen and coworkers reported in 2014 the transesterification of triglycerides catalyzed by amine-functionalized MOFs.[147] MOF-5, IRMOF-10 and MIL-53Al-NH_2 were selected as catalysts. The MOFs were modified with amines using i) dative modification (grafting) of ethylenediamine (ED) or 4-dimethylaminopyridine (DMAP) to unsaturated metal sites located at the secondary building units of MOFs and (ii) covalent modification of the amine-tagged organic linkers within MIL-53Al-NH_2 by alkylation with 2-dimethylaminoethyl chloride.

The ethylenediamine-grafted MOF-5 and IRMOF-10 catalysts exhibited high conversions in the liquid phase transesterification of glyceryl triacetate (both >99.9% after 3 h) and glyceryl tributyrate (both >99.9% after 6 h) with methanol. Upscaling of the reaction, starting from 302 mg glyceryl tributyrate to 2.1 g glyceryl tributyrate, led to a slight decrease in the conversion rate to 89% and 99%, respectively, after 10 h. MIL-53Al-NH_2 led to very low yields (4%) of converted glyceryl triacetate compared with 2-dimethylaminoethyl functionalized MIL-53Al-NH_2 (99.9 % yield). For the conversion of glyceryl tributyrate significant differences between the activity of amine functionalized MOFs can be measured (Figure 39a).[147] The catalytic activity (TOF) towards transesterification and the basic site density of amine-grafted MOFs revealed a linear correlation (Figure 39b).

The basic site density was determined by acid-base titration with aqueous HCl as titrant in aqueous KCl solution.[147] MOF-5 and other Zn-carboxylate based IRMOFs are, however, unstable in water,[44] so it is not clear how reliable the obtained values are.

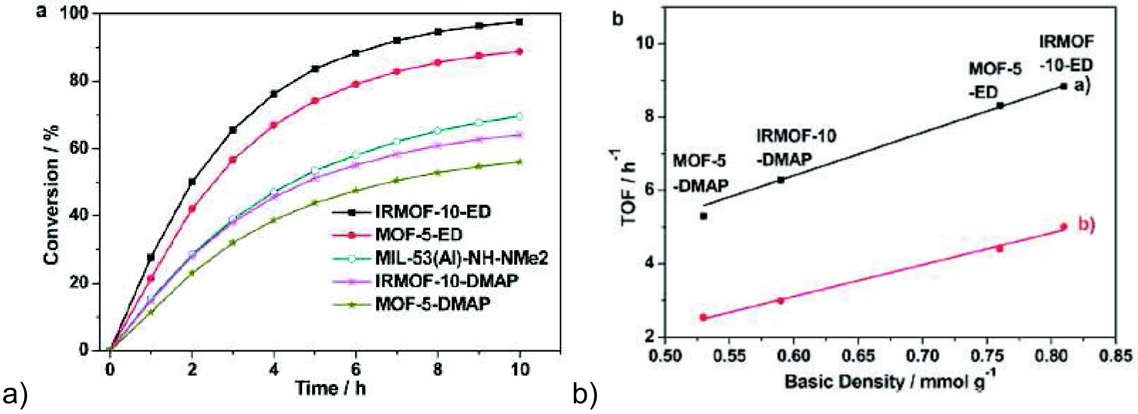

a) b)

Figure 39: a) comparison of the catalytic activities of amine-functionalized MOFs for the transesterification of glyceryl tributyrate with methanol (reaction conditions: glyceryl tributyrate (2.1 g); methanol (8.0 mL); catalyst (80 mg), temperature 60 °C); b) linear correlations between the basic density of amine-functionalized MOFs with their catalytic activity in the transesterification of (a) glyceryl triacetate and (b) glyceryl tributyrate with methanol. Reprinted from ref. [147], Copyright 2014, with permission of the Royal Society of Chemistry.

Only the powder X-ray diffractogram for IRMOF-10-ED after the reaction was shown. This PXRD pattern was in agreement with the diffractogram of the parent IRMOF-10. Nevertheless, the cycling experiments revealed a loss in activity of about 37% from the first to the fourth cycle using IRMOF-10-ED. The authors explain this decrease with leaching of ethylenediamine.[147]

Often algae oil, sunflower oil or other natural feedstocks are used for transesterification. These natural products are not comparable to glyceryl triacetate as a model compound. This makes a fair comparison difficult. A. Zieba *et al.* described the activity of a heterogeneous Zn catalyst (Zinc hydroxy nitrate, $Zn_5(OH)_8(NO_3)_2 \cdot 2\ H_2O$) at similar conditions (5 wt% catalyst, glyceryl triacetate:methanol 1:29 molar ratio, 3 h, 50 °C) for the reaction of glyceryl triacetate with methanol. This Zn catalyst gave only 52% methyl acetate after 3 h which is lower than for grafted MOF-5, IRMOF-10 and for MIL-53Al-NH-NMe_2.[148]

Table 7: Feedstock furans

Catalyst	Substrate	Conditions (solvent, time, temperature, pressure)	Product (%)[a]	Byproducts	Ref
Ru/UiO-66Zr (0.1g)	furfural (0.1mL)	H_2O (9.9mL), 4 h, 20 °C, 5 bar H_2	furfuryl alcohol (95%)		[130]
FeCo/C(500) (20 mol%)	5-HMF (1 mmol, 0.5 mol/L)	toluene (2 mL), 6 h, 100 °C 1.0 MPa O_2, Na_2CO_3 (1mmol)	DFF (>99%)		[131]
MIL-101Cr-SO_3H(50) (0.1g)	GVL 10 mmol	ethanol (5.8 mL), 10 h, 200 °C, 3 MPa H_2	conversion (39%) ethyl 4-ethoxy pentanoate (66%)	(1) 4-hydroxy-ethylvalerate (20%) (3)ethyl pentenoate (14%)	[136]
MIL-101Cr-SO_3H(100) (0.1g)	GVL 10 mmol	ethanol (5.8 mL) 10 h 200 °CC, 3 MPa H_2	conversion (44%) ethyl 4-ethoxy pentanoate (70%)	(1) 4-hydroxy-ethylvalerate(14%) (3)ethyl pentenoate (16%)	[136]
Pd@MIL-101-SO_3H(50), (0.1g)	GVL 10 mmol	ethanol (5.8 mL), 10 h, 200 °C, 3 MPa H_2	conversion (35%) (2) ethyl 4-ethoxy pentanoate (55%)	(1) 4-hydroxy-ethylvalerate (19%); (4) ethyl valerate (26%)	[136]
Pd@MIL-101-SO_3H(100), (0.1g)	GVL 10 mmol	ethanol (5.8 mL), 10 h, 200 °C, 3 MPa H_2	conversion (51%) 2) ethyl 4-ethoxy pentanoate (66%)	(1) 4-hydroxy-ethyl-valerate (8%); (4) ethyl valerate (26%)	[136]
W/NC3 (W 3.56 μmol), catalyst:reactant 1:320	levulinic acid (1.14mmol)	methanol (20mL), 12 h, 130 °C, 0.1 MPa N_2	conversion (4%) methyl levulinate (42%)		[135]
W/NC1 (W 3.56 μmol), catalyst:reactant 1:320	levulinic acid (1.14mmol)	methanol (20mL), 12 h, 130 °C, 0.1 MPa N_2	conversion (25%) methyl levulinate (25%)		[135]
Ru/NC3 (Ru 8.64 μmol), catalyst:reactant 1:160	levulinic acid (1.36 mmol)	H_2O (20mL), 6 h, 130 °C, 2 MPa N_2	conversion (97%) γ-valerolactone (97%)		[135]
Ru/NC1 (Ru 8.64 μmol), catalyst:reactant 1:160	levulinic acid (1.36 mmol)	H_2O (20mL), 6 h, 130 °C, 2 MPa N_2	conversion (5%) γ-valerolactone (5%)		[135]
UiO-66 (1.8 mol%Zr with respect to LA)	levulinic acid (1mmol)	ethanol:LA 15:1, 4 h/8 h 78 °C	ethyl levulinate (4h:78%, 8h: 94%)		[138]
UiO-66-NH_2 (1.8 mol%Zr with respect to LA)	levulinic acid (1mmol)	ethanol:LA 15:1, 4 h/8 h 78 °C	ethyl levulinate (4h:78%, 8h: 95%)		[138]
UiO-66 (1.8 mol%Zr with respect to LA)	levulinic acid (1mmol)	ethanol:LA 5:1, 4 h 78 °C/100C	ethyl levulinate (78 °C: 49%, 100 °C: 73%)		[138]
MIL-53Al-NH-NMe_2 (30mg)	glyceryl triacetate (181 mg)	methanol (1mL), 4 h, 50 °C	conversion (100%) glycerol (100%) methylacetate (100%)		[147]
MIL-53Al-NH-NMe_2 (30mg)	glyceryl butyrate (302 mg)	methanol (1.2mL), 6 h, 60 °C	conversion (95%) glycerol, methylbutyrate		[147]
other heterogeneous catalysts					
Ag-OMS-2 (Ag 16.7 mol%)	5-HMF (0.063 mol/L)	isopropyl alcohol, 165 °C, 1.5 MPa, air	Conversion (99%) DFF (99%)		[132]
Ru/HT (0.1g, Ru 4.4 wt%)	5-HMF (1 mmol)	DMF (3 mL) 6 h, 120 °C, 0.1 MPa O_2	DFF (92%)	FFCA (3%)	[133]
Pd@C (0.1g,Pd 5 wt%)	5-HMF (1 mmol)	DMF (3 mL) 6 h, 120 °C, 0.1 MPa O_2	DFF (21%)	FFCA (2%)	[133]

Amberlyst (2.5wt%)	levulinic acid	ethanol/acid 5:1, 5h, 70 °C	ethyl levulinate (55%)		[139]
Sulfated TiO_2 (2.5wt%)	levulinic acid	ethanol/acid 5:1, 5h, 70 °C	ethyl levulinate (40%)		[139]
HZSM-5 (2.5wt%)	levulinic acid	ethanol/acid 5:1, 5h, 70 °C	ethyl levulinate (4%)		[139]
DTPA/DHZSM-5 catalyst to LA ratio: 0.25	levulinic acid	ethanol/acid 6:1, 4h, 78 °C	ethyl levulinate (82%)		[140]
Zn-5 catalyst (5 wt%)	glyceryl triacetate	glyceryl triacetate:methanol (1:29 molar ratio), 3 h, 50 °C	conversion (73%) methylacetate (52%)		[148]

a) If no conversion is stated, the data was not found in the literature. LA: Levulinic acid, DFF: 2,5-Diformylfuran, FFCA: 5-Formyl-2-furancarboxylic acid

1.7.3 Lignin as feedstock

Ether bond cleavage into phenol and arenes

V. Stavila *et al.* reported first about MOFs that are able to catalyze the hydrogenolysis of carbon− oxygen ether bonds, which are common linkages in biomass.[149] Phenylethylphenyl ether (PPE), benzylphenylether (BPE), and diphenyl ether (DPE) have been selected as model substrates (Figure 40), because they bear the lignin relevant β-O-4, α-O-4 and 4-O5 linkages.

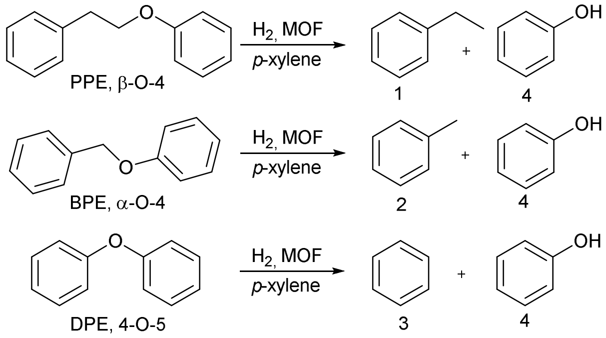

Figure 40: Reactions catalyzed by IRMOF-74(I, II). Redrawn with permission from ref [149]. Copyright 2016, American Chemical Society.

IRMOF-74(I) and IRMOF-74(II) were selected because of i) their sufficient thermal and chemical stability, ii) large enough channels for substrate diffusion and iii) high density of open metal sites (OMS) for C-O bond activation. Figure 41 shows the large channels of IRMOF-74(I)+(II) which have diameters of 1.4 and 2.2 nm, respectively. Crystal structures of all three substrates have been determined experimentally. The longest intramolecular distance was determined for IRMOF-74(I) to 1.2 nm and for IRMOF-74(II) to 1.4 nm (straight line between the blue-highlighted atoms, Figure 41). Therefore, the pores are large enough to accommodate all substrates.[149]

IRMOF-74(I) was build up from $Mg(NO_3)_2$ and 2,5-dihydroxyterephthalic acid with a mixture of DMF/ethanol and H_2O as solvents in a solvothermal reaction. IRMOF-74(II) contained also Mg as metal and 3,3'-dihydroxy-[1,1'-biphenyl]-4,4'-dicarboxylate was used as linker. Solvent stability tests, TGA, PXRD and an analysis of the supernatant reaction solution by elemental analysis showed that the MOF catalysts are stable under the applied conditions (45 mg catalyst, 5.0 mL *p*-xylene, 120 °C, 16 h, 10 bar H_2). It is noted that the authors reported partial dissolution of IRMOF-74(I) in H_2O. The authors did not provide information about substrate amounts; in consequence no statement about substrate to catalyst ratio can be made.

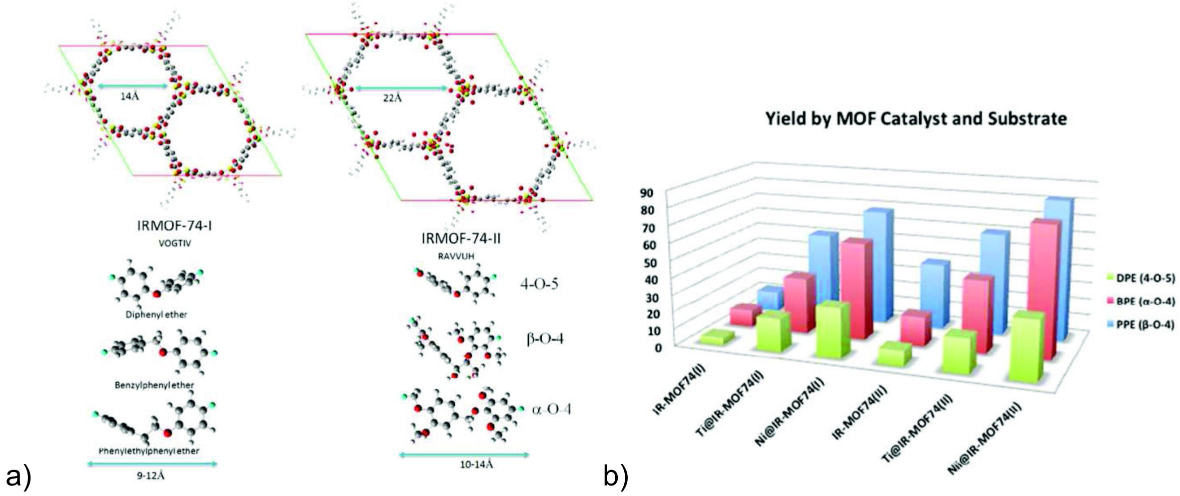

Figure 41: a) Pore diameters of IRMOF-74(I) and IRMOF-74(II) and largest intramolecular distances in the aromatic ether compounds, corresponding to a straight line between the blue-highlighted atoms in the optimized geometries; b) conversion efficiencies of the substrates into the corresponding hydrocarbon and phenol at 120 °C under 10 bar hydrogen. Reprinted with permission from ref [149]. Copyright 2016 American Chemical Society.

Results using IRMOF-74(I+II) catalysts revealed activity for the hydrogenolysis of ethers generating phenol and the corresponding aromatic hydrocarbon (Figure 40) for three substrates (Figure 41). Higher conversions were obtained using the IRMOF-74(II) catalyst with, for example, 39% conversion of PPE versus 12% with IRMOF-74(I) (Figure 41). Product selectivity is slightly higher for IRMOF-74(I) for all three substrates. For example product selectivity from PPE for **1** and **4** is 87 and 91% for IRMOF-74(I) versus 83% and 87% for IRMOF-74(II).

Based on the reaction stoichiometry, equal amounts of the two products would be expected. Selectivity distributions showed lower amounts of the alkyl benzenes **1**, **2** and **3** with respect to phenol. This was explained by volatility of the arene compounds and was experimentally verified by residual gas analysis (RGA). Although conversions of ethers with MOF catalysts are moderate to low, without catalyst no reaction occurred, supporting the role of MOFs as catalysts. The difference in surface area between the two MOFs is small, with 1627 m^2/g for IRMOF-74(I) and 1736 m^2/g for IRMOF-74(II). According to the authors the higher conversion rates using IRMOF-74(II) in comparison with IRMOF-74(I), indicated that the reactions occurred within the MOF´s pores. Therefore, DFT calculations were performed which led to the suggestion that the OMS in the MOF´s pores bind and orientate the substrate. Furthermore, the OMS were proposed to play a role in activating or orientating H_2. All findings indicated that substrate confinement may play a key role in MOF catalysis.

In addition to pure MOFs also $TiCl_x$ and Ni NPs have been encapsulated into the MOF pores, since they are known to catalyze aryl ether hydrogenolysis.[149] Substrate conversion was significantly enhanced up to 82% for Ni@IRMOF-74(II)) in case of PPE (overview see Figure 41) with high selectivities towards **1** of 96% and **4** of 98%. Conversion of PPE with pure Raney Ni as catalyst was similar (76%) to those of Ni@IRMOF-74(II), but the selectivity was lower: 81% of **1** and 75 % of **4**. Additionally, substantial amounts of cyclohexanol were found in reactions with Raney Nickel. This was not observed using MOF-based catalysts. Overall, the activity order for the three MOF-based catalysts was Ni@IRMOF-74 >Ti@IRMOF-74>IRMOF-74, independent of the substrate used. Ni@IRMOF-74 could be reused up to 5 times without loss in activity and, as confirmed by PXRD, it retained its structure through all 5 cycles.[149]

Vanillin into 2-methoxy-4-methyl phenol

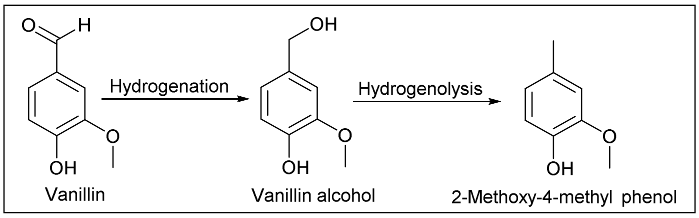

Scheme 12: Hydrodeoxygenation of vanillin to 2-methoxy-4-methyl phenol.

F. Zhang *et al.* reported the catalytic activity of Pd@MIL-101Cr-SO_3H[150] and Pd@ UiO-66Zr-NH_2[151] for the hydrodeoxygenation of vanillin. Both MOFs were prepared in a one pot synthesis procedure from SO_3H or NH_2 functionalized terephthalic acid. Following the incipient-wetness impregnation method, $Pd(acac)_2$ was dissolved in chloroform and added to MIL-101Cr-SO_3H. After aging overnight and drying, the solid was reduced using a gas flow containing a mixture of H_2 (10 vol%) in Ar for 4 h at 200 °C. The resulting catalyst Pd@MIL-101Cr-SO_3H, contained 2.0 wt% Pd.[150]

Catalytic conditions for vanillin conversion were vanillin (2 mmol), catalyst (50 mg), H_2O (20 mL), H_2 (0.5MPa) at 100 °C for Pd@MIL-101Cr-SO_3H and 90 °C for Pd@ UiO-66-NH_2.[150],[151] Vanillin was first hydrogenated to vanillin alcohol and then converted to 2-methoxy-4-methylphenol (Scheme 12). This was proven for both catalysts by gas chromatography (GC) analysis. The catalytic activity of Pd@MIL-101Cr-SO_3H and Pd@ UiO-66Zr-NH_2 is very similar, the latter one converted vanillin quantitatively to 2-methoxy-2-methylphenol within 1 h and Pd@MIL-101Cr-SO_3H with a selectivity of 91% (96% conversion). A reference experiment with Pd@MIL-101Cr gave a lower conversion (67%) and lower product selectivity (58% 2-methoxy-4-methylphenol).[150]

Moreover, the UiO-66Zr-NH_2 support showed a higher adsorption of the substrate and of the intermediate compared to UiO-66Zr. However, UiO-66Zr-NH_2 exhibited a lower BET surface area and pore volume than UiO-66Zr. It was suggested that the adsorption of vanillin or vanillin alcohol by amine-functionalized MOFs is enhanced by the hydrophilic nature of the substrate molecule as well as the interactions between the substrate molecule and the MOF support.

Both catalysts can be reused seven times without any loss in activity and selectivity. The presence of free amine moieties in the frameworks of Pd@UiO-66Zr-NH_2 is assumed to play a key role in the formation of uniform, well-dispersed and leaching resistant palladium nanoparticles on the support. For direct catalysis the amine moieties were proposed to interact with the substrate molecule but this suggestion was not proven.[151] Compared with other supported Pd catalysts such as Pd@CM170 (CM = carbonaceous microspheres, conversion >99%, 2-methoxy-4-methylphenol 48%) selectivity of Pd@UiO-66Zr-NH_2 (conversion 100%, 2-methoxy-4-methylphenol 100%) towards 4-methoxy-4-methyl phenol is higher (Table 8).[152]

Table 8: Feedstock Lignin

Catalyst	**Substrate**	**Conditions (solvent, time, temperature, pressure)**	**Product (%)**	**Byproducts**	**Ref.**
IRMOF-74(I) 45 mg	PPE (n.s)	*p*-xylene (5.0 mL), 16 h, 120 °C, 10bar H_2	conversion (12%) 1 (87%), 4 (91%)	no	[149]
IRMOF-74(II) 45 mg	PPE(n.s)	*p*-xylene (5.0 mL), 16 h, 120 °C, 10bar H_2	conversion (39%), 1 (83%), 4 (87%)	no	[149]
Ni@IRMOF-74(II) 45 mg	PPE (n.s)	*p*-xylene (5.0 mL), 16 h, 120 °C, 10bar H_2	conversion (82%), 1 (96%), 4 (98%)	no	[149]
Raney Ni (n.s.)	PPE (n.s)	*p*-xylene (5.0 mL), 16 h, 120 °C, 10bar H_2	conversion (76%), 1 (81%), 4 (75%)	cyclohexanol	[149]
Pd@MIL-101Cr (50 mg)	vanillin (2 mmol)	H_2O (20 mL), 1 h 100 °C, H_2 (0.5MPa),	conversion (67%) 2-methoxy-4-methylphenol (58%),	vanillin alcohol(42%)	[150]
Pd@MIL-101Cr-SO_3H (50 mg)	vanillin (2 mmol)	H_2O (20 mL), 1 h 100 °C, H_2 (0.5MPa),	conversion (96%) 2-methoxy-4-methylphenol (91%),	vanillin alcohol(9%)	[150]
Pd@UiO-66-NH_2 (50 mg)	vanillin (2 mmol)	H_2O (20 mL), °C, H_2 (0.5MPa),	conversion (100%) 2-methoxy-4-methylphenol (100%)		[151]
other heterogeneous catalysts					
Pd@C (2 wt%) S/C: 200;	vanillin (2 mmol)	H_2O (20 ml), 60 min, 100 °C; H_2 0.5 MPa.	conversion (55%) 2-methoxy-4-methylphenol(22%)	Vanillin alcohol (78%)	[150]
Pd@CM170 S/C:100	vanillin (155 mg)	H_2O (30 mL), 1 h, 100 °C, 1 MPa H_2	conversion (>99%) 2-methoxy-4-methylphenol(48%)	Vanillin alcohol (52%)	[152]

(n.s): not specified. PPE: Phenylethylphenyl ether; BPE: Benzylphenyl ether; DPE: Diphenyl ether.

1.7.4 Conclusion and perspective

From the presented studies it can be concluded that MOFs display a similar or better activity than comparable other heterogeneous catalysts such as zeolites or metal oxides. This is especially the case for MOFs in fructose dehydration in DMSO or in reactions where moderate acidity leads to the best results. In glucose dehydration and in cellulose hydrolysis MOFs cannot (yet) compete with other state-of-the-art catalysts. In metal@MOF catalyzed reactions, such as hydrogenations, MOFs do not only serve as support for the catalytically active metal, but also have a significant influence on product selectivity. This was, for example, the case in hydrodeoxygenation of vanillin to 2-methoxy-4-methylphenol with Pd@MIL-101Cr-SO_3H or Pd@UiO-66Zr-NH_2.[150],[151]

Especially, the following features distinguish MOFs from zeolites and metal oxides and are worthy of further development to enable new catalytic pathways leading to sustainable, biomass based fine chemicals:

- Tunable Lewis and Brønsted acidity owing to the type and degree of functionalization and defect engineering;
- Uniform nature of open metal sites (OMS) and other catalytically active sites within the MOF;
- Hydrogen bonding interactions through linkers and thereby anchoring and orienting substrates and intermediates;
- Modulation of hydrophilicity/hydrophobicity and acidity/basicity in terms of microenvironment in the pores, thereby controlling the adsorption of substrates/intermediates.

In order to develop efficient MOF catalysts for biomass catalysis, a better understanding has to be acquired regarding:

- Interplay between organic linker modifications and metal incorporation in MOF supports;
- Pore size versus pore confinement;
- Hierarchical meso/ macroporous MOFs for better mass transport;
- water stability of MOFs;
- Humin formation and solutions for prevention[153]
- Improving MOF characterization methods, regarding catalyst properties

Method development is fundamental, aiming a deeper understanding for instance in structure-property relations. There is the need of a reliable determination of acidity and basicity for MOFs. Currently, liquid acid or base titration is commonly used, but this usually involves proton exchange with sodium chloride. According to our experience this method does not lead to satisfactory results. Recently, R. C. Klet published the first detailed report about reliable acid base titration for MOFs.[154] On the contrary, for acidity/basicity measurements, most of the time MOF stability data (after titration) and measurement data (e.g. titration curves) are not reported. This makes it difficult to reconstruct if the MOF remained stable under the applied conditions.

Methods, such as temperature programmed desorption (usually performed with NH_3), have to be further developed to be applicable to temperatures below 300 °C. Also less basic probe molecules and new methods for acid-base characterization of MOFs have to be found.

Another critical issue is the free and accessible pore space. The usual characterization of a MOF pre-catalyst material involves PXRD for crystallinity and MOF identification, nitrogen volumetric sorption at 77 K for (BET) surface area measurement and pore volume determination and NMR digestion for the degree of linker functionalization. However, all three measurements give only an average value. The pore volume determined by N_2 sorption is seen as equally accessible, also for larger substrate molecules.

What about the distribution of functional groups within the MOF particle? For instance, (post-synthetic) functionalization could occur primarily only in the outer sphere of the MOF particle or within the pore mouths. Small dinitrogen molecules will diffuse through the entire MOF particle, but do larger molecules still enter the smaller functionalized pores? How many of the functional sites are really available for catalysis? How deep do the different molecules diffuse into the MOF particle? This has significant influence on catalyst activity, as TON and TOF values are usually calculated by assuming the number of active sites from the molecule formula. The diffusion path length of the substrates in the MOF would have consequences for particle size engineering. Therefore knowledge about minimum required particle size could reduce the amount of MOF material needed. Therefore, methods which offer spatial resolution within one MOF particle are necessary to gain a better understanding of MOF catalysis. In addition, a reliable method to quantify hydrophilicity or hydrophobicity of the pore size environment has, to the best of our knowledge, not been reported yet. This could help to optimize substrate uptake by MOFs as well as to investigate MOF substrate/intermediate interactions.

Taking the numerous possible applications of MOFs into account, there is an urgent need for MOFs which are stable in acidic or basic aqueous solution. Intensive research is going on, aiming at a better understanding of structure-property relations to improve hydrothermal stability in order to advance MOFs to real applications.[155],[36],[156]

Finally, we want to encourage the MOF community to boost work on MOF catalysis, especially in the context of biomass-based fine chemical production

2. Objectives of this work

This work targeted the application of prototypical metal-organic frameworks for heterogeneous catalysis and the investigation of different shaping strategies for metal-organic frameworks towards water vapor and combined CO_2/H_2O sorption.

The main objectives of this work are:

- Investigation of the influence of different properties, for instance functionalization of the linker, surface area and particle size of MOFs on catalytic activity. The acid catalyzed diacetalization of benzaldehyde with different alcohols was selected as model reaction. In addition, a deeper understanding in Brønsted vs. Lewis based MOF catalysis should be gained.

- Application of prototypical metal-organic frameworks as catalysts for the production of value added chemicals derived from biomass model compounds. The first challenge is the selection of an appropriate reaction for the investigation of the following criteria: a) potentially catalyzed by Brønsted acids; b) cascade reaction; c) selectivity by MOFs. The conversion of glucose into the platform chemical 5-hydroxymethylfurfural was identified to fulfill all requirements and was investigated using different functionalized MIL-101Cr MOFs.

- Summary and evaluation of state-of-the-art research developments in the area of biomass catalysis with metal-organic frameworks in form of a review as introduction.

- Shaping of metal-organic frameworks, which are usually obtained as powders, is an important challenge for industrial application, for instance in the field of gas sorption and catalysis. Therefore, in this work different strategies for shaping of MIL-101Cr and MIL-101Cr-NH_2 are investigated: a) mechanical shaping (cooperation project); b) deposition on glass substrates by spray coating (cooperation project) and c) application of resorcinol-formaldehyde polymers as binding agent. By using the latter technique the fabrication of stable MOF@xerogel monoliths is targeted with a special focus on retention of pore accessibility, which should be proven by nitrogen and water sorption experiments.

3. Cumulative part

Sections 3.1–3.3 present the published/submitted work of this thesis.

Each of the published or submitted work is self-contained with a discrete and short introductory part and a separate list of references. Before each section of this cumulative part, a short overview is given to integrate the results into the further context of this thesis. A statement about the author’s share of work is presented. Further unpublished work is illustrated in section 4 + 5.

3.1 Brønsted instead of Lewis acidity in functionalized MIL-101Cr MOFs for efficient heterogeneous (nanoMOF) catalysis in the condensation reaction of aldehydes with alcohols

A. Herbst, A. Khutia, C. Janiak,
Inorg. Chem. **2014**, *53*, 7319−7333
DOI: 10.1021/ic5006456, reference [71]
Impact factor 2014: 4.8

Metal-organic frameworks are promising materials for size- and shape-selective catalysis, because of the uniformity of the porous network and high tuneability. There is a current focus on the Lewis acidity/basicity in MOFs, whereas investigation of Brønsted acidity lags behind.[72] In this work MIL-101Cr and MIL-101Cr derivates have been investigated as heterogeneous catalysts for diacetal formation from benzaldehyde and methanol. Detailed characterization was performed to elucidate the reaction mechanism concerning Lewis- and Brønsted acidity. Furthermore, other aldehydes and longer chain alcohols were used. MIL-101Cr-NO_2 showed the highest activity with 99% conversion and 100% selectivity to the diacetal. After 90 min a turnover number of 114 was obtained. Properties such as surface area, acidity and particle size have been compared within different charges of MIL-101Cr and functionalized MIL-101Cr derivates. In addition, catalytic activity from nanoMOF particles with a diameter below 200 nm was investigated, too. From this work, insights to structure–property relations for MOF based acid catalysis could be obtained.

Author's share of work:

- Designing and performing of the synthetic work and catalytic reactions and evaluation of the results.
- The materials MIL-101Cr-NO_2 and MIL-101Cr-NH_2 were synthesized by Mr. Khutia
- Writing of the manuscript and drawing of the figures, graphs and tables except for figure 1 and S1 (done by Mr. Janiak).
- Editing of the manuscript regarding the reviewers' comments by Ms. Herbst and Mr. Janiak.

Inorganic Chemistry
Article
pubs.acs.org/IC

Brønsted Instead of Lewis Acidity in Functionalized MIL-101Cr MOFs for Efficient Heterogeneous (nano-MOF) Catalysis in the Condensation Reaction of Aldehydes with Alcohols

Annika Herbst, Anupam Khutia, and Christoph Janiak*

Institut für Anorganische Chemie und Strukturchemie, Heinrich-Heine-Universität Düsseldorf, Universitätsstrasse 1, D-40225 Düsseldorf, Germany

Ⓢ *Supporting Information*

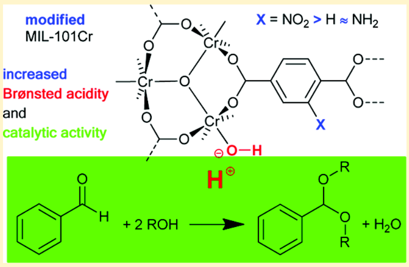

ABSTRACT: Porous chromium(III) 2-nitro-, 2-amino-, and nonfunctionalized terephthalate (MIL-101Cr) metal organic frameworks are heterogeneous catalysts for diacetal formation from benzaldehyde and methanol (B−M reaction) as well as other aldehydes and alcohols. MIL-101Cr-NO_2 obtained by direct reaction between CrO_3 and 2-nitro-terephthalate showed the highest activity with 99% conversion in the B−M reaction in 90 min and turnover numbers of 114. The activity decreased in the order MIL-101Cr-NO_2 > MIL-101Cr > MIL-101Cr-NH_2. Within different samples of nonfunctionalized MIL-101Cr the activity increased with surface area. Methanol gas sorption of the different MIL materials correlates with the BET surface area and pore volume but not with the diacetalization activity. Benzaldehyde adsorption from heptane showed no significant difference for the different MILs. Gas sorption studies of CD_3CN to probe for a higher Lewis acidity in MIL-101Cr-NO_2 remained inconclusive. A high B−M catalytic activity of wet MIL-101Cr-NO_2 excluded significant contributions from coordinatively unsaturated Lewis-acid sites. pH measurements of methanol dispersions of the MIL materials gave the most acidic pH (as low as 1.9) for MIL-101Cr-NO_2, which significantly increased over MIL-101Cr (3.0) to MIL-101Cr-NH_2 (3.3). The increase in acidity is of short range or a surface effect to the heterogeneous MIL particles as protons dissociating from the polarized aqua ligands (Cr−OH_2) have to stay near the insoluble counteranionic framework. The variation in Brønsted acidity of MIL-101Cr-NO_2 > MIL-101Cr ≈ MIL-101Cr-NH_2 correlates with the withdrawing effect of NO_2 and the diacetalization activity. The catalytic B−M activity of soluble, substitution-inert, and acidic $Cr(NO_3)_3\cdot 9H_2O$ supports the Brønsted-acid effect of the MIL materials. Filtration and centrifugation experiments with MIL-101Cr-NO_2 revealed that about 2/3 of the catalytic activity comes from nano-MOF particles with a diameter below 200 nm. The MIL-101Cr-NO_2 catalysts can be recycled five times with very little loss in activity. The diacetalization activity of MIL-101Cr-NO_2 decreases with the alcohol chain length from methanol over ethanol, *n*-propanol, *n*-butanol, to almost inactive *n*-pentanol, while conversions for benzaldehyde, paratolylaldehyde, 4-chlorobenzaldehyde, and cyclohexanone all reach 90% or more after 90 min.

■ INTRODUCTION

In recent years metal organic frameworks (MOFs), also known as porous coordination polymers (PCPs), have gained enormous attention due to promising applications such as gas storage,[1] gas and liquid separation processes,[2] sensing,[3] drug delivery,[4] luminescence,[5] magnetism,[6] heterogeneous catalysis,[7] heat transformation processes,[8] and hosts for metal nanoparticles.[9] MOFs are composed of metal ions or clusters, connected through organic linkers which lead to versatile topologies and architectures. MOFs surpass classical porous materials such as zeolite or activated carbon in their permanent porosities, high surface areas, tunable pore sizes, and topologies.[10] In MOFs BET surfaces range typically between 1000 and 4000 m^2/g and pore apertures or channel diameters from 0.3 to 3.4 nm with pore volumes of up to 1.5 or 2 cm^3/g.

Currently, MOFs are investigated as heterogeneous catalysts for various organic reactions.[11] An advantage of MOFs over other related porous materials toward catalysis should be their high order and uniformity of the porous network for size- and shape-selective catalysis.[12] There is a current focus on the Lewis acidity/basicity in MOFs. Catalytic reactions of MOFs include Lewis-acid catalysis, Lewis-base catalysis, enantioselective catalysis, etc. MOFs having coordinatively unsaturated metal centers can potentially interact with the substrate and act as Lewis-acid catalyst.[11d,13,14] The role and increase of active metal sites for catalysis with MOFs was studied and critically discussed by DeVos and co-workers.[15,16] The presence of suitable functional groups either in the organic linkers or attached to the metal center can also influence the Lewis acidity and catalytic activity of MOFs.[17−21]

MIL-101Cr is a three-dimensional chromium−terephthalate-based porous material with the empirical formula $[Cr_3(O)(BDC)_3(F,OH)(H_2O)_2]$ (where BDC = benzene-1,4-dicarboxylate).[22] Its structure resembles the augmented MTN zeolite topology with pore diameters of about 2.9 and 3.4 nm (Figure

Received: March 22, 2014
Published: July 9, 2014

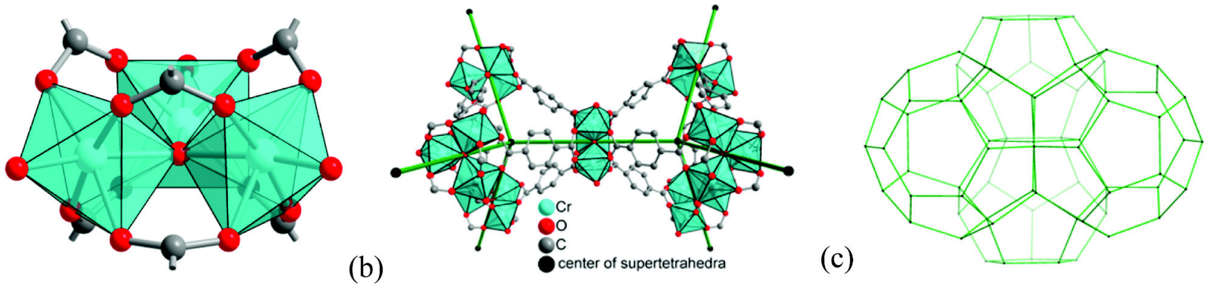

Figure 1. MIL-101Cr network with the (a) trinuclear $\{Cr_3(\mu_3\text{-}O)(O_2C-)_6(F,OH)(H_2O)_2\}$ building unit which forms the vertices of supertetrahedra (b). Vertex-sharing supertetrahedra (b) then form two types of mesoporous cages with pentagonal and hexagonal windows (c). For presentation of the pore and window size see Figure S1, Supporting Information.

1). MIL-101Cr has two terminal water molecules connected to the trinuclear $\{Cr_3(\mu_3\text{-}O)(O_2C-)_6(F,OH)(H_2O)_2\}$ building units with their octahedral Cr(III) ions (Figure 1a), which can be removed under high vacuum, thus creating Lewis-acid sites.[17,23] MIL-101Cr[8a] or its derivatives[8i] show remarkable stability toward water, which make them suitable for catalytic reactions involving water.

The catalytic activity of MIL-101Cr or its derivatives has been reported in the literature for various organic reactions such as oxidation of aryl sulfides to sulfoxides,[24] epoxidation of alkenes with H_2O_2,[25] or cyanosilylation of aldehydes.[26] Amine-grafted MIL-101Cr has proven to be a useful catalyst for Knoevenagel condensation reaction with high yield and high selectivity.[23,27] Pd loaded on amine-grafted MIL-101Cr has been used as catalyst for Heck reaction.[23] Similarly, Cu nanoparticles embedded in MIL-101Cr act as a high-performance catalyst for reduction of aromatic nitro compounds.[28] Recently, MIL-101Cr and its phospho-tungstic acid (PTA) composite material have been proven as efficient catalysts for aldehyde−alcohol reactions, including the benzaldehyde dimethyl acetal formation (cf. Scheme 1), albeit of low activity for MIL-101Cr only (24 h for 80% conversion).[29]

Scheme 1. Diacetalization of Benzaldehyde with Different Alcohols[a]

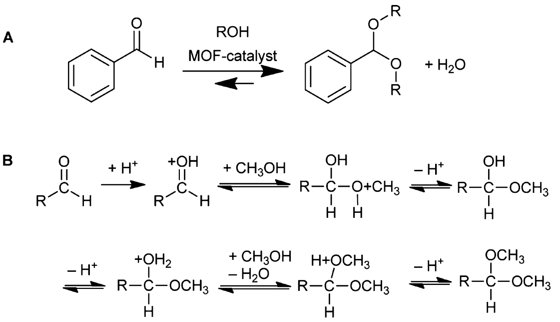

[a]R = Me, Et, ^nPr, ^nBu, $^nC_5H_{11}$, $PhCH_2$ and the Brønsted-acid (proton) catalyzed acetalization mechanism.[30,31]

Acetalization is an important technique to protect aldehyde or ketone groups in organic transformation reactions (Scheme 1). In homogeneous phase the reaction between the carbonyl substrate and the alcohol or trialkyl orthoformates as reagents is normally carried out in the presence of Brønsted acids (Scheme 1)[30,31] or Lewis-acidic transition-metal catalysts (Scheme 2).[32] The water formed in the equilibrium reaction has to be removed for quantitative conversion, which is typically done either azeotropically in a Dean−Stark apparatus or using trialkyl orthoformate as a water scavenger. The Lewis-acid catalysis mechanism is proposed as a simultaneous activation of the alcohol and the aldehyde by coordination at two available cis coordination sites (Scheme 2). Alcohol or alkoxide addition to the carbonyl group is then an intramolecular concerted reaction leading to a complexed hemiacetal or hemiacetalide (Scheme 2A or 2B, respectively). The reaction can proceed either through formation of an oxocarbenium ion, which subsequently undergoes external addition of ROH (Scheme 2A),[33] or by nucleophilic attack of ROH on the chelating hemiacetalide (Scheme 2B).[34] The intermediate metal hydroxide is then transformed to the metal aqua species by the protonated alcohol, and subsequently, the aqua ligand is substituted by the aldehyde.[34]

Irrespective of the mechanistic details, transition metals seem to be catalytically active when (a) two “active sites” in cis positions can easily be generated, e.g., by the presence of weakly coordinated ligands, and (b) the bonds between the metal center and the O donors are labile.[32−34] Also, a high charge of the metal ion is advantageous as it facilitates polarization of the metal−carbonyl substrate bond and promotes deprotonation of the coordinated ROH reagent. Both effects favor nucleophilic attack onto the coordinated C═O group.[32] For chromium(III) and MIL-101Cr the application of these principles creates a dilemma: If two cis positions are needed the Cr ions in MIL-101Cr will not have two “active sites” in cis position unless one assumes missing dicarboxylate linkers. Such missing linkers in MOFs can be possible as recently demonstrated for UiO-66.[20,35] For the moment we are not aware of similar studies on linker deficiencies in MIL-101Cr as for UiO-66. However, from coordination chemistry principles it can be envisioned that construction faults during the metal−ligand assembly in inert Cr(III) MOFs cannot easily be corrected as in labile Zn(II) MOFs with a pronounced dissociation equilibrium. Thus, there will be a certain degree of imperfections, such as missing linkers also in Cr(III) MOFs. However, one could also imagine that only the carbonyl compound is activated on one Lewis-acid site while the alcohol stays in the outer coordination sphere. Even then, Cr(III) does not form labile but inert complexes. Even if there is initially a vacant Lewis-acidic site on chromium the released water from the condensation reaction will occupy the unsaturated metal sites. Then, the rate constant for the water exchange in $[Cr(H_2O)_6]^{3+}$ is a very small $2.4 \times 10^{-6}\ s^{-1}$ (at 298.15 K).[36] A recent comprehensive review on transition-metal complexes in the synthesis of acetals does not list chromium as a catalyst.

Scheme 2. Proposed Mechanisms for Transition-Metal-Catalyzed Acetal Formation[a]

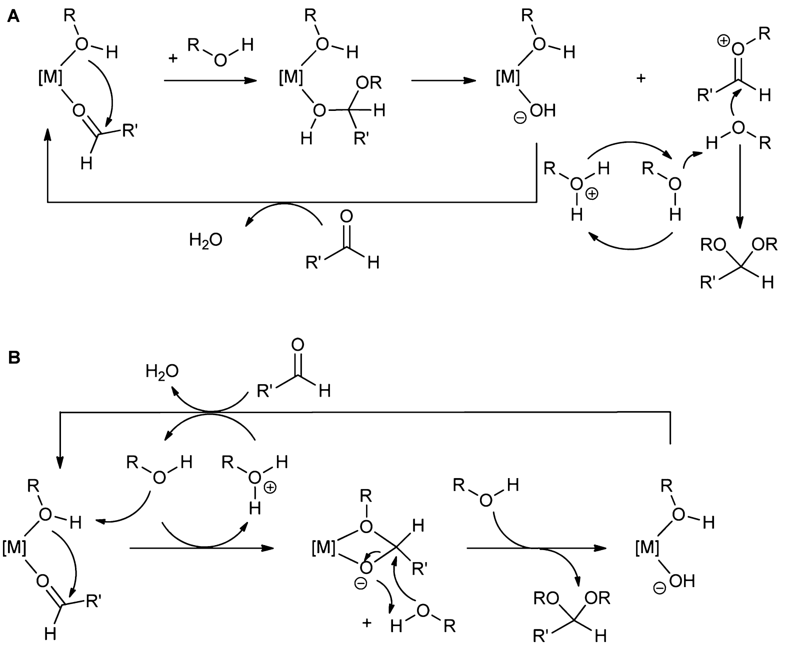

[a]Adapted from refs 32−34.

Table 1. Porosity and Particle Size Properties of MIL-101-Cr Materials

	BET surface area (m^2/g)[a]		total pore volume (cm^3/g)[b]			
materials	before	after catalysis[e]	before	after catalysis[e]	methanol loading (g/g)[c]	particle diameter ± standard deviation (σ) (nm)[d]
1a	3055	3100[e]	1.51	1.56	1.08	479 ± 150
1b	2763	2712	1.45	1.43	n.d.	330 ± 160
1c	2509	2749	1.15	1.42	n.d.	300 ± 70
2-NO$_2$-d	2429	2377, 2421[f]	1.32	1.35, 1.44[f]	0.89	380 ± 100
2-NO$_2$-ps	1353	1550	0.74	0.89	n.d.	280 ± 50
3-NH$_2$-ps	2920	2711[g]	1.60	1.53[g]	1.08	220 ± 30

[a]Calculated in the pressure range $0.05 < p/p_0 < 0.2$ from N_2 sorption isotherm at 77 K. BET error margin is 20−50 m^2/g. [b]Calculated from N_2 sorption isotherm at 77 K ($p/p_0 = 0.95$) for pores ≤ 20 nm. [c]Gravimetric methanol uptake capacity calculated from methanol sorption isotherm at 298 K (see also Figure 4 below) at $p/p_0 = 0.8$ (condensation effects possible at higher levels); n.d. = not determined. [d]Obtained by dynamic light scattering (DLS) of a particle suspension in methanol (see Figures S10−S12, Supporting Information). [e]After 90 min catalysis unless stated otherwise. See corresponding N_2 sorption isotherms as Figure S3, Supporting Information. [f]After five catalytic runs with 90 min each. [g]After a catalytic run for 24 h.

Rather, chromium is in a list of precursors noted as less or completely ineffective (see conclusions in ref 32).

Many solid materials such as zeolite,[37] silica gel,[38] and aluminosilicate[39] have been used as heterogeneous catalysts for the acetalization reaction of aldehydes with trimethyl orthoformate. Methanol has been reported for the condensation with aldehyde under refluxing condition, catalyzed by siliceous mesoporous material MCM-41.[40] Use of methanol in this condensation reaction would be advantageous because of its availability. Recently, MOF-catalyzed acetalization of aldehydes with methanol has been reported with $Cu_3(BTC)_2$[41] or MIL-101Cr/PTA composite materials.[29] In the present work, we study the effect of nitro and amino groups in MIL-101Cr (**1**) with its (postsynthetic) derivatives MIL-101Cr-NO$_2$ (**2-NO$_2$**) and MIL-101Cr-NH$_2$ (**3-NH$_2$-ps**) as heterogeneous catalysts for the condensation reaction of aldehydes with different alcohols (Scheme 1). Thereby, we also consider the effect of nano-MOFs in the catalytic activities of **2-NO$_2$-d**. The different porosity, particle size, and sorption properties **1**−**3** should contribute to a better understanding of how postsynthetic modifications influence the catalytic behavior of MOFs. We verify the Brønsted acidity of chromium MIL-101 which originates from aqua ligands versus the role of Lewis acidity of possible open metal sites. Lewis acidity has been the recent focus on the modification and tuning of MILs for catalytic applications[20,21,42] but does not seem to have taken into account the simultaneous Brønsted acidity of these MOFs.[43,44]

■ RESULTS AND DISCUSSION

Synthesis and Porosity. Three different batches of MIL-101Cr samples (**1a**−**c**) with different surface areas and pore volumes were reproducibly obtained by modifications in the synthesis route (Table 1). Sample **1a** was synthesized hydrothermally through a base-mediated reaction of $Cr(NO_3)_3$ and terephthalic acid.[45] MIL **1b** and **1c** were prepared through reaction of $Cr(NO_3)_3$ and terephthalic acid under acidic hydrothermal conditions[22] but differ in the washing part of their activation procedure (see below). The different batches of **1a–c** were each obtained reproducibly 2–3 times.

From the reaction of CrO_3 with 2-nitroterephthalic acid, MIL-101Cr-NO_2 (**2-NO_2-d**) was synthesized directly under hydrothermal conditions as reported in the literature.[8b] In addition, the postsynthetic modification of MIL-101Cr yielded also MIL-101Cr-NO_2 (**2-NO_2-ps**) and MIL-101Cr-NH_2 (**3-NH_2-ps**).[46,47] The suffix "-d" denotes direct synthesis, and "-ps" denotes postsynthetic synthesis. Organic linkers bearing functional groups may be incompatible for reaction under hydrothermal condition. Postsynthetic modification (PSM) is an alternative technique to introduce suitable functional groups in the material.[48] Here, we used nitration of MIL-101Cr with mixed acid (conc. HNO_3/conc. H_2SO_4) to yield **2-NO_2-ps**. MIL-101Cr-NH_2 (**3-NH_2-ps**) was then prepared through subsequent reduction of **2-NO_2-ps** with $SnCl_2$ and conc. HCl (Scheme 3).

Scheme 3. Schematic Representation of the Synthesis of MIL-101Cr-NO_2 (2-NO_2-ps, 2-NO_2-d) and MIL-101Cr-NH_2 (3-NH_2-ps) through Postsynthetic (-ps) Modification of MIL-101Cr or by Direct (-d) Synthesis

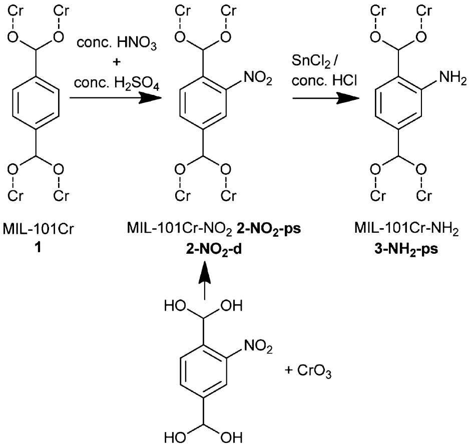

Analyses and catalytic studies were carried out on samples which were purified (activated) as follows: Compounds **1a–c** were purified by washing with H_2O, DMF, and ethanol, followed by 12 h stirring in DMF at room temperature and 6 h at 110 °C, concluded by 12 h stirring in ethanol at room temperature and 3–5 h at 90 °C with a final washing with water. Compound **1c** was additionally treated with boiling water for 12 h. The amount of solvent was 90 mL per washing cycle (see Supporting Information for details). Compounds **2-NO_2-d** and **-ps** as well as **3-NH_2-ps** were activated by washing three times with water (see Supporting Information for details). Finally, the materials **1–3** were collected by centrifugation and dried at 70 °C overnight. For use in catalysis the materials **1–3** were dried in vacuum (10^{-6} Torr) for 48 h at 30 °C and stored under nitrogen unless stated otherwise. Activation of MOF materials is particularly important to obtain materials with high surface area and pore volume. Different synthesized batches of MOF samples may have different surface area. Many parameters such as crystal defects and phase purity or the presence of guest molecules may influence the surface area of the materials. Previous studies[17] showed the presence of a significant amount of unreacted terephthalic acid within the pores of MIL-101Cr, which is very difficult to remove from the pores, leading to a decrease in surface area.

All compounds were characterized by powder X-ray diffractometry (PXRD) and surface area analysis. PXRD patterns match well with the simulated MIL-101Cr patterns (Figure 2a), which suggest retention of framework structures after postsynthetic modification. N_2 sorption isotherms showed typical type I isotherms, characteristic of a microporous material (Figure S2, Supporting Information). BET surface areas were calculated from N_2 sorption isotherms at 77 K. MIL-101Cr (**1a**) from base-mediated synthesis has a significantly higher BET surface area and pore volume than the acid-synthesized materials **1b** and **1c** (Table 1). The higher surface area of **1a** can be ascribed to the better solubility of terephthalic acid in alkaline aqueous solution. Purification of **1b** and **1c** differs by an additional final overnight washing cycle in hot water for **1c** (see Supporting Information for details).

Thermogravimetric analyses of **1–3** (dried at 10^{-6} Torr for 48 h at 30 °C) in Figure 2b showed that up to 200 °C a weight loss of less than 8% occurred.

Catalytic B–M Reaction. Conversion of benzaldehyde with methanol to benzaldehyde dimethyl acetal (B–M reaction) in the presence of different catalysts (Scheme 1) was screened, and conversion was followed by gas chromatography. The alcohol was added in excess with the ratio between alcohol to benzaldehyde as 50:1. For all experiments 10 mg of the catalyst was used, which corresponds to a molar ratio of chromium to benzaldehyde of 1:80. The materials **1–3** were tested under identical conditions.

For the three nonfunctionalized MIL-101Cr materials **1a–c** it can be stated that a higher surface area leads to higher conversion of benzaldehyde to dimethylacetal (Figure 3, Table 2). After 90 min, the highest surface area sample **1a** (S_{BET} = 3055 m^2/g) shows a conversion of 73%. A notably higher activity could be observed for the functionalized samples **2-NO_2-d** and **3-NH_2-ps** (Figure 3, Table 2). After only 20 min a conversion of 83% and after 90 min a quantitative conversion of 99% was measured for **2-NO_2-d**. The higher activity of **2-NO_2-d** indicates a positive effect on the catalytic activity by the NO_2 group because the surface area of 2429 m^2/g of **2-NO_2-d** is 20% lower than the surface area of **1a** (3055 m^2/g). The material **2-NO_2-ps** with the lowest surface area of 1352 m^2/g among all samples **1–3** shows a lower catalytic activity than **1a** (73%), but with 56% conversion after 90 min its activity is still higher than for the lower surface materials **1b** (35%) and **1c** (19%). In the UiO-66Zr-catalyzed cyclization of (+)-citronellal to isopulegol and its isomers and - conversion of geraniol in the Oppenhauer oxidation with furfural the activity of UiO-66Zr-NO_2 was also strongly increased over the nonfunctionalized parent compound.[21] Also, the Meerwein reduction of 4-*tert*-butylcyclohexanone with isopropanol proceeded much faster with UiO-66Zr-NO_2.[20] Molecular modeling studies suggested that the nitro group lowers the adsorption and activation free energy of the reaction.[21]

Compound **3-NH_2-ps**, which is functionalized with NH_2 groups, shows a slightly higher catalytic activity (77%) than the nonfunctionalized MILs **1a** (73%) but lower than **2-NO_2-d** (99%), although **3-NH_2-ps** has a higher surface area than **2-NO_2-d** (cf. Table 1). This finding contrasts with the observed lowest activity for UiO-66Zr-NH_2 in the UiO-66Zr-X-catalyzed cyclization of (+)-citronellal to isopulegol and its isomers. There, the activity of UiO-66Zr-NH_2 was slightly lower than that of the parent compound UiO-66Zr.[21] In the UiO-66-Zr-

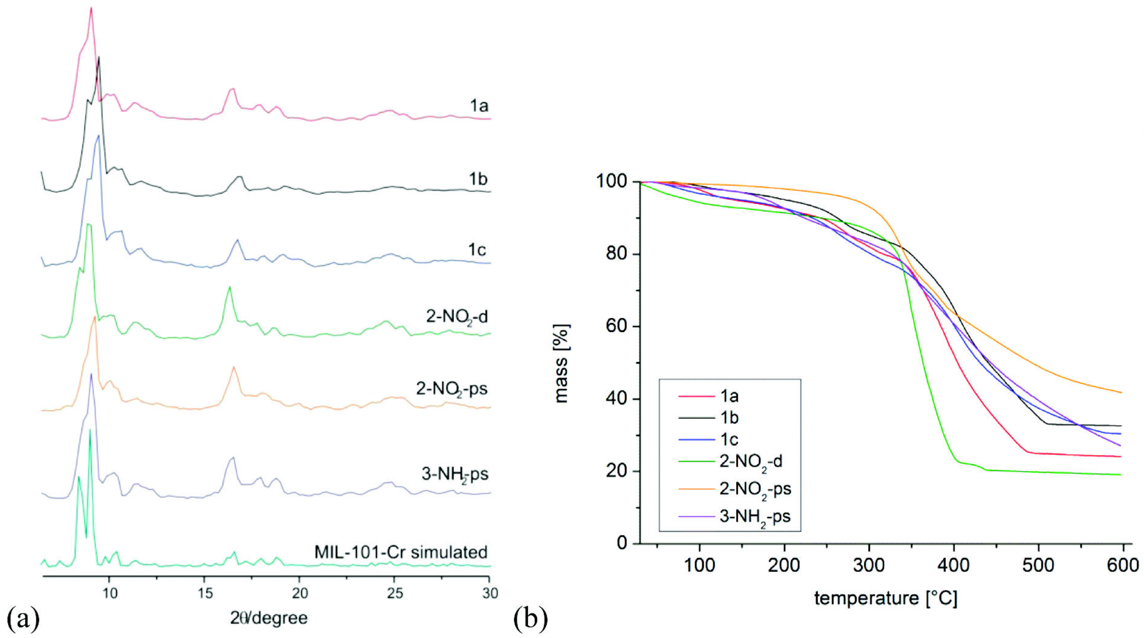

Figure 2. (a) PXRD patterns of MIL-101Cr samples. (b) Thermogravimetric analysis of **1**−**3**.

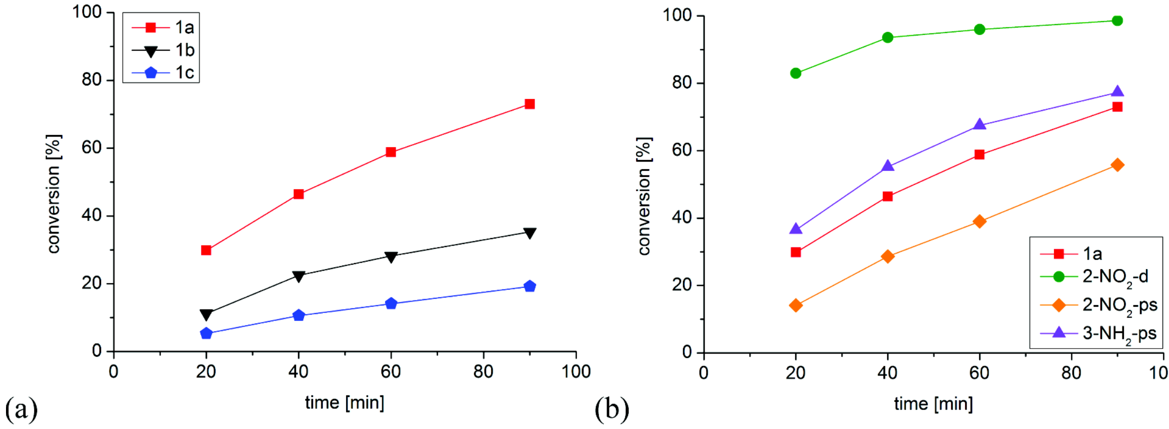

Figure 3. Time-dependent conversion of benzaldehyde to dimethyl acetal over 90 min: (a) Nonfunctionalized MIL **1a**−**c** and (b) **1a** and functionalized MIL-101 derivatives **2-NO$_2$-d**, **2-NO$_2$-ps**, and **3-NH$_2$-ps** (right).

Table 2. Catalytic Activities in the Acetalization of Benzaldehyde with Methanol with Different MIL-101Cr Catalysts[a]

materials	conversion [%]	TON[b]	TOF [h^{-1}][c]
1a	73	84	56
1b	35	40	27
1c	19	22	15
2-NO2-d	99	114	76
2-NO2-d-wet	74	85	57
2-NO2 ps	56	65	43
3-NH2 ps	77	89	59

[a] Standard reaction conditions: reaction time 90 min, benzaldehyde (340 μL, 3.34 mmol), methanol (6.7 mL, 166 mmol), total volume 7.04 mL, catalyst (10 mg =2.9×10^{-2} mmol chromium (2/3 of total n(Cr) = 0.043 mmol)). Every reaction was performed at least in duplicate to ascertain reproducibility. [b] TON = mol of product/mol of chromium. [c] TOF = mol of product/(mol of chromium·time(h))

catalyzed cyclization of citronellal the activity as log k_x shows a strong correlation with Hammett's σ values for the linker.[21]

The BET surface areas of **1**−**3** were determined again after the catalytic runs and found to be largely unchanged within experimental error (**1a**, **1b**, **2-NO$_2$-d**) or even slightly increased (**1c**, **2-NO$_2$-ps**), and only for **3-NH$_2$-ps** there was a slight decrease (Table 1). The increase of the surface area can be assigned to the soaking and washing of the MIL material with methanol during and after the catalysis run before drying for the sorption measurement. Clearly, the materials **1**−**3** retain their porosity (Table 1). Also, the phase identity and crystallinity **1**−**3** was unchanged after the catalytic runs as evidenced by powder X-ray diffraction (compare Figure 2 and Figures S4 and S15, Supporting Information).

For material **3-NH$_2$-ps** the NH$_2$ groups on the terephthalate ligand could react with benzaldehyde in a Schiff base reaction. This possibility was, however, not supported by IR spectroscopy (Figure S6, Supporting Information). In the IR spectrum of **3-NH$_2$-ps** no additional signal for a N=C bond could be detected after the catalytic run (which would have been expected as a very strong band between 1600 and 1630 cm^{-1}). The XRD stayed unchanged and confirmed that material **3-NH$_2$-ps** was still intact and crystalline after catalysis (Figure S6, Supporting Information) and the surface area decreased only slightly (Table 1).

Methanol and Benzaldehyde Adsorption. From all catalysts **2-NO$_2$-d** shows by far the best performance with near quantitative conversion in less than 90 min, so that we studied its properties in more detail in comparison to the other materials. If the catalytic reaction takes place inside the pores then the kinetics and thermodynamics of the substrate adsorption and product desorption may also determine the conversion rate. In order to rule out or support this effect, methanol gas ad- and desorption isotherms (Figure 4), which reflect the thermodynamic sorption behavior, were collected for **1a**, **2-NO$_2$-d**, and **3-NH$_2$-ps** on a Quantachrome iQ MP with all gas option (see Supporting Information for experimental details). The maximum MeOH uptake correlates with the BET surface area and pore volume (Table 1). There are slight differences in the onset of MeOH uptake (Figure 4). MIL **1a** and **3-NH$_2$-ps** reach the uptake of 0.15 g MeOH/g MIL already at $p/p_0 < 0.05$, while MIL **2-NO$_2$-d** shows this uptake not until $p/p_0 > 0.05$. Still, the differences in the MeOH gas uptake are not significant enough and do not follow the activity order **2-NO$_2$-d** > **3-NH$_2$-ps** > **1a**.

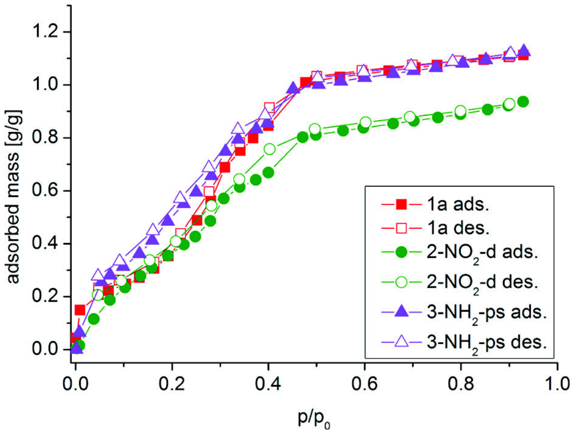

Figure 4. MeOH gas sorption isotherms (closed symbols for adsorption, and open symbols for desorption).

Considering that MeOH is present in 50-fold excess compared to benzaldehyde, the uptake of benzaldehyde may have a more significant effect on the activity. In the acetaldehyde–phenol condensation with MIL-101/PTA the acetaldehyde uptake capacity PTA > MIL-101/PTA > MIL-101 correlated with the activity.[29] Therefore, the time-dependent liquid-phase adsorption of benzaldehyde from a heptane solution was measured with gas chromatography (Figure 5).

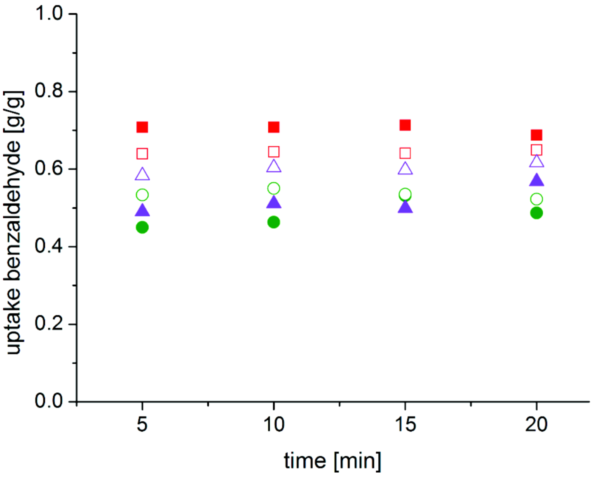

Figure 5. Benzaldehyde adsorption from heptane solution: (red squares) **1a**, (green circles) **2-NO$_2$-d**, and (purple triangles) **3-NH$_2$-ps**; filled symbols belong to 5 mg of MIL and the empty symbols to 10 mg of MIL sample. Uptake was calculated from the gas chromatogram peak area (initial benzaldehyde amount − benzaldehyde left after equilibration) per mass of MIL. *n*-Dodecane was used as internal standard. The molar ratio of benzaldehyde to Cr was 10:1 for 5 mg of MIL and 5:1 for 10 mg of MIL sample (see Supporting Information for experimental details).

The different MILs show an uptake of benzaldehyde between 0.45 (**2-NO$_2$-d**) and 0.71 g/g (**1a**). The benzaldehyde adsorption occurs within the first 5 min and does not change anymore over the next 15 min. The slight fluctuation over time in Figure 5 indicates the experimental error, so that small differences, e.g., between the 5 and 10 mg samples, should not be overinterpreted. The uptake in the general order **1a** > **3-NH$_2$-ps** > **2-NO$_2$-d** follows the trend in surface area (cf. Table 1).

Thus, the methanol and benzaldehyde adsorption studies do not provide evidence that the substrate adsorption has a decisive influence on the catalytic activity. In consequence, the high catalytic activity of **2-NO$_2$-d** compared to **1a** and **3-NH$_2$-ps** should be reasoned by electronic effects from the nitro group.

Lewis Acidity and Brønsted Acidity. The nature of the active sites in MIL-101Cr is still an open question here: Lewis-acid vacant Cr(III) sites or Brønsted-acid sites from polarized acidic aqua ligands (Cr–OH$_2$), perhaps enhanced by the acid treatment of MIL-101Cr upon modification?[15] Metal ions polarize and thereby increase the acidity of their aqua ligands. For $[Cr(H_2O)_6]^{3+}$,[36,49] $[CrBr(en)(H_2O)_3]^{2+}$,[50] $[Cr(en)(NH_3)(H_2O)_3]^{3+}$,[51] and some other Cr(III) aqua–amine complexes[52] the first dissociation constant is estimated at $pK_a \approx 4$. The first acid dissociation constants for $[Cr(III)(NH_3)_n(OH_2)_{6-n}]^{3+}$ lies between 4.4 and 5.3 depending on the number of aqua ligands, their cis, trans, fac, or mer orientation.[53] The acidity constant of *cis*-$[Cr(C_2O_4)_2(NCS)(H_2O)]^{2-}$ has been determined spectrophotometrically to $pK_a = 7.06 \pm 0.18$.[54] It has been shown that both Lewis and Brønsted acidity and thereby the catalytic activity of MIL-100Fe can be further enhanced via creation of additional active sites using a postsynthesis acid treatment.[15,55]

For the materials **1**–**3** we have to decide here if the activity of the benzaldehyde acetalization depends on the Lewis or Brønsted acidity of the vacant Cr or aqua-ligand Cr–OH$_2$ sites, respectively. Before reaction each catalyst was activated under identical conditions (drying under high vacuum of 10^{-6} Torr for 48 h at 30 °C unless stated otherwise) and stored in a glovebox under anhydrous and anaerobic conditions. Thus, we can assume that the number of dehydrated and hydrated chromium sites is very similar in **1**–**3**. Therefore, we suggest, so far, that the Lewis or Brønsted acidity of the Cr(–OH$_2$) sites gets stronger with an electron-withdrawing $-NO_2$ group on the linker and close to the metal site (see below).[19]

Lewis Acidity. Chemisorption of CD_3CN has been used to measure the number and strength of the Lewis-acid sites.[20] The C≡N stretching frequency is increased by about 40 cm^{-1} for CD_3CN chemisorbed at a Lewis-acid chromium site (Cr-$NCCD_3$) compared to physisorbed CD_3CN. For **1a** and the nitro-modified material **2-NO_2-d**, chemisorption of CD_3CN was investigated by infrared spectroscopy following sample activation as for catalysis (drying under high vacuum of 10^{-6} Torr for 48 h at 30 °C) (Figure 6, see Supporting Information for more details).

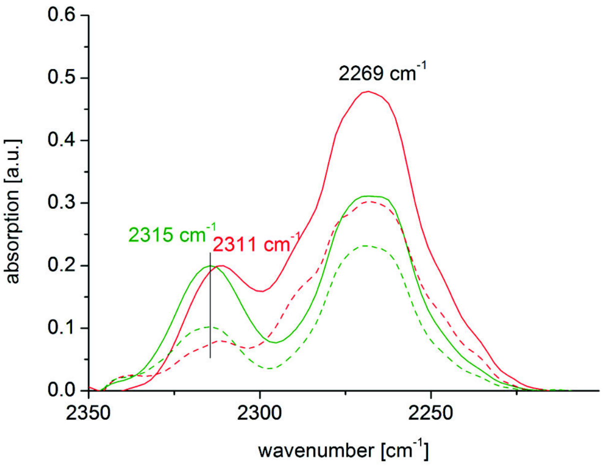

Figure 6. Time-dependent IR spectra for the CD_3CN chemisorption on **1a** (red) and **2-NO2-d** (green). Spectra start at 30 min after the beginning of CD_3CN exposure and are measured every 10 min up to 2 h: (dotted line) measured after 30 min, (solid line) measured after 2 h (bands at intermediate times are not shown for clarity).

Spectra show a time-dependent increase of adsorption both for physisorbed CD_3CN at 2269 cm^{-1} (overlaps with the band for free, gaseous CD_3CN) and for chemisorbed CD_3CN at 2311 and 2315 cm^{-1} for **1a** and **2-NO_2-d** respectively. For chemisorbed CD_3CN the CN stretching frequency was reported to be 2326–2321, 2304, 2305, and 2298 in MIL-100Al, Fe, Cr, and UiO-66, respectively.[20,44] The large hypsochromic frequency shift versus free CD_3CN for MIL-100Al is associated with the high Lewis-acid strength of Al^{3+}.[44] Assuming the same molar amount of Lewis-acid sites in **1a** and **2-NO_2-d**, normalization of the chemisorbed bands then shows a higher CD_3CN physisorption for **1a** due to its higher surface area (cf. Table 1). The slight hypsochromic shift of the signal of **2-NO_2-d** versus **1a** may signify stronger Lewis-acid properties for the nitro-modified material.[44] We note that coordination of CD_3CN like coordination of CO to the H atom of an aqua ligand[43] will also result in a hypsochromic shift with respect to free CD_3CN. Thus, the acetonitrile test showed the same amount (by absorption) and a very similar strength (by wavenumber) of Lewis-acid sites in **1a** and **2-NO_2-d**. Thereby, we conclude from the test that the catalytic difference cannot be explained by differences in Lewis acidity as these could not be verified.

Acetalization of aldehydes is a condensation reaction, generating water within each formula conversion. From adsorption studies of water on MOFs it is known that the metal centers are coordinated first by the water molecules.[8e] Thus, even if the catalyst exhibits coordinative unsaturated sites (CUS) at the beginning, in the course of the reaction they will be coordinated by the released water, thereby blocking initially active Lewis-acid sites.[43] Hence, for the most active catalyst **2-NO_2-d** the effect of wetting (wetness effect) was tested. For this experiment 10 mg of vacuum-dried **2-NO_2-d** was suspended in H_2O (5 mL) and stirred for 20 min at room temperature. The solid was separated by centrifugation, and the supernatant solution was removed. The powder was dried in air at room temperature for 48 h. After this drying period the material **2-NO_2-d-wet** still contained about 48 wt % water, determined by thermogravimetry (see Figure S16, Supporting Information), and was employed as a catalyst under otherwise identical reaction conditions (Figure 7).

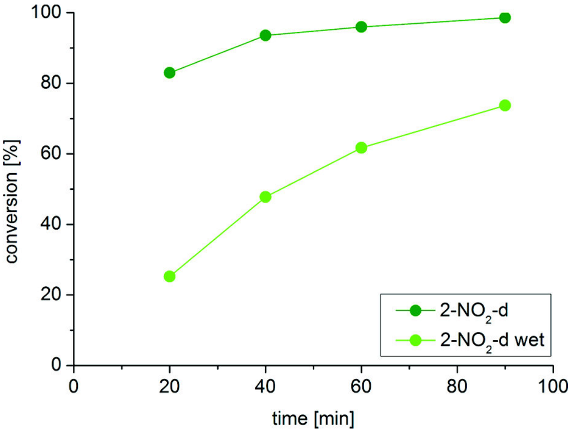

Figure 7. Activity of **2-NO_2-d** after an additional wetting with water.

After wetting, **2-NO_2-d-wet** shows reduced catalytic activity, especially at the beginning of the reaction, but reaches 74% conversion after 90 min, which still puts **2-NO_2-d-wet** among the high active materials (cf. Table 2). The loss in activity can be ascribed to the initial pore filling with water and, in part, to the adverse effect of water in the equilibrium formation of the product.[56] However, from the still high activity of this water-filled MOF it becomes quite clear that vacant Lewis-acid chromium sites are not needed for catalytic activity.

When the B–M reaction was carried out with the corresponding amount of chromium(III) nitrate nonahydrate as a catalyst under otherwise identical but homogeneous conditions even faster reaction rates and higher conversions were observed (see also Figure 13 below and Figure S9, Supporting Information). Hexaaquachromium(III) is very inert to ligand substitution with a rate constant for the water exchange in $[Cr(H_2O)_6]^{3+}$ of 2.4 × 10^{-6} s^{-1} (at 298.15 K).[36]

These last two observations lend strong support to the already indicated Brønsted-acid catalysis from deprotonation of the aqua ligands (see above) rather than Lewis-acid catalysis.

The high activity of $Cr(NO_3)_3{\cdot}9H_2O$ also excludes that the higher activity of dry versus wet **2-NO_2-d** (cf. Figure 7) is due to the known water uptake capacity of about 1 g H_2O/g MIL-101.[8i] The hydrated Cr(III) salt with the hexaaquachromium(III) cation lacks a significant water binding capacity.

Brønsted Acidity and pH. A Brønsted acid should be verifiable by its pH change to a solvent. Consequently, the pH value of catalysts **1a**, **2-NO_2-d**, and **3-NH_2-ps** were measured in methanol. The pH was assessed using two different procedures.

First, the pH was measured in slowly stirred suspensions of the dried MIL-101 powders in methanol. For the second procedure methanol was dropped onto MIL-coated KBr disks, and the pH of the wetted MIL surface was measured with a flat membrane electrode. Both methods show the same trend of pH value, that is, the pH is highest for **3-NH$_2$-ps** intermediate for **1a** and lowest for **2-NO$_2$-d** (Table 3). A higher concentration of MIL probes (10 mg of MIL in 6.7 mL of methanol versus 1 mg of MIL in 4 mL of methanol) approached the pH of the surface measurement of the MIL-coated KBr disk. Noteworthy, the pH values were only lowered in the near vicinity of the MIL particles. This explains the lower pH of the more concentrated suspension and of the wetted MIL-KBr coating. The pH values immediately rose for the supernatant MeOH solvent upon sedimentation of the particles when stirring was stopped. The suspensions were also filtered through a syringe filter and afterward centrifuged at 22 000 rpm for 40 min. By DLS it could be shown that the MIL material was completely removed. For the filtrates a much higher pH value was measured than with MIL sample, which shows clearly that the acidity originates from the MIL framework. Protons dissociating from the aqua ligands (Cr−OH$_2$) will leave a negatively charged hydroxyl group (Cr−OH$^-$). Thus, the insoluble framework will be the counteranion of the proton. By the electroneutrality principle the proton has to stay near the anionic framework. Hence, the Brønsted acidity of the MIL-101 compounds is a surface effect. At least in methanol it was verified that the acidity did not leach much into the surrounding liquid (see Supporting Information for pH measurements of the MIL materials in water). In methanol the variation in Brønsted acidity of **3-NH$_2$-ps** <**1a** < **2-NO$_2$-d** follows the electron-donating effect of NH$_2$ and the electron-withdrawing effect of NO$_2$.

Table 3. pH Values of the MIL-101 Materials and Cr(NO$_3$)$_3$ 9H$_2$O in Methanol[a]

	pH value	
material	methanol suspension	KBr disk coated with material
methanol	7.6	
KBr, not coated		6.6
1a	3.9,[b] 5.9[c]	3.0
2-NO$_2$-d	2.6,[b] 5.3[c]	1.9
3-NH$_2$-ps	–,[b] 6.6[c]	3.3
filtrate from **1a**[d]	6.2	
filtrate from **2-NO$_2$-d**[d]	6.3	
Cr(NO$_3$)$_3$ 9H$_2$O[e]	1.4	

[a] See Supporting Information for more details. [b] A 10 mg amount of MIL in 6.7 mL of MeOH. [c] A 1 mg amount of MIL in 4 mL of MeOH. [d] Fitrate of a suspension of 10 mg of MIL sample in 6.7 mL of MeOH (0.2 μm syringe filter, centrifuged at 22 000 rpm for 40 min). [e] A 12 mg amount in 6.7 mL of MeOH.

Also, chromium nitrate nonahydrate in methanol yields a very acidic solution (Table 3) such that its high catalytic activity (see below) is due to the large proton concentration of the solution.

Brønsted acidity arising from coordinated hydroxyl groups, belonging to the framework, or water molecules was investigated by infrared spectroscopic studies of interaction of CO with monomeric or multimeric water species in the case of MIL-100Al.[44] pH measurements of the MIL-101 probes support the assumption that the high activity of, especially, **2-NO$_2$-d** orginates from the Brønsted-acid nature of the catalysts.

Filtration Tests. The MIL materials in this study were introduced as heterogeneous catalysts. In order to prove that no leaching occurs, the materials were tested in filtration experiments. After approximately 50% conversion the catalyst was separated by centrifugation at 6000 rpm and subsequent filtration from the reaction mixture using a 0.2 μm (200 nm) syringe filter. The possible increase in conversion was continued to be monitored on the visually clear solution by GC. For the solution from MIL **2-NO$_2$-d** the reaction did indeed continue with only a slightly lower conversion rate than for the nonfiltered reaction (Figure 8a). In contrast, for **1a** and **1b** the catalytic reaction came to a stop after filtration of the solid MIL compound (**1c** was not tested due to the low conversion rate). Reaction with **2-NO$_2$-ps** showed only a slight increase of 7% conversion after filtration (Figure S8, Supporting Information). Additionally, the B−M acetalization reaction was performed without MIL catalysts but under otherwise identical conditions. No conversion was observed for the first 3 h. After 24 h reaction time 26% 1,1-dimethoxytoluene had formed

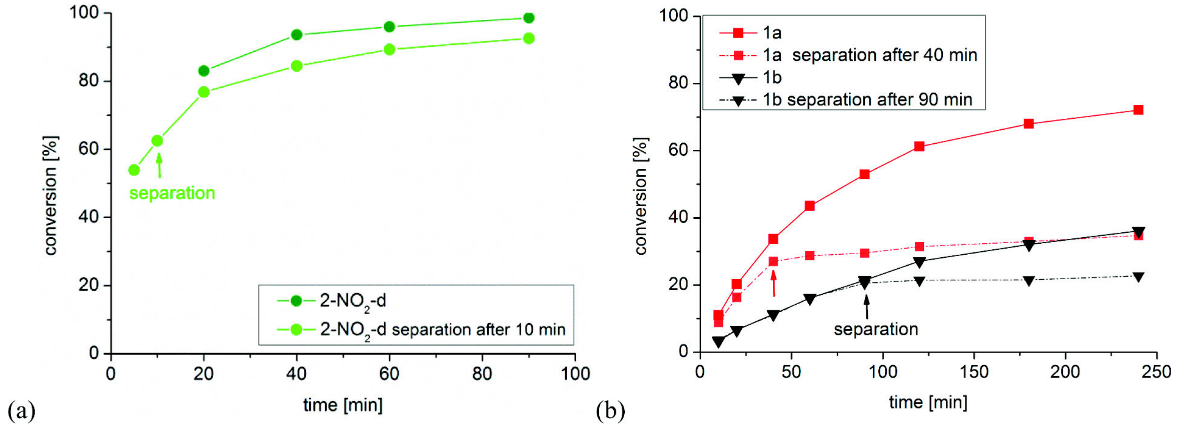

Figure 8. (a) Time conversion plot for **2-NO$_2$-d** and **2-NO$_2$-d** with attempted separation (6000 rpm centrifugation plus 0.2 μm filtration) of the catalyst completed after 5 min. (b) Time conversion plot for **1a** and **1b**; separation of **1a** completed after 40 min and of **1b** completed after 90 min (marked by arrows).

(Figure S7, Supporting Information). This observation is consistent with previous studies.[29,41]

Two explanations are possible. On one hand, some leaching of Cr(III) species could have occurred. In a comparative test experiment with 4.2 × 10^{-5} mol of $Cr(NO_3)_3$, which corresponds to the amount of chromium(III) in 10 mg of MIL, a conversion of 94% was measured after 20 min (Figure S9, Supporting Information). As a consequence, soluble Cr(III) species have a high catalytic activity for acetalization of benzaldehyde. On the other hand, it is also comprehensible that some of the MIL particles are smaller than the 200 nm (0.2 μm) pore size of the syringe filter. Such nano-MOFs could form a clear colloidal solution and further act as catalyst system. DLS measurements have shown that the particle diameter distribution is quite broad (Table 1, Figure S10 and S11, Supporting Information). SEM pictures show that the particles of **2-NO_2-d** are smaller than **1a** (Figure 9).

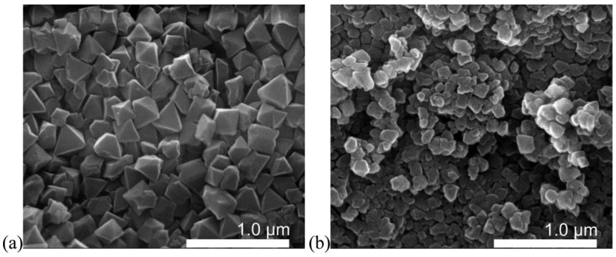

Figure 9. SEM pictures of (a) **1a** and (b) **2-NO_2-d**.

As a consequence, the filtrates of the reaction solutions were checked by DLS, TEM, and atomic absorption spectroscopy (AAS) for their particle and chromium content (Table 4, Figure 10). It is evident that the functionalized MILs **2-NO_2-d, -ps,** and **3-NH_2-ps** give rise to smaller particles which can pass through 200 nm filters.

Table 4. DLS and AAS Results of Filtrates

materials	time of filtration (min)[a]	DLS particle diameter ± standard deviation (σ) (nm) in filtrate[b]	AAS Cr(III) concentration (mg/L) in filtrate[c]
1a	90	n.d.	n.d.
1b	90	n.d.	n.d.
1c	90	n.d.	n.d.
2-NO_2-d	5	245 ± 117[c]	Cr detected, ~0.003
2-NO_2-d	90	131 ± 52[c]	0.04
2-NO_2-d	90 in 5th run	187 ± 66[c]	0.02
2-NO_2-ps	90	161 ± 57[c]	0.005
3-NH_2-ps	90	171 ± 54[c]	0.02

[a] From MeOH/benzaldehyde dispersion at 25 °C, filtered with a 0.2 μm (200 nm) syringe filter. [b] See Figure S13, Supporting Information. [c] n.d. = not detected; the detection limit for AAS is 0.003 mg/L.

By AAS, chromium could only be detected in the filtrates of **2-NO_2-d**, **2-NO_2-ps**, and **3-NH_2-ps** but not in **1a**–**c**, which explains why the reaction went on after filtration for these catalysts. The results of TEM and DLS clearly show MOF particles smaller than 200 nm. Besides, the presence of nanoparticles could be shown by the Tyndall effect (Figure 10c). Together with the DLS and AAS data, it is reasonable that nano-MOF particles are responsible for the ongoing reaction. Still, the above centrifugation and filtration experiments cannot fully exclude the possibility of leaching.

Therefore, if only nano-MOFs are indeed responsible for the continued conversion after filtration, it should be possible to separate the nano-MOF particles using an ultracentrifuge with a higher speed of rotation. Reaction of **2-NO_2-d** with methanol and benzaldehyde was run for 1 min to 12% conversion. Then the solution was carefully filtered with a syringe filter as before and additionally centrifuged at 24 000 rpm for 5 min. This procedure lasted 19 min, during which solid **2-NO_2-d** was still in contact with the reaction mixture so that the catalytic reaction could continue. Separation was complete after a total of 20 min. After this 20 min the conversion was monitored on the clear solution in a new vial by GC (Figure 11a). The reaction between MeOH and benzaldehyde came to a stop after removal of solid **2-NO_2-d** through ultracentrifugation. Therefore, we can rule out any leaching of soluble Cr(III) species. This result is supported by DLS measurements of the filtrate after ultracentrifugation, where no particles could be detected anymore.

In order to assess the activity of the **2-NO_2-d** nano-MOF particles, the following experiment was carried out: first, methanol (6.7 mL) was added to **2-NO_2-d** (10 mg), and the resulting suspension was stirred for 10 min. Then the suspension was filtered with the 0.2 μm syringe filter, and benzaldehyde (3.3 mmol) was added to the clear filtrate solution. The catalytic reaction was monitored as before under standard conditions. DLS measurements showed the nano-MOF particles in solution (Figure S14, Supporting Information). The amount of nano-MOF was determined from the filtrate after filtration with the 0.2 μm syringe filter. This filtrate was centrifugated at 24 000 rpm, and the residual solid was weighed to much less than 1 mg. The activity of **2-NO_2-d** after separation of the larger particles (cf. Figure 9) can be compared with the activity of the **2-NO_2-d** nanoparticles alone (Figure 11b). After separation of the larger particles conversion with the remaining nano-MOF particles increased from 63% to 93% over the next 80 min. The amount of less than 1 mg of **2-NO_2-d** nano-MOF alone enables a conversion of 68% in 90 min (Figure 11b). Thus, the small amount of nano-MOFs is much more active than the larger MIL particles.

In conclusion, a much lower sample amount of **2-NO_2-d** (less than 1 mg) can catalyze the acetalization reaction to about 60% conversion after 90 min (Figure 11b), which is nearly the same conversion as achieved for 10 mg of **1a**. This observation can be transferred to the small particle size in **3-NH_2-ps**, which leads to a slightly increased activity despite the lower Brønsted acidity compared to **1a** (Tables 2 and 3).

Recycling/Multiple Run Experiments. The possibility of catalyst recycling was tested for **1a** and **2-NO_2-d** over 5 runs. Catalyst runs were carried out for 90 min each for **1a** and **2-NO_2-d**. For less active **1a** the runs were also extended over 15 h each to achieve nearly quantitative conversion. After the first and fifth runs a PXRD spectrum was recorded to check for catalyst stability (Figure 12).

Catalysts **1a** and **2-NO_2-d** have a relatively stable catalytic activity over 5 runs of 15 h and 90 min, respectivly (Figure 12a). For **1a** the catalytic conversion drops from 73% to 50% for the 90 min runs. After the runs the materials were analyzed for their porosity and crystallinity. The results of the BET surface areas after five runs (90 min each) are for **1a** 3100 m^2/g and for **2-NO_2-d** 2421 m^2/g, (Table 1, Figure S2, Supporting Information), so that the materials retain their initial porosity.

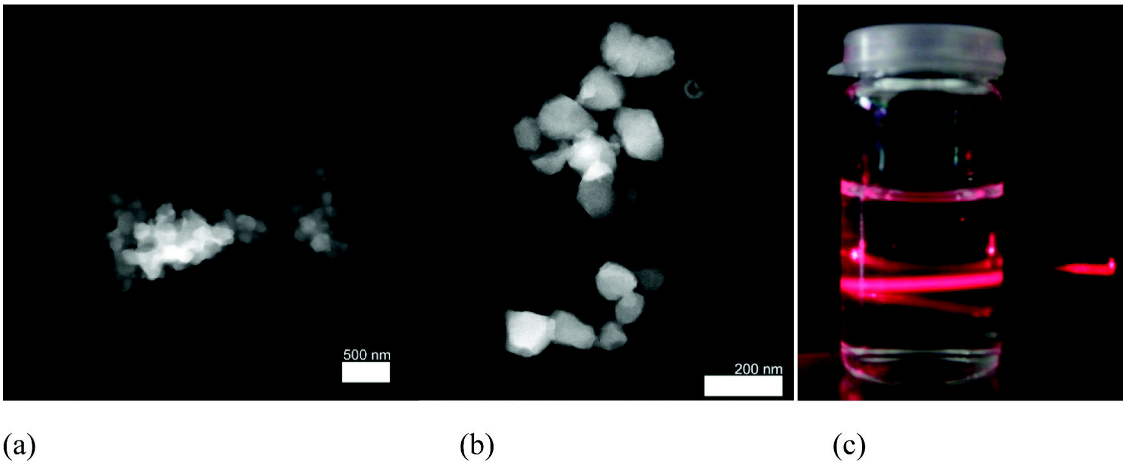

Figure 10. TEM image of the filtrate of **2-NO$_2$-d** filtered with a 0.2 μm (200 nm) syringe filter after (a) 5 and (b) 10 min. (c) Filtered solution of **2-NO$_2$-d** showing the Tyndall effect upon 650 nm laser irradiation.

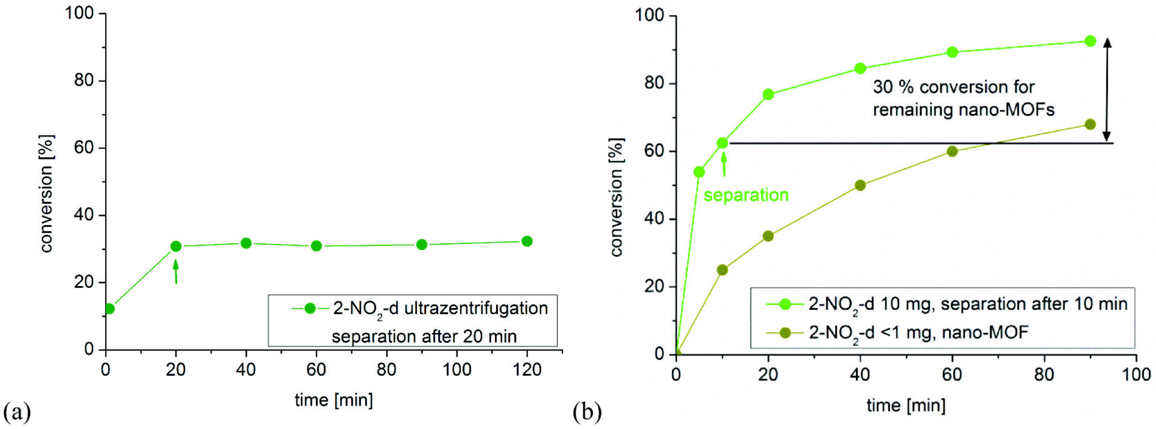

Figure 11. Time conversion plot for (a) **2-NO$_2$-d** after separation (0.2 μm filtration and 24 000 rpm centrifugation) completed after 20 min and (b) **2-NO$_2$-d** with attempted separation (6000 rpm centrifugation plus 0.2 μm filtration) of the catalyst completed after 5 min (cf. Figure 9a) and **2-NO$_2$-d** nano-MOF.

At the same time, the PXRD analysis shows some deterioration of the microcrystallinity and possibly a phase change for **1a** after the five 15 h runs and substantial crystal deterioration and phase change for **2-NO$_2$-d** after the five 90 min runs (Figure 12b). Yet, **1a** still retains its structure after the five 90 min runs; hence, the nonfunctionalized MOF **1a** is more stable than **2-NO$_2$-d** under the catalytic conditions. SEM pictures after 5 runs for **1a** and **2-NO$_2$-d** did not show any significant changes (Figure S15, Supporting Information).

Acetalization Reactivity of 2-NO$_2$-d with Other Alcohols. MOFs are discussed in terms of heterogeneous catalysts which can possess the selectivity properties of homogeneous catalysts.[20,57] The pores of the MOF are viewed as a "reactor", which can exert selectivity, e.g., by size exclusion effects.[41,58,59] If the reaction does indeed take place mainly inside the pores then the reaction rate should be influenced by the size and shape of the reagents. For larger substrates the diffusion of reagents and products through the pores and pore windows of the MOF material is expected to be slower, and in consequence, the catalyst activity should decrease. MIL-101Cr has pore sizes of 2.9 and 3.4 nm, which are accessible through cage windows of 1.2−1.6 nm (Figure S1, Supporting Information).[22] In order to investigate the effect of the size of the alcohol, the conversion rate with **2-NO$_2$-d** in the benzaldehyde acetalization reaction is compared in Figure 13a for methanol, ethanol, 1-propanol, 1-butanol, and 1-pentanol.

A decrease of conversion rate with increasing chain length of the homologous *n*-alcohol series can be observed. These results support our expectation and are in agreement with the studies of García and co-workers, who investigated the catalytic activity of $Cu_3(BTC)_2$ in the acetalization of benzaldehyde. Hence, the decrease of conversion rate with increasing alcohol chain length can be ascribed mostly to steric hindrances for substrate diffusion in the pore system.[41] Taking into account that the cage windows of MIL-101Cr with 1.2 and 1.6 nm are bigger compared than the ones of $Cu_2(BTC)_3$ (0.8 nm),[41] this is another important factor for the higher catalyst activity of MIL-101Cr.

Still, even under homogeneous conditions in the absence of steric hindrance on the catalyst center, a longer chain alcohol would be expected to react more slowly. Therefore, the benzaldehyde acetalization reactions were run under homogeneous but otherwise identical conditions with $Cr(NO_3)_3{\cdot}9H_2O$ as catalyst, with the equivalent molar amount of chromium to 10 mg of MIL-101Cr (Figure 13b). After 90 min conversion for all alcohols except pentanol is higher than 82%. A slight

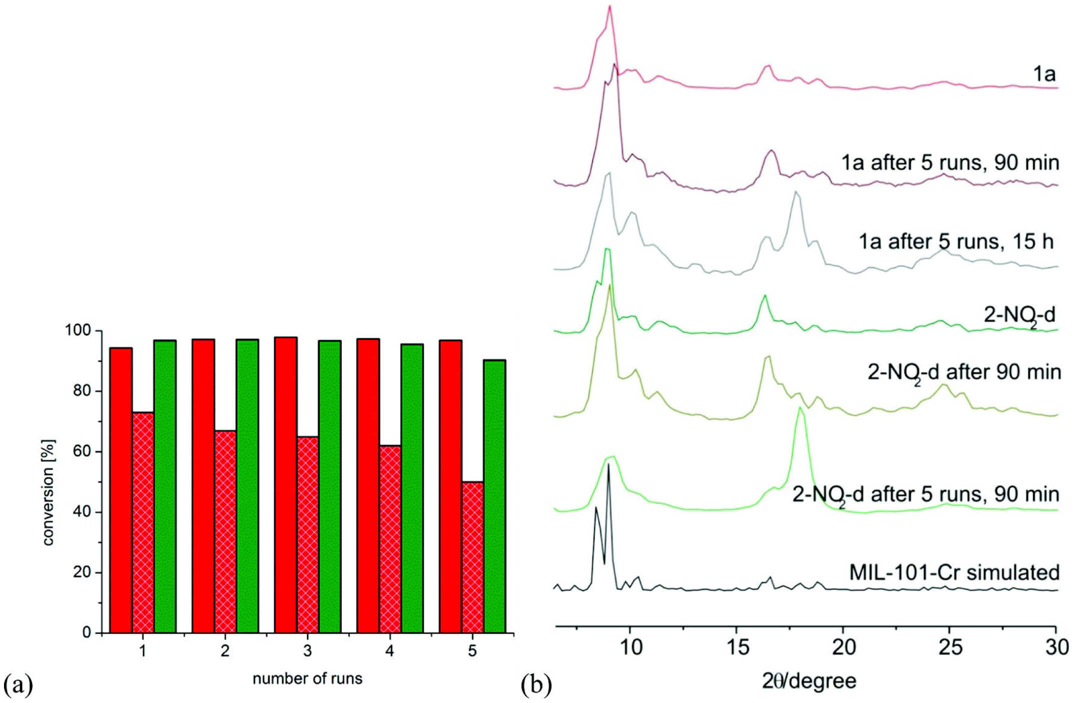

Figure 12. (a) Conversions in catalyst recycling experiments for **1a** (red, each run 15 h; red squared, each run 90 min) and **2-NO_2-d** (green bars). (b) XRD spectra of **1a** and **2-NO_2-d** before and after the catalytic runs.

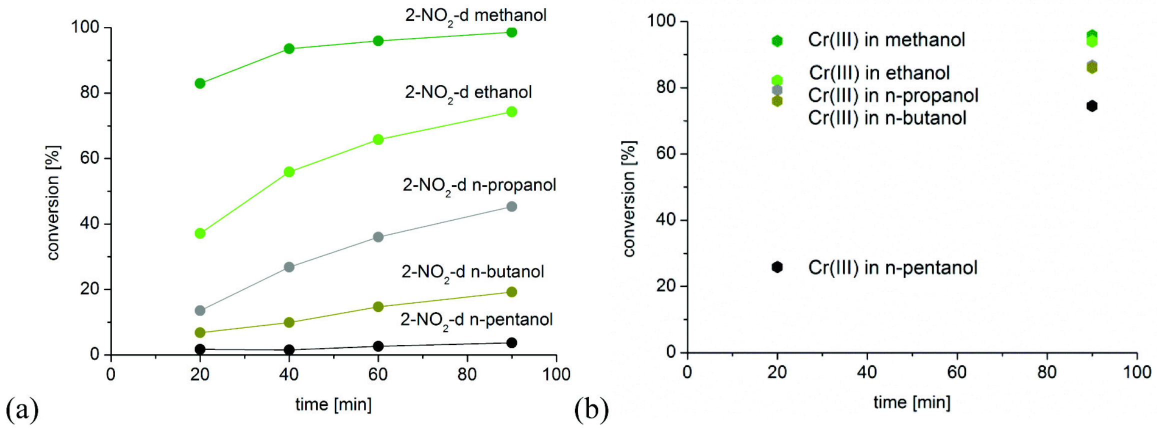

Figure 13. (a) Catalysis of **2-NO_2-d** or (b) chromium(III) nitrate nonahydrate with benzaldehyde in methanol, ethanol, *n*-propanol, *n*-butanol, and *n*-pentanol.

decrease of conversion is seen with increasing alcohol chain length. Yet, even *n*-pentanol gives 75% conversion after 90 min with $Cr(NO_3)_3{\cdot}9H_2O$, compared to only 4% with **2-NO_2-d** (Table S2, Supporting Information). The strong decrease of conversion rate with increasing chain length of the alcohol for **2-NO_2-d** supports the assumption that catalysis occurs mainly inside the pores of the MIL material.

Similarly, different aldehydes were tested under the same standard conditions with **2-NO_2-d** and $Cr(NO_3)_3{\cdot}9H_2O$ as catalyst (Figure 14, Table 5). All benzaldehyde derivatives and cyclohexanone show high and rapid conversion under heterogeneous and homogeneous conditions. Under heterogeneous conditions *p*-chlorobenzaldehyde reacts slower but also reaches over 90% conversion after 90 min. For cyclohexanone the conversion is fast and reaches the final value already after 20 min, where it remains unchanged to 90 min under both hetero- and homogeneous conditions. Noteworthy, conversion of cyclohexanone is higher with **2-NO_2-d** (90%) than with $Cr(NO_3)_3{\cdot}9H_2O$ (84%) as catalyst (Figure 14). Significant is the very low conversion for cyclohexylmethylketone, which is faster with the MIL than in homogeneous solution (Figure 14). The +I effect of the ketone leads to a reduced rate for the attack on the carboxyl carbon atom. It is reported that also for acetophenone and benzophenone no acetalization occurs.[32] Perhaps the higher and faster conversion of the aliphatic ketones cyclohexanone and cyclohexylmethylketone with **2-NO_2-d** compared to $Cr(NO_3)_3{\cdot}9H_2O$ are evidence for a water binding effect of the MIL network.

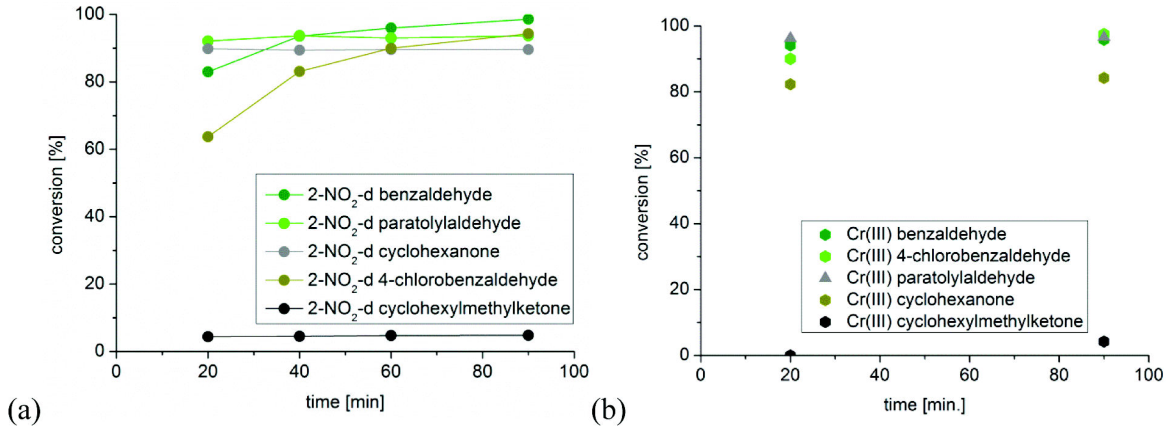

Figure 14. (a) Catalysis of **2-NO$_2$-d** or (b) chromium(III) nitrate nonahydrate with methanol and different aldehydes or ketones.

Table 5. Reaction of Different Aldehydes and Ketones in Methanol with 2-NO$_2$-d as Catalyst[a]

Entry	Reagent	Product	Time (min)	Conversion (%)	TON	TOF [h^{-1}]	Conversion (%)[b]
1	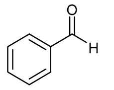	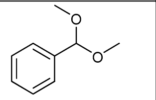	90	99	114	76	96
2	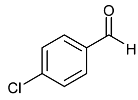	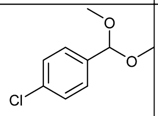	90	94	108	72	98
3	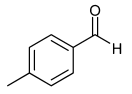	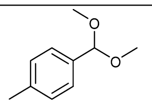	90	94	108	72	97
4	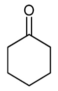	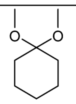	90	90	83	55	84
5	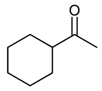	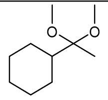	90	5	6	4	4

[a] Standard reaction conditions: aldehyde (3.3 mmol), methanol (166 mmol), catalyst (10 mg); every reaction was performed at least in a duplicate. [b] Conversion after 90 min is stated; 4.2 × 10^{-5} mol $Cr(NO_3)_3 \cdot 9H_2O$ was used under otherwise identical conditions.

In comparison with other catalysts, the material **2-NO$_2$-d** displays excellent activity, surpasses other MOFs, and can compete with the homogeneous catalyst $TiCl_4$ (Table 6).

Compared with the results for $Cu_3(BTC)_2$[41] and MIL-100Fe, MIL-101Cr-NO$_2$ (**2-NO$_2$-d**) shows a significantly higher catalytic activity for acetalization of benzaldehyde as well as for other aldehydes and alcohols (not shown in Table 6). In particular, for reaction of *p*-tolylaldehyde with methanol **2-NO$_2$-d** shows 94% conversion after 90 min, which is a significant improvement compared to $Cu_3(BTC)_2$ (ca. 30% after 24 h). These results could be obtained in a shorter time with a much lower catalyst loading and a higher amount of aldehyde (3.3 vs 1 mmol).

■ CONCLUSIONS

In the diacetalization of aldehydes and ketones with alcohols the high surface area of MIL-101Cr materials is not the decisive factor for high catalytic activity. Introduction of a nitro, $-NO_2$, group to the terephthalate ligand of MIL-101-Cr enhanced the catalytic activity significantly, although the BET surface area of the nitro modification **2-NO$_2$-d** is lower than that of the nonfunctionalized materials, e.g., **1a**. Compound **2-NO$_2$-d** is an efficient and a reusable heterogeneous solid catalyst for formation of dimethyl acetals. A possible stronger Lewis acidity through nitro modification is not the primary reason for the excellent activity of **2-NO$_2$-d**. Instead, pH measurements show that the activity can be explained by Brønsted-acid catalysis from deprotonation of the polarized aqua ligands, which is

Table 6. Comparison of Different Catalysts for Acetalization of Benzaldehyde in Methanol (B−M reaction)

catalyst	amount of catalyst (mg/mmol metal)[a]	molar ratio benzaldehyde:methanol	temperature (°C)	time (h)	conversion (%)	TOF (h^{-1})[b]	ref
MIL-101/PTA_{imp}	10/0.001 PTA + 0.043 mmol Cr(III)	3.3:166	25	24	93	2.9	29
PTA (phospho-tungstic acid)	0.003[c]	3.3:166	25	24	93	43	29
$Cu_3(BTC)_2$ (HKUST-1, Basolite C300)	50/0.25	1:74	rt	2; 24	63; 88	1.2; 0.2	41
Fe(BTC) (Basolite F300)	50/0.19	1:74	rt	2; 24	49; 71	1.3; 0.2	41
$Al_2(BDC)_3$ (MIL-53Al, Basolite A100)	50/0.24	1:74	rt	24	66	0.12	41
MIL-100Fe	10/0.046	3.0:123	40	5; 21	79:84	10.3; 2.6	57
MIL-101Cr-NO_2, **2-NO_2-d**	10/0.043	3.3:166	rt	1.5	99	50.7	this work
MIL-101Cr-NO_2, **2-NO_2-d**	10/0.043	3.3:166	rt	0.7	94	103	this work
MIL-101-NO_2, **2-NO_2-d** nano-MOF	1/0.0043	3.3:166	rt	1.5	68	348	this work
$TiCl_4/NH_3$	1 mol %/ 0.05 mmol	5.0:246	0	0.5	98	196	33

[a] The milligram amount refers to the total mass of catalyst used; the $mmol_{metal}$ amount refers to the total molar amount of metal in the catalyst mass. No corrections for coordinative unsaturated sites were made. [b] TOF = $mol_{product}/(mol_{metal} \cdot time)$. [c] Total amount PTA in solution (6.7 mL methanol)

strongly enhanced for **2-NO_2-d**. In addition it could be shown that very small amounts of nanoscale MIL particles of **2-NO_2-d** (<200 nm) result already in a high conversion compared with the bulk material. The effect of particle size then increases the activity of the amino modification **3-NH_2-ps** over the nonfunctionalized material **1a** despite a slightly lower Brønsted acidity of the former. By comparing a series of longer chained alcohols with homogeneous $Cr(NO_3)_3$ catalyst it could be shown that catalysis takes place inside the pores of the MIL materials. Therefore, MIL-101Cr and possibly other MILs can be active heterogeneous Brønsted-acid catalysts whose activity can be enhanced by electron-withdrawing linker modifications and small particle size.

■ ASSOCIATED CONTENT

Ⓢ Supporting Information

Synthesis and catalytic procedure details, N_2 sorption isotherms, powder X-ray diffractograms, IR spectra, additional catalytic data, DLS measurements, SEM images, thermogravimetic analysis. This material is available free of charge via the Internet at http://pubs.acs.org.

■ AUTHOR INFORMATION

Corresponding Author

*E-mail: janiak@uni-duesseldorf.de.

Notes

The authors declare no competing financial interest.

■ ACKNOWLEDGMENTS

Our work was supported by the Deutsche Forschungsgemeinschaft (DFG grant Ja466/25-1) and the University of Düsseldorf. We thank Mr. Hajo Meyer for providing the TEM images.

■ DEDICATION

Dedicated to Prof. Christel Marian on the occasion of her 60th birthday.

■ REFERENCES

(1) (a) Collins, D. J.; Zhou, H.-C. *J. Mater. Chem.* **2007**, *17*, 3154−3160. (b) Dincă, M.; Long, J. R. *Angew. Chem., Int. Ed.* **2008**, *47*, 6766−6779. (c) Lin, X.; Jia, J.; Hubberstey, P.; Schröder, M.; Champness, N. R. *CrystEngComm* **2007**, *9*, 438−448. (d) Ma, S.; Zhou, H.-C. *Chem. Commun.* **2010**, *46*, 44−53. (e) Morris, R. E.; Wheatley, P. S. *Angew. Chem., Int. Ed.* **2008**, *47*, 4966−4981. (f) Murray, L. J.; Dincă, M.; Long, J. R. *Chem. Soc. Rev.* **2009**, *38*, 1294−1314. (g) Suh, M. P.; Park, H. J.; Prasad, T. K.; Lim, D.-W. *Chem. Rev.* **2012**, *112*, 782−835. (h) Getman, R. B.; Bae, Y.-S.; Wilmer, C. E.; Snurr, R. Q. *Chem. Rev.* **2012**, *112*, 703−723.

(2) (a) Tanh Jeazet, H. B.; Staudt, C.; Janiak, C. *Dalton Trans.* **2012**, *41*, 14003−14027. (b) Hunger, K.; Schmeling, N.; Tanh Jeazet, H. B.; Janiak, C.; Staudt, C.; Kleinermanns, K. *Membranes* **2012**, *2*, 727−763. (c) Tanh Jeazet, H. B.; Staudt, C.; Janiak, C. *Chem. Commun.* **2012**, *48*, 2140−2142. (d) Li, J.-R.; Sculley, J.; Zhou, H.-C. *Chem. Rev.* **2012**, *112*, 869−932. (e) Zhang, Z.; Zhao, Y.; Gong, Q.; Li, Z.; Li, J. *Chem. Commun.* **2013**, *49*, 653−661. (f) Férey, G.; Serre, C.; Devic, T.; Maurin, G.; Jobic, H.; Llewellyn, P. L.; De Weireld, G.; Vimont, A.; Daturi, M.; Chang, J. S. *Chem. Soc. Rev.* **2011**, *40*, 550−562. (g) Zornoza, B.; Tellez, C.; Coronas, J.; Gascon, J.; Kapteijn, F. *Microporous Mesoporous Mater.* **2013**, *166*, 67−78. (h) Dong, G. X.; Li, H. Y.; Chen, V. K. *J. Mater. Chem. A* **2013**, *1*, 4610−4630.

(3) (a) Kreno, L. E.; Leong, K.; Farha, O. K.; Allendorf, M.; Van Duyne, R. P.; Hupp, J. T. *Chem. Rev.* **2012**, *112*, 1105−1125. (b) Janiak, C.; Vieth, J. K. *New J. Chem.* **2010**, *34*, 2366−2388.

(4) (a) Horcajada, P.; Chalati, T.; Serre, C.; Gillet, B.; Sebrie, C.; Baati, T.; Eubank, J. F.; Heurtaux, D.; Clayette, P.; Kreuz, C.; Chang, J.-S.; Hwang, Y. K.; Marsaud, V.; Bories, P.−N.; Cynober, L.; Gil, S.; Férey, G.; Couvreur, P.; Gref, R. *Nat. Mater.* **2010**, *9*, 172−178. (b) Horcajada, P.; Gref, R.; Baati, T.; Allan, P. K.; Maurin, G.; Couvreur, P.; Férey, G.; Morris, R. E.; Serre, C. *Chem. Rev.* **2012**, *112*, 1232−1268. (c) Keskin, S.; Kızılel, S. *Ind. Eng. Chem. Res.* **2011**, *50*, 1799−1812.

(5) (a) Allendorf, M. D.; Bauer, C. A.; Bhakta, R. K.; Houk, R. J. T. *Chem. Soc. Rev.* **2009**, *38*, 1330−1352. (b) Cui, Y.; Yue, Y.; Qian, G.; Chen, B. *Chem. Rev.* **2012**, *112*, 1126−1162.

(6) (a) Kepert, C. J. *Chem. Commun.* **2006**, *21*, 695−700. (b) Kurmoo, M. *Chem. Soc. Rev.* **2009**, *38*, 1353−1379. (c) Maspoch, D.; Ruiz-Molina, D.; Veciana, J. *J. Mater. Chem.* **2004**, *14*, 2713−2723.

(7) (a) Farrusseng, D.; Aguado, S.; Pinel, C. *Angew. Chem., Int. Ed.* **2009**, *48*, 7502−7513. (b) Lee, J. Y.; Farha, O. K.; Roberts, J.; Scheidt, K. A.; Nguyen, S. T.; Hupp, J. T. *Chem. Soc. Rev.* **2009**, *38*, 1450−1459. (c) Ranocchiari, M.; van Bokhoven, J. A. *Phys. Chem. Chem. Phys.* **2011**, *13*, 6388−6396. (d) Dhakshinamoorthy, A.; Alvaro, M.; Garcia, H. *Chem. Commun.* **2012**, *48*, 11275−11288. (e) Dhakshinamoorthy, A.; Opanasenko, M.; Čejka, J.; Garcia, H. *Adv. Synth. Catal.* **2013**, *355*, 247−268.

(8) (a) Henninger, S. K.; Jeremias, F.; Kummer, H.; Janiak, C. *Eur. J. Inorg. Chem.* **2012**, 2625−2634. (b) Akiyama, G.; Matsuda, R.; Sato, H.; Hori, A.; Takata, M.; Kitagawa, S. *Microporous Mesoporous Mater.* **2012**, *157*, 89−93. (c) Akiyama, G.; Matsuda, R.; Kitagawa, S. *Chem. Lett.* **2010**, *39*, 360−361. (d) Jeremias, F.; Khutia, A.; Henninger, S. K.; Janiak, C. *J. Mater. Chem.* **2012**, *22*, 10148−10151. (e) Küsgens, P.; Rose, M.; Senkovska, I.; Fröde, H.; Henschel, A.; Siegle, S.; Kaskel, S. *Microporous Mesoporous Mater.* **2009**, *120*, 325−330. (f) Ehrenmann, J.; Henninger, S. K.; Janiak, C. *Eur. J. Inorg. Chem.* **2011**, 471−474. (g) Seo, Y.-K.; Yoon, J. W.; Lee, J. S.; Hwang, Y. K.; Jun, C.-H.; Chang, J.-S.; Wuttke, S.; Bazin, P.; Vimont, A.; Daturi, M.; Bourrelly, S.; Llewellyn, P. L.; Horcajada, P.; Serre, C.; Férey, G. *Adv. Mater.* **2012**, *24*, 806−810. (h) Henninger, S. K.; Habib, H. A.; Janiak, C. *J. Am. Chem. Soc.* **2009**, *131*, 2776−2777. (i) Khutia, A.; Urs Rammelberg, H.; Schmidt, T.; Henninger, S.; Janiak, C. *Chem. Mater.* **2013**, *25*, 790−798. (j) Jeremias, F.; Lozan, V.; Henninger, S.; Janiak, C. *Dalton Trans.* **2013**, *42*, 15967−15973.

(9) (a) Moon, H. R.; Kim, J. H.; Paik Suh, M. *Angew. Chem., Int. Ed.* **2005**, *44*, 1261−1265. (b) Hermes, S.; Schröder, M.-K.; Schmid, R.; Knodeir, L.; Muhler, M.; Tissler, A.; Fischer, R. W.; Fischer, R. A. *Angew. Chem., Int. Ed.* **2005**, *44*, 6237−62411261. (c) Sabo, M.; Henschel, A.; Froede, H.; Klemm, E.; Kaskel, S. *J. Mater. Chem.* **2007**, *17*, 3827−3832. (d) Müller, M.; Hermes, S.; Kähler, K.; Van den Berg, M. W. E.; Muhler, M.; Fischer, R. A. *Chem. Mater.* **2008**, *20*, 4576−4587. (e) Dhakshinamoorthy, A.; Garcia, H. *Chem. Soc. Rev.* **2012**, *41*, 5262−5284.

(10) Stock, N.; Biswas, S. *Chem. Rev.* **2012**, *112*, 933−969.

(11) (a) Lee, J. Y.; Farha, O. K.; Roberts, J.; Scheidt, K. A.; Nguyena, S. T.; Hupp, J. T. *Chem. Soc. Rev.* **2009**, *38*, 1450−1459. (b) Phan, N. T. S.; Nguyen, T. T.; Ho, P.; Nguyen, K. D. *ChemCatChem* **2013**, *5*, 1822−1831. (c) Huang, Y.; Liu, T.; Lin, J.; Lü, J.; Lin, Z.; Cao, R. *Inorg. Chem.* **2011**, *50*, 2191−2198. (d) Horike, S.; Dincă, M.; Tamaki, K.; Long, J. R. *J. Am. Chem. Soc.* **2008**, *130*, 5854−5855.

(12) Dhakshinamoorthy, A.; Alvaro, M.; Corma, A.; Garcia, H. *Dalton Trans.* **2011**, *40*, 6344−6360.

(13) (a) Alaerts, L.; Seguin, E.; Poelman, H.; Thibault-Starzyk, F.; Jacobs, P. A.; De Vos, D. E. *Chem.—Eur. J.* **2006**, *12*, 7353−7363. (b) Gándara, F.; Gomez-Lor, B.; Gutiérrez-Puebla, E.; Iglesias, M.; Monge, M. A.; Proserpio, D. M.; Snejko, N. *Chem. Mater.* **2008**, *20*, 72−76.

(14) Schlichte, K.; Kratzke, T.; Kaskel, S. *Microporous Mesoporous Mater.* **2004**, *73*, 81−88.

(15) Valvekens, P.; Vermoortele, F.; De Vos, D. *Catal. Sci. Technol.* **2013**, *3*, 1435−1445.

(16) Van de, Voorde B.; Boulhout, M.; Vermoortele, F.; Horcajada, P.; Cunha, D.; Lee, J. S.; Chang, J.; Gibson, E.; Daturi, M.; Lavalley, J.; Vimont, A.; Beurroies, I.; De Vos, D. E. *J. Am. Chem. Soc.* **2013**, *135*, 9849−9856.

(17) Hwang, Y. K.; Hong, D.-Y.; Chang, J.-S.; Jhung, S. H.; Seo, Y.-K.; Kim, J.; Vimont, A.; Daturi, M.; Serre, C.; Férey, G. *Angew. Chem., Int. Ed.* **2008**, *47*, 4144−4148.

(18) Savonnet, M.; Ravon, U.; Aguado, S.; Bazer-Bachi, D.; Lecocq, V.; Bats, N.; Pinel, C.; Farrusseng, D. *Green Chem.* **2009**, *11*, 1729−1732.

(19) Gascon, J.; Aktay, U.; Hernandez-Alonso, M. D.; van Klink, G. P. M.; Kapteijn, F. *J. Catal.* **2009**, *261*, 75−87.

(20) Vermoortele, F.; Bueken, B.; Le Bars, G.; Van de Voorde, B.; Vandichel, M.; Houthoofd, K.; Vimont, A.; Daturi, M.; Waroquier, M.; Van Speybroeck, V.; Kirschhock, C.; De Vos, D. E. *J. Am. Chem. Soc.* **2013**, *135*, 11465−11468.

(21) Vermoortele, F.; Vandichel, M.; Van de Voorde, B.; Ameloot, R.; Waroquier, M.; Van Speybroeck, V.; De Vos, D. E. *Angew. Chem., Int. Ed.* **2012**, *51*, 4887−4890.

(22) Férey, G.; Mellot-Draznieks, C.; Serre, C.; Millange, F.; Dutour, J.; Surblé, S.; Margiolaki, I. *Science* **2005**, *309*, 2040−2042.

(23) Hong, D.-Y.; Hwang, Y. K.; Serre, C.; Férey, G.; Chang, J.-S. *Adv. Funct. Mater.* **2009**, *19*, 1537−1552.

(24) Hwang, Y. K.; Hong, J.-S.; Chang, D.-Y.; Seo, H.; Yoon, M.; Kim, J.; Jhung, S. H.; Serre, C.; Férey, G. *Appl. Catal. A: Gen.* **2009**, *358*, 249−253.

(25) (a) Granadeiro, C. M.; Barbosa, A. D. S.; Silva, P.; Almeida Paz, F. A.; Saini, V. K.; Pires, J.; de Castro, B.; Balula, S. S.; Cunha-Silva, L. *Appl. Catal. A: General* **2013**, *453*, 316−326. (b) Maksimchuk, N. V.; Kovalenko, K. A.; Arzumanov, S. S.; Chesalov, Y. A.; Melgunov, M. S.; Stepanov, A. G.; Fedin, V. P.; Kholdeeva, O. A. *Inorg. Chem.* **2010**, *49*, 2920−2930.

(26) Henschel, A.; Gedrich, K.; Kraehnert, R.; Kaskel, S. *Chem. Commun.* **2008**, 4192−4194.

(27) Hartmann, M.; Fischer, M. *Microporous Mesoporous Mater.* **2012**, *164*, 38−43.

(28) Wu, F.; Qiu, L.-G.; Ke, F.; Jiang, X. *Inorg. Chem. Commun.* **2013**, *32*, 5−8.

(29) Bromberg, L.; Hatton, T. A. *ACS Appl. Mater. Interfaces* **2011**, *3*, 4756−4764.

(30) Brückner, R. *Advanced Organic Chemistry: Reaction Mechanisms*; Harcourt/Academic Press: Burlington, MA, 2002; p 291.

(31) Miao, J.; Wan, H.; Shao, Y.; Guan, G.; Xu, B. *J. Mol. Catal. A: Chem.* **2011**, *348*, 77−82.

(32) Krompiec, S.; Penkala, M.; Szczubiałka, K.; Kowalska, E. *Coord. Chem. Rev.* **2012**, *256*, 2057−2095.

(33) Clerici, A.; Pastori, N.; Porta, O. *Tetrahedron* **1998**, *54*, 15679−15690.

(34) Jiang, Q.; Rüegger, H.; Venanzi, L. M. *Inorg. Chim. Acta* **1999**, *290*, 64−79.

(35) Vermoortele, F.; Ameloot, R.; Vimont, A.; Serre, C.; De Vos, D. *Chem. Commun.* **2011**, *47*, 1521−1523.

(36) Xu, F.-C.; Krouse, H. R.; Swaddle, T. W. *Inorg. Chem.* **1985**, *24*, 267−270.

(37) Corma, A.; Climent, M. J.; García, H.; Primo, J. *J. Appl. Catal.* **1990**, *59*, 333−340.

(38) Kamitori, Y.; Hojo, M.; Masuda, R.; Yoshida, T. *Tetrahedron Lett.* **1985**, *26*, 4767−4770.

(39) Climent, M. J.; Corma, A.; Iborra, S.; Navarro, M. C.; Primo, J. *J. Catal.* **1996**, *161*, 783−789.

(40) Tanaka, Y.; Sawamura, N.; Iwamoto, M. *Tetrahedron Lett.* **1998**, *39*, 9457−9460.

(41) Dhakshinamoorthy, A.; Alvaro, M.; García, H. *Adv. Synth. Catal.* **2010**, *352*, 3022−3030.

(42) Srirambalaji, R.; Hong, S.; Natarajan, R.; Yoon, M.; Hota, R.; Kim, Y.; Ko, Y. H.; Kim, K. *Chem. Commun.* **2012**, *48*, 11650−11652.

(43) Vimont, A.; Leclerc, H.; Mauge, F.; Daturi, M.; Lavalley, J.; Surble, S.; Serre, C.; Férey, G. *J. Phys. Chem. C* **2007**, *111*, 383−388.

(44) Volkringer, C.; Leclerc, H.; Lavalley, J.; Loiseau, T.; Férey, G.; Daturi, M.; Vimont, A. *J. Phys. Chem. C* **2012**, *116*, 5710−5719.

(45) Yang, J.; Zhao, Q.; Li, J.; Dong, J. *Microporous Mesoporous Mater.* **2010**, *130*, 174−179.

(46) Bernt, S.; Guillerm, V.; Serre, C.; Stock, N. *Chem. Commun.* **2011**, *47*, 2838−2840.

(47) Modrow, A.; Zargarani, D.; Herges, R.; Stock, N. *Dalton Trans.* **2012**, *41*, 8690−8696.

(48) (a) Cohen, S. M. *Chem. Rev.* **2012**, *112*, 970−1000. (b) Valtchev, V.; Majano, G.; Mintova, S.; Pérez-Ramírez, J. *Chem. Soc. Rev.* **2013**, *42*, 263−290.

(49) Emerson, K.; Graven, W. M. *J. Inorg. Nucl. Chem.* **1959**, *11*, 309−313.

(50) Hughes, R. G.; Garner, C. S. *Inorg. Chem.* **1968**, *7*, 1988−1993.

(51) Williams, T. J.; Garner, C. S. *Inorg. Chem.* **1969**, *8*, 1639−1645.

(52) Basolo, F.; Pearson, R. G. *Mechanisms of Inorganic Reactions*, 2nd ed.; John Wiley & Sons, Inc.: New York,1967; p 32.

(53) Andersen, P.; Døssing, A.; Glerup, J.; Rude, M. *Acta Chem. Scand.* **1990**, *44*, 346−352.

(54) Ashley, K. R.; Kulphrathipanja, S. *Inorg. Chem.* **1972**, *11*, 444−447.

(55) Vermoortele, F.; Ameloot, R.; Alaerts, L.; Matthessen, R.; Carlier, B.; Fernandez, E. V. R.; Gascon, J.; Kapteijn, F.; De Vos, D. E. *J. Mater. Chem.* **2012**, *22*, 10313−10321.

(56) Capeletti, M. R.; Balzano, L.; de la Puente, G.; Laborde, M.; Sedran, U. *Appl. Catal., A* **2000**, L1−L4.
(57) Dhakshinamoorthy, A.; Alvaro, M.; Horcajada, P.; Gibson, E.; Vishnuvarthan, M.; Vimont, A.; Greneche, J.; Serre, C.; Daturi, M.; García, H. *ACS Catal.* **2012**, *2*, 2060−2065.
(58) Luo, Q.; Ji, M.; Lu, M.; Hao, C.; Qiu, J.; Li, Y. *J. Mater. Chem. A* **2013**, *1*, 6530−6534.
(59) Hermannsdörfer, J.; Friedrich, M.; Kempe, R. *Chem.—Eur. J.* **2013**, *19*, 13652−13657.

Supporting Information

Brønsted instead of Lewis acidity in functionalized MIL-101Cr MOFs for efficient heterogeneous (nano-MOF) catalysis in the condensation reaction of aldehydes with alcohols

Annika Herbst, Anupam Khutia, Christoph Janiak*

Institut für Anorganische Chemie und Strukturchemie, Heinrich Heine Universität Düsseldorf, Universitätsstraße 1, D-40225 Düsseldorf, Germany

Corresponding author email: janiak@uni-duesseldorf.de
Additional emails: annika.herbst@hhu.de
anupam.khutia@uni-duesseldorf.de

Materials

Reagents were purchased from the following distributors and used without further purification. Chromium(III) nitrate nonahydrate (99 %), terephthalic acid (99+ %), p-tolylaldehyde (99+ %) from Acros Organics. Tetramethylammoniumhydroxide (TMAOH, 25 % in H_2O) from Alfa Aesar. N, N-Dimethylformamide (99.9 %) from VWR. Methanol, Ethanol (99.9 %), and cyclohexylmethylketone (>96 %) from Merck. 1-propanol,, benzyl alcohol (98 %), 1-butanol (99.5 %), 1-pentanol (99 %) and benzaldehyde (99 %) were all obtained from AppliChem. 4-Chlorobenzaldehyde (97 %) from Aldrich. Cyclohexanone (99.5 %) from Grüssing.

Synthesis

All MIL-101Cr materials were synthesized hydrothermally, utilizing an autoclave oven heat supply according to literature procedures.[c,d]

MIL-101Cr (**1a**): Terephthalic acid (0.66 g, 4.0 mmol) was added to an aqueous solution of TMAOH (20 mL, 0.05 mol/L) and stirred for 10 min at room temperature. $Cr(NO_3)_3 \cdot 9H_2O$ (1.6 g, 4.0 mmol) was added and the mixture was stirred again for 20 min. The suspension was transferred into a Teflon lined autoclave and was heated to 180 °C for 24 h (heating ramp 10 h; cooling ramp 18 h).

MIL-101Cr (**1b**): A suspension containing terephthalic acid (2.0 g, 12 mmol), $Cr(NO_3)_3 \cdot 9H_2O$ (4.8 g, 12 mmol) and H_2O (60 mL) was transferred into a Teflon lined autoclave and was heated to 210 °C for 6 h (heating ramp 1 h.; cooling ramp 8 h).

---

[c] Yang, J.; Zhao, Q.; Li, J.; Dong, J. *Microporous Mesoporous Mater.* **2010**, *130*, 174–179.

[d] Férey, G.; Mellot-Draznieks, C.; Serre, C.; Millange, F.; Dutour, J.; Surble, S.; Margiolaki, I. *Science*, **2005**, *309*, 2040-2042.

MIL-101Cr (**1c**): A suspension containing terephthalic acid (2.0 g, 12 mmol), $Cr(NO_3)_3 \cdot 9H_2O$ (4.8 g, 12 mmol) and H_2O (60 mL) was transferred into a Teflon lined autoclave and was heated to 210 °C for 8 h (heating ramp 1 h; cooling ramp 13 h).

Activation procedure for **1a** – **1c**: The green solid was washed (in the order) with 90 mL H_2O, 90 mL DMF and 90 mL ethanol. After the water washing procedure, the centrifuged product was stirred in 90 mL DMF overnight at room temperature and then heated in the dispersion for 6 h at 110 °C. After cooling to room temperature the powder was centrifuged off and re-suspended in 90 mL ethanol. The mixture was stirred again at room temperature overnight and then heated for 3-5 h at 90 °C. Then the products were washed with 90 mL H_2O. Compound **1c** was additionally heated in H_2O at 100 °C overnight. The amount of solvent was typically ca. 90 mL per washing cycle. The heating time varied from 3 to 5 h, unless stated otherwise. Finally, the products were collected by centrifugation and dried at 70 °C overnight (yield **1a**: 0.73 g 47 %, **1b**: 2.42 g, 52 %, **1c**: 2.81 g, 60 %)

MIL-101Cr-NO_2 (**2-NO_2-d**, **2-NO_2-ps**) and MIL-101Cr-NH_2 (**3-NH_2-ps**) were synthesized according to literature procedures.[e,f] Briefly, **2-NO_2-d** was synthesized from the reaction of CrO_3 with 2-nitroterephthalic acid under hydrothermal condition. The material (1g) was activated from water (40 mL, 3 times) at 40 °C and then with methanol (25 mL) at room temperature. The material was dried in air at 70 °C overnight. Compound **2-NO_2-ps** was synthesized from MIL-101Cr using nitrating agent. The material was then washed with water several times (15 mL, 4-5 times) at room temperature and dried in air at 70 °C overnight. Compound **3-NH_2-ps** was again activated from water (25 mL, 3 times) at room temperature and dried at 70 °C overnight. (Yield **2-NO_2-d**: 0.8 g, **2-NO_2-ps**: 0.56 g, **3-NH_2-ps**: 0.41 g).

For catalyst activation the materials **1-3** were dried in vacuum (10^{-6} Torr) for 2 days at 30 °C and stored under nitrogen unless stated otherwise.

The material **3-NH_2-ps** was found to still contain small amounts of tin, shown by X-ray photoelectron spectroscopy. The peak at 488 eV was assigned to the 3d orbital of tin and quantified against Cr (2p) with a molar ratio Sn:Cr = 15:85.

---

[e] Akiyama, G.; Matsuda, R.; Sato, H.; Hori, A.; Takata, M.; Kitagawa, S. *Microporous Mesoporous Mater.* **2012**, *157*, 89–93.

[f] Bernt, S.; Guillerm, V.; Serre, C.; Stock, N. *Chem. Commun.* **2011**, *47*, 2838–2840.

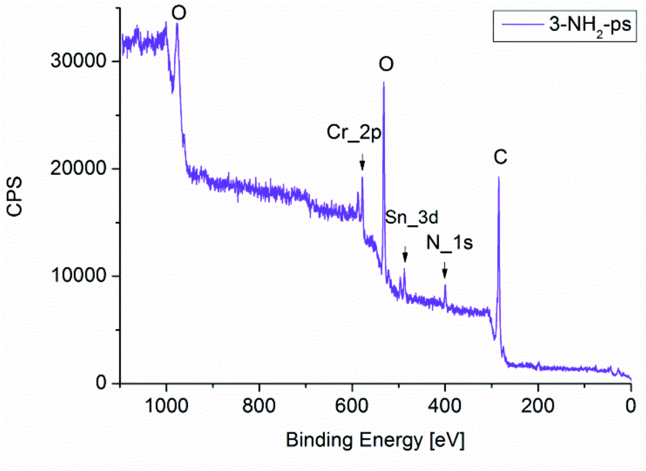

XPS Measurement of **3-NH$_2$-ps**. The experimental ratio of Sn to Cr is 15:85.

Instrumentation

Powder X-ray diffraction, PXRD patterns were recorded on a Bruker AXS D2 Phaser using Cu Kα1/α2 radiation with λ = 1.5418 Å).

Infrared spectra were measured on a Bruker Tensor 37 FT-IR Spectrometer with KBr disks.

The N_2 adsorption/desorption measurements from which the BET surface area is obtained were performed on a Quantachrome NOVA 4000 instrument at 77 K. The samples were degassed under high vacuum (10^{-5} Torr) at 120 °C (functionalized MILs) and at 200 °C (non-functionalized MILs) for at least 4 h, prior to each measurement. The BET surface area was calculated from adsorption isotherm data points in the pressure range p/p_0 = 0.05 – 0.2.

Dynamic light scattering, DLS experiments were carried out with a Malvern Zetasizer Nano S instrument working at 633 nm wavelength. Note that DLS measures the hydrodynamic radius which is larger than the individual dimensions of a particle.

Thermogravimetric analysis was performed with a Netzsch TG209 F3 Tarsus instrument.

X-ray photoelectron spectroscopy, XPS-(ESCA-)measurement was performed with a Fisons/VG Scientific ESCALAB 200X xp-spectrometer, operating at room temperature, a pressure of $1.0\cdot10^{-9}$ bar and a sample angle of 30°. Using this spectrometer, electron spectra were recorded using polychromatic Al-Kα excitation (14 kV, 20 mA) and an emission angle of 0°. Calibration of the XPS was carried out by recording spectra, using Al K_{alpha} X-rays, from clean samples of copper, silver and gold, at 20 eV and 10 eV pass energies and comparison with reference values.

Gas chromatographic (GC) studies were done with a GC-2014 Shimadzu instrument coupled with a flame ionization detector, and a GC-MS on a Finnigan Trace DSQ with Finnigan Trace GC Ultra System. GC Parameters: Autosampler injection volume 1.0 µl, rinses with solvent pre-run 1x, post-run 2x, rinses with sample 2x; injector temperature 240 °C; column information: Ultra 2, length 25 m, inner diameter 0.20 mm, film thickness 0.11 µL, column temperature 50 °C, maximum temperature 320 °C; column oven program: start at 50 °C, heating 8 °C/min until 230 °C, 22.5 min or until 150 °C, 12.3 min.

Atom absorption spectroscopy (AAS) was conducted with a Perkin Elmer AAnalyst100 instrument (flame AAS, acetylene/air as firing gas, burner head length: 10 cm). $Cr(NO_3)_3 \cdot 9 H_2O$ was chosen as material for the preparation of the Cr(III) standards in methanol. The concentrations of the standards were 0.1 ppm and 0.5 ppm, which correspond to absorptions of 0.005 and 0.053, respectively.

Transmission electron microscopy, TEM measurements were conducted with a FEI Tecnai G2 f20 with a FEG operated at 200 kV at the Ernst-Rusca centrum of Forschungszentrum Jülich.

Scanning electron microscopy, SEM measurements were done with an ESEM Quanta 400 FEG (University of Essen, Dipl.-Ing. S. Boukercha). Nano-MOF particles were separated with a high-performance centrifuge Allegra 64R, Beckmann Coulter with custom made PTFE vials.

Methanol uptake from gas phase

Methanol adsorption was measured on a Quantachrome iQ MP instrument with all gas option at 25 °C (outgassing conditions: 2 h, 120 °C).

Benzaldehyde uptake from solution

MIL powders were activated as for catalysis. Liquid phase adsorption experiments were performed at 298 K in glass vials filled with 5 or 10 mg of MIL and benzaldehyde (0.21 mmol) in heptane. Total volume of the reaction was 1 ml. The molar amount of benzaldehyde (n = 0.21 mmol) corresponded to the 10 fold amount of n(Cr(III)) in 5 mg MIL and to the 5 fold for 10 mg MIL. Dodecane was used as internal standard. Uptakes were calculated from gas chromatography data in % from the peak area according to [(initial benzaldehyde amount – benzaldehyde left after equilibration) / initial benzaldehyde amount] × 100%.

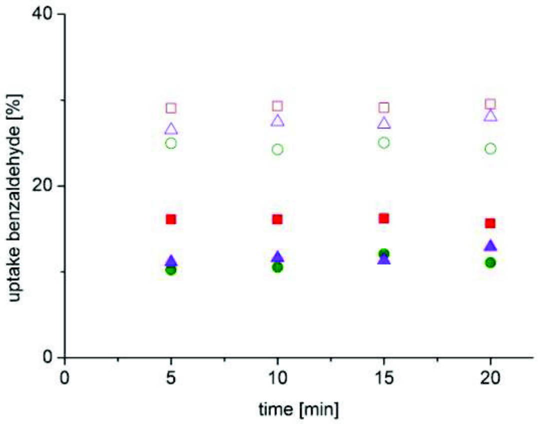

Benzaldehyde adsorption from heptane solution. ■ **1a**, ● **2-NO$_2$-d**, ▲ **3-NH$_2$-ps**, filled symbols belong to 5 mg MIL and the empty symbols to 10 mg MIL sample.

pH measurements were done with a flat-membrane electrode (Metrohm No. 6.0256.100) in methanol and water

Measurement in methanol:

The electrode was calibrated with Metrohm buffers (pH = 4.00 and 9.00). The pH of pure methanol was determined as the average of five measurements to 7.6±0.1. Before each measurement the electrode was equilibrated in methanol until a pH of 7.6±0.1 was reached. For the measurement in diluted suspensions, 1 mg of the MIL compound was suspended in 4 mL of methanol. The suspension was stirred for at least 3 h and treated for 30 min in an ultrasonic bath. For the surface measurements a KBr disk was prepared (300 mg) and coated on one side with the MIL (10 mg). Then two drops of methanol were added onto the disk coating and the measurement was done. Each measurement was done at least three times to ensure reproducibility.

For the filtration experiment a suspension of 10 mg MIL in 6.7 mL of methanol was prepared as described above. The suspension was filtered through a syringe filter and afterwards centrifuged at 22 000 rpm for 40 min. DLS measurement confirmed the absence of particles in the supernatant solution. The pH was measured of the suspension before centrifugation and of the filtrate after centrifugation.

Measurement in water:

The electrode was calibrated with Metrohm buffers (pH = 4.00 and 9.00). The pH of deionized (Millipore) water was determined as the average of five measurements to 6.1±0.1 probably due to dissolved carbon dioxide. Before each measurement the electrode was equilibrated in water until a pH of 6.1±0.1 was reached. For the measurement in diluted suspensions, 10 mg of the MIL compound was suspended in 6 mL of water. The suspension was stirred for at least 3 h and treated for 30 min in an ultrasonic bath. For the surface measurements a KBr disk was prepared (300 mg) and coated on one side with the MIL (10 mg). Then two drops of water were added onto the disk coating and the measurement was done. Each measurement was done at least two times to ensure reproducibility.

The pH values of the suspensions as well as of the coated disks decrease significantly. The experiment shows the same trend between **1a** and **2-NO$_2$-d** as in methanol dispersion for the coated disk, whereas only a small pH difference is observed in the water suspension. After centrifugation the pH values for **1a** and **2-NO$_2$-d** are only slightly enhanced. The samples were centrifugated for 4 h at 22 000 rpm. By DLS measurements for **1a** it was confirmed that no particles left in solution, whereas for **2-NO$_2$-d** still nano-MOF particles were found. In contrast to the results in methanol, it must be stated that in water the acidity leaches into the surrounding liquid.

Material	pH value water suspension [a]	pH value filtrate of water suspension [b]	pH value KBr disk coated with material [c]
1a	3.31	3.60	2.81
2-NO_2-d	3.24	3.46	1.69
H_2O (Millipore)	6.05	-	-

[a] 10 mg MIL in 6.0 mL of H_2O; [b] 0.2 µm syringe filter, centrifuged at 22 000 rpm for 4 h. [c] 10 mg MIL on KBr disk with 8 drops H_2O.

Catalytic di-acetalization of benzaldehyde

General procedure

All reactions were performed at 25 °C. The temperature was kept constant through a thermostated stirred water bath around the reaction vial. The catalysts are additionally dried under high vacuum (10^{-6} Torr for 48 h at 30 °C). The catalytic experiments were conducted in Pyrex glass vials equipped with a cap and a stirrer. The accuracy of the MIL sample weight was 10.1±0.1 mg. Every experiment was performed at least in a duplicate and in triplicate in case of larger deviations to ensure reproducibility. The standard reaction conditions of this work have been oriented towards the study of Hatton and Coworkers[g]

In a typical experiment the MIL catalyst (10 mg) was suspended in a mixture of methanol (6.7 mL, 166 mmol, d = 0.79 g/cm^3) and benzaldehyde (340 µL, 3.34 mmol, d = 1.04 g/cm^3) with a total volume of 7.04 mL. Thus, the initial MeOH and benzaldehyde concentrations were 23.6 mol/L and 0.474 mol/L, respectively. For experiments with ethanol a total volume of 9.6 mL and for *n*-propanol, *n*-butanol, *n*-pentanol and benzyl alcohol a total volume of 9 mL was used. The composition of the reaction mixture was determined by GC and GC-MS. Every experiment was performed at least in duplicate.

To collect the GC samples the vials were centrifuged for 5 to 10 min at 5000 rpm, until the supernatant solution was clear. Then 12 µL of the supernatant solution were diluted with 488 µL of the respective alcohol as solvent.

The conversion was calculated by dividing the peak area of the product signal through the peak area of product and reagent.

Catalytic data as TON and TOF was calculated as follows:

TON = $mol_{product}/mol_{cat}$ (mol_{cat} = mol(2/3 of total Cr) = 0.029 mmol)

TOF = $mol_{product}/(mol_{cat} \cdot time)$ with time in hours

---

[g] Bromberg, L.; Hatton, T. A. *ACS Appl. Mater. Interfaces* **2011**, *3*, 4756–4764.

The ideal activated MIL formula (where BDC = benzene-1,4-dicarboxylate) can be calculated with or without aqua ligands on the trinuclear chromium SBU:

$[Cr_3(O)(BDC)_3(F,OH)(H_2O)_2]$ = $C_{24}H_{17}Cr_3O_{16}$: M = 717.384 g/mol. The amount of 10 mg MIL-101 corresponds to 0.0139 mmol (13.94 µmol).

$[Cr_3(O)(BDC)_3(F,OH)]$ = $C_{24}H_{13}Cr_3O_{14}$: M = 681.354 g/mol. The amount of 10 mg MIL-101 catalyst corresponds to 0.0147 mmol (14.68 µmol).

For the sake of simplification an average value of 700 g/mol, corresponding to 0.0143 mmol of MIL was used.

This translates into 3 x n(MIL) for the Cr_3 content: 0.043 mmol Cr or 0.0061 mol(Cr)/L (6.1 mmol/L) for the total volume of 7.04 mL.

Lewis-acid catalysis: By assuming only 2/3 of the Cr(III) as active Lewis centers after the removal of the two aqua ligands from each Cr_3-SBU, the active chromium "catalyst" amount is at the most 0.029 mmol Cr.

Brønsted-acid catalysis: There are two aqua ligands available for deprotonation on each Cr_3-SBU, yielding at the most 0.029 mmol of protons.

Thus, for both Lewis-acid and Brønsted-acid catalysis the number of active chromium centers can be taken as 2/3 of the total chromium amount, that is, 0.029 mmol in 10 mg MIL sample.

Table S1. Retention times of reagents and products in GC measurements.[a]

Compound	Retention time [min]	Compound	Retention time [min]
MeOH	0.9	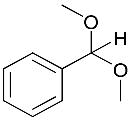	5.2
EtOH	1.0	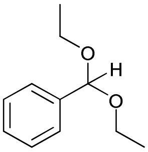	7.1
n-Propanol	1.1	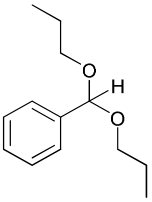	9.9
Benzyl alcohol	5.7	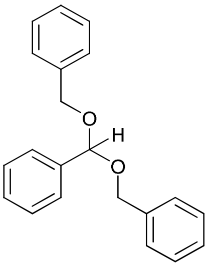	-
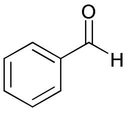	3.0	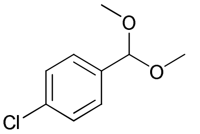	8.7
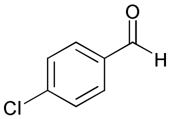	5.8	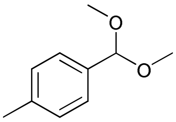	7.4
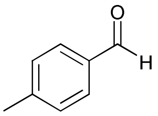	5.1	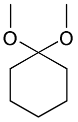	3.7
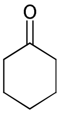	2.4	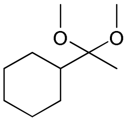	6.7
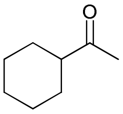	4.2		

[a] GC-2014 Shimadzu instrument with a flame ionization detector. GC Parameters: Autosampler injection volume 1.0 µl, rinses with solvent pre-run 1x, post-run 2x, rinses with sample 2x; injector temperature 240 °C; column information: Ultra 2, length 25 m, inner diameter 0.20 mm, film thickness: 0.11 µL, column temperature 50 °C, maximum temperature 320 °C; column oven program: start at 50 °C, heating 8 °C/min until 230 °C, 22.5 min or until 150 °C, 12.3 min.

Filtration test

After running the reaction for the chosen time, the catalyst was separated by centrifugation. The clear supernatant solution was filtered with a syringe filter of the type RC 0.2 µm. The reaction was continued with the filtrate in a new reaction vial under identical reaction conditions for at least 2.5 h. The filtrate was analyzed by GC, DLS, and TEM.

Recycling test

For experiments with multiple runs each catalytic reaction was run for the stated time (15 h for MIL-101Cr **1a**, 90 min for MIL-101-Cr-NO_2 (**2-NO_2-d**)) and centrifuged until the supernatant solution was visibly clear. The clear solution was collected for GC analysis. Then the catalyst was washed two times with methanol (9 ml) and dried at room temperature (20 °C) for ca. 6 h at 1.6 mbar vacuum. After that a new reaction was started under the standard conditions stated above. This procedure was repeated for 5 runs, after which PXRD was measured (cf. Fig. S4). The composition of the reaction mixture was determined by GC.

Reactions with $Cr(NO_3)_3$ 9 H_2O as catalyst

10 mg MIL is equivalent to 0.043 mmol Cr (see above). A stock solution (50 ml) of $Cr(NO_3)_3 \cdot 9\ H_2O$ with $c = 8.34 \cdot 10^{-3}$ mol/L was prepared in the respective alcohol and 5 ml were used for the reactions. Standard conditions were applied.

Table S2. Catalytic di-azetalization with **2-NO_2-d** and chromium(III) nitrate nonahydrate of benzaldehyde in methanol, ethanol, n-propanol, n-butanol and n-pentanol

	2-NO_2-d 20 min	**2-NO_2-d 90 min**	**$Cr(NO_3)_3 \cdot 9\ H_2O$ 20 min**	**$Cr(NO_3)_3 \cdot 9\ H_2O$ 90 min**
alcohol	Benzaldehyde conversion (%)			
methanol	83	99	94	96
ethanol	37	74	82	94
n-propanol	14	45	79	87
n-butanol	7	19	76	86
n-pentanol	2	4	26	75

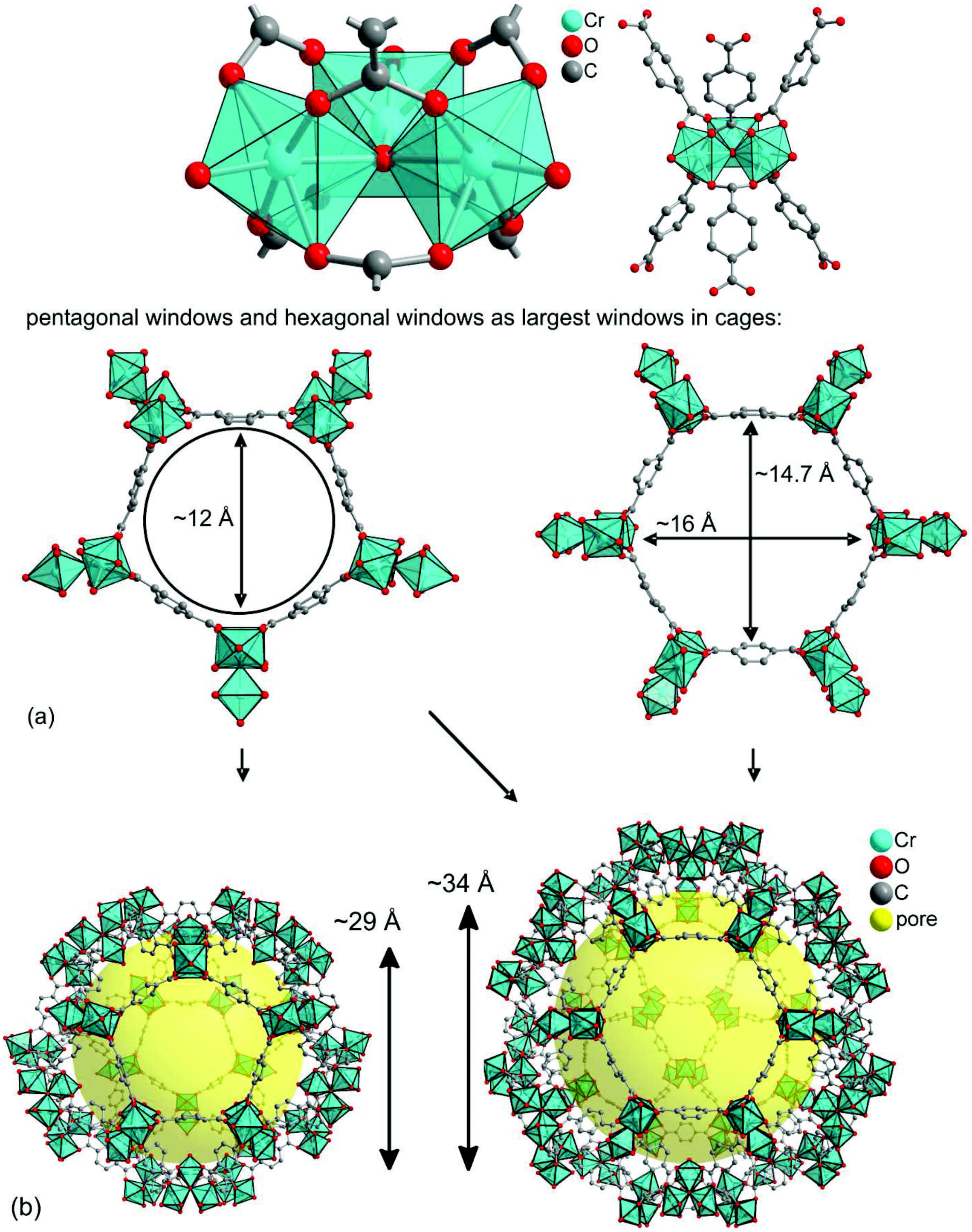

Figure S1. Building blocks for MIL-101, $[Cr_3(\mu_3\text{-}O)(F,OH)(BDC)_3(H_2O)_2]$, generated from the deposited X-ray data file at the Cambridge Structure Database (CSD-Refcode OCUNAK) [d] using the program DIAMOND [h]. Trinuclear $\{Cr_3(\mu_3\text{-}O)(F,OH)(H_2O)_2(O_2C\text{-})_6\}$ building units and bridging benzene-1,4-dicarboxylate ligands form pentagonal and hexagonal rings (a) which are assembled into mesoporous cages. The yellow spheres in the mesoporous cages with diameters of 29 or 34 Å, respectively, take into account the van-der-Waals radii of the framework walls (water-guest molecules are not shown). The different objects in this figure are not drawn to scale.

---

h Brandenburg, K. *Diamond* (Version 3.2), crystal and molecular structure visualization, Crystal Impact. K. Brandenburg, H. Putz, Bonn, Germany, **2007-2012**.

Nitrogen sorption isotherms

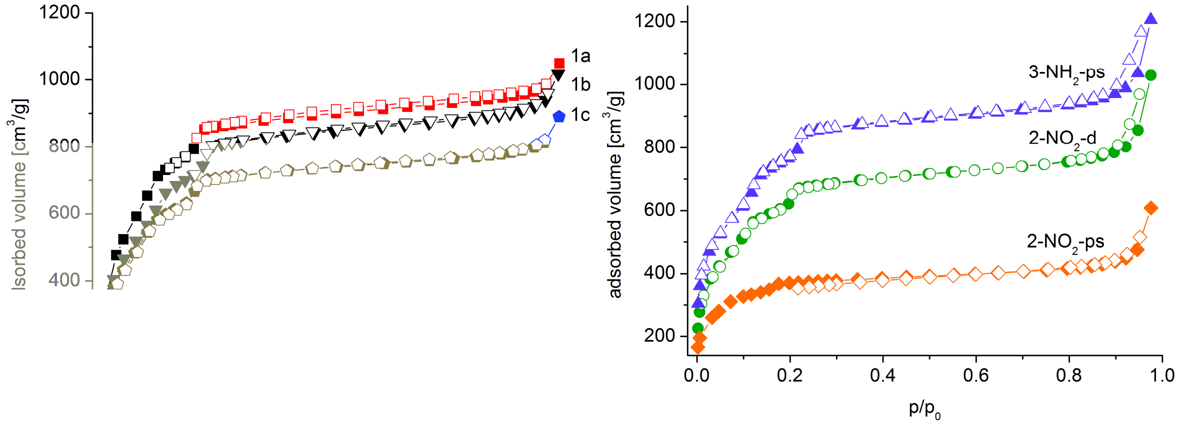

Figure S2. Nitrogen sorption isotherms of unfunctionalized MIL-101Cr (**1a** – **1c**, left) and functionalized MIL-101Cr (**2-NO$_2$-d**, **2-NO$_2$-ps** and **3-NH$_2$-ps**, right). Filled symbols are for adsorption, empty symbols are for desorption.

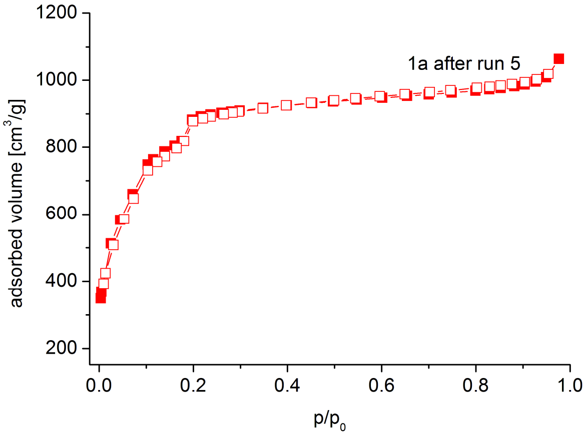

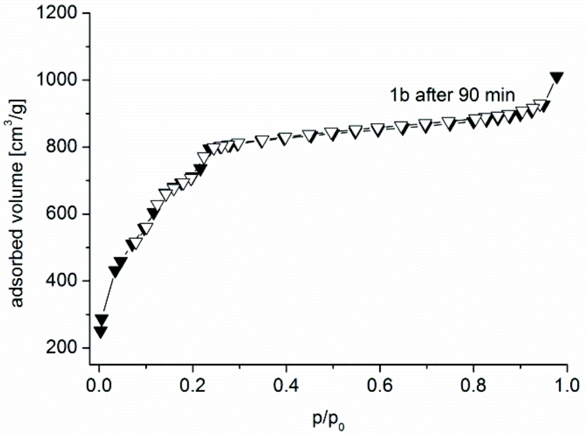

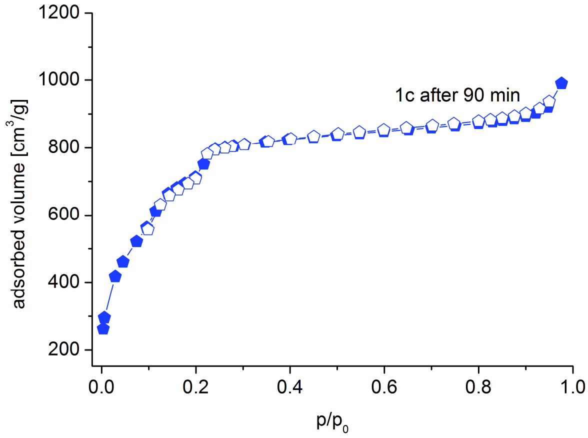

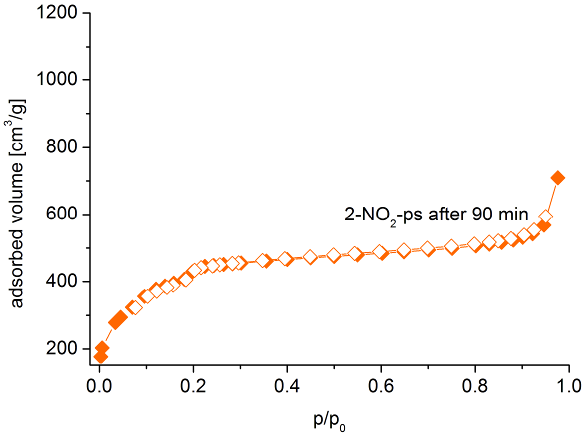

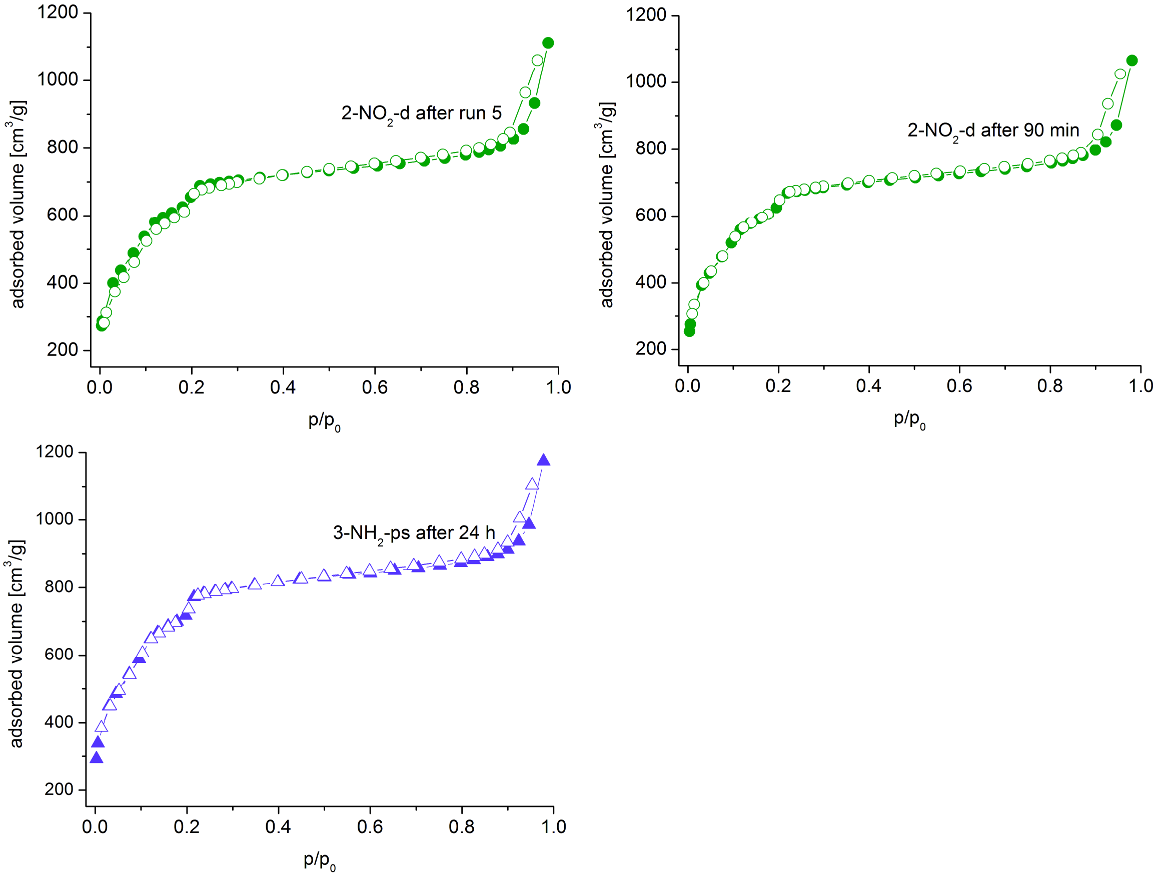

Figure S3. Nitrogen sorption isotherms of **1a** after 5 runs (90 min.), **1b**, **1c**, **2-NO$_2$-d** and **2-NO$_2$-ps** after 1 run (90 min.), **3-NH$_2$-ps** after 24 h reaction and **2-NO$_2$-d** after 5 runs, 90 min. each. Filled symbols are for adsorption, empty symbols are for desorption.

Table S3. Surface area of MIL samples after the catalytic reaction.

MIL **sample**	**S_{BET} (m^2/g)**
1a after 5 runs of 90 min.	3100
1b after 90 min.	2712
1c after 90 min.	2749
2-NO$_2$-d after 90 min.	2377
2-NO$_2$-d after 5 runs of 90 min.	2421
2-NO$_2$-ps after 90 min.	1550
3-NH$_2$-ps after 24 h	2711

Powder X-ray diffractograms, PXRD

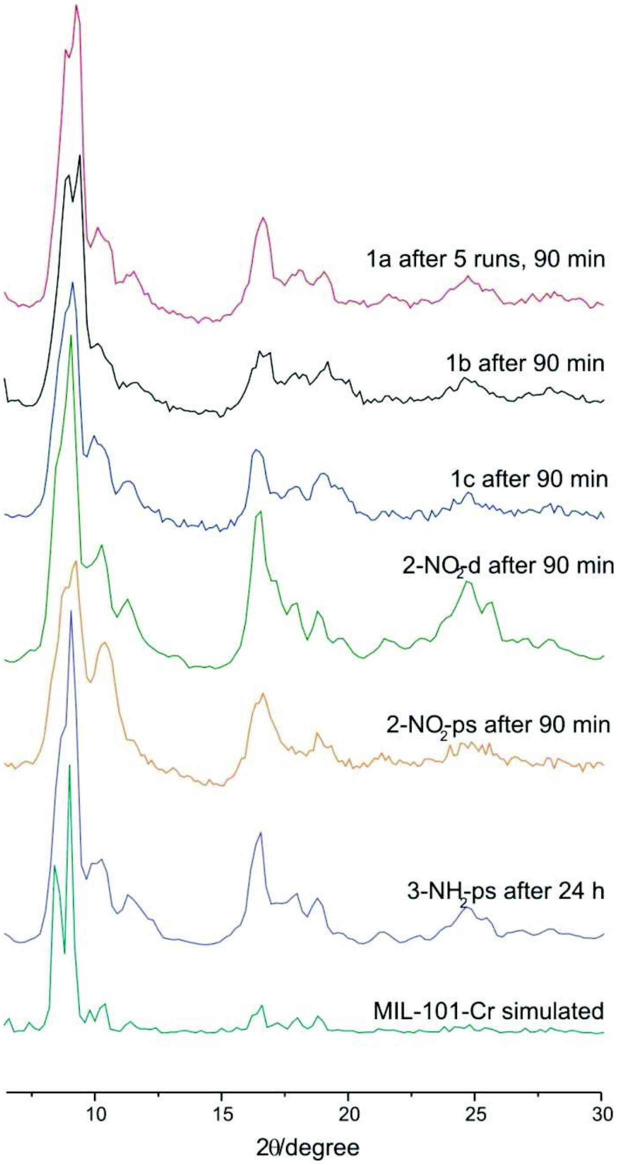

Figure S4. Powder X-ray diffractograms of MIL samples after catalytic reactions as indicated, that is, after 5 runs for 90 min for **1a** and after 1 run, **1b**, **1c**, **2-NO$_2$-d**, **2-NO$_2$-ps** after 90 min, **3-NH$_2$-ps** after 24 h.

IR Spectroscopy

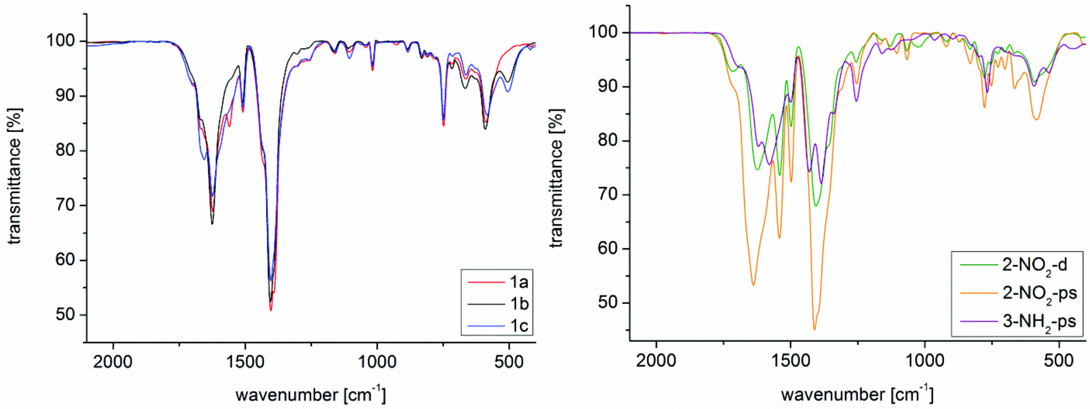

Figure S5. FT-IR spectra of non-functionalized MIL-101Cr (**1a – 1c**, left) and functionalized MIL-101Cr (**2-NO$_2$-d**, **2-NO$_2$-ps** and **3-NH$_2$-ps**, right).

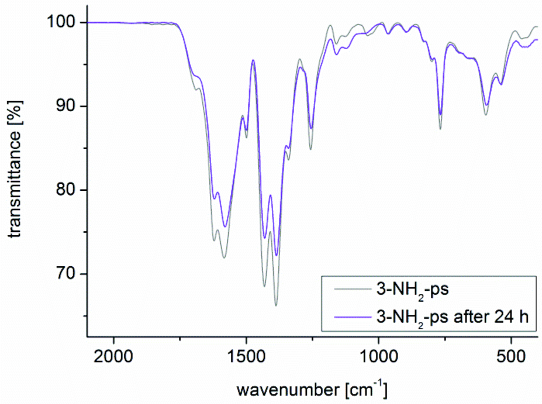

Figure S6. FT-IR spectra of MIL-101Cr-NH$_2$, **3-NH$_2$-ps**, before and after 24 h catalytic reaction.

Additional data from catalytic di-acetalization reactions

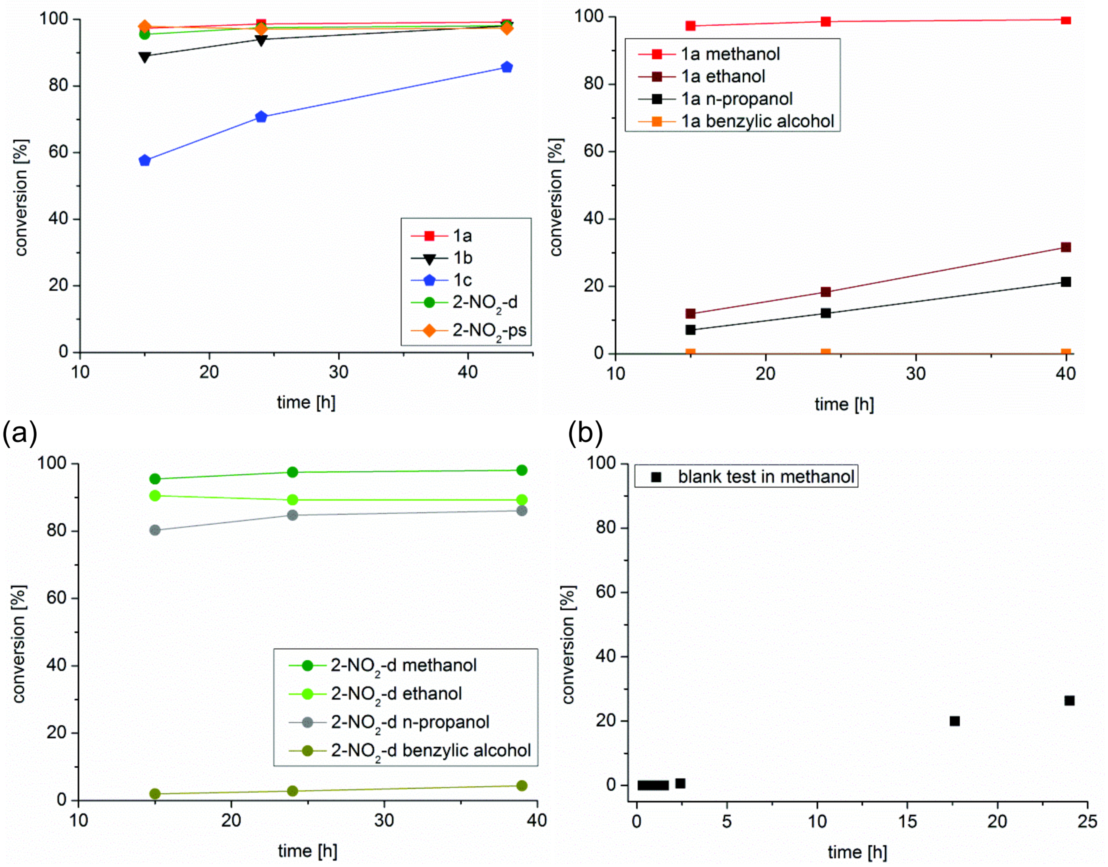

(a) (b)

(c) (d)

Figure S7. Extended time measurements of the catalytic di-acetalization of benzaldehyde with methanol with different MIL catalysts (a) and in different alcohols for **1a** (b) and **2-NO$_2$-d** (c). Blank test of benzaldehyde in methanol (d).

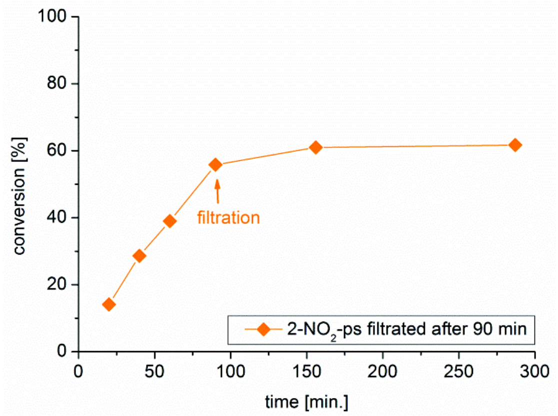

Figure S8. Filtration test with **2-NO$_2$-ps**. After filtration the conversion increased only by 7 %.

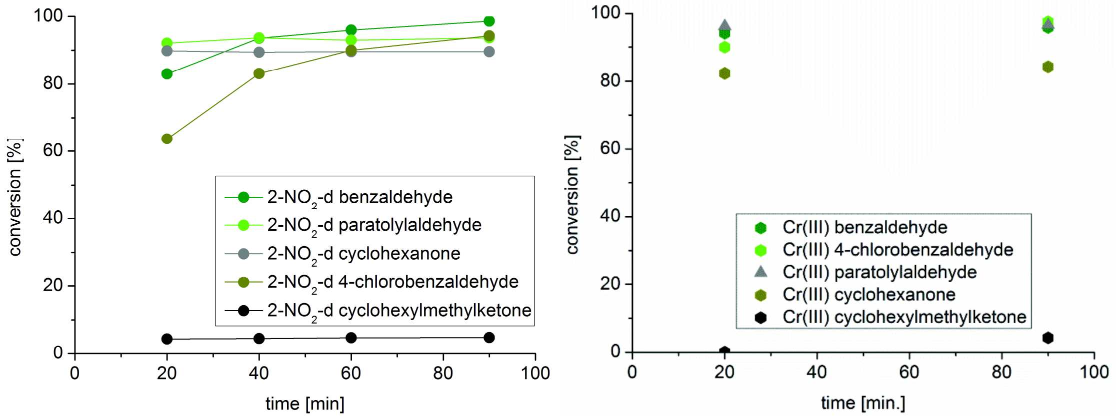

Figure S9. Reaction of **2-NO$_2$-d** in methanol with different aldehydes (left). Reaction of chromium(III) nitrate nonahydrate with different aldehydes (right).

DLS measurements

The measurements were conducted at 25 °C in methanol. For the detection of nanoparticles in the filtrate of the reaction, each experiment consisted of 3 measurements with 11 runs for different time periods in order to obtain the best data quality. The average of the maximum of the three measurements is given. In Figures S10 and S11 typical distributions for **1a** and **2-NO$_2$-d** are shown. Note that DLS measures the hydrodynamic radius which is larger than the individual dimensions of a particle.

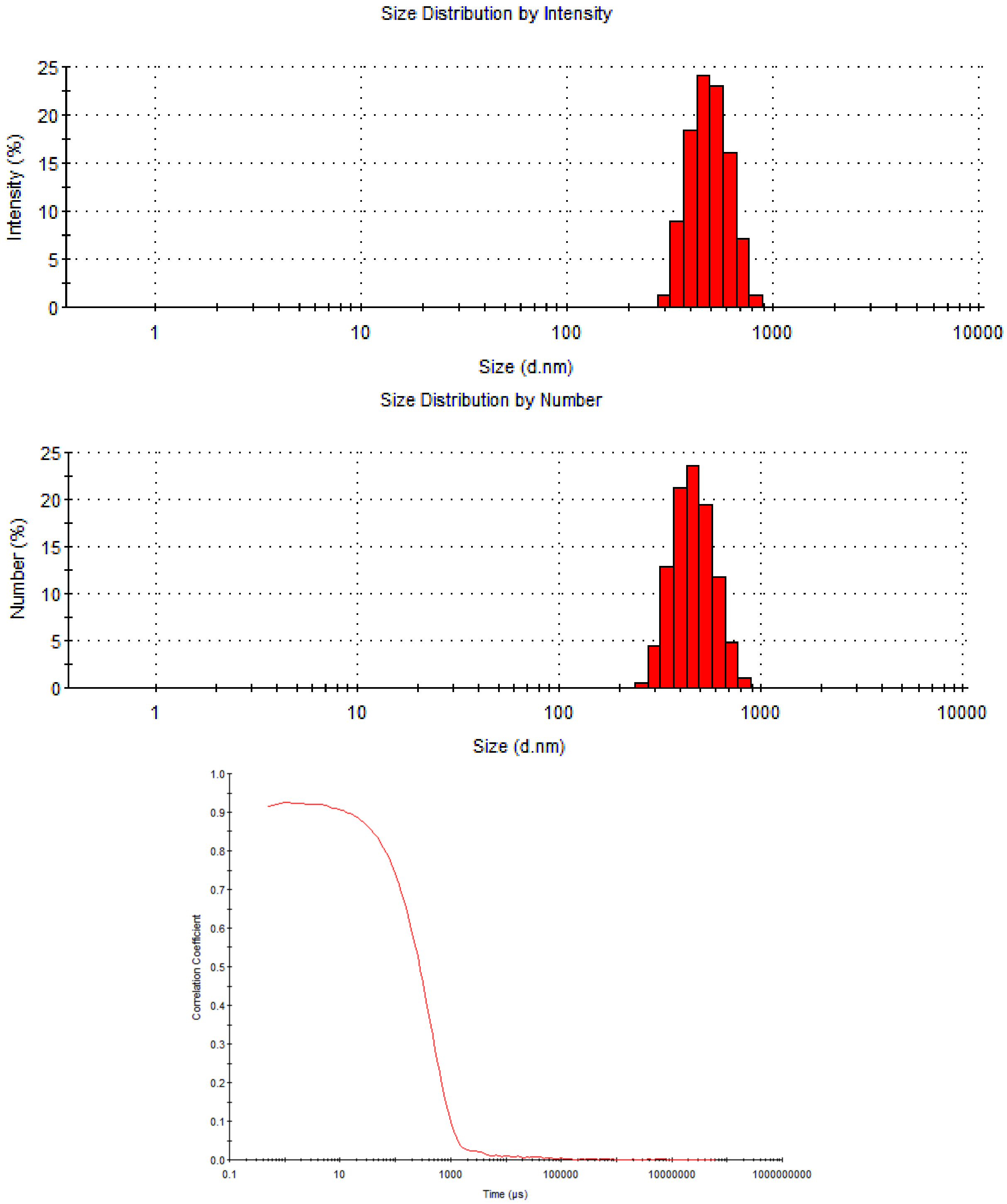

Figure S10. DLS measurements for **1a** with size distribution by number, intensity and the correlation diagram. Note that DLS measures the hydrodynamic radius which is larger than the individual dimensions of a particle.

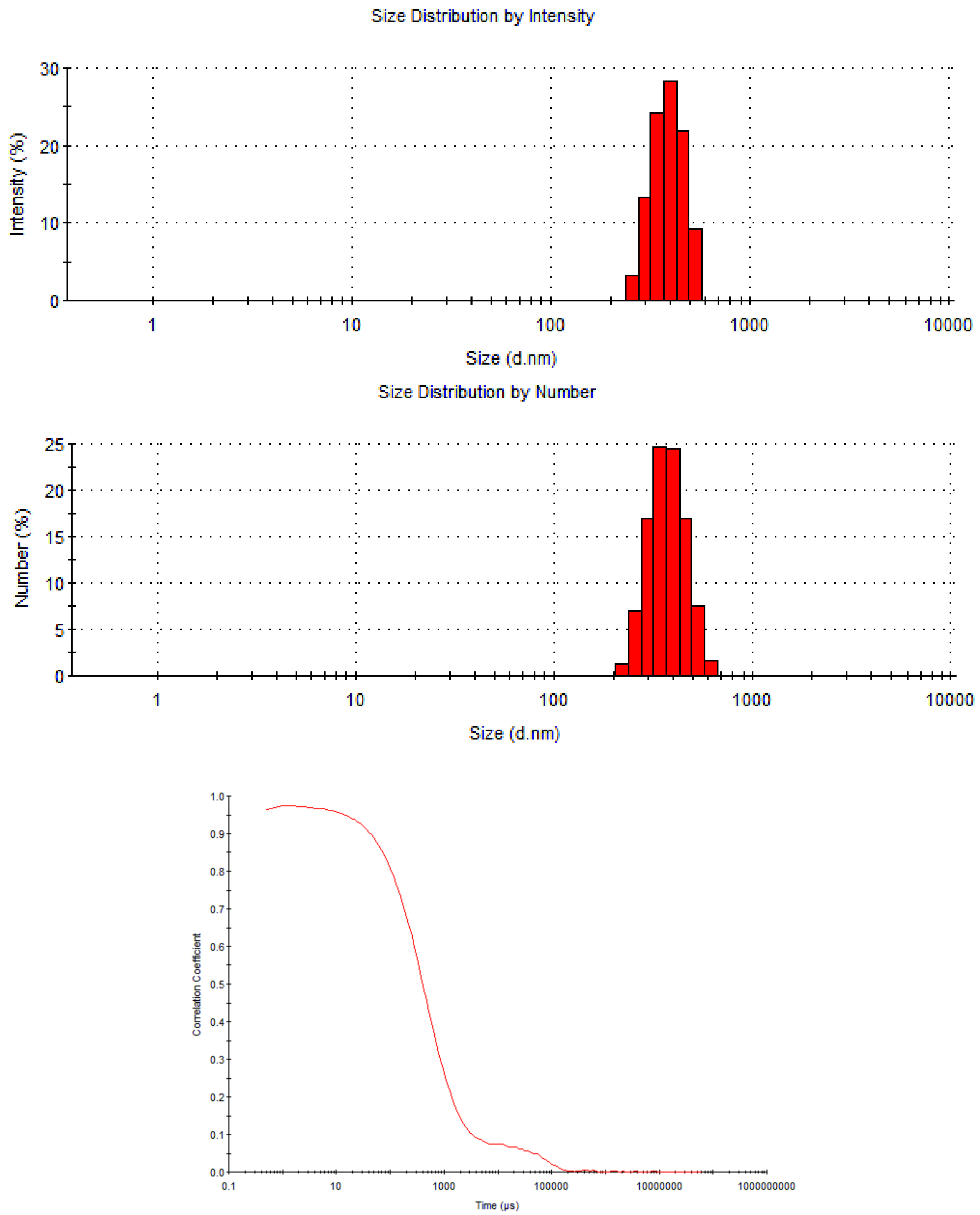

Figure S11. DLS measurements for **2-NO$_2$-d** with size distribution by number, intensity and the correlation diagram. Note that DLS measures the hydrodynamic radius which is larger than the individual dimensions of a particle.

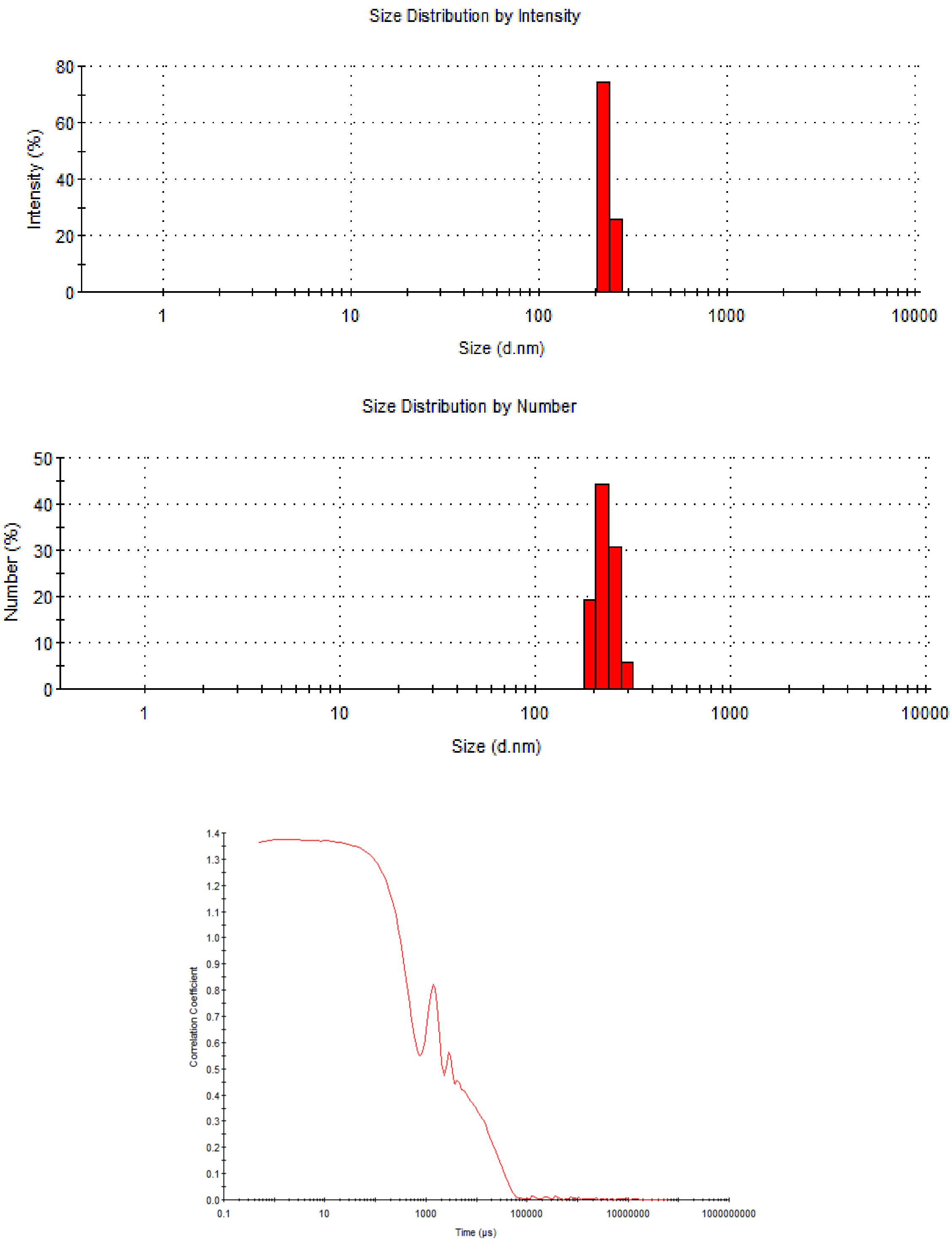

Figure S12. DLS measurements for **3-NH$_2$-ps** with size distribution by number, intensity and the correlation diagram. Note that DLS measures the hydrodynamic radius which is larger than the individual dimensions of a particle.

(a)

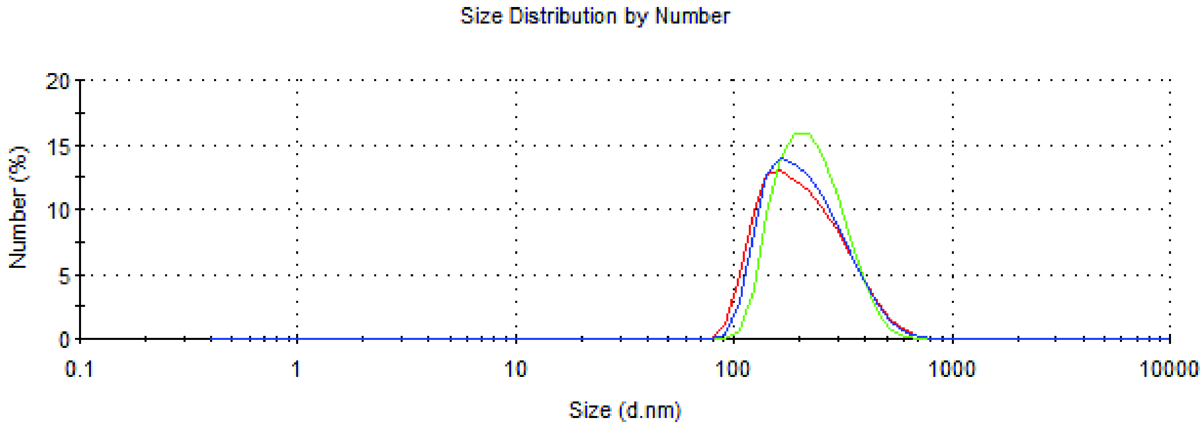
Size Distribution by Number
Number (%)
20
15
10
5
0
0.1
1
10
100
1000
10000
Size (d.nm)

(b)

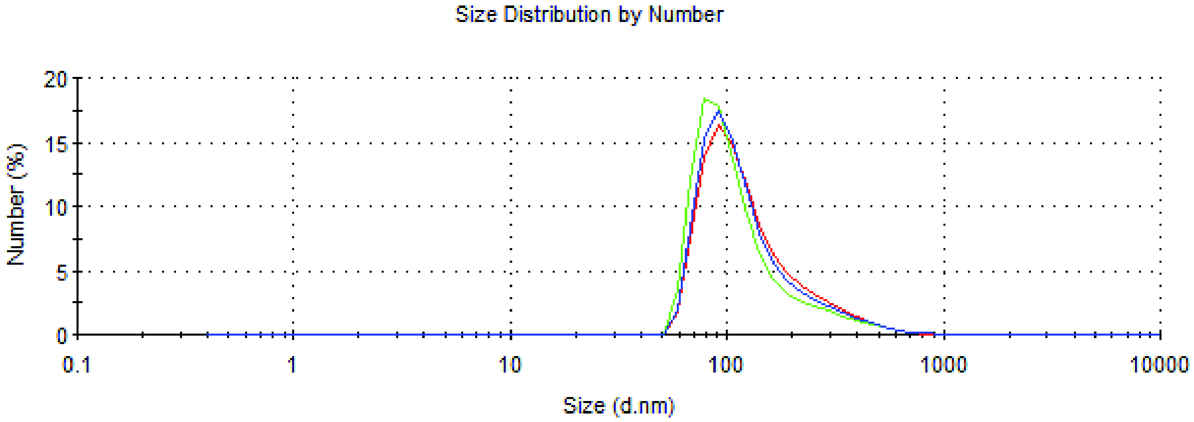
Size Distribution by Number
Number (%)
20
15
10
5
0
0.1
1
10
100
1000
10000
Size (d.nm)

(c)

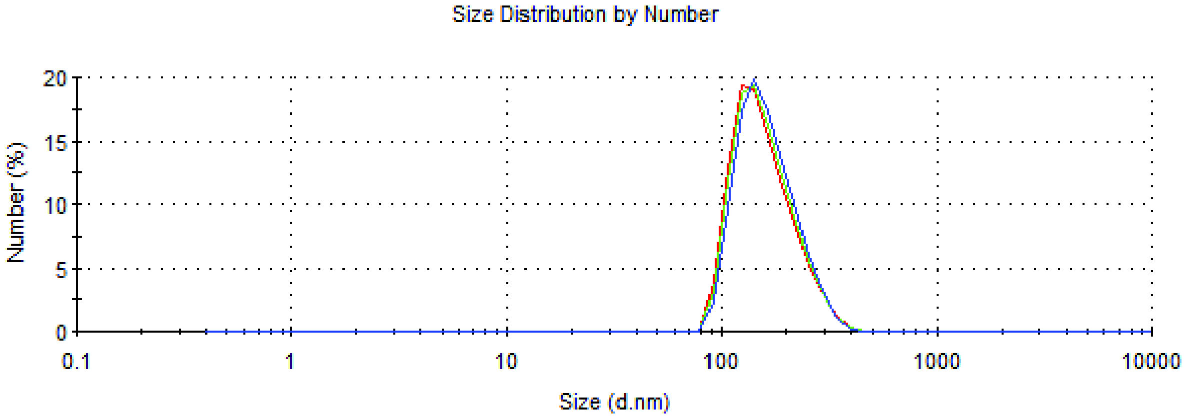
Size Distribution by Number
Number (%)
20
15
10
5
0
0.1
1
10
100
1000
10000
Size (d.nm)

(d)

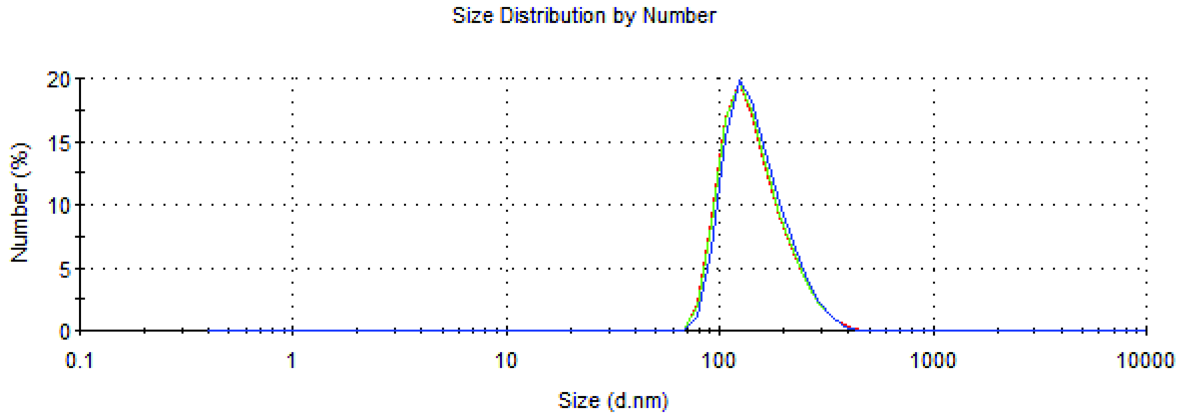
Size Distribution by Number
Number (%)
20
15
10
5
0
0.1
1
10
100
1000
10000
Size (d.nm)

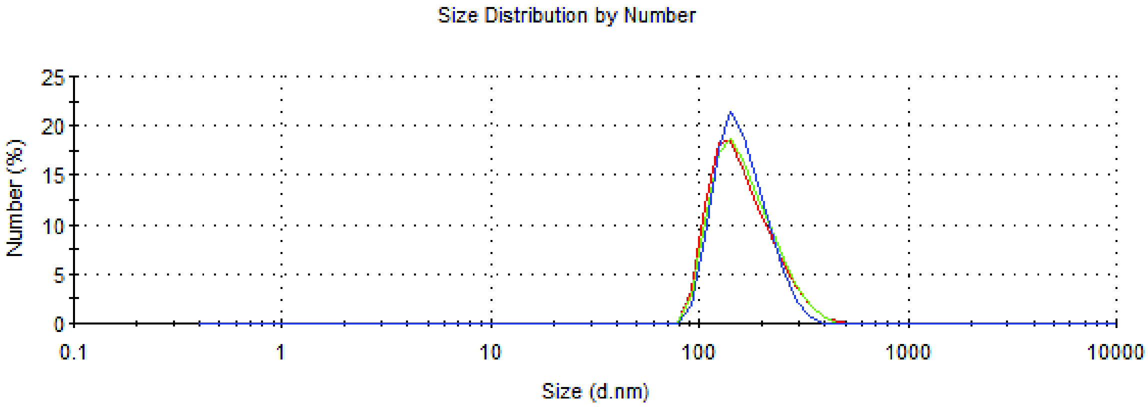

(e)

Figure S13. DLS measurements for the filtered solutions during or after catalytic runs: (a) **2-NO$_2$-d** after 5 min, (b) **2-NO$_2$-d** after 90 min, (c) **2-NO$_2$-d** after 5 runs, with 90 min each, (d) **2-NO$_2$-ps** after 90 min, (e) **3-NH$_2$-ps** after 90 min. Note that DLS measures the hydrodynamic radius which is larger than the individual dimensions of a particle.

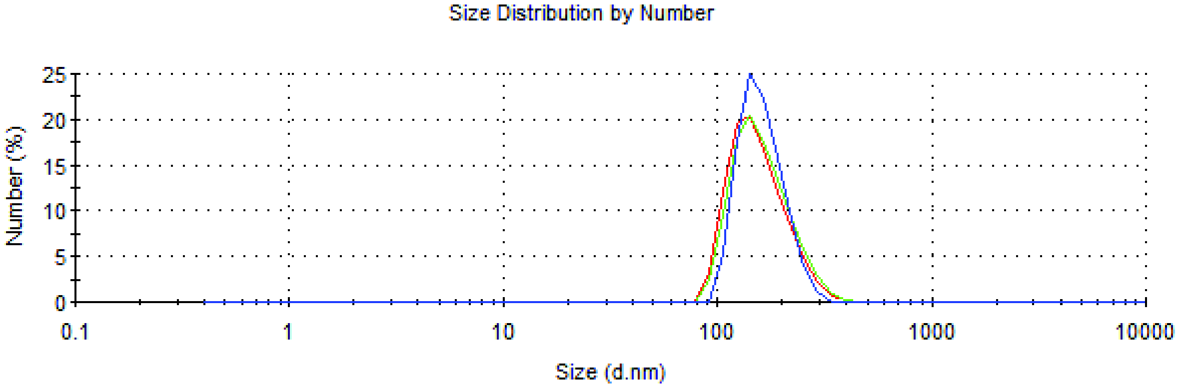

Figure S14. DLS measurement for **2-NO$_2$-d** nano-MOF. The measurement was performed after filtration and before addition of benzaldehyde.

Scanning electron microscopy, SEM images

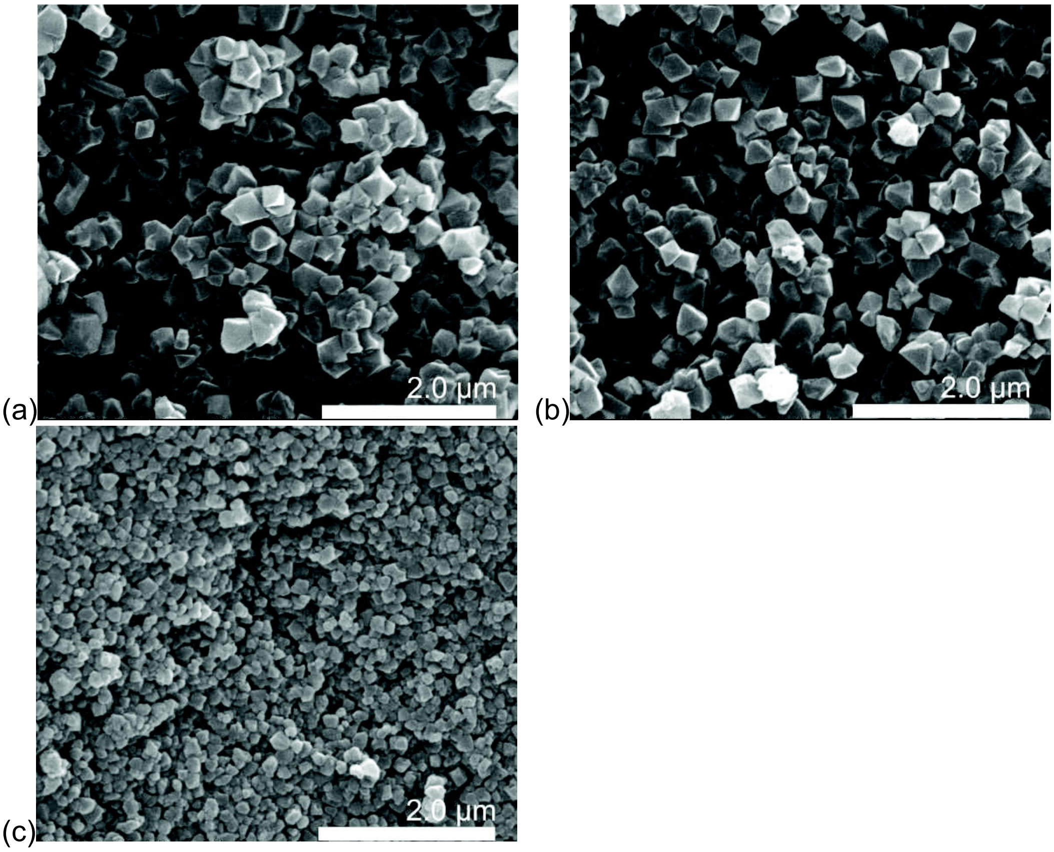

Figure S15. SEM images of (a) **1a** after 5 catalytic runs of 90 min each, (b) **1a** after 5 runs of 15 h each, (c) **2-NO$_2$-d** after 5 runs of 90 min each.

Infrared spectroscopic investigation of CD$_3$CN adsorption

MOF powders were activated as for catalysis. Samples were prepared by coating of a KBr disk (300 mg) with the MOF powder (9-10 mg) under argon atmosphere. The disk was adjusted in a sample holder and placed in a gas cell, equipped with KBr windows. The cell was connected to a vacuum line for evacuation ($P = 6\cdot10^{-3}$ mbar) and to a CD$_3$CN reservoir for introducing gaseous CD$_3$CN. The experiments were conducted at room temperature. After evacuation of the gas cell, the connection to the CD$_3$CN reservoir was opened for 10 min. Then spectra (256 scans per spectrum) were recorded over 2 h every 5 or 10 min. IR spectra are absorption spectra and the notation used is a.u. for absorption units. The resolution of the spectra was 4 cm^{-1}. The coated disk strongly absorbs the IR light between 1300 and 1650 cm^{-1} (region of the carboxylate stretching vibrations). CD$_3$CN has been used to avoid Fermi resonance interactions of the u(CN) vibration.[i]

---

[i] Volkringer, C.; Leclerc, H.; Lavalley, J.; Loiseau, T.; Férey, G.; Daturi, M.; Vimont, A. *J. Phys. Chem. C* **2012**, *116*, 5710-5719.

Thermogravimetric analysis

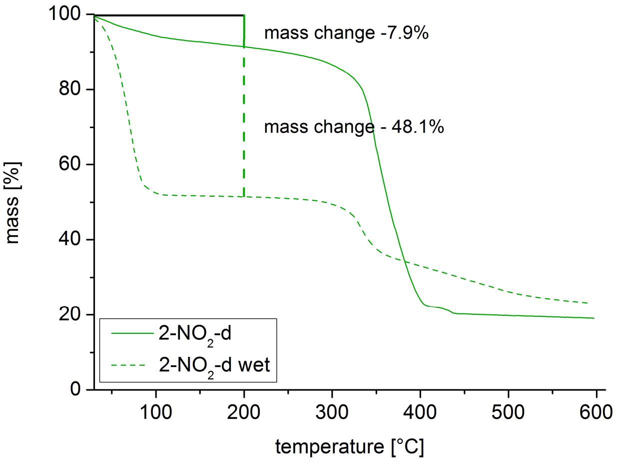

Figure S16. Thermogravimetric analysis of **2-NO$_2$-d** before and after wetting with water.

3.2 Selective glucose conversion to 5-hydroxymethylfurfural (5-HMF) instead of levulinic acid with MIL-101Cr MOF-derivatives

A. Herbst, C. Janiak
Submitted, reference [118]

The platform chemical 5-HMF is of great interest and production from glucose using low boiling solvents is highly desirable, since it opens access to important biomass feedstocks.[5] MOFs are a promising class of heterogeneous catalysts, which were applied previously in several acid catalyzed reactions. In this work, we investigated the scope of MOFs in the transformation of glucose to 5-HMF. The formation of 5-HMF from glucose was reported with several solid acid catalyst, but glucose conversion with MOFs is little investigated. New mechanistic insights from homogeneous catalysis and molecular simulations showed that purely Brønsted acid catalyzed conversion of glucose to 5-HMF is possible.[115],[116] MIL-101Cr-SO_3H was applied in a THF/H_2O mixture (v:v 39:1) at 130°C and was found to convert glucose achieving a 5-HMF yield of 29% after 24 h. The performance of MIL-101Cr-SO_3H was compared to other functionalized MIL-101Cr derivates. Different solvent mixtures were investigated with regard to 5-HMF yield and selectivity towards 5-HMF and levulinic acid. Results have been compared to the activity and selectivity of Amberlyst-15 and sulfuric acid. The formation of insoluble humins was observed and an alternative strategy to avoid this byproduct was constructed.

Author's share of work:

- Designing and performing of the synthetic work and catalytic reactions and evaluation of the results.
- Writing of the manuscript and drawing of the figures, graphs and tables except for figure 3 and S1 (done by Mr. Janiak).
- Editing of the manuscript regarding the reviewers' comments by Ms. Herbst and Mr. Janiak.

Journal Name

Selective glucose conversion to 5-hydroxymethylfurfural (5-HMF) instead of levulinic acid with MIL-101Cr MOF-derivatives†

Received 00th January 20xx,
Accepted 00th January 20xx

DOI: 10.1039/x0xx00000x

www.rsc.org/

Annika Herbst and Christoph Janiak*

The catalytic conversion of glucose to 5-hydroxymethylfurfural (5-HMF) is highly desirable, but the 5-HMF yield with hetereogenous catalysts is still low compared to homogenenous catalysts, and the mechanism is not elucidated completely. In addition isolation and purification of 5-HMF still presents a challenge as degradation reactions take place and side products form. The formation of 5-HMF from glucose was reported with several solid acid catalyst, still metal-organic framework (MOF) catalysts could, so far, catalyze the cascade reaction of glucose to 5-HMF only in low yields of less than 16%. Glucose conversion with MOFs is little investigated and here sulfonated MIL-101Cr (MIL-SO_3H) was found to achieve 29% conversion of glucose to 5-HMF after 24 h in a THF:H_2O (v:v 39:1) mixture. Conversion of maltose resulted in 50 % 5-HMF yield (saccharide solutions were 5 wt%). When the reaction with MIL catalysts was carried out in pure THF no product was formed, revealing the indispensability of water for the glucose-to-5-HMF conversion. Importantly, MIL-SO_3H preferentially leads to 5-HMF over levulinic acid (molar ratio 1:0.3) while the catalysts Amberlyst-15 and sulfuric acid form mostly levulinic acid in 5-HMF to levulinic acids ratios of 1:3 and 1:10, respectively. At the same time MIL-NO_2 is most selective yielding only 5-HMF and showing no formation of levulinic acid. Using 5-HMF as substrate did not result in any conversion to levulinic acid with MIL-SO_3H, thereby ruling out the catalytic formation of levulinic acid from 5-HMF. Catalyst recycle experiments showed that MIL-SO_3H stays porous and crystalline, but becomes deactivated through fouling by humin formation. With the use of ethanol as alternative reaction medium the formation of insoluble humins could be prevented, but the yield of 5-HMF and 5-ethyl-HMF decreased.

Introduction

Biomass is highly attractive as a source for valuable chemicals and fuels, to save fossil fuels and reduce CO_2 emissions therefrom.[1,2] Especially “waste” biomass from by-product streams (e.g. in agroindustry, food sector, paper manufacturing and recycling) is investigated as feedstock for platform chemicals, e.g., 5-hydroxymethylfurfural (5-HMF) (Fig. 1), which can replace the petro-based chemicals and create new valuable products.[3] Biomass of plants or algae consists mainly of lignocelluloses, which in turn contains cellulose, lignin and hemicelluloses. Cellulose represents the largest part with up to 50 weight%.[4] Therefore the conversion of cellulose, respectively its glucose subunits is of broad interest. The chemical conversion of glucose can proceed via acid-catalyzed dehydration, which presents challenging requirements to the catalyst, since a variety of products can be obtained (e.g. fructose, levoglucosan, other C5 or C6 monosaccharides, 5-HMF, furfural, lactic acid, levulinic acid and formic acid) (cf. Fig. 2).2

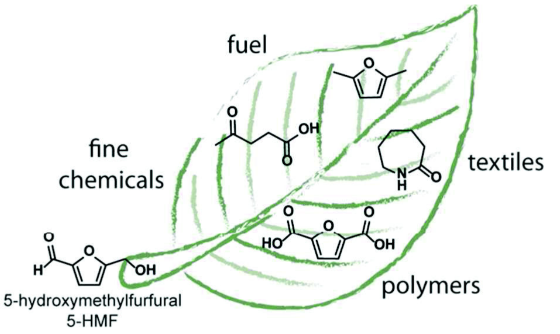

Fig. 1 5-HMF as precursor platform molecule for different products relevant to various industries.

Among these glucose-dehydration products 5-hydroxymethylfurfural (5-HMF) is of special interest because it can be converted to important polymer precursors such as 2,5-furan dicarboxylic acid (replacement of terephthalic acid), 1,6-hexanediol, caprolactam and 2,5-dimethylfuran, which is interesting as a fossil fuel alternative (Fig. 1).[5] Consequently, an enormous research interest arose with the aim of 5-HMF synthesis from glucose. During the last two years and also very

Institut für Anorganische Chemie und Strukturchemie, Heinrich-Heine Universität Düsseldorf, Universitätsstraße 1, D-40225 Düsseldorf, Germany. Email: janiak@uni-duesseldorf.de

† Electronic Supplementary Information (ESI) available: Details of synthesis, methods, catalysis, NMR spectra, SEM images, powder X-ray diffractograms, N_2 sorption isotherms, potentiometric titrations. See DOI: 10.1039/x0xx00000x

recently, a number of excellent reviews have been published on this topic and provide a thorough overview.4[,6]

5-HMF can be synthesized from glucose in aqueous media, DMSO, ionic liquids and in biphasic systems. Numerous catalysts have been tested which can be roughly classified in homogeneous Brønsted and Lewis acids (H_2SO_4, $CrCl_3$ or $AlCl_3$) and solid acids (zeolites, resins and metal organic frameworks). A brief reactions sequence of glucose to HMF is depicted in Fig. 2. Generally, 5-HMF is accessible via Lewis-acidic isomerization of glucose to fructose and Brønsted acidic conversion to 5-HMF.[7] Tessonnier *et al.* also investigated the selective isomerization to fructose via base catalysis, using amines, and found the same performance as the state-of-the-art Lewis acid catalysts with a yield of 32% and a selectivity to fructose of 63% after 20 min at 100°C.[8,9] Huber et al. recently proposed a new mechanistic pathway for the formation of 5-HMF from cellulose and glucose which is based on acid catalysis through the intermediate levoglucosan instead of fructose (Fig. 2).[10]

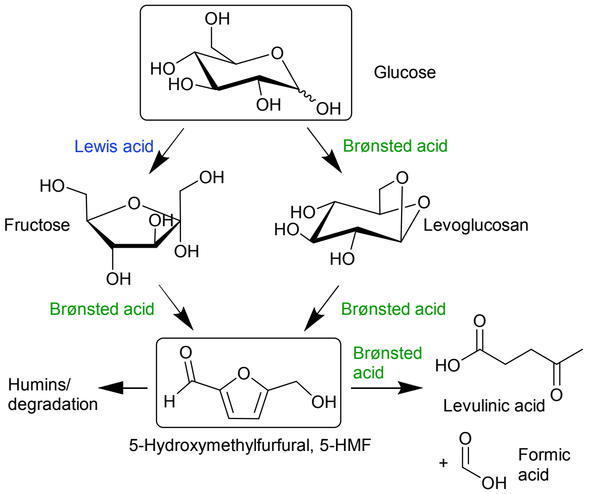

Fig. 2 Reaction scheme for 5-HMF production from glucose.[10]

Interestingly, the best 5-HMF yield of 44% from cellulose was reported for a mixture of THF/water 40:1, using H_2SO_4 as catalyst at 190 °C. As postulated by Vlachos et al. the first step of glucose dehydration to levoglucosan in the Brønsted acidic mechanism is a protonation step (see section on mechanistic aspects in ESI†).[11]

It would be a further improvement to use separable and recyclable solid Brønsted acid instead of homogenous acid catalysts in terms of green chemistry or green catalysis[12] which requires that catalysts be designed for easy separation from the reaction products and multi-time efficient reuse/recycling.[13,14,15]

Metal-organic frameworks (MOFs), built from organic ligands (linkers) and metal nodes, are intensively investigated as heterogeneous catalysts.[16,17] Usually, metal-organic frameworks are known for their Lewis acidity, which originates from open metal sites at the secondary building units (SBU).[18] From their porous structure, there are different possibilities to introduce Brønsted acid functionalities, discussed in a detailed review of Jiang and Yaghi.[19] These include encapsulation of Brønsted acidic molecules in the cavity of a MOF, ligation of Brønsted acid groups to metal open sites or (post)synthetic functionalization of linkers with acidic moieties. There are examples for all three types of Brønsted acid functionalities in MOFs with subsequent catalysis.[19] At present there are only a handful of studies dealing with the conversion of biomass using MOFs. Li and Hensen *et al*. demonstrated the Brønsted acidic conversion of fructose and glucose to 5-HMF in DMSO by encapsulating phosphotungstic acid (PTA) in MIL-101Cr, albeit with very low yield of 2% from glucose.[20] Hatton reported a MOF/polymer composite material from MIL-101Cr and poly(N-bromomaleimide) which was able to convert fructose to 5-HMF in 87% yield.[21] A hybrid material containing PTA and ruthenium immobilized on MIL-100Cr was used for the conversion of cellulose and cellobiose into sorbitol.[22] Matsuda and Kitagawa showed that linker functionalization in MIL-101Cr with SO_3H enabled the hydrolysis of cellulose into monosaccharides in water.[23] The same group studied the glucose to fructose isomerization ability of MIL-101Cr derivatives (with bdc-NO_2, -NH_2, -SO_3H; bdc = benzene-1,4-dicarboxylate) in water. MIL-101Cr can have open metal sites that could act as catalysts for glucose to fructose isomerization. The highest activity was found for the NO_2- and the SO_3H-functionalized MIL-101Cr (18.4 and 21.6% conversion to fructose, respectively, after 24 h, 100 °C, 0.2 g catalyst and 25 mg glucose in 2.0 g H_2O).[24] Chen et al. investigated the activity of different SO_3H-functionalized MOFs (MIL-101Cr-SO_3H, UiO-66Zr-SO_3H and MIL-53Al-SO_3H) for the conversion of fructose into 5-HMF in DMSO with a maximum conversion of 90%.[25] To the best of our knowledge, until now no conversion of glucose to 5-HMF using MOF catalysts with yields higher than 16% has been reported. The glucose conversion of 16% was achieved with MIL-101Cr-PMAi-Br with a MIL-101Cr catalyst loading of 6 mol% (or 21 wt%) after 6 h in the solvent DMSO which made product separation difficult (PMAi-Br = poly(N-bromomaleimide-co-divinylbenzene)).[21]

The isomerization of glucose to fructose can be carried out enzymatically but consumes over 10 million tons of glucose isomerase annually, representing the largest industrial use of immobilized enzymes.[26] Glucose isomerase has a narrow operating window concerning pH and temperature.[26] Therefore, it would be highly desirable to carry out a one-pot glucose-to-5-HMF transformation without the need of a separate glucose-to-fructose isomerization.

Recently, we showed that the catalyst activity of nitro-modified MIL-101Cr in benzaldehyde acetalization reaction originates from Brønsted acidity.[27] It has been concluded that inside the pores of MIL-101Cr there exists high proton acidity through polarized chromium-coordinated water molecules (aqua ligands). It is a logical extension to investigate the activity of functionalized MIL-101Cr in the acid catalyzed glucose-to-5-HMF dehydration. We are aware of the better catalytic performance of other heterogeneous catalysts like sulfated ZrO_2 or zeolite-beta,[28] but our aim here is to investigate the potential of MOFs for this cascade reaction. Further, the chosen reaction media is THF/water in order to avoid high boiling solvents (DMSO) and to facilitate separation of 5-HMF. MIL-101Cr and its derivatives are known for their high water stability and uptake.[29,30] MIL-101 is also often used as a catalyst support, e.g., for metal[31] or metal oxide nanoparticles.[32]

In this work we have examined four functionalized MIL-101Cr derivatives for the acid catalyzed conversion of glucose to 5-HMF using a THF/water system. For the first time using a metal-organic framework catalyst a significant conversion of 29% of glucose to 5-HMF has been achieved. In addition the selectivity between the formation of 5-HMF and levulinic acid has been investigated and compared with sulfuric acid and Amberlyst-15 as catalysts.

Experimental

Characterization of catalysts

Powder X-ray diffraction, PXRD patterns were recorded on a Bruker D2 phaser diffractometer in the Bragg-Brentano configuration with Cu- Kα1/α2 radiation (λ = 1.54184 Å), nickel filter and stationary flat-panel low background sample holder in the range 2θ = 5–50° (step width 0.02° in 2θ). Simulated powder patterns were based on single-crystal data and calculated using the STOE Win^{XPOW} software package[33] or Mercury v. 3.3 software[34]. Scanning electron microscopy, SEM images were measured on a JSM6510 with LaB6 cathode. The N_2 sorption measurements were performed on a Quantachrome NOVA 4200e instrument at 77 K. The samples were degassed under high vacuum (10^{-5} Torr) at 150 °C for 3 h, prior to each measurement. The BET surface area was calculated from adsorption isotherm data points in the pressure range $p/p_0 = 0.05 – 0.2$.

Preparation of catalysts

All MIL-101Cr materials were synthesized hydrothermally, utilizing an autoclave and programmable oven according to literature procedures.[30,35] MIL-SO_3H is described here as an example: CrO_3 (3.0 g, 30 mmol), H_2bdc-SO_3Na (6.0 g, 30 mmol) and 12 mol/L HCl (2.2 g, 60 mmol) were dissolved in H_2O and split into four batches of 30 mL each which were transferred into four Teflon-lined stainless steel autoclaves. The solutions were heated at 180 °C for 6 days (heating ramp 5 h; cooling ramp 15 h). For more details see ESI†.

Standard procedure for catalytic reactions

In a typical experiment the MIL-101 catalyst (50 mg) was suspended in a solvent mixture (39:1) of tetrahydrofuran (without stabilizer) (4.875 mL) and water (125 μL) with a total volume of 5 mL. The standard glucose loading was 5.0 wt% (223 mg, 1.24 mmol). The temperature was kept constant at 130 °C through a stirred oil bath around the reaction vial. The reaction was stopped by cooling the reaction mixture to 0 °C. The MIL catalysts were separated with a centrifuge at 4800 rpm for 10 min. and the solution was passed through a syringe filter (0.2 μm diameter).

Standard conditions: catalyst $5.22 \cdot 10^{-5}$ mol, glucose 223 mg (1.24 mmol), solvent 5 mL (THF:H_2O (v:v) 39:1), 130 °C, 24 h.

Concentrations of 5-HMF in the organic THF phase were quantified by GC with external standard calibration (R^2 = 0.9991, R = 0.9995). For more details see ESI†.

Results and discussion

Synthesis and porosity of MOFs

MIL-101Cr[36] is a three-dimensional micro- to mesoporous material based on chromium-terephthalate linkages with the empirical formula $[Cr_3(O)X(bdc)_3(H_2O)_2]$ (bdc = benzene-1,4-dicarboxylate, X = OH or F, depending on synthesis, here X = OH).[37] MIL-101Cr has inner cages of 29 Å and 34 Å diameters with pore aperture windows diameter of up to 16 Å (Fig. 3, Fig. S1 in ESI†).[36] Two of the three Cr(III) octahedra in the trinuclear building unit have terminal aqua ligands, which can potentially be Lewis acid sites.[38,39]

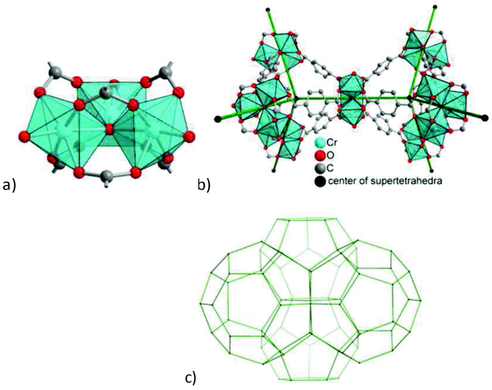

Fig. 3 (a) Trinuclear $\{Cr_3(\mu_3\text{-}O)(OH/F)(H_2O)_2(O_2C\text{-})_6\}$ building unit which is assembed with bridging benzene-1,4-dicarboxylate ligands into (b) vertex-sharing supertetrahedra whose centers form the corners of (c) mesoporous cages with diameters of 29 or 34 Å shown here in a zeolite-type framework presentation with the topological connectivity (in green) of the centers of the vertex-sharing supertetrahedra. Not-to-scale drawings (additional ones in Fig. S1, ESI†) were generated from the deposited X-ray data file at the Cambridge Structure Database (CSD-Refcode OCUNAK)[36] using the program DIAMOND.[40]

MIL-101Cr and its linker-modified derivatives[30,41] show remarkable stability towards water which make them most suitable for applications in the presence of moisture/water.[29,30] In addition, 2-nitro and 2-sulfo-terephthalic acid were selected to compare the influence of different functional groups. The strong electron-withdrawing effect of 2-nitro-modified MIL-101Cr on the catalyst activity was already shown in the diacetalization of benzaldehyde.[27] All modified MIL-101Cr materials were synthesized directly from the linker (2-nitro- or 2-sulfo-terephthalic acid) and CrO_3 under acidic hydrothermal conditions (details in ESI†).[30,35] For mixed-linker MILs a molar ratio of 1:1 of the linkers H_2bdc-NO_2/ H_2bdc-SO_3Na and H_2bdc/H_2bdc-SO_3Na was used in the synthesis. The effective linker ratio was then determined by digestive dissolution and ^1H NMR analysis (Table 1) (spectra in Fig. S ESI†).

The MIL-101 structure of the linker-modified compounds was verified by positive matching of the simulated and measured powder X-ray diffractograms (Fig. S4, ESI†). N_2 sorption isotherms at 77 K showed the typical MIL-101 curvature with two steps up to $p/p_0 = 0.25$ in the otherwise Type Ib isotherm, characteristic for a wider microporous material (Fig. S5, ESI†).[42] BET surface areas and pore volumes were calculated from these N_2 sorption isotherms. Among the four tested catalysts, MIL-NO_2 (2058 m^2/g) has the highest and MIL-SO_3H, (1333 m^2/g) the lowest surface area. In our earlier contribution on the diacetal formation with MIL-101Cr derivatives it could be shown that surface area is not the decisive factor for high catalytic activity, but particle size as well as electron withdrawing or donating functionalities have a higher influence on conversion.[27]

Table 1 Porous properties of MIL-X materials

Materials	BET surface area (m^2/g)[a]	Total pore volume (cm^3/g)[b]	Exp. ratio NO_2:SO_3H or bdc:SO_3H[c]	Number of Brønsted acid sites, in formula unit[d]	Particle diameter ± standard deviation (σ) (nm)[e]
MIL-101Cr	3049	1.50	--	2	174 ± 35
MIL-NO_2	2058	1.18	--	2	168 ± 30
MIL-NO_2/SO_3H	1480	0.75	1:1	3.5	160 ± 41
MIL-SO_3H(0.33)	1633	0.93	2:1	2.99	n.d.[f]
MIL-SO_3H	1333	0.70	--	5	152 ± 43

[a] Calculated in the pressure range $0.05 < p/p_0 < 0.2$ from N_2 sorption isotherm at 77 K. The BET error margin is 20–50 m^2/g. [b] Calculated from N_2 sorption isotherm at 77 K ($p/p_0 = 0.95$) for pores ≤40 nm. [c] Determined by digestion of MOF and ^1H-NMR (see Fig S2, ESI†). [d] From molecular formula based on the possible number of protic H atoms per formula unit (see ESI†) of MIL = $[Cr_3(O)(OH)(bdc\text{-}X)_3(H_2O)_2]$. [e] Obtained from SEM measurements, minimum of 50 particles were counted. [f] Particles are extremely agglomerated, particle size could not be determined (Fig. S3c, ESI†).

Conversion of glucose to 5-HMF

Due to the high importance of platform chemicals derived from biomass, several solid acid catalysts have been investigated for the conversion of glucose to 5-HMF.[19,28] Metal-organic frameworks were investigated for a number of acid-catalyzed reactions,[43] including conversion of fructose and glucose, albeit in a yield of maximum 16% for the latter.[21] Therefore this work focuses on the conversion of glucose to 5-HMF using MOF catalysts.

The conversion of glucose to 5-HMF was performed in the presence of each of the four functionalized MIL catalysts (Fig. 4) and conversion was followed by gas chromatography (GC). In a typical experiment 1.24 mmol glucose (223 mg) in 5 mL THF/water (v:v 39:1),[10] giving a 5 wt% glucose solution, was heated in the presence of catalyst ($5.22 \cdot 10^{-2}$ mmol) for a chosen time at 130 °C in a Pyrex glass vial. For all experiments 4.0 mol% MIL catalyst with respect to glucose was used. In the literature similar glucose or fructose substrate to MOF-catalyst ratios were used.[20,21,25] When glucose was kept in THF/water under the same conditions but in the absence of MIL material no formation of 5-HMF or any other products could be detected which shows that the MIL material is necessary for the catalytic reaction.

Comparing the catalytic activity of the four MIL-101Cr derivatives, the completely SO_3H-functionalized MIL has the highest activity. With 29% yield of 5-HMF (determined by calibrated GC after workup), this result is, to the best of our knowledge, the highest 5-HMF yield obtained with MOFs for the formation of 5-HMF from glucose. Interestingly, the other MOFs MIL-NO_2, MIL-SO_3H(0.33) and MIL-NO_2/SO_3H give lower, but among them very similar HMF yields of about 12 to 13%. Pure MIL-101Cr shows a very low 5-HMF yield of only 2% (standard conditions, 24 h) (Fig. 4a). Interestingly, MIL-NO_2, which has not obvious additional Brønsted acid sites than MIL-101Cr, shows a significant higher 5-HMF yield, probably due to the stronger polarized aqua ligands through the electron-withdrawing nitro groups (Fig. 4a). Hence, the electron-withdrawing effect of the NO_2 and additional acidic SO_3H groups seem to have a strong influence on the catalytic activity of the MIL-101 platform. MIL-SO_3H gives the highest yield of 5-HMF and, therefore, this catalyst has been investigated in more detail.

If we assume that Brønsted acid (BA) catalysis is taking place in the glucose to 5-HMF conversion and we normalize for the number of protons per formula unit (cf. Table 1) the activity becomes highest for MIL-NO_2 with just two BA sites (Fig. 4b). We have tried to determine the number of accessible acidic sites by potentiometric titration according to literature procedures.[44] Typically, the MIL is stirred in a saturated solution of sodium chloride in order to exchange the protons with sodium. Our experiments revealed that MIL materials are not stable under these conditions (see ESI†), since two inflection points were observed although by the backtitration method only one acid strength (HCl/H_2O) should be present. We also followed a recently published approach from Klet and coworkers who used sodium nitrate for proton exchange (see ESI†).[45] Attempts to quantify the amount of available or accessible acid sites remained inconclusive (see ESI†), which is why the theoretical number of acid sites was used (Table 1). We can only state from titration experiments that the amount of accessible protons is much smaller than what is calculated from the formula unit.

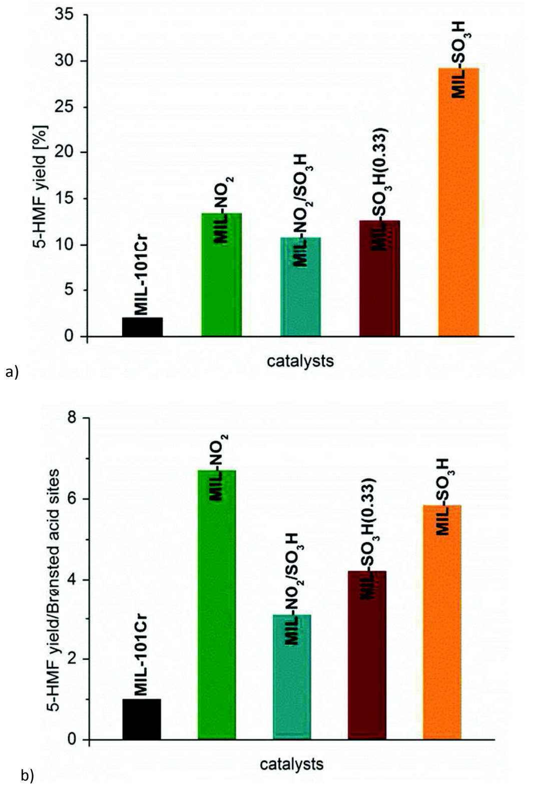

Figure 4 a) Conversion of glucose to 5-HMF with functionalized MIL-X (catalyst $5.22 \cdot 10^{-5}$ mol, 223 mg glucose, 130 °C, 5 mL THF:H_2O (v:v) 39:1, 24 h). b) Normalized to theoretical number of Brønsted acid (BA) sites (cf. Table 1).

Stability and recycling test

In order to prove that no leaching occurs, MIL-SO_3H was tested in a filtration experiment. The reaction was stopped by cooling to 0 °C after 5 hours and the catalyst was separated by centrifugation at 6000 rpm and subsequent filtration of the filtrate using a 0.2 µm syringe filter. The reaction was continued with the filtrate under identical conditions for different times, followed by the standard workup. No further formation of 5-HMF takes place over a time of 18:45 h (Table 2). Small differences of 1% are within experimental error of the reaction procedure, since for every measuring point a new reaction was started.

Table 2 Filtration experiment with MIL-SO_3H

Time (h)	Yield of 5-HMF (%)[a]
5 (reaction was stopped)	10
10	9
12	10
14	12
18.45	11

MIL-SO_3H $5.22 \cdot 10^{-5}$ mol, 223 mg glucose, 130 °C, 5 mL THF:H_2O (v:v) 39:1; new batch was started for every entry at t = 0 h..

Multiple run experiments showed that MIL-SO_3H can be re-used up to 3-4 times with a loss in 5-HMF yield from 29% to 13-16% (Table S3 in ESI†).In a first series of recycle experiments MIL-SO_3H was re-used without any intermediate washing or reactivation steps. In the fourth run the 5-HMF yield was reduced to 13%. Therefore, the experiment was repeated such that after each run the catalyst was washed with water and methanol and dried before re-use. After three runs, a 5-HMF yield of 16% was measured. After three runs the PXRD still shows crystalline MIL-SO_3H (Fig. 5a). The surface area was reduced to half after the first run (443 m^2/g) and essentially lost after four runs (91 m^2/g) (Fig. 5b). The surface area increased only negligibly from 91 m^2/g to 120 m^2/g after washing the MIL-SO_3H material after the third run with HCl (2 mol/L) at 85 °C for 20 h, followed by water and drying (140 °C, 15 h) .

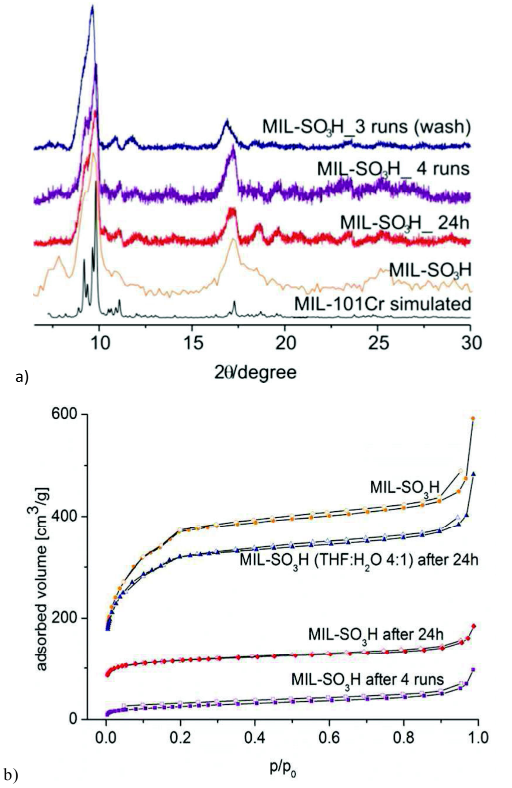

Figure 5 a) PXRD of MIL-SO_3H before and after one catalytic run (24h),4 runs without washing, and after 3 runs with washing (see text). (standard conditions). b) Nitrogen sorption isotherms (Filled symbols for adsorption, empty symbols for desorption) of MIL-SO_3H before and after catalysis with one run (24h), after one run (24h) using an additional 1mL of H_2O in the reaction and after 4 runs without washing. Standard conditions MIL-SO_3H $5.22 \cdot 10^{-5}$ mol, 223 mg glucose, 130 °C, 5 mL THF:H_2O (v:v) 39:1, except for THF:H_2O (v:v) 4:1

Effect of water amount on 5-HMF yield

It was suggested in a molecular simulation study, that MIL-101Cr is able to adsorb glucose from an aqueous solution.[46,47] Since the MIL material is known for its high uptake of water,[29] this might be a driving force for glucose to diffuse into the pores, due to the much better solubility of glucose in water over THF.

In order to elucidate the effect of water on the conversion of glucose, the water content was increased gradually from 39:1 to 1:1. The results in Table 3 show that with increasing water content the yield of 5-HMF becomes lower.

Table 3 Conversion of glucose to 5-HMF with different amounts of water

Ratio THF:water (v:v)[a]	Yield 5-HMF [%][b]
39:1	29
9:1	24
4:1	13
2.3:1	7
1:1	5
pure H_2O	6
pure THF	0

a) Conditions: 50 mg MIIL-SO_3H, 5 wt% glucose, 5 mL solvent, 24 h, 130 °C. [b] Determined by GC

In pure water only very low formation of 5-HMF was detected (6%) and in pure THF no 5-HMF (and no other products) could be detected by GC. Therefore, a small amount of water is not only beneficial, but even necessary for 5-HMF formation. In this respect, our reaction system differs significantly from the sulfuric acid study of Huber and coworkers, since for conc. (water-free) H_2SO_4 also in water-free THF, formation of 5-HMF was detected.[10] A possible explanation might be that the development of full acid strength of the MOF catalyst involves the polarization of water at the chromium centers of the MOFs. Glucose is more soluble in water than in THF. When water is adsorbed by the MIL catalyst this might be the driving force resulting in higher 5-HMF yield, at low amounts of water, having a higher local concentration of glucose in the MIL environment. The glucose concentration in the MOF vicinity would be lowered further with too much or only water as solvent. Additionally, THF is known to stabilize 5-HMF and prevent the formation of levulinic acid.[48] Abu-Omar et al. showed that using NaCl in a THF/H_2O mixture as phase separator, the 5-HMF yield from glucose could be increased from 52% to 61% in comparison to the system without NaCl (catalyst $AlCl_3$, HCl, 160 °C). Since the reaction takes place in water a good phase separation and a good continuous transfer of 5-HMF to the organic THF phase, is necessary.[48] In case of MIL-SO_3H catalysis in THF:H_2O (v:v 39:1) these requirements are apparently fulfilled best.

Formation of humins and deactivation pathways

The degradation of carbohydrates to humins plays a crucial role in glucose conversion and catalyst degradation. This kind of deactivation can be classified as fouling.[49] The formation of humins is not well investigated. Generally, unidentified soluble or insoluble degradation products are called humins.[5b,d,50] Recently, Vlachos et al. investigated the effect of reaction conditions, 5-HMF conversion and acid concentration on the molecular structure and formation of humins, using FTIR spectroscopy, SEM and in–situ dynamic light scattering, DLS.[51] It was concluded that combined effects from aldol condensation and etherification reactions as well as nucleophilic attack from 5-HMF and aggregation effects lead to insoluble polymers, especially at high 5-HMF formation.[51] These by-products can block the pores that no substrate can migrates in and no product can form or migrate out anymore.

If the degradation products are also formed inside the pores, they block the MOF pores, which lead to deactivation.

With increasing amount of water in the reaction solvent the yield of 5-HMF became lower (see Table 3). Yet, with increasing water fraction also less insoluble humin products are formed as evidenced from the color retention of the MIL and weight of the solid materials after the reaction (Fig. S6 and Table S2 in ESI†). To determine the amount of insoluble humins which have formed, the solid material was separated by centrifugation and dried (120 °C, overnight). The weights are listed in Table S2. Also, with increasing water fraction the BET surface area of MIL-SO_3H is diminished less after one catalytic run (Fig. 5b). When the catalytic reaction was carried out in a THF/water mixture of 4:1, the MIL-SO_3H catalyst, still had a BET surface area of 1161 m^2/g after the first run.

Another way to inhibit the formation of insoluble humans may be to deactivate the polymerizable sites of 5-HMF. Therefore, experiments were performed using ethanol in a mixture with THF and water (Table 4). In the presence of ethanol also the formation of 5-ethoxymethylfurfural (5-Ethyl-HMF) was observed in addition to 5-HMF. The higher the amount of ethanol the higher was the yield of 5-Ethyl-HMF.

Table 4 Product distribution in different solvent mixtures.

Solvent mixture (v:v)[a]	Yield 5-HMF [%] [b] 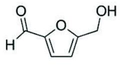	Yield 5-Ethyl-HMF [%] [b] 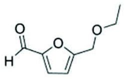	MIL-SO_3H surface area S_{BET} [m^2/g] after reaction
THF/H_2O (39:1)	29	0	443
THF/EtOH/H_2O (23:16:1)	13	7	1028
EtOH/H_2O (39:1)	5	11	1239

a) Conditions: MIIL-SO_3H 50 mg, glucose 223 mg, 5 mL solvent, 24 h, 130 °C. b) Determined by calibrated GC

The amount of insoluble humins seemed to be reduced when the reaction was carried out in ethanol/H_2O, evidenced by the retention of the MIL porosity, its color and amount of catalyst (Fig. S6, S7, Table S2 in ESI†). Unfortunately, in EtOH/H_2O the overall yield and product selectivity is much lower than in the THF:H_2O (v:v 39:1) mixture (Table 4).

Time profile

The yield of 5-HMF slowly approaches the determined value over the maximum allowed reaction time of 24h under our standard conditions (Fig. 6). The space-time yield is much lower than with other catalysts such as sulfuric acid,[10] $AlCl_3$,[52] montmorillonite K-10 clay[53] or beta zeolites[54], where saturation is observed within 40 min to 5 h. This difference in reaction rate can give a hint on the reaction mechanism, since it was suggested with homogeneous $AlCl_3$/solvent/H_2O that the catalysis proceeds by glucose to fructose isomerization (Lewis acid catalyzed) and subsequent dehydration to 5-HMF.

This reaction route seems much faster than only Brønsted acid catalyzed conversion by homogeneous sulfuric acid.[11,55]

Glucose signals were still detected after 8 and 15 h when the reaction was stopped by cooling after 8, 15 and 24 h and analyzed by NMR in D_2O (Fig. S9, ESI†). After 24 h no saccharide signals were seen anymore in the NMR spectrum (Fig. 9).

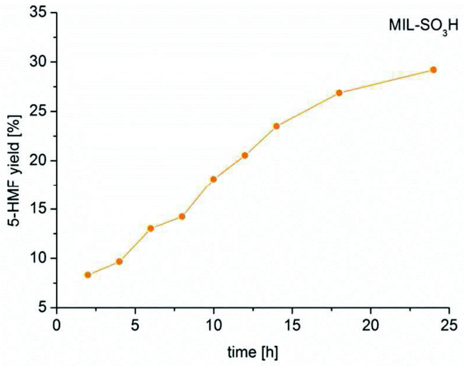

Figure 6 Time dependent conversion of glucose to 5-HMF. Standard conditions: catalyst 50 mg, glucose 223 mg, 5mL THF:H_2O (v:v) 39:1, 130 °C.

Assuming that the conversion of glucose takes place inside the pores or at least in the pore mouths of the MOF, diffusion limitations can be the reason for the slow conversion.

When decreasing the temperature to 100 °C under standard conditions the formation of 5-HMF is even slower, after 24 h only 8% can be detected. At 100 °C only formation of 5-HMF and the starting material is visible from NMR (in D_2O); no by-products are formed (Figure S8d).

Conversion of other substrates to 5-HMF

Reaction of maltose (5 wt%, 0.65 mmol) with MIL-SO_3H resulted in a conversion of 50% to 5-HMF. Maltose is a glucose-dimer with the two monomer units connected through a glycosyl-bond. The same mass of maltose contains almost the same amount of glucose monomer units as in 223 mg glucose used in our standard conditions. Since the 5-HMF yield from maltose is higher than from glucose, it seems that the (unknown) intermediate state is easier accessible from the dimer maltose. Also, the possible intermediates levoglucosan and fructose were used as starting materials and the reaction was performed under standard conditions (50 mg MIL-SO_3H, 1.24 mmol sugar, THF:H_2O (v:v) 39:1, 130 °C). With levoglucosan after 8 h a 5-HMF formation of 12% and after 24 h of 28% was measured with GC. It is evident, that 5-HMF can be formed also from levoglucosan, but only to a similar extent as from glucose.

It has already been shown by several groups that fructose can be converted to 5-HMF in good yields by Brønsted acidic MOF materials in other solvents.[20,25] In our study, a maximum yield of 5-HMF of 47% was obtained after 8 h under standard conditions. As expected the conversion of fructose proceeds much faster than the conversion of glucose. The formation of humins was also observed with fructose, levoglucosan and maltose by color and weight change.

Cellulose with MIL-SO_3H shows almost no formation of 5-HMF (1 %). This could indicate that the long polymer chains of cellulose cannot enter the pores of MIL-SO_3H for conversion or alternatively, that the chains are not cleaved to a sufficient extent.

Formation of 5-HMF versus levulinic acid

When 5-HMF is dissolved in THF/water (v:v 39:1) and reacted at 130 °C for 24 h with the catalyst MIL-SO_3H, no reaction is observed, only the starting material 5-HMF can be detected by GC or GC-MS. ^1H NMR of the reaction solution (without workup) showed only trace amounts of levulinic acid (molar ratio 5-HMF to levulinic acid 1:0.04). The catalyst also retained its green color instead of changing to brown, which indicates no formation of humins as in the glucose conversion. In contrast Dumesic and coworkers showed that other catalysts as for instance H_2SO_4, Amberlyst-70 or zeolites will give levulinic acid from furfuryl alcohol in THF/H_2O solutions with levulinic acid yields of over 70%.[57]

The selectivity of the glucose-to-5-HMF conversion concerning the formation of levulinic acid as by-product was analzyed by NMR. Since levulinic acid is very good soluble in water, the complete reaction solution was dried in vacuum, the residue re-disolved in deuterated solvent and then measured. All reactions have been performed under standard conditions for 24 h, unless stated otherwise.

With MIL-SO_3H and glucose the selectivity towards 5-HMF over levulinic acid is 80%, since the molar ratio between 5-HMF and levulinic acid is 1 to 0.25 after 24 h (Table 5, Fig. 7).

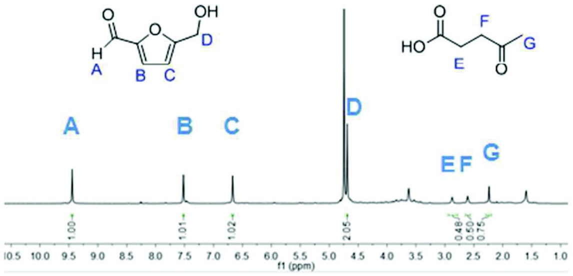

Figure 7 ^1H NMR spectrum of the soluble reaction products from glucose (50 mg MIL-SO_3H, 223 mg glucose, 5mL THF:H_2O (v:v) 39:1, 130 °C, 24 h) (NMR solvent D_2O). The 5-HMF to levulinic acid ratio was based on the integral ratio of the of the CH_2 groups, that is, the D and the average of the E and F signals.

After 8 h and 15 h reaction time the selectivity towards 5-HMF over levulinic acid is even higher (88% and 86%, respectively) and decreases with time (Table 5 and Fig. S9). This indicates that 5-HMF also slowly converts to levulinic acid. As pure 5-HMF with MIL-SO_3H shows only a very low conversion over 24 h (see above) other reaction products may assist in this conversion.

Table 5 Time dependent analysis of reaction mixture by NMR.[a]

Time (h)	Integral ratio 5-HMF vs. levulinic acid[d]	Selectivity of 5-HMF over levulinic acid
8	1:0.13	88%
15	1:0.16	86%
24	1:0.25	80%
24h[b]	1:0.09	92%
24h[c]	1:0.21	83%

[a] Conditions: 50 mg MIIL-SO_3H, 5 wt% glucose, 5 mL THF:H_2O (v:v) 39:1, 130 °C. Determined by ^{1}H-NMR in D_2O. [b] Fructose as substrate (1.24 mmol).[c] Levuglucosan as substrate (1.24 mmol). [d] Integral ratio of CH_2 groups: D (5-HMF) and the average of the E and F signal (levulinic acid), see Fig. 9.

For comparison MIL-SO_3H is also reacted with levoglucosan (1.24 mmol) and fructose (1.24 mmol) as substrate and similar ratios between 5-HMF and levulinic acid were obtained (Figure S8a,b, Table 5). Interestingly, the ^{1}H NMR of the glucose conversion with MIL-NO_2 shows signals of 5-HMF, but no levulinic acid is found. Only some signals of unidentified products can be found (Figure S8c). In summary, MIL-SO_3H shows the highest yield of 5-HMF which correlates with the highest potential number of acid sites of the MIL-materials (Fig. 4), whereas MIL-NO_2 shows a very selective formation of 5-HMF since no levulinic acid was found.

For comparison chromium(III) nitrate, sulfuric acid and Amberlyst-15 have been tested as catalysts ($1.57 \cdot 10^{-4}$ mol) for the formation of 5-HMF under the same conditions as the MIL-materials (THF:H_2O (v:v) 39:1, 130 °C, 223 mg glucose) for 24 h. $CrCl_3$ is known to catalyze the isomerization from glucose to fructose. Also formation of 5-HMF, levulinic acid and formic acid was observed with $CrCl_3$.7[a,56] In contrast to MIL-SO_3H the yield of 5-HMF from glucose catalyzed by $Cr(NO_3)_3$ is only 6% after 24 h. Interestingly. no levulinic acid was detected, but a high amount of unidentified products can be observed by NMR and GC-MS. The high formation of by-products in case of Cr^{3+} salts is supported by a comprehensive study of Vlachos et al.7[a]

Comparing the product distribution using MIL-SO_3H as catalyst or H_2SO_4 as homogenous catalyst or the strong acidic resin Amberlyst-15, starting from glucose a significant change can be observed (Fig. 8 and S10). For Amberlyst-15 the selectivity is strongly directed to levulinic acid, with a ratio of 5-HMF to levulinic acid 1:3 (5-HMF selectivity only 25%). For sulfuric acid as catalyst the major dominant product is also levulinic acid. The ratio between 5-HMF and levulinic acid is 1:10 (5-HMF selectivity 9%).

Recently, Dumesic et al. reported the conversion of furfuryl alcohol into levulinic acid using different solid acids (including Amberlyst-70 and H-ZSM-5) as well as sulfuric acid in a similar THF/water system.[57] Huber et al. reported the formation of levulinic acid as by-product from glucose conversion to 5-HMF with sulfuric acid (catalyst).[10]

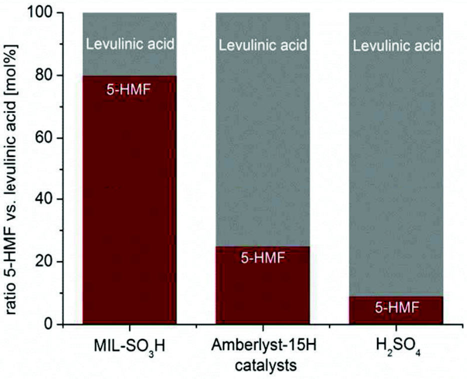

Figure 8 Ratio between 5-HMF and levulinic acid from ^{1}H-NMR. Comparison between MIL-SO_3H, H_2SO_4 and Amberlyst-15H. Conditions: catalyst MIL-SO_3H $5.22 \cdot 10^{-5}$ mol, glucose 223 mg, 5ml THF:H_2O (v:v) 39:1, 130 °C. For H_2SO_4 and Amberlyst-15 the reaction was conducted with $1.57 \cdot 10^{-4}$ mol of the catalyst under the same conditions. The estimated amount of acid of MIL-SO_3H, Amberlyst-15 and sulfuric acid is 0.46 mmol H^+/g (see Table S4), 4.7 mmol H^+/g (AMBERLYST^{TM} product information) and 10.2 mmol H^+/g, respectively.

It is evident that the ratio of 5-HMF to levulinic acid inversely proportional to the acidity of the catalyst. The significantly lower actual acidity of MIL-SO_3H compared to Amberlyst-15 and H_2SO_4 explains the low high ratio of 5-HMF to levulinic acid. The even lower acidity of MIL-NO_2 then explains the absence of levulinic acid. At present it is not fully clear if 5-HMF is converted to levulinic acid. Levulinic acid could also form through a 5-HMF independent pathway (see section on mechanistic aspects in ESI†).[11]

The 5-HMF yield varies only slightly, essentially within experimental error, with the amount of MIL-SO_3H catalyst (Fig. 9).

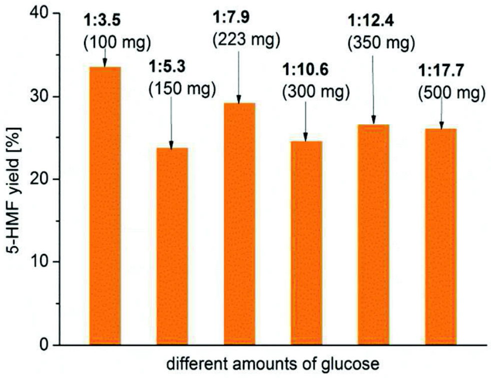

Figure 9 Conversion of glucose to 5-HMF with different amounts of glucose and MIL-SO_3H as catalyst (given is the molar Cr(III) ($1.57 \cdot 10^{-4}$ mol) to glucose ratio (catalyst $5.22 \cdot 10^{-5}$ mol, 130 °C, 5 mL THF:H_2O (v:v) 39:1, 24 h).

Increasing the ratio of MIL-SO_3H to glucose from the standard of 1:7.9 (223 mg glucose) to 1:3.5 (100 mg glucose) gives a yield of 5-HMF of 34% (up from 29%). Decreasing the ratio of MIL-SO_3H to glucose to 1:17.7 (500 mg), a slight decrease in 5-HMF formation to 26% can be observed (Fig. 9). These results show that the catalyst remains active also at higher concentration of glucose and the percentage yield does not change significantly with a moderate variation of the substrate ratio.

The scope of using MOFs as catalyst in the synthesis of fine chemicals is summarized elsewhere[16,58], but the advantage of selective catalysis in 5-HMF formation is already obvious. Synergistic effects due to reactions catalyzed in confined space are highlighted in literature[59] and could be an important factor explaining the selectivity towards 5-HMF using MILs as catalysts. A defined solvent microenvironment due to preferred uptake of water by the MIL catalyst can also play a role.

Conclusions

For different nitro- and sulfo-modified MIL-101Cr compounds MIL-SO_3H gives the highest yield of 5-HMF from glucose with 29% after 24 h. This yield is lower than results obtained with other solid acid catalysts,[28] but at present the highest value reported for the glucose-to-5-HMF conversion catalyzed by metal-organic frameworks. Importantly, it could be shown, that the reaction only proceeds with a small amount of water. In pure THF no product formation was observed. Furthermore, also from pure 5-HMF as reactant, only very little production of levulinic acid could be detected, in contrast to results in literature using sulfuric acid[10] or Amberlyst-70.[57] Under the same conditions MIL-SO_3H, sulfuric acid and Amberlyst-15 show significantly different 5-HMF/levulinic acid product distributions. MIL-SO_3H preferentially forms 5-HMF over levulinic acid in contrast to the other catalysts. Reactivation of the MOF catalyst remains a challenge, since pore blocking effects have been observed in multiple run experiments. Derivatisation to 5-Ethyl-HMF is a promising way, avoiding the formation of insoluble humins. At present the 5-Ethyl-HMF yield is low, awaiting the development of more active MOF-based acidic catalysts.

Acknowledgements

The work was funded in part by the Deutscher Akademischer Austauschdienst, DAAD through PPP-project no 57053987 (China 2j ab 14).

References

1 a) P.Gallezot, *Chem. Soc. Rev*., 2012, **41**, 1538–1558; b) S. Dutta and S. Pal, *Biomass and Bioenergy*, 2014, **62**, 182–197; c)
2 C. Chatterjee, F. Pong and A. Sen, *Green Chem.*, 2015, **17**, 40–71.
3 a) A. A. Koutinas, A. Vlysidis, D. Pleissner, N. Kopsahelis, I. L. Garcia, I. K. Kookos, S. Papanikolaou, T. H. Kwan and C. S. K. Lin, *Chem. Soc. Rev*, 2014, **43**, 2587–2627; b) D. Esposito and M. Antonietti, *Chem. Soc. Rev.*, 2015, **44**, 5821–5835.
4 T. Wang, M. W. Nolte and B. H. Shanks, *Green Chem.*, 2014, **16**, 548–572.
5 R. Beerthuis, G. Rothenberg and N. R. Shiju, *Green Chem.*, 2015, **17**, 1341–1361.
6 a) B. Saha and M. M. Abu-Omar, *Green Chem.*, 2014, **16**, 24–38; b) R. van Putten, J. C. van der Waal, E. de Jong, C. B. Rasrendra, H. J. Heeres and J. G. de Vries, *Chem. Rev.*, 2013, ***113***, 1499–1597; c) S. P. Teong, G. Yi and Y. Zhang, *Green Chem.*, 2014, **16**, 2015–2026; d) A. A. Rosatella, S. P. Simeonov, R. F. M. Frade, C and A. M. Afonso, *Green Chem.*, 2011, **13**, 754–793.
7 a) V. Choudhary, S. H. Mushrif, C. Ho, A. Anderko, V. Nikolakis, N. S. Marinkovic, A. I. Frenkel, S. I. Sandler and D. G. Vlachos, *J. Am. Chem. Soc.* 2013, **135**, 3997–4006; b) J. Tang, X. Guo, L. Zhu, and C. Hu, *ACS Catal.*, 2015, **5**, 5097–5103.
8 C. Liu, J. M. Carraher, J. L. Swedberg, C. R. Herndon, C. N. Fleitman and J. Tessonnier, *ACS Catal.*, 2014, **4**, 4295–4298.
9 J. M. Carraher, C. N. Fleitman and J. Tessonnier, *ACS Catal.*, 2015, **5**, 3162–3173.
10 R. Weingarten, A. Rodriguez-Beuerman, F. Cao, J. S. Luterbacher, D. Martin Alonso, J. A. Dumesic and G. W. Huber, *ChemCatChem*, 2014, **6**, 2229–2234.
11 L. Yang, G. Tsilomelekis, S. Caratzoulas and D. G. Vlachos, *ChemSusChem*, 2015, **8**, 1334–1341.
12 R. A. Sheldon, *Chem. Commun.*, 2008, **29**, 3352-3365.
13 P. Wasserscheid and T. Welton in *Ionic Liquid in Synthesis*, 2007, **1**, Wiley-VCH, Weinheim, 325–350.
14 P. Wasserscheid and W. Keim, *Angew. Chem. Int. Ed.*, 2000, **39**, 3773-3789; *Angew. Chem.*, 2000, **112**, 3926–3945.
15 C. van Doorslaer, Y. Schellekens, P. Mertens, K. Binnemanns and D. De Vos, *Phys. Chem. Chem. Phys.*, 2010, **12**, 1741–1749.
16 P. Garcia-Garcia, M. Müller and A. Corma, *Chem. Sci.*, 2014, **5**, 2979–3007.
17 J. Gascon, A. Corma, F. Kapteijn and F. X. Llabres i Xamena, *ACS Catal.*, 2014, **4**, 361–378.
18 a) F. Vermoortele, M. Vandichel, B. Van de Voorde, R. Ameloot, M. Waroquier, V. Van Speybroeck and D. E. De Vos, *Angew. Chem. Int. Ed.*, 2012, **51**, 4887–4890; b) P. Valvekens, F. Vermoortele and D. De Vos, *Catal. Sci. Technol*., 2013, **3**, 1435–1445.
19 J. Jiang and O. M. Yaghi, *Chem. Rev.*, 2015, **115**, 6966–6997.
20 Y. Zhang, V. Degirmenci, C. Li, E. and J. M. Hensen, *ChemSusChem*, 2011, **4**, 59–64.
21 L. Bromberg, X. Su, and T. A. Hatton, *Chem. Mater.*, 2014, **26**, 6257–6264.
22 J. Chen, S. Wang, J. Huang, L. Chen, L. Ma, X. Huang, *ChemSusChem*, 2013, **6**, 1545–1555.
23 G. Akiyama, R. Matsuda, H. Sato, M. Takata and S. Kitagawa, *Adv. Mater*., 2011, **23**, 3294–3297.
24 G. Akiyama, R. Matsuda, H. Sato and S. Kitagawa, *Chem. Asian J.*, 2014, **9**, 2772–2777.
25 J. Chen, K. Li, L. Chen, R. Liu, X. Huang and D. Ye*, Green Chem.* 2014, **16**, 2490–2499.
26 R. DiCosimo, J. McAuliffe, A. J. Poulose and G. Bohlmann, *Chem. Soc. Rev*., 2013, **42**, 6437–6474
27 A. Herbst, A. Khutia and C. Janiak, *Inorg. Chem.*, 2014, **53**, 7319–7333.
28 a) T. D. Swift , H. Nguyen, Z. Erdman, J. S. Kruger, V. Nikolakis and D. G. Vlachos, *J. Catal.*, 2016, **333**, 149–161; b) I. Jiménez-Morales, A. Teckchandani-Ortiz, J. Santamaría-González, P. Maireles-Torres and A. Jiménez-López, *Appl. Catal. B,* 2014, **144**, 22–28; c) J. Wang, J. Ren, X. Liu, J. Xi, Q. Xia, Y. Zu, G. Lu and Y. Wang, *Green Chem.*, 2012, **14**, 2506-2512; d) H. Yan, Y. Yang, D. Tong, X. Xiang and C. Hu, *Catal. Commun*., 2009, **10**, 1558–1563.
29 a) A. Khutia, H. Urs Rammelberg, T. Schmidt, S. Henninger and C. Janiak, *Chem. Mater*., 2013, **25**, 790−798; b) J. Ehrenmann, S. K. Henninger and C. Janiak, *Eur. J. Inorg. Chem*., 2011, **4**, 471–474.
30 G. Akiyama, R. Matsuda, H. Sato, A. Hori, M. Takata and S. Kitagawa, *Micropor. Mesopor. Mater.*, 2012, **157**, 89–93.

31 M. Trivedi, Bhaskaran, A. Kumar, G. Singh, A. Kumar and N. P. Rath, *New J. Chem.*, 2016, **40**, 3109-3118; N. Cao, T. Liu, Jun Su, X. Wu, W. Luo and G. Cheng, *New J. Chem.*, 2014, **38**, 4032-4035;

32 M. Saikia, D. Bhuyan and L. Saikia, *New J. Chem.*, 2015, **39**, 64-67.

33 STOE WinXPOW Version 1.10; STOE and Cie GmbH, Darmstadt, Germany, 2002.

34 Mercury - Program for Crystal Structure Visualisation, Exploration and Analysis, The Cambridge Crystallographic Data Centre (CCDC), Version 3.3.1.

35 Y. Lee, Y. Chung and W. Ahn, *RSC Adv.*, 2014, **4**, 23064–23067.

36 G. Férey, C. Mellot-Draznieks, C. Serre, F. Millange, J. Dutour, S. Surble and I. Margiolaki, *Science*, 2005, **309**, 2040–2042.

37 T. Zhao, F. Jeremias, I. Boldog, B. Nguyen, S. K. Henninger and C. Janiak, *Dalton Trans*., 2015, **44**, 16791–16801.

38 Y. K. Hwang, D.-Y. Hong, J.-S. Chang, S. H. Jhung, Y.-K. Seo, J. Kim, A. Vimont, M. Daturi, C. Serre and G. Férey, *Angew. Chem. Int. Ed.*, 2008, **47**, 4144–4148.

39 D.-Y. Hong, Y. K. Hwang, C. Serre, G. Férey and J.-S. Chang, *Adv. Funct. Mater.,* 2009, **19**, 1537–1552.

40 K. Brandenburg, Diamond (Version 3.2), crystal and molecular structure visualization, *Crystal Impact*, K. Brandenburg & H. Putz Gbr, Bonn, Germany, 2007–2012.

41 M. Lammert, S. Bernt, F. Vermoortele, D. E. De Vos and N. Stock, *Inorg. Chem.*, 2013, **52**, 8521–8528.

42 a) M. Thommes, K. Kaneko, A. V. Neimark, J. P. Olivier, F. Rodriguez-Reinoso, J. Rouquerol and K. S. W. Sing, *Pure Appl. Chem.*, 2015, **87**, 1051–1069; b) K. S. W. Sing, D. H. Everett, R. A. W. Haul, L. Moscou, R. A. Pierotti, J. Rouquerol and T. Siemieniewska, *Pure Appl. Chem*., 1985, **57**, 603–619.

43 A. Dhakshinamoorthy, M. Opanasenko, J. Cejka and H. Garcia, *Catal. Sci. Technol.*, 2013, **3**, 2509–2540.

44 a) J. Chen, K. Li, R. Liu, X. Huang and D. Ye, *Green Chem.,* 2014 **16**, 2490–2499; b) S. Chen, T. Yokoi, C. Tang, L. Jang, T. Tatsumi, J. C. C. Chan and S. Cheng, *Green Chem*., 2011, **13**, 2920–2930; c) Y. Zang, J. Shi, F. Zhang, Y. Zhong and W. Zhu, *Catal. Sci. Technol.*, 2013, **3**, 2044–2049. d) Z. Hasan, J. W. Jun and S. H. Jhung, *Chemical Engineering Journal*, 2015, **278**, 265–271.

45 R. C. Klet, Y. Liu, T. C. Wang, J. T. Hupp and O. K. Farha, *J. Mater Chem. A.*, 2016, **4**, 1479–1485.

46 K. M. Gupta, K. Zhang and J. Jiang, *Scientific Reports*, 2015, **5**, 12821–12830.

47 P. Bai and J. I. Siepmann*, AIChE Journal,* 2013, **59**, 3523-3529.

48 Y. Yang, C. Hu and M. M. Abu-Omar, *Green Chem.,* 2012, **14**, 509–513.

49 I. Sádaba, M. López Granados, A. Riisager and E. Taarning, *Green Chem*., 2015, **17**, 4133–4145.

50 J. Lange, *Angew. Chem.,* 2015, **127**, 13382–13394

51 G. Tsilomelekis, M. J. Orella, Z. Lin, Z. Cheng, W. Zheng, V. Nikolakis and D. G. Vlachos, *Green Chem*., 2016, **18**, 1983-1993.

52 Y. J. Pagan-Torres, T Wang, J M. R. Gallo, B H. Shanks and J. A. Dumesic, *ACS Catal.*, 2012, **2**, 930–934.

53 Z. Fang, B. Liu, J. Luo, Y. Ren, Z. Zhang, *Biomass and Bioenergy*, 2014, **60**, 171–177.

54 R. Otomo, T. Yokoi, J. N. Kondo and T. Tatsumi, *Appl. Catalysis A: General*, 2014, **470**, 318–326.

55 R.van Putten, J. N. M. Soetedjo, E. A. Pidko, J. C. van der Waal, E. J. M. Hensen, E. de Jong and H. J. Heeres, *ChemSusChem*, 2013, **6**, 1681–1687.

56 P. Wrigstedt, J. Keskiväli, M. Leskelä and T. Repo, *ChemCatChem*, 2015, **7**, 501–507.

57 M. A. Mellmer, J. M. R. Gallo, D. M. Alonso and J. A. Dumesic, *ACS Catal.*, 2015, **5**, 3354–3359.

58 A. Dhakshinamoorthy and H. Garcia, *ChemSusChem*, 2014, **7**, 2392–2410

59 a) C. Yu and J. He, *Chem. Commun*., 2012, **48**, 4933–4940; b) R. De Clercq, M. Dusselier, C. Christiaens, J. Dijkmans, R. I. Iacobescu, Y. Pontikes and B. F. Sels, *ACS Catal.*, 2015, **5**, 5803–5811; c) S. H. A. M. Leenders, R. l. Gramage-Doria, B. de Bruin and J. N. H. Reek, *Chem. Soc. Rev.*, 2015, **44**, 433–448.

Supporting Information

Selective glucose conversion to 5-hydroxymethylfurfural (5-HMF) instead of levulinic acid with MIL-101Cr MOF-derivatives

Annika Herbst and Christoph Janiak*
Institut für Anorganische Chemie und Strukturchemie, Heinrich Heine Universität Düsseldorf, Universitätsstraße 1, D-40225 Düsseldorf, Germany

Corresponding author email: janiak@uni-duesseldorf.de

Additional emails: annika.herbst@hhu.de

Materials

Reagents were purchased from the following distributors and used without further purification, except for THF which was distilled prior to use, to remove the stabilizer and except for the Amberlyst resin, which was dried at 110 °C before use.

Chromium(III) nitrate nonahydrate (99 %), terephthalic acid (99+ %), 2-nitroterephthalic acid (99+%) and 5-hydroxymethylfurfural (98%) from Acros Organics. *N,N*-Dimethylformamide (99.9 %), sulfuric acid (95%) from VWR. Methanol and ethanol (99.9 %) from Merck.

Monosodium 2-sulfoterephthalic acid (>98.0%) and levoglucosan (>99.0 %) from TCI

D-(+)-glucose, >99.5% (GC), cellulose (microcrystalline, powder) and levulinic acid (98%) from Sigma Aldrich, D(+)-maltose (>95%) from Roth, Amberlyst-15(H), wet from Alfa Aesar.

Synthesis

All MIL-101Cr materials were synthesized hydrothermally, utilizing an autoclave and programmable oven for heating according to literature procedures.[j]

MIL-101Cr-NO_2 (**MIL-NO_2**): CrO_3 (0.75 g, 7.5 mmol), $H_2BDC-NO_2$ (1.58 g, 7.5 mmol) and 12 mol/L HCl (1.1 g, 30 mmol) were dissolved in H_2O (30 mL), then transferred into a Teflon-lined stainless steel autoclave. This acidic solution was heated at 180 °C for 6 days (heating ramp 5 h; cooling ramp 15 h).

MIL-101Cr-SO_3H(0.33) (**MIL-SO_3H(0.33)**): CrO_3 (0.75 g, 7.5 mmol), $H_2BDC-SO_3Na$ (1.00 g, 3.75 mmol), H_2BDC (0.62 g, 3.75 mmol) and 12 mol/ HCl (1.02 g, 28 mmol) were dissolved in H_2O (34 mL), then transferred into a Teflon-lined stainless steel autoclave. This acidic solution was heated at 180 °C for 6 days (heating ramp 5 h; cooling ramp 15 h).

---

[j] Y. Lee, Y. Chung and W. Ahn, *RSC Adv.* 2014, **4**, 23064–23067. G. Akiyama, R. Matsuda, H. Sato, A. Hori, M. Takata and S. Kitagawa, *Micropor. Mesopor. Mater.*, 2012, **157**, 89–93.

MIL-101Cr-NO_2/SO_3H (**MIL-NO_2/SO_3H**): CrO_3 (0.75 g, 7.5 mmol), H_2BDC-SO_3Na (1.00 g, 3.75 mmol), H_2BDC-NO_2 (0.79 g, 3.75 mmol) and 12 mol/L HCl (1.02 g, 28 mmol) were dissolved in H_2O (34 mL), then transferred into a Teflon-lined stainless steel autoclave. This acidic solution was heated at 180 °C for 6 days (heating ramp 5 h; cooling ramp 15 h).

MIL-101Cr-SO_3H (**MIL-SO_3H**): CrO_3 (3.0 g, 30 mmol), H_2BDC-SO_3Na (6.00 g, 30 mmol) and 12 mol/L HCl (2.2 g, 60 mmol) were dissolved in H_2O (4x30 mL), then transferred into 4 Teflon-lined stainless steel autoclaves. This acidic solution was heated at 180 °C for 6 days (heating ramp 5 h; cooling ramp 15 h).

Activation procedure for above MIL materials: The green solids were stirred overnight with 80 mL of H_2O. After the water washing procedure, the centrifuged product was stirred in 150 mL of ethanol at reflux overnight. The solid was centrifuged off, suspended in fresh ethanol (150 ml) and stirred at reflux for 3 days. The procedure was repeated again with 150 mL of fresh ethanol. Finally, the products were collected by centrifugation and dried at 110 °C overnight.

Yields

MIL-NO_2: 1.06 g, 17 %,

MIL-SO_3H(0.33): 1.32 g, 21%,

MIL-SO_3H/NO_2: 1.32 g, 20 %,

MIL-SO_3H: 9.2 g, 32 %.

MIL-101Cr: Terephthalic acid (0.66 g, 4.0 mmol) was added to an aqueous solution of TMAOH (20 mL, 0.05 mol/L) and stirred for 10 min at room temperature. $Cr(NO_3)_3 \cdot 9H_2O$ (1.6 g, 4.0 mmol) was added and the mixture was stirred again for 20 min. The suspension was transferred into a Teflon-lined autoclave and was heated to 180 °C for 24 h (heating ramp 10 h; cooling ramp 18 h).

Activation procedure: The green solid was washed (in the given order) with 90 mL H_2O, 90 mL DMF and 90 mL ethanol. After the water washing procedure, the centrifuged product was stirred in 90 mL DMF overnight at room temperature and then heated in the dispersion for 6 h at 110 °C. After cooling to room temperature the powder was centrifuged off and re-suspended in 90 mL ethanol. The mixture was stirred again at room temperature overnight and then heated for 2 d at 90 °C in ethanol. Finally, the products were collected by centrifugation and dried at 70 °C overnight

Yield: 0.73 g 47 %.

For catalyst activation the materials were dried prior to each experiment at 140 °C for 15 h in air.

Characterization techniques

NMR spectra were measured on a Bruker Avance III – 600 and 300 and a Bruker Avance DRX 500 spectrometer. ^{1}H shifts were referenced to the deuterated solvent signals for $CDCl_3$ ^{1}H: $\delta = 7.26$ ppm and for spectra in D_2O ^{1}H shifts were referenced to the signal of 3-(trimethylsilyl)propionic-2,2,3,3-d_4 acid sodium salt with $\delta = 0$ ppm.

NMR reaction control experiments

The ratio between 5-HMF and levulinic acid was determined by ^{1}H NMR in $CDCl_3$. Also NMR spectra in D_2O have been measured, to identify all reaction products. All NMR spectra for determination of 5-HMF vs. levulinic acid were measured with D1 = 20 sec. If not stated otherwise the complete reaction solution was dried *in vacuo* and then dissolved in the deuterated solvent, without any workup.

The ratio of mixed linkers in $\underline{\text{MIL-SO}_3\text{H(0.33)}}$ and $\underline{\text{MIL-SO}_3\text{H/NO}_2}$ was determined by digestion of the MIL material in D_2O/NaOD. First the MIL (40 mg) was dissolved in 1 mL of D_2O with 0.15 mL of NaOD/D_2O (40%). To the resulting green solution HCl (conc.) was added adjusting the pH to 10-11. After separation of the main part of precipitated Cr(III)-hydroxide salts by centrifugation, the supernatant solution was measured. It was not possible to improve the quality of NMR spectra by precipitation and resolvation of the linker, because 2-sulfo-terephtalic acid is very good soluble in basic and acidic aqueous solution.

Catalytic conversion of glucose

Standard procedure

The MIL samples were dried at 140 °C for 15 h in air prior to each experiment. The catalytic experiments were conducted in Pyrex glass vials equipped with a cap and a stirrer. The accuracy of the MIL sample weight was 50±0.2 mg. Every experiment was performed at least in duplicate to ensure reproducibility. For every measurement point a new reaction had to be started due to the necessary work up procedure. From every reaction two samples were taken and each sample was measured with GC three times. From the resulting two values the average was taken.

Standard conditions: catalyst $5.22 \cdot 10^{-5}$ mol, glucose 223 mg (1.24 mmol), solvent 5 mL (THF/H_2O 39:1), 130 °C, 24 h.

For other MIL catalysts, the mass (mg) corresponding to $5.22 \cdot 10^{-5}$ mol was used:

MOF	**Mass [mg] corresponding to $5.22\cdot10^{-5}$ mol**
MIl-NO_2	44.3
MIL- NO_2/SO_3H	46.9
MIL-SO_3H(0.33)	41
MIL-SO_3H	50
MIl101Cr	37.4

Analysis of products

Gas chromatographic (GC) analyses were done with a GC-2014 Shimadzu instrument coupled with a flame ionization detector (FID) and a GC-MS Finnigan Trace DSQ with Finnigan Trace GC Ultra System. GC Parameters: Autosampler injection volume 1.0 µL, rinses with solvent pre-run 2x, post-run 1x, rinses with sample 2x; injector temperature 240 °C; column information: Ultra 2 (Ø 0.2 mm x 25 m, 5%-Phenyl)-methylpolysiloxane), column maximum temperature: 320 °C; column oven program: start at 60 °C, hold time 0.30 min, heating 7 °C/min until 115 °C, hold time 1.0 min °C, heating 12°C/min until 200 °C, hold time 0.30 min. Total program time 16.54 min.

Concentrations of 5-HMF in the organic THF phase were quantified by GC with external standard calibration (R^2 = 0.9991, R = 0.9995). It was already shown that at least 93% of 5-HMF is present in the THF phase.[k] Phase separation has been achieved by extracting the reaction mixture with 5 mL saturated sodium chloride solution.

Conversion HMF = (moles of 5-HMF/moles of initial glucose loading) · 100 as determined by GC.

For the 5-HMF conversion only the yields detected by GC in the THF phase after workup are given in the main article.

Possible corrections for maximum yield: Since only 93% of 5-HMF is present in the THF phase (the rest remains in the H_2O phase),[k] the conversion will even be slightly higher. Another factor is the uptake of reaction mixture from MIL-SO_3H itself. Therefore, after the catalyst was separated and the supernatant removed, new THF was added to the catalyst. The mixture was stirred for 1 h and separated again by centrifugation. The supernatant THF solution was analyzed by GC again. After 24h reaction an additional 5-HMF yield of 1.3 % was found.

50 mg MIL-SO_3H (M = 956.7 g/mol) corresponds to $5.22\cdot10^{-5}$ mol, multiplied with three for each Cr atom in the {Cr_3} formula unit gives $1.57\cdot10^{-4}$ mol.

formula unit: $[Cr_3(H_2O)_2(OH)O(O_2CC_6H_3(SO_3H)CO_2)_3]$

---

[k] Y. J. Pagán-Torres, T. Wang, J. M. R. Gallo, B. H. Shanks and J. A. Dumesic, *ACS Catal.*, 2012, **2**, 930–934.

The reference experiments with chromium(III) nitrate nonahydrate, Amberlyst 15 and sulfuric acid were conducted with $1.57 \cdot 10^{-4}$ mol.

Theoretical calculation of Brønsted acid sites of MIL-materials

For each mol of activated and dried MIL-101 formula unit of $[Cr_3(O)(OH)(bdc\text{-}X)_3(H_2O)_2]$ we assume a potential maximum of

2 mol of Brønsted acid sites for X = NO_2 (namely the two terminal H_2O ligands),

5 mol of Brønsted acid sites for X = SO_3H (two terminal H_2O and three SO_3H),

2.99 mol of Brønsted acid sites for X = $SO_3H(0.33)$ (two terminal H_2O and 3x0.33 SO_3H),

3.5 mol of Brønsted acid sites for X = $NO_2(0.5)/SO_3H(0.5)$ (two terminal H_2O and 3x0.5 SO_3H)

Table S1 Retention times of reagents and products in GC measurement

Compound	Retention time [min]	Compound
THF	1.03	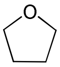
HMF	6.97	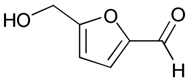
Levulinic acid	4.5	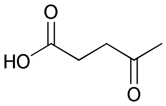

Filtration test

After running the catalytic glucose to 5-HMF reaction for the chosen time, the mixture was cooled to 0 °C and the catalyst was separated by centrifugation. The clear supernatant solution was filtered with a syringe filter of the type RC 0.2 µm. The reaction was continued with the filtrate in a new reaction vial under identical reaction conditions for at least 18:45 h. Then the standard workup procedure was performed and the filtrate was analyzed by GC.

Recycling test

For experiments with multiple runs each catalytic reaction was run for 24 h, stopped by cooling to 0 °C and centrifuged until the supernatant solution was visibly clear (10 min). With the clear solution the standard workup procedure was performed and a sample for GC analysis was collected.

The catalyst was washed one time with THF (4 ml) and dried at 140°C for ca. 2 h in vacuum. After that a new reaction was started under the standard conditions stated above. This procedure was repeated for 3 to 4 runs, after which PXRD and nitrogen sorption analysis was measured. In a second set of experiments the conversion was determined following the same procedure, but implement further washing steps with water and ethanol. Additionally, it was tried to reactivate the material by stirring in hydrochloric acid. After the treatment with acid the solution has been washed with water until a neutral pH was achieved in the filtrate.

Structural elements of MIL-101Cr

pentagonal windows and hexagonal windows as largest windows in cages:

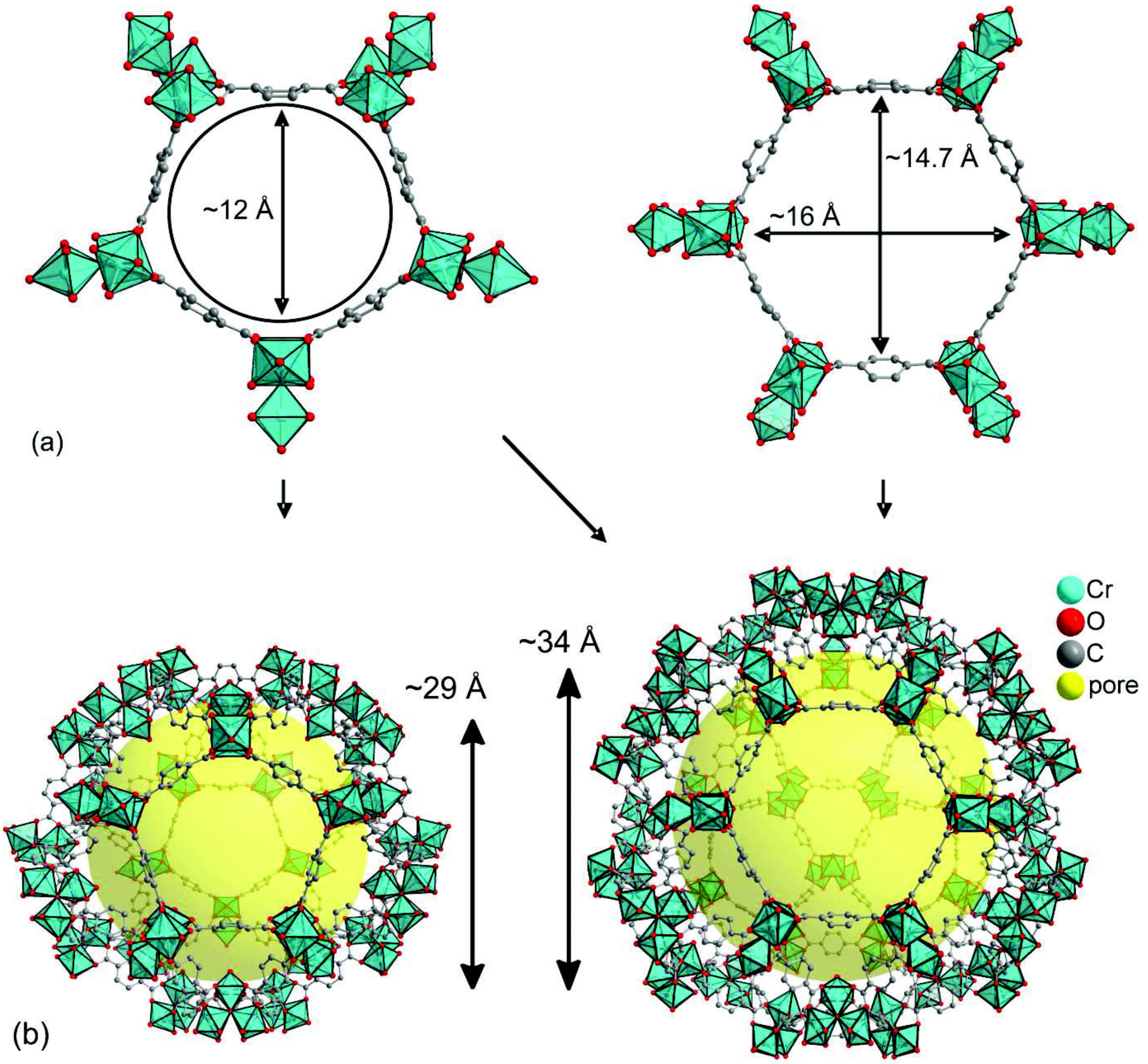

Figure S1 Building blocks for MIL-101, $[Cr_3(\mu_3\text{-}O)(F,OH)(BDC)_3(H_2O)_2]$, generated from the deposited X-ray data file at the Cambridge Structure Database (CSD-Refcode OCUNAK)[l] using the program DIAMOND.[m] Trinuclear $\{Cr_3(\mu_3\text{-}O)(F,OH)(H_2O)_2(O_2C\text{-})_6\}$ building units and bridging benzene-1,4-dicarboxylate ligands form pentagonal and hexagonal rings (a) which are assembled into mesoporous cages. b) The yellow spheres in the mesoporous cages with diameters of 29 or 34 Å, respectively, take into account the van-der-Waals radii of the framework walls (water-guest molecules are not shown). The different objects in this figure are not drawn to scale.

---

[l] G. Férey, C. Mellot-Draznieks, C. Serre, F. Millange, J. Dutour, S. Surble and I. Margiolaki, *Science*, 2005, **309**, 2040–2042.

[m] Brandenburg, K. *Diamond* (Version 3.2), crystal and molecular structure visualization, Crystal Impact. K. Brandenburg, H. Putz, Bonn, Germany, 2007-2012.

NMR spectra of digested MILs

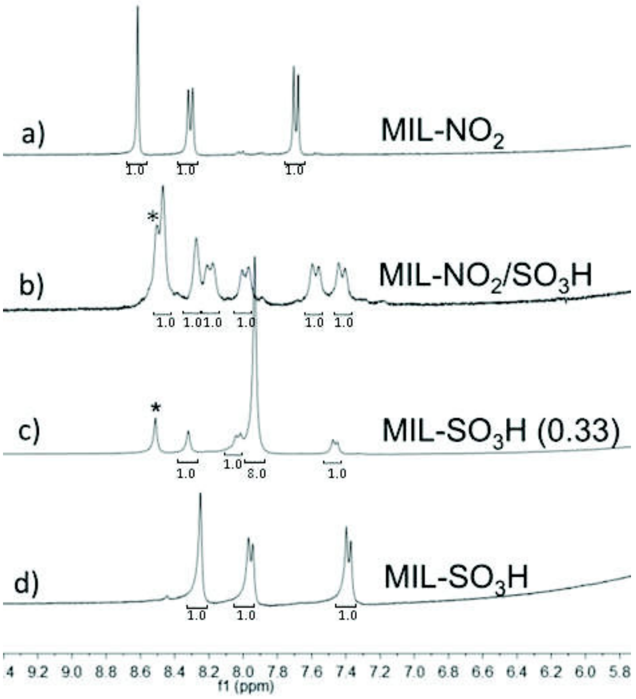

Figure S2 ^{1}H NMR spectra (300 MHz) after digestion of MILs in D_2O/NaOD. a) MIL-NO$_2$, b) MIL-NO$_2$/SO$_3$H, c) MIL-SO$_3$H(0.33) (*artefact signal from solvent) and d) MIL-SO$_3$H. Slight shifts in different spectra a versus b and c versus d can be induced by residual Cr^{3+} species.

Scanning electron microscopy (SEM)

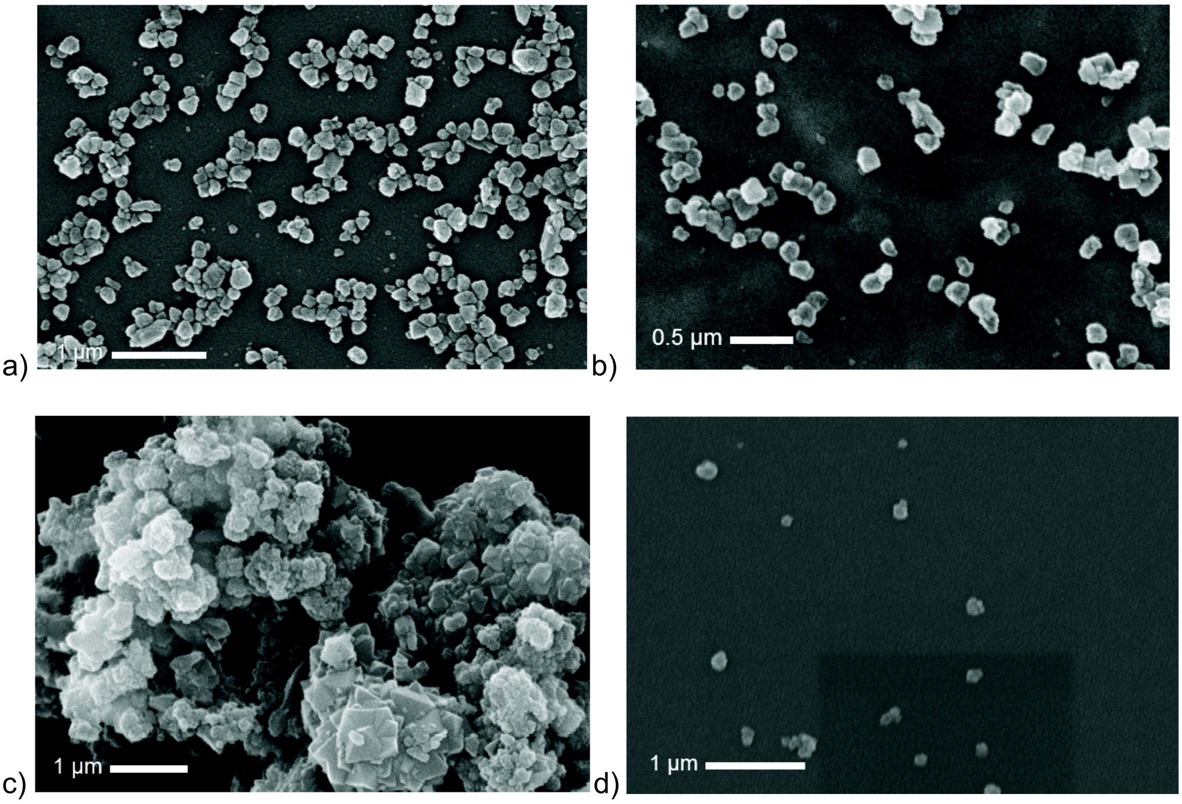

Figure S3 Scanning electron microscopy images of a) MIL-NO_2, b) MIL-NO_2/SO_3H, c) MIL-SO_3H(0.33) and d) MIL-SO_3H.

Powder X-ray diffraction

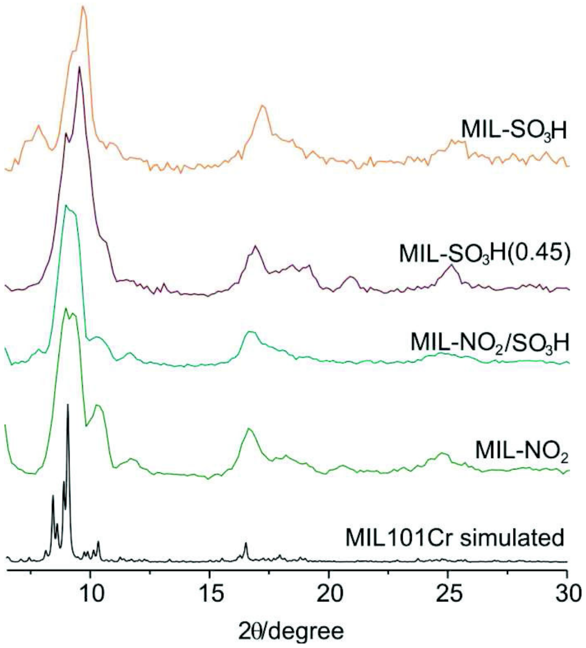

Figure S4 Powder X-ray diffractograms of MIL-NO_2, MIL-NO_2/SO_3H, MIL-SO_3H(0.33) and MIL-SO_3H. Measured for 2 h.

Nitrogen sorption isotherms

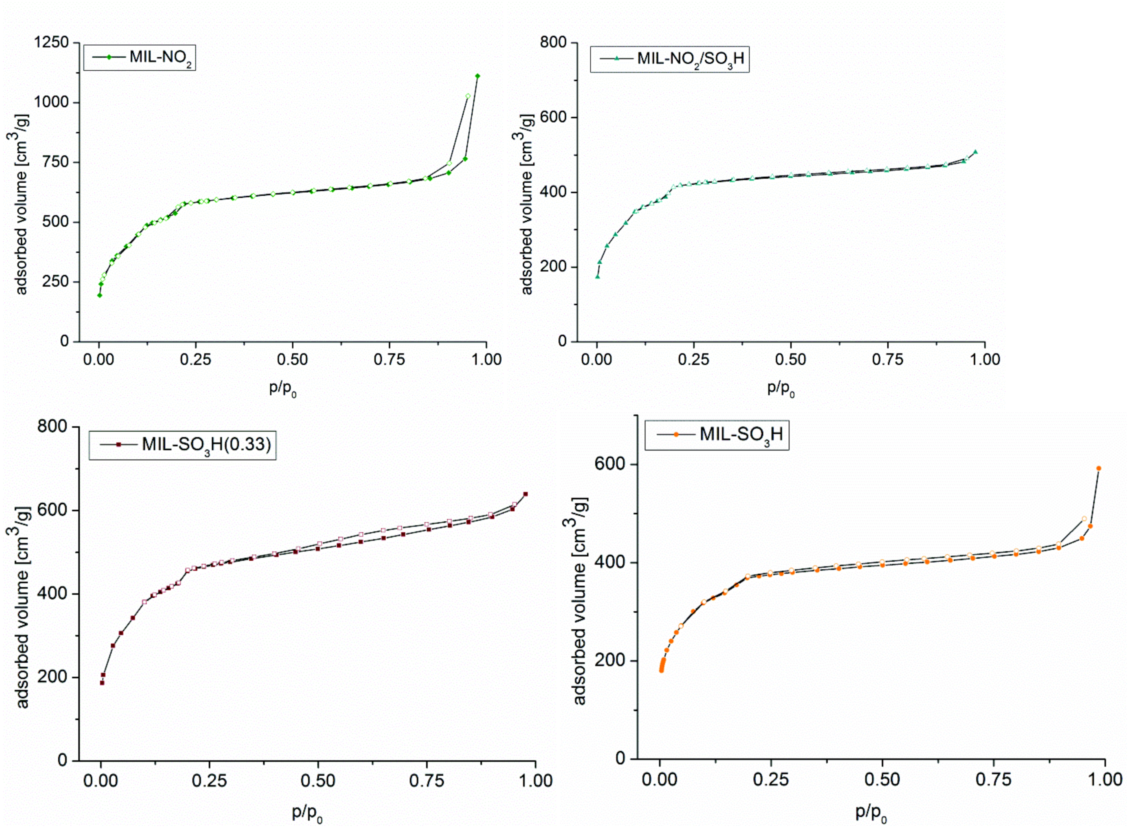

Figure S5 Nitrogen sorption isotherms of MIL-NO$_2$, MIL-NO$_2$/SO$_3$H, MIL-SO$_3$H(0.33) and MIL-SO$_3$H. Filled symbols are for adsorption, empty symbols are for desorption.

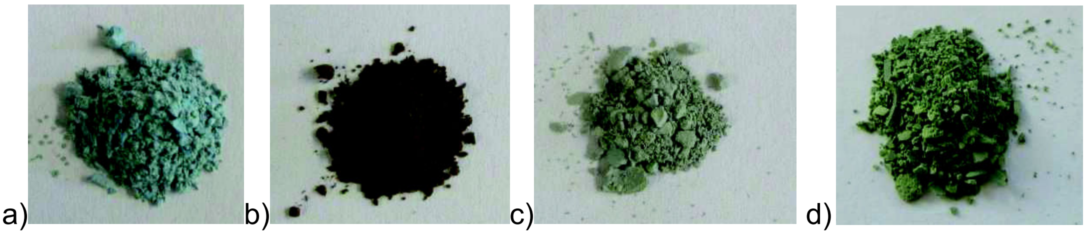

Figure S6 pictures of a) pure MIL-SO$_3$H powder; b) MIL-SO$_3$H after 24 h catalysis under standard conditions with THF:H$_2$O (v:v) 39:1; c) MIL-SO$_3$H after catalysis in THF:H$_2$O (v:v) 4:1 c) d) reacted in EtOH/H$_2$O.

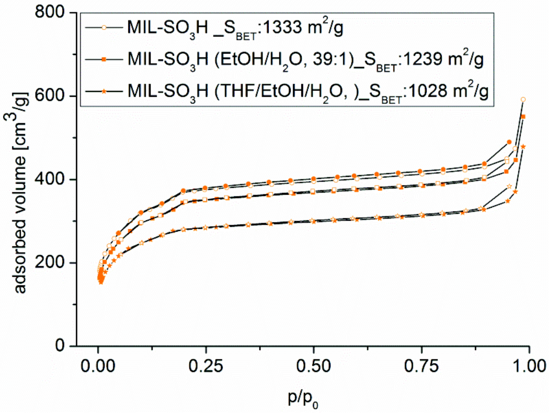

Figure S7 Nitrogen sorption isotherms of MIL-SO$_3$H after the catalytic reaction under standard conditions for 24 h in EtOH/H$_2$O 39:1, THF/EtOH/H$_2$O (23:16:1) and before catalysis.

Table S2 Weights of different catalytic materials together with insoluble humins after the reaction (24 h, 130 °C, 50 mg catalyst (or $4.7 \cdot 10^{-4}$ mol for H_2SO_4 and $Cr(NO_3)_3$). Samples have been dried at 120 °C overnight.

Catalytic material	**Weight of insoluble material after catalytic reaction [mg]**
MIL-SO_3H	91
MIL-SO_3H with substrate levoglucosan	85
MIL-SO_3H after 3 runs	72
H_2SO_4	70
$Cr(NO_3)_3$	132
MIL-SO_3H in EtOH/H_2O	53

Table S3 Multiple run experiments with MIL-SO_3H

Run number	**Yield of 5-HMF [%]**[a]
1	29
2	24
3	19
4	13
With washing steps	
2	18
3	16

a) Determined by GC.

NMR data of reaction products from catalytic substrate conversion

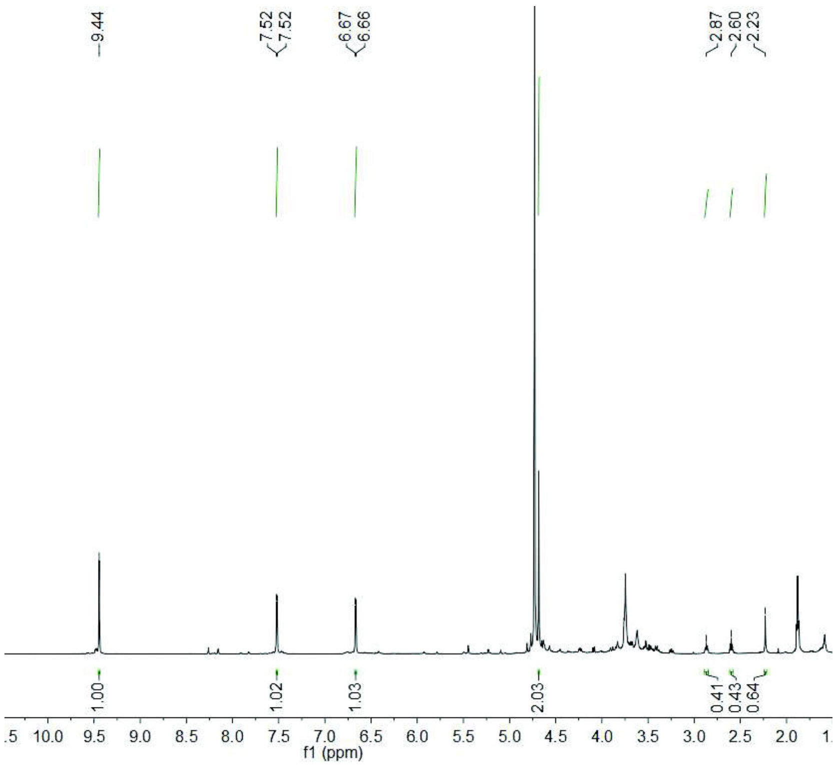

a)

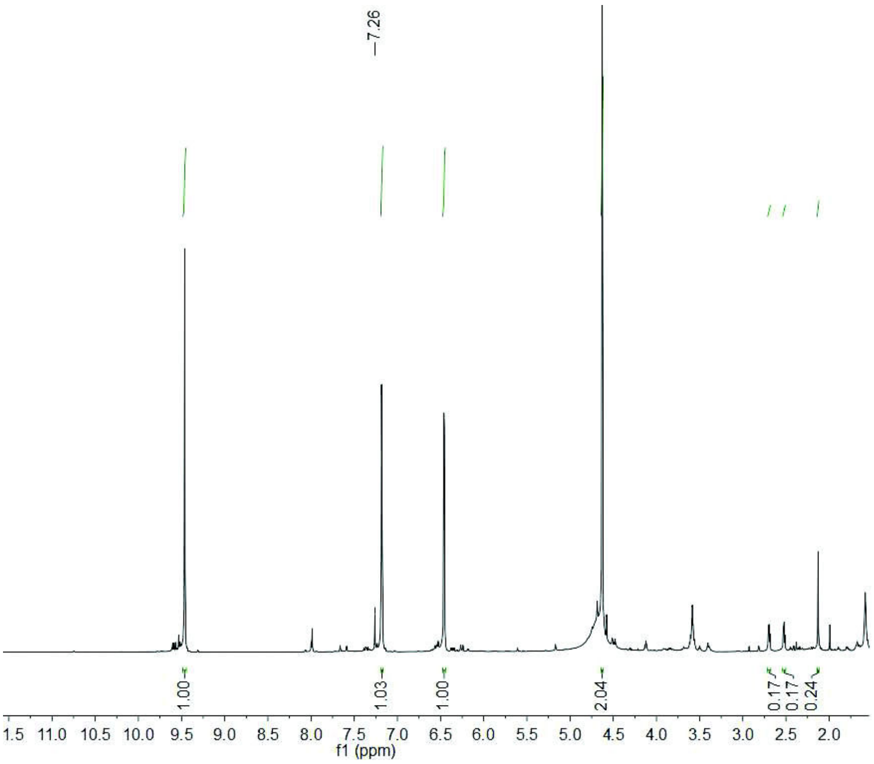

b)

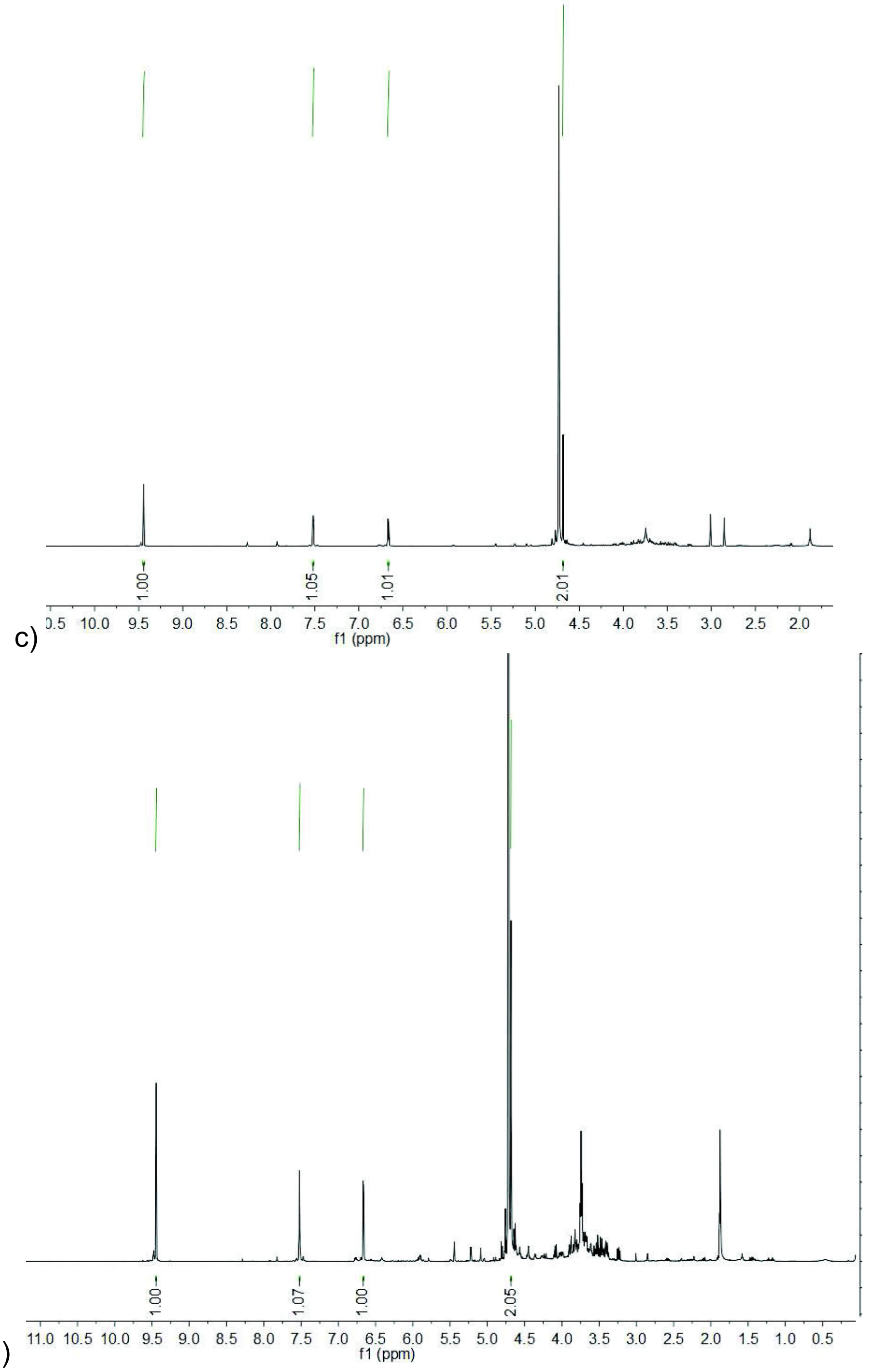

Figure S8 ^{1}H NMR data of the reaction products of

a) MIL-SO_3H with levoglucosan (conditions: levoglucosan 1.24 mmol, MIL-SO_3H $5.22{\cdot}10^{-5}$ mol, THF/H_2O 5mL, (v:v) 39:1, 130 °C, 24 h), spectrum in D_2O;

b) MIL-SO_3H with fructose (conditions: fructose 1.24 mmol MIL-SO_3H $5.22{\cdot}10^{-5}$ mol, THF/H_2O 5 mL, (v:v) 39:1, 130 °C, 24 h), spectrum in $CDCl_3$;

c) MIL-NO_2 with glucose (conditions: glucose (1.24 mmol), MIL-NO_2 $5.22{\cdot}10^{-5}$ mol, THF/H_2O 5mL, (v:v) 39:1, 130 °C, 24 h), spectrum in D_2O;

d) MIL-SO_3H with glucose reacted at 100 °C (conditions: glucose 1.24 mmol, MIL-SO_3H $5.22{\cdot}10^{-5}$ mol, THF/H_2O 5mL, (v:v) 39:1, 100 °C, 24 h), spectrum in D_2O.

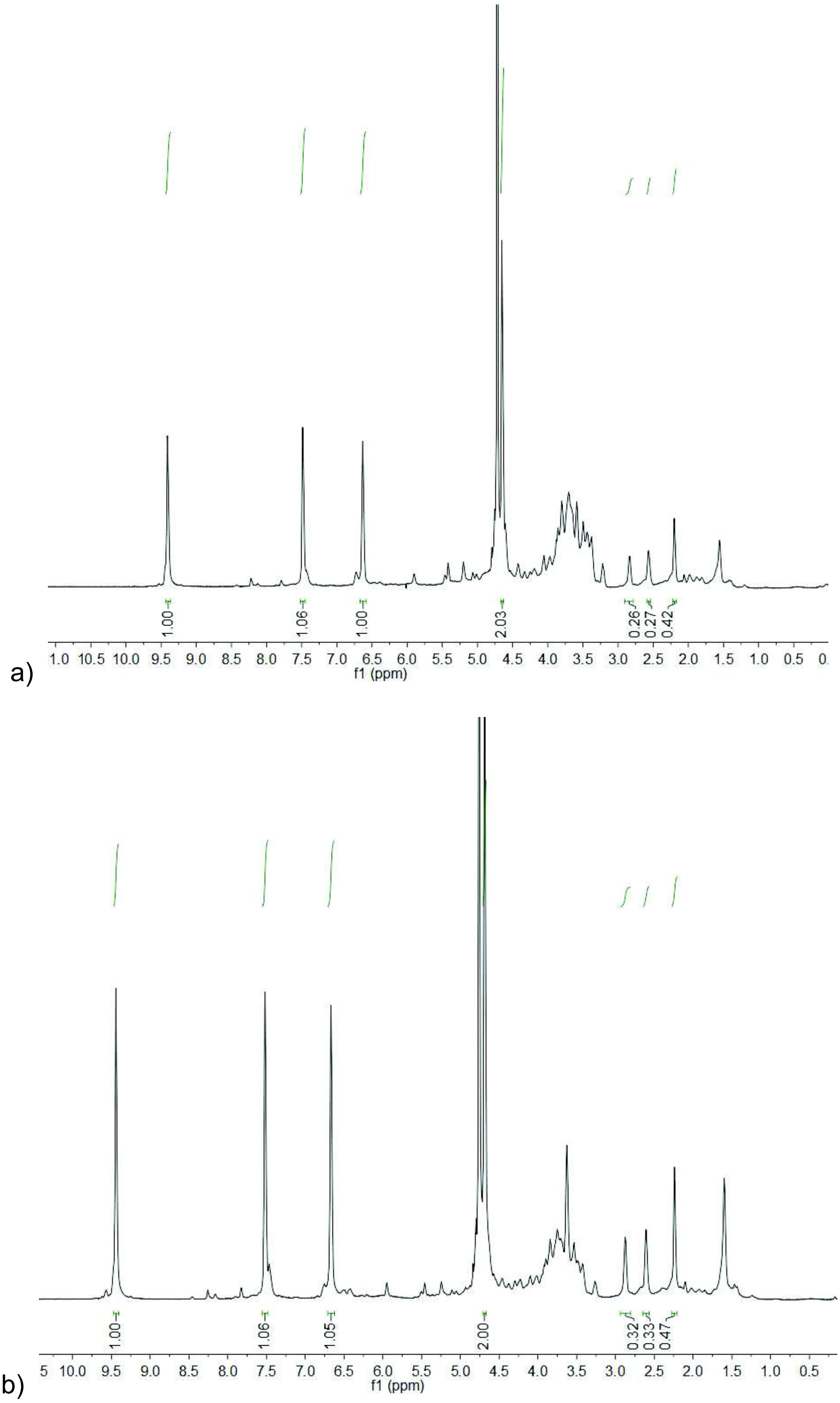

Figure S9 a) MIL-SO_3H with glucose after 8 h (conditions: glucose 223 mg, MIL-SO_3H $5.22\cdot10^{-5}$ mol, TF/H_2O 5ml, 39:1, 130°C, 8 h), spectrum in D_2O; b) MIL-SO_3H with glucose after 15 h (conditions: glucose 223 mg, MIL-SO_3H $5.22\cdot10^{-5}$ mol, THF/H_2O 5ml, 39:1, 130°C, 15 h), spectrum in D_2O.

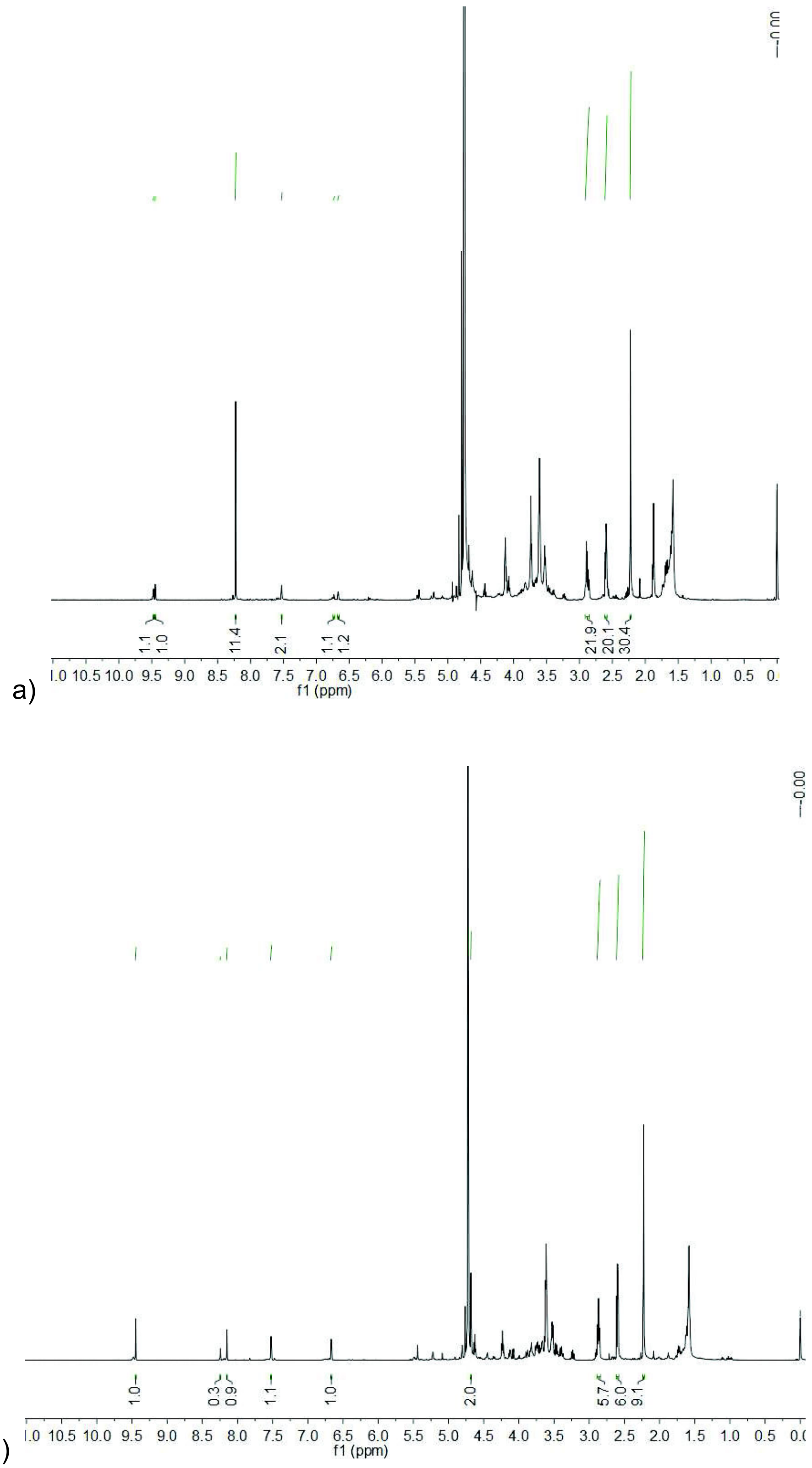

Figure S10 ^{1}H NMR of the reaction solution of a) H_2SO_4 and b) Amberlyst-15 with glucose. Conditions: glucose 223 mg, THF/H_2O 5 mL (v:v 39:1), 130 °C, 24 h. For H_2SO_4 and Amberlyst-15 reaction was conducted with $1.57 \cdot 10^{-4}$ mol each. Spectra in D_2O.

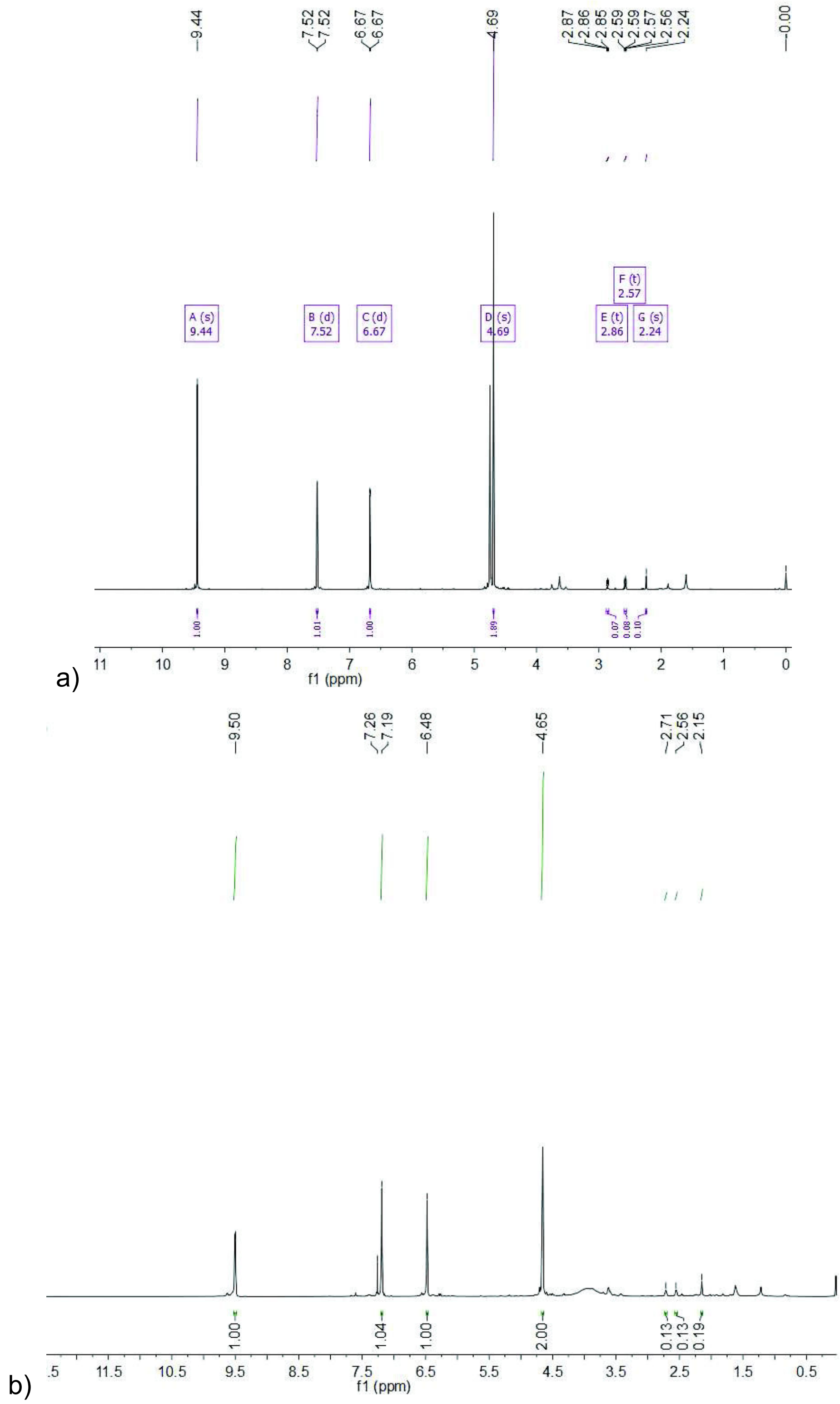

Figure S11 ^{1}H NMR spectra of the reaction solution of a) 5-HMF with MIL-SO_3H (conditions 5-HMF 1.03 mmol, MIL-SO_3H $5.22 \cdot 10^{-5}$mol, THF/H_2O 5 ml (39:1), 130 °C, 24 h), spectrum in D_2O b) glucose with MIL-SO_3H, only the THF phase after workup procedure (conditions: MIL-SO_3H $5.22 \cdot 10^{-5}$mol, glucose 223 mg, THF/H_2O 5 ml (39:1), 130 °C, 24 h), spectrum in $CDCl_3$. Normally the whole THF/H_2O solution was used for NMR (after centrifugation of the MIL catalyst). Here, it was seen that the 5-HMF to levulinic acid ratio is higher as workup leaves the latter partly in the aqueous phase.

Potentiometric titration experiments

Potentiometric titration experiments were conducted with a Titrino plus 848 (Metrohm). Dynamic equivalence point titration was used. Program details for experiments using sodium chloride as exchange agent (backtitration): dynamic equivalence point titration, signal drift 1 mV/min, waiting time minimum 10 sec, maximum 300 s, temperature 21 °C.

Equivalence points have been determined by maxima of ERC value (Equivalence point recognition criterion), which uses the first derivative of the titration curve. Titrations were performed at least in a triplicate and with varying concentrations of MIL-MOF and NaOH.

Program details for experiments with using sodium nitrate as exchange agent (backtitration): dosing rate 0.2 mL/min, signal drift 30 mV/min, minimum increment 0.05 mL, maximum increment 0.2 mL; temperature 21 °C.

Experiment using NaCl as exchange agent

The acidity of MIL-materials has been determined by acid-base backtitration using NaCl as ion exchange agent. For direct titration with MOFs no equilibrium of values could be found, also not after adding very small amounts of base (50 µL) and long waiting times (5 min). The results of experiments were not reproducible. Besides, MIL materials are known to decompose in basic milieu and it cannot be sure at which pH this process starts. For this reason backtitration method was used. Based on literature procedures,[n] in a typical experiment 50 mg or 100 mg of MOF was suspended in saturated NaCl aqueous solution (10 mL). The mixture was stirred for 20 h, centrifugated and washed with 10 mL of water (stirring time 20 min.). The filtrate was titrated with NaOH with a concentration of 0.001 mol/L or 0.005 mol/L. For all solutions Millipore water was used, additionally the solutions have been treated in an ultrasonic bath and with gaseous nitrogen. The saturated NaCl solution was heated and cooled to room temperature under inert atmosphere to minimize carbon dioxide in solution.

---

[n] a) J. Chen, K. Li, R. Liu, X. Huang and D. Ye, *Green Chem.*, 2014 **16**, 2490-2499; b) S. Chen, T. Yokoi, C. Tang, L. Jang, T. Tatsumi, J. C. C. Chan and S. Cheng, *Green Chem.*, 2011, **13**, 2920–2930; c) Y. Zang, J. Shi, F. Zhang, Y. Zhong and W. Zhu, *Catal. Sci. Technol.*, 2013, **3**, 2044-2049; d) Z. Hasan, J. W. Jun and S. H. Jhung, *Chem. Eng. J.*, 2015, **278**, 265–271.

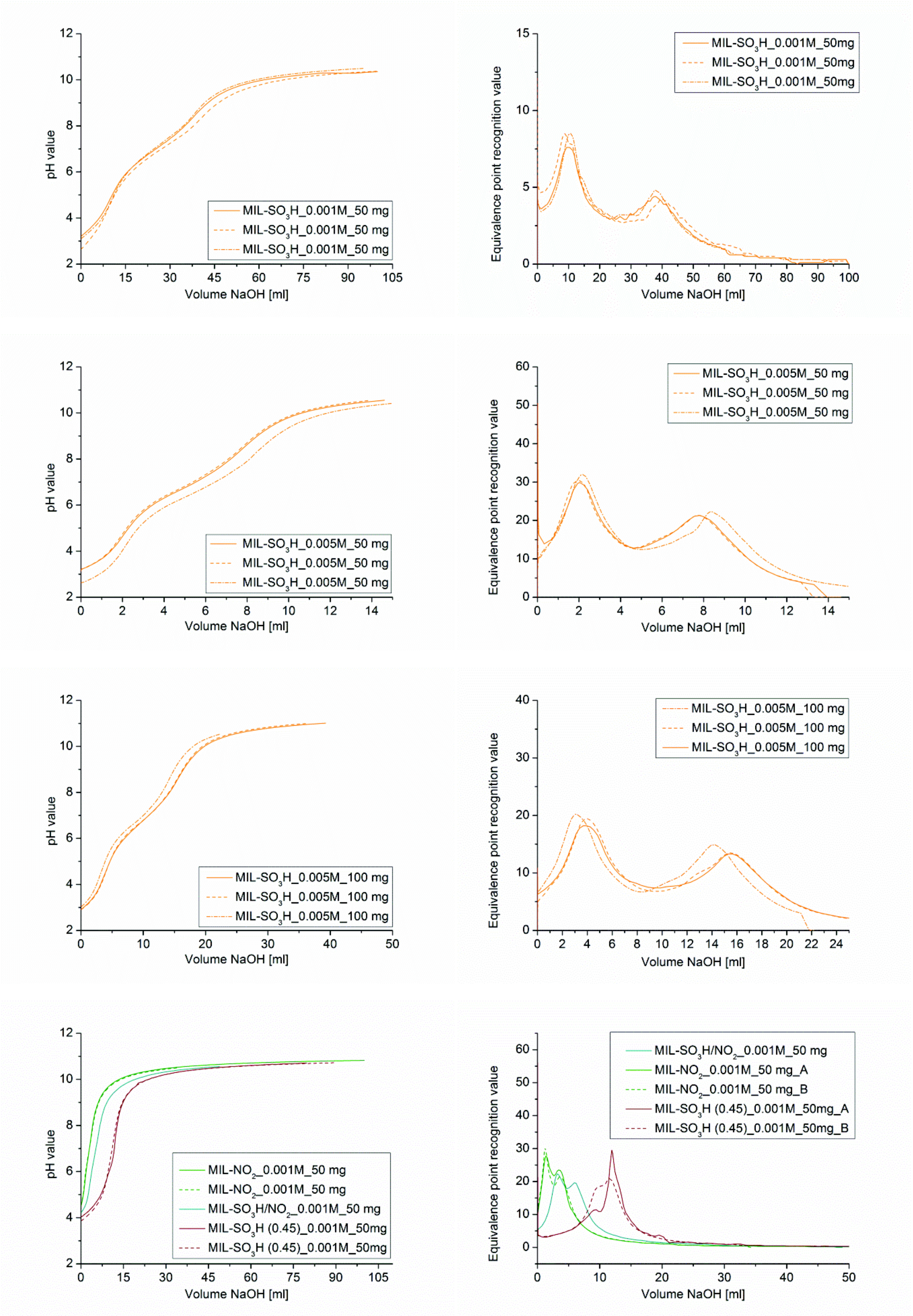

Figure S12 Titration of MIL-X with NaOH (different concentrations)

The titration curve of MIL-SO_3H shows 2 steps which is unexpected, since there should be only one kind of acidic protons. Therefore reference titrations have been performed. First only the pure saturated NaCl solution was titrated (Fig. S13). As expected the pH rises immediately very fast.

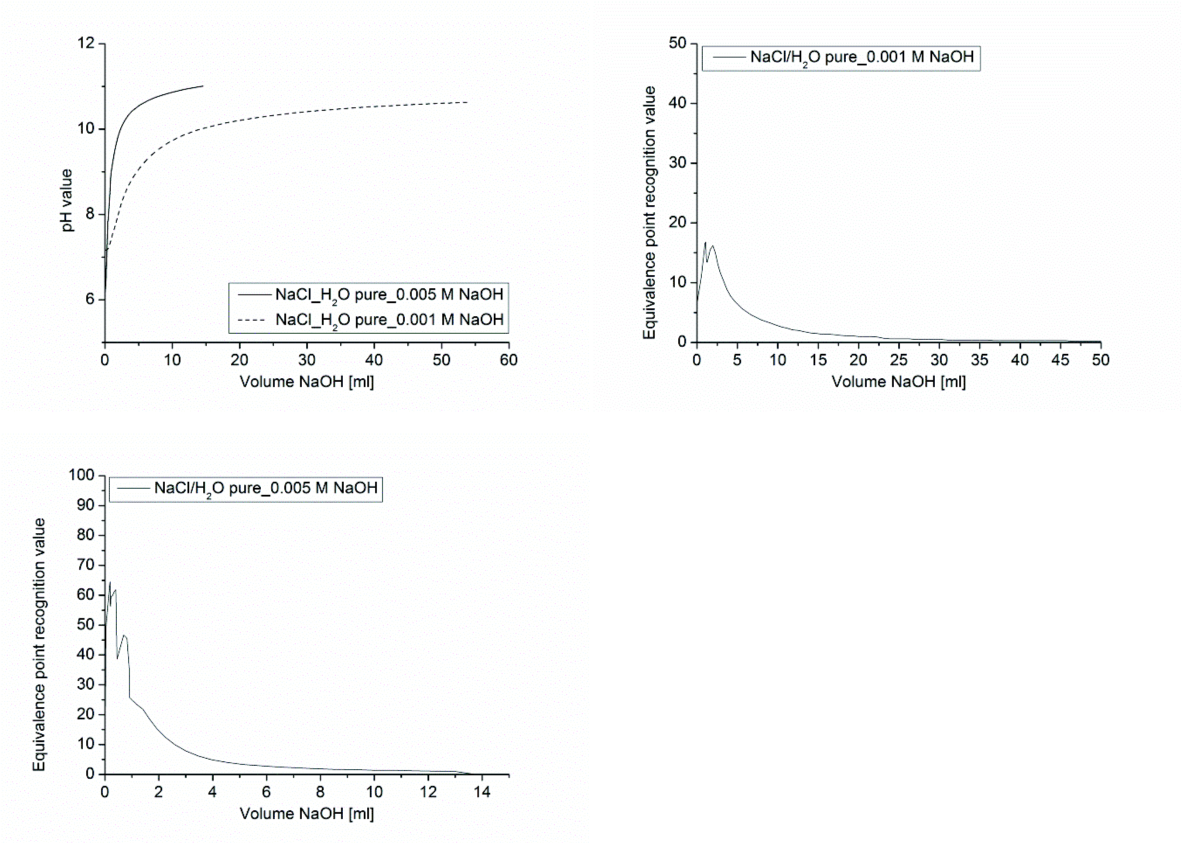

Figure S13 Reference experiments of NaCl pure without catalyst with 0.001 M and 0.005M NaOH solution.

It was taken into account, that the unexpected behavior can originate from leaching of the linker 2-sulfoterephtalate or chromium metal ions into solution). Titration of both 2-sulfoterephtalate (5 mg, $2.0 \cdot 10^{-5}$mol) or chromium nitrate ($1.57 \cdot 10^{-4}$ mol in 25 ml H_2O) with 0.005 M NaOH shows that the linker is a strong acid whereas chromium nitrate is a weak acid. The strong rise in pH at a volume of ca. 90 ml is coming from insoluble chromium hydroxide which precipitated from the solution.

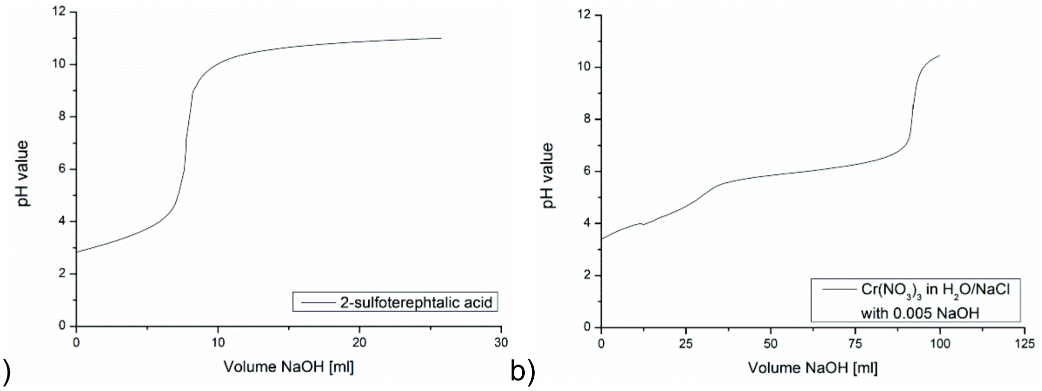

a) b)

Figure S14 Titration of a) 2-sulfoterephtalic acid and b) chromium nitrate in NaCl/H_2O with 0.005 M NaOH.

Assuming linker leaching from linkers inside the pores, which are not coordinated to metal, it can be proposed that the surface area should be enhanced after washing with NaCl. Therefore MIL-SO_3H (50 mg) was stirred in saturated NaCl for 20 h. Then the MOF was washed three times with water (40 mL each). From N_2 sorption experiments it could be shown that the surface area decreased to 1040 m^2/g.

If the acidity is coming from leaching of residual linkers or chromium nitrate, those should also leach in pure water, since both are good soluble in water. Therefore MIL-SO_3H (50 mg) was stirred for 20 h in pure water, and after centrifugation the solution was backtitrated with NaOH (0.005 M) (Figure S15). The pH of the solution rises immediately and a behavior similar to pure NaCl/H_2O solution was found. No leaching occurs.

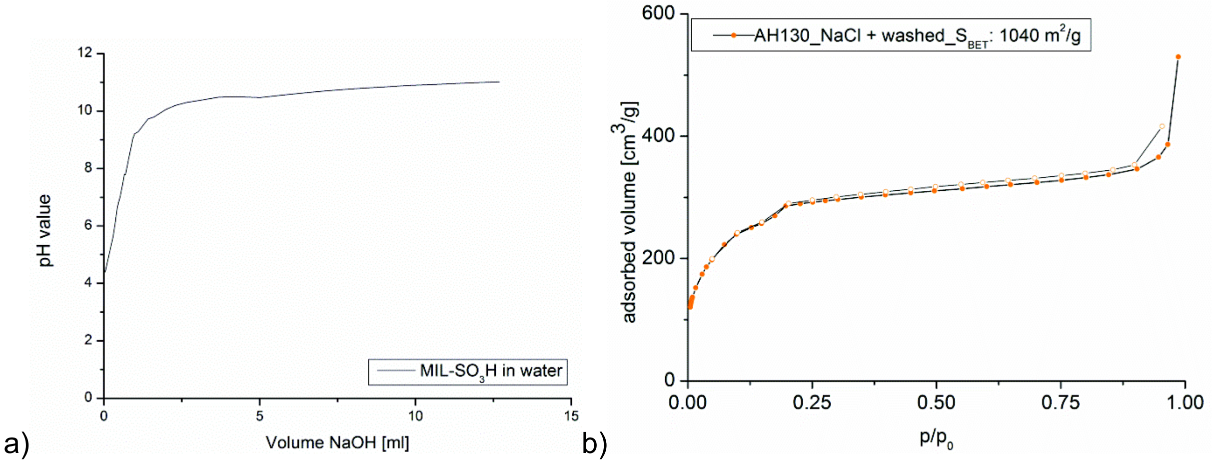

Figure S15 a) MIL-SO_3H (50 mg) stirred in pure water, centrifuged and titrated back with 0.005 M NaOH, b) N_2 sorption isotherme of MIL-SO_3H stirred in saturated NaCl solution for 20 h, centrifugated and washed 3 times with water.

In conclusion, it can be proposed, that saturated NaCl solution gives rise to partial decomposition of MIL catalyst and is not suitable for the determination of acidity.

Experiment using $NaNO_3$ as exchange agent

Since it was concluded that sodium chloride is not suitable for determination of acidic sites, according to a modified procedure following the work of R. C. Klet *et al.* titration was repeated using sodium nitrate (0.01 M).[o] For direct titration with MOFs no equilibrium of values could be found, also not after adding very small amounts of base (50 µL) and long waiting times (5 min). The results of experiments were not reproducible. Besides, MIL materials are known to decompose in basic milieu and it cannot be sure at which pH this process starts. For this reason backtitration method was used.

In a typical experiment 50 mg of MIL was suspended in $NaNO_3$ aqueous solution (0.01 M, 40 mL). The mixture was stirred for 20 h, centrifugated and the filtrate was titrated with NaOH

---

[o] R. C. Klet, Y. Liu, T. C. Wang, J.T. Hupp and O. K. Farha, *J. Mater Chem. A*, 2016, **4**, 1479-1485.

with a concentration of 0.001 mol/L or 0.005 mol/L. For all solutions Millipore water was used.

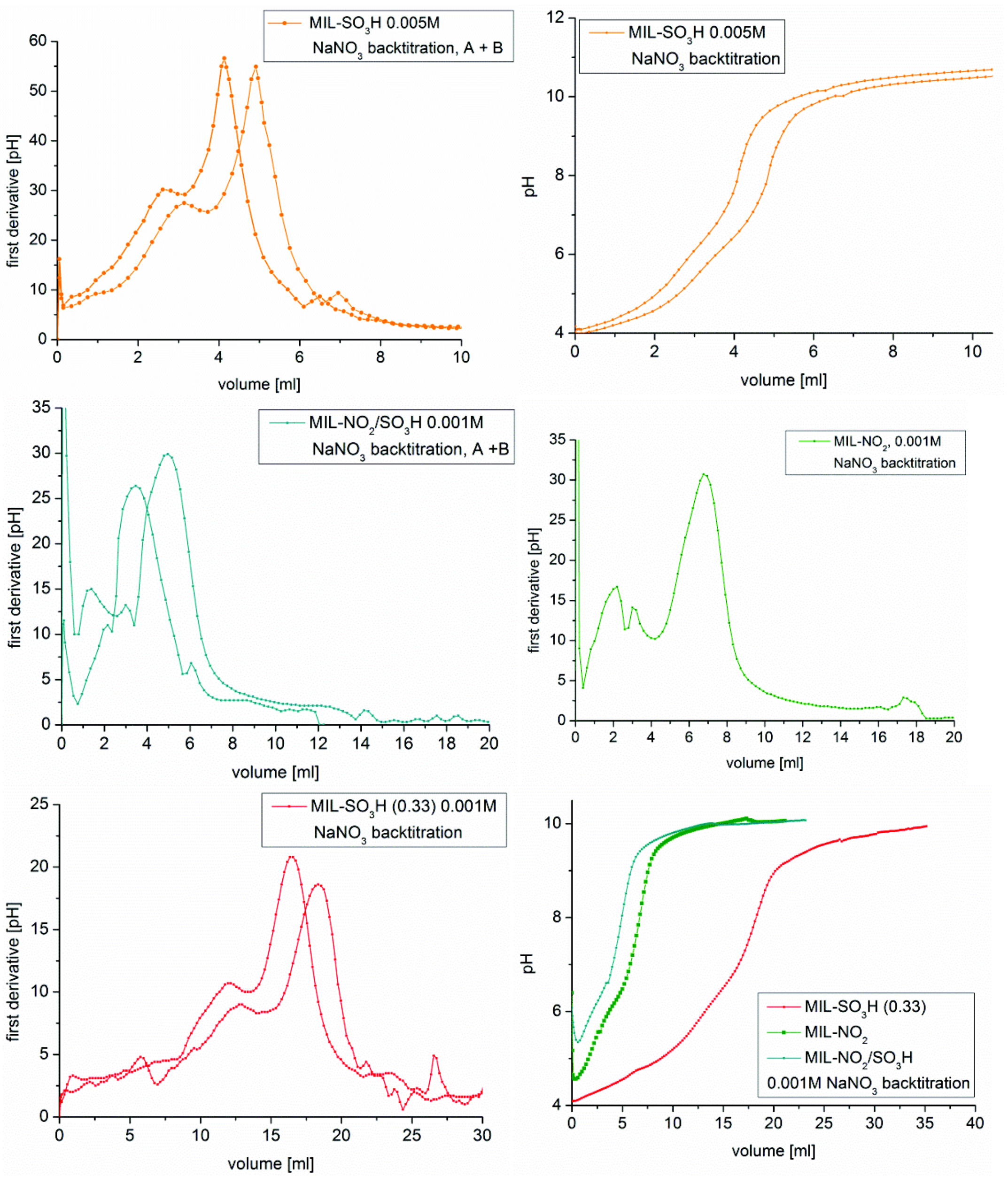

Fig. S16 Titration of MIL-X, using $NaNO_3$ (0.001M), backtitration method.

Taking the largest maximum into account, the molar fraction was calculated (Table S3). When two titrations were performed the values have been averaged.

Table S4 Amount of acid sites, determined by potentiometric titration with NaOH (0.001 mol/L).

MIL-X	**Volume [a] [ml]**	**mmol H^+ (for 50 mg MIL)**	**Mol H^+/mol MIL**	**Calc. value mol H^+/mol MIL**	**Amount %**
MIL-SO_3H [b]	4.52	0.023	0.43	5	8.6%
MIL-SO_3H(0.33)	17.45	0.017	0.28	3	9.3%
MIL-NO_2/SO_3H	4.21	0.004	0.076	3.5	2.2%
MIL-NO_2	6.76	0.007	0.12	2	6%

[a] volume for highest maximum in first derivative curve. [b] NaOH 0.005 mol/L was used.

Since the results from experiments are not really reproducible and remained inconclusive, our attempts are documented here, but not discussed further.

Mechanistic aspects of 5-HMF formation from glucose

Several pathways for the formation of 5-HMF from glucose are under discussion and especially for porous heterogeneous systems it is very difficult to elucidate exact mechanisms. Therefore a brief overview over recent insights in 5-HMF formation from glucose is given here (Fig. 8, cf. Fig. 2). The Brønsted base catalyzed glucose isomerization to fructose followed by the Brønsted acid catalyzed glucose dehydration to 5-HMF and a tandem Lewis/ Brønsted acid route have been discussed recently.[p,q,r] Although all these studies refer to aqueous homogeneous systems, valuable information can be gained. Thiel and coworkers developed criteria for good metal catalysts in the glucose to fructose isomerization and identified Cr(III) and Al(III) as best candidates. One of the most important criteria is moderate Lewis and Brønsted acidity (pK_a = 4-6).[rb] Detailed kinetic studies using Cr(III)-salts led to the conclusion that the Brønsted acidity of metal-aqua complexes has significant impact on glucose conversion.[rc] $[Cr(H_2O)_5OH]^{2+}$ has been identified as the most active Cr-species in glucose to fructose isomerization; aqua ligands are displaced by glucose to enable ring-opening and isomerization (Fig. S17b).[rc] Recently, Vlachos and coworker showed that in the aqueous $CrCl_3$-HCl system adjusting the concentration of both $CrCl_3$ and HCl has a higher influence on 5-HMF yield than the change of temperature or $CrCl_3$ concentration. The rate limiting step can change from fructose dehydration to glucose isomerization with an increase of Brønsted acid concentration.[ra]

Following the model of only Brønsted acid conversion of glucose, the first step is the protonation of hydroxyl groups and in consequence, the rate limiting step involves this first dehydration (Fig. S17a). Vlachos and coworker conclude from experimental and theoretical data that also the direct dehydration to levulinic acid and formic acid without 5-HMF formation is possible. Besides they identified two intermediate species composed of five-membered rings. Their study further confirms the strong dependence of dehydration rate on temperature and pH and suggests a reaction mechanism via a cyclic intermediate (Fig. S17a).[q]

An important difference is the reaction time scale, whereas conversion involving Lewis acid formation of fructose and dehydration to 5-HMF (Fig. S17b) is fast, in comparison

---

[p] J. M. Carraher, C. N. Fleitman and J. Tessonnier, *ACS Catal.*, 2015, **5**, 3162–3173

[q] L. Yang, G. Tsilomelekis, S. Caratzoulas and D. G. Vlachos, *ChemSusChem*, 2015, **8**, 1334–1341

[r] a) T. D. Swift, H. Nguyen, A. Anderko, V. Nikolakis and D. G. Vlachos, *Green Chem.*, 2015, **17**, 4725–4735; b) C. Loerbroks, J. van Rijn, M. Ruby, Q. Tong. F. Schüth and W. Thiel, *Chem. Eur. J.*, 2014, **20**, 12298–12309; c) V. Choudhary, S. H. Mushrif, C. Ho, A. J. Anderko, V. Nikolakis, N. S. Marinkovic, A. I. Frenkel, S. I. Sandler and D. G. Vlachos, *J. Am. Chem. Soc.*, 2013, **135**, 3997–4006

to purely Brønsted acid dehydration which is slow.[q,ra,s] Very recently Huber *et al.* presented a new mechanism for Brønsted acid dehydration of cellulose and glucose involving the intermediate Levoglucosan (Fig. S17c).[t]

Having a closer look to heterogeneous catalyst systems, especially Sn-Beta zeolite has been investigated for the formation of 5-HMF from glucose.[u] From deuterium labeling experiments at the C2 position of glucose it was suggested that a hydrogen shift from the C2 to C1 positions is the rate-limiting step. In consequence a Lewis acid isomerization to fructose and Brønsted acid dehydration was postulated (Fig. S17b). In more detail it was proposed, that the OH group at the Sn-site lowers the energy barrier for the initial deprotonation step, which in turns activates the following Lewis acid catalyzed intramolecular hydride shift.[ud]

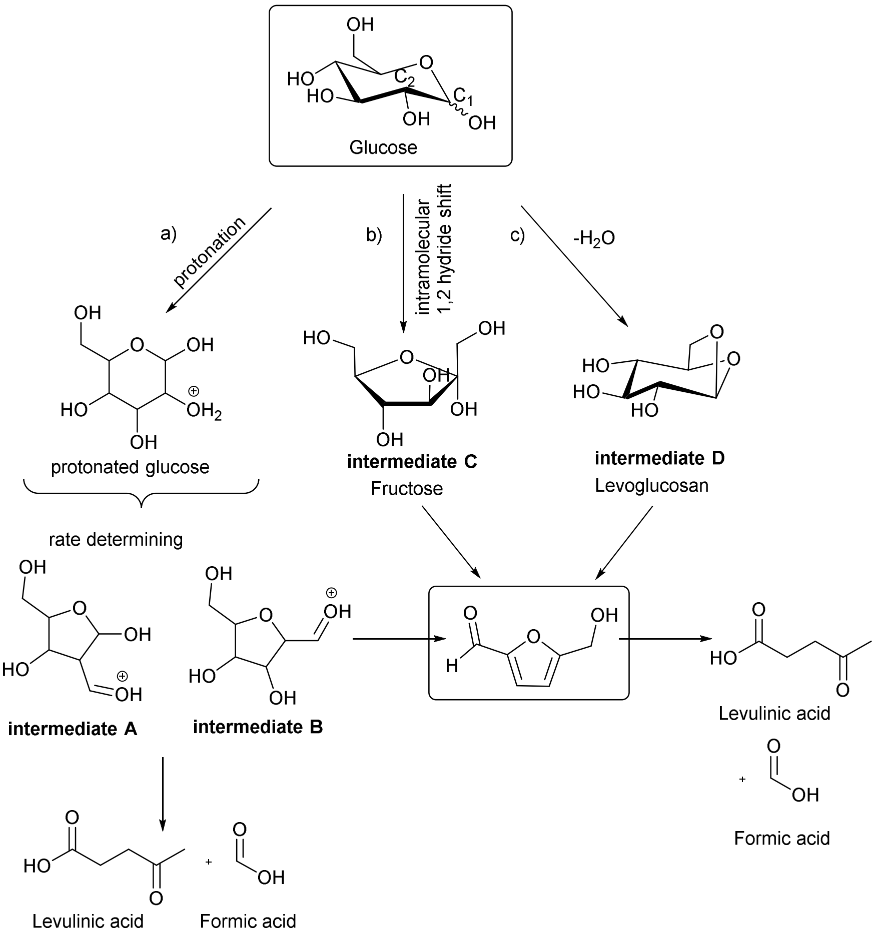

Figure S17 Possible reaction pathways and intermediates for glucose to 5-HMF conversion.[q,t,u]

---

[s] R. van Putten, J. N. M. Soetedjo, E. A. Pidko, J. C. van der Waal, E. J. M. Hensen, E. de Jong and H. J. Heeres, *ChemSusChem*, 2013, **6**, 1681–1687

[t] R. Weingarten, A. Rodriguez-Beuerman, F. Cao, J. S. Luterbacher, D.Martin Alonso, J. A. Dumesic, G. W. Huber, *ChemCatChem* 2014, *6*, 2229 – 2234.

[u] a) Y. Li, M. Head-Gordon and A. T. Bell, *ACS Catal.*, 2014, **4**, 1537–1545; b) G. Yang, E. A. Pidko and E. J. M. Hensen, ChemSusChem, 2013, **6**, 1688–1696; c) R. Bermejo-Deval, M. Orazov, R. Gounder, S. Hwang and M. E. Davis, *ACS Catal.*, 2014, **4**, 2288–2297; d) V. Choudhary, A. B. Pinar, R. F. Lobo, D. G. Vlachos and S. I. Sandler *ChemSusChem,* 2013, **6**, 2369–2376.

Now all these findings should be interpreted taking the present MIL catalyst system into account. Most importantly the mechanism of 1,2 hydrogen shift includes two neighboring open metal sites, which can coordinate to the oxygen atoms of glucose.[ud] This is not given in the MIL-101Cr structure (Fig. 3). Defect formation in MIL-101Cr leading to cis-open metal sites which is in principle conceivable, is not reported in literature.

3.3 Hierarchical MOF-xerogel monolith composites from embedding MIL-100(Fe,Cr) and MIL-101(Cr) in resorcinol-formaldehyde based xerogels for water adsorption applications

M. Wickenheisser, A. Herbst, R. Tannert, B. Milow, C. Janiak

Microporous and Mesoporous Materials **2015**, *215*, 143-153.

DOI:10.1016/j.micromeso.2015.05.017, reference [157]

Impact factor 2014: 3.5

Appropriate shaping of MOFs is a key issue towards industrial application. With regard to the mechanical properties of most MOFs, it becomes clear that methods using high-pressure shaping will not be an option.[1] Therefore, coating or composite based strategies have to be further explored. In this work, resorcinol-formaldehyde xerogels were used as binding agents, in combination with different water stable MOFs (MIL-101Cr, MIL-100Fe, Cr), for the formation of monolithic materials. The resulting mechanically stable MOF@xerogel materials have been characterized by PXRD, nitrogen- and water sorption measurements. A pre-polymerization method was developed to avoid pore blocking effects. Sorption measurements revealed accessible pores and almost no loss of BET surface area, with best results for the MIL-101Cr@xerogel composites.

Author's share of work[v]:

- Designing, performing of the synthetic work and evaluation of the results for MIL-101Cr@xerogel composites. Work resulting in MIL-100Cr@xerogel and MIL-100Fe@xerogel composites was done by Mr. Wickenheisser.
- Development of method with additional water for MIL-101Cr@xerogel composites
- Writing of the introduction part of the manuscript and drawing of figures 1 and 2. Main part of the manuscript was written by Mr. Wickenheisser and figure S16 was done by Mr. Janiak.

Reprinted from ref. 157, Copyright 2015, with permission from Elsevier.

---

[v] The xerogel project was worked out in cooperation with Martin Wickenheisser, Sebastian Glomb, Tian Zhao and co-workers of the DLR in Cologne. We thank Marina Schwan and Jessica Laskowski from DLR for the kind introduction to xerogel syntheses. Pre-polymerization experiments, performing of pure xerogel syntheses with different parameters (variation of R/C, R/F and R/W ratios) and initial MIL@R,F-xerogel syntheses were done together with Martin Wickenheisser (MIL-100Cr, Fe), Sebastian Glomb (HKUST-1) and Tian Zhao (MIL-101Al-NH_2).

Microporous and Mesoporous Materials 215 (2015) 143–153

Contents lists available at ScienceDirect

Microporous and Mesoporous Materials

journal homepage: www.elsevier.com/locate/micromeso

Hierarchical MOF-xerogel monolith composites from embedding MIL-100(Fe,Cr) and MIL-101(Cr) in resorcinol-formaldehyde xerogels for water adsorption applications

Martin Wickenheisser [a], Annika Herbst [a], René Tannert [b], Barbara Milow [b], Christoph Janiak [a, *]

[a] *Institut für Anorganische Chemie und Strukturchemie I, Universitätsstraße 1, 40225 Düsseldorf, Germany*
[b] *Deutsches Zentrum für Luft- und Raumfahrt (DLR), Institut für Werkstoff-Forschung, Aerogele, Linder Höhe, 51147 Köln, Germany*

ARTICLE INFO

Article history:
Received 16 April 2015
Received in revised form
7 May 2015
Accepted 9 May 2015
Available online 20 May 2015

Keywords:
Metal-organic framework
Resorcinol-formaldehyde xerogels
Monoliths
Water adsorption
Heat transformation

ABSTRACT

Shaping of otherwise powdery metal-organic frameworks is recognized as a more-and-more important issue to advance them to the application stage. Monolithic MOF composites were synthesized using micro-to-mesoporous MIL-100(Fe,Cr) and MIL-101(Cr) as thermally and chemically stable MOFs together with a mesoporous resorcinol-formaldehyde based xerogel as binding agent. The monolithic bodies could be loaded with up to 77 wt% of powdery MIL material under retention of the MIL surface area and porosities (from N_2 adsorption) by pre-polymerization of the xerogel solution. The obtained monoliths are mechanically stable and adsorb close to the expected water vapor amount according to the MIL weight percentage. There is no loss of BET surface area, porosity and water uptake capacity especially for the MIL-101(Cr) composites. Water vapor adsorption isotherms show that the 77 wt% MIL-101(Cr) loaded composite even features a slightly increased water vapor uptake compared to pure MIL-101(Cr) up to a relative vapor pressure of $P \cdot P_0^{-1} = 0.5$. These hydrophilic monolithic composites could be applied for heat transformation application such as thermally driven adsorption chillers or adsorption heat pumps.

1. Introduction

MOFs (metal-organic framework) are potentially porous coordination networks based on metal ions or metal clusters, connected by organic ligands [1]. Metal-organic frameworks are often three-dimensional networks and have uniform micropore structures with high surface areas and large pore volumes. Research tries to advance MOFs towards applications [2,3], such as catalysis [4–6], gas storage [7–9], and gas separation [10–13]. Many review articles are evidence to the increasing interest in MOF chemistry over the last years [14–18].

Recently, MOFs are investigated as microporous materials for cycling water sorption for heat transformation: During hot seasons in large part of cities energy consumption caused by electric air-conditioning represents 30–50 % of total electric energy consumed [19]. Therefore, it would be beneficial to use a cooling system based on adsorption chilling running on solar thermal energy. In this context sorption-based heat transformations attracted growing interest during the last years [20–23].

A schematic diagram of a thermally driven adsorption chiller or adsorption heat pump is depicted in Fig. 1. Bed 1 and Bed 2 contain the porous (MOF-) material in combination with a heat exchange device and are switched between the working and regeneration cycle. During the working cycle, adsorption of the working fluid (*e.g.* water) takes place in the bed until the desired loading is reached. At the same time the other bed is regenerated by applying heat to desorb the working fluid. The desorbed vapor is liquefied in the condenser and the liquid working fluid then flows back to the evaporator, where again evaporation takes place. The heat of condensation (Q_{out}^{cond})) and the heat of adsorption (Q_{out}^{ads}) can be used in a heating application or are dissipated to the environment. From the heat of evaporation (Q_{in}^{evap}) either useful cold is generated for the cooling application or it is the low-temperature heat (blue) which is converted to medium temperature levels (green) by means of the driving heat of desorption $Q_{in}^{drive,des}$ (red). When the water loadings in bed 1 and 2 reach the same level, the two beds are interchanged with respect to regeneration and working cycle by closing and opening the respective valves [24].

---

* Corresponding author.
E-mail address: janiak@uni-duesseldorf.de (C. Janiak).

http://dx.doi.org/10.1016/j.micromeso.2015.05.017
1387-1811/

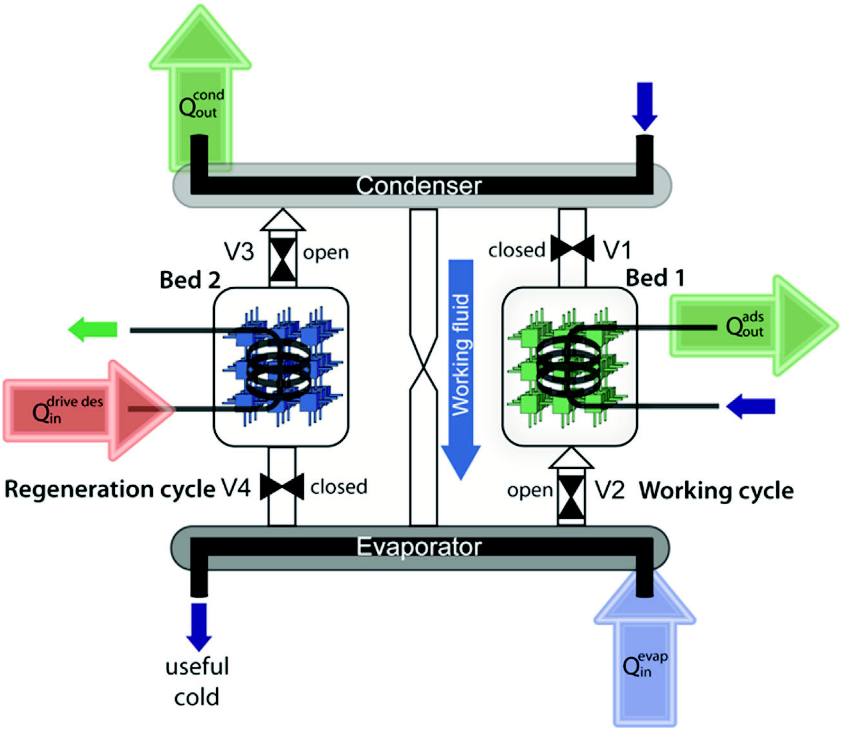

Fig. 1. Thermodynamic principle for adsorption chillers or heat pumps. Bed 1 (here in working cycle) and bed 2 (here in regeneration cycle) contain the porous adsorbent [24]. $Q_{in}^{drive,des}$ driving heat of desorption at a high temperature level (red), Q_{out}^{cond} and Q_{out}^{ads}, heat of condensation and heat of adsorption at a medium temperature level (green), Q_{in}^{evap} heat of evaporation at a low temperature level (blue). (For interpretation of the references to color in this figure legend, the reader is referred to the web version of this article.)

The key part of the system is the sorption material which should have a high water loading lift in the ideal interval $0.05 < P \cdot P_0^{-1} < 0.35$. Water is the working fluid of choice because of its high evaporation enthalpy (2440 kJ kg^{-1} at 25 °C) and non-toxicity despite the need to work under vacuum because of the low vapor pressure of only 3.17 kPa at 25 °C [15,25,26]. During the last years significant progress has been made in the development of MOF-based sorption materials [27]. Various materials, predominately of the MIL (Materials of Institute Lavoisier) family, have been investigated for water adsorption [28,29] and also different strategies of tuning prototypical MOFs to enhance the water uptake have been examined [30,31]. Long term and cycle measurements have been performed to ensure the required water stability [32–34]. Three of these MOFs, namely MIL-100(Fe,Cr) and MIL-101(Cr), were selected for the present study due to their good water sorption properties and stability [31,35].

MIL-100 $\{M_3(\mu_3\text{-}O)(X)(H_2O)_2(BTC)_2 \cdot nH_2O\}_n$ (M = Cr [36,37], Fe [38–41]; X = OH, F; BTC = 1,3,5-benzene tricarboxylate) possesses two types of mesopores with cages of 25 Å and 29 Å in diameter consisting of hexagonal (8.6 Å) and pentagonal windows (4.7–5.5 Å) (Fig. A.17, Fig. 2) [38]. MIL-101(Cr) [42] $\{Cr_3(\mu_3\text{-}O)(F,OH)(H_2O)_2(BDC)_3 \sim 25H_2O\}_n$ is a micro- and mesoporous material, having 1,4-benzene dicarboxylate (BDC) as linker, with hexagonal (15–16 Å) and pentagonal windows (12 Å) and inner free cages of 29 Å and 34 Å in diameter (Fig. A.16, Fig. 2). The water uptake of MIL-100(Cr), MIL-100(Fe) and MIL-101(Cr) are in the range of 0.6–0.7 g g^{-1}, 0.65–0.75 g g^{-1} and 1.0–1.5 g g^{-1}, respectively [33].

MOFs are typically obtained as crystalline fine powders, yet almost every application requires an appropriate shaping, *e.g.*, monolithic structures, of the used materials without diminishing its useful properties [43,44].

Different strategies of shaping MOFs have been investigated so far [43,45,46]: One possibility is to press the material into tablets or pellets [47]. MOF-177 has been mechanical compressed to a monolithic structure, resulting in enhanced hydrogen storage capacity, but also leading to an amorphous material [48]. An alternative strategy is the preparation of pure MOF monoliths, although there are often difficulties in obtaining phase pure MOFs and retaining porosity [49]. More studies have been performed on MOF composites where an organic or inorganic additive acts as binder to shape the material [17,50–53]. The resulting monoliths or membranes were tested for example in separation processes [54,55].

Aerogels are characterized by high porosity and high surface area as well as a low density and low thermal conductivity [56,57]. To obtain an aerogel with these properties supercritical drying with CO_2 is a necessary step [56,58]. Resorcinol-formaldehyde based gels can be dried under atmospheric conditions, if the ratio of resorcinol to basic catalyst is high enough leading to mechanically stable xerogels with negligible shrinking during the drying procedure [59]. In the following, the term xerogel is defined as subcritically dried and aerogel is used for supercritical dried materials. Easily obtainable resorcinol-formaldehyde aero- and xerogels are well investigated and can be tuned by several parameters. For example, the ratio of resorcinol and catalyst as well as the pH of the solution influences the properties of the gel material [60–62]. A major advantage, in terms of embedding porous materials, is the possibility of pre-polymerizing the polymer, which was reported first by Czakkel et al. [63]. By applying this method to MOF polymer composites, pore-blocking effects, which often occur in composite syntheses, could be avoided in order to retain the porous properties of the MOFs [43,45,53].

In this work, we present for the first time the embedding of three different metal-organic frameworks (MIL-100(Fe, Cr) and MIL-101(Cr)) in resorcinol-formaldehyde xerogels and investigate the resulting monoliths for their porosity and water-sorption behavior.

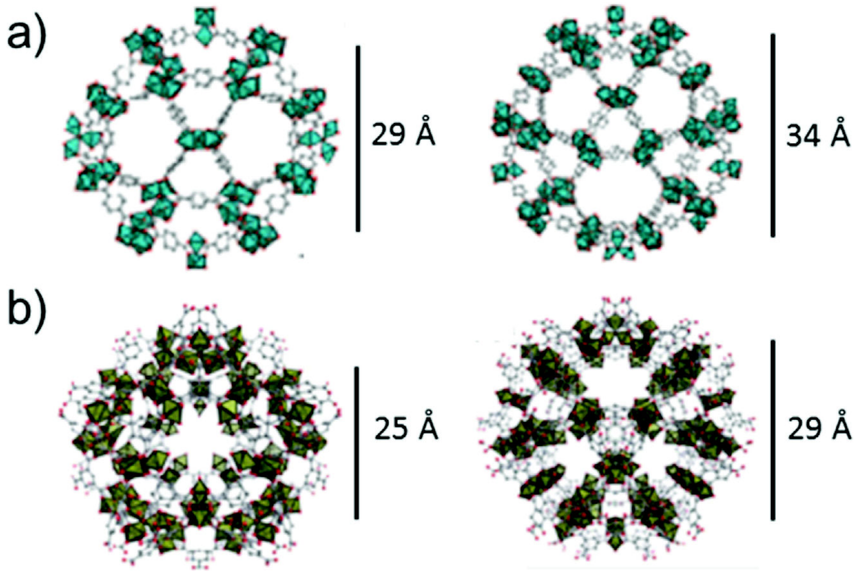

Fig. 2. a) MIL-101(Cr) small and large cages (CSD-Refcode OCUNAK [42]). b) Small cage and large cage in MIL-100(Fe) (CSD-'Refcode CIGXIA [38]) (different objects are not drawn to scale). Hydrogen atoms and solvent molecules of crystallization are not shown. MIL-100(Cr) is isostructural to MIL-100(Fe). See Fig. A.16 and Fig. A17 for further details.

2. Experimental section

2.1. Materials and methods

All chemicals were obtained commercially and were used without further purification: Fe^0 powder (Riedel-de Haën, >99%), CrO_3 (Alfa Aesar, 99%), $Cr(NO_3)_3$ $9H_2O$ (Acros Organics, 99%), hydrofluoric acid (Acros Organics, 48–51 wt% in H_2O), HNO_3 (Grüssing, 65 wt%), 1,3,5-benzenetricarboxylic acid (H_3BTC) (Alfa Aesar, 98%), 1,4-benzenedicarboxylic acid (H_2BDC) (Acros Organics, >99%), tetramethylammonium hydroxide (TMAOH) (Alfa Aesar, 25 wt% in water), resorcinol (Acros Organics, 98%), Na_2CO_3 (Riedel-de Haën, >99.8%)), formaldehyde (VWR, 24 wt% in water), acetic acid (VWR, 99.9%), N,N'-dimethylformamide (DMF) (VWR, p.a.), ethanol (VWR, p.a.). All experimental work was performed in air.

2.2. Physical measurements

Powder X-ray diffraction (PXRD) diffractograms were obtained at ambient temperature on a Bruker D2 Phaser with a flat sample holder using Cu-Kα radiation ($\lambda = 1.54182$ Å). Fourier transform infrared spectra were done on a Bruker TENSOR 37 IR spectrometer at ambient temperature in a KBr disk in a range of 4000 to 500 cm^{-1}. Nitrogen physisorption isotherms were carried out on a Nova 4000e from Quantachrome at 77 K. Water physisorption isotherms were measured volumetrically on a Quantachrome Autosorb iQ MP at 293 K. For measuring the isotherms the materials were loaded into glass tubes capped with septa. The weighed tubes were attached to the corresponding degassing port of the sorption analyzer, degassed under vacuum at elevated temperature, weighed again and then transferred to the analysis port of the sorption analyzer. BET surface areas were calculated from the nitrogen physisorption isotherms. DFT calculations for the pore size distribution curves were done with the native NovaWin 11.03 software using the 'N_2 at 77 K on carbon, slit pore, nonlinear density functional theory (NLDFT) equilibrium' model [64–66]. Scanning electron microscopic images were done on a LEO 1430 VP (native xerogel, MIL-100(Fe)@xerogel), on a LEO 982 (77 wt%, MIL-101(Cr)@xerogel-H_2O) both from Zeiss and on a JSM-6510 (MIL-100(Cr)@xerogel; 35 wt%, MIL-101(Cr)@xerogel) from Jeol. The samples were coated with Au for 180 s at 30 mA by an AGAR sputter coater (LEO 1430 VP), sputtered with chromium (approx. 10 nm thickness, LEO 982) or with Au for 20 s at 35 mA by an Jeol JFC-1200 sputter (JSM-6510). The thermogravimetric analysis (TGA) curve of native R,F-xerogel was measured on a TG 209 F3 Tarsus from Netzsch in the temperature range between 303 and 873 K, with heating rate of 3 K min^{-1}.

2.3. Synthesis of MIL-100(Fe,Cr) and MIL-101(Cr)

MIL-100(Fe), MIL-100(Cr) and MIL-101(Cr) were hydrothermally synthesized according to the literature [67–69]. Typical batch sizes of 665 mg Fe^0 powder (11.9 mmol), 1.65 g H_3BTC (7.85 mmol), 0.83 mL hydrofluoric acid (24 mmol; 48–51 wt% in H_2O), 0.5 mL HNO_3 (7 mmol; 65 wt%) and 60 mL of deionized H_2O (for *MIL-100(Fe)*), 1.20 g CrO_3 (12.0 mmol), 2.52 g H_3BTC (12.0 mmol), 0.42 mL hydrofluoric acid (12 mmol; 48–51 wt% in H_2O) and 58 mL of deionized H_2O (for *MIL-100(Cr)*) and 4.80 g (12.0 mmol) $Cr(NO_3)_3$ $9H_2O$, 1.98 g (11.9 mmol) H_2BDC, 1.1 mL TMAOH (3.1 mmol; $\rho = 1.014$ g mL^{-1} ; 25 wt% in H_2O) and 60 mL of deionized water (for *MIL-101(Cr)*) yielded the raw MILs. For further activation the MILs were purified through a consecutive washing procedure with DMF, EtOH and deionized water (See Supplementary Data for details). 1.50, 3.18 and 2.34 g of purified MIL-100(Fe), MIL-100(Cr) and MIL-101(Cr) were isolated (41, 69 and 50% yield based on Fe or Cr), as orange-brown (MIL-100(Fe)) and green powders (MIL-100/101(Cr)) with BET surface areas and pore volumes shown in Table 1. Pore volumes (measured at $P \cdot P_0^{-1} = 0.95$) and BET surface areas were calculated from the type I N_2 sorption isotherms (Fig. A.2a, A.4a, A.6a, Table 1). Experimental, theoretical powder X-ray patterns and the IR-spectra are shown in Fig. A.1, A.3, A.5.

2.4. Synthesis of native R,F-xerogel

The polycondensation reaction of resorcinol and formaldehyde is initiated by the basic catalyst Na_2CO_3, which first leads to deprotonation of the acidic phenol groups followed by addition of formaldehyde to the phenol ring. The formed hydroxymethyl functionalities (-CH_2OH) undergo a condensation reaction forming a methylene (–CH_2–)- and methylene ether (–CH_2OCH_2–)-bridged polymer illustrated in Scheme 1. For gelation (polymerization)

Table 1
Nitrogen and water vapor sorption measurements.

Sample[a]	Textural data			Water adsorption value[e]		
	S(BET) meas.[b] ($m^2\ g^{-1}$)	*S*(BET) calc.[c] ($m^2\ g^{-1}$)	*V*(pore),[d] ($cm^3\ g^{-1}$)	meas.[e] ($g\ g^{-1}$)	calc.[f] ($g\ g^{-1}$)	Rel. to surface area[g] ($x\ 10^{-3}\ g\ m^{-2}$)
R,F-xerogel	100	–	0.16	0.10	–	
MIL-100(Fe)	2200[h]	–	0.94	0.76[i]	–	0.35
Composites:						
43 wt%	590	1000	0.31	0.26	0.38	0.44
50 wt%	730	1150	0.39	0.33	0.43	0.45
58 wt%	770	1320	0.41	n.d.[j]		
MIL-100(Cr)	1560[k]		0.85	0.60[l]		0.38
Composites:[m]						
41 wt%	400	700	0.28	0.23	0.31	0.57
51 wt%	550	850	0.35	0.28	0.36	0.51
56 wt%	570	920	0.40	n.d.[j]		
MIL-101(Cr)	3060[n]		1.45	1.06[o]		0.35
Composites:[p]	Standard/with water added		Standard/with water added	Standard/with water added		
35 wt%	960/1340	1140	0.54/0.69	n.d/0.41	0.44	0.31
46 wt%	1160/1420	1460	0.62/0.72	n.d./0.50	0.54	0.35
50 wt%	1350/1500	1580	0.72/0.76	n.d.		
77 wt%	-/2530	2380	-/1.27	-/0.88	0.84	0.35

[a] wt% refers to MIL amount in the composites.

[b] *S*(BET) measured from N_2 sorption isotherm 77 K with a standard deviation ± 20 $m^2\ g^{-1}$ (calculated at $0.05 < P \cdot P_0^{-1} < 0.2$).

[c] *S*(BET) calculated (estimated) as the sum of the mass-weighted surface areas of the MILs (MIL-100(Fe) = 2200 $m^2\ g^{-1}$; MIL-100(Cr) = 1560 $m^2\ g^{-1}$; MIL-101(Cr) = 3060 $m^2\ g^{-1}$) and R,F-xerogel (100 $m^2\ g^{-1}$) from the following formula (I): $\text{BET calc} = \frac{\text{wt\% of xerogel}}{100} \times 100\ m^2\ g^{-1} + \frac{\text{wt\% of MIL}}{100} \times 2200\ (\text{MIL} - 100\text{Fe})\ \text{or}\ 1560\ (\text{MIL} - 100\text{Cr}\ \text{or}\ 3060\ (\text{MIL} - 101\text{Cr})\ m^2\ g^{-1}$.

[d] Total pore volume V(pore) calculated from N_2 sorption isotherm at 77 K ($P \cdot P_0^{-1} = 0.95$) for pores ≤20 nm.

[e] Water adsorption value measured from water sorption isotherm at 293 K ($P \cdot P_0^{-1} = 0.9$).

[f] Water adsorption value calculated (estimated) as the sum of the mass-weighted uptakes at $P \cdot P_0^{-1} = 0.9$ of the MILs (MIL-100(Fe) = 0.76 $g\ g^{-1}$; MIL-100(Cr) = 0.60 $g\ g^{-1}$; MIL-101(Cr) = 1.06 $g\ g^{-1}$) and R,F-xerogel (0.10 $g\ g^{-1}$) from the following formula (II); $\text{Water adsorption calc} = \frac{\text{wt\% of xerogel}}{100} \times 0.10\ g\ g^{-1} + \frac{\text{wt\% of MIL}}{100} \times 0.76\ (\text{MIL} - 100\text{Fe})\ \text{or}\ 0.60\ (\text{MIL} - 100\text{Cr})\ \text{or}\ 1.06\ (\text{MIL} - 101\text{Cr})\ g\ g^{-1}$.

[g] Water adsorption value calculated relative to the measured BET surface area of the MIL or MIL@xerogel composite according to the following formula (III): $\text{Water adsorption calculated relative to surface area} = \frac{\text{Water adsorption measured in g g}^{-1}}{\text{S(BET) measured in m}^2\ \text{g}^{-1}}\ [g\ m^{-2}]$ for example: for MIL-100(Fe): 0.76 $g\ g^{-1}$/2200 $m^2\ g^{-1} = 0.00035\ g\ m^{-2} = 0.35 \times 10^{-3}\ g\ m^{-2}$; 43 wt% MIL-100(Fe)@xerogel composite: 0.26 $g\ g^{-1}$/590 $m^2\ g^{-1} = 0.00044\ g\ m^{-2} = 0.44 \times 10^{-3}\ g\ m^{-2}$.

[h] In literature 1550–2050 $m^2\ g^{-1}$ [38,39].

[i] In literature 0.65–0.75 $g\ g^{-1}$ [35,40].

[j] n.d. = not determined.

[k] In literature 1770–1980 $m^2\ g^{-1}$ [38,39].

[l] In literature 0.6–0.7 $g\ g^{-1}$ [37].

[m] MIL-100(Cr)@xerogel without any pre-polymerization of the xerogel solution yielded a BET surface area of 20 $m^2\ g^{-1}$ and a total pore volume of 0.03 $cm^3\ g^{-1}$ (see Supplementary Data for details).

[n] In literature 2060–4100 $m^2\ g^{-1}$ [29,42].

[o] In literature 1.0–1.5 $g\ g^{-1}$ [29,41].

[p] The first value refers to the standard syntheses of MIL-101(Cr)@xerogel, the second value to the synthesis of MIL-101(Cr)@xerogel-H_2O composites where additional water was used.

typically resorcinol (R) and formaldehyde (F) are dissolved in a basic, aqueous Na_2CO_3 solution (C, $c = 2.1 \cdot 10^{-3}$ mol L^{-1}). The base C is essential for the formation of the R anions, which are more active towards the addition of F compared to uncharged, neutral R. After a short period of stirring (5 min), the so-called sol mixture, is transferred into an appropriate mold and cured for 7 days at 333 K. The curing of the sol leads to a monolithic product, which is then placed for 1 day in dilute acetic acid solution to increase the crosslinking of the residual hydroxymethyl groups. The monolithic resorcinol-formaldehyde polymers are washed in ethanol several times and finally dried subcritically by conventional evaporation of the solvent at atmospheric pressure (See Supplementary Data for details). The obtained brown-colored polymers are called "xerogels". Supercritical drying with CO_2 would lead to so-called "aerogels". The choice of the catalyst concentration, the initial gel pH, the concentration of R and F in the sol, dilution effects and the way of drying the monoliths all influence the particle size, density, surface area and mechanical strength of the final monoliths. For a detailed analysis of these factors the reader is referred to other literature [56,60,61].

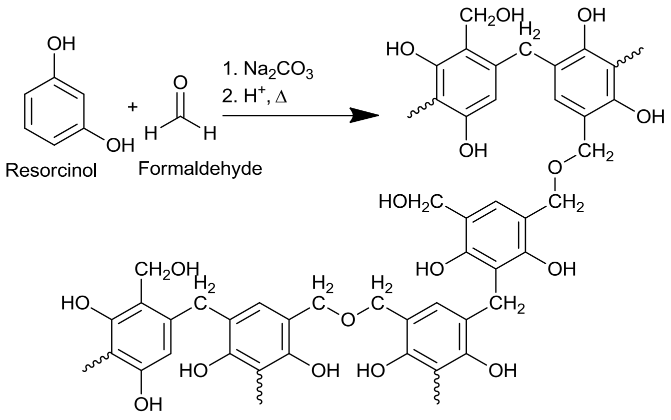

Scheme 1. Schematic presentation of the polymerization reaction of resorcinol (R) with formaldehyde (F) in the presence of a base (C).

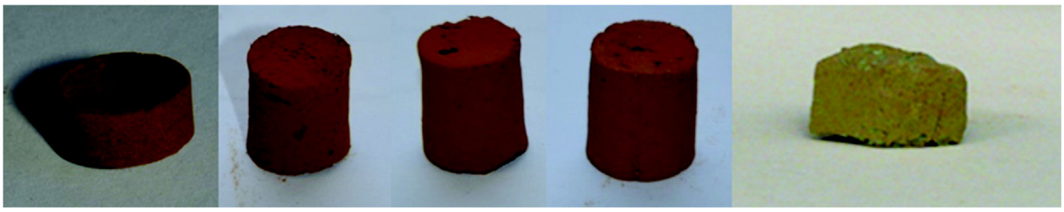

Fig. 3. From left to right: Pure R,F-xerogel, MIL@xerogel composites with 58 wt% MIL-100(Fe), 41 wt% MIL-100(Cr), 50 wt% MIL-101(Cr) and 77 wt% MIL-101(Cr) (77 wt%, MIL-101(Cr)@xerogel-H_2O). Dimensions (diameter × height) are 13 × 8 mm for pure R-F-xerogel; 10 × 13 mm for both MIL-100@xerogel; 10 × 14 mm for MIL-101(Cr)@xerogel (50 wt%) and 15 × 10 mm for MIL-101(Cr)@xerogel-H_2O (77 wt%). MIL-101(Cr)@xerogel-H_2O was cut to show the MIL distribution inside the monolith.

2.5. *Syntheses of MIL-100(Fe,Cr)@xerogel and MIL-101(Cr)@xerogel*

MIL@xerogel with different wt% of MILs were synthesized by homogenization of the MIL powders with the pre-polymerized R,F-xerogel solution. The prepared R,F-xerogel solution was filled into syringes (approx. 1 g per syringe), which were cut off from the cannula side, properly sealed by several layers of polyethylene- and aluminum foil and pre-polymerized for 5 h at 343 K. During this step the native R,F-xerogel changed from a clear, almost colorless solution to a honey-like, viscous material (Fig. A.11). Various amounts of well-ground MIL-100(Fe), MIL-100(Cr) and MIL-101(Cr) powders (100, 150 and 180 mg) were added to the pre-polymerized R,F-xerogel. After homogenization of the mixtures directly in the syringes by means of a spatula, curing, washing, and drying, brown monoliths with MIL contents between 35 and 58 wt% were isolated. To maximize the amount of MOF powder in the composites, one MIL-101(Cr)@xerogel-H_2O with 77 wt% of MIL was synthesized by additional usage of water to the pre-polymerized xerogel for proper homogenization of the MIL@xerogel mixture yielding a green monolith (Fig. 3). The suffix $-H_2O$ is added to MIL@xerogel when additional water was used in the composite syntheses. MIL-101(Cr)@xerogel-H_2O (35, 46, 50 wt%) were also obtained using additional water during the synthetic procedure (see Supplementary Data for details). If no additional water was used, the term ‘standard synthesis’ was used.

3. Results and discussion

3.1. *Native R,F-xerogel*

Infrared data (Fig. 4a) of the native or bulk resorcinol-formaldehyde based xerogel reveal the expected organic functional groups (*cf.* R,F-xerogel structure in Scheme 1). The broad band between 3700 and 3000 cm^{-1} is associated with the ν(O–H) stretching vibrations, originating from the phenol groups and water molecules in the hydrophilic xerogel. Aliphatic stretching vibrations $\nu(CH_2)$ can be assigned to the band at 2931 cm^{-1}. The corresponding $\delta(CH_2)$ deformation vibration is located at

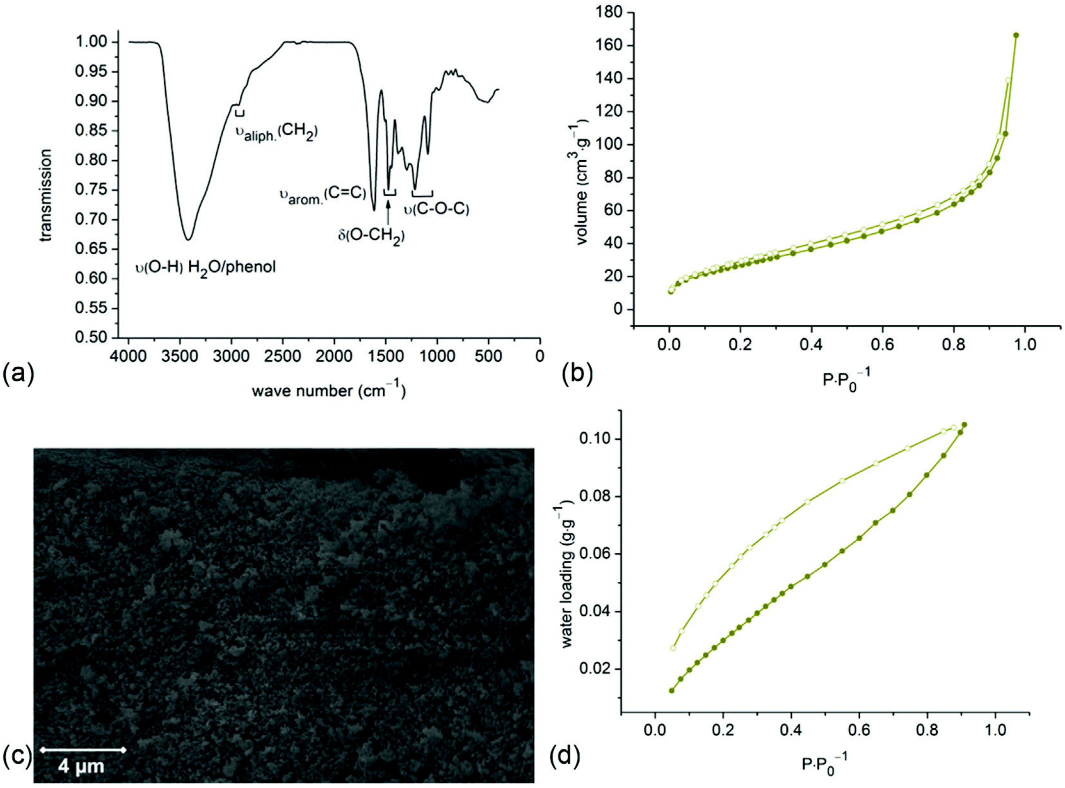

Fig. 4. Native or bulk R,F-xerogel (a) IR-spectrum (KBr), (b) N_2-sorption isotherm (degassing conditions: 3 h, 423 K), (c) scanning electron microscopy (SEM) image, (d) water vapor sorption isotherm (degassing conditions: 3 h, 423 K). Adsorption is depicted with filled, desorption with empty symbols.

1474 cm^{-1}. The band at 1613 cm^{-1} corresponds to the aromatic ring stretching vibration ν(C=C) and valence vibration bands at 1217 and 1092 cm^{-1} reveal the presence of the methylene ether bridges ν(C–O–C). The IR-spectrum is consistent with other literature data [70].

The porous nature of the xerogel is verified by N_2 sorption experiments (Fig. 4b). The N_2 sorption isotherm exhibits a mixture of type II (macroporous) shape together with type IV (mesoporous) shape, due to the hysteresis between adsorption and desorption isotherm [71]. The pore volume of 0.16 $cm^3\ g^{-1}$ and the BET surface area of 100 $m^2\ g^{-1}$, both calculated from the N_2 adsorption isotherm, are typical values for subcritically dried R,F-xerogels with the following molar ratios of the starting materials: resorcinol/formaldehyde = 0.73, resorcinol/Na_2CO_3 = 1000, resorcinol/water = 0.031 (Table 1) [60,70,72].

Scanning electron microscopy (SEM) images displays the typical morphological surface known for resorcinol-formaldehyde xerogels with low catalytic Na_2CO_3 concentrations (high resorcinol/Na_2CO_3 molar ratios of R/C = 1000) (Fig. 4c). The morphology can be described as interconnected colloidal-like particles, which do not possess porosity themselves, but generate porosity between the gaps of the particles [60,70].

Thermogravimetric analysis of the native xerogel shows a first mass loss of approximately 10 wt% up to temperature of 473 K, which can be assigned to the loss of physisorbed water (Fig. A.7a). The R,F-xerogel is thermally stable up to 493 K. The first mass loss of 10 wt% of water together with the shape of its water adsorption isotherm, showing an almost linear rise of water vapor with a total water uptake of 0.10 g g^{-1} at $P \cdot P_0^{-1} = 0.9$, indicates a hydrophilic character, which is comparable to silica gels (Fig. 4d, Table 1).

3.2. *Embedding MIL-100(Fe,Cr) and MIL-101(Cr) into R,F-xerogel monoliths*

Monolithic composites, consisting of a metal-organic framework (*e.g.* MILs) and an organic polymer (*e.g.* R,F-xerogel), can be synthesized in two different ways: (i) The synthesized MIL powder can either be mixed together with the just prepared xerogel solution, followed by curing, washing and drying steps ('direct route'). (ii) The MIL can be synthesized *in situ* into the already cured, porous system of a R,F-xerogel monolith by impregnating it with the corresponding starting materials (metal source and linker) followed by an appropriate temperature program ('in-situ route'). Through the direct route the ratio of MIL and R,F-xerogel in the final monolithic product can easily be predetermined by varying the amount of MIL powder and xerogel solution, which is not that realizable in the in-situ route. A disadvantage of the direct route is that the micro- and mesopores of the MOF can be blocked by the monomers or oligomers of the xerogel precursors. This pore blocking is accompanied by a pronounced decrease of the total surface area of the monolith. In this paper, we describe how to avoid pore blocking by pre-polymerization of the xerogel solution, resulting in highly porous and therefore active monolithic MIL@xerogel composites through the direct route.

In a first experiment aimed to synthesize a highly porous composite, MIL-100(Cr) powder was mixed together with an excess of the just prepared R,F-xerogel solution without any pre-polymerization. To maximize the amount of MIL in the monolithic composite, the powder was sedimented for one day followed by curing. After washing and drying steps the resulting monolith consisted of a brown bottom layer containing MIL and xerogel and a top brown layer, which represents the pure xerogel (Fig. A.8a). Powder X-ray diffraction pattern and infrared spectrum reveal the unchanged presence of the MIL-100(Cr) phase in the composite material (Fig. A.8b,c), but the N_2-sorption isotherm and the corresponding pore size distribution curve showed only a small residual porosity of 20 $m^2\ g^{-1}$, indicative of complete blockage of the micro- and mesopores of MIL-100(Cr) in the monolithic composite (Fig. A.9a,b) (see Supplementary Data for details). The disappearance of the MIL pores in the composites occurs through the initial filling of the micro- and mesopores or at least the pore mouths by resorcinol and formaldehyde molecules followed by polycondensation inside these MIL pores or pore mouths.

For the synthesis of highly porous monolithic MOF@xerogel composites the MIL pores have to be protected during the synthesis. To avoid, or at least minimize polymerization reactions of resorcinol and formaldehyde inside the MIL pores, the xerogel solution has to be pre-polymerized before adding the MIL powder to create larger resorcinol-formaldehyde oligomers or small polymer strands. Those larger oligomers should be less prone to diffuse into and block the MIL pores.

Similar experiments were carried out here on MIL-100(Fe)@xerogel composites. Identical amounts of just prepared xerogel solution were placed for 3, 4 and 5 h into an oven at 343 K. After 3, 4

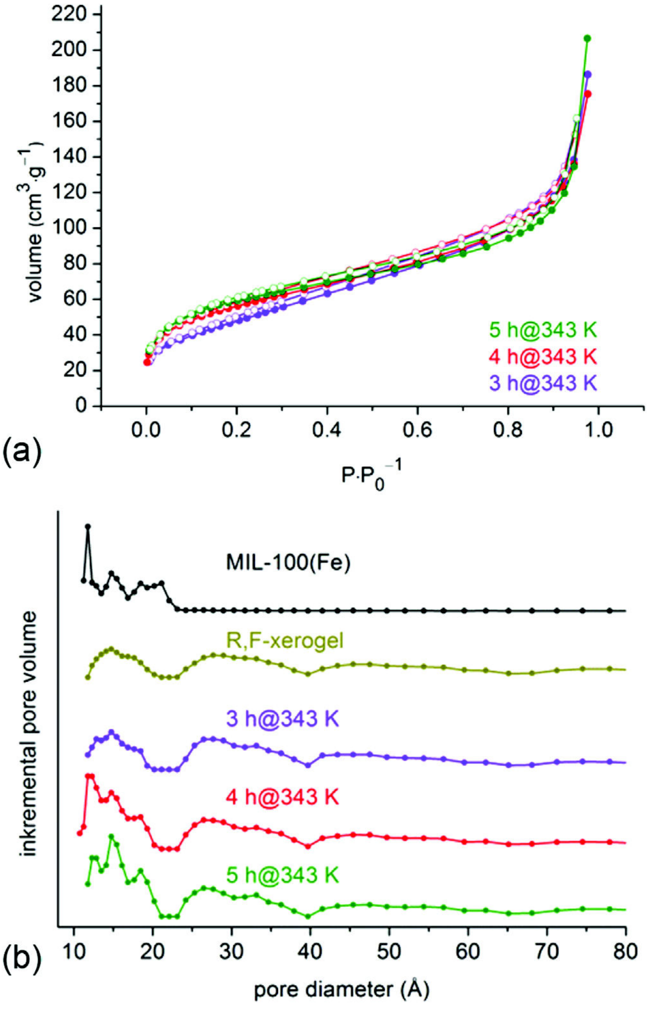

Fig. 5. (a) N_2-sorption isotherms of MIL-100(Fe)@xerogel with 11 wt% MIL-100(Fe). MIL-100(Fe) powders were added to the R,F-xerogel solutions after 3, 4 and 5 h of pre-polymerization time at 343 K, respectively (degassing conditions: 3 h, 423 K, S(BET) = 180 $m^2\ g^{-1}$ (3 h), 210 $m^2\ g^{-1}$ (4 h), 220 $m^2\ g^{-1}$ (5 h)). (b) Pore size distribution curves of native MIL-100(Fe), native R,F-xerogel and MIL-100(Fe)@xerogel with 11 wt% MIL-100(Fe) (3, 4 and 5 h of polymerization at 343 K). Adsorption is depicted with filled, desorption with empty symbols.

and 5 h of pre-polymerization time the viscous solutions were mixed together with 100 mg of MIL-100(Fe) powder, respectively. Homogenization, curing, washing and drying were done according to the native R,F-xerogel synthesis yielding brown monoliths each with 11 wt% of MIL-100(Fe) (See Supplementary Data for details). X-ray diffraction patterns and infrared spectra prove the existence of MIL-100(Fe) in all three composites (Fig. A.12a,b). The weight-averaged estimated BET surface area of the composite would be $= \frac{\text{wt\% of xerogel}}{100} \times 100\ \text{m}^2\ \text{g}^{-1} + \frac{\text{wt\% of MIL}}{100} \times 2200\ (\text{MIL} - 100\text{Fe})\ \text{m}^2\ \text{g}^{-1}$. For 11 wt% of MIL-100(Fe) the estimated BET surface of the composite would then be ~330 $m^2\ g^{-1}$. The corresponding N_2-sorption isotherms yield increased BET surface areas by elongation of the pre-polymerization time of the xerogel solution: 180 $m^2\ g^{-1}$ for 3 h, 210 $m^2\ g^{-1}$ for 4 h, 220 $m^2\ g^{-1}$ for 5 h (Fig. 5a). Pore size distribution curves also confirm the increasing fraction of the MIL-100(Fe) micropores with elongation the pre-polymerization rate (Fig. 5b). After 3 h the MIL-100(Fe) pores between 12 and 21 Å are hardly visible in the composite material, whereas 4 and 5 h of pre-polymerization time leads to more accessible, clearly observable micropores.

The pre-polymerization rate is not only controllable by temperature and time. Also the amount of xerogel solution at a given concentration is an important parameter. A larger amount of a xerogel solution needs more time for curing at a given temperature. It has been found that the maximum pre-polymerization time for 1 g of xerogel solution at 343 K is 5 h. With a longer temperature treatment the MIL powder and pre-polymerized xerogel solution cannot be homogenized properly any more.

Different, mechanically stable, monolithic MIL@xerogel composite materials were synthesized using well-ground MIL-100(Fe), MIL-100(Cr) and MIL-101(Cr) powder (100–460 mg) respectively and 1 g of pre-polymerized (5 h, 343 K) xerogel solution for each monolith. Fig. 3 shows the pure R,F-xerogel monolith together with MIL-100(Fe)@xerogel (43 wt%), MIL-100(Cr)@xerogel (41 wt%) MIL-101(Cr)@xerogel (50 wt%) and MIL-101(Cr)@xerogel-H_2O (77 wt%) (from left to right). To maximize the amount of MOF in the composite, a small amount of water was added to the pre-polymerized xerogel to reach a proper homogenization with 77 wt% MIL-101(Cr) in the composite material (See Supplementary Data for details). Increasing the amount of MIL-101(Cr) powder up to 77 wt% yielded a monolith with the typical green color of MIL-101(Cr). Other monolithic composites using lower weight percentages of orange-brown MIL-100(Fe) or green MIL-100/101(Cr) powders yielded brown monoliths. Mechanical stability tests have been carried out on the pure R,F-xerogel and three representative composites in a shaking incubator for 3 h to determine the abrasion under mechanical treatment (See Supplementary Data for details, Fig. A.18). Pure R,F-xerogel shows the lowest degree of abrasion with only 1.1 wt% of mass loss. The composites feature more abrasion (6.8–19.5 wt% mass loss) due to the MIL content, but fortunately none of the tested monoliths did break into granules through shaking for 3 h.

Representative scanning electron microscopy images of MIL-100(Fe)@xerogel (43 wt%) and MIL-101(Cr)@xerogel-H_2O (77 wt %) (Fig. 6a–d) show the typical octahedral MIL morphologies with particle sizes between 2 and 5 μm for MIL-100(Fe) and 300–500 nm for MIL-101(Cr) in the composites [69,73]. MIL octahedra and xerogel substrate are well grown together to a physical mixture with the xerogel surrounding the MIL particles and with both components showing a reasonable adherence (Fig. 6). The increasing amount of MIL octahedra in the composites is obvious by comparing Fig. 6a–b (43 wt% MIL) with Fig. 6c–d (77 wt% MIL). The embedding of MOF particles leads to a high dispersion of MIL crystallites in the xerogel matrix.

Powder X-ray diffraction patterns of MIL@xerogel compounds demonstrate the unchanged, crystalline phase of the respective MILs in the composites (Fig. A.19a–c) although the reflections of MIL-101(Cr) composites are slightly broadened compared to bulk MIL-101.

Infrared spectra of the composite materials represent an additive overlap of the individual spectra of the corresponding components (MILs and xerogel) (Fig. A.20a–c). With increasing loading of MIL in the MIL@xerogel composites, the intensities of bands, coming from the MIL components are enhanced. The regions highlighted by square brackets in Fig. A.20 show the increasing bands for the asymmetric [$\nu_{as}(R\text{-}CO_2)$, region 1] and symmetric

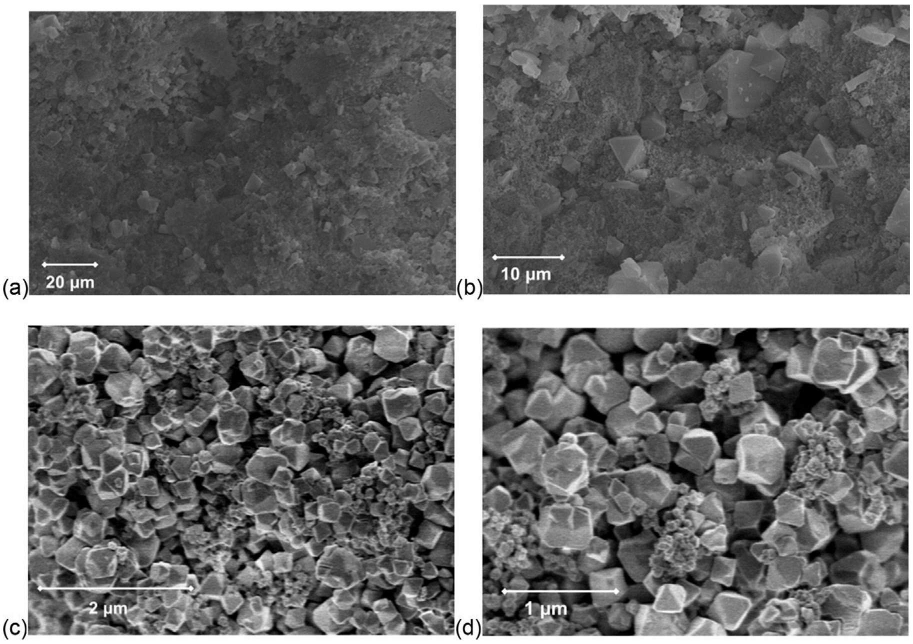

Fig. 6. Scanning electron microscopy (SEM) images of (a)–(b) MIL-100(Fe)@xerogel (43 wt% MIL-100(Fe)) and (c)–(d) MIL-101(Cr)@xerogel-H_2O (77 wt% MIL-101(Cr)) composites.

[ν_s(R-CO_2), region 2] valence-vibrations of the coordinated BDC- or BTC-ligand of the MILs. Region 3 displays the deformation-vibration of the carboxyl groups [δ(R-CO_2)].

3.3. N_2- and water sorption studies

N_2 sorption measurements have been carried out for all pre-polymerized MIL@xerogel composites (Fig. 7a, c, e). The nitrogen adsorption capacities increase continuously with increasing the MIL content. The composites feature a transition from type II/IV for the bulk R,F-xerogel to type I-shaped N_2 isotherms with the MIL additive and its free and accessible micropores. The steep rise at low relative pressures, typical for type I isotherms, becomes more pronounced with increasing MIL ratios. BET surface areas increase with the amount of MIL in the monolithic composites (Table 1). The relevant comparison is to the estimated mass-weighted surface areas of bulk MIL and xerogel using Formula (I) from Table 1. MIL-100(M)@xerogel (M = Fe, Cr) composites reach approximately 60% of the estimated surface areas. MIL-101(Cr)@xerogel composites with MIL loading between 35 and 50 wt% achieve nearly 83% of the expected values. The higher BET surface areas for MIL-101 composites, compared to the MIL-100 composites, can be explained by pronounced pore blocking effects in the MIL-100 containing composites. The xerogel-binding agent can more easily diffuse and therefore block the smaller MIL-100 pores due to the smaller windows size of MIL-100 (4.7–5.5 Å, 8.6 Å) compared to the windows of MIL-101 (12 Å, 15–16 Å) (Fig. A.16, Fig. A.17, Fig. 2). In other words: Smaller pores are more difficult to protect than larger pores.

As stated above, to maximize the amount of MIL-101(Cr) in the monolithic composite a small amount of additional water was added to the pre-polymerized xerogel solution together with MIL-101 powder to achieve a proper homogenized mixture (See Supplementary Data for details). The resulting monolith with 77 wt% of MIL-101(Cr) shows a BET surface which is even slightly

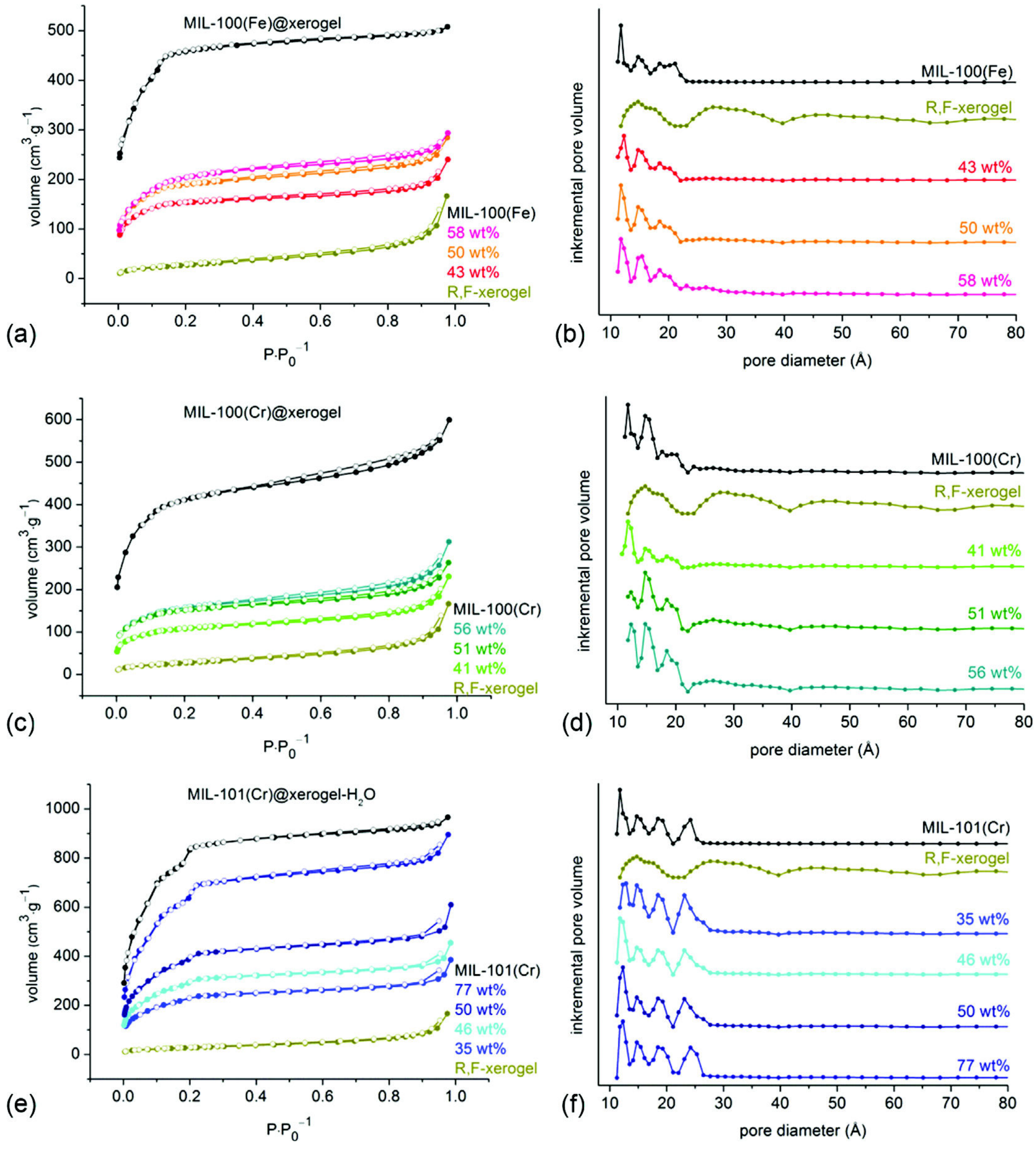

Fig. 7. N_2-sorption isotherms and pore diameter distribution of R,F-xerogel, MILs and MIL@xerogel composites. See Table 1 for BET surface areas and total pore volumes. (a,b) MIL-100Fe, (c,d) MIL-100Cr, (e,f) MIL-101Cr (a–d: MIL-100@xerogel; e,f: MIL-101(Cr)@xerogel-H_2O). For enlarged pore size distribution curve of bulk MILs see Fig. A.2c, A.4c, A.6c (degassing conditions: 3 h, 423 K). Adsorption is depicted with filled, desorption with empty symbols. N_2 sorption data of MIL-101(Cr)@xerogel without water addition is shown in Fig. A.13(a,b).

higher (+150 $m^2 g^{-1}$) than the estimated BET (Table 1). The addition of water with the MIL could lead to formation of a water layer around the MIL crystallites; thereby prevent pore blocking by the xerogel. This assumption is supported by comparison of the SEM images of 35 wt% MIL-101(Cr)@xerogel-H_2O (Fig. A.15) and 35 wt% MIL-101(Cr)@xerogel, in which no water was added (Fig. A.14). The 35 wt% MIL-101(Cr)@xerogel-H_2O has the MIL crystallites slightly more separated from the xerogel, while the 35 wt% MIL-101(Cr)@xerogel (no H_2O) shows the MIL and xerogel more intimately mixed.

Subsequent addition of water also significantly increased the surface areas and total pore volumes in case of the 35, 46 and 50 wt% MIL-101(Cr)@xerogel-composites (Table 1).

Pore size distribution curves of the bulk MILs can be calculated from the nitrogen adsorption isotherms (Fig. 7) using NLDFT models and show pores sizes of 12, 15, 18–19 and 20–21 Å for *MIL-100(Fe)* and *MIL-100(Cr)*. The pore regions of 18–19 and 20–21 Å correspond to the MIL-100 cages (Fig. A.17).

The pore size distribution curve of bulk MIL-101(Cr) shows pores of 12 and 15 Å in diameter, which are consistent with the pentagonal (12 Å) and hexagonal windows (14.7–16 Å) (Fig. A.16) [42]. The larger pores of 19 and 24 Å belong to the cages with diameters of 29 and 34 Å (Fig. A.16) [42]. Differences to the cage size from X-ray structure refinement can be explained by residual impurities of non-coordinated ligand and metal-ligand fragments inside the pores [74].

Pore size distribution curves of the MIL@xerogel composites match those of the respective bulk MIL. Thus, from N_2 sorption isotherms, BET surface area and pore diameter distribution it is obvious that all monolithic composite materials largely retain the accessibility to the micro- and mesopores of the MIL. This is, however, only true for the materials based on pre-polymerized xerogel solutions. In contrast, a MIL-100(Cr)@xerogel composite without any pre-polymerization of the xerogel solution, presents a material which appears non-porous or without any accessible porosity (Table 1, see ‘l’; Fig. A.8, A.9, A.10).

Other MOF composite materials show similar differences between experimental and estimated BET surface areas (Table 2). HKUST-1, embedded in porous carbon monoliths achieves only 40% of the estimated BET surface areas [45]. Composites like UiO-66@polyurethane or HKUST@HIPE reach about 60% of the calculated values [53,75,76]. These values are comparable to our pre-polymerized MIL-100(M)@xerogel (M = Fe, Cr) compounds. Yet, metal-organic frameworks in inorganic silica templates, such as HKUST-1 incorporated in silica aerogels or HKUST-1 in macro-/mesoporous silica match or even exceed the estimated BET values similar to the MIL-101(Cr)@xerogel composites with added water reported here [52,58].

In order to evaluate the monolithic composites as potential adsorbents for heat transformation applications, water sorption experiments were carried out to quantify their hydrophilic behavior. Water sorption isotherms of different MIL@xerogel materials are shown together with the adsorption isotherm of bulk MIL and R,F-xerogel (Fig. 8a–c). MIL-100@xerogel composites display the same stepwise adsorption isotherm, as for bulk MIL-100(M) (M = Fe, Cr) (Fig. 8a–b, Fig. A.2b, Fig. A.4b). This specific shape relates to the stepwise filling of the different MIL-100 cages. Mesopores larger than 20 Å (2 nm) for MIL-100(Cr)@xerogel samples probably influence the water adsorption characteristics of these composites (Table 1, Fig. 7).

Water loading capacities at $P \cdot P_0^{-1} = 0.9$ of the MIL@xerogel compounds can be estimated (calculated) from the MIL wt% based on the water uptake of bulk MIL using formula (II) in Table 1. MIL-100(M)@xerogel (M = Fe, Cr) compounds reach approximately 74% of the calculated values. The MIL-101(Cr)@xerogel monoliths with 35 and 46 wt% of MIL loading achieve 93% of the estimated water uptake capacities. Compared to the BET analyses given above, the MIL-101(Cr) water uptakes are closer to the calculated expected

Table 2
Comparison of N_2 sorption data of similar composite materials from the literature.

Composites	Experimental $S(BET)$ ($m^2 g^{-1}$)	Estimated $S(BET)$ ($m^2 g^{-1}$)[f]	wt% of MOFs and quantification method	Possible application	Ref.
HKUST-1 @PAM[a]	654[d]	667	62 wt%; N_2 sorption data + TGA	no application investigated	[76]
HKUST-1 monolith[b]	484[e]	–	No wt% given	no application investigated	[51]
HKUST-1 @porous carbon monoliths	270; 455; 516	816; 988; 1198	19 wt%; 41 wt%; 68 wt%; Weighing method	CO_2 storage; Gas separation (CO_2/N_2)	[45]
HKUST-1 @silica aerogel	1025; 1036; 1138	944; 955; 1056	4.2 wt%; 16.3 wt%; 30.5 wt%; Weighing method	no application investigated	[58]
HKUST-1 @macro-/mesoporous silica	971	907	25 wt%; TGA	catalysis	[52]
UiO-66@ polyurethane	511[d]; 427[d]	834; 752	71 wt%; 64 wt%; TGA	adsorption of organic vapors	[75]
HKUST-1 @HIPE	570	846	62.3 wt%; TGA	no application investigated	[53]
CAU-1@PMMA[c]	423	–	No wt% given	open-tubular capillary electro-chromatography	[69]

[a] PAM = polyacrylamide. We notice that MOF wt% determination in HKUST-1@PAM composites was calculated from nitrogen sorption data based on the assumption that all of the native MOF surface area is still accessible in the composite material.

[b] Binding agent: methoxy functionalized siloxane ether; plasticizer: methyl hydroxyl propyl cellulose.

[c] PMMA = polymethyl methacrylate.

[d] BET surface areas of pure binding agents are not considered in calculations due to the their absence in the corresponding literature.

[e] Values decreased after several months to 287 $m^2 g^{-1}$.

[f] BET surface area as the sum of the mass-weighted surface areas of MOFs and porous binding agents calculated from the following formula: $\text{BET (estimated)} = \frac{\text{wt\% of MOF}}{100} \times \text{BET of pure MOF} + \frac{\text{wt\% of binding agent}}{100} \times \text{BET of pure binding agent}$.

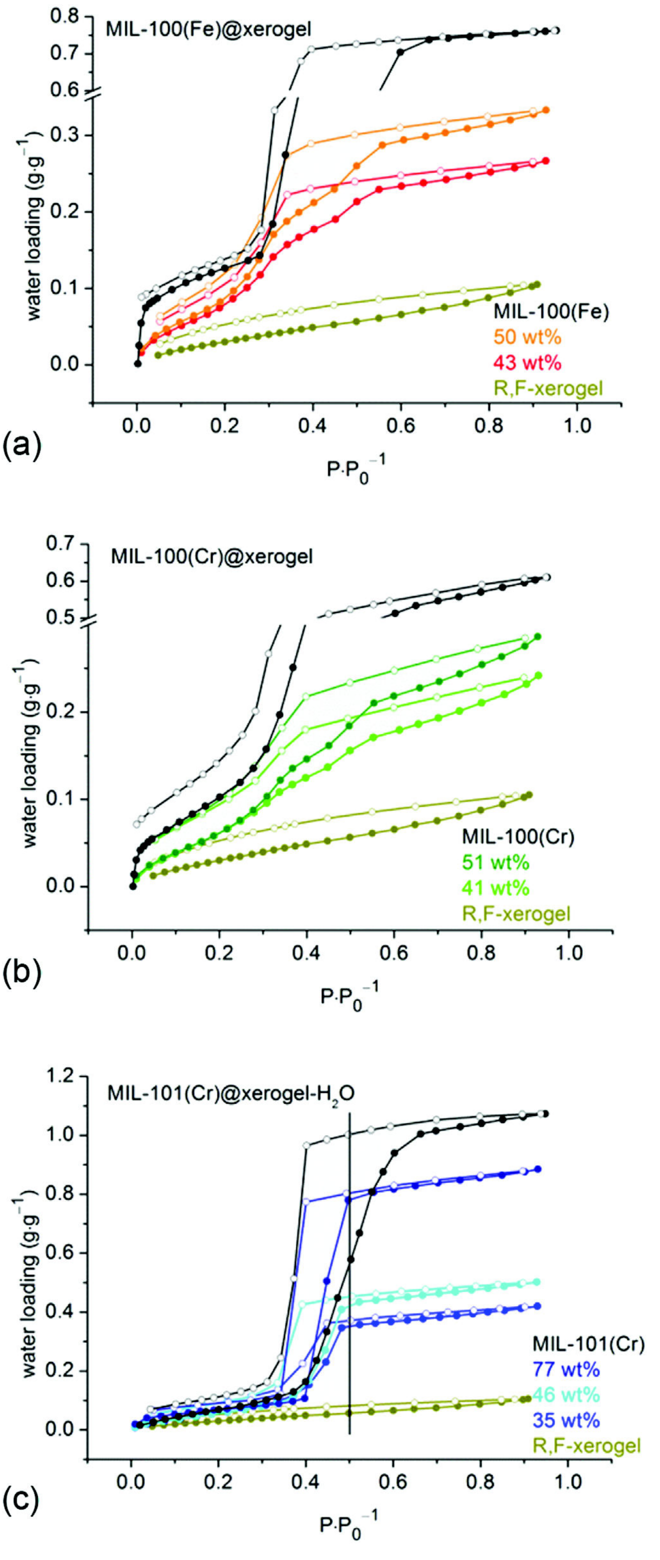

Fig. 8. Water vapor sorption isotherms of R,F-xerogel, MILs and MIL@xerogel composites. (a) MIL-100(Fe)@xerogel, (b) MIL-100(Cr)@xerogel, (c) MIL-101(Cr)@xerogel-H_2O (degassing conditions: 3 h, 423 K). Adsorption is depicted with filled, desorption with empty symbols.

values. The 77 wt% loaded MIL-101(Cr)@xerogel-H_2O matches or even slightly exceeds the estimated water uptake capacity as a result of the higher BET surface area (Table 1). As an indication of the hierarchical nature the 35 and 46 wt% MIL-101(Cr) composites achieve a near to maximum water loading already at $P \cdot P_0^{-1} = 0.5$ (Fig. 5c). The 77 wt% MIL-101(Cr)@xerogel-H_2O composites already realizes 0.79 g g^{-1} water uptake at $P \cdot P_0^{-1} = 0.5$ (Fig. 5c). In contrast, for bulk MIL-101(Cr) only 0.57 g g^{-1}, corresponding to ~50% water uptake, could be achieved at $P \cdot P_0^{-1} = 0.5$.

When calculating the water adsorption value relative to the surface area measured in the MIL@xerogel composite (last column in Table 1) the following trends became apparent: For the iron and chromium MIL-100@xerogel composites the surface-based water adsorption is higher than for the MIL-100 alone. This suggests that our method of encapsulation of MOFs leads to a high dispersion of the MILs in the xerogel matrix. For the MIL-101(Cr) composite (prepared with added water) and bulk MIL-101(Cr) the surface area-based water uptake values of 0.35×10^{-3} g m^{-2} are mostly the same. This is in agreement with the good match between the measured and calculated (mass-weighted) BET values for the composites prepared with added water. There is no pore blocking for the MIL-101(Cr)@xerogel-H_2O materials. The MIL-100(Cr) composite has a significantly higher surface area-based water adsorption value than the MIL-100(Fe) composite. This is explained by the hierarchical contribution of the xerogel matrix which adds significantly with diameters >20 Å for the chromium and less for the iron material according to the pore diameter distribution plots in Fig. 8d and b (see Supporting Information).

4. Conclusion

We presented new composite materials in monolithic shape based on a metal-organic framework part (MIL-100(M)/101(Cr), (M = Fe, Cr)) and a polymerized resorcinol-formaldehyde xerogel as the binding agent. Mesoporous resorcinol-formaldehyde (R,F-) xerogels are easily obtainable, highly tunable and the second most investigated xerogels (after silica xerogels). The MIL@xerogel composites were characterized by powder X-ray diffraction, infrared spectroscopy, nitrogen- and water sorption and scanning electron microscopy. Embedding up to 77 wt% of MIL particles is possible without the loss of the mechanical stability of the monoliths. Pore blocking effects of the MILs through the binding agent could largely be avoided by pre-polymerization of the native xerogel solution before embedding of the MILs. The larger MIL-101(Cr) pores remain more open than the smaller MIL-100 pores during the monolith syntheses. The expected BET surface areas and water uptakes could be reached when the MIL was added together with water to the pre-polymerized xerogel solution. Formation of a water film around the MIL particles may be responsible to avoid pore blocking. These MIL-101(Cr)@xerogel-H_2O composites then match the wt%-correlated BET values and water uptakes within experimental error. As an indication of the hierarchical nature the 77 wt% MIL-101(Cr)@xerogel-H_2O composite achieves 0.79 g g^{-1} water uptake at $P \cdot P_0^{-1} = 0.5$ while for bulk MIL-101(Cr) only 0.57 g g^{-1} water uptake could be achieved at $P \cdot P_0^{-1} = 0.5$. Also, the surface area-based water adsorption is higher for the MIL-100@xerogel composites than for MIL-100 alone.

Acknowledgments

Support by the DAAD with PPP-project no 57053987 ("hierarchical structured metal-based nanocomposites“) and the University of Düsseldorf through its strategic research fund (SFF) is gratefully acknowledged. We thank Mr. Steffen Köhler for help with the SEM images. Marina Schwan and Jessica Laskowski from DLR, Cologne for the kind introduction to xerogel syntheses. We thank one of the referees for emphasizing the water adsorption value relative to the surface area.

Appendix A. Supplementary data

Supplementary data related to this article can be found at http://dx.doi.org/10.1016/j.micromeso.2015.05.017.

References

[1] (a) S.R. Batten, N.R. Champness, X.-M. Chen, J. Garcia-Martinez, S. Kitagawa, L. Öhrström, M. O'Keeffe, M.P. Suh, J. Reedijk, CrystEngComm 14 (2012) 3001–3004;
(b) S.R. Batten, N.R. Champness, X.-M. Chen, J. Garcia-Martinez, S. Kitagawa, L. Öhrström, M. O'Keeffe, M.P. Suh, J. Reedijk, Pure Appl. Chem. 85 (2013) 1715–1724.
[2] J.R. Long, O.M. Yaghi, Chem. Soc. Rev. 38 (2009) 1213–1214.
[3] C. Serre, S. Kitagawa, P.D.C. Dietzel, Microporous Mesoporous Mater. 157 (2012) 1–2.
[4] M. Yoon, R. Srirambalaji, K. Kim, Chem. Rev. 112 (2012) 1196–1231.
[5] A. Herbst, A. Khutia, C. Janiak, Inorg. Chem. 53 (2014) 7319–7333.
[6] F.X. Llabrés i Xamena, F.G. Cirujano, A. Corma, Microporous Mesoporous Mater. 157 (2012) 112–117.
[7] R.B. Getman, Y.-S. Bae, C.E. Wilmer, R.Q. Snurr, Chem. Rev. 112 (2012) 703–723.
[8] Z. Chen, S. Xiang, H.D. Arman, P. Li, S. Tidrow, D. Zhao, B. Chen, Eur. J. Inorg. Chem. 24 (2010) 3745–3749.
[9] L. Wu, M. Xue, S.-L. Qiu, G. Chaplais, A. Simon-Masseron, J. Patarin, Microporous Mesoporous Mater. 157 (2012) 75–81.
[10] Z. Zhang, Y. Zhao, Q. Gong, Z. Li, J. Li, Chem. Commun. 49 (2013) 653–661.
[11] J.-R. Li, Y. Ma, M.C. McCarthy, J. Sculley, J. Yu, H.-K. Jeong, P.B. Balbuena, H.-C. Zhou, Coord. Chem. Rev. 155 (2011) 1791–1823.
[12] Z.R. Herm, R. Krishna, J.R. Long, Microporous Mesoporous Mater. 157 (2012) 94–100.
[13] M.G. Plaza, A.F.P. Ferreira, J.C. Santos, A.M. Ribeiro, U. Müller, N. Trukhan, J.M. Loureiro, A.E. Rodrigues, Microporous Mesoporous Mater. 157 (2012) 101–111.
[14] C. Janiak, Dalton Trans. 14 (2003) 2781–2804.
[15] C. Janiak, J.K. Vieth, New J. Chem. 34 (2010) 2366–2388.
[16] G. Férey, Chem. Soc. Rev. 37 (2008) 191–214.
[17] N. Stock, S. Biswas, Chem. Rev. 112 (2012) 933–969.
[18] M. Gaab, N. Trukhan, S. Maurer, R. Gummaraju, U. Müller, Microporous Mesoporous Mater. 157 (2012) 131–136.
[19] C. Li, J. Zhou, Y. Cao, J. Zhong, Y. Liu, C. Kang, Y. Tan, Appl. Energy 117 (2014) 149–156.
[20] (a) Y.I. Aristov, Int. J. Refrig. 32 (2009) 675–686;
(b) B.B. Saha, A. Chakarborty, S. Koyama, Y.I. Aristov, Int. J. Heat Mass Transf. 52 (2009) 516–524;
(c) R.E. Critoph, Z. Tamainot-Telto, S.J. Metcalf, Int. J. Refrig. 32 (2009) 1212–1229;
(d) J.V. Veselovskaya, R.E. Critoph, R.N. Thorpe, S. Metcalf, M.M. Tokarev, Y.I. Aristov, Appl. Therm. Eng. 30 (2010) 1188–1192.
[21] K. Habib, B.B. Saha, A. Chakraborty, S.T. Oh, S. Koyama, Appl. Therm. Eng. 50 (2013) 1582–1589.
[22] A.A. Askalany, M. Salem, I.M. Ismael, A.H.H. Ali, M.G. Morsy, B.B. Saha, Renew. Sust. Energ. Rev. 19 (2013) 565–572.
[23] D. Fröhlich, S.K. Henninger, C. Janiak, Dalton Trans. 43 (2014) 15300–15304.
[24] S.K. Henninger, H.A. Habib, C. Janiak, J. Am. Chem. Soc. 131 (2009) 2776–2777.
[25] S.K. Henninger, F. Jeremias, H. Kummer, C. Janiak, Eur. J. Inorg. Chem. (2012) 2625–2634.
[26] F. Jeremias, L. Lozan, S.K. Henninger, C. Janiak, Dalton Trans. 42 (2013) 15967–15973.
[27] J. Canivet, A. Fateeva, Y. Guo, B. Coasne, D. Farrusseng, Chem. Soc. Rev. 43 (2014) 5594–5617.
[28] J. Canivet, J. Bonnefoy, C. Daniel, A. Legrand, B. Coasne, D. Farrusseng, New J. Chem. 38 (2014) 3102–3111.
[29] J. Ehrenmann, S.K. Henninger, C. Janiak, Eur. J. Inorg. Chem. (2011) 471–474.
[30] M. Wickenheisser, F. Jeremias, S.K. Henninger, C. Janiak, Inorg. Chim. Acta 407 (2013) 145–152.
[31] G. Akiyama, R. Matsuda, H. Sato, A. Hori, M. Takata, S. Kitagawa, Microporous Mesoporous Mater. 157 (2012) 89–93.
[32] A. Khutia, H.U. Rammelberg, T.S. Schmidt, S. Henninger, C. Janiak, Chem. Mater. 25 (2013) 790–798.
[33] J.B. De Coste, G.W. Peterson, B.J. Schindler, K.L. Killops, M.A. Browe, J.J. Mahle, J. Mater. Chem. A 1 (2013) 11922–11932.
[34] F. Jeremias, D. Fröhlich, C. Janiak, S.K. Henninger, New J. Chem. 38 (2014) 1846–1852.
[35] F. Jeremias, A. Khutia, S.K. Henninger, C. Janiak, J. Mater. Chem. 22 (2012) 10148–10151.
[36] G. Férey, C. Serre, C. Mellot-Draznieks, F. Millange, S. Surble, J. Dutour, I. Margiolaki, Angew. Chem. Int. Ed. 43 (2004) 6296–6301.
[37] G. Akiyama, R. Matsuda, S. Kitagawa, Chem. Lett. 39 (2010) 360–361.
[38] P. Horcajada, S. Surble, C. Serre, D.-Y. Hong, Y.-K. Seo, J.-S. Chang, J.-M. Grenèche, I. Margiolaki, G. Férey, Chem. Commun. 27 (2007) 2820–2822.
[39] J.S. Lee, S.H. Jhung, J.W. Yoon, Y.K. Hwang, J.-S. Chang, J. Ind. Eng. Chem. 15 (2009) 674–676.
[40] L. Kurfiřtová, Y.-K. Seo, Y.-K. Hwang, J.-S. Chang, J. Čejka, Catal. Today 179 (2012) 85–90.
[41] P. Küsgens, M. Rose, I. Senkovska, H. Fröde, A. Henschel, S. Siegle, S. Kaskel, Microporous Mesoporous Mater. 120 (2009) 325–330.
[42] G. Férey, C. Mellot-Draznieks, C. Serre, F. Millange, J. Dutour, S. Surble, I. Margiolaki, Science 309 (2005) 2040–2042.
[43] B. Böhringer, R. Fischer, M.R. Lohe, M. Rose, S. Kaskel, P. Küsgens, in: D. Farrusseng (Ed.), Metal-organic Frameworks: Applications from Catalysis to Gas Storage, first ed., Wiley-VCH Verlag GmbH & Co. KGaA, Weinheim, 2011, pp. 353–381 (chapter 15).
[44] (a) F. Jeremias, S.K. Henninger, C. Janiak, Chem. Commun. 48 (2012) 9708–9710;
(b) F. Jeremias, D. Fröhlich, C. Janiak, S.K. Henninger, RSC Adv. 4 (2014) 24073–24082.
[45] D. Qian, C. Lei, G. Hao, W. Li, A. Lu, ACS Appl. Mater. Interfaces 4 (2012) 6125–6132.
[46] M. Wickenheisser, C. Janiak, Microporous Mesoporous Mater. 204 (2015) 242–250.
[47] V. Finsy, L. Ma, L. Alaerts, D.E. De Vos, G.V. Baron, J.F.M. Denayer, Microporous Mesoporous Mater. 120 (2009) 221–227.
[48] R. Zacharia, D. Cossement, L. Lafi, R.J. Chahine, Mater. Chem. 20 (2010) 2145–2151.
[49] M.R. Lohe, M. Rose, S. Kaskel, Chem. Commun. (2009) 6056–6058.
[50] H.B. Tanh Jeazet, C. Staudt, C. Janiak, Chem. Commun. 48 (2012) 2140–2142.
[51] P. Küsgens, A. Zgaverdea, H. Fritz, S. Siegle, S. Kaskel, J. Am. Ceram. Soc. 93 (2010) 2476–2479.
[52] A. Sachse, R. Ameloot, B. Coq, F. Fajula, B. Coasne, D. De Vos, A. Galarneau, Chem. Commun. 48 (2012) 4749–4751.
[53] M.G. Schwab, I. Senkovska, M. Rose, M. Koch, J. Pahnke, G. Jonschker, S. Kaskel, Adv. Eng. Mat. 10 (2008) 1151–1155.
[54] H. Huang, C. Lin, C. Wu, Y. Cheng, C. Lin, Anal. Chim. Acta 779 (2013) 96–103.
[55] (a) H.B. Tanh Jeazet, C. Staudt, C. Janiak, Dalton Trans. 41 (2012) 14003–14027;
(b) H.B. Tanh Jeazet, C. Janiak, in: L.R. MacGilivray, C.M. Lukehart (Eds.), Metal-organic Framework Materials, John Wiley & Sons, Ltd, Chichester, 2014, pp. 1–15.
[56] N. Hüsing, U. Schubert, Angew. Chem. 110 (1999) 22–47.
[57] (a) J. Li, J. Li, H. Meng, S. Xie, B. Zhang, L. Li, H. Ma, J. Zhang, M. Yu, J. Mater. Chem. A 2 (2014) 2934–2941;
(b) M.A. Aegerter, N. Leventis, in: M.M. Koebel (Ed.), Aerogels Handbook, Springer, New York, 2011.
[58] Z. Ulker, I. Erucar, S. Keskin, C. Erkey, Microporous Mesoporous Mater. 170 (2013) 352–358.
[59] U. Fischer, R. Saliger, V. Bock, R. Petricevic, J. Fricke, J. Porous Mater. 4 (1997) 281–285.
[60] S.A. Al-Muhtaseb, J.A. Ritter, Adv. Mater. 15 (2003) 101–114.
[61] J. Laskowski, B. Milow, L. Ratke, Microporous Mesoporous Mater. 197 (2014) 308–315.
[62] (a) N. Rey-Raap, J. Angel Menéndez, A. Arenillas, Microporous Mesoporous Mater. 195 (2014) 266–275;
(b) C. Lin, J.A. Ritter, Carbon 35 (1997) 1271–1278;
(c) S. Mulik, C. Sotiriou-Leventis, N. Leventis, Chem. Mater. 19 (2007) 6138–6144;
(d) M. Reuß, L.J. Ratke, Sol-Gel Sci. Technol. 47 (2008) 74–80;
(e) M. Schwan, L. Ratke, J. Mater. Chem. A 1 (2013) 13462–13468.
[63] B. Nagy, O. Czakkel, K. László, Microporous Mesoporous Mater. 185 (2014) 66–71.
[64] L.D. Gelb, K.E. Gubbins, R. Radhakrsihan, M. Sliwinska-Bartowiak, Rep. Prog. Phys. 62 (1999) 1573–1659.
[65] N.A. Sedron, J.P.R.B. Walton, N. Quirke, Carbon 27 (1989) 853–861.
[66] A. Vishnyakov, P. Ravikovitch, A.V. Neimark, Langmuir 16 (2000) 2311–2320.
[67] J.W. Yoon, Y.-K. Seo, Y.K. Hwang, J.-S. Chang, H. Leclerc, S. Wuttke, P. Bazin, A. Vimont, M. Daturi, E. Bloch, P.L. Llewellyn, C. Serre, P. Horcajada, J.-M. Grenèche, A.E. Rodrigues, G. Férey, Angew. Chem. Int. Ed. 49 (2010) 5949–5952.
[68] A. Vimont, J.-M. Goupil, J.-C. Lavalley, M. Daturi, S. Surblé, C. Serre, F. Millange, G. Férey, N. Audebrand, J. Am. Chem. Soc. 128 (2006) 3218–3227.
[69] J. Yang, Q. Zhao, J. Li, J. Dong, Microporous Mesoporous Mater. 130 (2010) 174–179.
[70] A. Awadallah-F, A.M. Elkhatat, S.A. Al-Muhtaseb, J. Mater. Sci. 46 (2011) 7760–7769.
[71] K.S.W. Sing, D.H. Everett, R.A.W. Haul, L. Moscou, R.A. Pierotti, J. Rouquerol, T. Siemieniewska, Pure Appl. Chem. 57 (1985) 603–619.
[72] R. Saliger, V. Bock, R. Petricevic, T. Tillotson, S. Geis, J. Fricke, J. Non-Cryst. Solids 221 (1997) 144–150.
[73] W. Chen, Z. Zhang, W. Bao, Y. Lai, J. Li, Y. Gan, J. Wang, Electrochim. Acta 134 (2014) 293–301.
[74] R. Canioni, C. Roch-Marchal, F. Sécheresse, P. Horcajada, C. Serre, M. Hardi-Dan, G. Férey, J.-M. Grenèche, F. Lefebvre, J.-S. Chang, Y.-K. Hwang, O. Lebedev, S. Turner, G.J. Van Tendeloo, Mater. Chem. 21 (2011) 1226–1233.
[75] M.L. Pinto, S. Dias, J. Pires, Appl. Mater. Interfaces 5 (2013), 2360–1263.
[76] L.D. O'Neill, H. Zhang, D.J. Bradshaw, J. Mater. Chem. 20 (2010) 5720–5726.

Supplementary data

Hierarchical MOF-xerogel monolith composites from embedding MIL-100(Fe,Cr) and MIL-101(Cr) in resorcinol-formaldehyde xerogels for water adsorption applications

Martin Wickenheisser [a], Annika Herbst [a], René Tannert [b], Barbara Milow [b], Christoph Janiak [a,*]

[a]*Institut für Anorganische Chemie und Strukturchemie I, Universitätsstraße 1, 40225 Düsseldorf, Germany*

[b]*Deutsches Zentrum für Luft- und Raumfahrt (DLR), Institut für Werkstoff-Forschung, Aerogele, Linder Höhe, 51147 Köln, Germany*

Contact Emails:
martin.wickenheisser@uni-duesseldorf.de
annika.herbst@uni-duesseldorf.de
rene.tannert@dlr.de
barbara.milow@dlr.de
janiak@uni-duesseldorf.de

Experimental Section

Synthesis of the starting materials

MIL-100(Fe) {$Fe_3(\mu_3\text{-}O)(F,OH)(H_2O)_2(BTC)_2\cdot{\sim}14.5H_2O\}_n$: MIL-100(Fe) was prepared according to the literature [w]. 665 mg of Fe^0 powder (11.9 mmol), 1.65 g H_3BTC (7.85 mmol), 0.83 mL hydrofluoric acid (24 mmol; 48-51 wt% in H_2O), 0.5 mL HNO_3 (7 mmol; 65 wt%) and 60 mL of deionized H_2O were placed in a 90 mL Teflon-liner. The Teflon-liner was inserted in a steel autoclave and heated to 423 K within 2 h. After 12 h the autoclave was cooled to r.t. within 2 h. The powder was centrifuged off and washed consecutively with DMF (2 x 120 mL), EtOH (2 x 120 mL) and deionized H_2O (2 x 180 mL). Between each washing step the powder was centrifuged off and dried for 24 h at 373 K. For further activation the powder was first stirred for 12 days in 420 mL DMF at r.t., then additional 6 h at 383 K. After centrifugation and stirring for 2 days in 500 mL EtOH at r.t., the solid was further washed for 3 h at 333 K. The powder was centrifuged off, stirred again for 4 h in 500 mL of deionized water at 353 K and additional 22 h at r.t.. After centrifugation the solid was dried for 24 h at 343 K. 1.50 g of an orange-brown powder was isolated (1.64 mmol, 41 % for $Fe_3(\mu_3\text{-}O)(F)(H_2O)_2(BTC)_2\cdot 14.5H_2O$ ($C_{18}H_{10}FFe_3O_{15}\cdot H_{29}O_{14.5}$, 914.02 g·mol^{-1})).

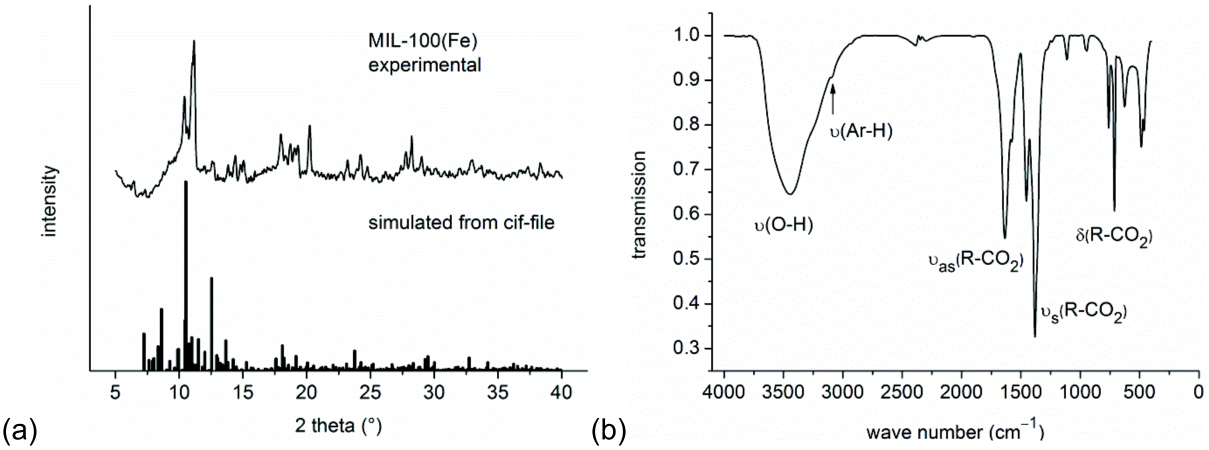

Fig. A.1. (a) Experimental powder X-ray diffraction (PXRD) pattern of activated MIL-100(Fe) and PXRD pattern simulated from the cif-file of MIL-100(Fe), CSD-'Refcode CIGXIA [x]. (b) IR-spectrum (KBr) of activated MIL-100(Fe).

---

[w] J.W. Yoon, Y.-K. Seo, Y.K. Hwang, J.-S. Chang, H. Leclerc, S. Wuttke, P. Bazin, A. Vimont, M. Daturi, E. Bloch, P.L. Llewellyn, S. Serre, P. Horcajada, J.-M. Grenèche, A.E. Rodrigues, G. Férey, Angew. Chem. Int. Ed. 49 (2010) 5949–5952.

[x] P. Horcajada, S. Surble, C. Serre, D.-Y. Hong, Y.-K. Seo, J.-S. Chang, J.-M. Grenèche, I. Margiolaki, G. Férey, Chem. Commun. 27 (2007) 2820–2822.

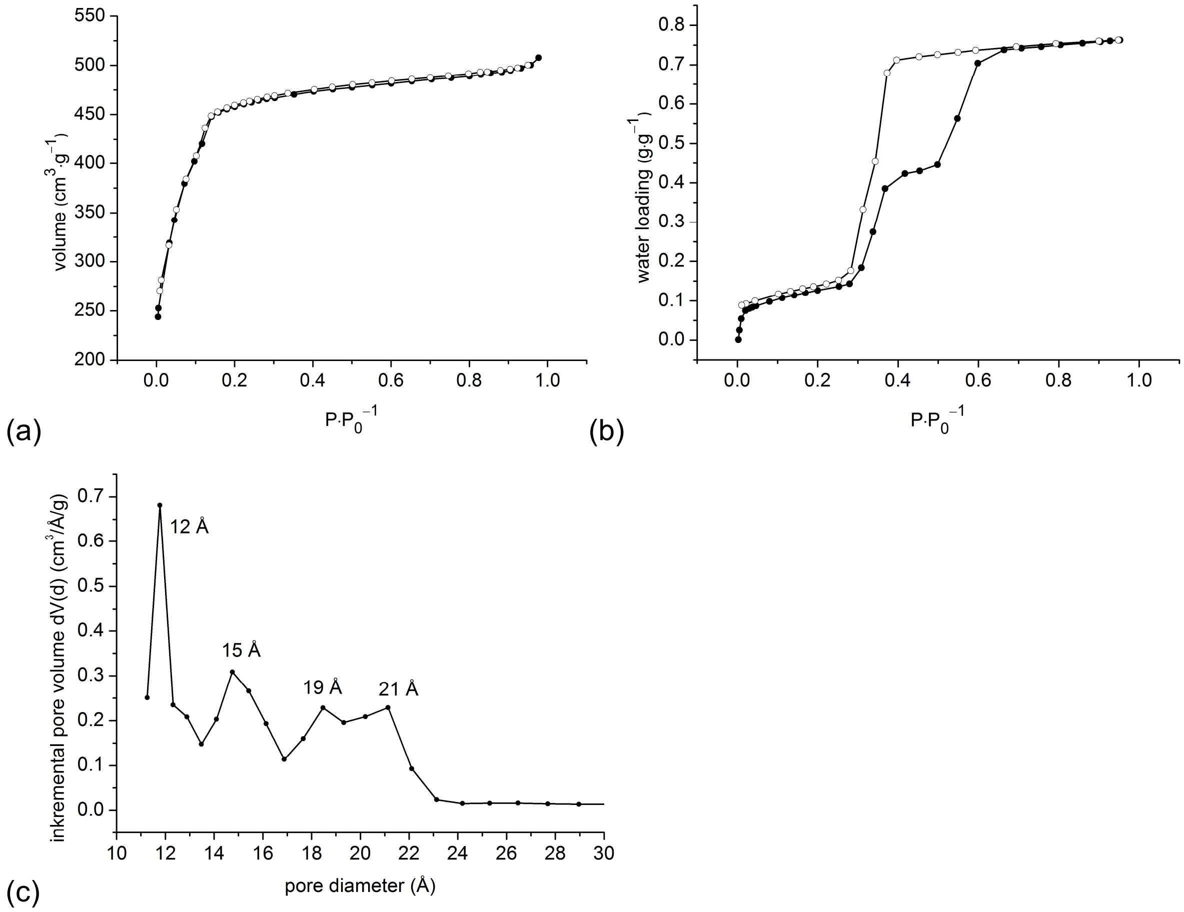

Fig. A.2. (a) N_2-sorption isotherms of activated MIL-100(Fe) (degassing conditions: 2.5 h, 423 K, BET = 2200 $m^2 \cdot g^{-1}$). (b) Water sorption isotherm of activated MIL-100(Fe) (degassing conditions: 2 h, 423 K). Adsorption is depicted with filled, desorption with empty symbols. (c) Pore size distribution curve of activated MIL-100(Fe) from 'N_2 at 77 K on carbon, slit pore, NLDFT equilibrium' model [y,z,aa].

---

[y] L.D.Gelb, K.E. Gubbins, R. Radhakrsihan, M. Sliwinska-Bartowiak, Rep. Prog. Phys. 62 (1999) 1573–1659.

[z] N.A. Sedron, J.P.R.B. Walton, N. Quirke, Carbon 27 (1989) 853–861.

[aa] A. Vishnyakov, P. Ravikovitch, A.V. Neimark, Langmuir 16 (2000) 2311–2320.

MIL-100(Cr) $\{Cr_3(\mu_3\text{-}O)(F,OH)(H_2O)_2(BTC)_2\cdot\sim28H_2O\}_n$: MIL-100(Cr) was prepared according to the literature [bb]. 1.20 g CrO_3 (12.0 mmol), 2.52 g H_3BTC (12.0 mmol), 0.42 mL hydrofluoric acid (12 mmol; 48-51 wt% in H_2O) and 58 mL of deionized H_2O were placed in a 90 mL Teflon-liner. The Teflon-liner was inserted in a steel autoclave and heated to 473 K within 2 h. After 96 h the autoclave was cooled to r.t. within 2 h. The powder was centrifuged off and washed consecutively with DMF (2 x 120 mL), EtOH (2 x 120 mL) and deionized H_2O (2 x 180 mL). Between each washing step the powder was centrifuged off and dried for 2 h at 373 K. For further activation the powder was first stirred for 42 h in 500 mL DMF at r.t., then additional 4 h at 383 K. After centrifugation and stirring for 45 h in 500 mL EtOH at r.t., the solid was further washed for 4 h at 333 K. The powder was centrifuged off, stirred again for 69 h in 500 mL of deionized water at r.t. and additional 3 h at 353 K. After centrifugation the solid was dried for 18 h at 343 K. 3.18 g of a light green powder was isolated (2.78 mmol, 69 % for $Cr_3(\mu_3\text{-}O)(F)(H_2O)_2(BTC)_2\cdot28H_2O$ ($C_{18}H_{10}Cr_3FO_{15}\cdot H_{56}O_{28}$, 1145.68 g·mol^{-1})).

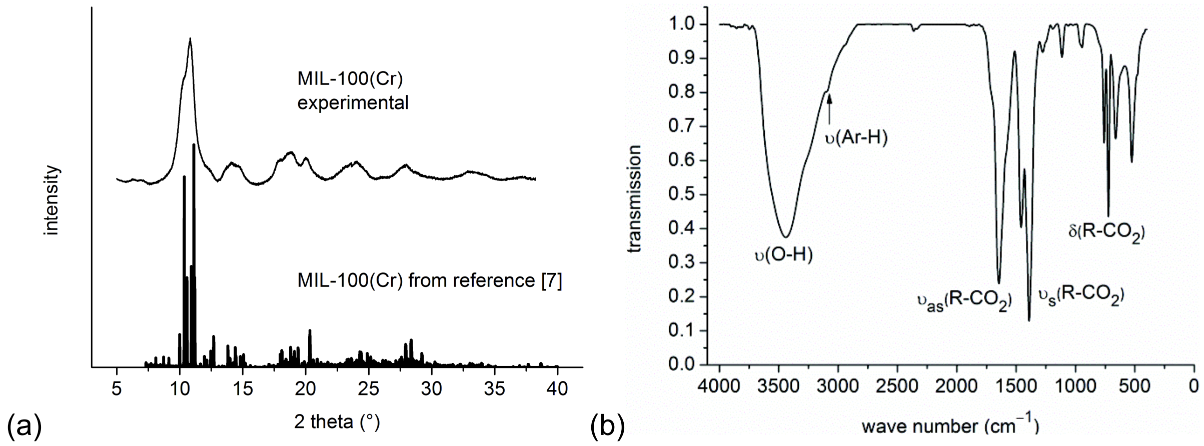

Fig. A.3. (a) Experimental powder X-ray diffraction pattern of activated MIL-100(Cr) and PXRD pattern from reference [cc]. (b) IR-spectrum (KBr) of activated MIL-100(Cr).

[bb] A. Vimont, J.-M. Goupil, J.-C. Lavalley, M. Daturi, S. Surblé, C. Serre, J.-C. Millange, G. Férey, N. Audebrand J. Am. Chem. Soc. 128 (2006) 3218–3227.

[cc] G. Férey, C. Serre, C. Mellot-Draznieks, F. Millange, S. Surble, J. Dutour, I. Margiolaki, Angew. Chem. Int. Ed. 43 (2004) 6296–6301.

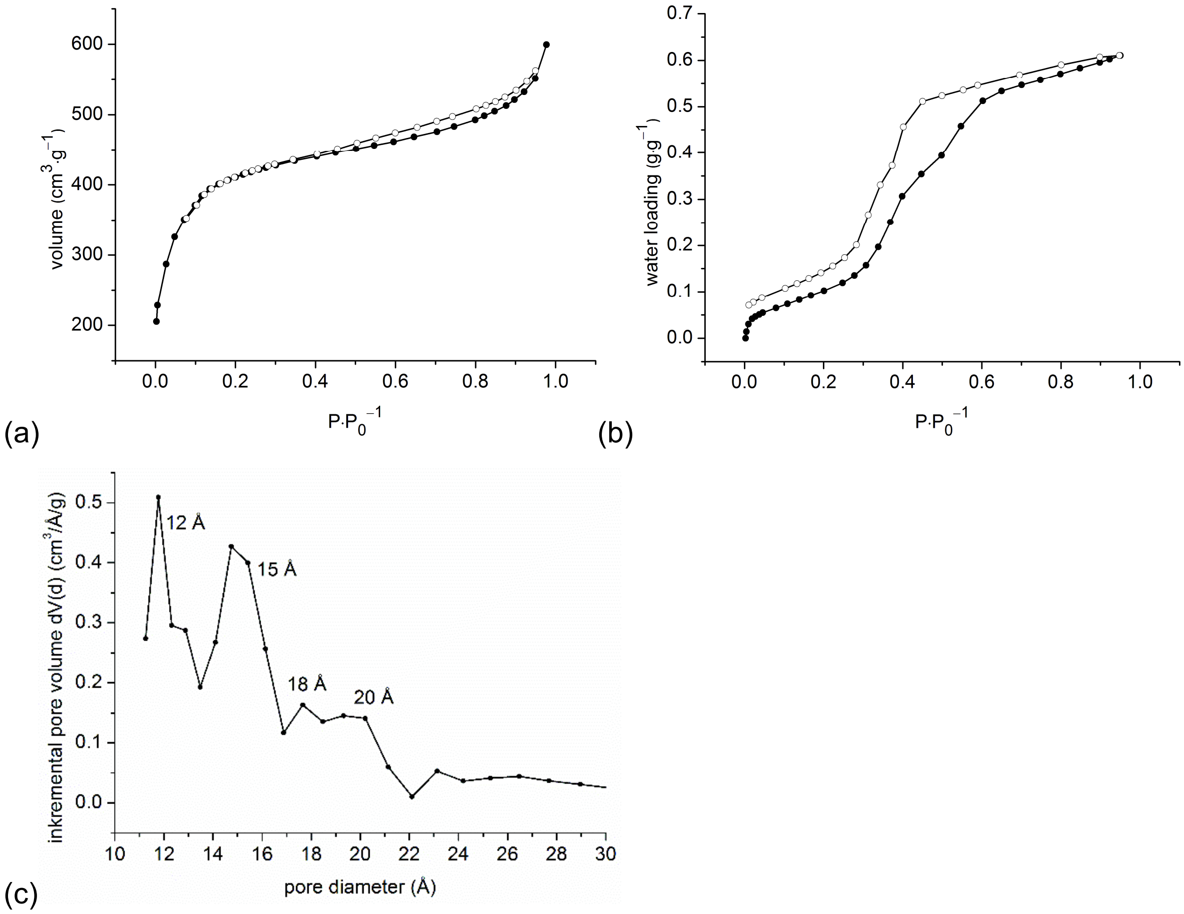

Fig. A.4. (a) N_2-sorption isotherms of activated MIL-100(Cr) (degassing conditions: 2.5 h, 473 K, BET = 1560 m^2·g^{-1}). (b) Water sorption isotherm of activated MIL-100(Cr) (degassing conditions: 2.5 h, 273 K). Adsorption is depicted with filled, desorption with empty symbols. (c) Pore size distribution curve of activated MIL-100(Cr) from 'N_2 at 77 K on carbon, slit pore, NLDFT equilibrium' model.

MIL-101(Cr) $\{Cr_3(\mu_3\text{-}O)(F,OH)(H_2O)_2(BDC)_3\cdot{\sim}25H_2O\}_n$: MIL-101(Cr) was prepared according to the literature [dd]. 4.80 g $Cr(NO_3)_3\cdot 9H_2O$ (12.0 mmol), 1.98 g H_2BDC (11.9 mmol), 1.1 mL TMAOH (tetramethylammonium hydroxide) (3.1 mmol; $\rho = 1.014\ g\cdot mL^{-1}$; 25 wt% in H_2O) and 60 mL of deionized H_2O were placed in a 90 mL Teflon-liner. The Teflon-liner was inserted in a steel autoclave and heated to 453 K within 10 h. After 24 h the autoclave was cooled to r.t. within 18 h. Before heating $Cr(NO_3)_3\cdot 9H_2O$ and H_2BDC was first stirred in deionized H_2O for 5 min, then TMAOH was dropped dropwise to the mixture and the suspension was stirred for 20 min. The green powder was centrifuged off and washed consecutively with DMF (1 x 240 mL), EtOH (1 x 240 mL) and deionized H_2O (1 x 240 mL). Between each washing step the powder was centrifuged off and dried for 22 h at 373 K. For further activation the powder was first stirred for 20 h in 400 mL DMF at 383 K. After centrifugation and stirring for 19 h in 400 mL EtOH at 333 K, the green powder was centrifuged off and stirred again for 19 h in 400 mL of deionized water at 353 K. After centrifugation the solid was dried for 24 h at 373 K. 2.34 g of a green powder was isolated (2.00 mmol, 50 % for $Cr_3(\mu_3\text{-}O)(F)(H_2O)_2(BDC)_3\cdot 25H_2O$ ($C_{24}H_{16}Cr_3FO_{15}\cdot H_{50}O_{25}$, 1169.74 $g\cdot mol^{-1}$)).

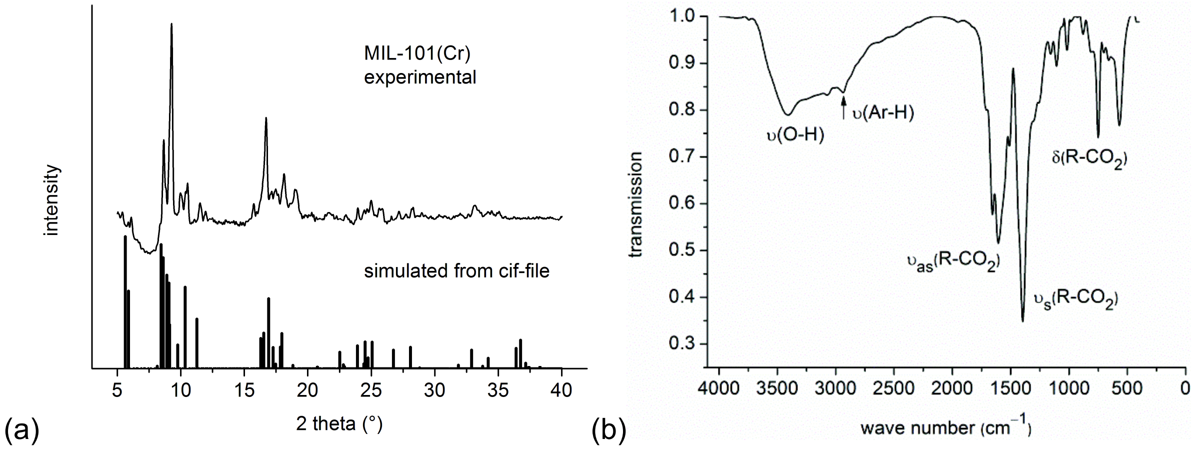

Fig. A.5. (a) Experimental powder X-ray diffraction pattern of activated MIL-101(Cr) and PXRD pattern simulated from the cif-file of MIL-101(Cr), CSD-Refcode OCUNAK) [ee]. (b) IR-spectrum (KBr) of activated MIL-101(Cr).

[dd] J. Yang, Q. Zhao, J. Li, J. Dong, Micropor. Mesopor. Mater. 130 (2010) 174–179.

[ee] G. Férey, C. Mellot-Draznieks, C. Serre, F. Millange, J. Dutour, S. Surblé, I. Margiolaki, Science 309 (2005) 2040–2042.

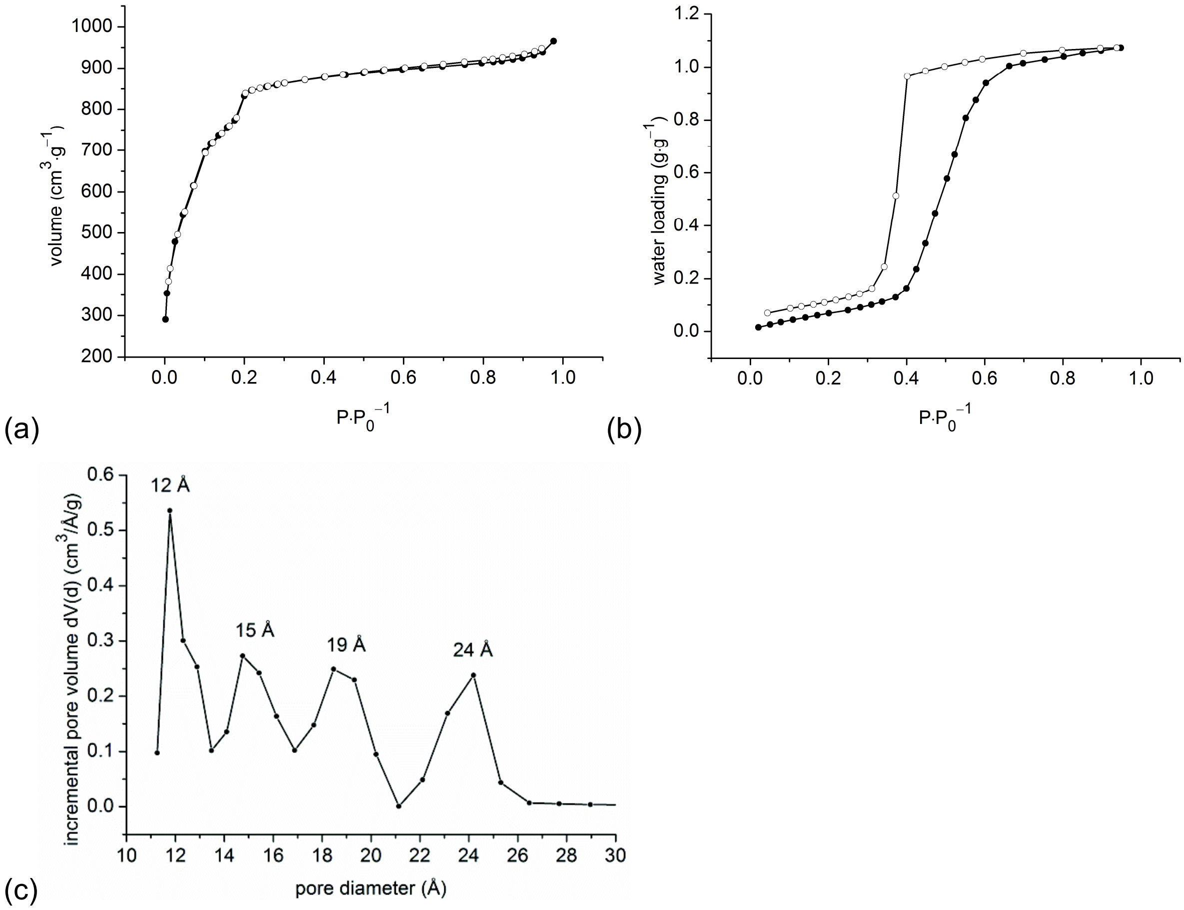

Fig. A.6. (a) N_2-sorption isotherms of activated MIL-101(Cr) (degassing conditions: 2.5 h, 473 K, BET = 3060 $m^2 \cdot g^{-1}$). (b) Water sorption isotherm of activated MIL-101(Cr) (degassing conditions: 3 h, 473 K). Adsorption is depicted with filled, desorption with empty symbols. (c) Pore size distribution curve of activated MIL-101(Cr) from 'N_2 at 77 K on carbon, slit pore, NLDFT equilibrium' model.

R,F-xerogel: The synthesis was prepared according to the literature [ff]. 2.29 g resorcinol (20.8 mmol) was dissolved in 9.87 g of an aqueous Na_2CO_3 solution ($2.1 \cdot 10^{-3}$ mol·L^{-1}; 0.021 mmol Na_2CO_3). Then 3.57 g of a formaldehyde solution (28.5 mmol; $\rho = 1.06$ g·mL^{-1}; 24 wt% in H_2O) was added and the solution was stirred for 5 min. The molar ratios of the starting materials were: resorcinol/formaldehyde = 0.73, resorcinol/Na_2CO_3 = 1000, resorcinol/water = 0.031. The clear solution was filled into a plastic syringe, which was cut off from one side (side where the cannula is normally attached), sealed and cured for 7 days at 333 K. The brown monolith was stored in 50 mL of acetic acid (10 wt% in water) for 24 h, followed by storing it in EtOH (3 x 50 mL, min. 7 h each washing step) and drying at 313 K (21 h), 333 K (71 h) and 353 K (24 h). 820 mg of a brown monolith was isolated.

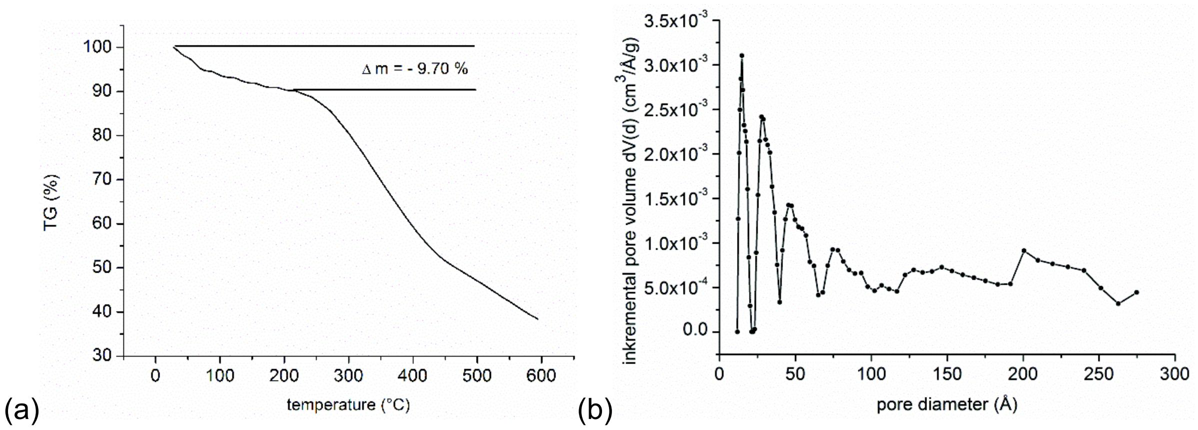

Fig. A.7. (a) Thermogravimetric analysis of R,F-xerogel. (b) Pore size distribution curve of R,F-xerogel from 'N_2 at 77 K on carbon, slit pore, NLDFT equilibrium' model.

[ff] S.A. Al-Muhtaseb, J.A. Ritter, Adv. Mater. 15 (2003) 101–114.

Synthesis of the composite materials MIL-100(Cr)@xerogel without pre-polymerization of the R,F-xerogel solution

150 mg of well ground MIL-100(Cr) powder was filled into a plastic syringe, which was cut off from side (side where the cannula is normally attached). Then the just prepared, entire R,F-xerogel solution of low viscosity (Fig. A11, left picture) (same amounts and same procedure like described before), was dropped onto the MIL powder. After sealing the syringe by several layers of polyethylene- and aluminum foil to avoid evaporation of the solution, homogenization of the suspension by vigorous shaking of the syringe and sedimentation of the green powder for 1 day, the reaction mixture was cured for 7 days at 333 K. The resulting monolith was light brown colored at the bottom (MIL and xerogel) and brown colored at the top (pure xerogel) (Fig. A8a). Both phases were separated and the light brown monolith from the bottom layer was stored in 40 mL of acetic acid (10 wt% in water) for 24 h, followed by storing it in EtOH (3 x 40 mL, min. 6 h each washing step) and drying at 313 K (17 h), 333 K (17 h) and 353 K (24 h). A brown monolith was isolated.

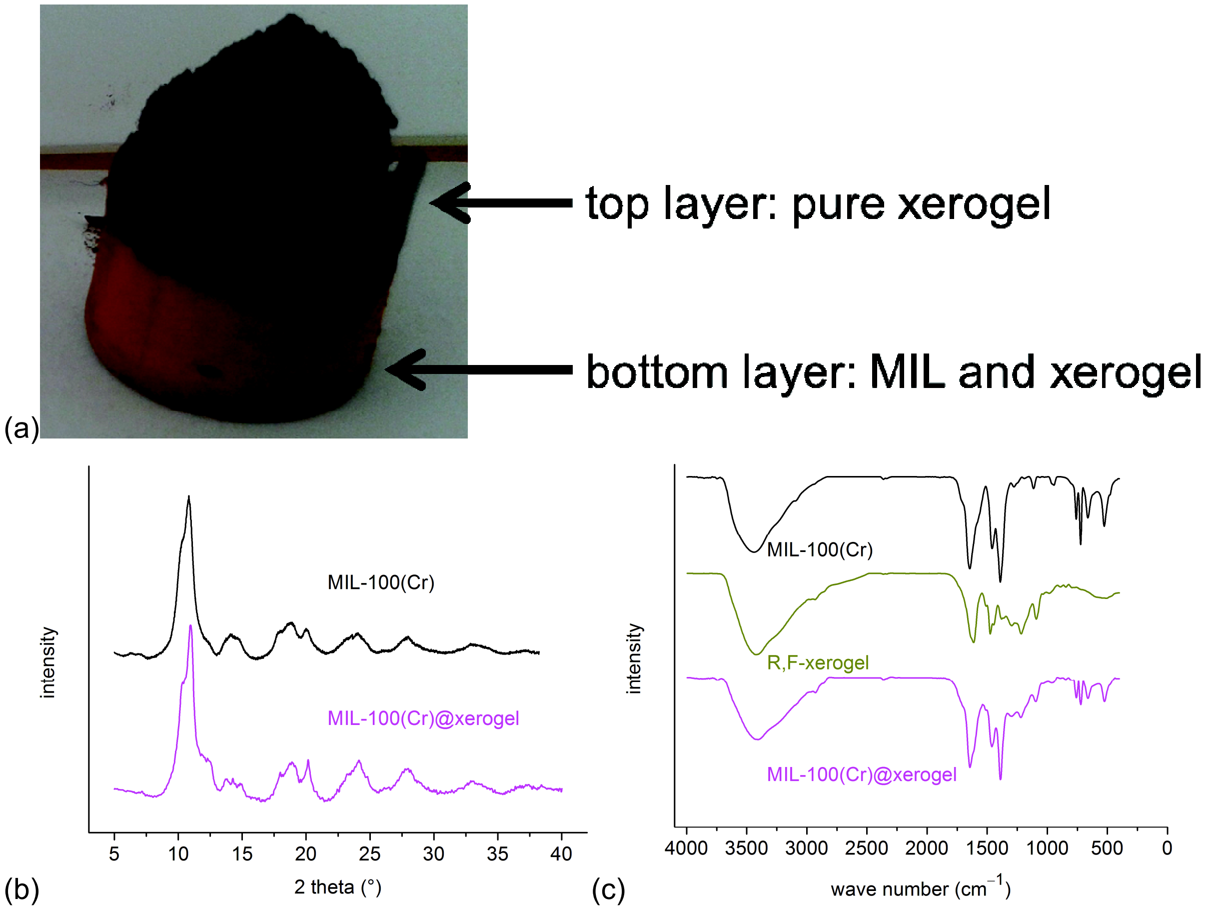

Fig. A.8. (a) Monolithic product of MIL-100(Cr)@xerogel at the bottom layer and residual parts of the pure xerogel at the top layer. (b) Experimental powder X-ray diffraction patterns of MIL-100(Cr) and MIL-100(Cr)@xerogel (bottom layer). (c) IR-spectra (KBr) of MIL-100(Cr), R,F-xerogel and MIL-100(Cr)@xerogel (bottom layer).

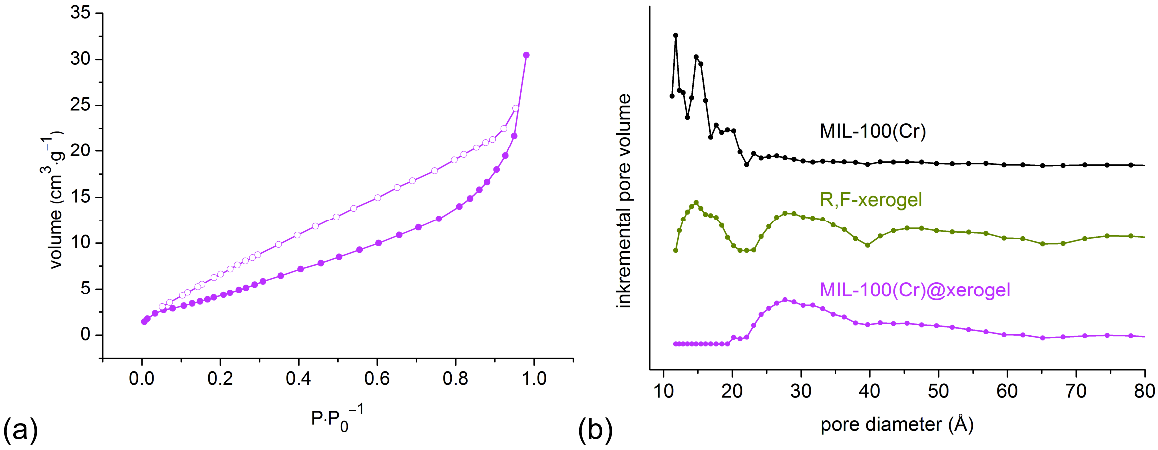

Fig. A.9. (a) N_2-sorption isotherms of MIL-100(Cr)@xerogel (bottom layer) (degassing conditions: 3 h, 423 K, BET = 20 m^2·g^{-1}). Adsorption is depicted with filled, desorption with empty symbols. (b) Pore size distribution curves of MIL-100(Cr), R,F-xerogel and MIL-100(Cr)@xerogel (bottom layer) from 'N_2 at 77 K on carbon, slit pore, NLDFT equilibrium' model.

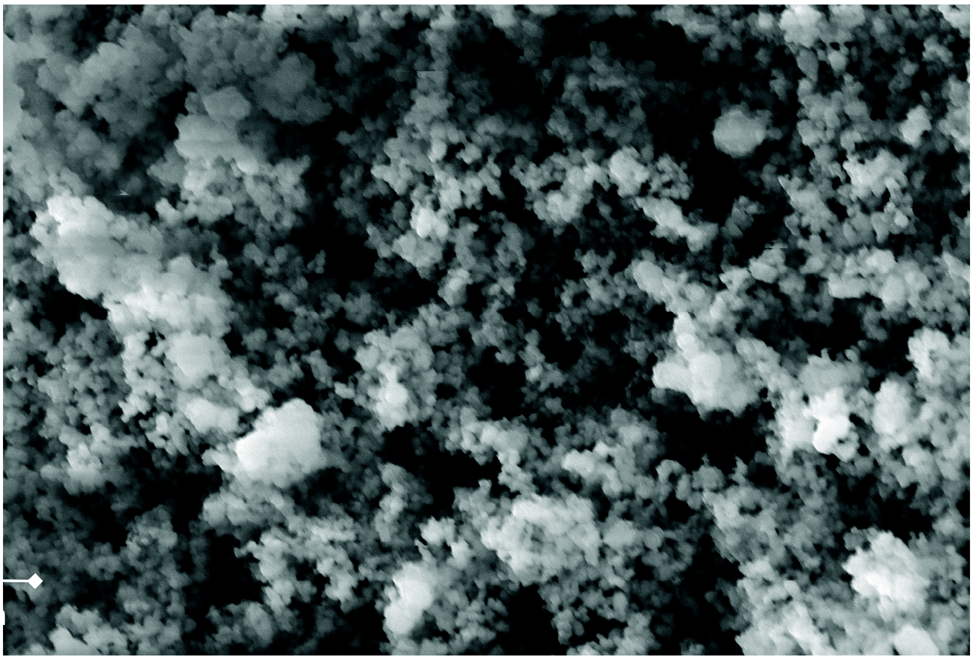

Fig. A.10. Scanning electron microscopic (SEM) image of MIL-100(Cr)@xerogel (bottom layer) without pre-polymerization of the xerogel solution.

Pre-polymerization experiments of MIL-100(Fe)@xerogel with 11 wt% MIL-100(Fe)

4.59 g Resorcinol (41.7 mmol) was dissolved in 19.74 g of an aqueous Na_2CO_3 solution ($2.1\cdot10^{-3}$ $mol\cdot L^{-1}$; 0.042 mmol Na_2CO_3). Then 7.14 g of formaldehyde solution (57.1 mmol; $\rho = 1.06$ $g\cdot mL^{-1}$; 24 wt% in H_2O) was added and the solution was stirred for 5 min. The molar ratios of the starting materials are: R/F = 0.73, R/C = 1000, R/W = 0.031. The clear solution was filled into three plastic syringes (4.71 g R,F-xerogel solution per syringe), which were cut off from one side (side where the cannula is normally attached), sealed by several layers of polyethylene- and aluminum foil and cured for 3 h (syringe 1), 4 h (syringe 2) and 5 h (syringe 3) at 343 K respectively. Thermal treatment of the R,F-solutions yielded an enhanced viscosity (Fig. A11). 100 mg of well ground MIL-100(Fe) powder was then added to each syringe and the mixtures were stirred well by a spatula until homogeneous appearance is reached. After compressing and curing for 7 days at 333 K each monolith was stored in 50 mL of acetic acid (10 wt% in water) for 23 h. The monoliths were stored in EtOH (3 x 40 mL, min. 7 h each washing step) and drying at 313 K (21 h), 333 K (71 h) and 353 K (24 h). 906 mg (**11 wt%**, syringe 1), 873 mg (**11 wt%**, syringe 2) and 899 mg (**11 wt%**, syringe 3) of brown monoliths were isolated. The loading of MIL-100(Fe) in MIL-100(Fe)@xerogel was calculated from formula S1.

Fig. A.11. Pre-polymerization steps of pure R,F-xerogel solution (approx. 1 g) at 343 K. The first picture refers to the initial solution before heat treatment. The last one shows the pre-polymerized dispersion after 5 h.

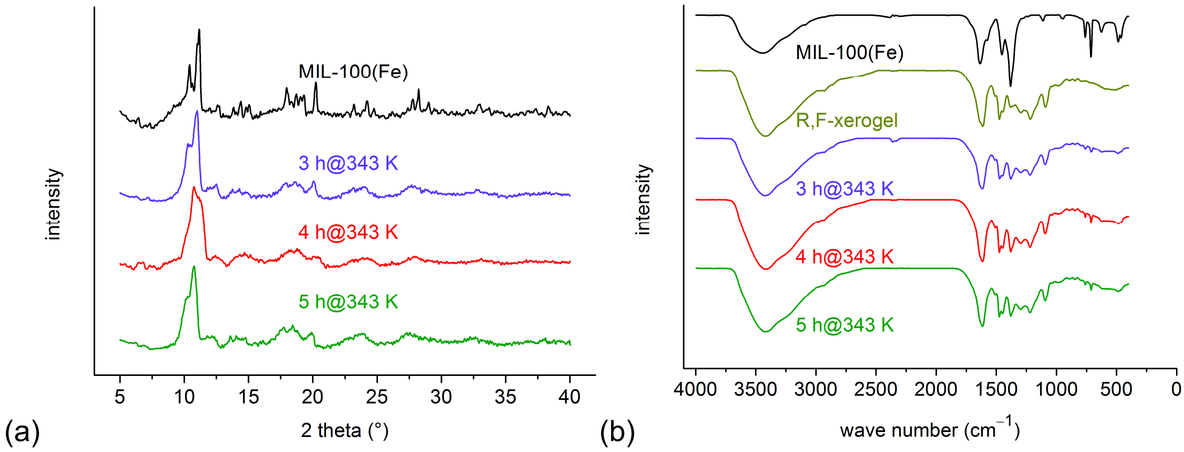

Fig. A.12. (a) Experimental powder X-ray diffraction patterns of MIL-100(Fe) and MIL-100(Fe)@xerogel with 11 wt% MIL-100(Fe). MIL-100(Fe) powders were added to the R,F-xerogel solutions after 3, 4 and 5 h of pre-polymerization time at 343 K respectively. (b) IR-spectra (KBr) of MIL-100(Fe), R,F-xerogel and MIL-100(Fe)@xerogel with 11 wt% MIL-100(Fe) (3, 4 and 5 h of polymerization at 343 K).

Formula A.1. Used for calculations of wt% MIL in MIL@R,F-xerogel.

$$\text{wt\% (MIL in MIL@R, F– xerogel)} = \frac{\text{m (weighted MIL)}}{\text{m (MIL@R, F– xerogel)}} \times 100$$

Standard syntheses of pre-polymerized MIL@xerogel without additional water

Standard syntheses of the composite materials MIL-100(Fe)@xerogel (no additional water) with 43, 50 and 58 wt% of MIL-100(Fe) with pre-polymerization of the R,F-xerogel solution

2.29 g resorcinol (20.8 mmol) was dissolved in 9.87 g of an aqueous Na_2CO_3 solution ($2.1 \cdot 10^{-3}$ mol·L^{-1}; 0.021 mmol Na_2CO_3). Then 3.57 g of formaldehyde solution (28.5 mmol; $\rho = 1.06$ g·mL^{-1}; 24 wt% in H_2O) was added and the solution was stirred for 5 min. The molar ratios of the starting materials are: R/F = 0.73, R/C = 1000, R/W = 0.031. The clear solution was filled into a three plastic syringes (1.01 g per syringe), sealed by several layers of polyethylene- and aluminum foil and pre-polymerized for 5 h at 343 K obtaining in highly viscous solutions. 100, 150 and 180 mg of well ground MIL-100(Fe) powders were added into the syringes, stirred well by a spatula until homogenous appearance is reached, compressed and cured for 7 days at 333 K. Each monolith was stored in 40 mL of acetic acid (10 wt% in water) for 20 h. The monoliths were stored in EtOH (3 x 40 mL, min. 7 h each washing step) and drying at 313 K (21 h), 333 K (71 h) and 353 K (24 h). 230 mg (**43 wt%**, syringe 1), 300 mg (**50 wt%**, syringe 2) and 313 mg (**58 wt%**, syringe 3) of brown monoliths were isolated. The loading of the MILs in MIL@xerogel was calculated from formula S1.

Standard syntheses of the composite materials MIL-100(Cr)@xerogel (no additional water) with 41, 51 and 56 wt% of MIL-100(Cr) with pre-polymerization of the R,F-xerogel solution

The preparation, pre-polymerization of the R,F-xerogel solution, washing and drying of the monoliths are described before. 100, 150 and 180 mg of well ground MIL-100(Cr) was used yielding 246 mg (**41 wt%**), 297 mg (**51 wt%**) and 319 mg (**56 wt%**) of brown monoliths. The loading of the MILs in MIL@xerogel was calculated from formula S1.

Standard syntheses of the composite materials MIL-101(Cr)@xerogel (no additional water) with 35, 46 and 50 wt% of MIL-101(Cr) with pre-polymerization of the R,F-xerogel solution

The preparation, pre-polymerization of the R,F-xerogel solution, washing and drying of the monoliths are described before. 100, 150 and 180 mg of well ground MIL-101(Cr) was used yielding 285 mg (**35 wt%**), 325 mg (**46 wt%**) and 358 mg (**50 wt%**) of brown monoliths. The loading of the MILs in MIL@xerogel was calculated from formula S1.

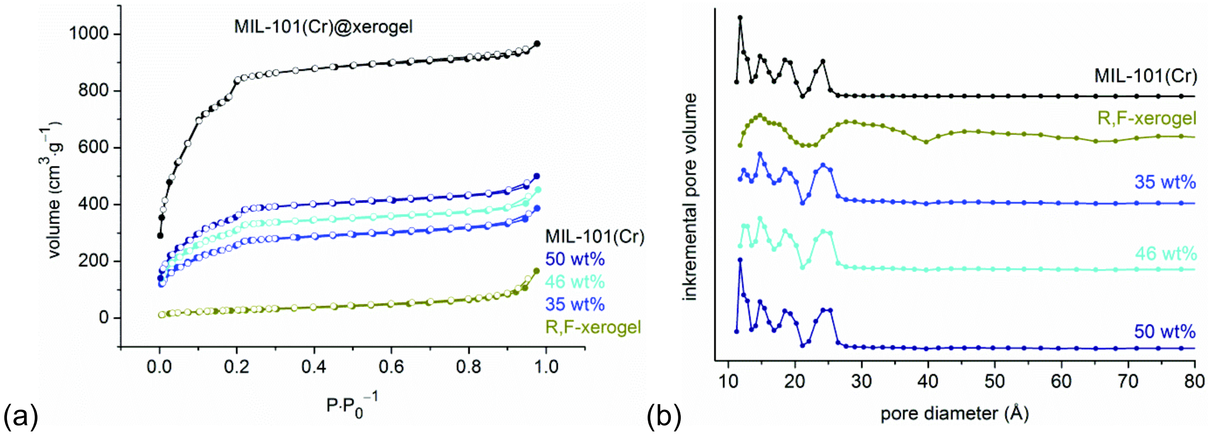

Fig. A.13. (a-b) N_2-sorption isotherms and pore diameter distribution of R,F-xerogel, MIL-101(Cr) and MIL-101(Cr)@xerogel composites (degassing conditions: 3 h, 423 K). Adsorption is depicted with filled, desorption with empty symbols.

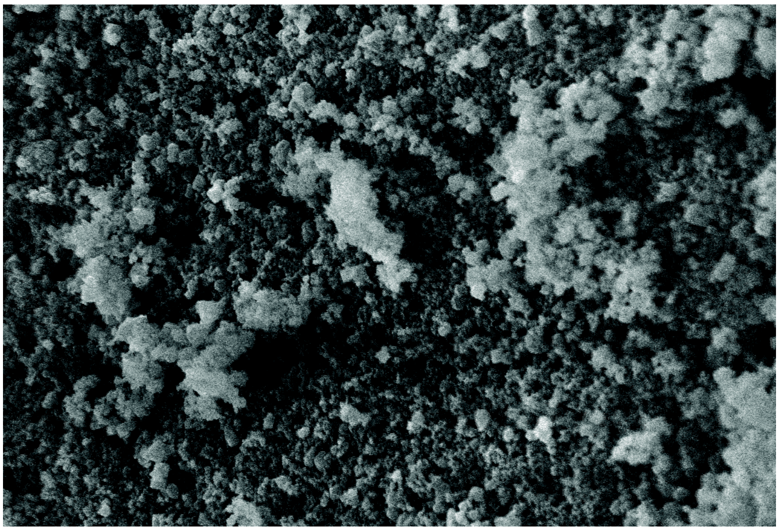

Fig. A.14. Scanning electron microscopic (SEM) images of MIL-101(Cr)@xerogel (35 wt%) with pre-polymerization of the xerogel solution.

Syntheses of MIL-101(Cr)@xerogel-H_2O with additional water

Syntheses of the composite material MIL-101(Cr)@xerogel-H_2O (with additional water) with 35, 46 and 50 wt% of MIL-101(Cr) with pre-polymerization of the R,F-xerogel solution

The preparation, pre-polymerization of the R,F-xerogel solution, washing and drying of the monoliths are described before for the standard syntheses. 100, 150 and 180 mg of well ground MIL-101(Cr) powders were used together with 0.6 mL of deionized water per syringe yielding brown monoliths in all cases: 288 mg (**35 wt%**), 323 mg (**46 wt%**) and 358 mg (**50 wt%**) for MIL-101(Cr) composites. The loading of the MILs in MIL@xerogel was calculated from formula S1.

Synthesis of the composite material MIL-101(Cr)@xerogel-H_2O (with additional water) with 77 wt% of MIL-101(Cr) with pre-polymerization of the R,F-xerogel solution

6.88 g resorcinol (62.5 mmol) was dissolved in 29.6 g of an aqueous Na_2CO_3 solution ($2.1 \cdot 10^{-3}$ mol·L^{-1}; 0.063 mmol Na_2CO_3). Then 10.7 g of formaldehyde solution (85.5 mmol; $\rho = 1.06$ g·mL^{-1}; 24 wt% in H_2O) was added and the solution was stirred for 1 h. The molar ratios of the starting materials are: R/F = 0.73, R/C = 1000, R/W = 0.031. The clear solution was pre-polymerized for 5 h at 343 K until it was almost solid and cooled to room temperature. The gel can be stored at 278 K and was used for several experiments. To the pre-polymerized gel (1.03 g) well ground MIL-101Cr powder (0.46 g) and deionized water (0.6 mL) were added. The suspension was stirred for 30 min with a mechanical stirrer in a custom-made, closable glass vial, to achieve a homogenous distribution. Then the vial was closed and the gel was cured for 7 days at 343 K. The brown monolith was stored in 50 mL of acetic acid (10 wt% in water) for 24 h, followed by storing it in EtOH (3 x 50 mL, min. 7 h each washing step) and drying it without cap for 3 days at 333 K. The MIL-101Cr@xerogel composite (0.60 g, **77 wt%**) was isolated as a green monolithic solid. The loading of the MILs in MIL@xerogel was calculated from formula S1.

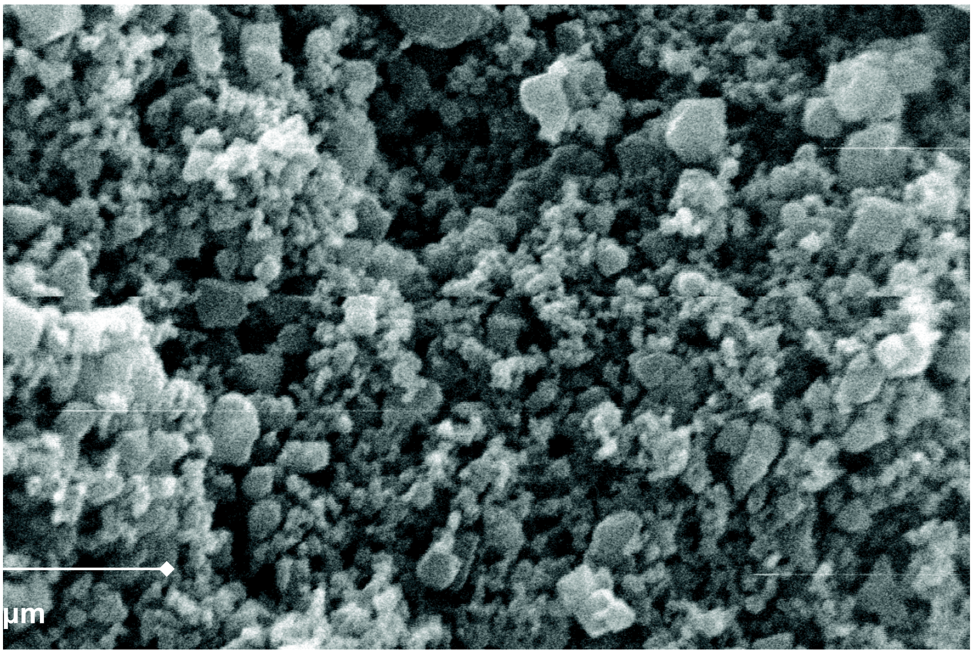

Fig. A.15. Scanning electron microscopic (SEM) images of MIL-101(Cr)@xerogel-H_2O (35 wt%) with pre-polymerization of the xerogel solution.

Porous structure of MIL-101(Cr)

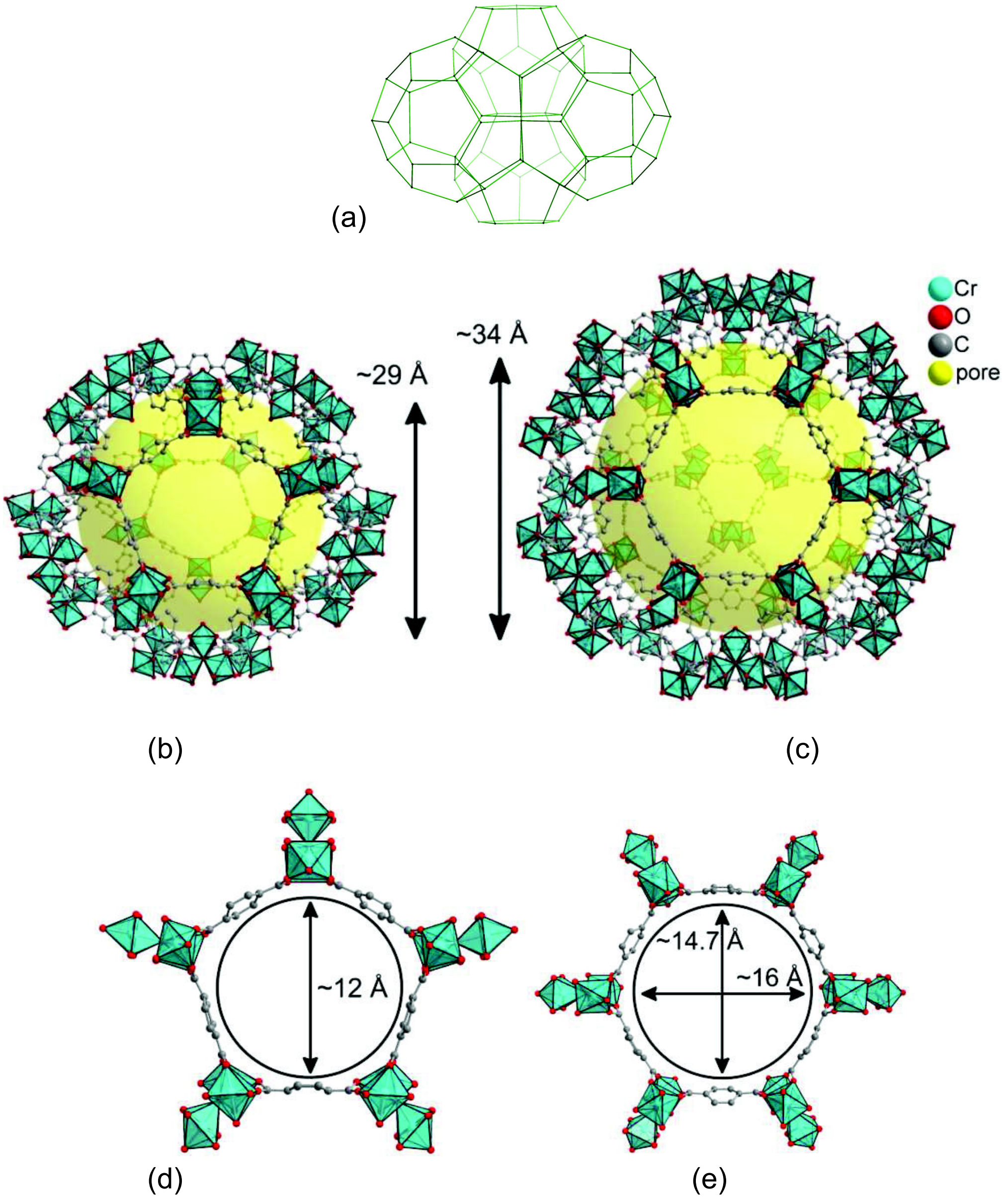

Fig. A.16. MIL-101(Cr), $\{Cr_3(\mu_3\text{-}O)(F,OH)(H_2O)_2(BDC)_3{\cdot}{\sim}25H_2O\}_n$ (BDC = 1,4-benzene dicarboxylate) presents a 3D framework constructed by two mesopores (in a 2:1 ratio) with diameter of 29 and 34 Å (a-c). The small cage (b) has an inner diameter 29 Å and only pentagonal windows (d). The large cage (c) has an inner diameter of 34 Å and both pentagonal and hexagonal windows (e). The MIL-101(Cr) structure is redrawn from the deposited cif file at the Cambridge Structure Database (CSD-Refcode OCUNAK [gg]) using the software DIAMOND [hh]. Different objects are not drawn to scale and water of crystallization is not shown.

[gg] G. Férey, C. Mellot-Draznieks, C. Serre, F. Millange, J. Dutour, S. Surblé, I. Margiolaki, Science 309 (2005) 2040–2042.

[hh] K. Brandenburg, Diamond (Version 3.2), crystal and molecular structure visualization, Crystal Impact. K. Brandenburg & H. Putz Gbr, Bonn, Germany, 2007–2012.

Porous structure of MIL-100(Fe)

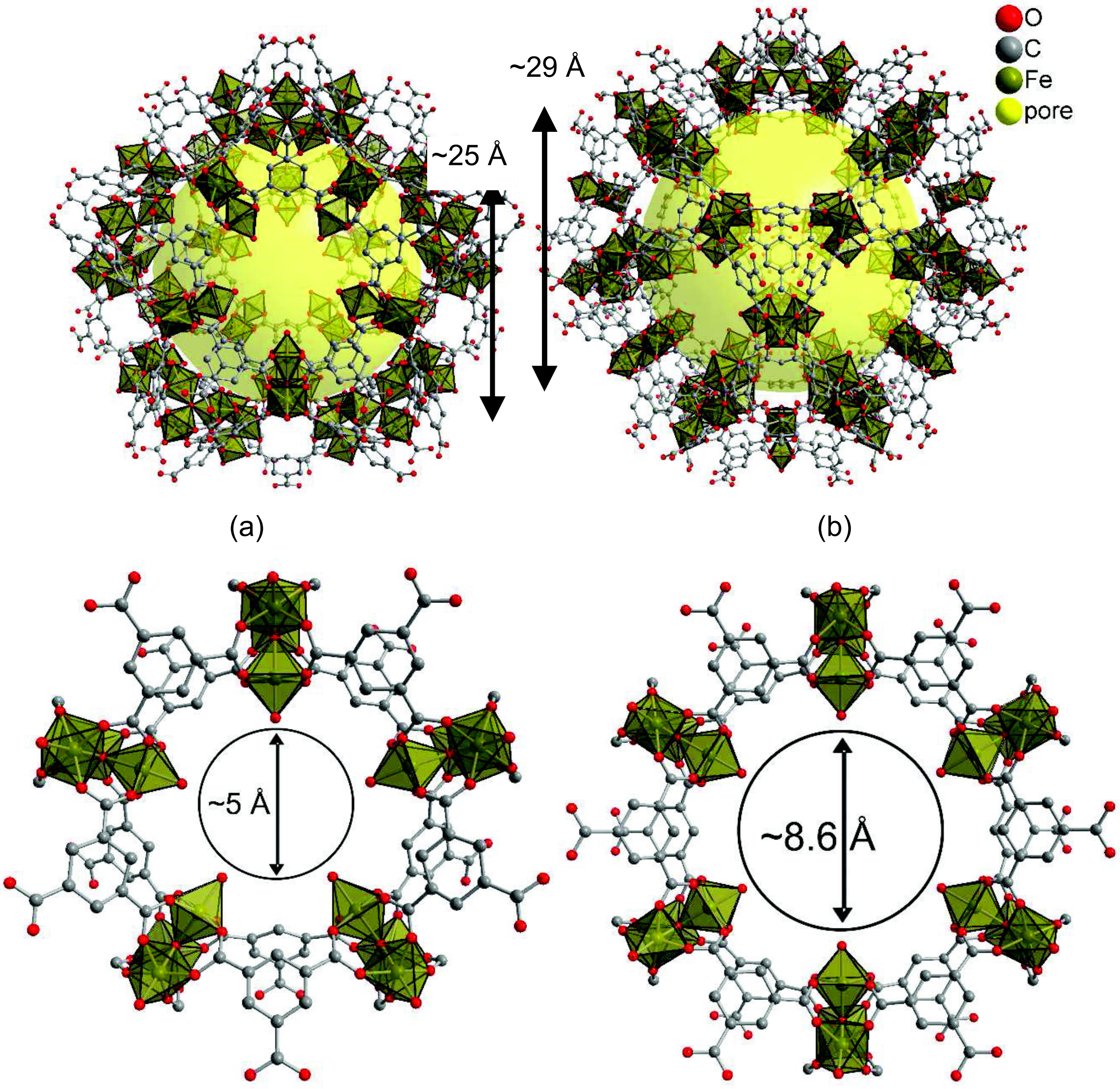

(a) (b)

(c) (d)

Fig. A.17. MIL-100(Fe) (isostructural to MIL-100(Cr), $\{Fe_3(\mu_3\text{-}O)(F,OH)(H_2O)_2(BTC)_2\}\cdot\sim 14.5H_2O$ (BTC = 1,3,5-benzene tricarboxylate) presents a 3D framework constructed by two mesopores (in a 2:1 ratio) with diameter of 25 and 29 Å (a-b). The small cage (a) has an inner diameter 25 Å and only pentagonal windows (c). The large cage (b) has an inner diameter of 29 Å and both pentagonal and hexagonal windows (d). The MIL-100(Fe) structure is redrawn from the deposited cif file at the Cambridge Structure Database (CSD-Refcode CIGXIA [x]) using the software DIAMOND [hh]. Different objects are not drawn to scale and water of crystallization is not shown.

Mechanical stability test of native R,F-xerogel and composites

Monolithic, pure R,F-xerogel (177 mg), MIL-100(Fe)@xerogel (58 wt%, 159 mg), MIL-100(Cr)@xerogel (56 wt%, 161 mg) and MIL-101(Cr)@xerogel (50 wt%, 160 mg) were placed into 25 mL beakers and treated in a shaking incubator (GFL 3032) at maximum rotation (250 min^{-1}) for a time period of 3 hours. After 5, 10, 20, 40, 60, 120 and 180 min, the monoliths were weighed to determine the mechanical abrasion.

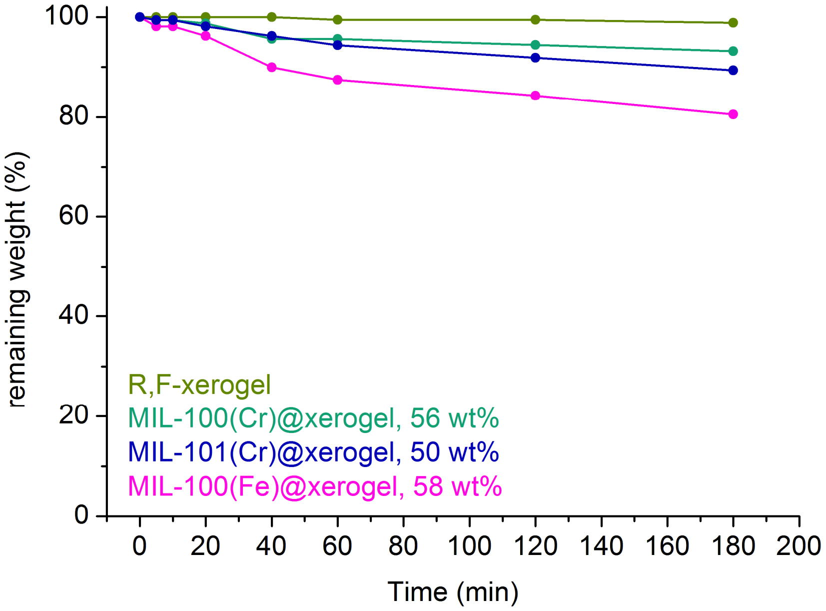

Fig. A.18. Mechanical stability test of pure R,F-xerogel and three representative MIL@xerogels in a shaking incubator at 250 rounds/min. The initial weights are set to 100 %. Mechanical abrasion after 3 hours: Pure R,F-xerogel (–1.1 wt%), MIL-100(Cr)@xerogel, 56 wt% (–6.8 wt%), MIL-101(Cr)@xerogel, 50 wt% (–10.6 wt%), MIL-100(Fe)@xerogel, 58 wt% (–19.5 wt%).

Powder X-Ray diffraction patterns

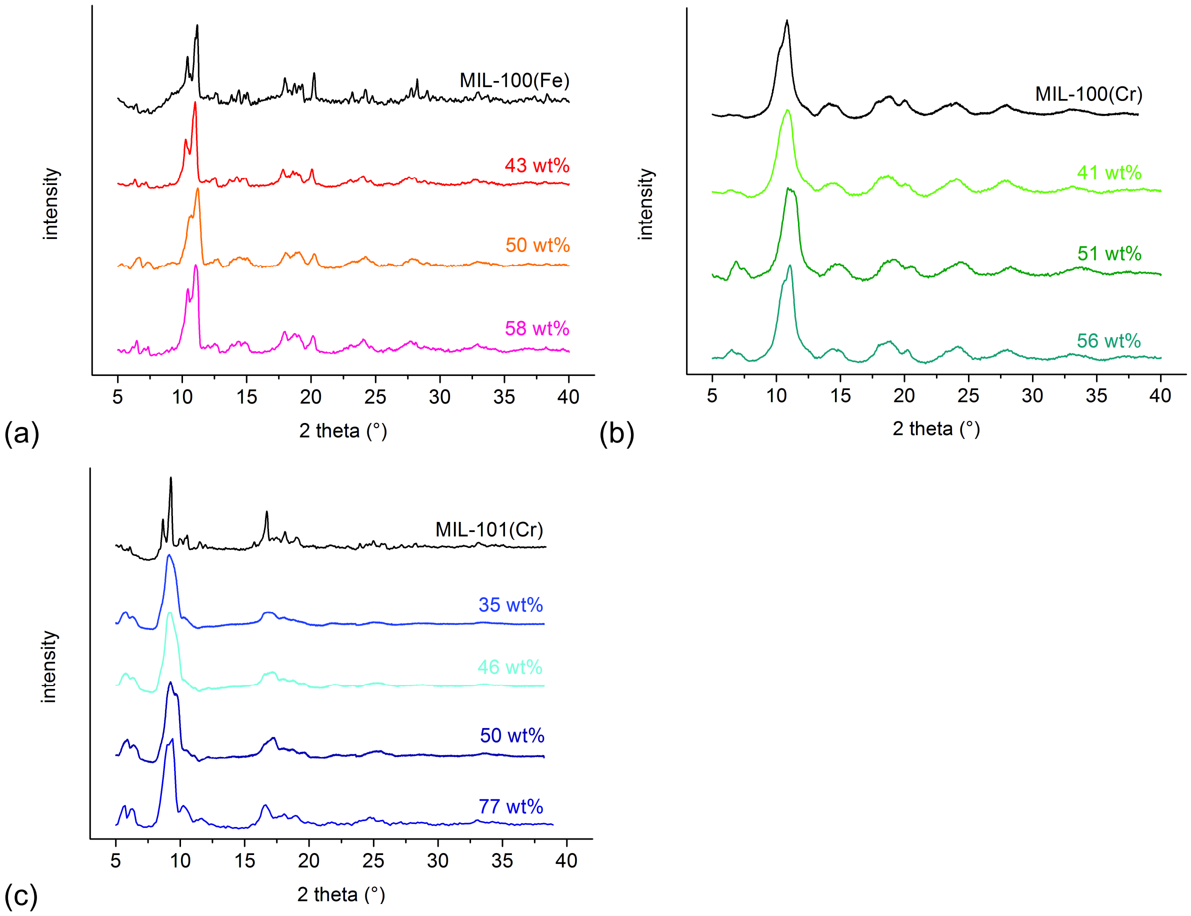

Fig. A.19. Experimental powder X-ray diffraction patterns of (a) MIL-100(Fe) and MIL-100(Fe)@xerogel with 43, 50 and 58 wt% MIL-100(Fe). (b) MIL-100(Cr) and MIL-100(Cr)@xerogel with 41, 51 and 56 wt% MIL-100(Cr). (c) MIL-101(Cr) and MIL-101(Cr)@xerogel with 35, 46, 50 and 77 wt% MIL-101(Cr). 77 wt% MIL containing MIL-101(Cr)@xerogel-H_2O was obtained using additional water in the synthesis.

Infrared spectra

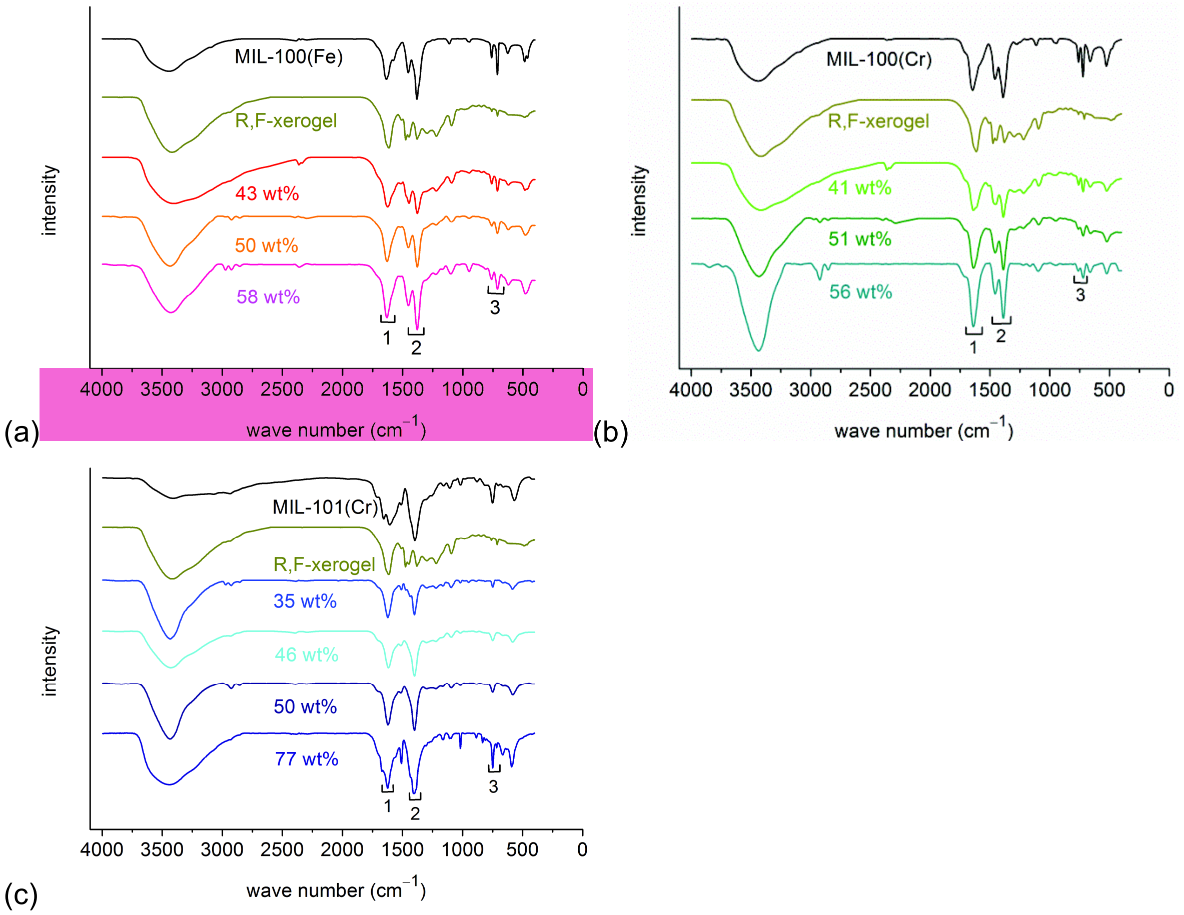

Fig. A.20. IR-spectra (KBr) of (a) MIL-100(Fe), R,F-xerogel and MIL-100(Fe)@xerogel with 43, 50 and 58 wt% MIL-100(Fe). (b) MIL-100(Cr), R,F-xerogel and MIL-100(Cr)@xerogel with 41, 51 and 56 wt% MIL-100(Cr). (c) MIL-101(Cr), R,F-xerogel and MIL-101(Cr)@xerogel with 35, 46, 50 and 77 wt% MIL-101(Cr). Square brackets (1, 2, 3) indicate the bands of the MILs in the composite materials. 77 wt% MIL containing MIL-101(Cr)@xerogel-H_2O was obtained using additional water in the synthesis.

4. Unpublished work

4.1 Catalysis and separation – synthesis of a glucose modified terephthalic acid linker towards chiral metal-organic frameworks

Introduction

Up to the present day metal-organic frameworks cannot compete with the chemical and thermal stability of zeolites. Otherwise, the mild synthesis conditions of MOFs (compared to zeolites) and the infinite number of possible building blocks offer new ways, for example the synthesis of chiral MOFs. Chiral MOFs combine the advantages of heterogeneous catalysts, for example the easy handling, with well-defined chiral functionalities. They are investigated intensively in asymmetric catalysis and enantiomeric separations.[35],[158],[159] Chiral MOFs can be prepared by following different strategies, as depicted in Figure 42.[160] K. Bisht and coworkers differentiate between direct and indirect synthesis methods. The direct methods include the use of chiral linkers or chiral auxiliaries, indirect methods lead to enantiopure MOFs by chiral influence of solvents or additives as well as chiral induction methods.[160]

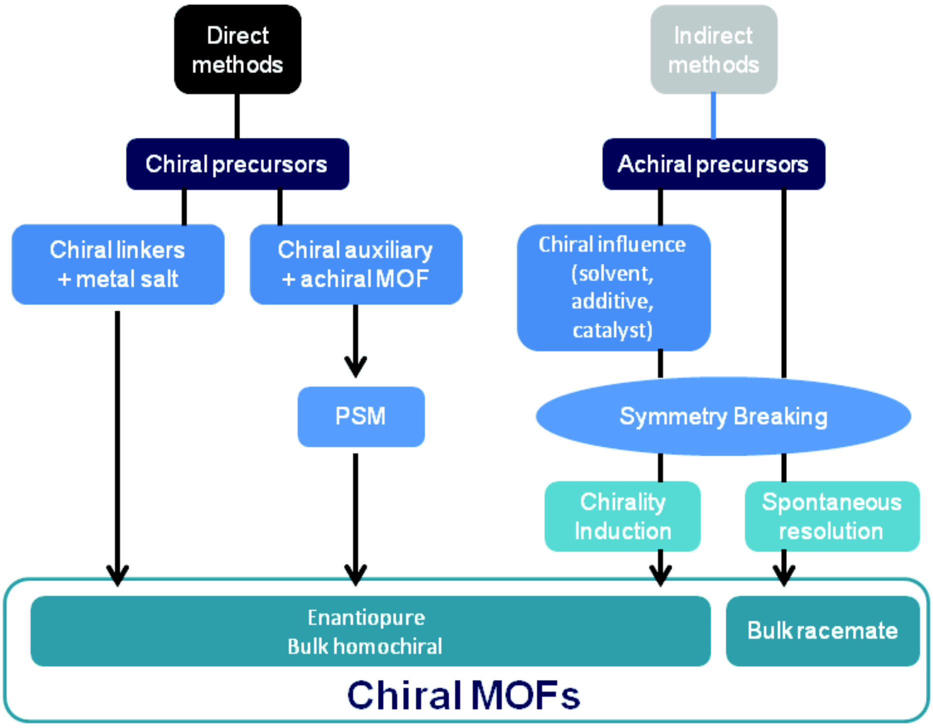

Figure 42: General overview of synthetic routes leading to chiral MOFs. Redrawn from ref. [160], Copyright 2015, with permission from the Royal Society of Chemistry.

A number of reviews reported the current state-of-the-art research.[160],[161],[162],[163] Related to the aim of this project an example for homochiral MOF synthesis using direct methods was given and accompanying challenges have been pointed out.

D. J. Lun and coworkers reported that the direct synthesis of a MOF-5 analogon using a L-proline functionalized ligand ($H_2$2) was not possible. In consequence, they developed a protection strategy in which the MOF was synthesized using the di-*tert*-butyldicarbonat (boc)-protected analogue of the ligand ($H_2$1). Deprotection was achieved by simple heating due to the thermolabile nature of boc-protecting group.[164] Due to the steric demand of the bulky boc-protection group the resulting IRMOF structure exhibit a non-interpenetrated structure. Pore accessibility was confirmed by dye uptake experiments. However, by N_2 sorption experiments the structure was found to collapse upon drying. The chiral MOF was tested as catalysts in asymmetric aldol reaction of acetone and nitro-benzaldehyde. The measured ee values for the MOF catalyst (ee: 29%) are low compared with the pure organocatalyst (ee: 52%). The results are explained by a less marked organization of the substrate transition state.[164]

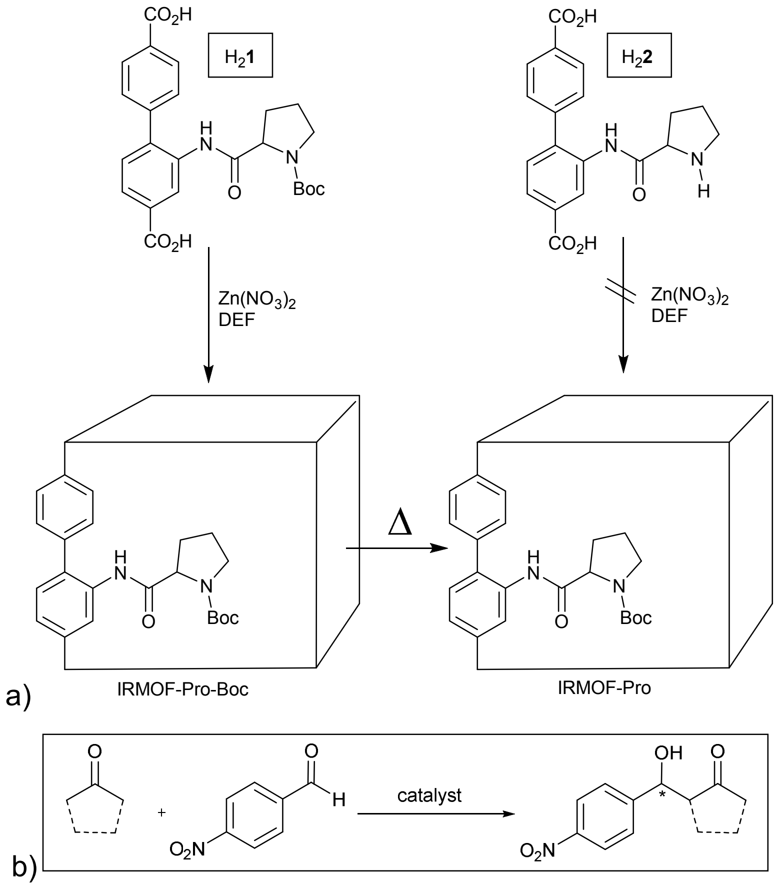

Figure 43: a) Conversion of ligand $H_2$1 to a cubic MOF, IRMOF-Pro-Boc, followed by thermolytic expulsion of the Boc moiety to generate IRMOF-Pro; b) aldol reaction catalyzed by IRMOF-Pro. Redrawn with permission from ref. [164]. Copyright 2011 American Chemical Society.

Exemplarily by this work, several challenges for chiral MOF catalysts can be pointed out:

- hydrolytic stability of the MOF is of critical importance
- sufficient diffusion of substrates has to be ensured, which can be achieved by larger pores
- the larger the pores are, the lower is the effect of spatial confinement

Nevertheless, when overcoming the mentioned challenges, especially the incorporation of chiral metal- or organocatalysts can provide manifold opportunities to multifunctional chiral MOF catalysts.**[161]**

Single site heterogeneous catalysis with MOFs

Following the concept of J. M. Thomas single-site heterogeneous catalysts (SSHCs) are materials "*in which the active centres are energetically equivalent and spatially isolated from one another, and are uniformly distributed over an internal and accessible surface which is exceptionally large (e.g. ca.* $10^3\ m^2\ g^{-1}$*) and three-dimensional (3D).*"[165],[166]

Metal-organic frameworks can fulfill the requirement of SSHC. In general, metal sites can be introduced to MOFs applying three different methods:

i) Framework design considering accessible or coordinative unsaturated metal sites.

In this case a major challenge is the accessibility and the constrained coordination environment of the metal cluster, due to framework geometry. Especially, in Lewis acid catalysis *cis*-connected open metal sites are necessary for transition states but are often not present in MOFs, as for example in MIL-101Cr (Figure 44).[167] A higher amount of open metal sites can be generated by defect engineering, but defects are not distributed homogeneously over the whole material.[168]

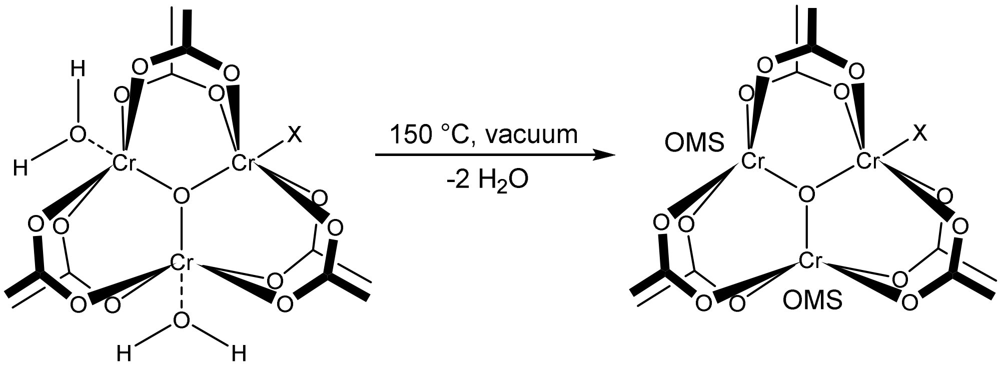

Figure 44: Depiction of MIL-101Cr SBU. X = F, OH; OMS = open metal sites.[51]

ii) Formation or introduction of metal nanoparticles inside the pores of a MOF.

The encapsulation of metal nanoparticles into MOF pores is an intensively investigated approach. Up to now the MOF mainly served as support, not as active catalyst. Through incorporation in the MOF, the nanoparticles are well distributed and agglomeration can be prevented. This topic is not within the scope of this work, Therefore, the reader is referred to the literature.[30],[169]

iii) Incorporation of metal complexes through functionalized ligands.

This method allows a high degree of control over the coordination mode of active sites, ending up with a tailor made, highly functionalized catalyst.[35]

Table 9 gives an overview of advantages of heterogeneous and homogeneous catalysts. SSHCs combine the advantages of both. A good general overview of porous materials for this application is given by C. Copéret and coworkers.[170]

Table 9: Advantageous of heterogeneous and homogeneous catalysts.[170]

Advantages heterogeneous catalyst	Advantages homogeneous catalyst
Easy separation	Active at lower temperatures
Applicability to continuous flow processes	Higher selectivities
recyclability	well defined active sites
Thermal and chemical stable	Better designable

Generating MOF single site catalysts by immobilizing metal complexes, can be achieved using different strategies. First, the linker, which contains an additional catalyst-metal binding site, can be part of the one-pot synthesis where the metal complex is coordinated directly (Figure 45a) or after deprotecting the linker (Figure 45c). Secondly, the MOF can be functionalized using post-synthetic methods either by chemical modification of the linker or a linker exchange following the SALE approach (Figure 45b+d).[58]

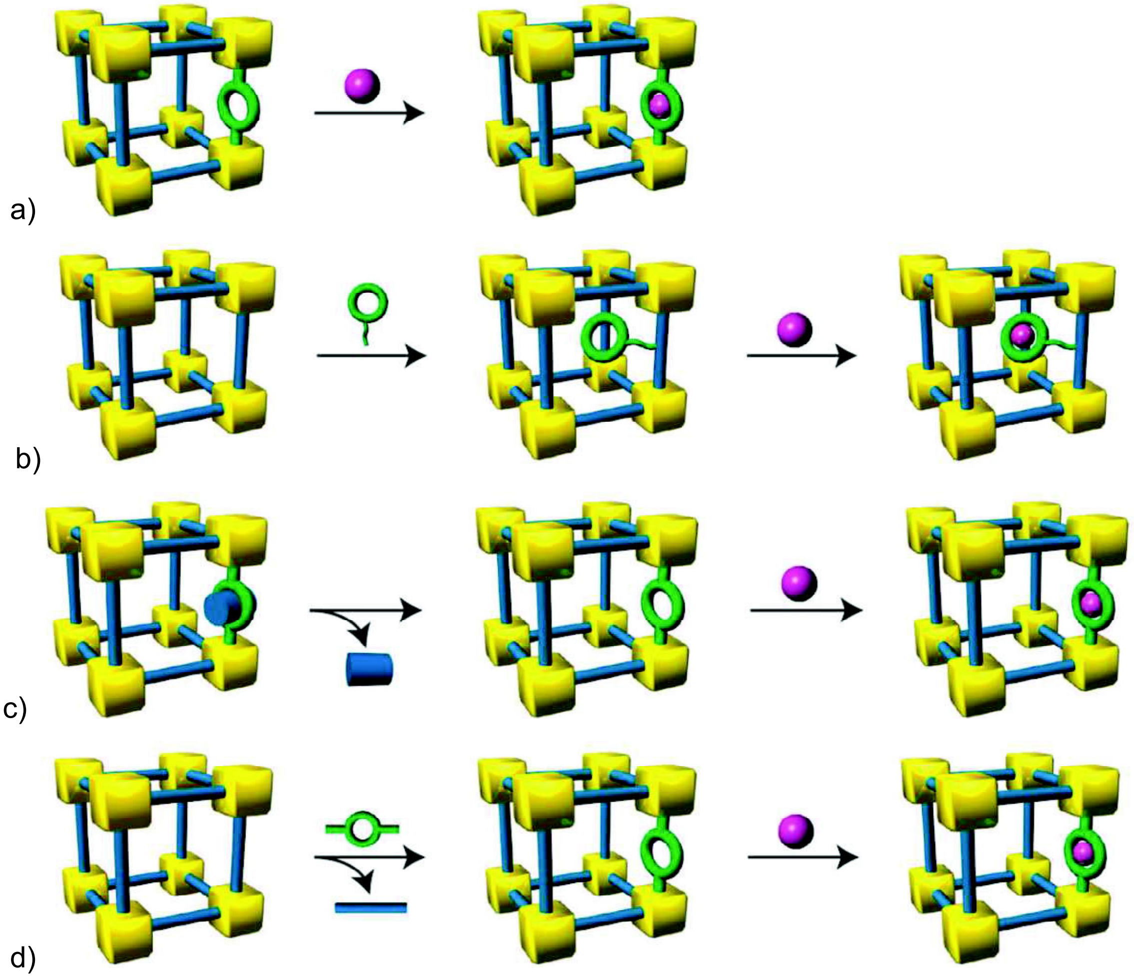

Figure 45: Strategies for metal-ion immobilization in MOFs (a) coordination of a metal ion to a functionalized linker. (b) construction of a binding site at the linker by PSM. (c) liberating binding groups by an orthogonal deprotection step or (d) solvent assistant linker exchange (SALE). Reprinted from ref. [58], Copyright 2014, with permission of the Royal Society of Chemistry.

More detailed information is given by J. D. Evans and coworkers in their recent review “*Post-synthetic metalation of metal–organic Frameworks*”.[58] In the following two selected examples are presented, for more detailed information the reader is referred to the literature.[171],[172],[173],[174]

In 2013, J. Canivet and coworkers functionalized MIL-101Fe with a molecular nickel(II)complex and investigated the resulting SSHC in the dimerization of ethylene (Figure 46).[175]

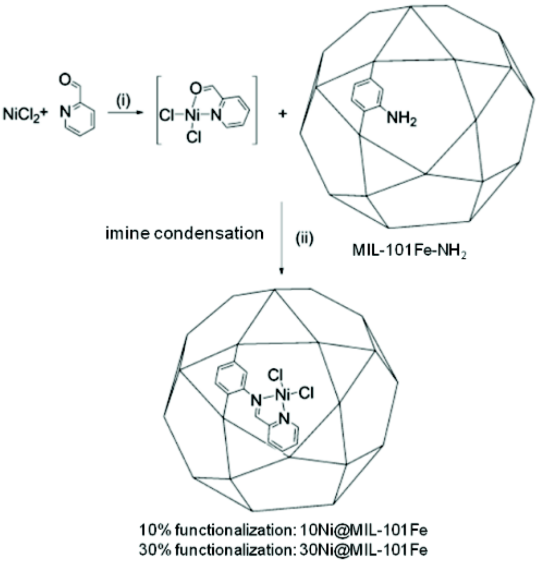

Figure 46: One-pot synthesis of the MOF-anchored nickel-complex Ni@MIL-101Fe. Reprinted with permission from ref [175]. Copyright 2013 American Chemical Society.

The nickel-complex was introduced post-synthetically. First, a precursor complex was formed by the N-coordination of the pyridyl group to the Ni(II) salt. The precursor Ni-complex should prevent the coordination of the ligand to the open iron sites of the MIL. The Ni-precursor complex was immobilized by the reaction of framework 2-aminoterephthalate with 2-pyridine carboxaldehyde resulting in a pyridine methanimino group (Figure 46).

10% and 30% functionalization was evidenced by NMR and EDX measurements. PXRD revealed the crystalline nature after modification. Nitrogen sorption experiments showed a significant decrease of surface for the 30% functionalized MOF from 1884 m^2/g (MIL-101Fe) to 155 m^2/g. The authors attributed the decrease of surface area to the high degree of functionalization with the Ni-complex. Otherwise, it has not been shown how the Ni-complex is distributed within the MOF particle. Since the post-synthetic functionalization is based on diffusion, it can be assumed that in the shell of a single MOF particle the degree of functionalization is much higher than in the core of the particle. This has to be regarded critically and is often overlooked in literature.

Nevertheless, the SSHC MOF catalyst was explored for the oligomerization of ethylene. The MOF catalysts containing 10 or 30% Ni-complex displayed, in addition to high TOF values (up to 10455 h^{-1}, at 25% and 30 bar), a higher selectivity to 1-butene than comparable molecular catalysts, which outlines the promising perspective for SSHCs.[175]

A second interesting study combines chiral ligand design with anchoring of metal complexes. J. M. Falkowski and coworkers synthesized a BINAP derived dicarboxylate linker which forms a UiO-66 type structure including $Zr_6O_4(OH)_4(O_2CR)_{12}$ Cluster as secondary building units. Post synthetic coordination of ruthenium and rhodium complexes resulted in highly enantioselective MOF catalysts (Figure 47).[176]

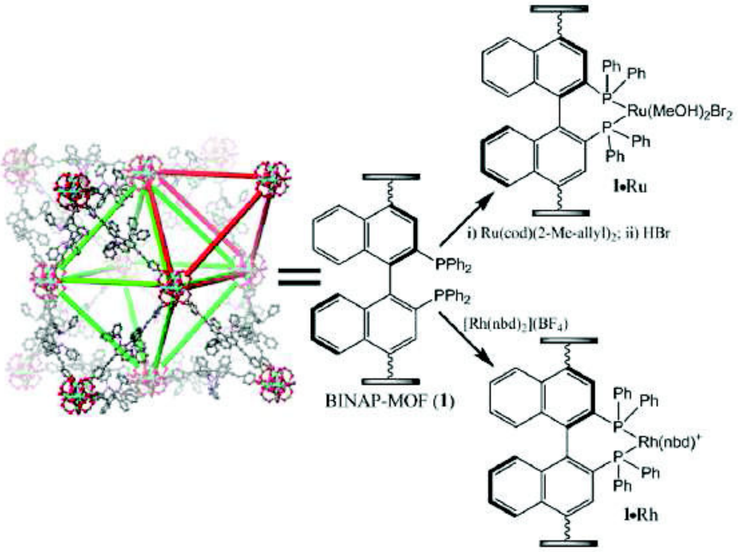

Figure 47: Post-synthetic metalation of BINAP-MOF (1) to form 1·Ru and 1·Rh. Reprinted with permission from ref [176]. Copyright 2014 American Chemical Society.

Unfortunately the BINAP MOF is not stable upon removal of solvent, hence the experimental surface area could not be determined. Liquid adsorption of dye molecules showed the accessibility of the pores. Although single crystals of BINAP MOF were obtained, the environment of metal ion could not be determined due to rotational disorder of the ligands. Instead using X-ray absorption fine structure spectroscopy (XAFS) it was confirmed nearly identical coordination environment comparing BINAP MOFs and the molecular complex.[176] The BINAP MOF successfully catalyzed various asymmetric transformations, as for instance the asymmetric hydrogenation of β-keto esters with *ee* values between 94-97%.[176]

Although several examples are reported in the literature, this field of MOF catalysis is still in its infancy.[170] Especially, effects as cooperative catalysis, synergistic effects and selectivity studies in relation to pore confinement effects bear a high potential for future research.

Project

It has been shown that the variation of pore size and pore environment of a metal-organic framework has a significant impact on catalyst activity and separation efficiency.[1],[177] Nevertheless, the active open metal sites often are not well accessible, since coordination is impeded through secondary building units and bulky ligands. Taking into account that open metal sites are important for the majority of reactions, a new ligand has been designed which can accomplish the following requirements:

i) coordination of metal precursors
ii) chiral coordination (Figure 48)
iii) the resulting MOF should be stable and permanently porous
iv) the reagent should be cheap
v) the method should be applicable to various kinds of MOF structures.

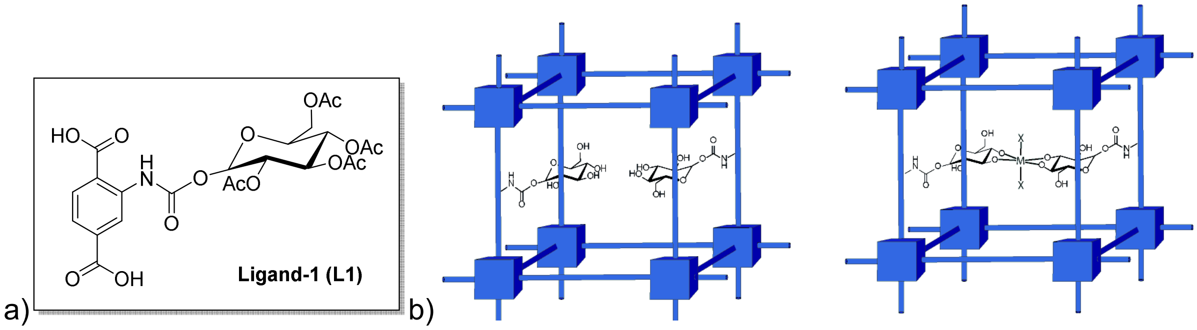

Figure 48: a) Depiction of the targeted Ligand 1 (L-1); b) schematic drawing of the coordination of a metal ion by ligand 1.

As shown in Figure 48b depending on the amount of Ligand-1 (L1) the metal precursor could be coordinated through one linker or be chelated by two linkers. The latter coordination mode outlines the higher stability of the metal ion and could minimize leaching effects (Figure 48b). It was already shown, that a variety of metals are able to form stable complexes with carbohydrates.[178],[179] In principle, by choice of metal ion and reaction conditions various structures can be accessible as for instance MIL-101, MIL53, MIL88, UiO-66, allowing the comparison of free pore volumes. As seen before a judicious choice between large pore volume for diffusion and pore restrictions for high selectivity has to be considered.[164]

Ligand-1-protected was synthesized as part of the Bachelor thesis of Serkan Gökpinar. Single syntheses of compounds A - C (Figure 49) are known in the literature and have been reproduced, whereas Ligand-1-protected is a new compound. First α-D-glucose was acetylated using acetic anhydride with 1,4-Diazabicyclo[2.2.2]octane (DABCO) as a base catalyst.[180] The product A could be obtained in high yield (90 %). For selective deprotection at the C1 position two literature known methods have been tested.[181],[182] The deprotection using iron(III)chloride in acetonitrile gave the better yield of 40 % after column chromatographic purification (Figure 49).

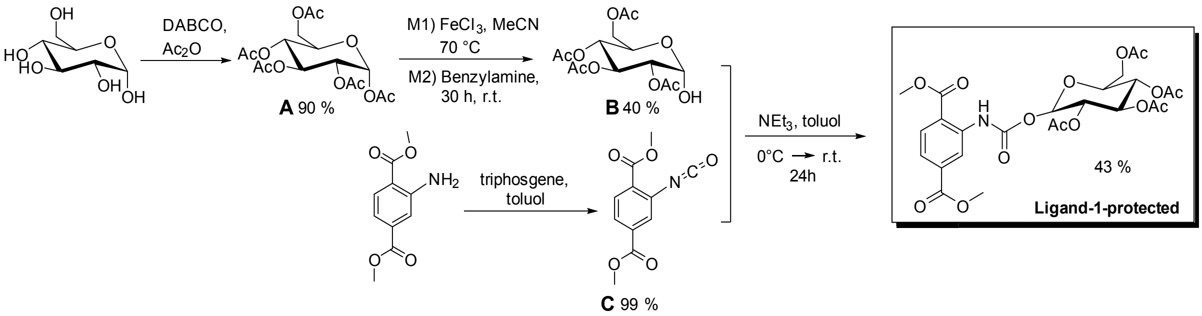

Figure 49: Synthesis of Ligand 1-protected.

The second building block of Ligand-1-protected was dimethyl-2-isocyanatoterephtalate (C) (Figure 49). Using an in situ approach following H. Knölker *et al.* dimethyl-2-aminoterephthalic acid was reacted with 4-dimethylaminopyridine and di-*t*-butyl dicarbonate (Figure 50)[183]. Dimethyl-2-isocyanatoterephtalate could be detected by mass-spectrometry, but neither the isocyanate nor the final product could be isolated. Therefore, in a second approach dimethyl-2-isocyanatoterephtalate was synthesized in toluol using triphosgene (Figure 49).[184] The desired product C was obtained in quantitative yield. Finally the two buildings blocks were combined, using an equimolar amount of triethylamine for deprotonation of the hydroxyl moiety in toluol.[185] Ligand-1-protected precipitated from the reaction solution after cooling to 0 °C.

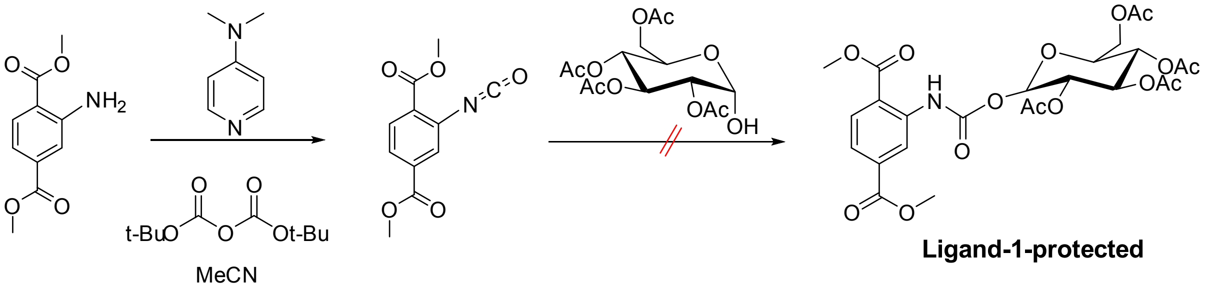

Figure 50: Attempts to synthesize ligand-1-protected using DMAP.

Crystals of Ligand-1-protected could be obtained by dissolving Ligand-1-protected in tetrahydrofuran (THF) and evaporation by air (Figure 51).

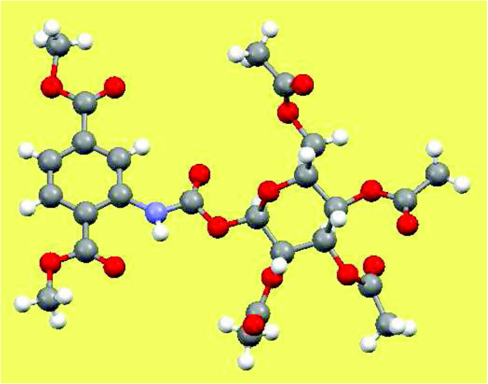

Figure 51: Single-X-ray structure of Ligand-1-protected.

In order to build up metal-organic frameworks with Ligand-1-protected, the carboxylate groups must be deprotected. Also for incorporation of Ligand-1 following the SALE approach a deprotection of the carboxylate groups is a prerequisite. For SALE incorporation of Ligand-1 MOF-5 was chosen, since for this MOF it has been already reported that linker can be exchanged post-synthetically. In addition, the incorporation can be confirmed via single-crystal X-ray crystallography. MOF-5 single crystals were prepared following S. Han *et al.*[186] BET surface area for the colorless MOF-5 crystals was determined as 3136 m^2/g (Figure 52).

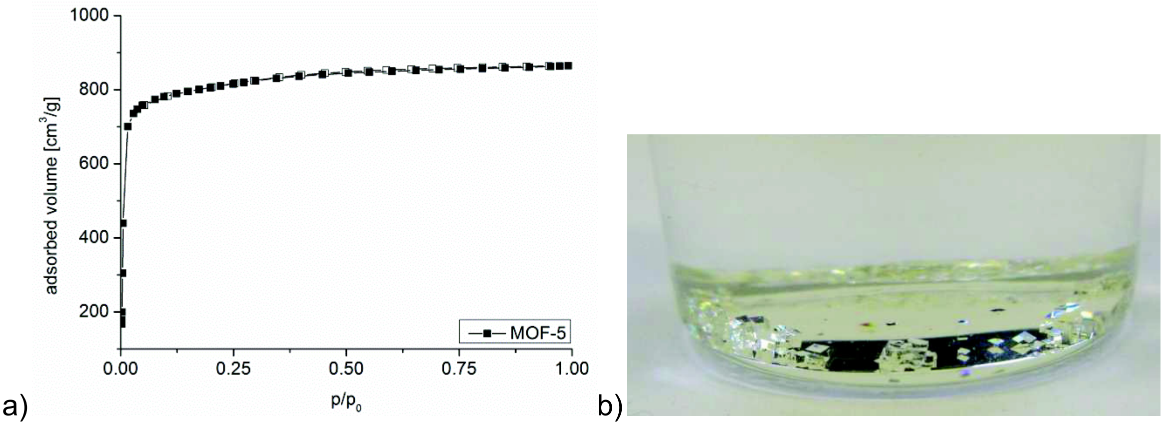

Figure 52: a) N_2 sorption isotherm of MOF-5 single crystals. B) Images of MOF-5 crystals.[186]

Unfortunately, all deprotection attempts of the carboxylate moiety failed, because the ester group of the urethane moiety was cleaved under the applied conditions.

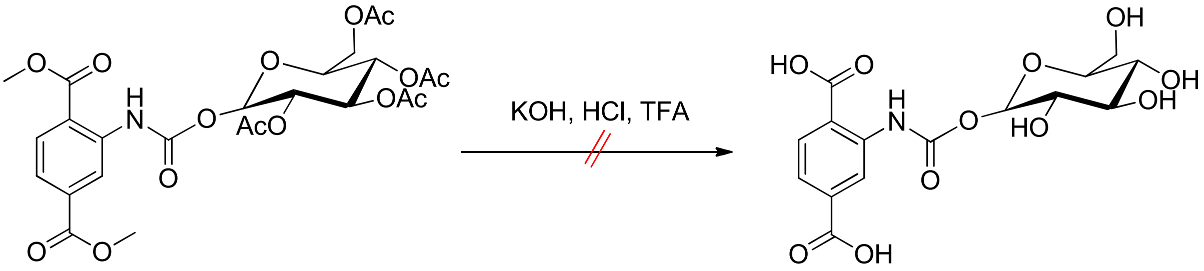

Figure 53: Deprotection experiments of Ligand-1-protected.

As alternative protecting group instead of methyl moieties, for instance, benzyl-groups or tert-butyl groups could be applied. Benzyl groups can be cleaved using Pd@C under H_2 pressure. Otherwise the ester functionality can be exchanged to a more stable carbamid moiety. The second method was applied using commercially available 1,3,4,6-*Tetra-O*-acetyl-2-amino-2-deoxy-*β*-D-glucopyranose (2-amino-glucopyranose) (Figure 54).

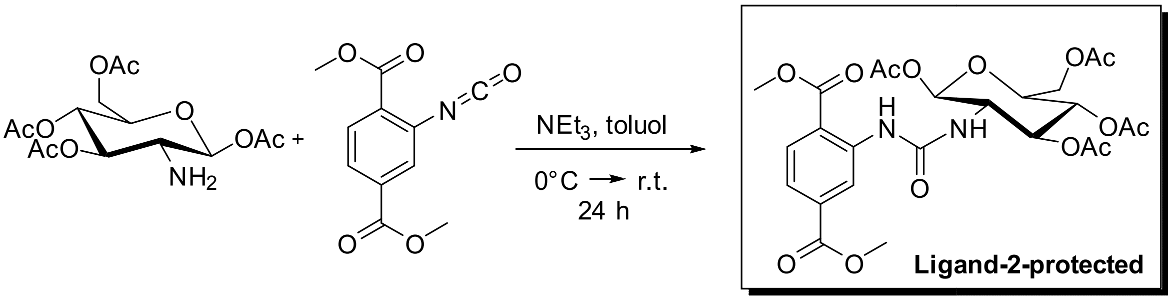

Figure 54: Synthesis of Ligand-2-protected.

As shown by ^{1}H-NMR spectrum Ligand-2-protected was obtained in good purity following the same method as for Ligand-1-protected.

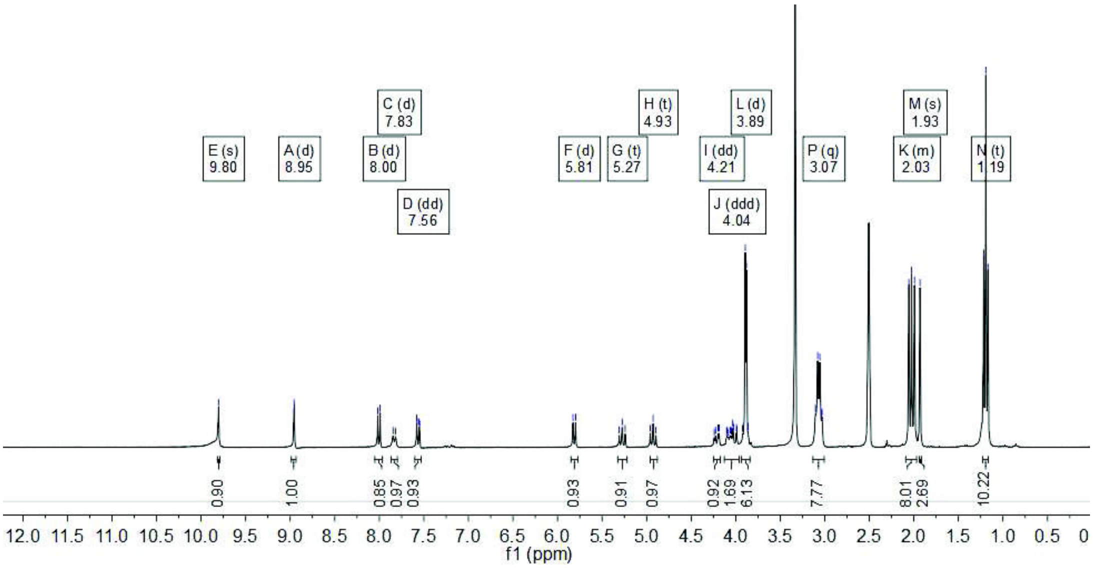

Figure 55: ^{1}H-NMR of Ligand-2-protected in DMSO-d_6.

Ligand-2-protected is very well soluble in a 1:1 mixture of THF/MeOH. After addition of NaOH (7 eq) and slow heating to 80 °C the color of the mixture turned from colorless to orange (Figure 56).

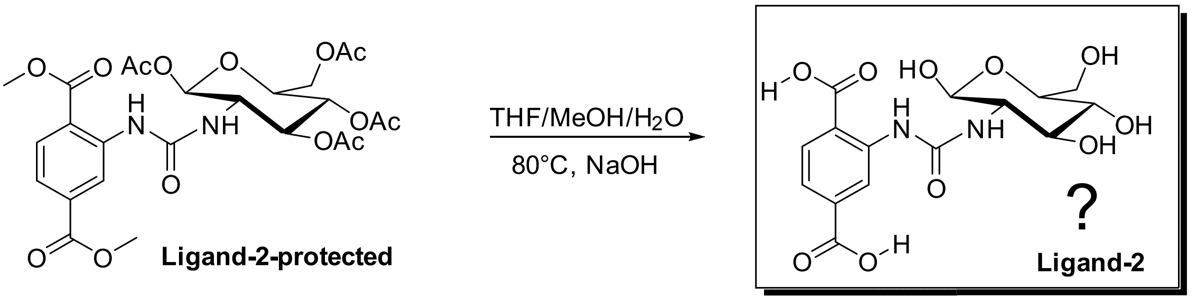

Figure 56: Deprotection attempt of Ligand-2-protected.

The large excess of NaOH was used, since the acetyl-protection groups can be removed more easily at slightly basic pH than the targeted carboxylate moieties. After stirring for 1h at 80 °C a solid has formed, the solvent was concentrated and the solid was separated by filtration. Ligand-2 is expected to be highly soluble in water. The solid was dissolved in dry acetone, to separate product from sodium chloride, which forms after the addition of HCl. Slowly, HCl (conc.) was added and a white solid precipitated. The remaining red solution was dried and the oily product was analyzed by ^{1}H-NMR (Figure 57).

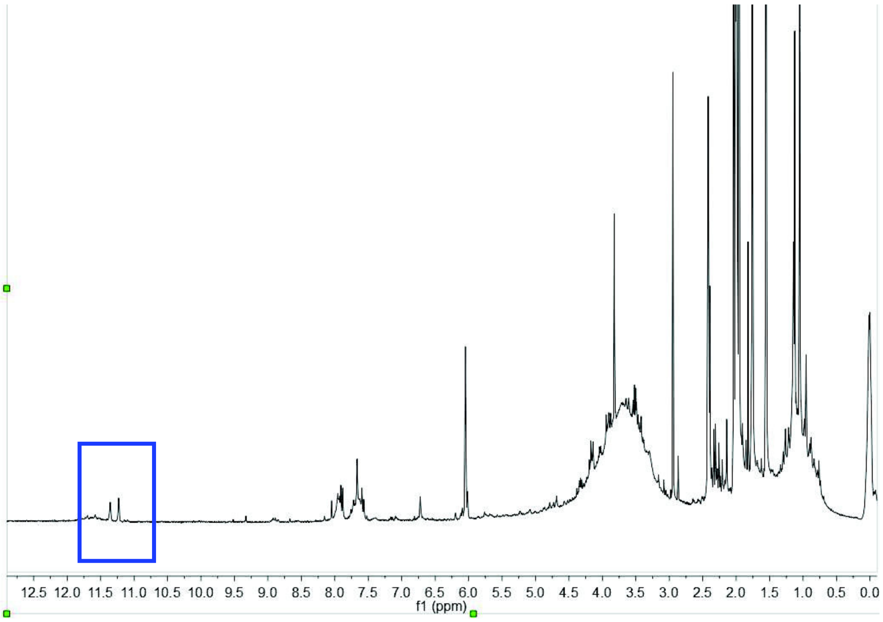

Figure 57: ^{1}H-NMR of deprotection attempt of Ligand-2-protected in DMSO-D$_6$.

The signals between 11 and 11.5 ppm can be assigned to carboxyl-protons indicting a successful deprotection. Isolation and further improvement of the reaction was not followed due to prioritization of the ongoing work.

Summary and outlook

In conclusion the designed Ligand-1 and Ligand-2 were synthesized in their protected form, but could not be isolated as deprotected ligands. Nevertheless, since it is known from MOFs as MIL-100Al that in some cases an in situ deprotection can occur[48], Ligand-1-protected was reacted with Cr(III) salts. The results are described in chapter 4.3.2.

Since deprotection and isolation of ligand-2 became apparently difficult, another synthesis pathway was planned. Instead of converting dimethyl-2-aminoterephtalate in water, 1,3,4,6-tetra-*O*-acetyl-β-D-glucosamine (TetraAc-2-glucosamine) can also be transformed to the isocyanate derivative, for instance following the method of M. Avalos (Figure 58).[187]

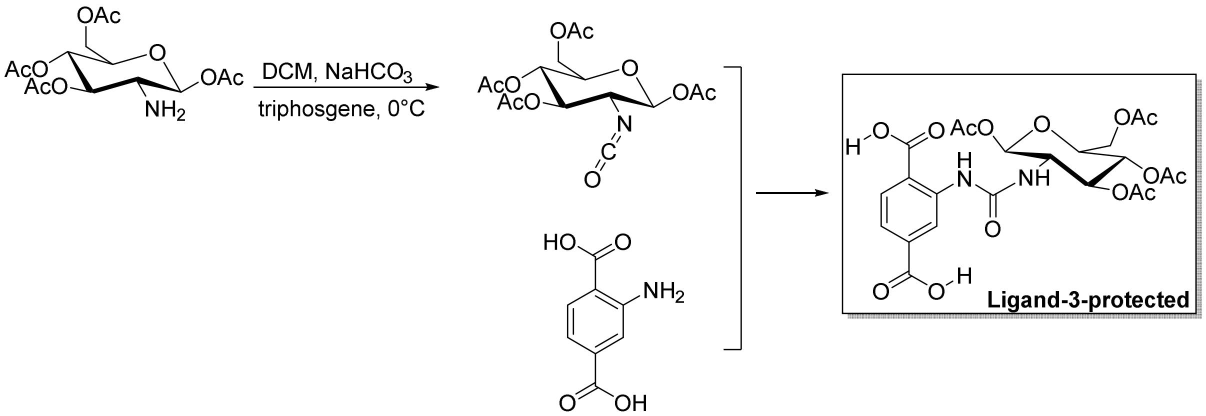

Figure 58: Synthesis strategy for ligand-3-protected.

This strategy avoids the need of protection since the primary amine preferably attacks the isocyanate moiety. Also advantageous is the preservation of the acetyl-protection of the glucose moiety, which makes the linker suitable for direct one-pot MOF synthesis in acidic conditions. The strategy is also suitable for post-synthetic modification of various amine-modified MOFs. Due to priority setting of projects this pathway could not be tested, but was followed by Serkan Gökpinar within the scope of his master thesis. Ligand-3-protected could be synthesized successfully and was obtained in good yields, but results are not reported within this work.

Ligand-3 and Ligand-3-protected are regarded as highly promising building blocks for MOFs. Therefore, an outlook of ideas which could be followed is given:

A) Solvent assisted linker exchange using Ligand-3.

The exchange of terephthalate ligands of single-crystalline MOF-5 (Figure 52) with Ligand-3 would be very interesting, since the occupied pore volume by glucose and the amount of replaced ligands (per unit cell) can be determined experimentally using single-X-ray crystallography. In a second step metal-ions could be coordinated to the glucose-moiety. Tracing the metal coordination by EDX measurements, insights about the deepness of linker exchange and metal coordination inside the crystal can be gained (Figure 59). In consequence, a core-shell material could be obtained.

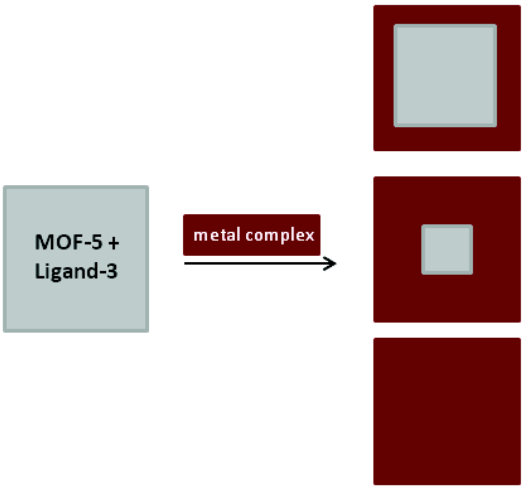

Figure 59: Schematic depiction of diffusion deepness after SALE process.

B) SALE, PSM or direct linker synthesis for incorporation of Ligand-3 into stable MOF structures.

The generation of single-site heterogeneous catalysts using Ligand-3 can be achieved by employing UiO-66 as parent MOF structure. For UiO-66 it is known that terephthalate linkers can be exchanged and the resulting MOFs can be stable enough for catalysis and sorption experiments.[171]

During the synthesis of Ligand-3 the amine-group of tetraAc-2-glucosamine is converted into an isocyanate moiety, this reagent can be used to functionalize a variety of amine based MOFs. The acetyl-protecting groups are stable in acidic environment up to certain degree, Therefore, also direct MOF synthesis is worth to perform and can be compared with post-synthetic procedures.

The resulting core-shell material can be investigated for cascade reactions. The terephthalic acid linkers of the MOF core could be functionalized with acidic moieties such as SO_3H groups, whereas the metal coordinated Ligand-3 shell can act as enantioselective hydrogenation catalyst. Also, cooperative effects or enantioselective acid catalysis can be investigated.

C) Ligand-3 based MOF as highly hydrophilic gas and vapor sorption material

Ligand-3 is highly soluble in polar solvents as acetone and water due to the connected glucose moiety containing four hydroxyl- and two amine- moieties. Therefore, a stable Ligand-3 functionalized MOF, for instance MIL-101Cr, UiO-66 or MIL-53Al might be able to absorb a high amount of polar compounds, water or also CO_2 due to hydrogen bonding groups.

D) Chiral separation with Ligand-3 functionalized MOF

HPLC columns with the best performance for enantioselective separations are mainly based on chiral polysaccharide functionalized materials (Figure 60).[188]

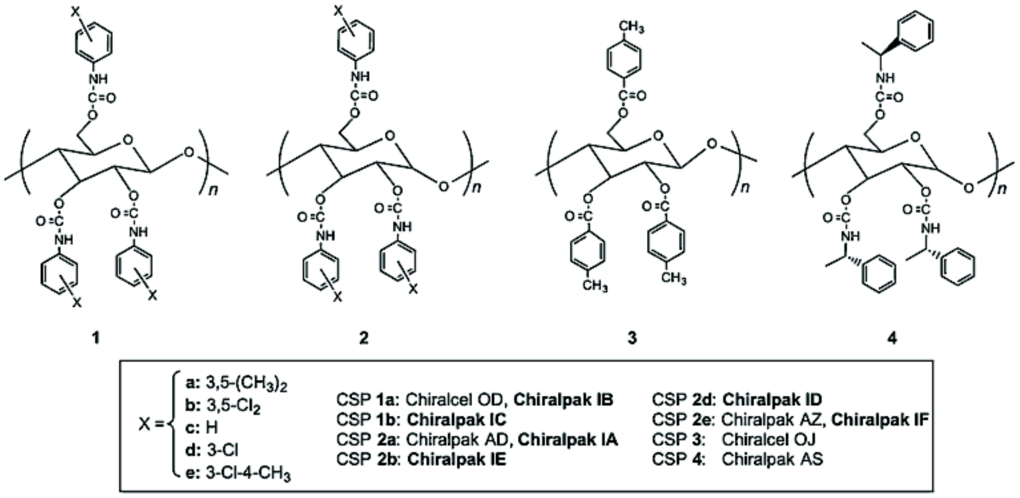

Figure 60: CSPs used in Daicel chiral columns. CSPs 1a, 2a and 2e have been commercialized with different brand names by several other companies. Reprinted from ref. [188], Copyright 2014, with permission of Elsevier.

For most separations good methods have been already developed, hence the question must be, in which case can the use of chiral MOFs really solve a problem?

A great challenge is the enantioselective separation of aryl- and alkyl halogenes (Figure 61).[ii]

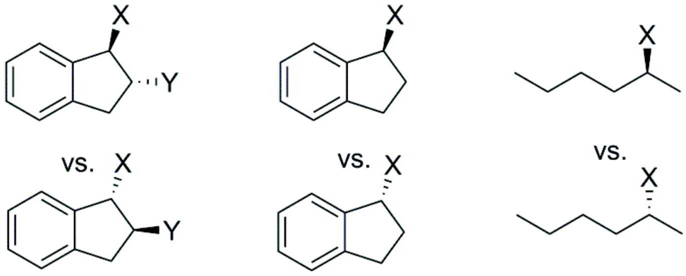

Figure 61: Examples for separations of aryl and alkyl halogenes.

There are already a lot of works dealing with the separation of isomers, as for instance hexane isomers[189] or different C5 hydrocarbons using MOFs.[190] An excellent review of B. van de Voorde and coworkers summarizes the state-of-the-art in 2014 for liquid phase adsorptive separations.[191] Still, to best of my knowledge, no experimental studies are reported about enantioselective separation of alkyl halogenes neither with MOFs nor with other materials. The difficulty for this kind of separation is the lack of interactions between the substrate (e.g. 2-chloropentane) and framework/adsorbent (Figure 61).

X. Bao *et al.* conclude from their molecular simulation study which focused on MOFs that "*high enantioselectivity is strongly correlated with a close match between the size of the pore and the size of the chiral sorbate molecule*".[192]

[ii] Idea generated in dialogue with Prof. Dr. Czekelius.

In consequence, a flexible MOF which adjusts its pore volume depending on the applied solvent or pressure might be suitable for investigation of the perfect size match.

T. Duerinck and J.F.M. Denayer critically discussed the potential of MOFs for chiral separations and separation of small molecules.[177] They outlined a concept, based on three-point interactions, for chiral resolution in nanoporous materials which can help to design better MOF materials for separations (Figure 62).

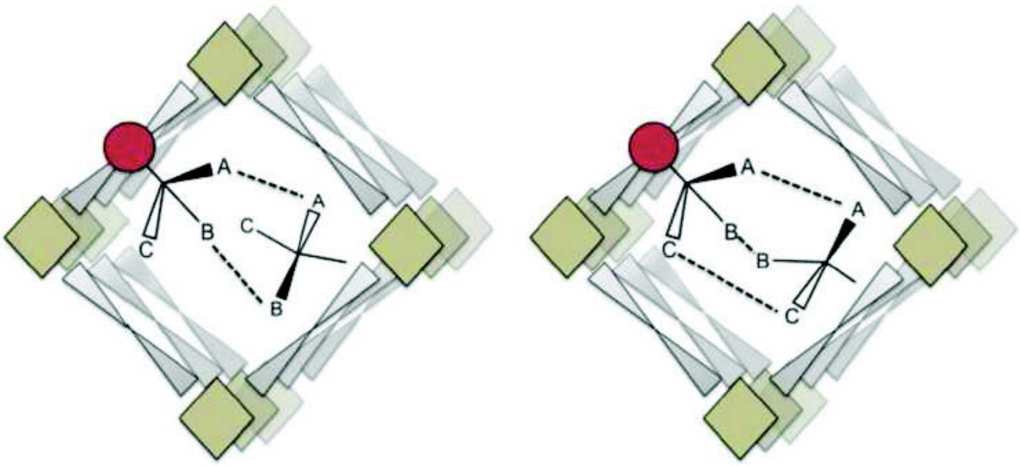

Figure 62: Three point interaction theory for chiral resolution in a nanoporous material: a) incomplete 2-point match (A,B) between host and guest; b) successful pairwise 3-point interaction of functional groups (A,B,C). Reprinted from ref. [177], Copyright 2015, with permission of Elsevier.

In chapter 4.3.3 the results of MOF@xerogel materials showed that a homogenous particle size and a certain macroporosity are necessary for HPLC columns in order to avoid too high resistances. Therefore, the growth of MOFs on silica spheres might be beneficial.[193]

E) TetraAc-2-glucosamine functionalization as anchoring point for carbohydrate based composites

If the functionalization of MOFs with Ligand-3 or the tetraAc-2-glucosamine moiety via post-synthetic methods can selectively occur in the surface region of a MOF particle, a novel kind of core-shell material can be obtained. The sugar moiety can be easily functionalized in order to improve adhesion in composites. In combination with carbohydrate based porous polymers or cellulose and chitin based hydrogels *in situ* polymerization might be possible.[194] The carbohydrate moiety on the MOF surface can also be used as (bioactive) sensor[195], at what the MOF itself can fulfill an additional task (loading of active species, acidity, catalysis, photoactivity) turning into a multifunctional system.

This project was forwarded to Serkan Gökpinar (Master student) in April 2016.

4.2 Catalysis - synthesis of MOF@metal oxide core-shell composites

Introduction

In the previous chapters selected aspects of MOF catalysis were highlighted, focusing on the challenges which are hard to overcome with known catalysts but maybe solved by MOFs. The supreme discipline in MOF catalysis is about combining the presented methods and strategies to generate a multi-functional solid catalyst which is able to catalyze reactions which are regarded as impossible until now.

"*Cascade or tandem reactions where two or more individual reactions are carried out in one pot constitute a clear example of process intensification, targeting the maximization of spatial and temporal productivity with mobilization of minimum resources.*"[37]

Cascade reactions or also multi-component reactions have several benefits as they reduce waste, solvents and number of reactions steps. From a chemical point of view, they can lead to higher selectivity and better yield (Figure 63).[37]

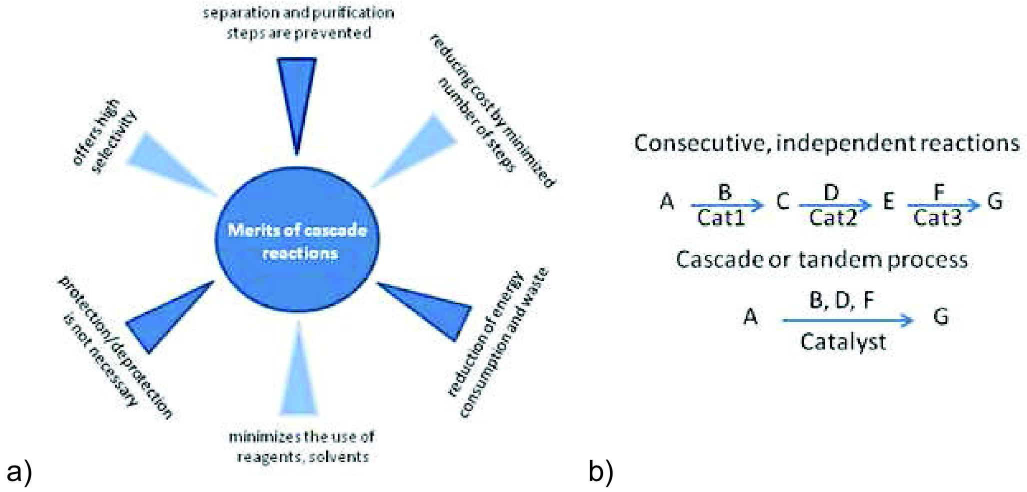

Figure 63: a) Advantages of cascade reactions; b) schematic depiction of the difference between consecutive and cascade reactions. Modified from ref.[37].

Cascade reactions require multifunctional catalysts. Multifunctionality in MOFs can be achieved by using molecular engineering combing the strategies, which were introduced in the chapters before. A very recent review of B. Li and coworkers describes state-of-the-art examples.[196] Multifunctionality can also originate from multi-component systems. A. D. Burrows defined multi-component systems again on the one hand within the single material level, as for example mixed-metal or mixed-linker MOFs[197],[198] but on the other hand also systems in which components are arranged segregated from each other (Figure 64).[199]

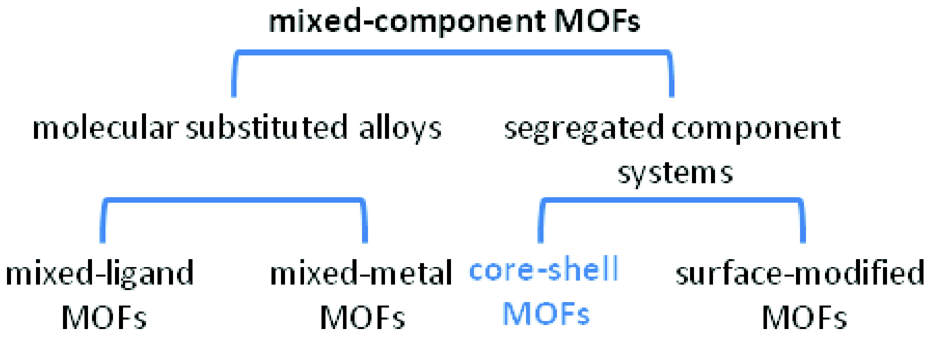

Figure 64: Different strategies to obtain mixed-component MOFs. Redrawn from ref. [199], Copyright 2011, with permission of the Royal Society of Chemistry.

The latter systems, named in the following core-shell materials, can be regarded as superior due to multiple levels of functionality.

Related to catalysis, MOF based core-shell systems are promising materials because the different catalysts can be incorporated in the same heterogeneous material. Core and shell of the same material can catalyze different steps of a cascade reaction.[35] Different size and shape selectivity can lead to better reaction control and easier separation. Shorter diffusion pathways can increase product yield.

In the following section the 3 main categories of core-shell materials will be presented: i) nanoparticle@MOF, ii) MOF@MOF, iii) MOF@silica/zeolite/metal oxides.

NP@MOF

Nanoparticles can be incorporated in metal-organic frameworks using different strategies. The reviews of A. Dhakshinamoorthy *et al.*[30], P. Hu *et al.*[200], C. Rösler *et al.*[201] and P. Falcaro[202] provide a thorough overview including tables about NP@MOF systems which have been used in catalytic reactions. Generally, different kinds of core-shell systems can be prepared which are illustrated in Figure 65. Taking the example of NP@MOF structures these are: (a) one core coated by a shell; (b) multiple cores encapsulated in a matrix particle; (c) "yolk−shell" or "bell" structures, consisting of a core encapsulated in a hollow shell with a void in between.[200]

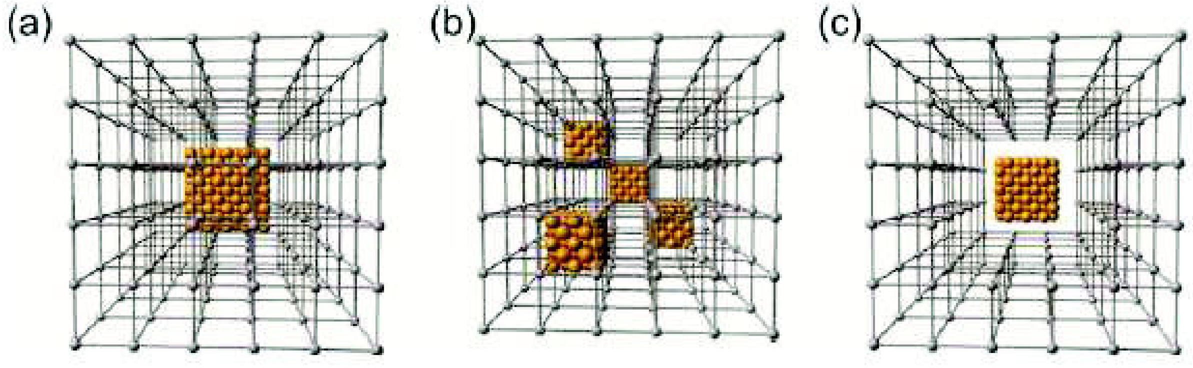

Figure 65: Various types of core-shell structures; a) single core-shell structure, b) multiple cores in one shell, c) yolk-shell structure. Reprinted with permission from ref [200]. Copyright 2014 American Chemical Society.

With regard to heterogeneous catalysis the use of MOFs as support for metal-nanoparticles was investigated first. Because of their high porosity and regular pores, MOFs are ideal candidates to prevent aggregation of nanoparticles. Numerous examples showed that nanoparticles or even nanocluster can be immobilized in MOFs and resulting composites exhibit good catalytic performances.[201]

An interesting example of how different kind of core-shell structures can differ in catalytic performance was reported by M. Zhao *et al.* in 2014. They prepared a core-shell structure containing a single Pd-NP core with a shell based on IRMOF-3 (Figure 66).

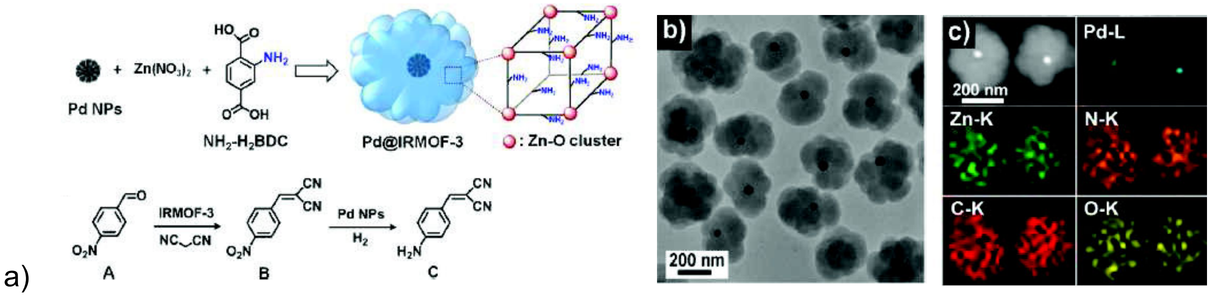

Figure 66: a) Synthetic route for the core−shell Pd@IRMOF-3 hybrid and model cascade reactions; b) TEM, HAADFSTEM image and c) corresponding EDX elemental mapping image of the nanocomposites. Reprinted with permission from ref [203]. Copyright 2014, American Chemical Society.

In the cascade reaction, IRMOF-3 catalyzed the Knoevenagel condensation of 4-nitrobenzaldehyde (A) and malononitrile into 2-(4-nitrobenzylidene)malononitrile (B) whereas the Pd NP core converted the nitro moiety by hydrogenation into the target product 2-(4-aminobenzylidene)-malononitrile (C). Carefully designed reference experiments showed the need of both – core and shell – for product formation. Comparison between single core-shell catalyst and multiple core-shell structures (Pd NP distributed within the MOF particle) revealed significant different product selectivity, whereas the single-core-shell material exhibited higher selectivity.[203]

The summary of reactions catalyzed by NP@MOFs shows a clear trend towards acid/base catalyzed reactions by MOFs and hydrogenation or oxidation reaction catalyzed by the metal-nanoparticle.[37]

MOF@MOF

In the area of core-shell MOF@MOF structures up to now the work focused mainly on understanding of crystal growth or sorption application instead of catalysis.[204],[205],[206]

Generally it can be distinguished between having different ligands[207] or metal ions[208] in the shell material.[199] Theoretically, also both, different metal and linker can be imagined, but after intense literature research no reports have been found.

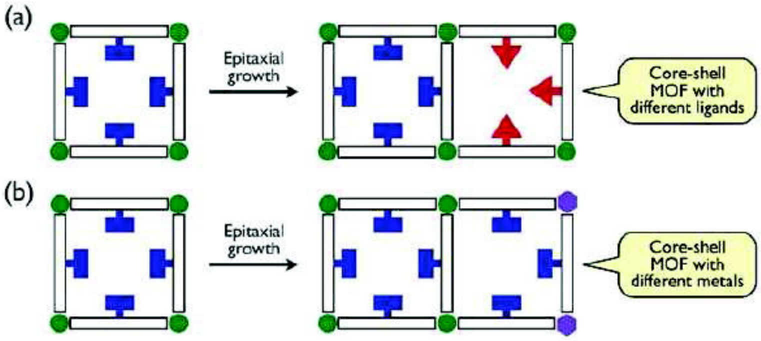

Figure 67: Schematic representation of the core–shell approach to forming MC-MOFs involving (a) different ligands and (b) different metals. Reprinted from ref. [199], Copyright 2011, with permission of the Royal Society of Chemistry.

K. Koh and coworkers presented in 2009 core-shell structures of IRMOF-3@MOF-5 and reverse MOF-5@IRMOF-3, where the core-shell structure was clearly visible from microscopic images.[207]

Recently, K. A. McDonald *et al.* reported a composite material based on the same IRMOF-3@MOF-5 structure which was additionally functionalized via post-synthetic modification with a polymer initiator (Figure 68).[209] By tethering the initiator selectively to the amine groups of IRMOF-3 only the pores of the shell are blocked through polymerization, whereas the high surface area of MOF-5 core could be preserved.[209]

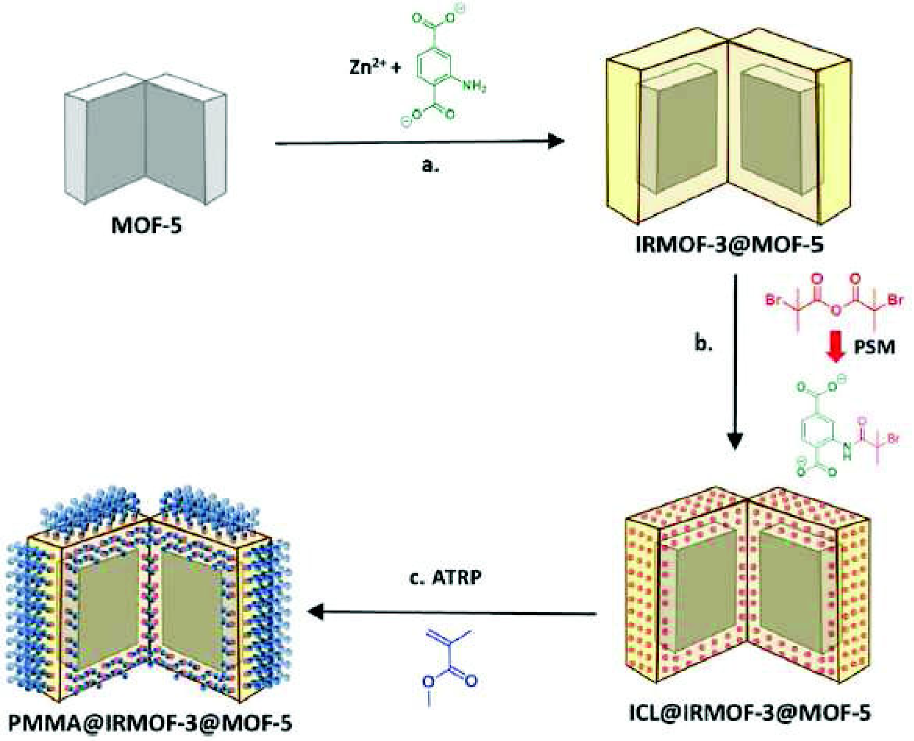

Figure 68: Synthetic route to PMMA@IRMOF-3@MOF-5 core-shell composites (a) IRMOF-3@MOF-5), (b) initiator carrying linker@IRMOF-3@MOF-5 (ICL@IRMOF-3@MOF-5) and (c) atomtransfer radical polymerization on ICL@IRMOF-3@MOF-5 with methyl methacrylate to generate PMMA@ IRMOF-3@MOF-5. Reprinted from ref. [209], Coyright 2015, with permission of the Royal Society of Chemistry.

In principle, also post-synthetic functionalization can generate core-shell materials, although the shell is much thinner in these cases. Besides also the SALE mechanism (solvent assistant linker exchange) can be used to synthesize mixed linker core-shell materials.[171]

MOF@silica/zeolites

The third group of core-shell materials is composed of mixed porous materials as for instance MOF@zeolite or MOF@silica structures. These materials are very interesting since by thorough choice of components hierarchical porous structures exhibiting micro- and mesoporosity are obtainable. The most studied materials are MOF@silica structures, whereas the silica shell protects the MOF core. The first example was a coordination polymer (indium)@SiO_2 composite, reported by C. Jo *et al.* in 2011.[210] Furthermore only a few examples of MOFs cased by a SiO_2 shell are known, as for instance ZIF-8[211] and HKUST[212] and MIL-88Fe-NH_2.[213] Reverse structures where the MOF is grown around a core of silica sphere also have been reported.[193],[214],[215] In 2016, S. Sorribas *et al.* reported the synthesis of SiO_2@MIL-53Al-NH_2 composites. It was observed that the pressure depended breathing behavior of MIL-53-NH_2 can control the access of gas molecules to the silica core, which makes the material promising for encapsulation or gas separation processes.[216]

G. Zhu *et al.* reported in 2014 the first example of a zeolite@MOF core-shell structure growing a MOF around a zeolites support, resulting in ZSM-5@UiO-66Zr-NH_2.[217] The composite material showed catalytic activity for the cascade conversion of malononitrile and benzaldehyde dimethyl acetal yielding benzylidene malononitrile. The process involves Brønsted acid catalyzed hydrolysis of the acetal and a Knoevenagel condensation reaction.[217]

An interesting example combining different strategies was reported by V. Pascanu and coworkers.[213] First they prepared a multiple NP@MOF material using Pd nanoparticle and the flexible MOF MIL-88Fe-NH_2 which was protected with a nano-SiO_2 shell afterwards. Remarkably, the multifunctional catalyst withstood a 7-day-continuous flow process in aerobic oxidation of benzylic alcohols (Figure 69).[213]

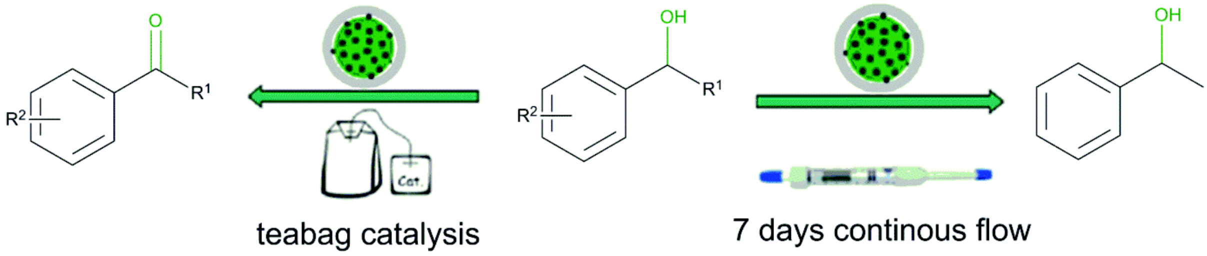

Figure 69: Pd@MIL-88Fe-NH_2@nano-SiO_2. Adapted with permission from ref [213]. Copyright 2014 American Chemical Society.

The vision of highly multifunctional MOFs was already put into words[196] and is often associated with the synthesis of artificial enzymes.[218] First attempts were already started, using the confined pockets of MOFs to protect catalytic centers and enhance substrate specificity.[219],[220]

Still, MOF systems are not a patch on enzymes. Instead, intensive research is going on at every single part of the puzzle, developing and improving methods and combining results little by little. There are already a lot of works combining one or two or three methods, as seen in Figure 69. Nevertheless, the systematic investigation of multifunctional MOFs as catalysts for cascade reactions, cooperative catalysis and catalysis of multi-step reactions is still in its fledgling stage, making this one of the hot topics of MOF research.

Project

The aim of the project is the synthesis of core-shell materials with different kinds of acids as well as active sites of different acid strength in order to investigate their activity in cascade reactions (e.g. biomass based conversions) and gain a better understanding about multifunctional catalysts.

In cooperation with Prof. Xiao-Yu Yangs group we worked on the **green synthesis of hierarchically structured metal-based nanocomposites with highly stable catalytic active sites.**[jj]

Porous metal oxides are interesting catalytic active materials, which have been investigated very intensively during the last years.[221],[222],[223],[224] Especially, a very good review about porous metal oxides of F. Wu and coworkers is recommended.[225]

To meet the objective of the common project, the preparation of hierarchical porous MOF@metal oxide core-shell structures was pursued (Figure 70).

Figure 70: Schematic depiction of core-shell cooperative catalyst material.

Two works dealing with MOF@nonporous TiO_2 were published parallel to the ongoing work, but targeting other applications.[226],[227]

To the best of my knowledge no single MOF-core@porous metal oxide shell structure is known yet. K. Bahranowski *et al.* measured stronger acidity for mixed metal Ti/Zr-montmorillonite in comparison with the single metal reference material[228]. Therefore, also mixed metal oxides have been investigated as shell materials.

MIL-101Cr was selected as core material since it exhibits good chemical stability and already showed good catalytic activity in a variety of reactions.[52],[45] Besides MIL-101Cr can be functionalized with a variety of functional groups, including Brønsted acidic SO_3H moieties.[229]

[jj] Cooperation with Prof. X. Yang of Wuhan University of Technology, China, part of the project was done in Wuhan within a visit abroad. Financial support given by German Academic Exchange Service (DAAD).

Additionally, the MOF should stay accessible when using for catalysis, hence the shell material must be porous, too. As shown by M. Sun and coworkers as well as Z. Yuan *et al.*, following template strategies, hierarchical porous zeolite and (mixed) metal oxide materials can be obtained (Figure 71).[223],[224]

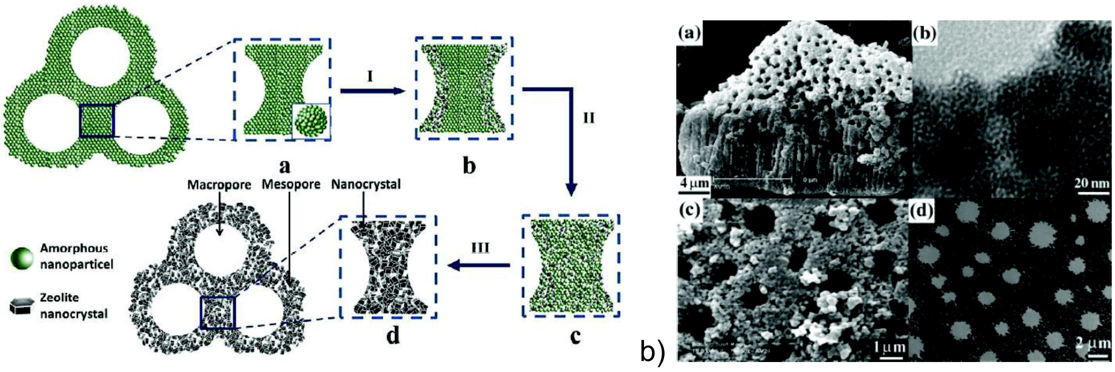

a) b)

Figure 71: a) Schematic representation of the crystallization transformation process to form hierarchically micro-meso-macroporous catalysts constructed from zeolite nanocrystals. Reprinted from ref. [223], Copyright 2013, with permission of Elsevier; b) SEM (a+c) and TEM (b+d) images of meso-macroporous Ti/Zr composites with ratios of Ti/Zr 1:1 and 4:1 Reprinted with permission from ref [224]. Copyright 2004 American Chemical Society.

Usually, metal oxide assemblies are calcined at high temperatures (up to 600 °C), in order to obtain crystalline materials. MIL-101Cr is thermally stable only up to 300-350 °C. Therefore, in cooperation with Mr. Ying Jie (Ph.D. student, Wuhan) a method for the synthesis of a MIL-101Cr@SiO_2 composite which retained the MOF surface area was developed. For the synthesis, well characterized MIL-101Cr and tetraethyl orthosilicate (TEOS) for the silica shell was used. After drying under ultrahigh vacuum and at 250 °C, nitrogen sorption and PXRD experiments revealed that the MIL-101Cr structure was retained. By TEM measurements the core-shell structure was confirmed. Mr. Ying Jie continued this project within his Ph.D. studies in Wuhan; the material was applied as oxidation catalyst.[kk]

Based on the experience acquired from this collaboration project, the synthesis of core-shell MOF@metal oxide materials using Ti/Zr precursor was started in Wuhan with the help of Wei Geng (Ph.D. student)[ll]

The difficulty in synthesis is the controlled hydrolysis of the metal precursors, since they hydrolyze very fast in water which makes it difficult to disperse the MOF material homogenously with the precursors. Additionally, cetyltrimethylammoniumbromid (CTAB) was used as porogen for the metal oxide which needs a pH of 2 to form micelles (Figure 72).

[kk] Manuscript is in preparation.

[ll] This project was started in Wuhan (China) and continued in Germany.

Figure 72: Synthetic procedure for MIL-101Cr@metal oxide core-shell (MOF@MO) compounds.

The general procedure was as following: MIL-101Cr was suspended in isopropanol and stirred for 20 h to obtain a homogeneous suspension. Since MIL-101Cr is acidic by itself, after stirring for 20 h the pH was controlled and set to 2 using hydrochloric acid. In order to obtain mesoporous metal oxide, CTAB was added, which is well soluble in isopropanol. Zr(propoxide) and Ti(isopropoxide) were also dissolved in isopropanol, added to the reaction mixture followed by heating at 60 °C for 48 h.

Following method A, concentrated hydrochloric acid (37%) and isopropanol were used in order to slow down hydrolysis. After heating, no hydrolysis has occurred, which could be observed from reference samples containing Ti-and Zr precursors in the reaction mixture without MOF. The reference samples were colorless, no solid has formed. The MIL-101Cr@metal oxide composite (in the following **MOF@MO-A**) was separated by centrifugation and suspended in ethanol. In order to hydrolyze all metal precursor potentially assembled around the MOF, H_2O was added. The mixture was stirred overnight, separated and dried at 100 °C for 15 h.

N_2 sorption isotherm shows that not all pores are accessible anymore, since the surface area decreased from 3049 m^2/g (pure MIL-101Cr) to 2036 m^2/g. Since no hysteresis and no change in pore size could be observed, either the metal oxide material is not porous at all or has not formed.

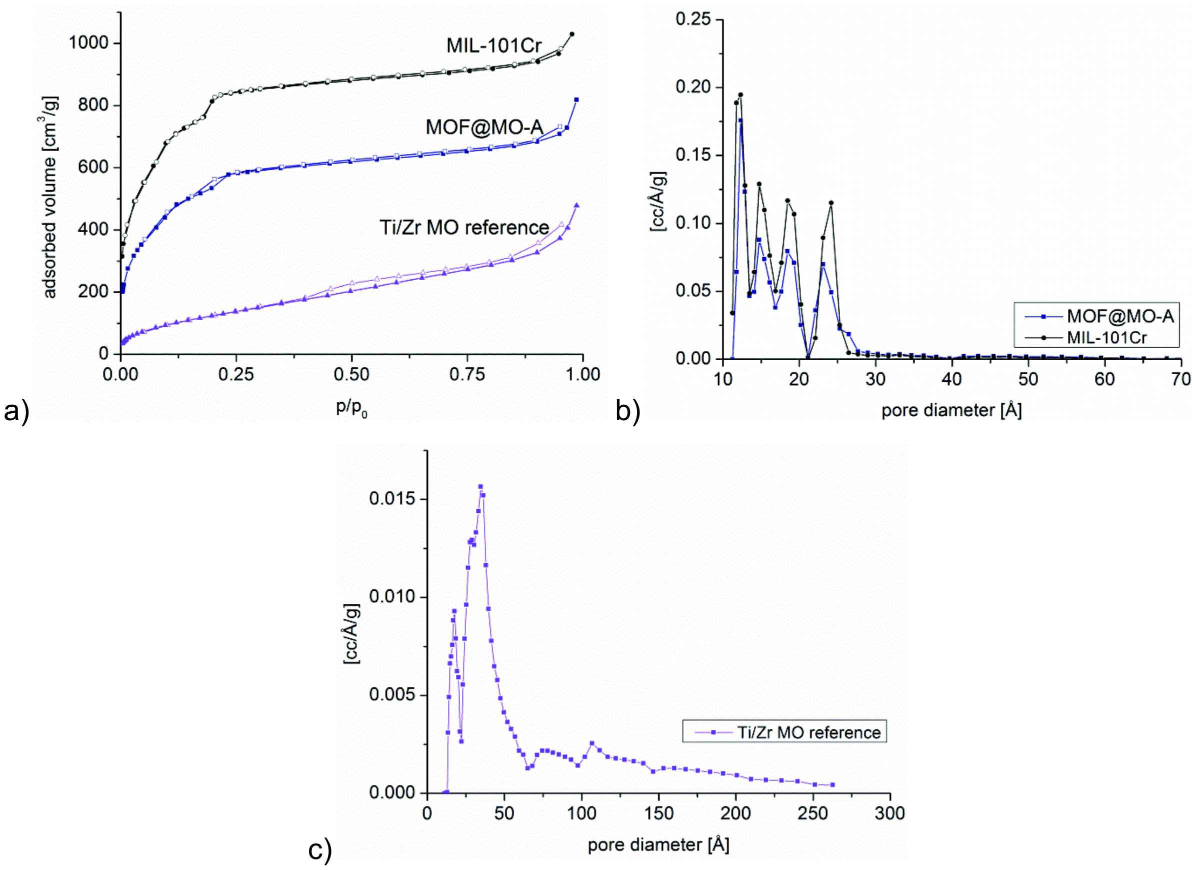

Figure 73: a) N_2-sorption isotherm and b) pore size distribution of MOF@MO-A (0.37) vs. MIL-101Cr (0.33) and c) Ti/Zr MO reference (1.71). Fitting error is given in % in brackets.

When adding water to the reference sample a white solid precipitated immediately. The solid was washed with ethanol and dried in air. From nitrogen sorption measurement a surface area of 502 m^2/g was measured and pores with a maximum volume adsorbed at a diameter of 3.5 nm were calculated (Figure 73). A more reliable evidence for mesopores is the slight hysteresis in the desorption curve of nitrogen isotherm.

On SEM pictures it becomes clear, that metal oxide particles are assembled and agglomerated together with MOF particles. Still the octahedral particle structure of MIL-101Cr can be found (Figure 74).

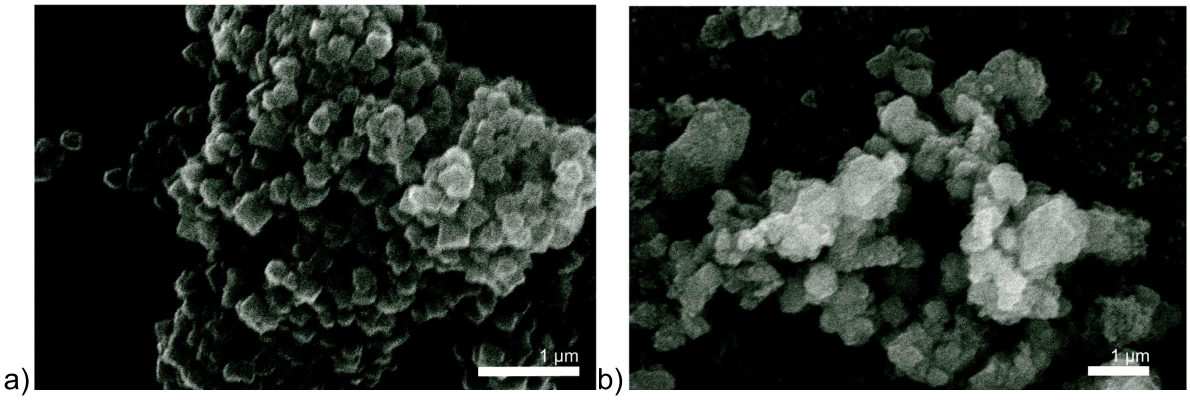

Figure 74: a) SEM picture of MOF@MO-A; b) SEM picture of Ti/Zr MO.

By EDX measurement of the reference sample Ti/Zr MO the ratio between titanium oxide and zirconium oxide was measured. From the molar ratio of 1:1 was set in synthesis, calculated from EDX was: 55:45 (Figure 75).

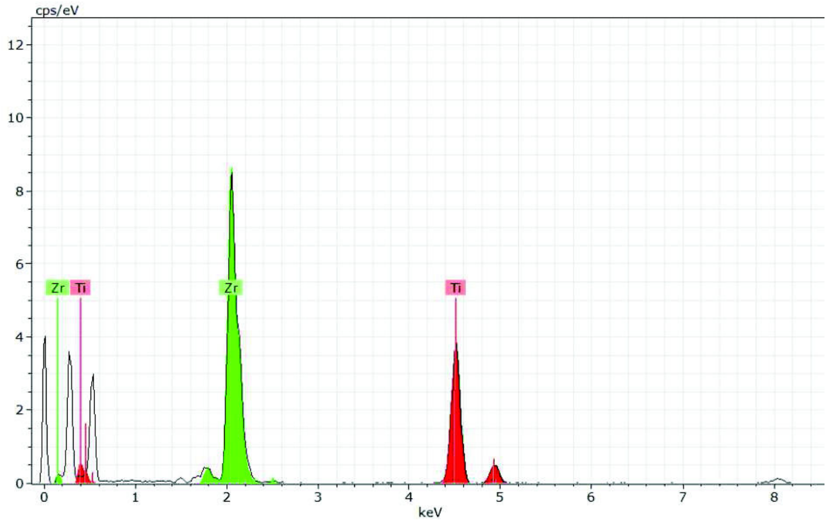

Figure 75: EDX of Ti/Zr MO reference sample. Sample was uncoated; background was subtracted by software of Jeol. Naming of N, O, C and Cu was omitted for clarity.

In consequence, no core-shell composite was formed. Therefore, method B was developed (Figure 72) which differs from method A in the addition of a small amount of water before heating. Moreover, sulfuric acid (conc.) instead of hydrochloric acid was used.

To precipitate the metal precursors slowly, but controlled, different amounts of water were tested for hydrolysis: (a) 0.5 mL, b) 1.5 mL, c) 3 mL; based on total volume of 30 mL). Using 1.5 mL and 3 mL water, after heating period a mixture of a white and green solid was observed, showing that hydrolysis occurred to a large extent and beside possible product also pure metal oxide was obtained. Using 0.5 mL water the reaction solution was turbid (Figure 76), but the green solid (MOF@MO-B.1) could be separated by sedimentation. MOF@MO-B.1 was washed with ethanol and resuspended in ethanol. After the second washing step MOF@MO-B.1 was separated via slow centrifugation until the supernatant solution was clear. After drying a surface area of 886 m^2/g and hysteresis in desorption curve was measured (Figure 76). The synthesis was also performed with MIL-101Cr-SO_3H and a similar shaped sorption isotherm of corresponding MOF@MO-B.2 was measured. The surface area of MOF@MO-B.2 is 592 m^2/g, thus lower than the surface area of MOF@MO-B.1. However, pure MIL-101Cr-SO_3H exhibited a BET surface area of 1333 m^2/g which explains the difference.

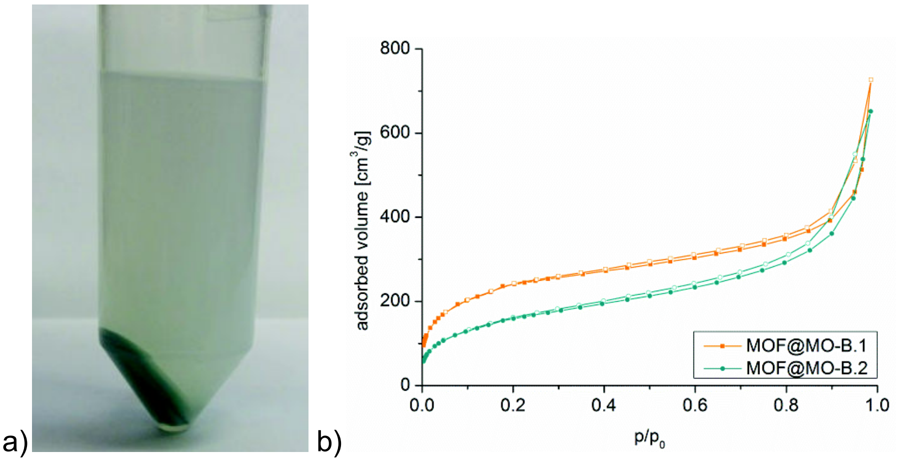

Figure 76: a) Picture of MOF@MO-B.1, the green solid was washed until the supernatant solution was clear; b) nitrogen sorption isotherm of MOF@MO-B.1 und MOF@MO-B.2.

From SEM pictures agglomerated particles have been found, hence it is not clear if the MOF@MO composite was formed. EDX shows a ratio based on atomic percent of Cr:Ti:Zr 4:16:80. TEM pictures revealed that at least some MOF particles seem to have a metal oxide shell (Figure 77). Still, also bulk metal oxide formed.

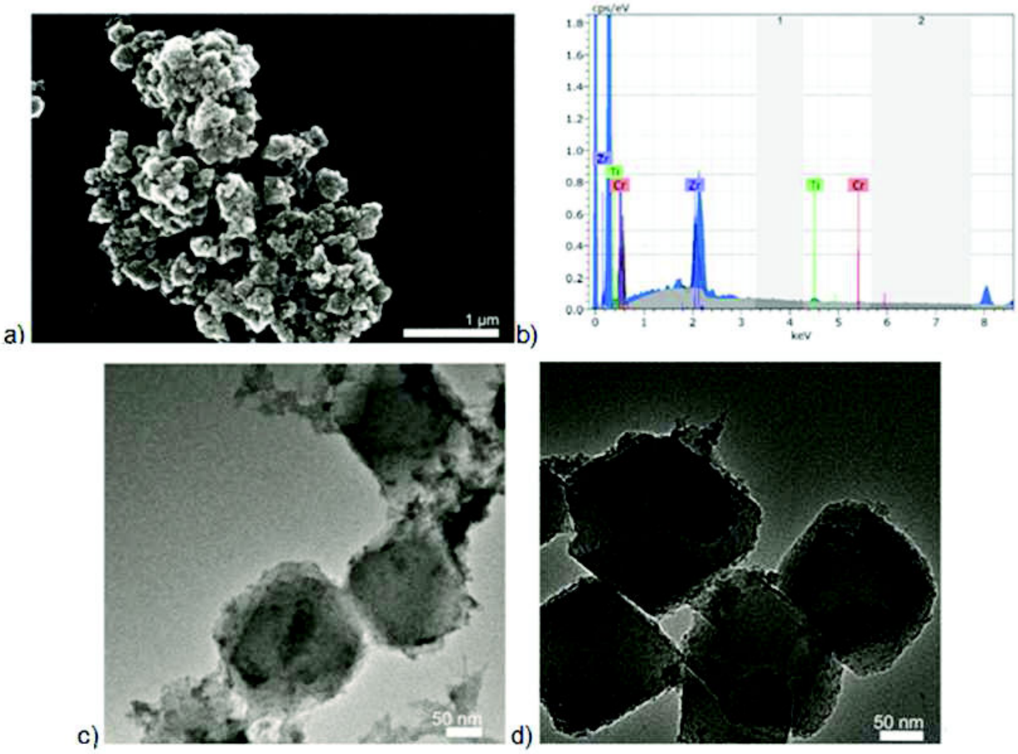

Figure 77: a) - d) SEM, EDX and TEM pictures of MOF@MO-B.1. For SEM the signal of gold from sputtering partly masked the signal of zirconium. Therefore, the Bruker EDX software was used to simulate peak area and calculate the elemental ratio.

PXRD of MOF@MO-B.2 containing MIL-101Cr-SO_3H shows the pattern of MIL-101Cr, although it has to be stated that the crystallinity in comparison to pure MIL-101Cr-SO_3H is quite low. This can be due to the amorphous shell formed around the MOF (Figure 78).

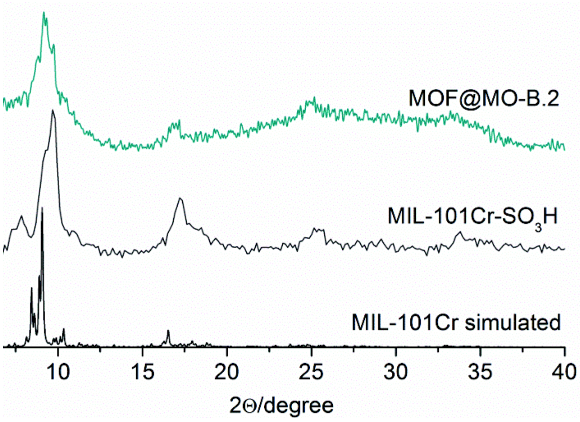

Figure 78: PXRD of MOF@MO-B.2 in comparison with MIL-101Cr-SO_3H and simulated pattern of MIL-101Cr.

In addition to bulk material also spherical shaped particles with a diameter of approximately 3 µm formed. The particles were analyzed by SEM and EDX. The spherical particles contained a large amount zirconium oxide and a small amount of titanium oxide. Besides sulfur was found which originates from the MOF linker 2-sulfo-terephthalic acid. The atomic ratio between Cr and S was found to be approximately 1:1 which is consistent with the molecular formula of MIL-101Cr-SO_3H (Figure 79). The atomic percentage (calculated by Bruker EDX software) of Cr:Zr was 2:1.

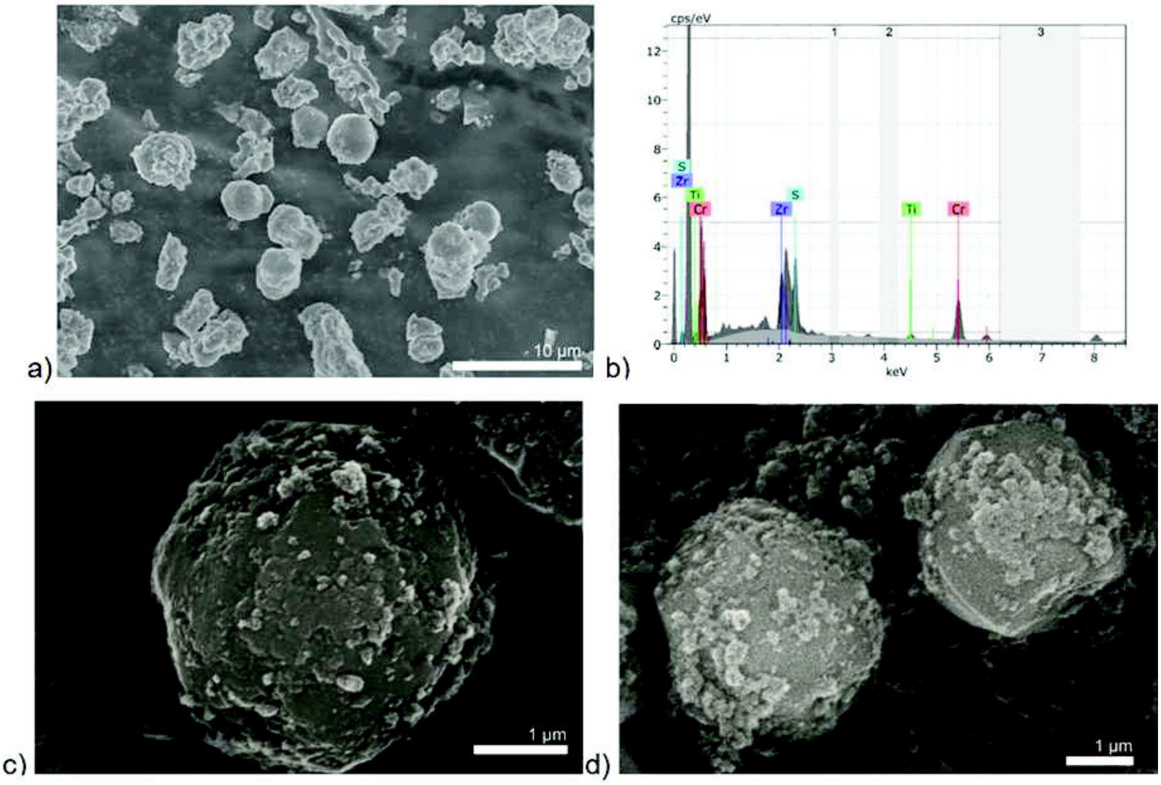

Figure 79: a), c), d) SEM pictures and b) EDX of MOF@MO-B.2. The signal of gold from sputtering partly masked the signal of zirconium. Therefore, the Bruker EDX software was used to simulate peak area and calculate the elemental ratio.

The distribution of elements within one particle by EDX mapping showed that Zr, Ti and Cr are present. Titanium (red) can also be found in the background of the particle (Figure 80).

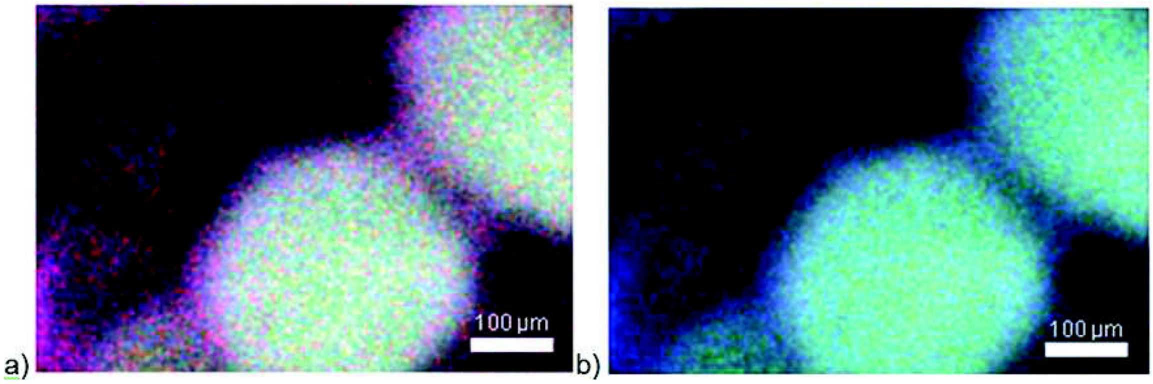

Figure 80: EDX mapping of a spherical particle of MOF@MO-B.2. Red: Ti, green: Cr, blue: Zr; a) Ti, Cr, and Zr: b) Cr and Zr.

The line scan allows scanning along a predefined way (yellow arrow on SEM picture of Figure 81) and monitoring of relevant elements. As supported by the results of normal EDX measurement the titanium oxide content is low. Importantly, in the center of the particle the chromium amount is highest, whereas the zirconium amount stayed constant at a lower level. The amount of zirconium raised a little bit earlier than the one of chromium and decreased a little bit later, from which it can be suggested that the MOF is successfully covered with zirconium oxide (Figure 81). It has to be regarded critically that the pure MIL-101Cr-SO_3H

particles have a size of 150 ± 40 nm.[118] MOF particles tend to agglomerate, which might be an explanation for the large diameter of the particle. For MIL-101Cr a similar kind of core-shell composite was not observed yet. The SO_3H-functionalized linker seems to have a strong influence on the precipitation of zirconium oxide, maybe due to acid catalyzed hydrolysis.

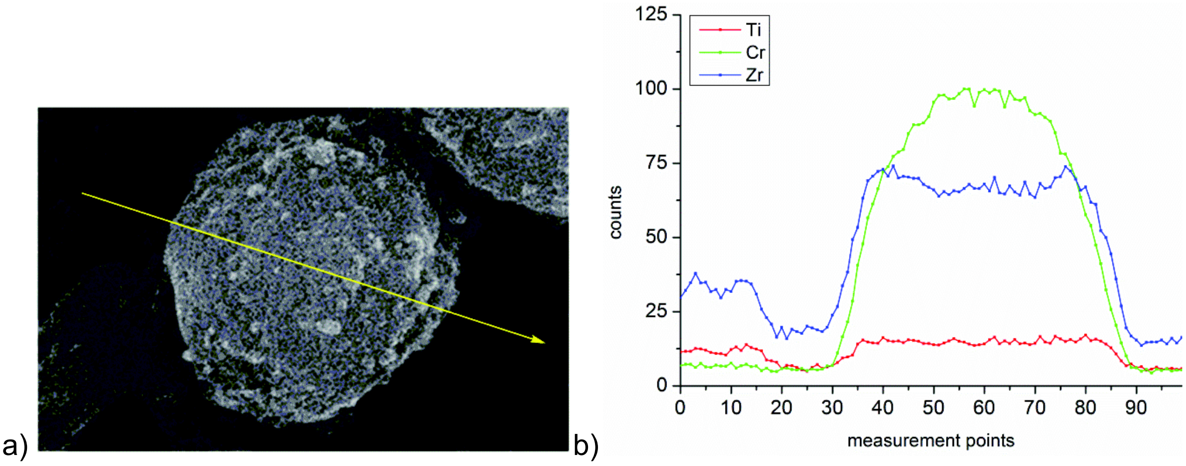

Figure 81: a) image of the pathway of the line scan; b) EDX line scan of MOF@MO-B.2.

Next, the ratio of CTAB and metal precursor to solvent was changed in order to optimize the shell thickness and porosity. For these experiments only titanium tetraisopropoxide was used as precursor, because it is easier to monitor via EDX (Table 10). The synthesis was performed following method B (H_2O was added (0.5 mL)). For each experiment 40 mg MIL-101Cr was used. The employed molar amounts of CTAB and titanium tetraisopropoxide for the synthesis of MOF@MO-B.3 is the same as for MOF@MO-A and B1+2, but with the difference that only titanium tetraisopropoxide was used.

Table 10: Different ratios of CTAB/Titanium tetraisopropoxide.

Material	**CTAB [mmol]**	**Ti(isoprop)$_4$ [mmol]**	**Ratio CTAB:Ti**	**Solvent^a [mL]**
MOF@MO-B.3	0.25	0.75	1:3	30
MOF@MO-B.4	0.75	2.3	1:3	30
MOF@MO-B.5	0.75	0.75	1:1	30

a) isopropanol

MOF@MO-B.3-5 composites exhibit clearly a lower surface area than the pure MOF material (Figure 82) The shape of the isotherms is more reminiscent to MIL-101Cr than the ones of MOF@MO-B.1+2, but they display a similar hysteresis in desorption which implies mesoporosity. In all cases in addition to the desired MOF@MO products, also titanium oxide precipitated (verified by SEM and color), making it meaningless to discuss about values of surface area.

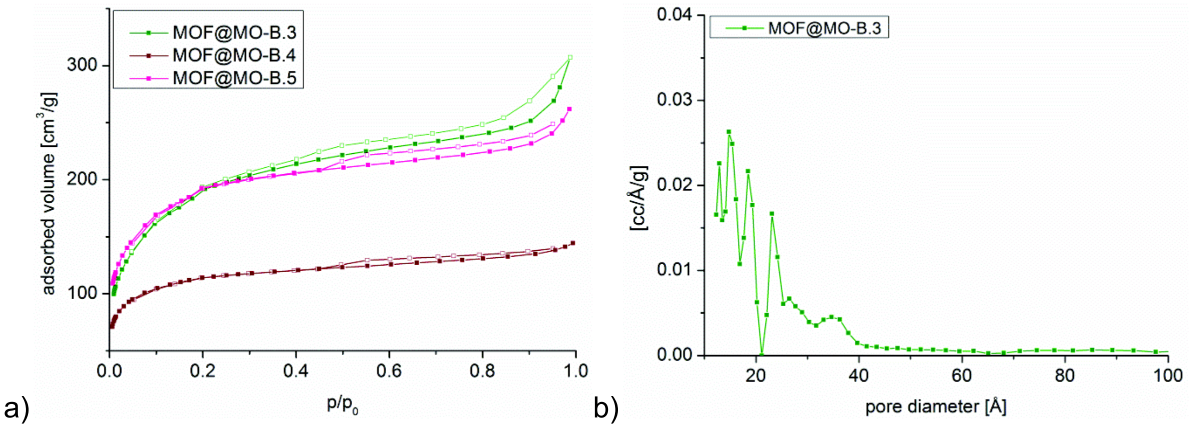

Figure 82: a) Nitrogen sorption isotherm of MOF@MO-B.3-5; b) pore size distribution of MOF@MO-B.3 (0.28). Fitting errors are given in % in brackets.

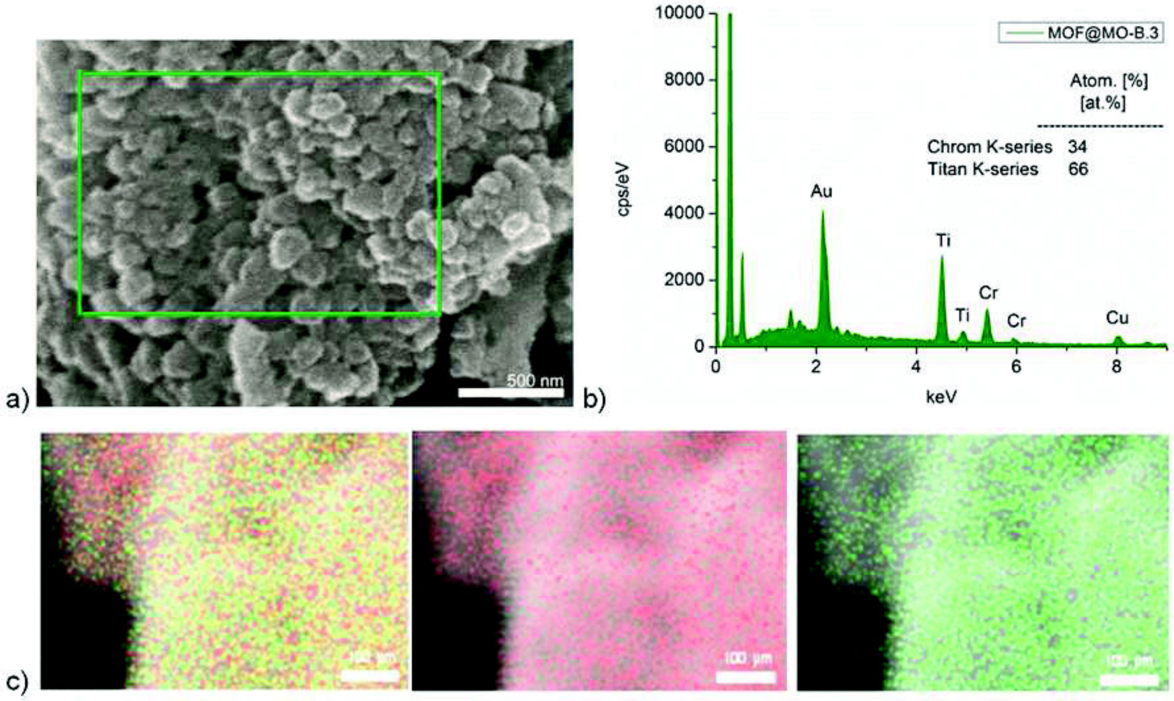

Figure 83: a) Section used for EDX measurement of MOF@MO-B.3. B) EDX measurement of section a) of MOF@MO-B.3; c) EDX mapping of titanium (red) and chromium (green) for MOF@MO-B.3.

Following Z. Yuan *et al.* [224], MOF@MO-B.3 was calcined at 500 °C for 30 min, although the MOF is expected to decompose at this temperature. Nitrogen sorption isotherm showed on the one hand a decrease in surface area, but on the other hand an increased mesoporosity (Figure 84). Although pore size distribution gives no “fixed values” (compare experimental part) an increase to higher pore diameters in general can be stated (Figure 84).

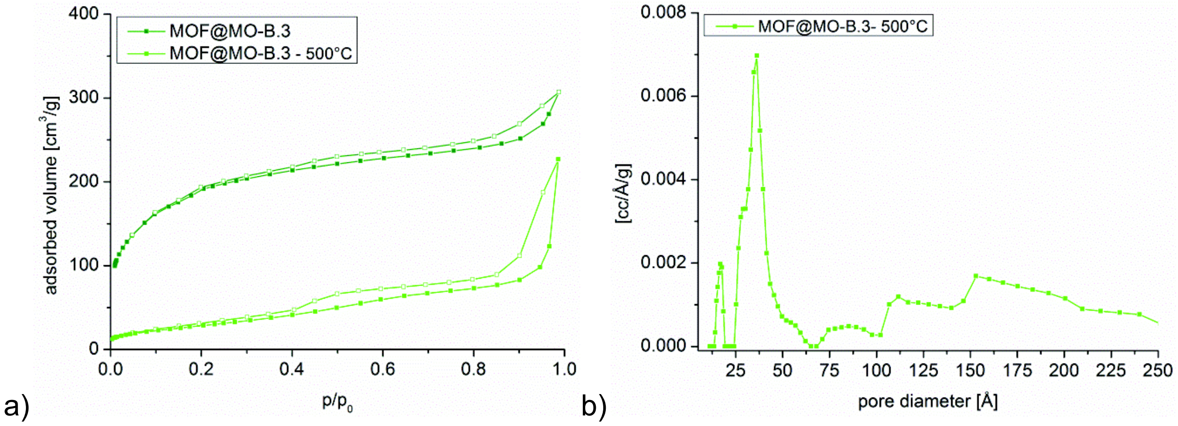

Figure 84: a) nitrogen sorption isotherm of MOF@MO-B.3 and MOF@MO-B.3-500 °C; b) pore size distribution MOF@MO-B.3-500 °C (1.25). Fitting errors are given in % in brackets.

Powder X-ray diffraction pattern of MOF@MO-B.3 shows a broad reflex at 10 2θ/degree, which is characteristic for MIL-101Cr. For the calcined sample MOF@MO-B.3-500 °C reflexes corresponding to anatase structure were measured in the range of 25 – 50 10 2θ, whereas the reflex at 10 2θ decreased significantly. As expected, MIL-101Cr decomposed under the applied conditions (Figure 85).

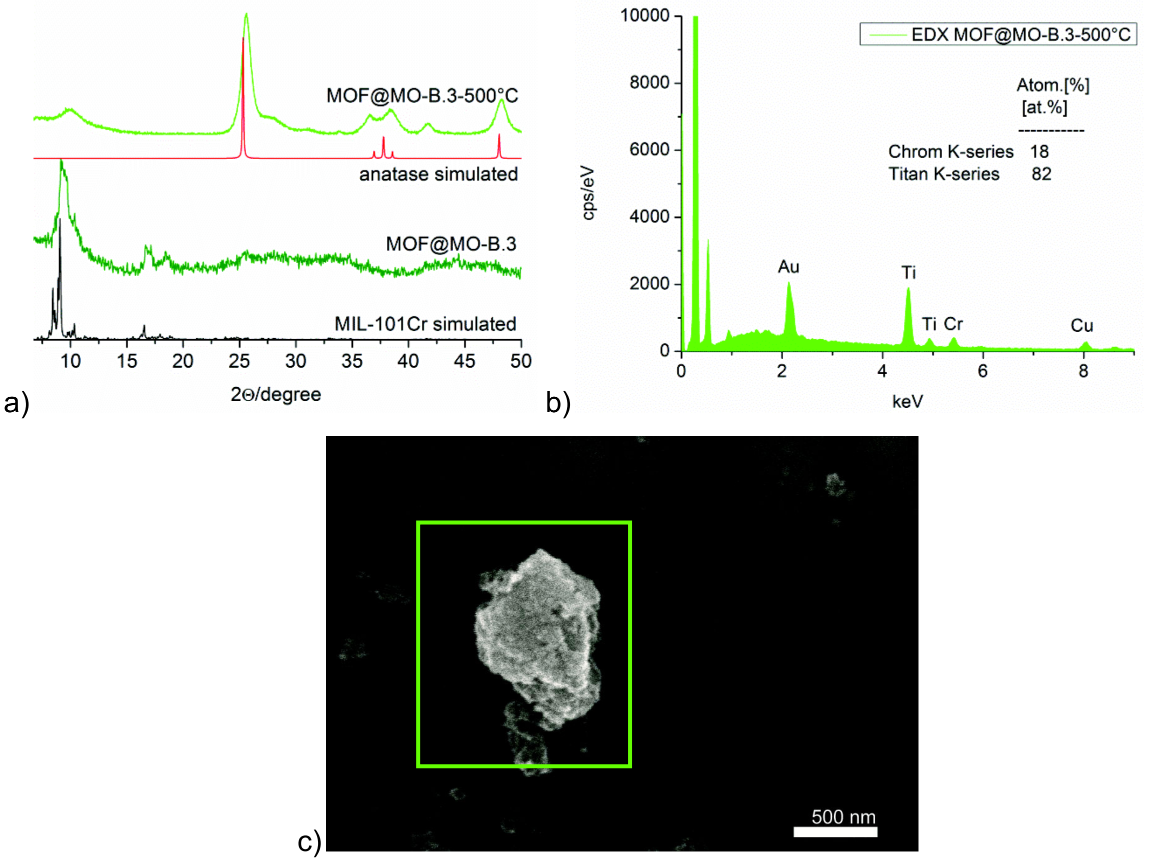

Figure 85: a) PXRD pattern of MOF@MO-B.3 and MOF@MO-B.3-500 °C and b) EDX spectrum of MOF@MO-B.3-500 °C. Au and Cu signals originated from sputtering and sample holder; c) section for EDX measurement.

The overall difficulty is the separation of MOF@MO from pure metal oxides. Probably the desired core-shell material formed to some extent, as visible by SEM and TEM pictures, but still there is also byproduct in the mixture.

By incorporation of a single magnetic nanoparticle, for instance Fe_3O_4, the resulting composite material can be separated from the bulk material through a strong magnet (Figure 86). This method is already used in a variety of applications as shown by R. Ricco *et al.*[230] and was tested for the previously presented system.

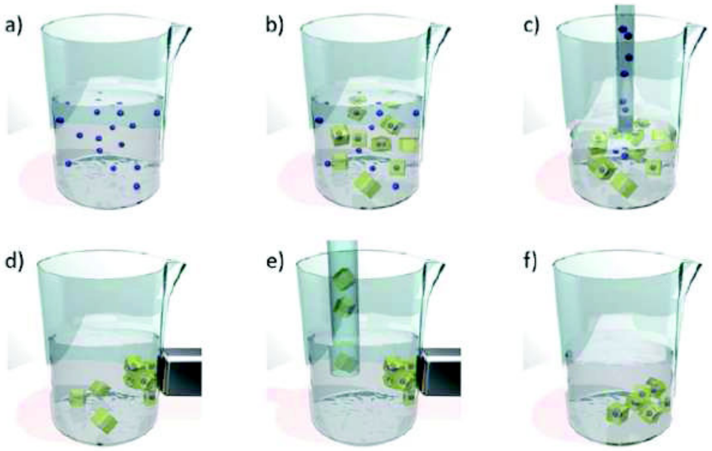

Figure 86: Procedure for the separation of magnetic framework composites from bulk magnetic particles and pure MOF crystals. Reprinted from ref. [230], Copyright 2013, with the permission of the Royal Society of Chemistry.

L-3,4-Dihydroxyphenylalanin functionalized Fe_3O_4 nanoparticles[mm] were suspended in H_2O and 2-aminoterephthalic acid as well as chromium nitrate were added. The mixture was reacted following the protocol of MIL-101Cr-NH_2 synthesis.[231] After washing with ethanol at room temperature and at 80 °C the product was obtained as green-brown powder. As depicted in Figure 86 pure nanoparticles can be separated from MOF, since they are much smaller and disperse easily in solution (Figure 86c) and MOF from NP@MOF can be separated by a magnet (Figure 86e + Figure 88).

Proved by SEM measurements particle size of MIL-101Cr-NH_2 is around 100 nm. By SEM it could not be shown if Fe_3O_4 NPs are incorporated as core or assembled around the MOF. In EDX measurements iron could be detected. The magnetic behavior of the powder supports the presence of magnetic iron particles (Figure 87+Figure 88).

[mm] The nanoparticles were kindly provided by Dr. Hajo Meyer.

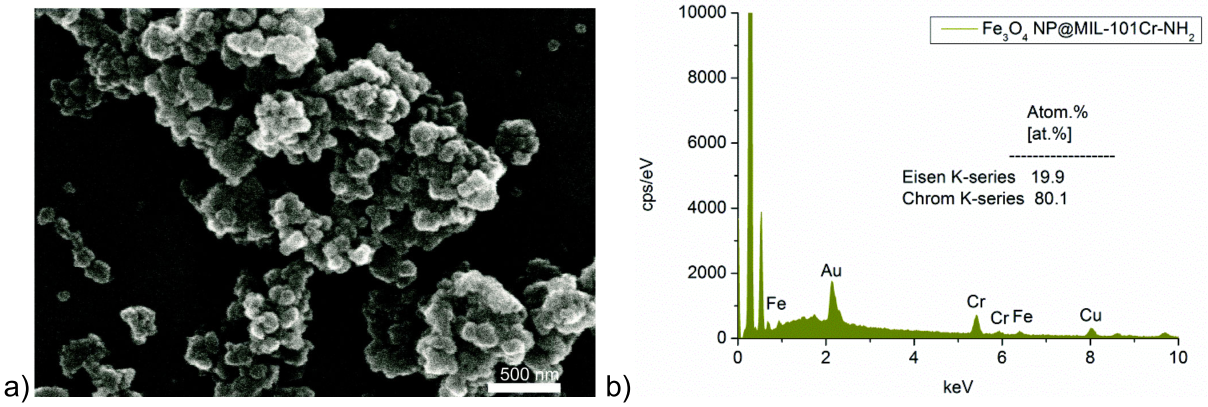

Figure 87: a) SEM picture of Fe_3O_4 NP@MIL-101Cr-NH$_2$; b) EDX spectrum of Fe_3O_4 NP@MIL-101Cr-NH$_2$.

The PXRD pattern shows no additional reflexes to the one of MIL-101Cr-NH$_2$ (Figure 88). Either the particles became amorphous during synthesis or the amount of NP which are incorporated in or assembled around the MOF is below the detection limit. TEM and nitrogen sorption measurements remained to be done.

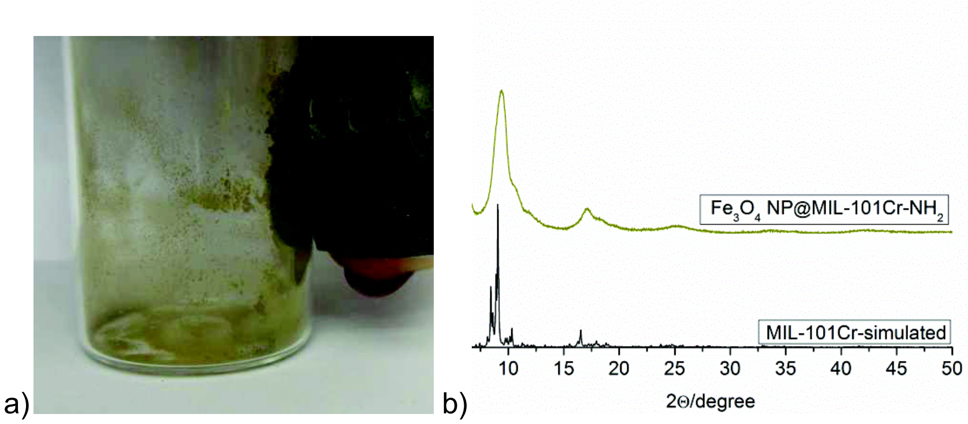

Figure 88: a) The magnetic behavior of NP@MOF composite is shown; b) PXRD pattern of Fe_3O_4 NP@MIL-101Cr-NH$_2$.

Summary and outlook

Promising first results were obtained which imply, that the synthesis of porous MOF@metal oxide core-shell composites is possible. In the case of MOF@MO-B.2 the core-shell formation of the spherical particles has been verified by SEM and EDX measurements. Therefore, it is supposed that hydrogen-bonding or acidic functional moieties at the MOF linker have an influence on core-shell formation.

Also the kind of metal precursor plays an important role. As seen from experiments using zirconium propoxide and/or titanium tetraisopropoxide, the rate of hydrolysis has a significant influence on composite formation. K. E. de Krafft used titanium(IV) bis(ammonium lactato)dihydroxide (TALH) as metal precursor.[226] TALH is stable in water and can be decomposed to TiO_2 by acid catalyzed hydrolysis. Therefore, shell thickness can be controlled much more precisely. In addition, the bulky lactate ligands can prevent diffusion into the MOF pores. Therefore, also TALH should be applied in combination with CTAB and presented synthesis route.

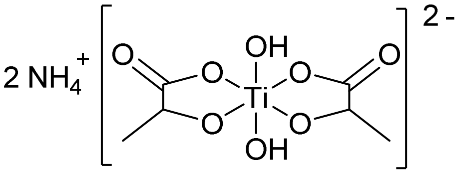

Figure 89: Structure of titanium(IV) bis(ammonium lactato)dihydroxide (TALH).

Calcination of MOF@MO-B.3 resulted in a crystalline TiO_2 phase, although the MOF decomposed. Here, a suitable solution has to be found, ideas are given below.

The separation of core-shell material from bulk material is the critical point of this project. A strict requirement for any application is the synthesis of the targeted material in pure form either by an optimized synthesis strategy or purification. The encouraging results from NP@MIL-101Cr-NH_2 synthesis showed, that a magnetic NP core can in principle be suitable for the separation of MOF@MO composites from bulk metal oxides. For future projects the synthesis procedures have to be reproduced and optimized.

The targeted MOF@MO composites are worth to develop further, hence an outlook of ideas which could keep track of is given.

1) Synthesis of magnetic NP@MOF composites for better product separation

By variation of precursor concentrations or layer-by-layer method[232] the shell thickness can be controlled. Concerning the application of MOF catalysts it is still under discussion to which extent the reaction takes place inside the pores of the MOFs or only at the surface.[1] How deep do substrates diffuse into MOFs and which influence can have the functionalization of MOF linker? Although core-shell systems have been successfully applied for separation or other applications[232],[233],[234] the increase of shell thickness in dependence on diffusion behavior as well as limits or ideal shell thickness for catalysis were not elucidated yet systematically. A system composed of a magnetic metal nanoparticle as catalysts and a MOF shell of varying thickness can serve as model system for the investigation of the described challenge (Figure 90). By selection of a reaction which is only catalyzed by the nanoparticle core, it can be monitored if and how deep the substrate diffuses through the MOF shell. In addition to shell thickness also functional group of MOFs as well as different substrates could be evaluated.

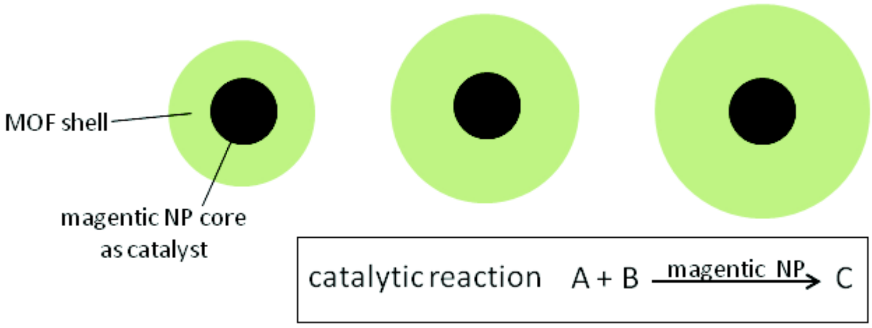

Figure 90: Schematic depiction of project design for NP@MOF materials.

2) Controlled calcinations of MOF@MO composites

Amorphous metal-oxides can be porous, too.[224] By calcination, organic template molecules are removed and crystalline materials can be obtained. Since MOFs usually are not stable at temperatures above 350 °C an alternative way has to be developed. For example with the aim to remove the template molecules of MO, drying at 250 °C in ultrahigh vacuum can be a promising way. This method was developed for MIL-101Cr@silica composites in cooperation with Ph.D. student Ying Jie.[nn]

Another possibility would be to have an additional porous heat insulating layer between metal oxide and MOF, which protects the MOFs against the high temperatures. Further investigations with the aim to develop a method to protect the MOF layer against decomposition are necessary.

At this point it has to be stated that even though the MOF decomposes the resulting material would be a core-shell hierarchical porous mixed metal oxide.

Pure MOF derived porous metal oxides currently attract much attention from research community due to their interesting properties and possible applications as electrochemical capacitors, sensors, in catalysis and in heat transformation. A state-of-the-art overview is given by Y. Song *et al.* and L. Lux *et al.*[63],[235] The field of hierarchical porous MOF@MO as well as hierarchical mixed metal oxides is still in its infancy and admits space for improvement.

3) MOF@MO composites as antifouling strategy

MOFs are promising materials for membrane based separation devices, purification of wastewater and gas sorption as well as for air quality management.[43],[236],[237],[238],[239]. A severe challenge for the previously mentioned applications is biofouling. For hygienic reasons applied materials have to accomplish strict requirements concerning growth of microorganisms.[oo]

[nn] Cooperation with the group of Prof. X.Yang of WHUT, China.

[oo] a) http://hygiene-institut.de/en/index.php5, Hygiene institut des Ruhrgebietes, 03.05.2016. b) https://www.vdi.de/technik/fachthemen/bauen-und-gebaeudetechnik/fachbereiche/technische-gebaeudeausruestung/richtlinienarbeit/richtlinienreihe-vdi-6022-raumLufttechnik-raumLuftqualitaet/ 03.05.2016

In 2008 the international maritime organization banned organotin compounds which were used as anti-biofouling agent for a long time for shipping due to acute harmful effects to the environment and non-target organisms.[240] Efficient alternatives are needed urgently.[240] Environmental friendly examples are functionalized chitosan based or silane/siloxane based coatings.[241],[242]

Microorganisms need nutrients to grow which can be any carbon source, used for metabolization. In consequence, for anti-biofouling coatings inorganic materials as siloxane based coatings are applied. Coatings often bear the risk of displaying defects which can be attacked by the microorganisms and facilitate growth.

Here a porous core-shell material has significant benefits with respect to a coating. The shell can be composed of an inorganic porous material as for instance porous TiO_2, and protects every single MOF particle whereby the risk of defects can be reduced.

This project was forwarded to Carsten Schlüsener (Master student) in April 2016.

4.3 Engineering MOF catalyst properties on the macroscopic scale

In the previous chapters the focus was put on molecular engineering of metal-organic frameworks. Bulk material of MOFs is usually obtained as polycrystalline fine powder with defined particle sizes and shapes. Tuning of the macroscopic properties of MOFs also includes i) tailoring of particle size for synthesis of nanoscale metal-organic frameworks, ii) synthesis of hierarchical ordered systems as well as iii) metal-organic framework composites. The latter is specifically important for the application of MOFs in industry. All three topics target the macroscopic tuning of MOF particles and can have a strong influence on catalyst performance. In the following, respective projects are presented.

4.3.1 Synthesis of nanoMOFs using microemulsion and ultrasound

Introduction

The particle size of metal-organic frameworks can vary from less than 100 nanometers to a few hundred micrometers. This can have a strong influence on diffusion behavior and reaction kinetics. From metal-nanoparticle synthesis it is known that metal-nanoparticles in the range of 1 – 100 nm show an enormous increase of external surface area which results in modified or new chemical and physical properties.[243] For MOFs it has to be taken into account that the pores themselves are relatively large (e.g. 0.34 nm in diameter for MIL-101Cr[51]) and a certain size might be necessary to generate a sufficiently stable material.

In context of catalysis, especially two properties can have a strong influence on catalyst activity: i) increased external surface area and associated more active sites on the MOF surface, ii) facilitated diffusion behavior.[244]

Therefore, it is highly desirable to synthesize MOF catalysts with a particle size of less than 100 nm. Figure 91 shows which energy source as well as modulation can be used in MOF synthesis.[245] The review of N. Stock and S. Biwas provide an excellent overview about different parameters in MOF synthesis.[245]

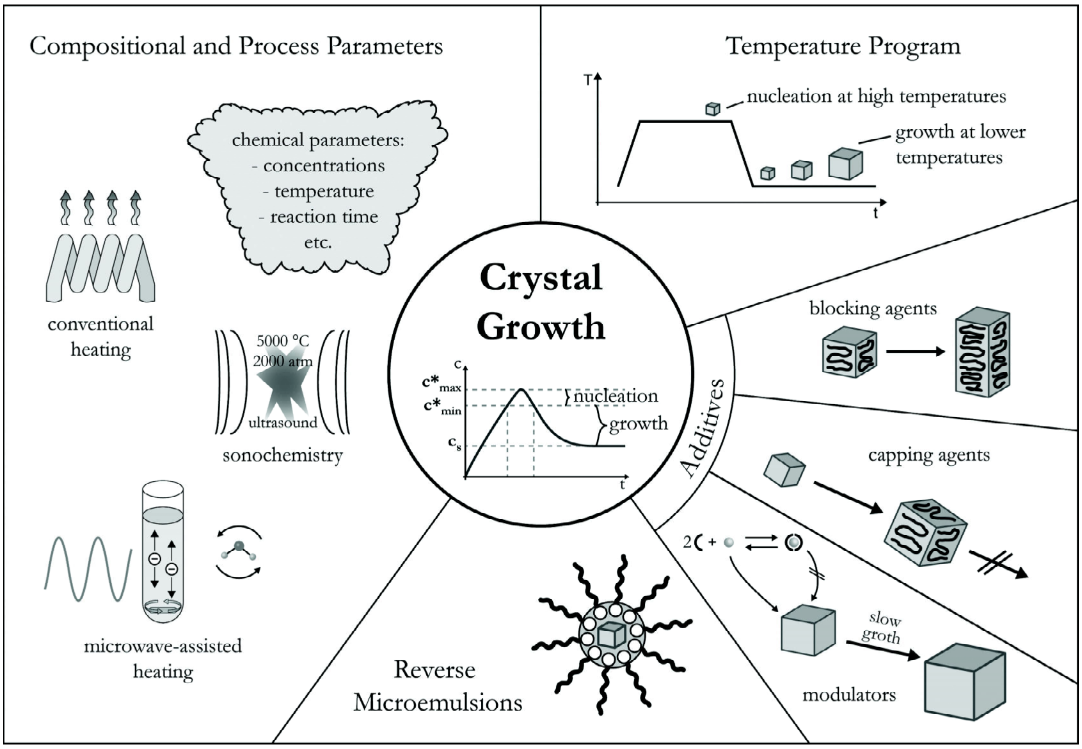

Figure 91: Energy sources and modulation tools for the synthesis of various morphologies of MOFs. Reprinted with permission from ref [245]. Copyright 2012 American Chemical Society.

Detailed reviews can be found elsewhere.[245],[246],[244],[247],[248],[249] With regard to the project work in this field the emphasis is put on three topics, namely ultrasound as energy source, capping agents and microemulsion.

High intensity ultrasound can be used for the synthesis of nano-structured materials. The ultrasonic wavelengths are much larger than molecular size scale (frequency from 20 kHz to 15 MHz). The effects arising from ultrasound are ascribed to acoustic cavitation. This includes the formation, growth and implosive collapse of bubbles which results finally in the formation of hot spots (Figure 92).[250]

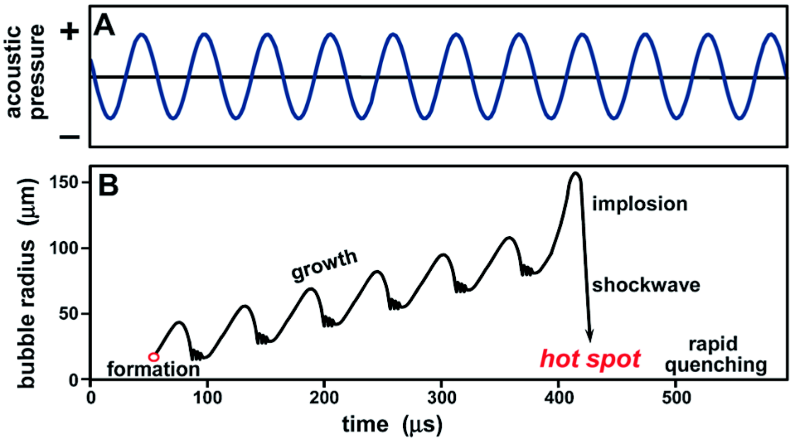

Figure 92: Schematic illustration of the process of acoustic cavitation: the formation, growth and implosive collapse of bubbles in a liquid irradiated with high intensity ultrasound. Reprinted from ref. [250], Copyright 2013, with permission of the Royal Society of Chemistry.

Advantages of ultrasonic energy for the formation of metal-organic frameworks are

- efficient isolation of phase-pure materials
- short reaction times
- homogeneous particle size and morphology
- suitable for preparation of nano-sized MOFs

However, the synthesis of large single crystals using ultrasound is difficult since the vibrations disrupt the formation of the same.[251]

Examples of MOFs, which have been synthesized using ultrasound are MOF-5[252], ZIF-MOFs[253], MIL-53Fe[254],[255] and MIL-88AFe[256].

Depending on reaction parameters as energy, temperature and time, for instance in case of MIL-88AFe particles in the size range of 300 nm until 1 µm were obtained. Dilution (0.008 mM iron precursor) or use of acetic acid as modulator led to smaller particle size, but also the yield decreased significantly to 4 – 6%.[256]

Capping agents can be added to the reaction mixture in order to modulate nucleation and crystallization rate. Modulators can be monocarboxylic acids as for example acetic or benzoic acid. For different zirconium based metal-organic frameworks UiO-X was shown that crystallinity can be significantly increased by adding a large excess of benzoic acid.[257]

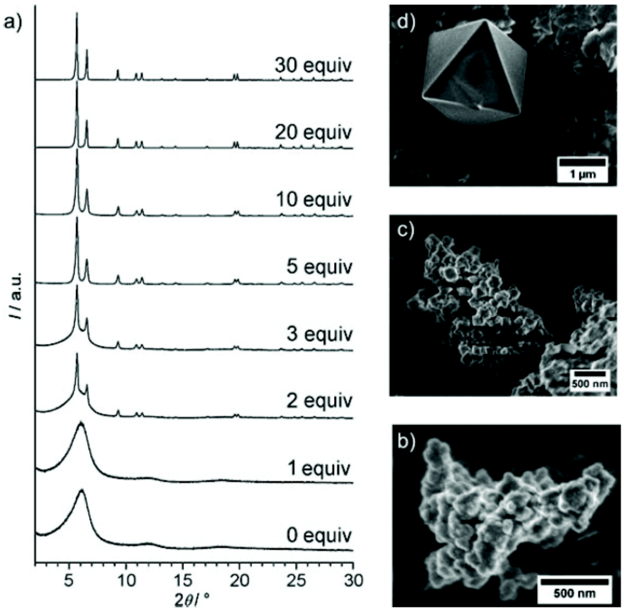

Figure 93: a) Powder XRD patterns of Zr–bpdc MOFs prepared with different amounts of benzoic acid as the modulator. The equivalents are given with respect to $ZrCl_4$. SEM images of Zr–bpdc samples synthesized in the presence of b) 0, c) 3 and d) 30 equivalents of benzoic acid. Reprinted from ref. [257], Copyright 2011, with permission of John Wiley and Sons.

J. M. Chin and corworkers investigated the control over morphology in case of MIL-53Al-NH_2 using acetic acid as modulator. Additionally, to competitive coordination of the mono-carboxylic acid, they also change the pH of reaction mixture and thereby the grade of protonation of the dicarboxylate linkers.[258] Similar works were performed with a copper imidazolate framework and ammonia as capping agent.[259]

D. Jiang and coworkers investigated the effect of different monocarboxylic acids on the particle size of MIL-101Cr in hydrothermal synthesis.[260] The results of their experiments revealed the higher the pKa value of the modulator, the smaller was the particle size (Figure 94). XRD measurements show very low crystallinity which is attributed to the small particle size, since surface areas are high (2600 – 2944 m^2/g). Although the yield was given by the authors with 49%, the low concentration of reactants can lead to difficulties in upscaling.

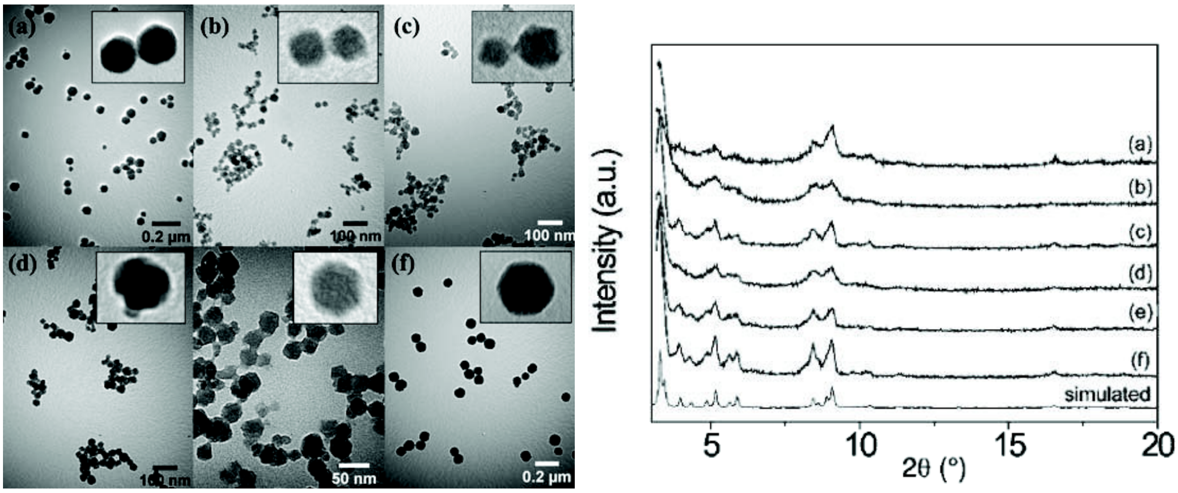

Figure 94: TEM images and PXRD pattern of the NMOFs with/without chemical additives: (a) no additive; (b) stearic acid; (c) 4-methoxybenzoic acid; (d) benzoic acid; (e) 4-nitrobenzoic acid; (f) perfluorobenzoic acid. The pattern simulated from the crystal structure of MIL-101(Cr) is shown for comparison. Reprinted from ref. [260], Copyright 2011, with permission of the Royal Society of Chemistry.

Not only mono-acids can act as modulator, also surfactants or polymers have been applied to control particle size. For example, A. Ranft *et al.* as well as M. Pham *et al.* used different polymers for the synthesis of small particle sized metal-organic frameworks.[261],[262] By addition of polyacrylic acid or CTAB (cetyltrimethylammoniumbromide) the morphology of HKUST-1 and IRMOF-3 could be controlled in a particle size range of 30 – 300 nm through varying modulator concentrations in a solvothermal synthesis.[261] MIL-88BFe-NH_2 was obtained as nanoMOFs with a size between 30 and 200 nm depending on concentration of tri-block-copolymer and acetic acid.[262]

Microemulsion are very interesting as they can serve as a “microreactor” in organic reactions as well as for the synthesis of nanostructured materials.[263],[264]

Generally it can be distinguished between water-in-oil (w/o) and oil-in-water (o/w) emulsions. Water-in-oil emulsions are also called reverse micelles, because the polar head group interacts with the water droplets whereas the hydrophobic tail points at the oily phase. Furthermore, only in a certain composition a microemulsion can be obtained, which depend on the ratio between water, oil phase and surfactant as well as temperature. A schematic phase diagram is depicted in Figure 95.

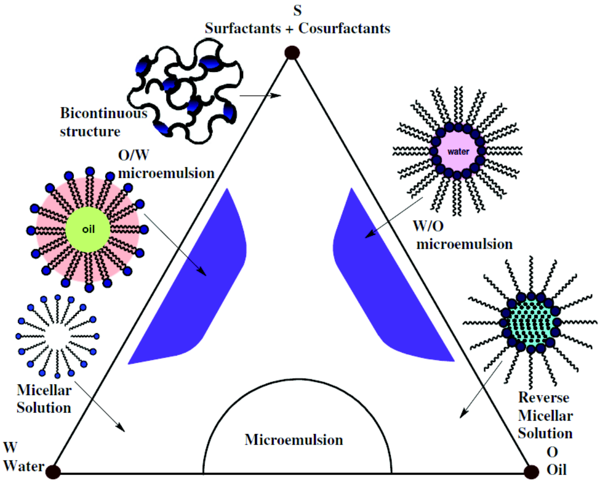

Figure 95: Hypothetical phase regions of a microemulsion system. Reprinted from ref. [264], Copyright 2012, with permission of Elsevier.

In case of MOF chemistry, not much is known about synthesis of MOFs using microemulsions, two examples are given.

W. Lin and coworkers used water in oil microemulsions of the composition: CTAB/1-hexanol/*n*-heptane/water for the synthesis of Gadolinium and manganese based MOF´s. The materials formed thin needles with a length of several hundered nanometers as well as cubic and octahedral particles of 100 – 200 nm size.[265],[266],[267]

J. Groll *et al.* investigated the effect of bulk and nanoMOF crystals on adsorption properties of a Zn MOF CID-1 (linker: isophtalic acid and bipyridine). By using a non-aqueous microemulsion system containing dioctyl sulphosuccinate sodium salt (AOT), *n*-heptane and *N, N*-dimethylformamide nanoMOF rods of several hundred nanometers and 10 – 20 nm thickness were obtained under ultrasonic radiation.[268] In comparison to the bulk material the amount of adsorbed methanol is almost the same, but regarding adsorption kinetics significant differences can be observed (Figure 96).

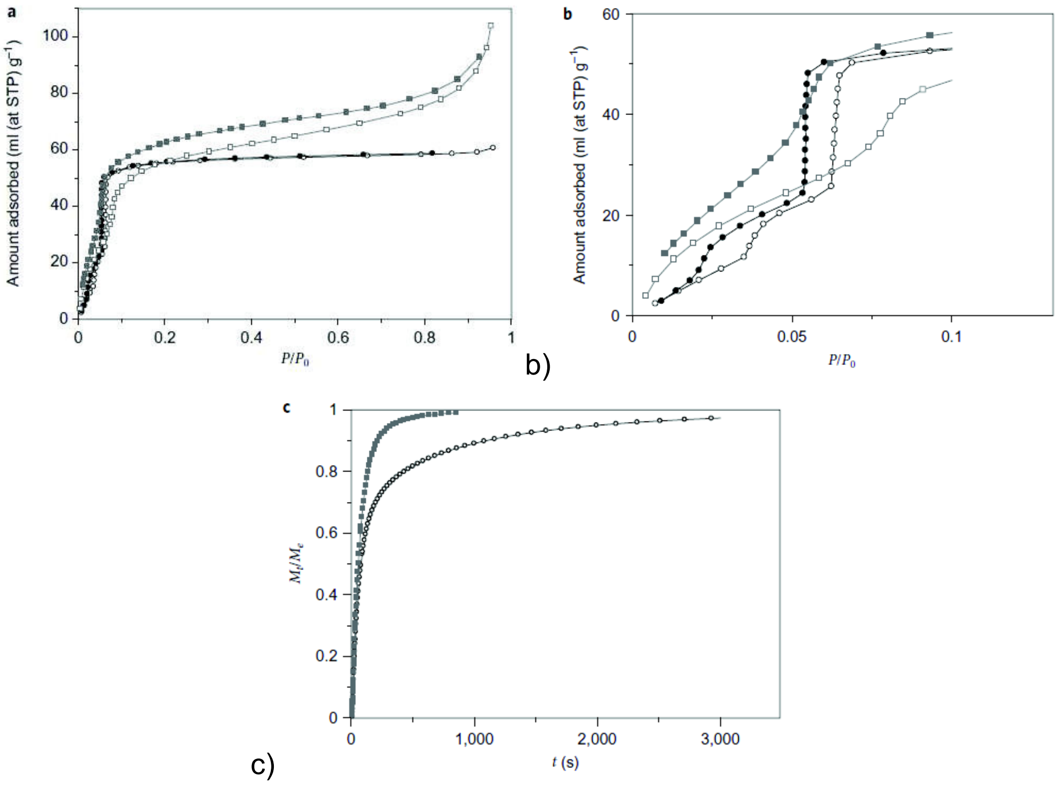

a)

b)

c)

Figure 96: Gas adsorption properties of bulk-CID-1 and NCID-1a; a) adsorption and desorption isotherms for methanol at 293 K on bulk-CID-1 (black circles) and NCID-1a (grey squares); b) adsorption in the low relative pressure region; c) kinetics of adsorption of methanol on bulk-CID-1 (black circles) and NCID-1a (grey squares) at 293 K. Reprinted from ref. [268], Copyright 2010, with permission of Nature publishing group.

The authors assign this change to the shorter diffusion ways in the nano-crystal compared to the bulk material as well as possible presence of surfactant at the surface of the nanoMOF crystal.[268]

Therefore, it is highly desirable to investigate deeply further tuning methods to obtain uniform nanoMOFs of prototypical MOFs and study their adsorption behavior as well as catalytic performance.

Project

The aim of this project was to develop a general strategy for the synthesis of MOF particles which are smaller than 100 nm (in the following called nanoMOFs). As mentioned in the introduction there are already strategies for the synthesis of nanoMOFs, but they are either very specific to a special kind of MOFs or have poor yields, since high dilution is necessary. Especially, for the family of MIL-MOFs only few studies are available.[245],[244]

Here, in a new combination approach was investigated which includes the combined application of ultrasound energy, microemulsions and capping agents (Figure 97). By this method the synthesis of nanoMOF particles with a size smaller than 100 nm as well as functionalization of the particle by the capping agent was targeted.

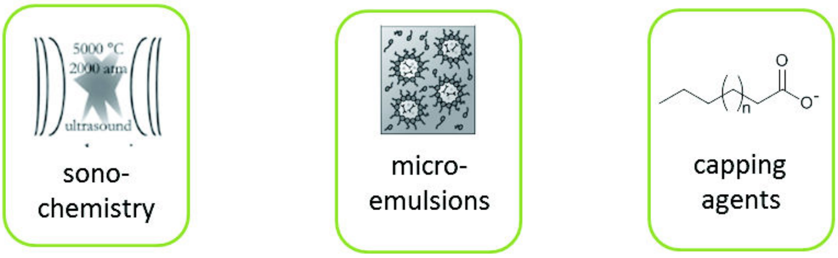

Figure 97: Combined application of ultrasound energy, microemulsions and capping agents for the synthesis of nanoMOFs

In comparison with batch synthesis and solvothermal synthesis, ultrasound was shown to accelerate reaction times in the formation of MOFs. As discussed in before also the generation of hot spots facilitates product formation and allows lower reaction temperatures[255],[269] which is the reason why this energy source was chosen.

For the synthesis of nanoMOF particles a water in oil microemulsion is used. Therefore, the system is applicable for all MOFs which can be synthesized in water. As surfactant monocarboxylic acids are used which act not only as surfactant, but also as a capping agent and are expected to strongly confine the particle growth.[260],[268] The MOF particles are expected to growth as long as they have space inside the water drops. As soon as the particles become large enough, the capping agents as well as the oil phase inhibit further growth. In consequence, by controlling the size of the water droplets in the microemulsion also the particle size could be controlled (Figure 98).

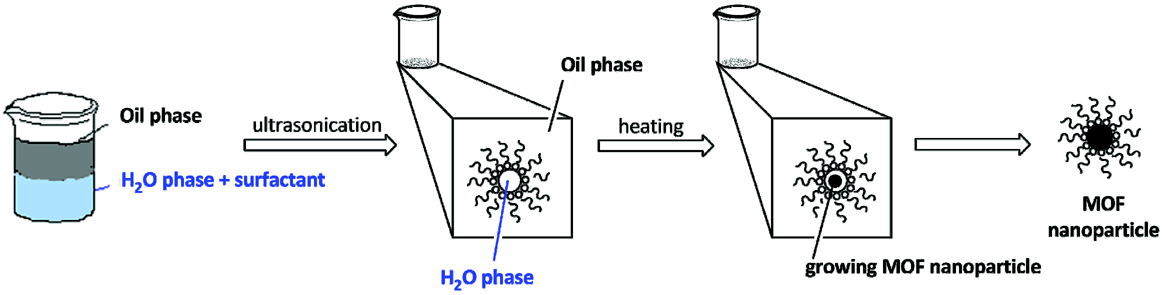

Figure 98: Synthesis strategy for nanoMOFs.

As seen in Figure 98, the product should be a surfactant functionalized MOF particle. The long chains of the surfactant can prevent particle aggregation and improve interactions with polymers. For instance in mixed matrix membrane fabrication, the long alkyl chains of the surfactant can improve the adhesion between MOF and polymer. Furthermore, also the surfactant can be functionalized post synthetically which opens doors to other application areas. In previous studies individual aspects have been investigated and the influence on particle size was investigated. Here, all three aspects (ultrasound, microemulsion and capping agents) are applied combined with the aim to control the MOF particle size below 100 nm as well as functionalization.

As proof of concept system MIL-88A Fe was chosen. This MOF is build up from fumaric acid and iron(III) chloride in water at a temperature of 100 °C following the hydrothermal synthesis strategy.[256] Since iron(III) is coordinated by carboxylates also the carboxylate moieties of the surfactant could coordinate to iron ions. MIL-88AFe was chosen, because it contains biocompatible iron as metal node, its synthesis can be carried out at comparatively low temperature and its breathing effect is interesting for further applications.

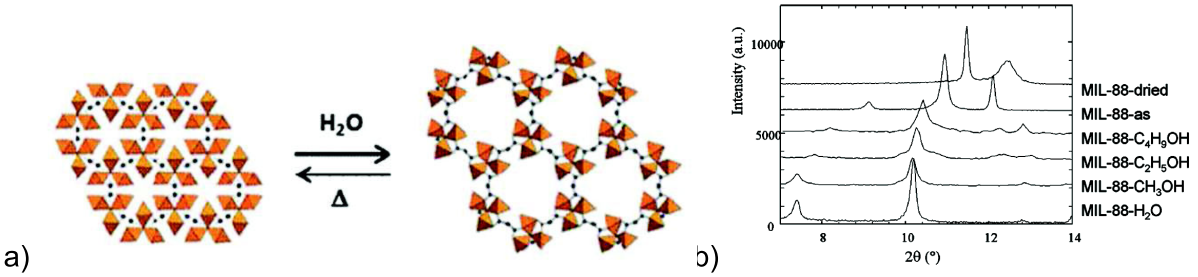

Figure 99: a) Schematic depiction of MIL-88A-Fe. Reprinted from ref. [256], Copyright 2011, with permission of the Royal Society of Chemistry; b) PXRD pattern of MIL-88AFe in different solvents, illustrating the breathing effect. Reprinted with permission from ref [270]. Copyright 2005 American Chemical Society.

Horcajada and coworkers already showed that MIL-88AFe can be synthesized with ultrasound. They used an ultrasound bath at 50 °C with different reaction times.[256] In this work an ultrasound horn type reactor was used, which provides better controlled reaction conditions (control of energy and temperature) and more power compared to an ultrasound bath (Figure 100).

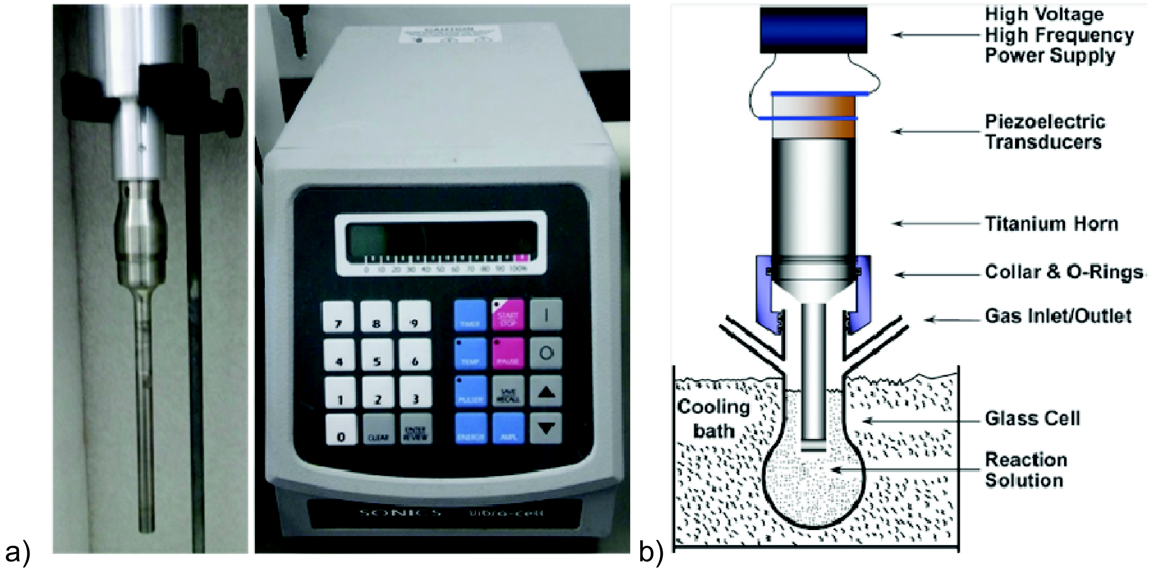

Figure 100: a) Ultrasound horn-type reactor (sonics, vibra-cell) used for nanoMOF synthesis. b) schematic depiction of a ultrasound horn-type reactor. Reprinted from ref. [250], Copyright 2013, with permission of the Royal Society of Chemistry.

By applying the same reaction conditions (50 °C, 90 min, 0.1 mol/L solution of reactants) as in literature with the only difference of horn type ultrasound source MIL-88AFe-1 was synthesized and compared to the literature results using a ultrasonic bath.

From XRD results it can be stated that crystallinity of MIL-88AFe-1 synthesized with horn-type reactor is higher than that from ultrasonic bath. Particle size from DLS is 571 ± 146 nm, which is in line with results of TEM pictures (Figure 101).

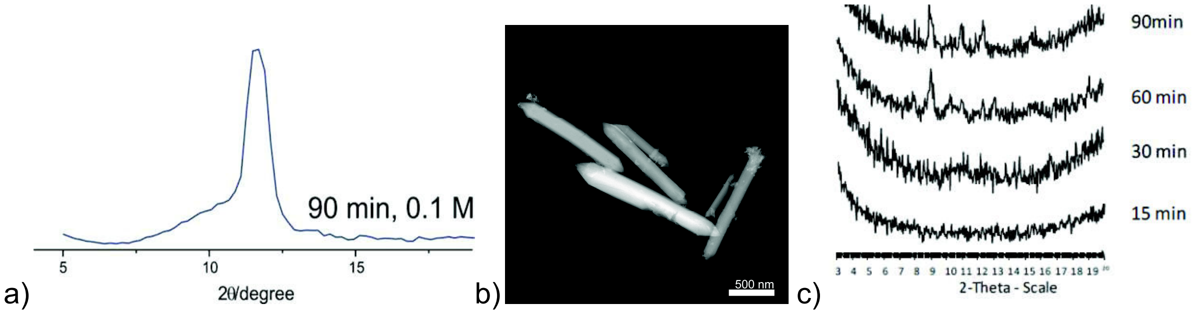

Figure 101: a) PXRD of MIL-88AFe-1 (50 °C, 90 min, 0.1 mol/L solution of reactants); b) TEM images of MIL-88AFe-1; c) PXRD pattern from MIL-88AFe (50 °C, 0.1 mol/L solution of reactants) taken from ref. [256], Copyright 2011, with permission of the Royal Society of Chemistry.

The next target was the development of the microemulsion system. Instead of using toxic surfactants as cetyltrimethylammoniumbromid (CTAB) or others, different fatty acids were investigated as surfactants because they contain carboxylate moieties as coordinating capping agents. In detail, sodium myristate, sodium stearate and sodium oleate were used in a *n*-heptane/water system (Figure 102). In principle due to the long chains of fatty acids microemulsion formation should be possible. In literature only a few reports deal with similar microemulsion systems e.g. an application for rare earth metal extractions was found.[271],[272],[273] Additionally, in his Ph.D. thesis K. Rottländer describes different sodium oleate based microemulsions.[274]. J. Xu reported a ternary system based on oleic acid, *n*-propanal and H_2O.[275]

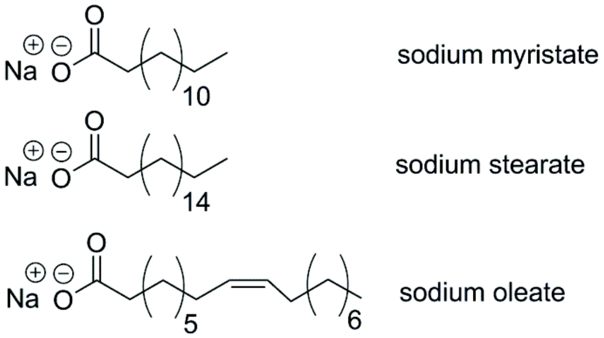

Figure 102: Structures of sodium myristate, sodium stearate and sodium oleate.

First tests with sodium myristate and sodium stearate revealed that they are not suitable as surfactants since it was not possible to achieve critical micelle concentration and in consequence, a stable microemulsion, when applying synthesis conditions. That is why the system was optimized using oleic acid, heptane and water.

The largest amount of water resulting in a clear microemulsion was figured out by adding small amounts of water (25 µL) to a suspension of sodium oleate in heptane. After a certain amount of water, the mixture became clear (Figure 103) and after adding more water the mixture became turbid again. The largest amount water forming a transparent and stable emulsion was determined as 3 vol%. The droplet size of the microemulsion was monitored by dynamic light scattering (DLS).[276]

200 µl H_2O
DLS: 45 [18] nm

350 µl H_2O
DLS: 58 [23] nm

Figure 103: Pictures of microemulsion water in oil using H_2O/heptane and sodium oleate with increasing amount of water from left to right.

Adding 3 Vol% water to the sodium oleate/heptane mixture yields a droplet size of 58 nm (Figure 103) (distribution by number, DLS). These tests were performed at 30 °C. Since the synthesis temperature for MIL-88AFe is 50 °C, the microemulsion was prepared again and treated at 50 °C for 40 min with ultrasound horn-type reactor (30% amplitude). DLS measurements after the reaction time gave a relative broad distribution, below 100 nm which is important for the synthesis of nanoparticles (Figure 104).

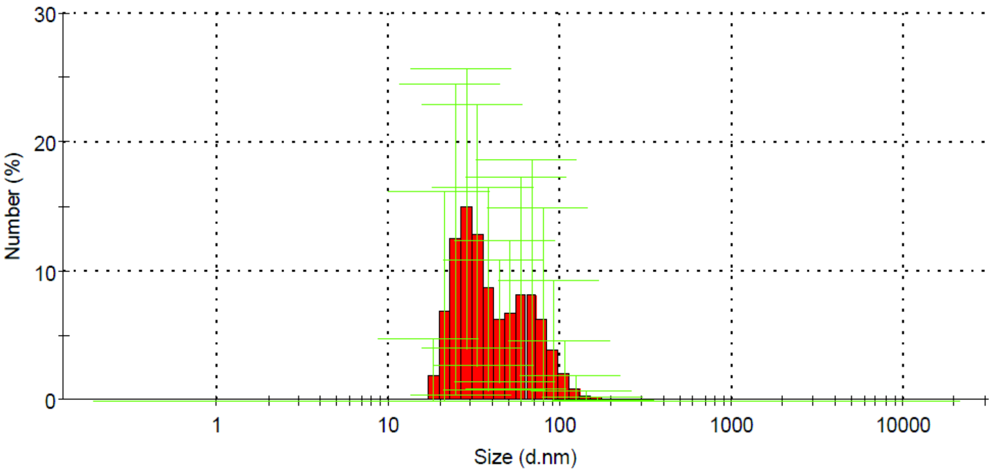

Figure 104: DLS distribution of w/o microemulsion after ultrasonic treatment for 40 min at 50 °C.

Next, nanoMOF synthesis of MIL-88AFe was performed with the microemulsion (MIL-88AFe-2). Synthetic details are reported in the experimental part (8.3.3). Two methods A and B were tested. First using **method A**, the microemulsion was formed using heptane, water and sodium oleate. Iron chloride and fumaric acid were dissolved in a small amount of water and added to the emulsion. The temperature of 50 °C was controlled with a stirring water bath and the reaction mixture was treated with ultrasound (30 % amplitude) for different times. Then ethanol was added which resulted in precipitation of an orange solid. The product was washed several times with water and ethanol and finally dried at 100 °C in air (Figure 105).

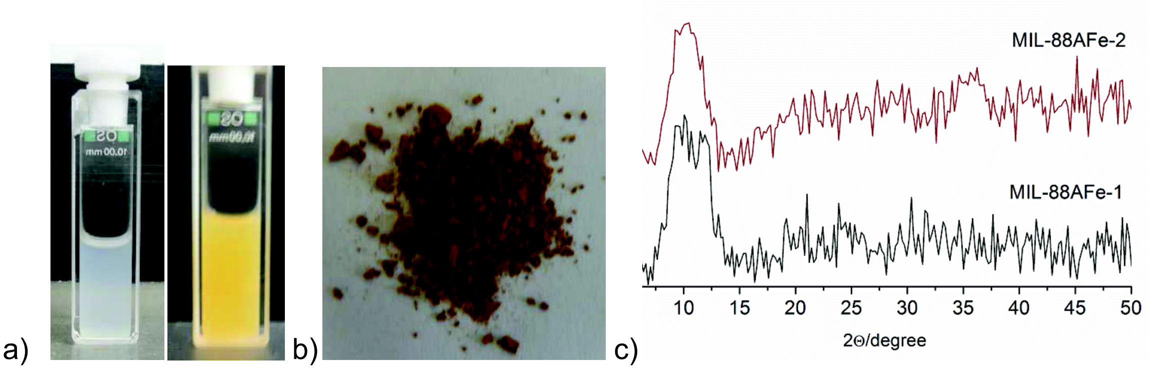

Figure 105: a) Microemulsion pure and after reaction (samples); b) dried product; c) PXRD of MIL-88AFe-2

PXRD patterns clearly revealed only very poor crystallinity. The reflex at 10 2θ is almost hidden behind the background reflexes. This might be due to small particle size, but can also point towards amorphous nature of the compound.

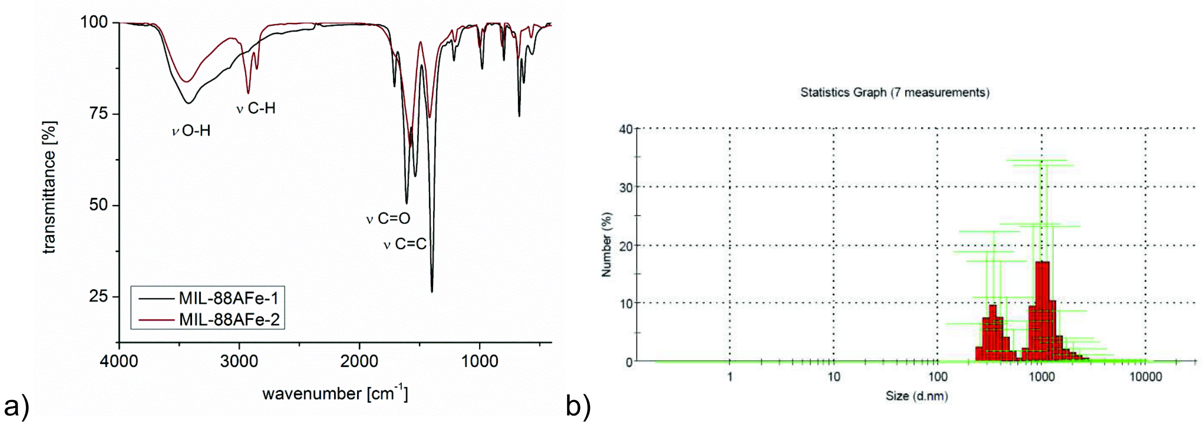

Figure 106: a) IR-spectrum of MIL-88AFe-1+2. B) DLS measurement of resuspended MIL-88AFe-2 in ethanol (average of 7 measurements, distribution by number).

IR spectrum of MIL-88AFe-1 in comparison with MIL-88AFe-2 shows additional C-H vibrations indicating the presence of sodium oleate. DLS measurement of the resuspended solid MIL-88AFe-2 after washing in ethanol shows a quite broad distribution of particles. To improve the particle size towards smaller particles, method B was developed.

Method B is refers to the procedure of W. J. Rieter *et al.* [265] and differs from method A regarding the addition of reactants. In method B two microemulsion are formed, one with $FeCl_3$ and the other one with fumaric acid. After mixing the two emulsions, the reaction started immediately when raising the temperature to 50 °C. The workup procedure was the same as for method A. As clearly visible from the PXRD measurement the purification of MIL-88AFe-3 has to be improved (Figure 107).

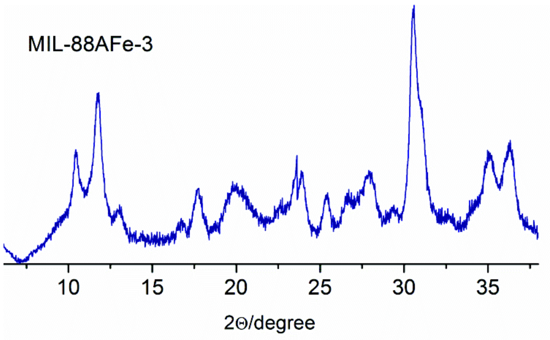

Figure 107: PXRD pattern of MIL-88AFe-3.

Nevertheless, from the reaction solution TEM samples were prepared and the pictures revealed that small particles below 100 nm formed. From EDX measurements it could be shown, that iron was found (Figure 108).

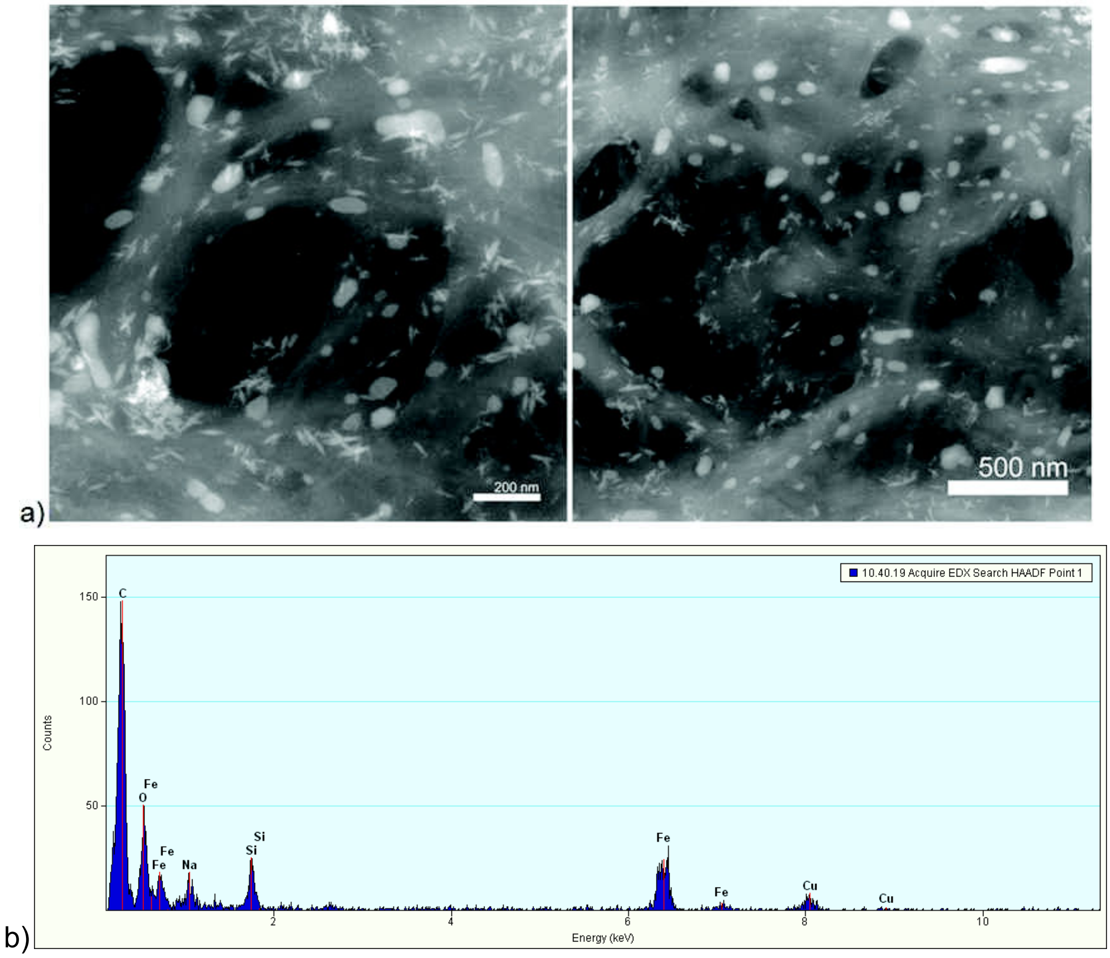

Figure 108: a) TEM pictures and b) EDX analysis of MIL-88AFe-3.

Additionally, after washing and drying, the particles were resuspended in DMF and the particle size was measured by DLS (Figure 109). A quite narrow distribution with particle size below 100 nm was obtained, which is in line with TEM measurements.

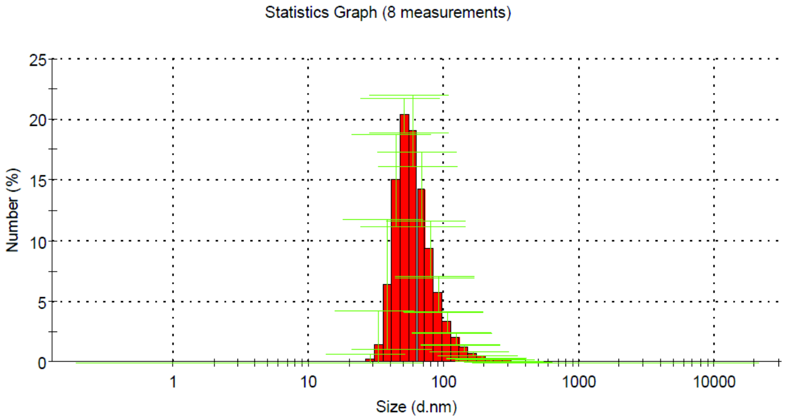

Figure 109: DLS measurement of resuspended MIL-88AFe-3 in DMF (average of 8 measurements, distribution by number).

As explained in the introduction, MIL-88AFe shows a breathing behavior. The dried form shows, due to closed pore structure, no experimentally detectable surface area. Therefore, water sorption was selected as method of choice to compare pore size accessibility of

MIL-88AFe-3 and MIL-88AFe-1. The water uptake of MIL-88AFe-3 (0.13 g/g) is much lower than the one of MIL-88AFe-1 (0.46 g/g; synthesized by ultrasound, only). This can be explained by the presence of hydrophobic sodium oleate. To determine if porosity was retained or if pores are simply blocked it would be interesting to measure the uptake of a hydrophobic compound. In addition, solid state NMR should be measured in future in order to determine if sodium oleate coordinates to the MOF.

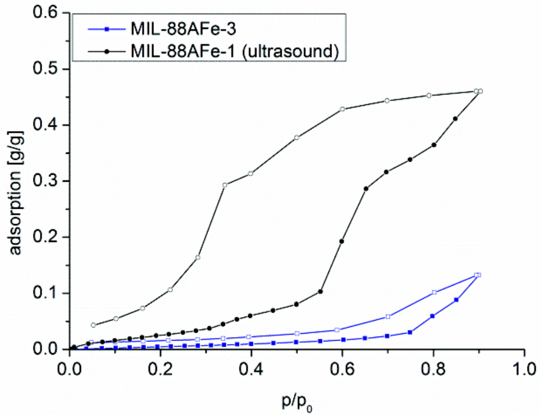

Figure 110: Water sorption of MIL-88AFe-3 and MIL-88AFe-1 (ultrasound).

In summary it could be shown that using ultrasound, microemulsion and capping agents can be used for the synthesis of MIL-88AFe with particle sizes below 100 nm. Further improvement of the reaction has to be done regarding purification and reproducibility. Additionally, the question is still open, if sodium oleate really coordinates to the MOF or only blocks the pores. It would be straightforward to employ the developed method on the synthesis of prototypical MOFs as MIL-101Cr where at the point of this project no reliable method is known.

This project was forwarded to Mrs. Irina Gruber as project for her diploma thesis in October 2013. The aim of her project was the validation of the results for MIL-88AFe as well as the method transfer to MOFs which are interesting for application of catalysis and water sorption, namely, MIL-101Cr and MIL-100Fe. This project is still under investigation.

Assuming that the synthesis and functionalization of nanoMOFs in microemulsions is successful, the materials could be applied as filler for mixed matrix membranes. Additionally, in a recent review M.S. Bakshi describes how surfactants can control crystal growth of metal nanoparticles and shows how to design the shape of the same using selected micelle architectures.[277] It would be interesting to investigate how this concept can be applied to MOF synthesis. Also the idea to functionalize the C–C double bond of sodium oleate in order to introduce additional, for example catalytic active or polymerizable, moieties makes this kind of materials very interesting.

4.3.2 Towards hierarchical micro-, meso and macroporous MOFs

Introduction

An ideal hierarchical structured porous material should contain a macropore system to enhance mass transport, mesopores for precise selectivity, and microporous structure to provide the catalytically active sites (Figure 111).[278] Hierarchical structures can be obtained by the design of multi-component systems, as for instance core-shell systems, which were presented before (chapter 4.2). Instead, synthetic strategies which lead to hierarchical porosity within a single material are introduced.

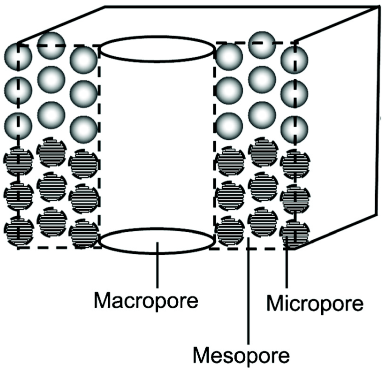

Figure 111: Schematic representation of the hierarchially micro–meso–macroporous material constructed from zeolite nanocrystals via quasi-solid state crystallization process. Reprinted from ref. [278], Copyright 2011, with the permission of the Royal Society of Chemistry.

Mostly metal-organic frameworks display pores in the microporous region up to 2 nm. This limits their application as catalysts regarding transformations of larger molecules as for example biomass derived compounds. Therefore, the expansion to materials possessing larger pores in the mesoporous region (2 – 50 nm) and even in macroporous pores is highly desirable.[279]

In 2012 W. Xuan and coworkers summarized the first developments of mesoporous MOFs.[280] They distinguished between cage type and channel type mesoMOFs, but both refer to mesopores arising from the molecular building unit of MOFs. Prominent examples of MOFs exhibiting micropores as well as mesopores larger than 2 nm are MIL-101Cr or IRMOF series (Figure 112).

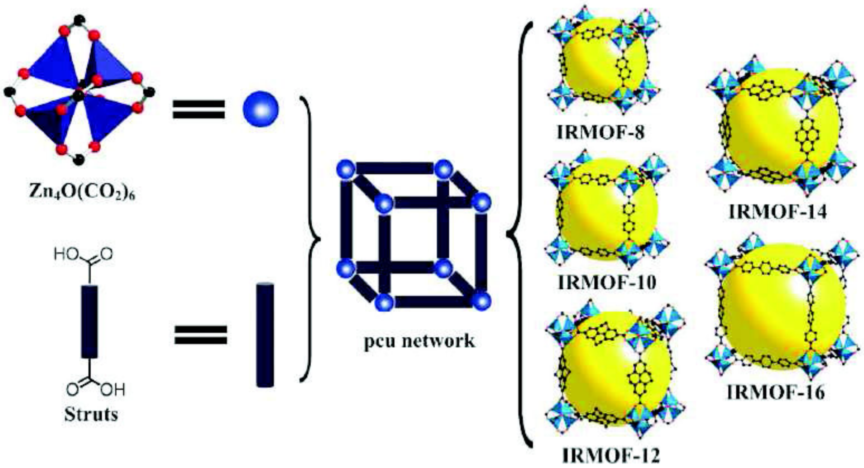

Figure 112: The expansion of IRMOFs-n based on ligand extension strategy. Reprinted from ref. [280], Copyright 2012, with permission of the Royal Society of Chemistry.

Nevertheless, entering the upper size region of mesopores or macropores additional strategies for MOF synthesis are necessary. Generally, D. Bradshaw *et al*. classified three kinds of hierarchical structured materials (Figure 113), a) mesoporosity coming from interparticle voids between nanoMOF particles of 50-100 nm in size, b) mesoporosity originated from template synthesis, resulting in the assembly of very small nanoMOF particles (approx. <20 nm) to meso or macroporous aggregates or c) mesoporosity from defect engineering.[279]

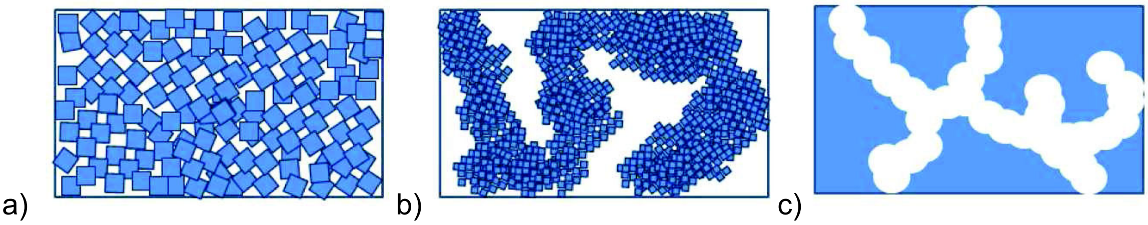

Figure 113: Different kinds of hierarchical mesoporosity (white) porosity in MOFs; a) mesoporosity in MOFs from interstices between MOF nanoparticles; b) via template guided aggregation and c) mesoporosity from specific defects or chemical etching. Reprinted from ref. [279], Copyright 2014, with permission of the Royal Society of Chemistry.

Typical adsorption isotherms for mesoporous materials are shown in Figure 114. The hysteresis in desorption originates from capillary condensation occurring in mesopores.[281] In 2015 the IUPAC recommendation for the classification of physisorption isotherms was refined, since during the last years new characteristic types of isotherms were identified. A close relationship between type of isotherm and pore structure is proposed.[281]

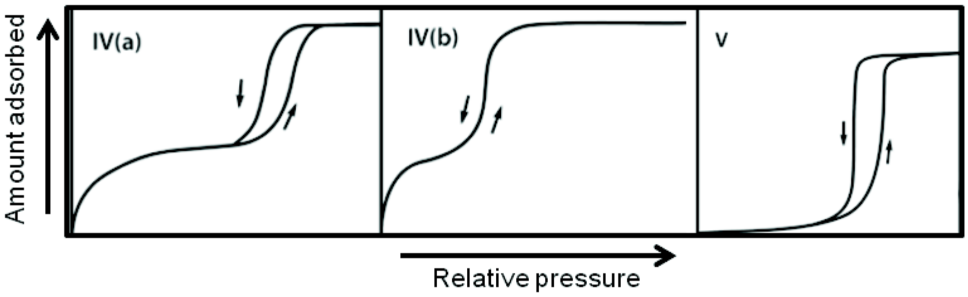

Figure 114: Type IV and V adsorption isotherms for mesoporous materials. Reprinted from ref. [281], Copyright 2015, with permission of IUPAC & De Gruyter.

Isotherm Iva and IV b differ in the critical width of mesopores. For IVa this size is exceeded, resulting in capillary condensation accompanied by hysteresis.[281]

Developments in the area of mesoporous metal-organic frameworks are reviewed detailed by D. Bradshaw and coworkers[279] as well as S. Furukawa and coworkers.[282]

In the following two selected examples are given. An early report adapted the common strategy for the synthesis of meso-structured silica compounds known as MCMs for HKUST-1.[283] Using CTAB as well as 1,3,5-trimethylbenzene as structure directing agents, mesopores were generated.[283] Figure 115 shows a TEM image of template directed assembly of nanoMOF particles revealing that mesoporosity originated from interparticle voids. Corresponding nitrogen sorption isotherms and pore size distributions indicated mesoporosity. Compounds 2A to 3 varied in the amount of template used (Figure 115).

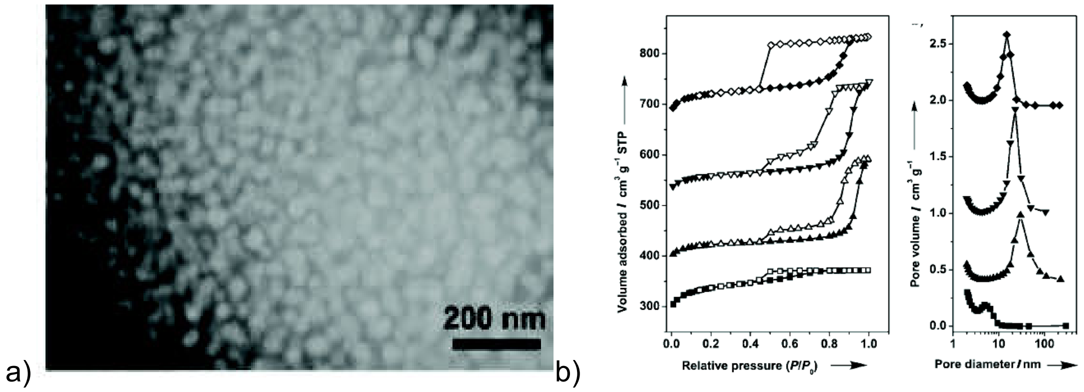

Figure 115: a) TEM image of the mesostructured MOF 2a; b) nitrogen sorption isotherms and pore-structure analysis of the hierarchically micro- and mesoporous MOFs 2A (▲), 2B (▼), 2C (■), and 3 (♦). The isotherms for 2A, 2B, and 3 are vertically offset by 250, 400, and 500 cm^3/g, respectively. Distributions of pore diameters obtained using the BJH method; the distributions for 2 A, 2B, and 3 are vertically offset by 0.4, 1.0, and 2.0 cm^3/g, respectively. Reprinted from ref. [283], Copyright 2008, with permission from John Wiley and Sons.

In 2013, S. Cao and coworkers reported the synthesis of stable bicontinuous hierarchically porous metal–organic frameworks. They used two different functional block co-oligomers, namely. poly(styrene)-block-poly(4-vinylpyridine) and poly(styrene)-block-poly(acrylic acid) in combination with the prototypical MOFs HKUST-1 and ZIF-8.[284]

The synthesis strategy is depicted in Figure 116, which involves the hierarchical assembly of block-co-polymer micelles, followed by MOF synthesis in the spacings and template removal by dissolution of the polymer in THF/DMF mixture.

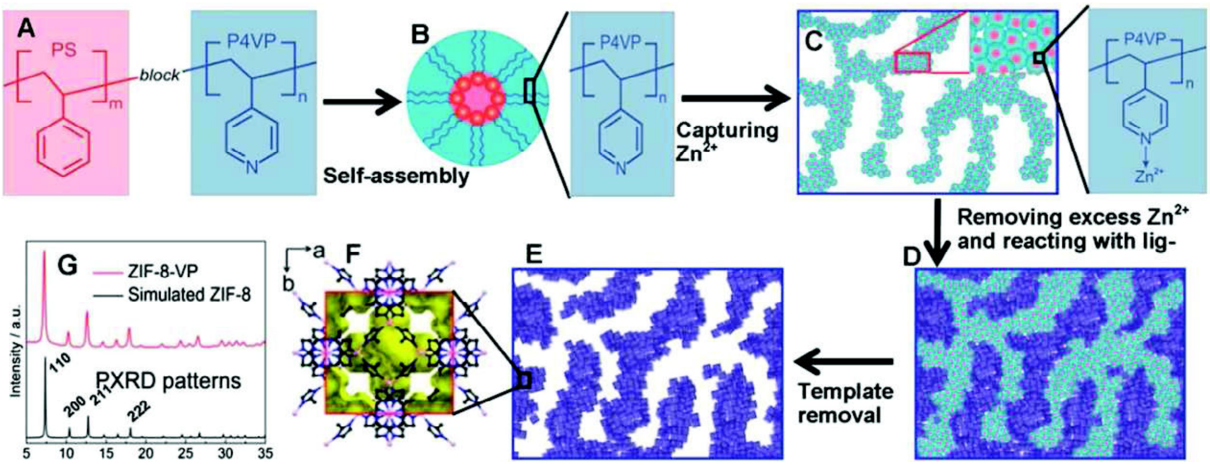

Figure 116: Synthesis of hierarchical ZIF-8-VP templated from PSty$_{14}$-b-P4VP$_{19}$ block co-oligomer micelles. Reprinted from ref. [284], Copyright 2013, with permission from the Royal Society of Chemistry.

The resulting materials exhibited interconnected porosities throughout the micro-, meso- and macroporous regions, as shown by electron microscopy images and pore size distribution analyses (Figure 117).[284]

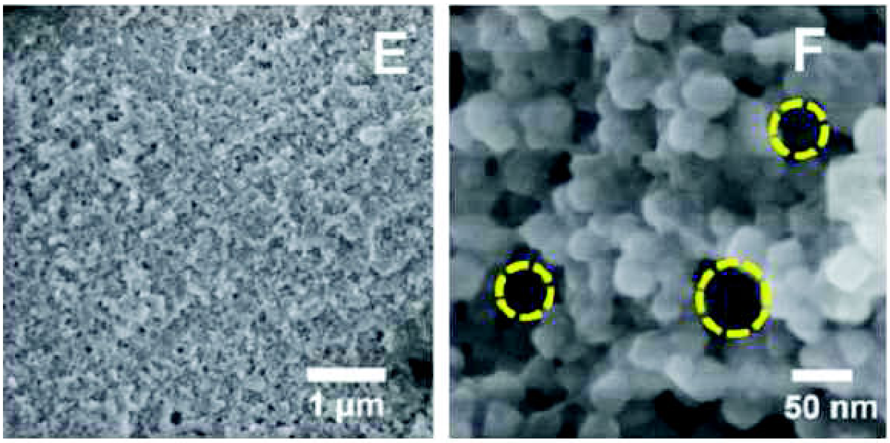

Figure 117: FEG-SEM of hierarchical ZIF-8-VP at different magnifications; the yellow dashed circles highlight the textural meso- and macro-porosities. Reprinted from ref. [284], Copyright 2013, with permission from the Royal Society of Chemistry.

Related to catalysis, the concept of “hierarchical catalyst” which describes a multifunctional catalyst with micro-, meso- and macropores, allows the integration of different catalytic processes to a single material. Due to increased physical closeness of reactants in the catalyst material, enhanced performances can be achieved. The number of steps in the production of a multistep reaction product can be reduced which is in line which a reduction of energy consumption and less waste products.

Project

Usually deprotected carboxyl acids are used to build up metal-organic frameworks, but for instance in the case of MIL-100Al the metal salt reacts with trimethyl-1,3,5-benzenetricarboxylate.[48] Acidic chromium nitrate together with hydrothermal conditions might be sufficient to deprotect also Ligand-1-protected, which was introduced in chapter 4.1. Therefore, Ligand-1-protected reacts together with dimethyl-2-aminoterephtalic acid (1:1) in a mixture of H_2O and DMF at 130 °C for 24 h. Dimethyl-2-aminoterephtalic acid was used instead of 2-aminoterephalic acid to ensure similar nucleation behavior, regarding deprotection as for Ligand-1-protected.

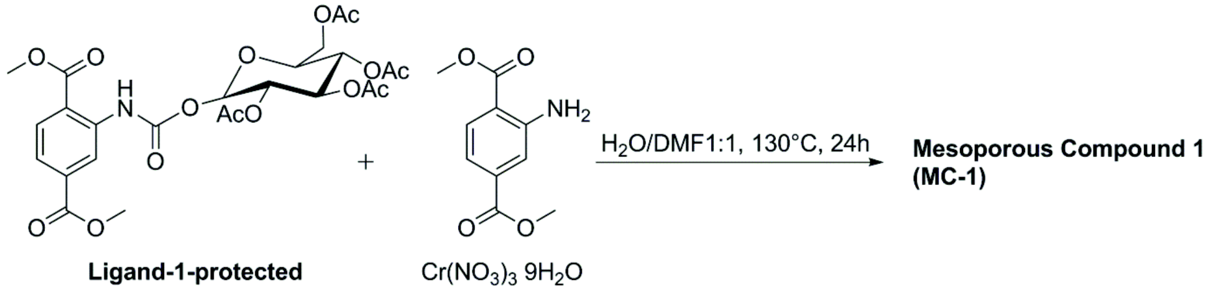

Figure 118: Synthesis of MC-1.

A dark brown gel-like compound was obtained which was suspended in different solvents (H_2O, DMF, THF and ethanol) stirred for 3 h, respectively and separated by centrifugation. Compound MC-1 was dried at 100 °C *in vacuo* which resulted in strong shrinkage (Figure 119).

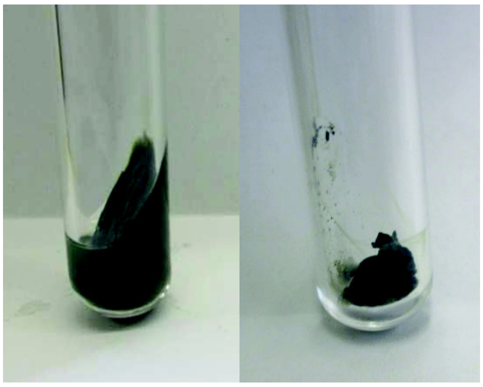

Figure 119: MC-1 after washing procedure and after drying.

Analysis of MC-1 by IR spectroscopy revealed good agreement of carboxylate vibrations with the carboxylate vibrations of MIL-101Cr-NH_2. Therefore, it can be assumed that carboxylate moieties of Ligand-1-protected are coordinated to chromium. Vibrations assigned to glucose or rather Ligand-1-protected can be found for MC-1 in the fingerprint regions (400 – 1300 cm^{-1}) (Figure 120).

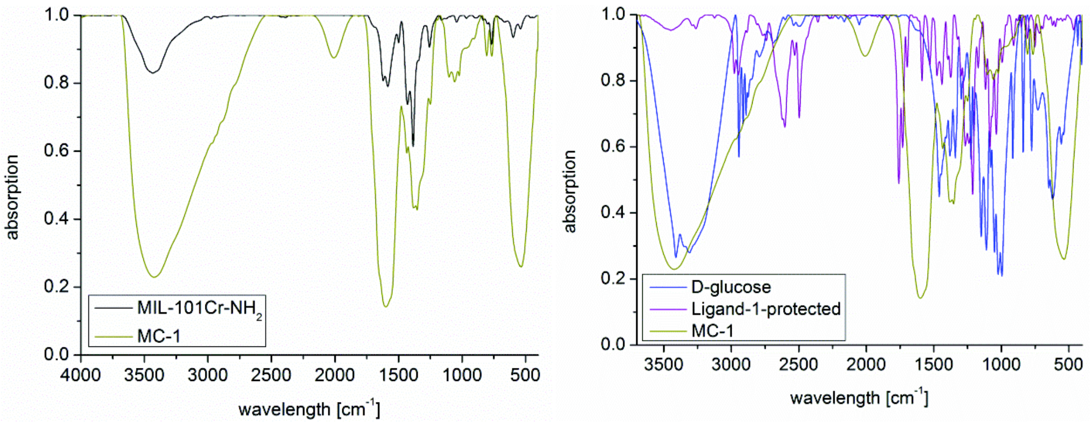

Figure 120: Infrared spectra of MC-1 and reference compounds.

PXRD pattern shows only pure crystallinity (Figure 121). It is known from MIL-101Cr-NH$_2$ that the smaller the particle size the worse is crystallinity and since MC-1 was synthesized in a similar way with similar precursors it can be proposed that pure crystallinity also originates from small particle size.[231] Otherwise it is assumed that MC-1 posses very pure crystallinity.

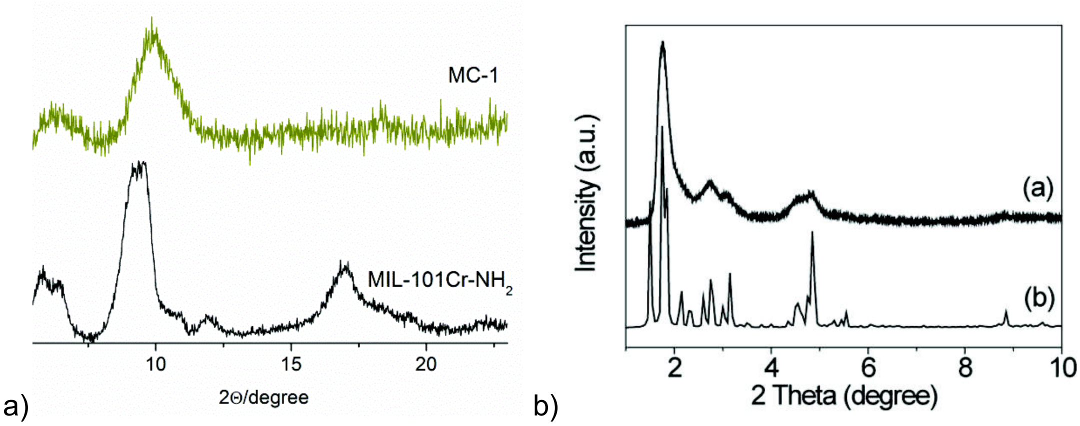

Figure 121: a) PXRD of MC-1 in comparison with MIL-101Cr-NH$_2$; b) high resolution PXRD pattern of MIL-101Cr-NH$_2$ and simulated MIL-101Cr pattern, taken from ref. [231], Copyright 2012, with permission of the Royal Society of Chemistry.

MC-1 showed relatively high porosity and depicted a BET surface area of 439 m^2/g. Nitrogen sorption measurement showed a type IV shaped isotherm. The pronounced hysteresis in desorption indicates the presence of mesopores (Figure 122).

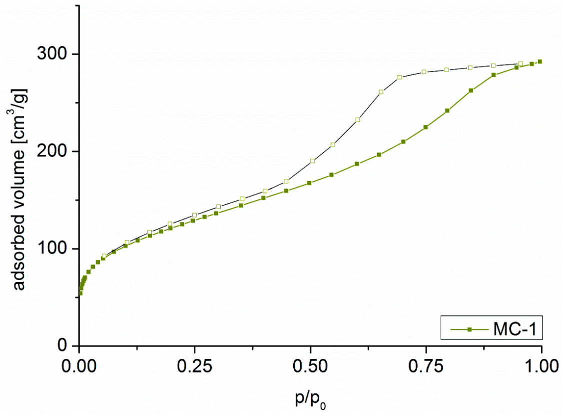

Figure 122: N_2 sorption isotherm of MC-1.

Indeed also from calculated pore size distribution, mesopores can be observed in the range of 2–6 nm (Figure 123). As described in the experimental part, calculated pore size distribution is not a reliable method, since no accurate DFT model for MOFs is available so far. Nevertheless, the fitting error for adsorption is below 1 % and also hysteresis in desorption points towards mesoporosity.

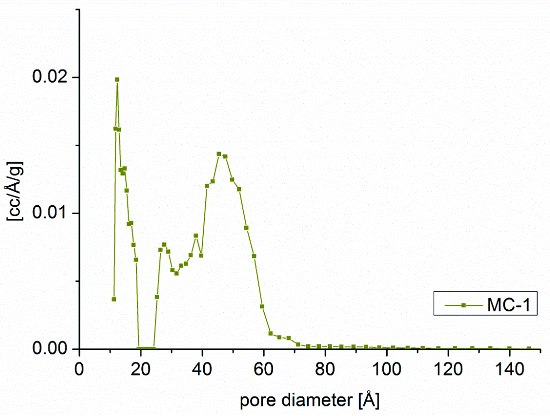

Figure 123: Pore size distribution for MC-1, fitting error 0.64%.

SEM measurements showed that particles of MC-1 are very small, around 10-20 nm. Even with a field emission SEM it was very difficult to obtain good quality pictures because the particles do not withstand the electron beam. Using TEM techniques, the same problems occurred, agglomerates of very small particles could be observed. EDX measurements show the presence of chromium, as well as nitrogen (Figure 124).

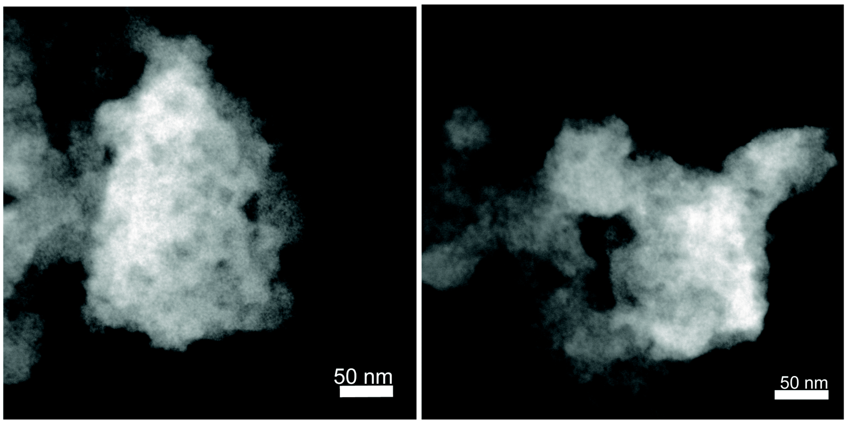

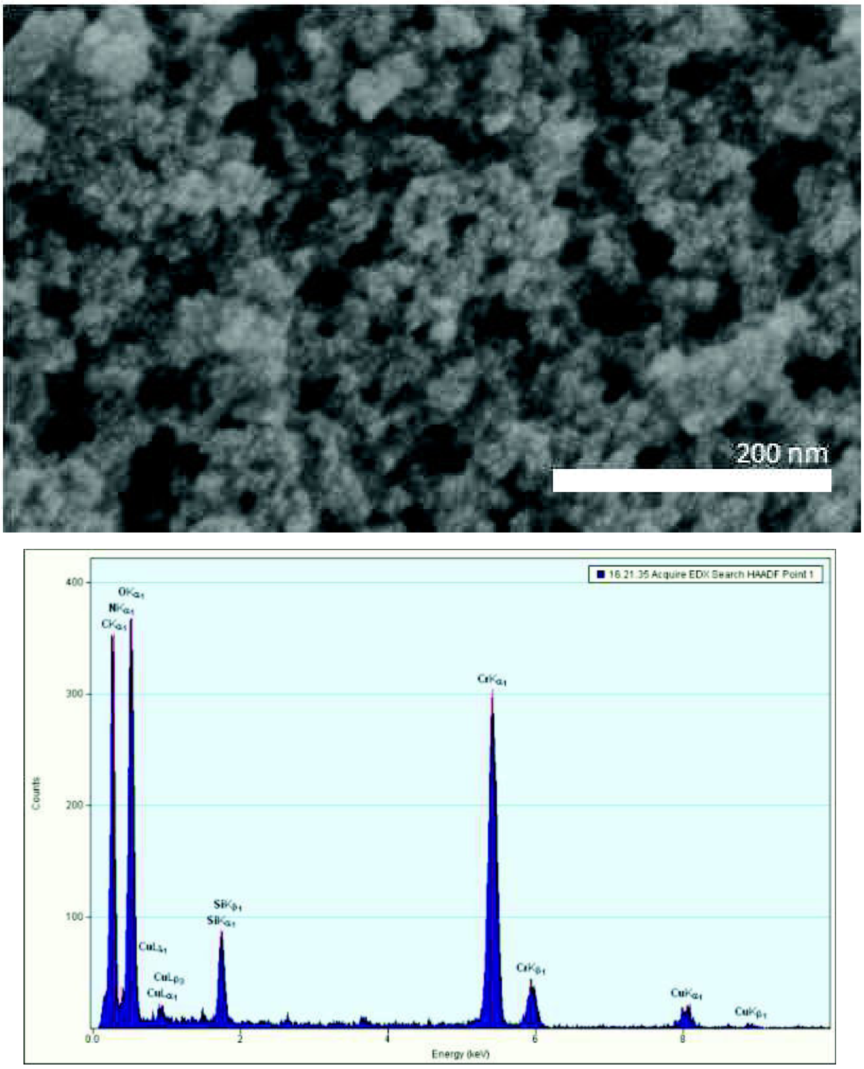

Figure 124: SEM and TEM pictures as well as EDX results for MC-1. [pp]

A second attempt was made where a thicker (approx. 2 nm) layer of platinum was sputtered on the sample.[qq] Although the small particles are not visible any more through the layer, pictures of the meso-structure could be obtained (Figure 125).

[pp] SEM picture was measured at WHUT, China

[qq] Measured with Merlin instrument (Zeiss), MPI für Eisenforschung, Düsseldorf, with kind support of Frau Niessen.

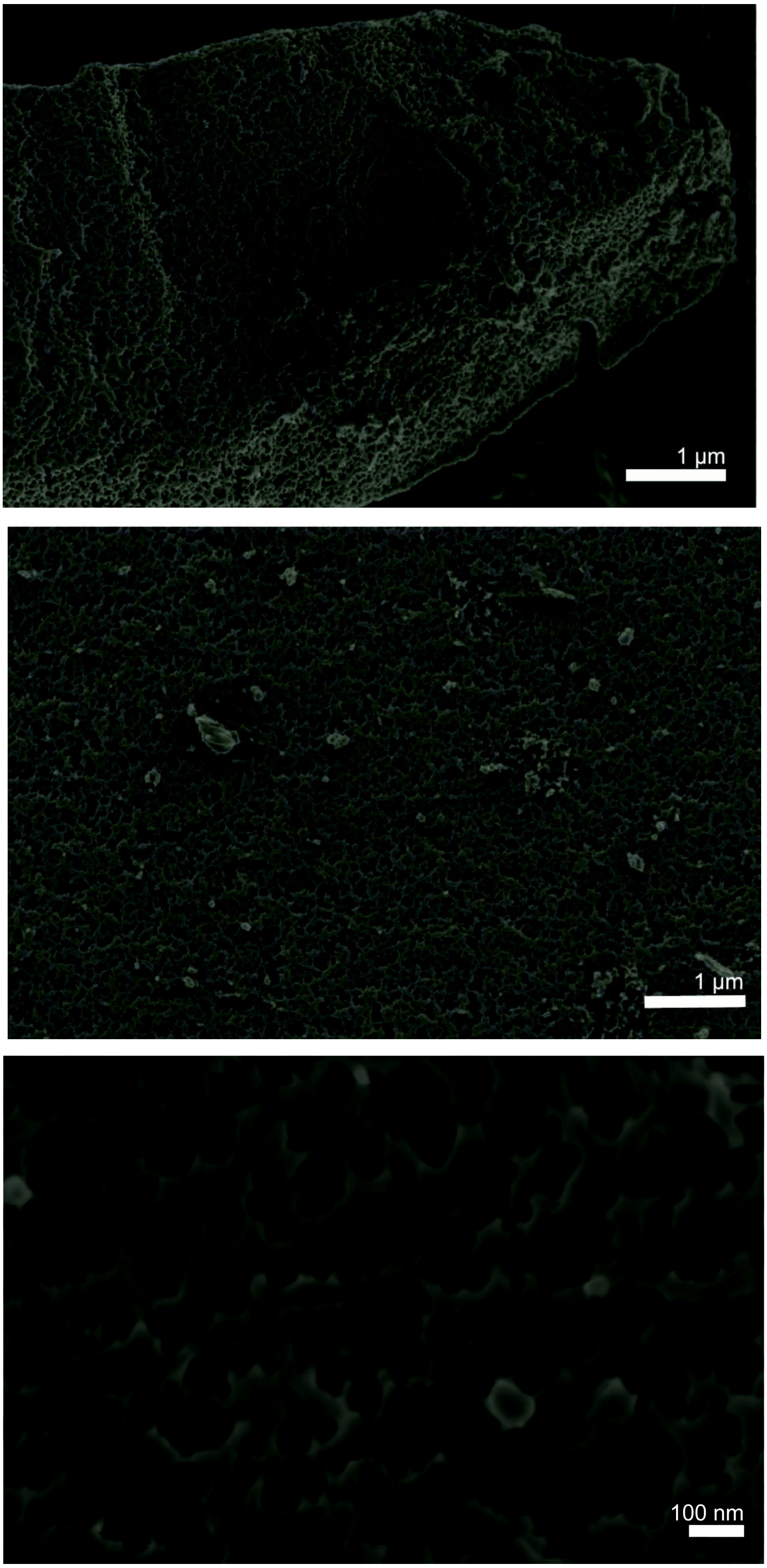

Figure 125: SEM pictures of MC-1, sputtered with platinum.

From SEM pictures a sponge like structure was observed. Pores of very different sizes were found ranging from 15 nm until 89 nm, whereas the larges pores (larger than 50 nm) can be already numbered as macropores. In order to furthermore verify the size and accessibility of mesopores, it would be necessary to perform mercury porosimetry measurements. The experiment using Ligand-1-protected was repeated successfully twice to ensure reproducibility. A number of reference experiments were performed to investigate this kind of materials and gain a deeper understanding of formation of meso and macropores. First, dimethyl-2-aminoterephtalate reacts with chromiumnitrate and D-glucose in order to find out if glucose can act as template as well (Figure 126).

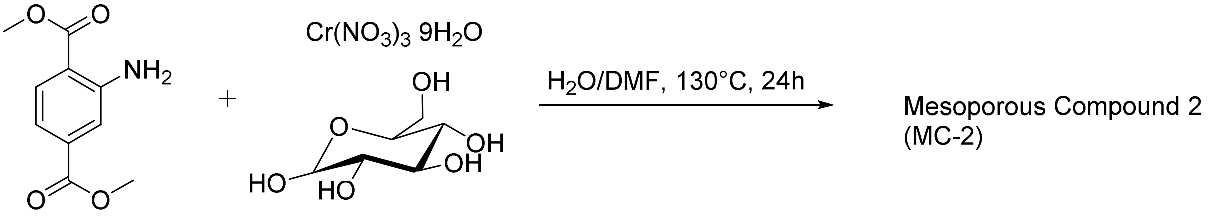

Figure 126: Synthesis of mesoporous compound 2 MC-2.

As seen from the N_2 sorption-isotherm and pore size distribution as well as from SEM pictures, again a mesoporous material was obtained. The BET surface area of MC-2 is 423 m^2/g. In comparison to MC-1 the pores are smaller (up to 38 Å from pore size distribution and visible by SEM images), showing that it makes a difference if glucose is bound to the linker or not (Figure 127).

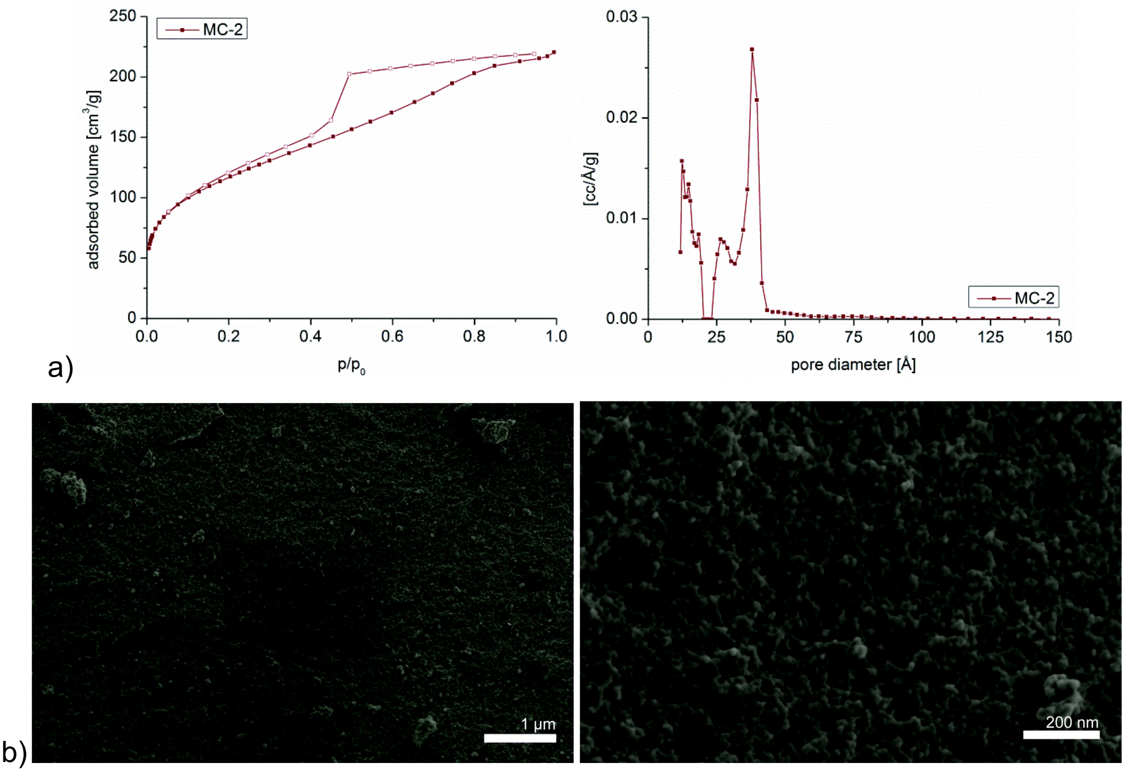

Figure 127: a) N_2 sorption isotherm and pore size distribution of MC-2, fitting error: 0.61%. b) SEM pictures of MC-2.

Since in Linker-1-protected the glucose is acetylated and pH can have a great influence on synthesis, also acetylated glucose was tested as additive (Figure 128).

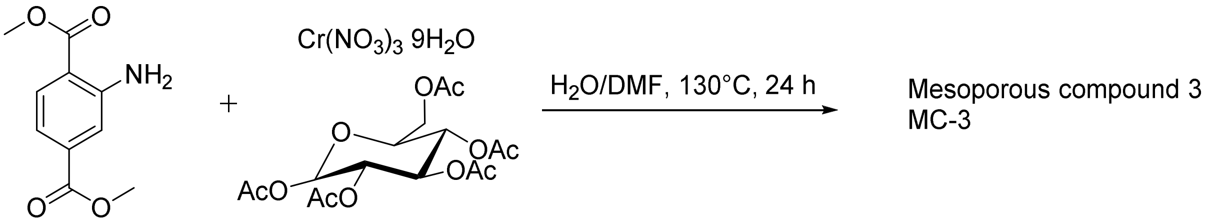

Figure 128: Synthesis of mesoporous compound 3 MC-3.

MC-3 displays a type V sorption isotherm and a very broad pore size distribution compared to MC-1 and 2. The BET surface area of MC-3 is with 436 m^2/g very similar to the others. In contrast SEM pictures show no mesopores, but agglomerated particles (Figure 129).

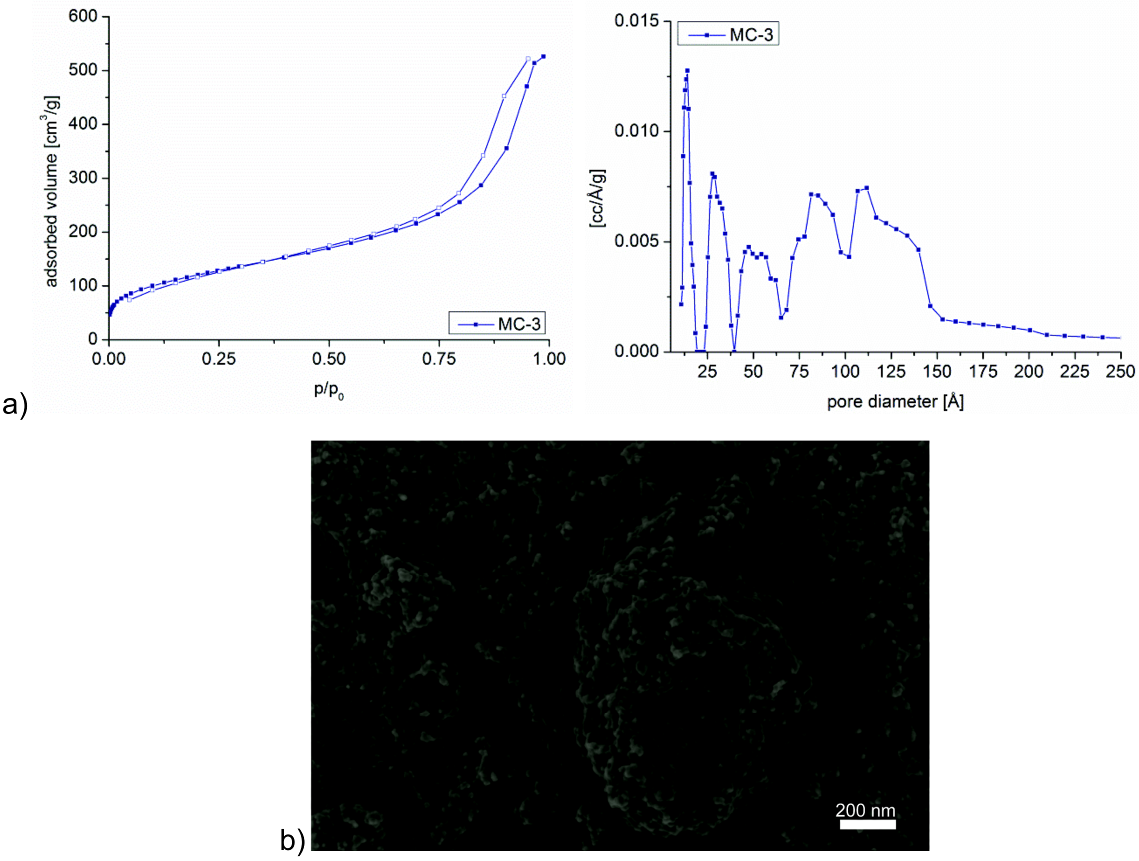

Figure 129: a) N_2 sorption isotherm and pore size distribution of MC-3, fitting error: 0.86%. b) SEM pictures of MC-3.

In all three cases mesoporous compounds could be obtained, whereas larger mesopores and macroporosity differs when using different template molecules as visible from SEM pictures. A series of experiments was performed varying glucose ratio as well as solvent. Also 2-aminoterephtalic acid was used. An overview about these experiments is given in the experimental part. In all cases from nitrogen sorption isotherm mesoporosity can be stated, although the hysteresis shape as well as calculated pore size distribution differs. PXRD analysis showed that crystallinity of all materials is low, probably attributed to small particle size.

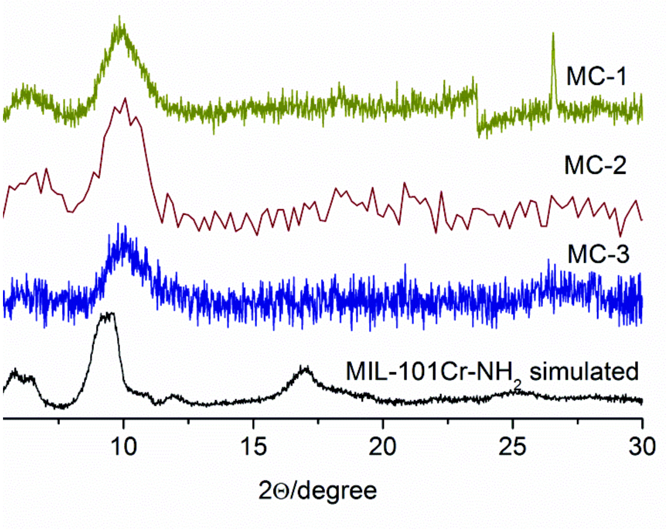

Figure 130: PXRD pattern of MC-1 , MC-2 and MC-3.

From the catalysis project described in chapter 3.2, it has to be taken into account that glucose might be converted to fructose, 5-HMF or levulinic acid and formic acid or also humins during synthesis, since high temperatures (130 °C) are applied. The chromium salt can act as catalyst and it was already shown, that chromium salts can convert glucose to various products.[285] The supernatant reaction solution after reaction forms two fractions, one containing more DMF and the other more H_2O. The dark red color of the H_2O phase was also observed in 5-HMF and humin formation (Figure 131). Since DMF cannot be used in mass spectroscopy and due to prioritization experiments were not followed.

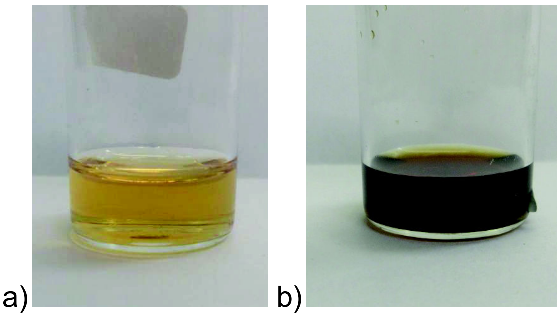

Figure 131: Supernatant reaction solution after synthesis. Two phases formed, a) DMF fraction, b) H_2O fraction.

As reference experiment, only chromium nitrate and glucose were reacted in H_2O/DMF 1:1, but no solid was formed. Additionally chromium nitrate and dimethyl-2-aminoterephtalic acid were reacted using standard synthesis conditions in order to see if MIL-101Cr-NH$_2$ is formed. Surprisingly, a different mesoporous material, MC-9, was obtained. MC-9 displayed a surface area of 457 m^2/g, which was comparable to MC-1, 2 and 3 (Figure 132). In contrast, reacting chromium nitrate and dimethyl-2-aminoterephtalic acid applying same molar ratios as before, but in pure water (instead DMF/H_20 1:1) MIL-101Cr-NH$_2$ exhibiting BET surface area of 1947 m^2/g is formed (here MC-10) (Figure 132). This proves at least that MIL-101Cr-NH$_2$ can be synthesized based on dimethyl-2-aminoterephtalic acid.

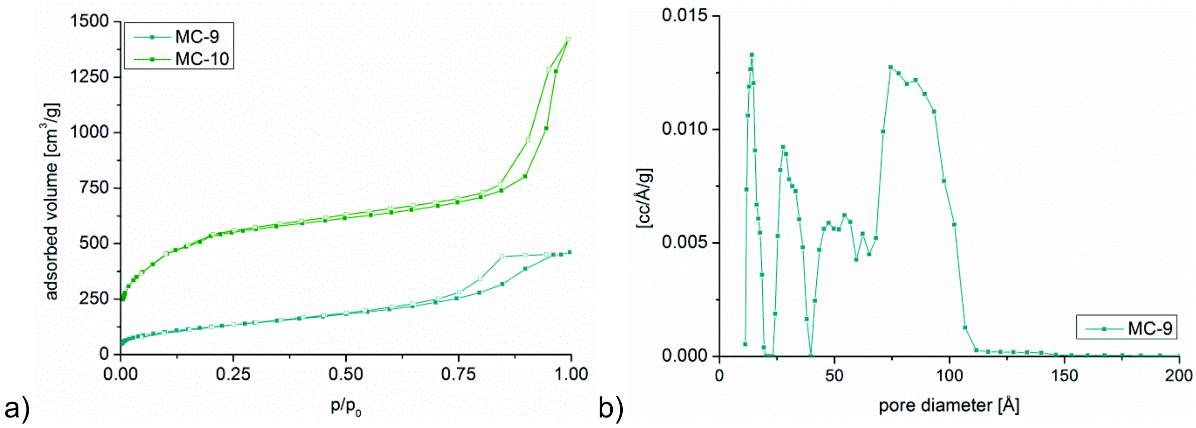

Figure 132: a) a) N_2 sorption isotherms of MC-9 and MC-10 and b) pore size distribution of MC-9, fitting error: 0.90%.

It would be very interesting to look at scanning electron microscope pictures to elucidate which kind of mesopores the material MC-9 displays. Unfortunately, at the time the project was worked on, no access to high resolution SEM was given. Without addition of glucose, also a kind of mesoporous compound was obtained. Therefore, it was proposed that solvent conditions, more precise the ratio of DMF/H_2O might influence the mesoporosity.

Two experiments were performed, using a ratio of H_2O/DMF 2:1 with glucose as template and without. Both times mesoporous compounds were obtained. Pore size distribution is very similar for pores smaller than 10 nm and varies with sizes larger than 10 nm (Figure 133).

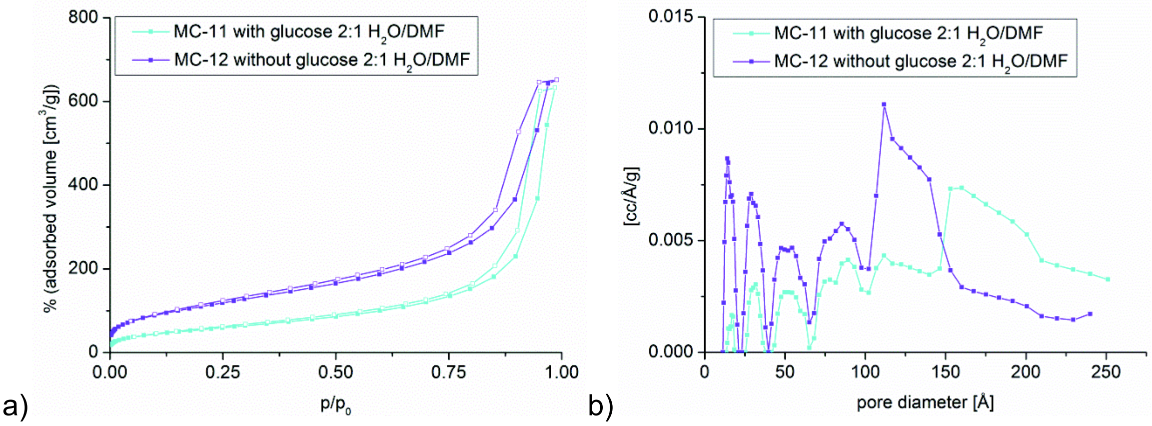

Figure 133: a) N_2 sorption isotherm and b) pore size distribution of MC-11 (1.7) and MC-12 (1.1); fitting error is given in brackets in %.

In conclusion, hierarchical micro-meso-macroporous compound MC-1 was obtained from Ligand-1-protected. From reference experiments a number of micro-mesoporous compounds could be obtained which show, as proved for MC-2 and MC-3 by SEM measurements, lower or no macroporosity. Therefore, the formation of macro pores is attributed to Ligand-1-protected.

A number of questions still have to be answered which was not possible within the scope of this work: A very critical point is that the structure of the obtained material is unknown. Although from SEM pictures nanoparticles can be observed, it is not sure if they have really

MIL-101Cr composition since XRD diffractogram is not convincing. For future measurements elemental analysis should be performed.

In addition, it has to be taken into account that the amid bond of Ligand 1-protected or ester bond can be cleaved under solvothermal synthesis conditions. In consequence, it should be elucidated if Ligand-1-protected stays intact or is decomposed during synthesis of MC-1.

Also further analysis by SEM of other MC compound could lead to a deeper understanding of formation of hierarchical pores. Confirmation of macropores for example by mercury porosimetry can be performed.

Contemporaneous to this work, X. Liu and coworkers published their work about NMOF gels.[286] They developed a strategy to synthesize permanent interparticle porosity, using different prototypical MOFs, through aggregation of sufficient small nanoMOFs.

By this strategy polymorphs of IPD-mesoMOFs can be obtained, which micropore aperture from the microporous MOF architecture is unchanged, while mesopore apertures derived from various levels of interparticle random loose packing (RLP) are changeable. They can be efficiently tuned by adding a variety of spherical organic molecules as interparticle-filler. A The authors tested polymorphs of an IPD-mesoMOF with large mesopores for biomolecule immobilization (Figure 134).[286]

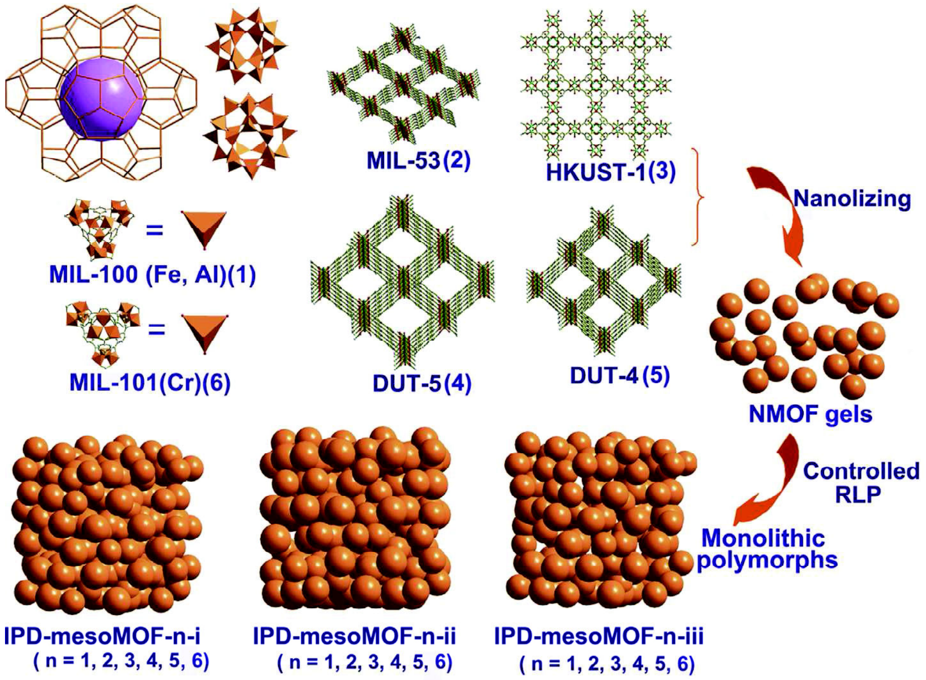

Figure 134: Schematic diagram of the interparticle porosity generated from the controlled random loose packing NMOFs. Reprinted from ref. [286], Copyright 2015, with permission of Elsevier.

The PXRD pattern depicted in Figure 135 clearly shows an amorphous structure of IPD-mesoMOF-6 (MIL-101Cr analogue). Nitrogen sorption isotherms show a slight hysteresis in desorption and on the SEM pictures a kind of interparticle porosity can be observed, which is less pronounced as for MC-1.

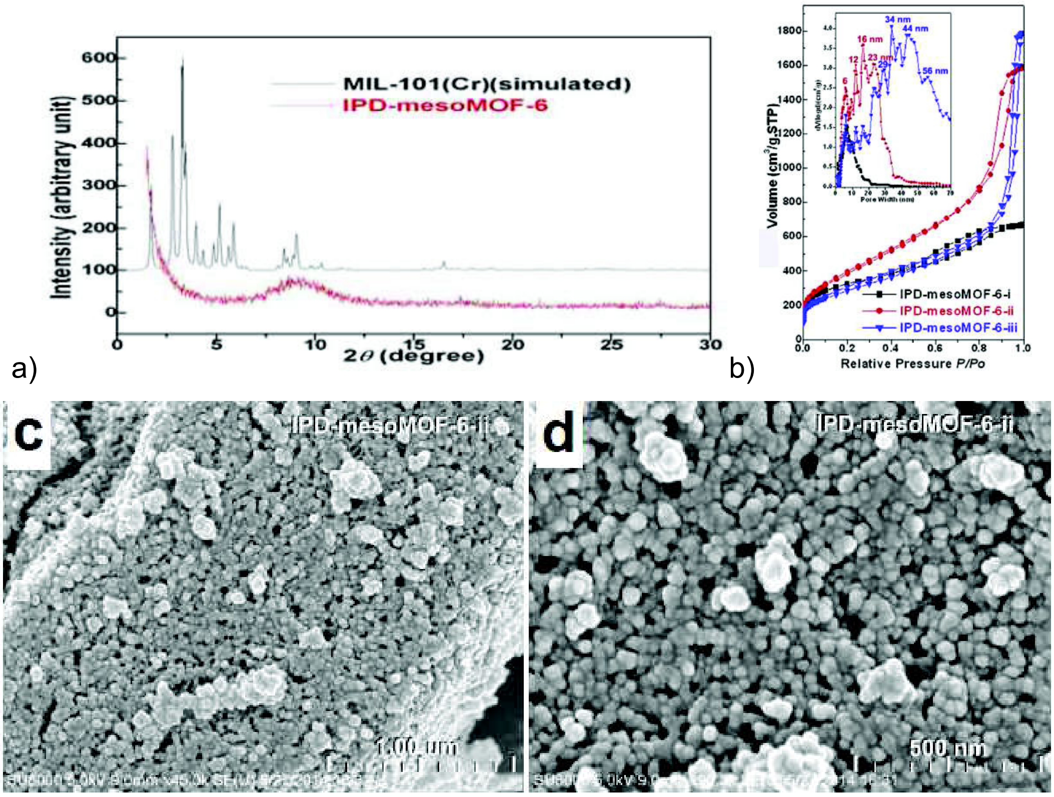

Figure 135: a) PXRD, b) N_2 sorption isotherms and c,d) SEM pictures of IPD-mesoMOF-6, MIL-101Cr analogue. Reprinted from ref. [286], Copyright 2015, with permission of Elsevier.

Compared to the experiments of X. Liu and coworkers, in our presented project also permanent interparticle porosity can be observed. The main effects are proposed to originate from solvent interactions, as well as *in situ* templating effect of glucose moiety at Ligand-1-protected. The templating effect seemed to be significantly more pronounced when using Ligand-1-protected than pure glucose (Figure 125, Figure 127).

Outlook

Keeping in mind the work of X. Liu *et al.* other combinations of linker and metal salts can be tested using optimized conditions in order to see whether the strategy can be adapted to other MOFs. In addition to the challenges addressed above, it can be investigated if variation of concentrations, temperatures or solvents the surface area as well as crystallinity can be improved. Also supercritical drying with CO_2 might be an interesting option to further increase crystallinity and surface area.

On the one hand to circumvent the problem of unknown structure and one the other hand recognizing the potential of the micro-meso-macroporous structures, carbonization could be performed with the MC materials. Hierarchical carbon and metal oxide structures, especially derived from MOFs attracted great interested during the last years due to their promising properties in the field of supercapacitors, electrode materials and catalysts.[63]

The development of stable meso- and macroporous MOFs is interesting, especially for catalysis, because also larger molecules could be converted. Besides larger pores offer more space for additional functionalization which is an improvement towards multifunctional catalysts.

4.3.3. Additional experiments with MOF@xerogel composites

Introduction

The properties of resorcinol-formaldehyde xerogels were already described in chapter 3.3. The focus of the published project was shaping of MOF´s for heat transformation purposes. In the following the application and challenges of polymer@MOFs composites for catalysis and liquid phase separations are introduced.

Generally, separations can be performed in the gas-phase or in the liquid phase. For both areas MOFs are promising materials, due to their chemical tuneability. Disadvantages are low thermal, chemical and solvent stability, hence the MOF material should be selected carefully.[287] Furthermore it has to be distinguished between separation of gases as for example CO_2/CH_4 and separation of organic molecules. In the area of gas separations, MOF based membranes and especially metal-organic framework mixed matrix membranes are intensively investigated.[236],[288],[289] Secondly, solid phase (micro)extraction (SPE)[290],[291] as well as (nano)filtration[292] serve great attention in research, since especially the purification of waste water is of emerging interest.[293],[238] Figure 136 depicts a general principle for solid phase extraction/enrichment and sample preparation.[294] The monolithic material is fabricated in a syringe and installed in a vacuum manifold. Due to vacuum the eluent as well as analyte can be loaded and flow through the monolithic material. Advantageous is the small amount of material needed for this kind of application.

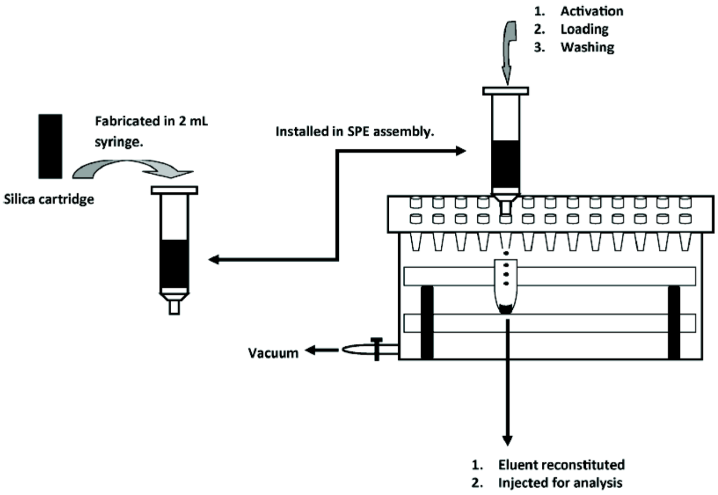

Figure 136: Principle of an solid phase extraction (SPE) manifold. Reprinted from ref. [294], Copyright 2014, with permission from Elsevier.

As already traced in chapter 4.1.2 HPLC separation of enantiomers with MOFs is another highly interesting field of research.[177] As stated by Denayer *et al.* column packed testing of MOF´s under real application conditions are rare and still in its infancy.[177]

One reason for this is common to all separation techniques involving a packed column. Pure MOF fine powder is generally not well suitable as packing material, since the MOF particle size is in the nanometer region which results in very high ram pressure. Besides, quite high amounts of MOF are necessary to fill a HPLC column under high pressure.[295] Even if the instrument (for instance UHPLC) can generate sufficient high pressure this can damage the MOF material (loss of surface area and crystallinity), since MOFs are not very stable under mechanical pressure (see chapter 5.2). Nearly the same challenges exist for industrial application in catalysis.[1]

Therefore, it would be beneficial to have a polymer@MOF composite which meets the following criteria: i) forms stable monoliths, ii) complete retention of porosity and properties of the MOF, iii) can serve as filler material for columns.

In literature mainly different methacrylate polymers are used so far as polymer for mixing with MOFs.[295],[296],[297]

For example, MIL-101Cr was incorporated into mixtures of ethylene dimethacrylate (EDMA), butyl methacrylate (BMA) and 2-acrylamido-2-methylpropane sulfonic acid (AMPS) and used as stationary phase for separation of small molecules (Figure 137).[296]

Figure 137: Schematic depiction of the preparation of MOF packed column and polymer@MOF based column. Reprinted from ref. [296], Copyright 2013, with permission from Elsevier.

Mixtures of different xylene and cymene isomers were separated well. Anyhow, the surface area of composite material (MIL-101Cr-poly-BMA-EDMA) was given with 732 m^2/g whereas 50% MIL-101Cr was added. In comparison the surface area of pure MIL-101Cr is given with 2938 m^2/g. Therefore, it becomes clear that surface area of the MOF or at least accessibility of the pores is strongly reduced.[296]

From these examples it becomes obvious that retention of MOF properties is not trivial and synthesis of composite materials still has to be improved.

Project

As described in chapter 3.3 a method for the embedding of MOFs in resorcinol-formaldehyde xerogels was developed.[rr] By following the method using additional water was added, the surface area of MIL-101Cr was retained completely (according to weight percent). Applying this method, the MIL-101Cr@xerogel material is superior over other MOF@polymer composites which usually suffer from significant surface area loss.[296],[298],[299]

Shaping is an important issue in catalysis and separation. As described before HPLC separation is the most used method for separation of enantiomers.[188] Therefore, the aim of this follow-up project was to investigate the use of MOF@xerogel composites as column filling material towards separation of small molecules. Since amino-modified MOFs were shown to be active catalysts in a variety of organic transformations[92] MIL-101Cr-NH_2 and MIL-101Al-NH_2 were investigated as filler material.

The project can be divided into the following steps

1) Investigation if amino-modified MOFs are suitable for MOF@xerogel composites
2) Preparation of a MOF@xerogel filled HPLC column
3) Separation of organic molecules on this column as proof of concept

1) Investigation if amino-modified MOFs are suitable for MOF@xerogel composites

Amino-modified MOFs have catalytic activity due to basic properties as well as hydrogen bonding interactions, but are also used as anchoring groups for a variety of modifications.[300],[301],[302] For composite synthesis MIL-101Al-NH_2, MIL-53Al-NH_2 and MIL-101Cr-NH_2 were investigated.

The synthesis of MOF@resorcinol-formaldehyde-xerogels was already introduced in chapter 3.3. Briefly, the resorcinol-formaldehyde polymer was pre-polymerized until a high viscous material was obtained. MOF powder and water were added and the mixture was stirred with a mechanical stirrer in a customized apparatus (see experimental part) After gelation for 7 days, the mixture was altered in acetic acid, washed with ethanol and finally dried at 60 °C.

[rr] The xerogel project was worked out in cooperation with Martin Wickenheisser, Sebastian Glomb, Tian Zhao and co-workers of the DLR in Cologne. Pre-polymerization experiments, performing of pure xerogel syntheses with different parameters (variation of R/C, R/F and R/W ratios) and initial MIL@R,F-xerogel syntheses were done together with Martin Wickenheisser (MIL–100Cr,Fe), Sebastian Glomb (HKUST-1) and Tian Zhao (MIL-101Al-NH_2).

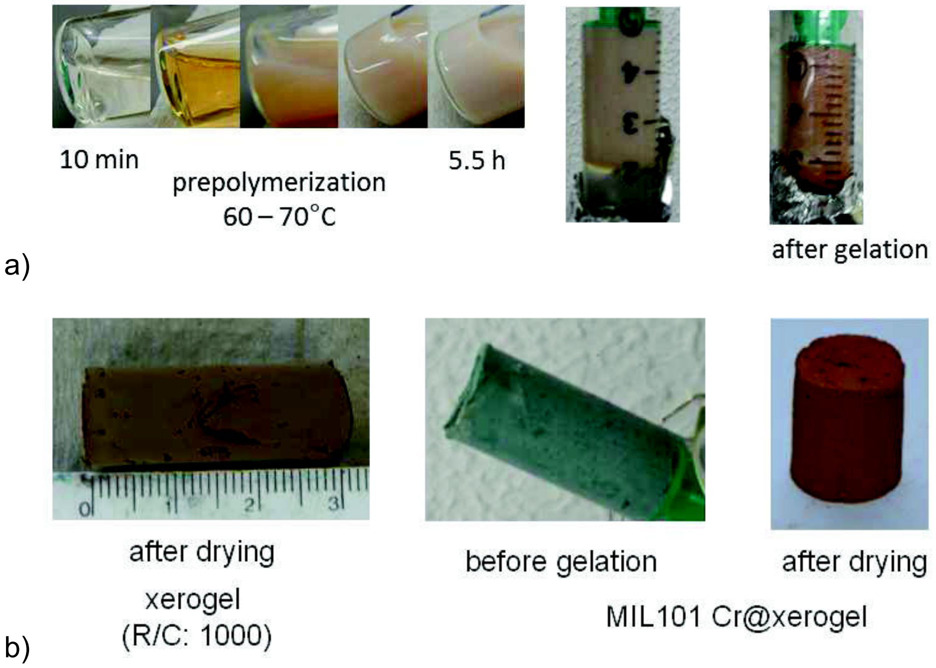

Figure 138: a) pictures of pre-polymerized solution at different times and R, F xerogel before and after gelation; b) pictures of xerogel after drying and MIL-101Cr@xerogel mixture before gelation and after drying.

Using this procedure, MOF@xerogel composites with MIL-101Al-NH_2, MIL-53Al-NH_2 and MIL-101Cr-NH_2 were prepared. The overview in Table 11 showed that for MIL-101Cr-NH_2 the experimental surface area was very close to the calculated one (based on wt%). Instead, for MIL-101Al-NH_2 the experimental surface area was much lower.

Table 11: Calculated and experimental BET surface area of composites

MOF material	Amount MOF based on weight **(%)**	**Calc.** **BET [m^2/g]** based on weight[a]	**Experimental BET [m^2/g]**
MIL-101Al-NH_2@xerogel	47	1053	120
MIL-53Al-NH_2@xerogel	47	241	169
MIL-101Cr-NH_2@xerogel	51	1302	1189

a) Surface area of pure MILs: MIL-101Al-NH_2 2240 m^2/g, MIL-53Al-NH_2 956 m^2/g, MIL-101Cr-NH_2: 2552 m^2/g

From XRD measurements it can be seen, that additional reflexes are observed in case of MIL-101Al-NH_2 which indicate that the material is not stable under synthetic conditions of xerogel synthesis. To be sure, more detailed experiments have to be performed. For HPLC column experiments the more stable MIL-53Al-NH_2 was used.

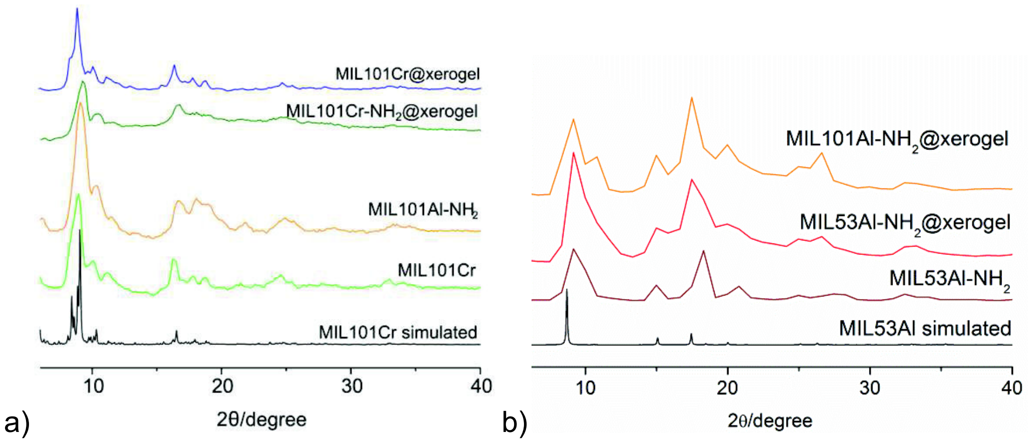

Figure 139: PXRD of different MOFs and MOF@xerogel composites (measuring time a) 2 h, b) 1 h).

2) Preparation of a MOF@xerogel filled HPLC column

For separation experiments it is important that the analytes are forced to flow through the column material. Cracks or shrinking of the composites need to be avoided. The MOF@xerogel mixture could be utilized in HPLC separations as well as in solid phase extraction experiments (SPE). Therefore, it was tested if it is possible to obtain a good adhesion between plastic syringes and the composite material. In Figure 140 different materials are shown before aging, after aging and after drying.

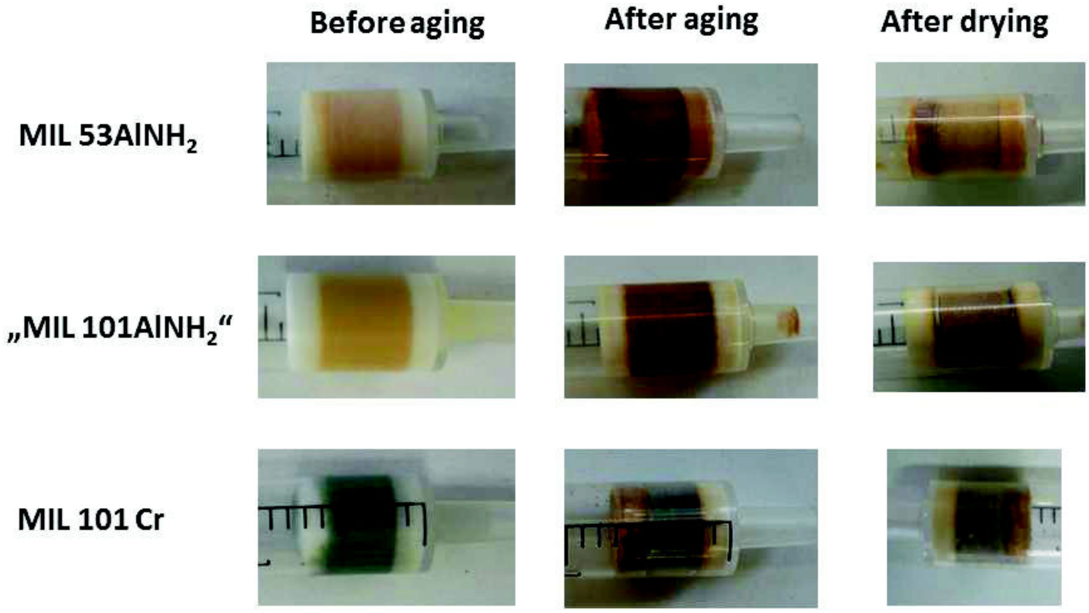

Figure 140: MOF@xerogel composites before and after aging as well as after drying.

After aging, the material showed no shrinking and seemed to be suitable for separations, whereas after drying significant shrinking occurred. Using a vacuum apparatus it was possible to wash the syringe composites with acetic acid and ethanol (Figure 141).

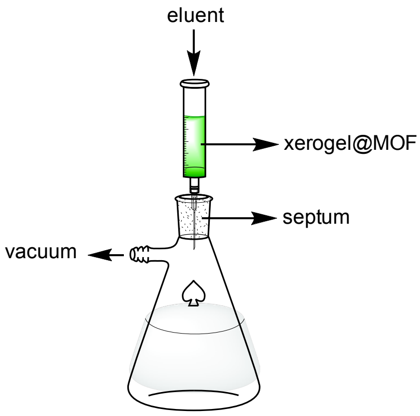

Figure 141: Vaccum apparatus for washing of MOF@xerogel composites.

As a next step, a commercially available empty HPLC column was filled with the pre-polymerized MIL-53Al-NH$_2$@xerogel mixture (Figure 142). The mixture was altered for 7 days as usual and it was taken care that the column material did not desiccated. The column was closed on both ends with PE frits.

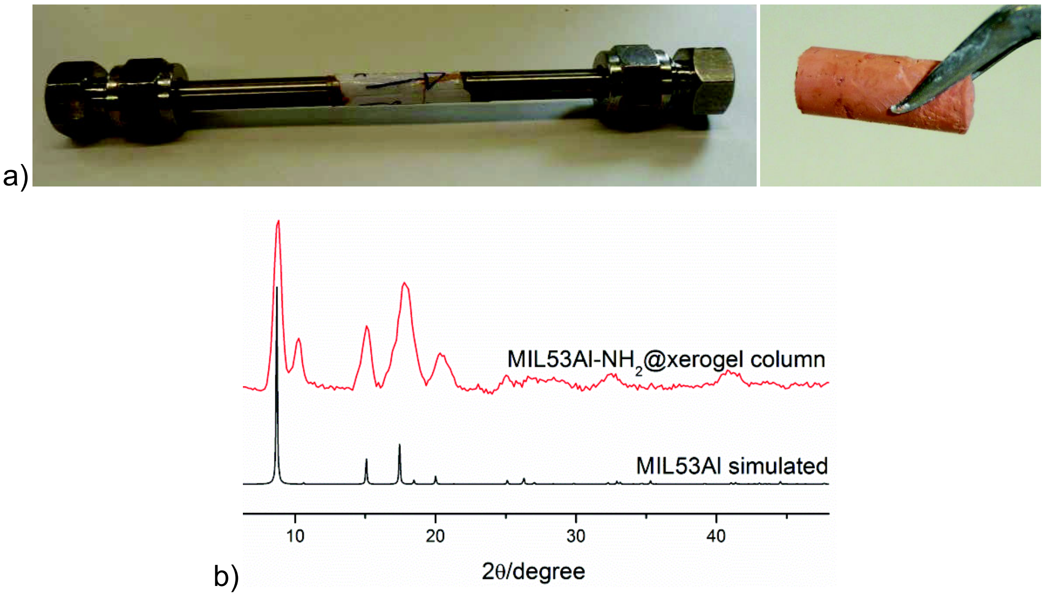

Figure 142: a) HPLC column filled with MIL-53Al-NH$_2$@xerogel and filling after drying; b) PXRD pattern of MIL-53Al-NH$_2$@xerogel.

It was tested if the filled column can be flushed with organic solvents using a standard HPLC system.[ss] Following the work of S. Liu, acetonitrile/H_2O mixtures were tested as eluents.[303] Unfortunately, the ram pressure increased constantly until it was too high to operate. As reference also the pure xerogel material was tested in a HPLC column with acetonitrile/H_2O mixtures as well as ethanol as eluent and the same effect was observed. Obviously the column packing is too dense. From SEM pictures (see ESI chapter 3.3) it is known that the particle size of the xerogel is very small and porosity of the xerogel is based on interparticular voids instead of intrinsic porosity. The use of higher MOF loading or additional porogens might be necessary to improve the system.

In conclusion the pre-polymerized MOF@polymer mixture could be altered successfully in a way that solvent is forced to pass through the MOF composite and cannot flow along the walls of the column. For application as HPLC column improvement of the system by using a polymer with intrinsic porosity or a porogen is necessary to reduce the high backpressure.

[ss] Tests on HPLC system were performed on the instruments and with the help of Prof. C. Czekelius.

5 Cooperation projects

5.1 Shaping of MIL-101Cr and MIL-101Cr-NH_2 for fixed bed adsorption of CO_2/H_2O mixtures

Cooperation with Herr Jens Möllmer, Institut für Nichtklassische Chemie, Leipzig

Background for this cooperation was a previous project, where MIL-101Cr and MIL-101Cr-NH_2 were investigated as CO_2 sorbents. Its large CO_2 uptake capacities, high adsorption enthalpy and high selectivity makes MIL-101Cr-NH_2 a suitable material for capturing CO_2 at low pressures.[304] An advantage with respect to other MOF materials, is the good water stability of MIL-101Cr-NH_2 which was proved in 40 cycles of water vapor ad- and desorption.[42]

For application in industry, specifically the CO_2 capture from flue gas is very interesting. Flue gas mostly contains a small amount of water. This water can be beneficial for CO_2 capture since when coordinating to open metal sites of the MOFs it increases the interaction with CO_2 (Lit.). On the other hand it can destroy the MOF structure in case of water labile MOFs. Therefore, the aim of this project was to investigate the CO_2/H_2O binary adsorption equilibriums for MIL-101Cr and MIL-101Cr-NH_2.

These kinds of measurements afford approximately 5 g of each material and are measured in a fixed bed column (Figure 143). The pellet size was asked to be in the range of 0.5 – 3 mm. The pellet size is important in terms of pressure and packing. If the pellets are bigger than 3 mm the packing is to loose and more material is needed, if the pellets are too small the ram pressure is too high for the measurement.

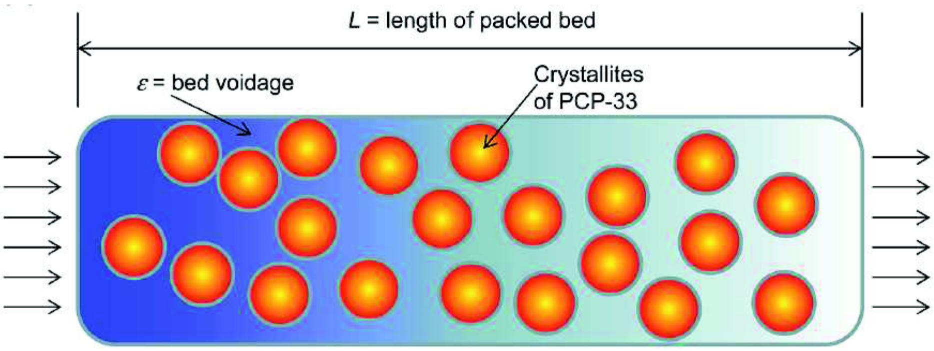

Figure 143: Schematic depiction of fixed bed adsorber for gas mixture separations. Reprinted from ref. [305], Copyright 2015, with permission from the Royal Society of Chemistry.

It is known from literature, that MOF do not withstand high pressures without loss of surface area. For example J. Ren and workers prepared spherical pellets of a Zr-MOF using 10% sucrose as binder and a centrifugal granulator. They report good mechanical stability for the resulting pellets, but surface area loss is about 50%.[306]

In this work it was shown, that both materials can be synthesized in the required quantity in good quality using hydrothermal batch procedures. Besides the mechanical stability of MIL compounds was investigated to develop a gently method which allows the shaping of powder MIL to pellets.

Each material was synthesized using multi-batch reaction process in an amount of 5 g. Characterization by TEM shows average particle sizes of 174 ± 35 nm for MIL-101Cr and 22 ± 5 nm for MIL-101Cr-NH_2 (Figure 144). Nitrogen sorption data as well as PXRD are shown in table XY and Figure 146.

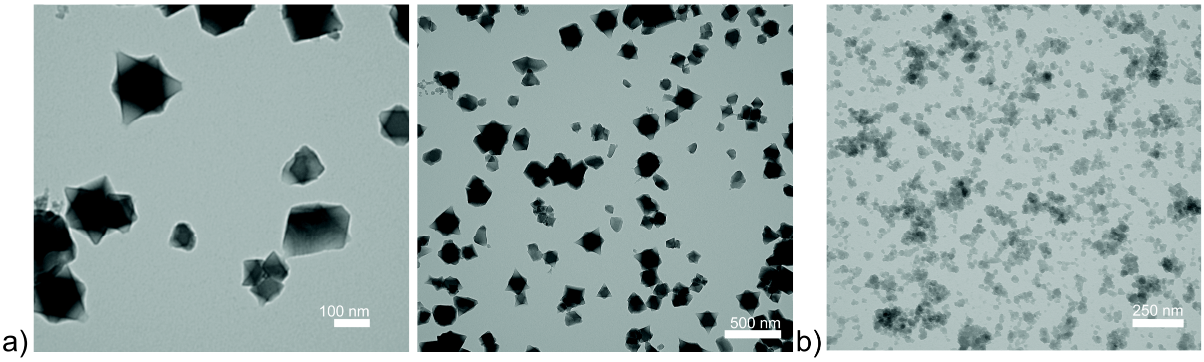

Figure 144: TEM pictures of a) MIL-101Cr and b) MIL-101Cr-NH_2

Pellets have been pressed with a common press for Infrared spectroscopy. The diameter of the sample holder comes to 1.2 cm. For each pellet 100 mg material was used. The powder was pressed at different pressures for 30 s. For sorption measurements the pellets were crushed and only bigger crumbs (no powder) were used for measurements (Figure 145).

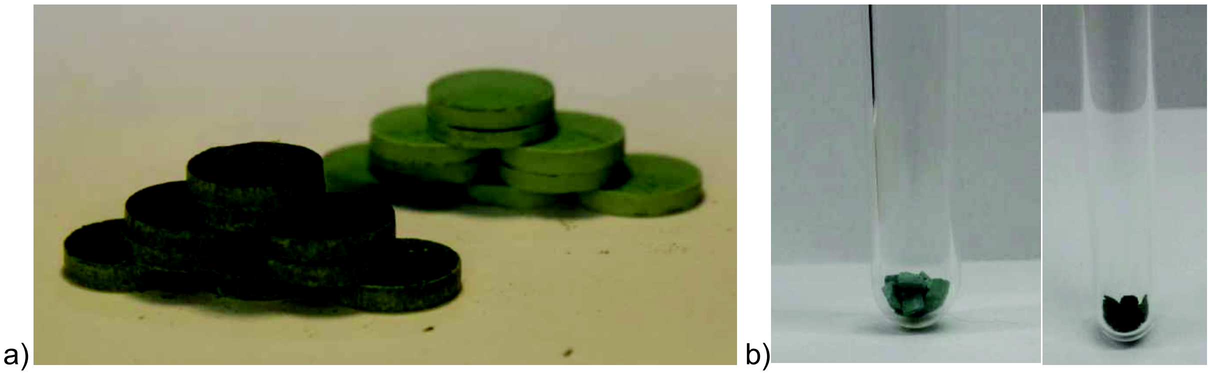

Figure 145: a) Pellets of MIL-101Cr and MIL-101Cr-NH_2 pressed at 0.5 kbar b) crumbs of MIL-101Cr and MIL-101Cr-NH_2 used for nitrogen sorption experiments.

Nitrogen sorption isotherms show significant decrease of surface area, whereas the decrease is more pronounced for MIL-101Cr as for MIL-101Cr-NH_2. Comparing the pellets pressed at 0.5 kbar, which is the lowest pressure which could be set, MIL-101Cr-NH_2 retained its surface area with 90%, whereas the porosity of MIL-101Cr was already decreased to 72% (Table 12).

Table 12: Properties of MIL-101Cr and MIL-101Cr-NH_2 pellets pressed at different pressures.

Material	S_{BET} [m^2/g]	Pore Volume^a [cc/g]	Surface area [%], related to parent material (100%)
MIL101Cr	3062	1.52	100
MIL101Cr_0.5kbar	2200	1.10	72
MIL101Cr_1kbar	1713	0.86	56
MIL101Cr_2kbar	971	0.50	32
MIL101Cr-NH_2	2463	1.47	100
MIL101Cr-NH_2-0.5kbar	2218	1.32	90
MIL101Cr-NH_2-1kbar	1904	1.13	77
MIL101Cr-NH_2-2kbar	1243	0.68	51

a) For pores smaller as 450 Å at $P/P_o = 0.95$.

The shape of sorption isotherms was mainly unchanged, except for MIL-101Cr-NH_2 at 2 kbar. Here, a kind of hysteresis can be observed during the desorption process. The calculated pore size distribution shows a new pore at 38 Å (Figure 146, Figure 147).

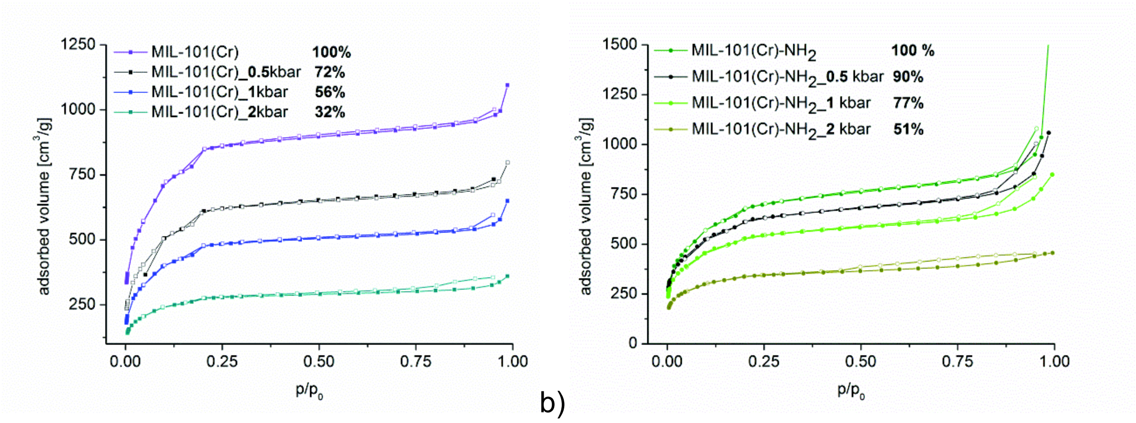

a) b)

Figure 146: N_2 sorption isotherms of a) MIL-101Cr and b) MIL-101Cr-NH_2 pellets using different pressures.

Also the crystallinity of samples decreased with rising pressure (Figure 147).

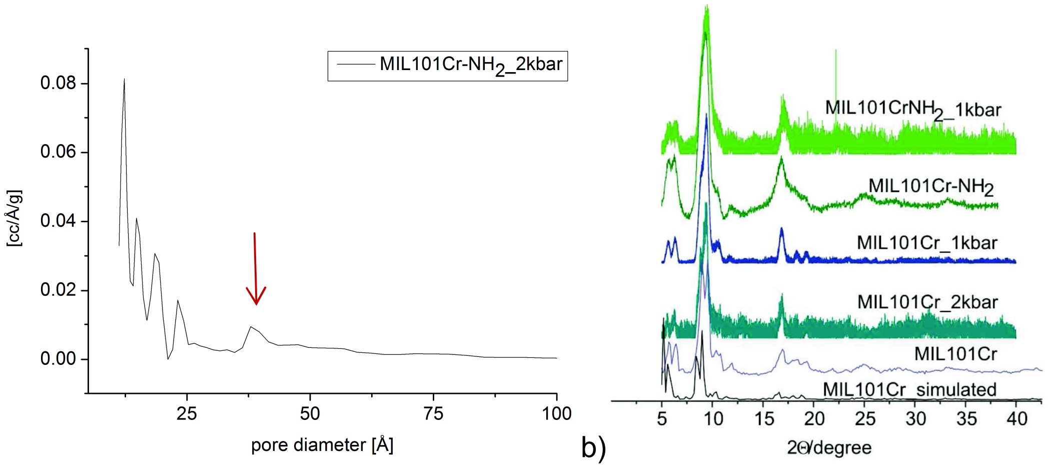

a) b)

Figure 147: a) pore size distribution for MIL-101Cr-NH_2_2kbar. b) PXRD pattern of MIL-101Cr and MIL-101Cr-NH_2 at different pressures.

In conclusion the mechanical stability of MIL-101Cr and MIL-101Cr-NH_2 was investigated at different pressures. Especially MIL-101Cr-NH_2 was found to be suitable for pellet formation at a pressure of 0.5 kbar on a surface of 1.2 cm in diameter, retaining its surface area up to 90%. With regard to the requirements for fixed bed adsorption, the pellets pressed at 0.5 kbar meet the challenge best, since they are sufficient stable and have the largest surface area.

The group of J. Möllmer performs the fixed bet adsorption measurements. This includes the CO_2 loading as well as mixed gas adsorption of CO_2 and H_2O. First results of CO_2 loadings are shown in Figure 148.

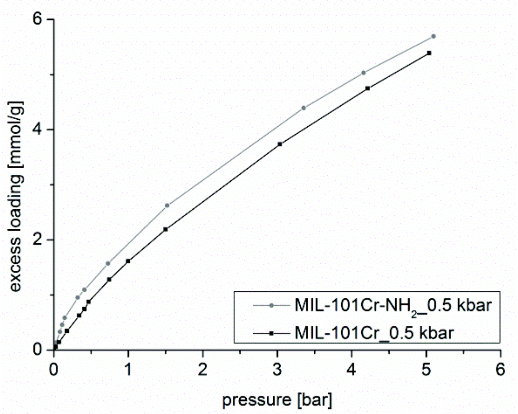

Figure 148: CO_2 at MIL-101Cr and MIL-101Cr-NH_2 crushed pellets at 25 °C.

Measurements are time consuming and are currently running.

5.2 Printing of defined patterns on substrates using nanoMOFs

Cooperation with Prof. Wim Defermé, TU Hasselt, Belgium

The aim of this project was to investigate the possibilities of immobilization of nanoMOF particles on different substrates. Using spray-coating and ink printing techniques a defined pattern should be produced on a glass or metal substrate.[307] According to instrument parameters, patterns with a line width of minimum 200 µm can be spray coated.
In general, there are two different strategies to generate thin films on surfaces, i) surface growth and ii) deposition on a surface. Growth of metal-organic framework thin films is an intensively investigated research area including also the family of SURMOF termed MOFs. A good overview is provided by reviews of A. Bétard[308], D. Bradshaw[309] and L. Heinke.[310]
To the best of my knowledge, only a few reports concerning the deposition of MOFs with printing techniques exist in the literature. Mostly substrates are immersed in precursor solutions and the MOF is formed by drying afterwards, as shown by J Zhuang and coworkers.[311]

An advantage using spray coating techniques for the deposition of nanoMOFs is that the pre-synthesized MOFs can be characterized completely, before suspended and deposited on the substrate. Hence, more control over the properties can be gained. Additionally, in principle every surface can be coated, for example metal, glass or also (flexible) polymer foils.

Unsatisfactory, no fixation on the substrate occurs as in the case of surface growth. Therefore, the adhesion between nanoMOF and substrate as well as further layers between nanoMOFs after spray coating has to be investigated and improved.

First nanoMOF particles of MIL-101Cr-NH_2 have been synthesized and characterized. MIL-101Cr-NH_2 exhibits a BET surface area of 1807 m^2/g. PXRD pattern shows the signals of MIL-101Cr, but signals are very broad, due to the small particle size (Figure 149).

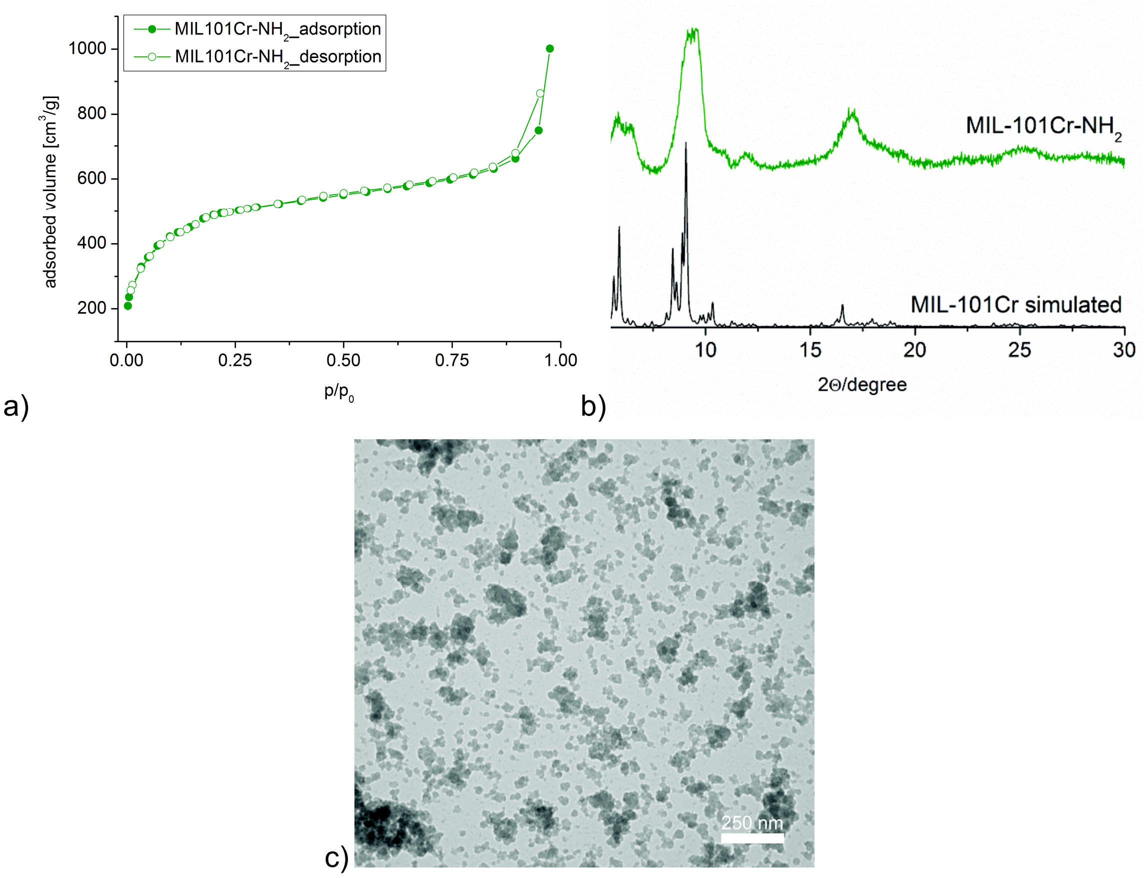

Figure 149: a) Nitrogen sorption isotherms, b) PXRD pattern and c) TEM images of nanoMOF MIL-101Cr-NH$_2$

By counting more than 50 particles, the particle size was determined to 22 ± 5 nm. Next, the MOF material was suspended in a mixture of water and sodiumdodecylsulfate (SDS) (Figure 150). The green suspension was treated with ultrasound and was stirred at room temperature overnight. It was observed that several minutes after stirring some MOF particles sedimented to the bottom. By adding the surfactant SDS the stability of suspension should be increased. Indeed, precipitation was slowed down.

Figure 150: a) Amount of MIL101Cr-NH$_2$ (0.9 g) which was suspended in H_2O (30 mL), b) suspension of 3 % MOF in 2 mL H_2O with SDS

After first spray coating experiments it turned out, that SDS interferes with the spray coating process and SDS had to be extracted from the mixture (sample 1). Therefore, the following suspensions were simply suspended in water (3%) (sample 2). For spray coating experiments glass substrates were used.

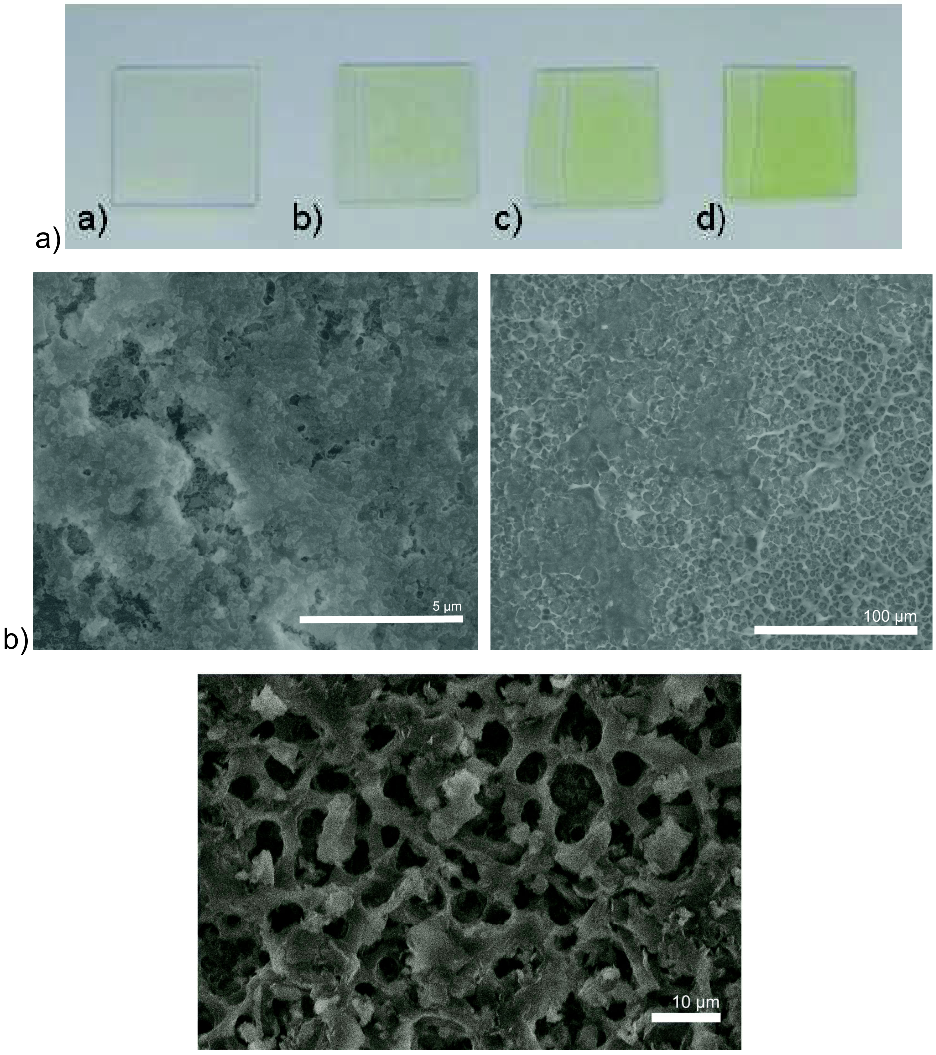

Figure 151: a) pictures of spray coated samples of MIL-101Cr-NH_2 on glass (sample 1a-d); b) SEM pictures of sample 1c.

From instrument parameters and nanoMOF concentration a rough estimation about the amount of material deposition can be stated (Figure 152).

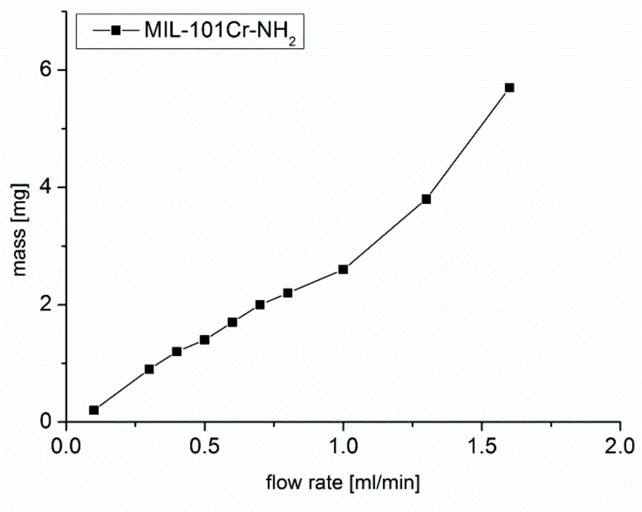

Figure 152: Estimation of the amount of MOF deposition [mg] in dependence of the flow rate (mL/min).

Next, it was proved if the nanoMOFs retain their properties after spray coating process, which is usually performed at higher temperatures between 100 – 200 °C. The substrate was too large for sample tubes of gas sorption and at least 10 – 20 mg of material is needed. Therefore, the coated nanoMOFs were separated from the substrate by ultrasonication in methanol. The suspension was dried and PXRD as well as nitrogen sorption were measured (Figure 153).

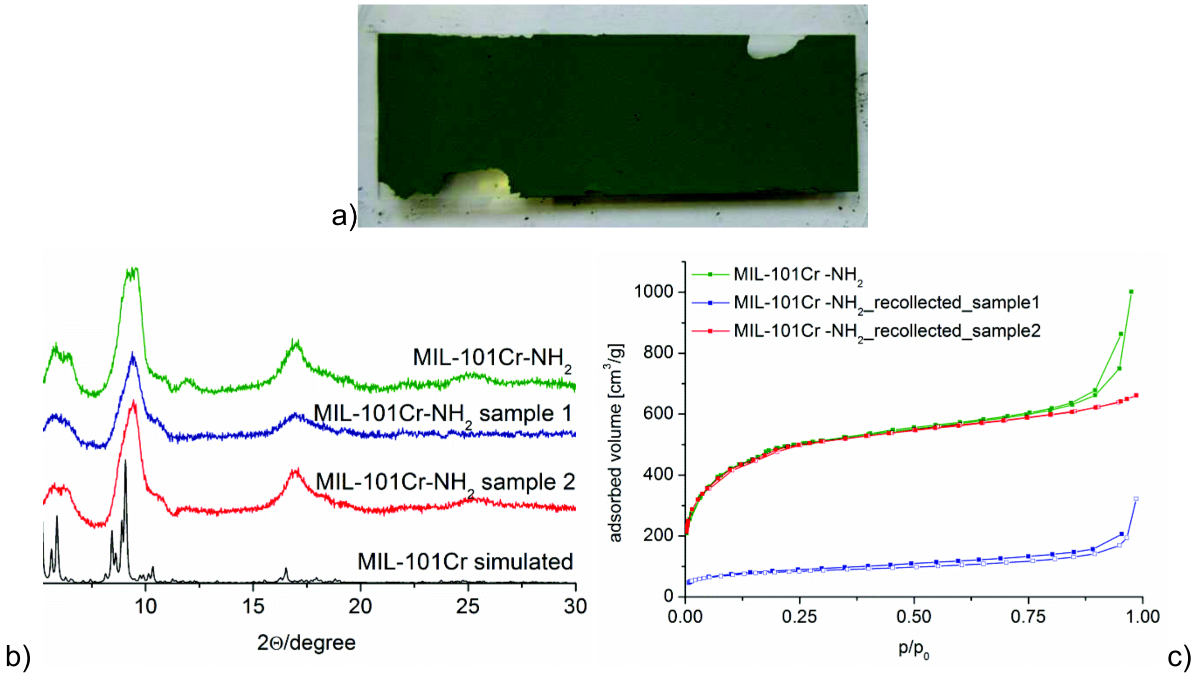

Figure 153: a) picture of sample 2, b) PXRD pattern and c) nitrogen sorption of recollected powder of sample 1 a-d; nitrogen sorption of pure MIL-101Cr-NH_2 (green), recollected sample 1 (blue) and recollected sample 2 (red).

As seen from PXRD pattern, crystallinity remained unchanged after spray coating for sample 1 and 2. In contrast, sample 1 shows a BET surface area of 298 m²/g due to pure porosity. The pure nanoMOFs exhibited a surface area of 1807 m²/g. Since sample 2 has a high surface area of 1744 m²/g, it can be concluded that SDS was not fully removed and influenced the accessibility of the MOF pores.

Using a suspension of nanoMOFs in water, porosity of the nanoMOF was retained after spray coating procedure (sample 2). Unfortunately, the MOF could be removed from the substrate very easily when rinsing with water or other solvents such as methanol. Obviously the adhesion between substrate and nanoMOF is not good enough. Therefore, two strategies were developed to improve the adhesion.

1) A binder can be applied to protect the nanoMOF layer. The binder has to be porous or at least open to diffusion in order to ensure accessibility. In context of heat transformation application several commercial available siloxane based binders were already tested for water vapour adsorption.[312],[313] The results are very promising since for the coated adsorbent the maximum adsorption capacity in comparison to the pure adsorbent could be retained.[313] Therefore, the binder Silikophen®[tt] is planned to be tested as stabilizer for nanoMOF coated glass substrates.

2) Together with Prof. Dr. Wim Defermé a second approach was developed which involves the covalent attachment of nanoMOF particles at the glass surface. Therefore, the glass surface is functionalized in a silanization procedure ending in a carboxylate moiety (Figure 154). By coupling of the amine group of the MOF linker and carboxylate of substrate through 1-Ethyl-3-(3-dimethylaminopropyl)carbodiimide (EDC) the nanoMOF can be attached covalently. A similar strategy was used for the attachment of MIL-53Al by B. Seoane *et al.*[314] *This attempt is pursued by the group of Prof. Wim Defermé.*

[tt] Silikophen ® was kindly supplied by Evonik.

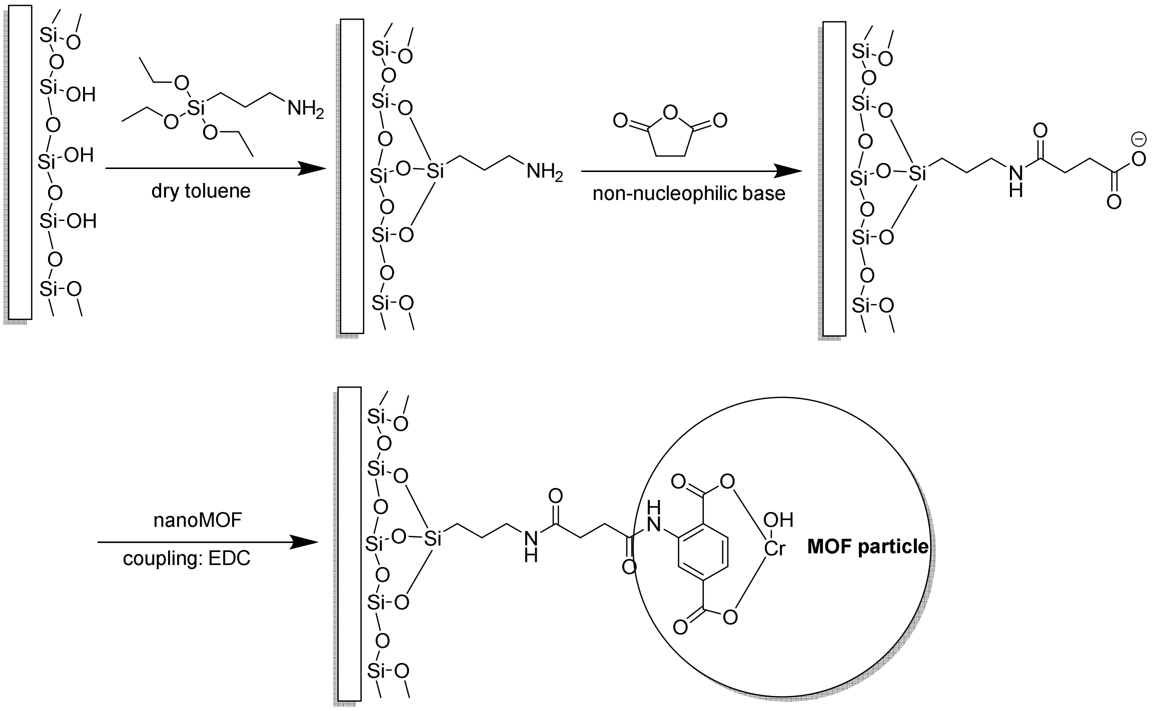

Figure 154: schematic depiction of covalent attachment of nanoMOF on the glass substrates.[uu]

Using the second approach a monolayer of nanoMOF on glass can be obtained. This is very interesting for catalysis. Furthermore, the adhesion between MOF particle layers still has to be improved. Both strategies can also be combined to improve the adhesion between substrate and nanoMOF as well as nanoMOF layers.

Unfortunately, the spray coating instrument broke at the end of September 2015. Therefore, due to hardware breakdown the project had to be paused. First attempts of coating with silanization were performed in April 2016, but could not be included in this work.

In summary, it was shown that nanoMOF particles of MIL-101Cr-NH_2 can be spray coated on glass substrates including retention of porosity. Further improvement of adhesion following the introduced strategies has to be done. Next step would be the spray coating of patterns on different substrates and evaluation of their mechanical stability (e.g. ISO 1519:2011, ISO 2409:2013, ISO 6272-1:2011-11).

The deposition of well characterized MOF particles is highly interesting for various applications since shaping of MOFs is a key issue for any industrial application.[251] In terms of catalysis, the immobilization of nanoMOF particles is interesting, since in previous projects (see chapter 3.1) it was shown that nanoMOFs have an increased catalytic activity, but their separation is difficult due the small size and low density. Here solvent stable immobilization on substrates with retention of pore accessibility can be the key.

[uu] Figure 154 was drawn by the group of Prof. Wim Defermé.

Contribution to the project: Done by Annika Herbst: Coordination of the project and elaboration of possible application fields. Synthesis of nanoMOF particles and suspension and characterization by PXRD, nitrogen sorption and partly SEM.
Done by Prof. Wim Defermé and coworkers: spray coating experiments and silanization (planned).

The project was forwarded to Irina Gruber in May 2016.

6. Summary

6.1 Catalysis with metal-organic frameworks

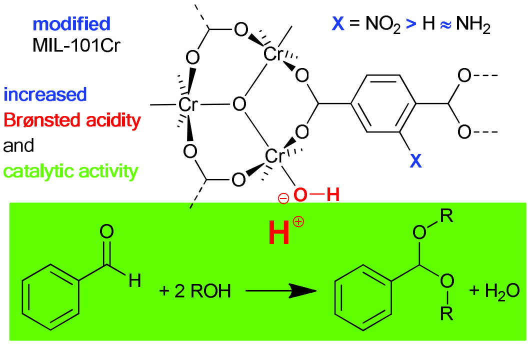

Figure 155: Investigation of determining factors for activity in diacetalization reaction in case of MIL-101Cr derivates. Reprinted with permission from ref.[71]. Copyright 2014 American Chemical Society.

On the basis of the diacetalization of aldehydes with alcohols as model reaction the influence of different tunable parameters of water stable MIL-101Cr derivatives on catalyst activity was investigated. The high surface area of MIL-101Cr materials was found to be not the decisive factor for high catalytic activity. Instead, the introduction of an electron withdrawing nitro-group to the terephthalate ligand of MIL-101Cr enhanced the catalytic activity significantly, although the BET surface area of the nitro modification MIL-101Cr-NO_2 (direct synthesis) was lower than that of the non-functionalized MIL-101Cr materials.

The heterogeneous nature of MIL-101Cr-NO_2 in the formation of dimethyl acetals was proven by filtration and multiple run experiments. In addition, it could be shown that very small amounts of nanoscale MIL particles of MIL-101Cr-NO_2 (<200 nm) already resulted in a high conversion compared with the bulk material. It was shown that about 2/3 of the catalytic activity comes from nanoMOF particles with a diameter below 200 nm. By comparing the activity of MIL-101Cr-NO_2 with homogeneous $Cr(NO_3)_3$ catalyst in a series of longer chained alcohols with benzaldehyde it could be shown that catalysis takes place inside the pores of the MIL materials. Investigation of Lewis vs. Brønsted acidity revealed that the activity can be explained by Brønsted-acid catalysis from deprotonation of the polarized aqua ligands, which is strongly enhanced for MIL-101Cr-NO_2.

The variation in Brønsted acidity of MIL-101Cr-NO_2 > MIL-101Cr ≈ MIL-101Cr-NH_2 correlated with the withdrawing effect of NO_2 and the diacetalization activity.

Therefore, MIL-101Cr and possibly other MILs can be active heterogeneous Brønsted-acid catalysts whose activity can be enhanced by electron-withdrawing linker modifications and small particle size.

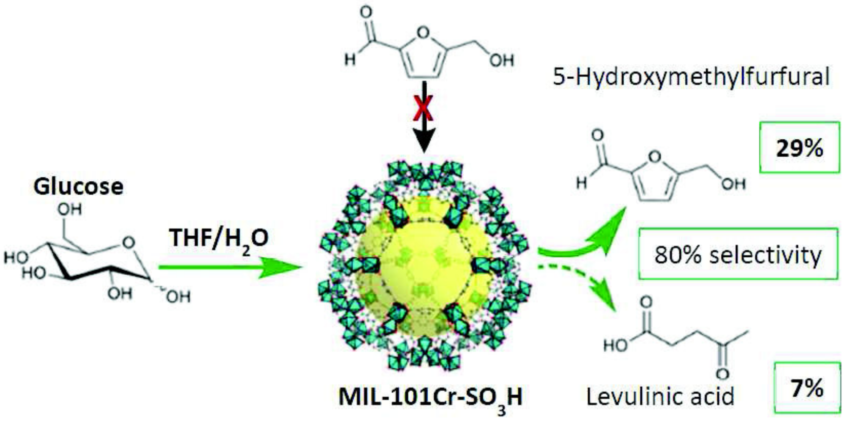

Figure 156: Investigation of MIL-101Cr derivatives for the cascade reaction of glucose to 5-HMF. Reprinted from ref. [118], Copyright 2016, with permission of the Royal Society of Chemistry.

Brønsted acid chemistry in MOFs, in comparison to the investigation of Lewis acid properties, just starts to attract attention, due to the limited amount of materials which are stable under highly acidic aqueous reaction conditions.

With the aim to contribute to the investigation of the scope of Brønsted acid chemistry in MOFs the gained experience was applied in a challenging reaction, the conversion of glucose to 5-HMF.

MIL-101Cr-SO_3H exhibiting electron withdrawing sulfonate groups as well as Brønsted acidic functionalities and a particle size below 200 nm was selected and compared with different nitro- and sulfo-modified MIL-101Cr compounds. From all four tested derivates MIL-101Cr-SO_3H gave the highest yield of 5-HMF from glucose, with 29% after 24 h. This yield is lower than results obtained with other solid acid catalysts, but at present the highest value reported for the glucose-to-5-HMF conversion catalyzed by metal-organic frameworks. MIL-101Cr derivatives have been regarded so far to be not able to catalyze this reaction due to missing *cis*-Lewis acid sites, here it was shown that a Brønsted acid pathway has to be taken into account. For the conversion of glucose to 5-HMF the presence of a small amount of H_2O is necessary, since in pure THF no product formation was observed. Interestingly, from pure 5-HMF as reactant, only very little production of levulinic acid could be detected, which is in contrast to results in literature using sulfuric acid or Amberlyst-70. The conversion of glucose, applying the standard reaction conditions and MIL-101Cr-SO_3H, sulfuric acid and Amberlyst-15 as catalysts, resulted in significantly different 5-HMF/levulinic acid product distributions. MIL-101Cr-SO_3H preferentially forms 5-HMF over levulinic acid in contrast to the other catalysts. The reactivation of the MOF catalyst remained a challenge, since pore blocking effects due to the formation of insoluble byproducts (humins) have been observed in multiple run experiments. Performing the reaction in ethanol led to partial derivatisation to 5-Ethyl-HMF, but yield of 5-Ethyl-HMF is still low. Nevertheless, the derivatisation of reactive groups of 5-HMF is a promising way, avoiding the formation of insoluble humins.

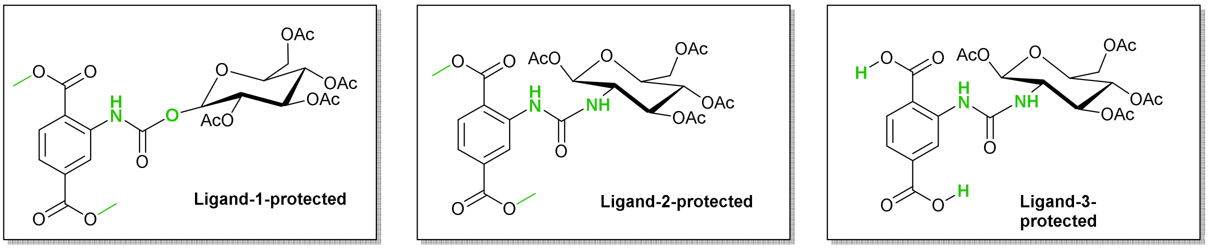

Figure 157: Development of linker design towards a chiral hydrophilic ligand, which is able to coordinate metal ions.

On the way to multifunctional MOFs, which are able to catalyze cascade reactions, it is necessary to combine different functionalities for catalysis. After identification of relevant attributes, Ligand-1 was designed, which is composed of terephthalic acid and glucose. Different synthetic strategies have been explored, which succeeded in the synthesis of Ligand-1-protected as well as Ligand-2-protected. Unfortunately, the deprotection turned out to be difficult. Therefore, the synthesis route was reevaluated and Ligand-3 was designed.

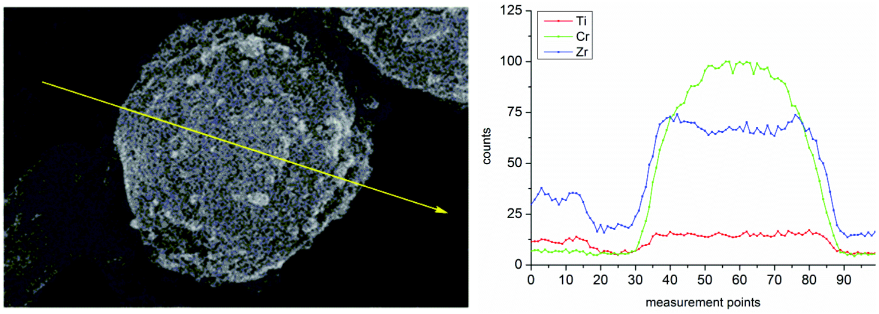

Figure 158: MIL-101Cr-SO_3H@metal oxide core-shell material.

In cooperation with Prof. X. Yangs group hierarchical core-shell systems of MOFs as core and metal oxides as well as silica as shell material have been developed. In addition to MIL-101Cr@SiO_2 composites (cooperation with PhD student Ying Jie), a method for the synthesis of MOF@metal oxide (MOF@MO) composites was developed. The influence of different concentrations was investigated. A method to slow down hydrolysis of the precursors was developed. The best results were obtained using MIL-101Cr-SO_3H, giving a porous MIL-101Cr-SO_3H@MO composite with a Cr:Zr ratio of 2:1 (atomic percent).

Unsatisfactory, the hydrolysis of metal oxides always lead to a significant formation of bulk material, which makes purification difficult. As strategy incorporation of metal nanoparticles as core was suggested and first attempts looked promising.

6.2 Shaping of metal organic frameworks

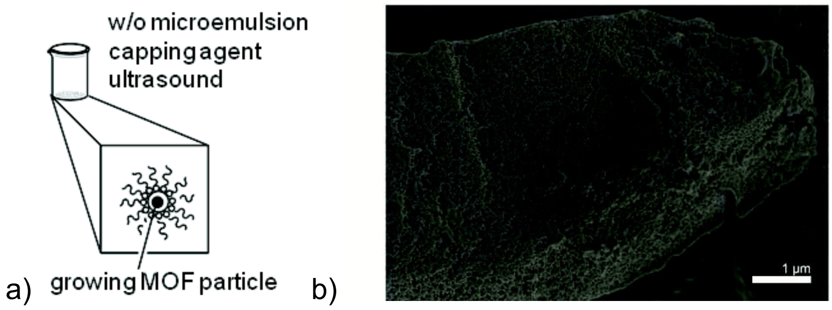

Figure 159: a) Bottom up approach for nanoMOF particle; b) hierarchical porosity in metallogels.

In a bottom up approach involving ultrasound energy, microemulsion and sodium oleate as capping agent, MIL-88AFe particles with a size below 100 nm have been obtained. Sodium oleate was investigated as surfactant for the formation of microemulsions and an optimized ratio of water/heptane and sodium oleate was determined. The synthesis method was optimized resulting in method B. Method B included the formation of two separate microemulsions which are finally added before processing with ultrasound.

A number of hierarchical micro-meso-macroporous compounds were obtained from Ligand-1-protected (MC-1) and chromium nitrate as well as from dimethyl-2-aminoterephthalate and glucose (MC-2) and dimethyl-2-aminoterephthalate with glucose penta-acetate (MC-3). MC-1 shows micro- and mesoporosity measured by nitrogen sorption as well as macroporosity, which was visible best from SEM images. In contrast MC-2 and MC-3 displayed lower or no macroporosity. Therefore, the formation of macro pores is attributed to the nature of Ligand-1-protected, although an explanation cannot be given at this point. All materials exhibited a pronounced hysteresis loop in nitrogen sorption measurements, but showed only very poor or no crystallinity. A number of reference experiments were performed in order to gain a better understanding of the material, whose molecular structure remained unclear. Finally, it was concluded that the solvent composition has a major effect on mesoporosity, but further experiments remain to be done.

Figure 160: a) Shaping of MOF powder into b) pellets or c) as coating on glass substrates.

Different shaping strategies in form of a) mechanical shaping (cooperation project); b) deposition on glass substrates by spray coating (cooperation project) and c) application of resorcinol-formaldehyde polymers as binding agent have been investigated. The resulting composites have been tested for mechanical stability and retention of properties in terms of accessibility of pores and crystallinity.

Mechanical shaping came along with a significant loss of surface area when applying pressures above 0.5 kbar. Deposition by spray coating resulted in a coating, which is tunable in thickness depending on the number of layers which are spray coated. The surface area of the material (MIL-101Cr-NH_2) was retained, but adhesion to the glass substrate was low. Two strategies (covalent attachment by silanization and fixation through a siloxane based coating) were conceptualized to improve adhesion. Due to hardware breakdown the project had to be paused and the ideas will be followed in future.

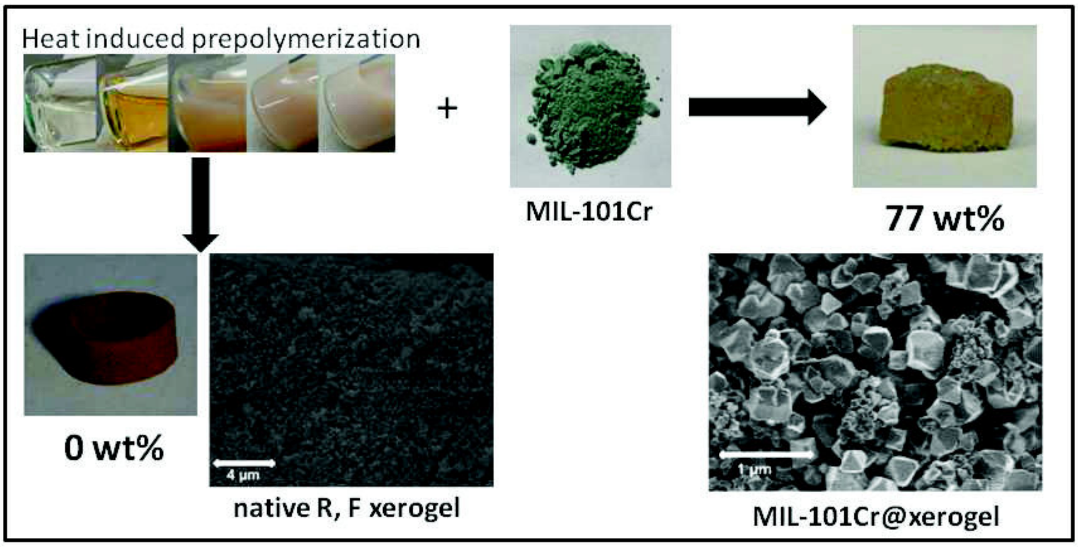

Figure 161: schematic depiction of synthesis of MIL-101Cr@xerogel composites.

A method for the synthesis of monolithic materials based on resorcinol-formaldehyde polymers as binding agent was realized successfully. MIL-101Cr@xerogel monoliths were obtained with variable weight percentages of MIL-101Cr. Embedding of the MOF, with largely avoiding pore blocking effects, was possible, because a heat induced pre-polymerization strategy was worked out. The MIL-101Cr@xerogel composites were characterized by powder X-ray diffraction, infrared spectroscopy, nitrogen- and water sorption and scanning electron microscopy. With the aim to embed as much MIL-101Cr as possible, the pre-polymerization strategy was amended by the addition of water during the mixing of MOF and polymer. In this way, embedding up to 77 wt% of MIL-101Cr particles was possible, yielding monoliths which matched the wt%-correlated BET values and water uptakes within experimental error. The hierarchical nature of the 77 wt% MIL-101Cr@xerogel-H_2O composite led to a higher water uptake at low pressures compared to bulk MIL-101Cr (0.79 g/g water uptake at $P/P_0 = 0.5$, for bulk MIL-101Cr 0.57 g/g water uptake at $P/P_0 = 0.5$). In addition, the synthesis of MOF@xerogels was extended to amine modified MOFs such as MIL-101Cr-NH_2, MIL-101Al-NH_2 and MIL-53Al-NH_2. Nitrogen sorption and PXRD measurements revealed that MOF@xerogel composites using MIL-101Cr-NH_2 and MIL-53Al-NH_2 were synthesized successfully, whereas MIL-101Al-NH_2 seemed to decompose under the applied conditions. The MOF@xerogel mixture could be altered successfully without shrinking, which is important for application as HPLC column material. The MIL-53Al-NH_2@xerogel composite was fabricated in a HPLC column to investigate the direct applicability. Unsatisfactory, the system was found to be not suitable because of too high ram pressure.

7. Outlook

Outlooks close to the respective projects of the unpublished part were already given at the end of each subchapter. At this point, an overall outlook for the areas of shaping of MOFs and catalysis with MOFs is given with respect to the presented projects (3.1-3.3).

Shaping of metal-organic frameworks

The synthesis of MOF@xerogel composites can be regarded as proof of concept for the successful formation of monolithic materials, where the MOF retains its porosity and pores remained accessible for vapor sorption. Nevertheless, for application regarding a) water sorption, b) catalysis and c) separation, the composites have to comply with additional requirements.

a) Application in water sorption

Gels can be dried with supercritical CO_2, the resulting aerogels have different properties than conventionally dried xerogels. This drying method could be investigated for the MOF-R,F composites. Maintaining the pre-polymerization strategy, resorcinol formaldehyde polymers should be replaced by more hydrophilic materials. As a consequence, more water can potentially be adsorbed through the contribution of the polymer material. Possible materials can be cellulose or chitin based xerogels and aerogels.[315],[316]

b) Application in catalysis

For application in catalysis the accessibility of pores not only for nitrogen or water, but also for larger molecules has to be given. Still, this should be investigated for the obtained composite materials. In addition, varying the hydrophilicity and hydrophobicity of the polymer part as well as of the MOF can have significant influence on substrate interactions and uptake and should be investigated more deeply.

c) Application in separation

Separation of compounds, for example in HPLC columns or solid phase extraction devices, also requires permeability for substrates. As learned from presented experiments, improvement of the system by using a polymer with intrinsic porosity or a porogen is necessary to reduce the high ram pressure. In addition, it would be beneficial to gain a better control about shrinking upon drying, which could be achieved by changing the kind of polymer.

Catalysis with metal-organic frameworks

With the objective of expanding the scope of reactions catalyzed by MOFs, due to their unique properties, still, intensive research is necessary.

The presented project revealed excellent catalytic activity for MIL-101Cr-NO_2 in the diacetalization of benzaldehyde. The filtration experiments showed that the small amount of MOF nanoparticles seemed to be responsible for the major activity in diacetalization. This rationale can be used to reduce the amount of catalyst material significantly. Associated with the small size of nanoMOF particles is a more difficult separation. It would be desirable to immobilize the nanoMOF particle on a support in order to facilitate their separation and in consequence also their application.

For the conversion of glucose to 5-HMF using MIL-101Cr-SO_3H promising results have been obtained with potential to be improved. With the aim to further optimize the acid strength of MIL-101Cr-SO_3H or other suitable MOFs, a deeper understanding of reaction mechanism in MOFs has to be gained. The long reaction time exceeding 24 h, together with the insight from the molecular formula of MIL-101Cr that no *cis* metal sites for isomerization from glucose to fructose exist, a Brønsted acid mechanism has to be considered.

In addition, other highly Brønsted acidic MOFs as UiO-66-SO_3H[70],[91], sulfated MOF 808[317] or recently developed NUS-6-Hf[108] could be investigated for the conversion of glucose to 5-HMF using the same reaction conditions. UiO-66 was previously shown to possess a tunable amount of open metal sites, generated by defect engineering, which can act as Lewis acid sites.[138] Therefore, UiO-66 and UiO-66-SO_3H might serve as reference materials for the elucidation of reaction mechanism.

A critical point in glucose conversion is the formation of humins, which is promoted by long reaction times. The reaction in ethanol led to the successful formation of 5-Ethyl-HMF, but resulted in low yields. Following this strategy of “protection” of the reactive groups of 5-HMF in course of the reaction can be a promising approach to enhance the overall yield and reduce the amount of humins. Hence, the MOF catalyst could be reused, which is a crucial point in heterogeneous catalysis. In consequence, the investigation and optimization of synthesis conditions using ethanol or other “protecting agents” should be continued.

Furthermore, the adjustable acidity of MOF catalysts could be used for other acid catalyzed biomass based transformations as highlighted in the introduction. Still, one of the main criticisms about MOF catalysis is stability of metal-organic frameworks, especially water stability. Although it is highly desirable to perform reactions in H_2O as a green solvent,[318] as pointed out in the beginning, the repertory of MOFs which are highly stable in water and acidic or basic conditions is rare.[44],[45] As the number of new MOF structures continuously grows, computational methods will gain in importance to analyze structure-property relations. Resources in form of several databases are available for screening of MOFs. Important developments are summarized by the group of R. Q. Snurr.[319],[320] Gaining profit from the experience of last 20 years of research it would be reasonable to make greater use of high-throughput screening and modeling instead of looking for a needle in a haystack.

Key challenges, but at once great potential when achieving predictability, are a better understanding of MOF/linker – substrate interactions, modulation of hydrophilicity/ hydrophobicity of the pore microenvironment as well as the investigation of hierarchical porous systems.

MOF catalyst design benefits of the toolbox of methods which have been developed during the last 20 years and ongoing attempts. Acid catalysis is predestinated for cascade reactions, for instance in combination with hydrogenation or oxidation reactions.

Regarding the variety of organic linkers, introduction of chirality as well as immobilization of metal catalysts are highlights and will serve even greater attention in future.

A smart approach of metal immobilization was described by S. A. Burgess *et al.*[321]

They constructed a porous carboxylate coordinated Zr MOF based on Pd aryl diphosphinite pincer complexes (Figure 162). The resulting MOFs exhibit a BET surface area of 1164 m^2/g. Via anion exchange the I^- was replaced by trifluoracetate which resulted in a decrease in surface area to of 594 m^2/g. The resulting MOF demonstrated good catalytic activity for transfer hydrogenation of aldehydes, whereas the analogues homogeneous complex turned out to be ineffective as a result of decomposition under the catalytic conditions.[321] On the one hand, this example illustrates the potential of rigid immobilization in the MOF framework towards new heterogeneous catalysts. On the other hand, the embedding of metals to the ligand design allows maintaining the accessible pore volume and can be combined with organic functionalities on other linkers which is reminiscent of the working principle of enzyme.

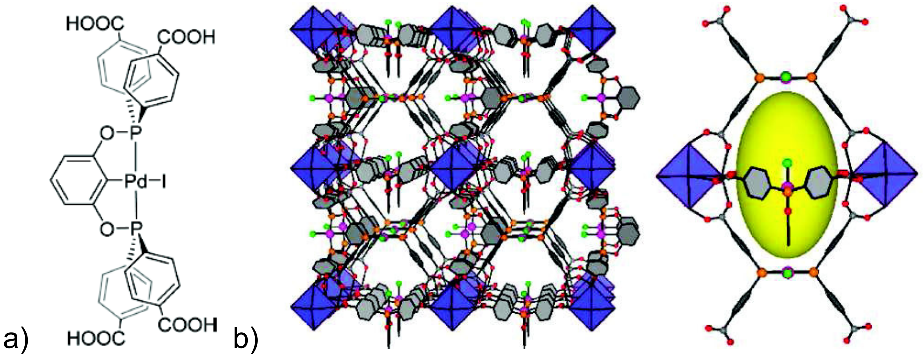

Figure 162: a) linker of the resulting MOF; b) framework structure of 1-X. and view of a portion of the framework showing ovoidal pores. Blue octahedra represent $[Zr_6O_4(OH)_4]^{12+}$ building units Reprinted with permission from ref [321]. Copyright 2016 American Chemical Society.

MOFs are often discussed as synthetic analogues for enzymes and development of biomimetic MOFs already started. Recent developments are summarized by Z. Gu *et al.*[219], M. Zhao *et al.*[220] and Y. Chen *et al.*[322]. M. D. Allendorf *et al.* compared the structural organization of proteins and MOFs.[323] Whereas enzymes catalyze numerous transformations with high selectivity and enzyme engineering attracted much interests during recent years in industrial applications[324], MOF catalysts are still in its infancy.

Theoretical studies of S. C. L. Kamerlin *et al.* revealed that the backbone or framework of for instance the alkaline phosphatase superfamily is a relatively rigid architecture, whereas the active sites are sensibly influenced by changes of the amino acids.[325]

Kamerlin *et al.* concluded: "*Examination of transition-state geometries and the contribution of individual residues to the calculated activation barriers suggest that the broad promiscuity of these enzymes arises from cooperative electrostatic interactions in the active site, allowing each enzyme to adapt to the electrostatic needs of different substrates. By comparing the structural and electrostatic features of several alkaline phosphatases, we suggest that this phenomenon is a generalized feature driving selectivity and promiscuity within this superfamily and can be in turn used for artificial enzyme design.*"[325]

Obvious similarities rule MOFs in as promising candidates for artificial enzymes. Hence, electrostatic interactions might be realized in a MOF based on coordinated anions to metal nodes as described by B. Manna *et al.*[326] or by cation/anion pairs, introduced by linker as depicted in Figure 163.

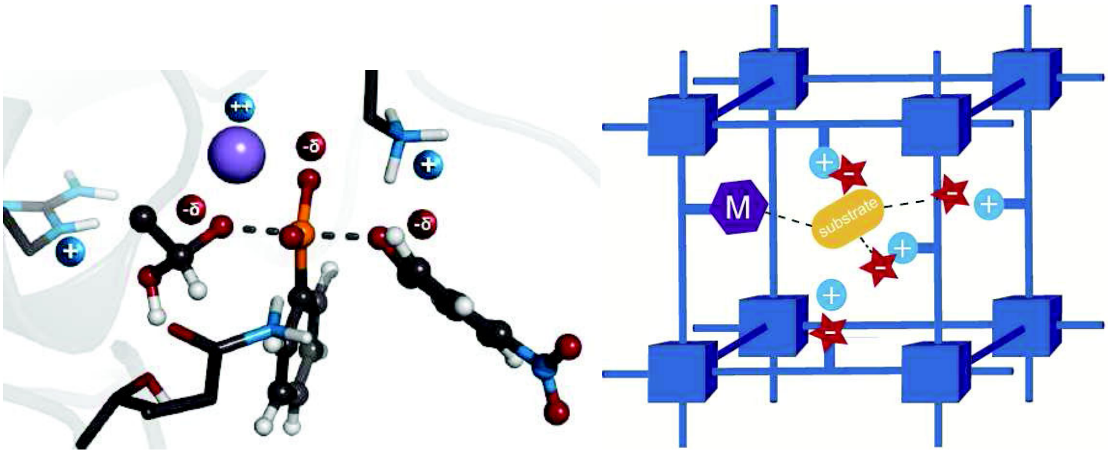

Figure 163: Active site model of alkali phosphatase[325] versus MOF model. Reprinted with permission from ref [325]. Copyright 2015 American Chemical Society.

The multipoint interaction through different coordination functionalities is a promising approach to orientate substrates and stabilize intermediates during the reaction.

A direct and fair comparison of multifunctional MOF catalysts in multi-cascade reactions, with the use of several MOFs, each able to catalyze one reaction, might help to elucidate determining parameters for new highly efficient catalysts (Figure 164). Examples for valuable products based on cascade reactions are for instance the reaction of 5-HMF to 1,6-hexandiol[327] or the direct synthesis of 2,5-furandicarboxylic acid.[328]

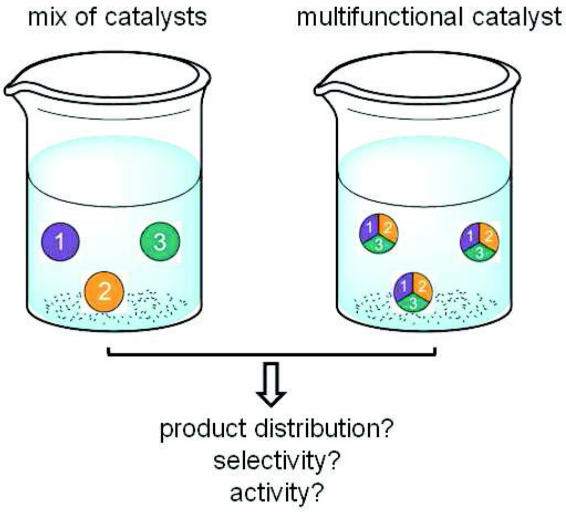

Figure 164: Schematic depiction of the comparison between mixing of catalysts with different functionalities (1-3) with multifunctional catalyst.

Which system is superior in terms of activity? Will they have the same selectivity towards products? Which impact have diffusion rate and pore confinement in this context? Questions which hopefully will be answered by research community in future.

8. Experimental part

8.1 General section

All experiments were carried out with exposure to air unless otherwise stated.
All glassware was cleaned by storage in a KOH/isopropanol bath overnight followed by storage in a diluted HCl bath overnight. Between both baths and after the HCl bath, the glassware where rinsed with deionized water and finally dried overnight in an oven at 373 K. Ultrasonic treatment for nanoMOF experiments were performed by a Vibra Cell horntype ultrasound reactoer (pictures see chapter 4.3.1) from Sonics. Centrifugation and filtration steps were carried out on centrifuges EBA 3S and Rotina 46 from Hettich as well as on high-performance centrifuge Allegra 64R, Beckmann Coulter. MOFs or MOF composites were hydrothermally or solvothermally synthesized using an oven from Memmert with programmable temperature ramps.

Chemicals and solvents (p.a. grade) were commercially purchased and additionally purified as noted in Table 10.

Table 10. Chemicals and solvents.

Chemicals	**Purity**	**Source**	**Additional purification**
Acetic anhydride	> 99 %	Riedel-de Haen	
2-Aminoterephthalic acid	> 99 %	Acros Organics	-
Cetyltrimethylammonium bromide	≥99 %,	Carl Roth	
$Cr(NO_3)_3 \cdot 9H_2O$	99 %	Acros Organics	-
CrO_3	99 %	Alfa Aesar	-
1.4-Diazobicyclo[2.2.2]octane	> 99 %	Sigma Aldrich	
4-Dimethylaminopyridin	> 99 %	Sigma-Aldrich	
Dimethyl-(2-amino)terephthalat	≥ 97 %	Sigma Aldrich	
Di-tert-butyldicarbonate	≥ 98 %	Fluka	
Formaldehyde	24 % in H_2O, not buffered	VWR	-
D-(+)-Glucose	> 99.5 %	Sigma Aldrich	
Hydrochloric acid	p.a., 37 % in H_2O	Fisher Chemical	-
Iron chloride-hexahydrate	≥ 98 %	AppliChem	
Na_2CO_3	≥ 99.8 %	Riedel-de Haën	-
$NaOD/D_2O$	40 % in D_2O	Sigma-Aldrich	
NaOH	99.99 %	VWR	-
Nitric acid	p.a., 65 % in H_2O	AppliChem	-
Resorcinol	98 %	Acros Organics	-
2-Sulfoterephtalic acid, monosodium salt	>98.0%	TCI	
Terephthalic acid	> 99 %	Acros Organics	-
Tetramethylammonium hydroxide	25 % in H_2O	Alfa Aesar	-
Titanium(IV)isopropoxide	≥ 97 %	Sigma Aldrich	
Triphosgene	98 %	Sigma-Aldrich	
Zirconium(IV)propoxide solution	70 wt. % in 1-propanol	Sigma-Aldrich	
Solvents	**Purity**	**Source**	**Additional purification**
Acetic acid	p.a., 99.9 %	VWR	-
Acetone	p.a., 99.9 %	VWR	-
Acetonitrile	p.a., 99.9 %	Fisher Chemical	or from solvent drying machine
DMF	p.a., 99.99 %	Fisher Chemical	-
Ethanol	p.a., 99.9 %	VWR	-
Ethyl acetate	p.a., 99.9 %	Fisher Chemical	
n-Heptane	p.a., 99.7 %	VWR	
n-Hexane	95 %	Acros Organics	

Methanol	p.a., ≥ 99.99 %	Fisher Chemical	-
THF	p.a., 99.6 %	VWR	Distillated to remove stabilizer
Toluene	p.a., 99.99 %	Fisher Chemical	Dried over molecular sieve (4 Å)

8.2 Analytical methods

Powder X-ray diffraction (PXRD)

Powder X-ray diffraction patterns were carried out at ambient temperature on a Bruker D2 phaser (300 W, 30 kV, 10 mA) using Cu-Kα radiation (λ = 1.54182 Å) between $5° < 2\Theta < 40°$ with a scanning rate of 0.006 °/s. The diffractograms were obtained on a flat "low background sample holder", in which at low angle the beam spot is strongly broadened so that only a fraction of the reflected radiation reaches the detector, hence the low relative intensities measured at $2\Theta < 7°$. Analyses of the diffractograms were carried out with the 'STOE WinXPOW 1.10' software and "Match" software.

Fourier transform infrared spectroscopy (FT-IR)

Infrared spectra were measured on a Bruker TENSOR 37 IR spectrometer at ambient temperature in a wavenumber region of 4000–500 cm^{-1}. Solid compounds were measured in a KBr disk. For preparation of the KBr disks, the samples were well ground with an excess of KBr (20–40 fold amount) in an agate mortar followed by pressure/vacuum treatment in a RIIC England/London 30 ton press (10 ton were used). Evaluations of the spectra were done with the software 'OPUS 7.2'. This instrument was also used for mechanical pressure shaping of MOFs.

Nitrogen, water and methanol sorption analyses

Nitrogen (purity 99.9990 %) physisorption isotherms were carried out on a Nova 4000e from Quantachrome at 77 K. Water and methanol physisorption isotherms were measured volumetrically on a Quantachrome Autosorb iQ MP at 293 K. Before measuring of the isotherms, the products were transferred into glass tubes capped with septa, which were weighted out before. These tubes were attached to the corresponding degassing port of the sorption analyzer, degased under vacuum at elevated temperature, weighted out again and then transferred to the analysis port of the sorption analyzer. For determination of the cold and warm free space of the sample tubes helium gas was used. BET surface areas were calculated from the nitrogen adsorption isotherms in the $P \cdot P_0^{-1}$ range of 0.05–0.2. Total pore volumes were calculated from the nitrogen sorption isotherm at $P \cdot P_0^{-1} = 0.95$. DFT calculations for the pore size distribution curves were done with the native 'NovaWin 11.03' software using the ‘N_2 at 77 K on carbon, slit pore, NLDFT equilibrium’ model.[vv] For vapor sorption measurements the ‘ASiQwin 3.01’ software was applied.

Supplement:

Pore size distributions are calculated values and different DFT models can be applied.

MIL-101Cr is the most used material in this work, Therefore, exemplarily the effect of different DFT models was compared. The measured adsorption volume is compared with the fitted volume from which the pore size distribution is calculated. The quality of calculation model was assessed by the fitting error (%). For MIL-101Cr two models were find to fit based: a) ‘N_2 at 77 K on carbon, slit pore, NLDFT equilibrium’ model, fitting error: 0.32 % and b) ‘N_2 at 77 K on silica, cylindr. pore, NLDFT equilibrium’ model, fitting error: 0.15 %. In Figure 165 the fitting curve vs. measured volume for both models is shown. Pore size distributions were calculated accordingly and have been compared in Figure 166.

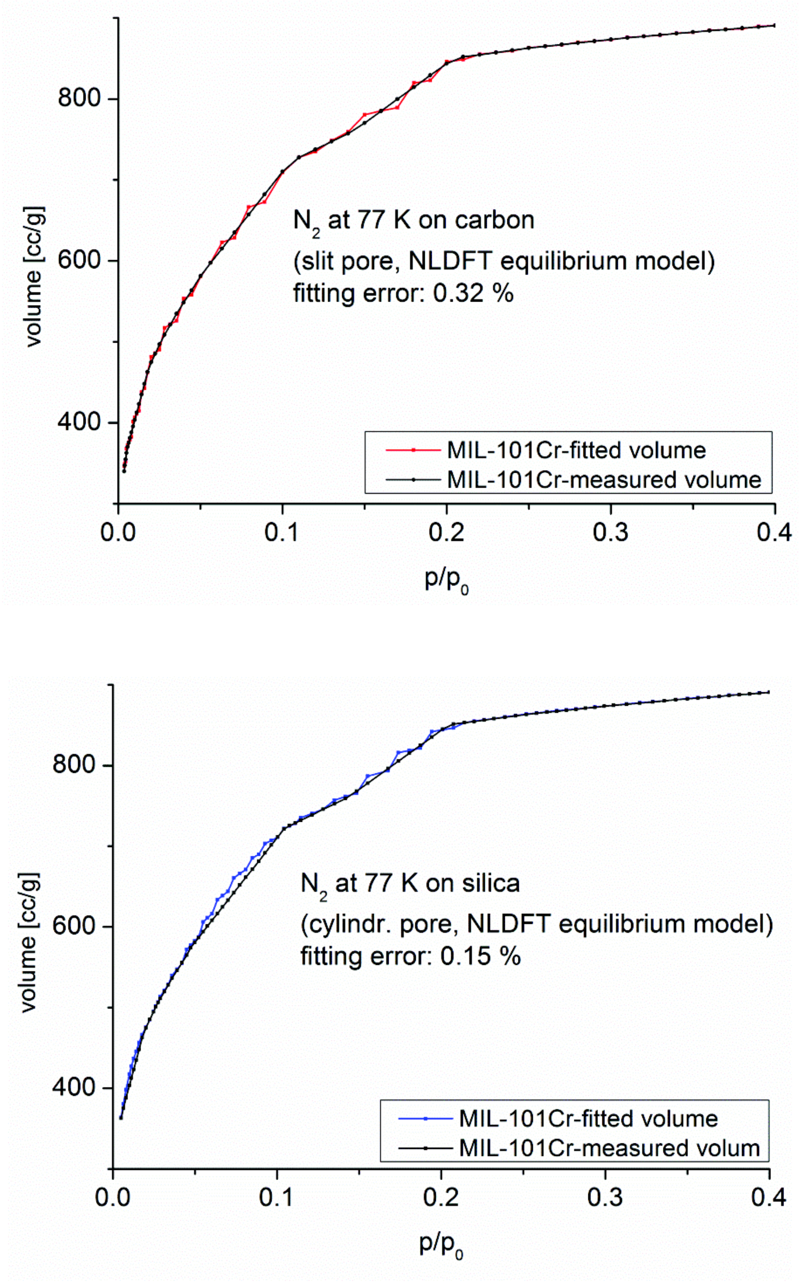

Figure 165: Fitting curve vs. measured volume for MIL-101Cr using different DFT models.

It is clearly visible that pore size differs significantly from each other. The given pores have different sizes as well as different amount volume. Although the fitting error is quite low in both cases, comparison, for example with literature, is not reliable if not the same model is used. Besides as also reported in literature a really reliable DFT method for MOFs is not yet developed.[329]

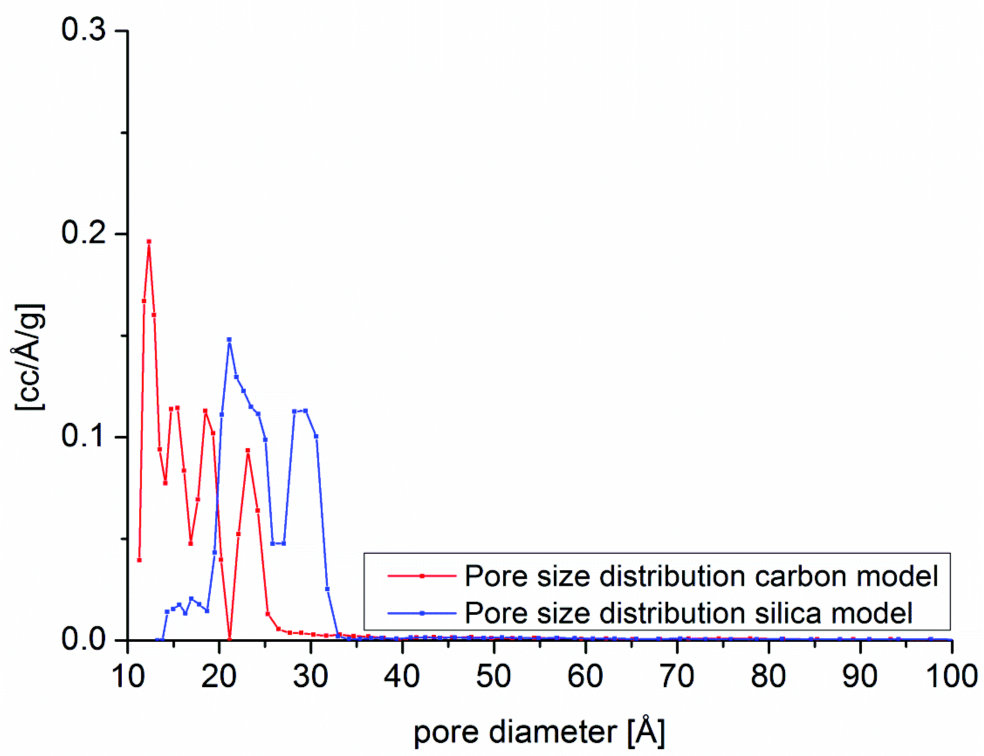

Figure 166: Pore size distribution for MIL-101Cr using different DFT models.

For this work for all pore size distributions the N_2 at 77 K on carbon, slit pore, NLDFT equilibrium' model was used. The fitting error is given in brackets for each measurement. With regard to the uncertainty of absolute pore sizes, this aspect is no given much importance.

NMR spectroscopy

Solution NMR spectra were recorded on a Bruker Avance DRX200 operating at 200 MHz for ^{1}H or a Bruker Avance III – 600 and 300 and a Bruker Avance DRX 500 spectrometer. The proton NMR spectra were calibrated against the residual proton resonances of the deuterated solvent relative to tetramethylsilane: D_2O/NaOD δ_H = 4.79 ppm, $CDCl_3$ ^{1}H: $\delta = 7.26$ ppm and DMSO-d_6 $\delta = 2.5$ ppm.
Preparation of the NMR tubes was carried out with exposure to air. Analysis of the ^{1}H NMR spectra was done with Mestrenova 10.0.

Scanning electron microscopy

Scanning electron microscopic images were recorded on following devices
(Information about sputtering of the samples before measuring is given in the brackets):
LEO 982 from Zeiss with a schottky field electron emission cathode (steaming with chromium; approximately 10 nm thickness).

LEO 1430 VP from Zeiss with a tungsten cathode (coating with Au for 180 sec at 30 mA by an AGAR sputter coater).
Quanta 400 FEG (ESEM) from Fei. Electrons are generated by field emission (coating with Au using an Emitech K550 sputter for 3 min at 15 mA).
JSM-6510 from Jeol with a LaB_6 or W cathode (coating Au for 15 - 20 sec at 35 mA by Jeol JFC-1200 sputter).

Transmission electron microscopy

TEM measurements were conducted with a FEI Tecnai G2 f20 with a FEG operated at 200 kV at the Ernst-Rusca centrum of Forschungszentrum Jülich.

Dynamic light scattering (DLS)

DLS experiments were carried out with a Malvern Zetasizer Nano S instrument working at 633 nm wavelength. Note that DLS measures the hydrodynamic radius which is larger than the individual dimensions of a particle.

X-ray photoelectron spectroscopy,

XPS-(ESCA-)measurement was performed with a Fisons/VG Scientific ESCALAB 200X xp-spectrometer, operating at room temperature, a pressure of $1.0 \cdot 10^{-9}$ bar and a sample angle of 30°. Using this spectrometer, electron spectra were recorded using polychromatic Al-Kα excitation (14 kV, 20 mA) and an emission angle of 0°. Calibration of the XPS was carried out by recording spectra, using Al K_{alpha} X-rays, from clean samples of copper, silver and gold, at 20 eV and 10 eV pass energies and comparison with reference values.

Gas chromatographic (GC)

GC studies were done with a GC-2014 Shimadzu instrument coupled with a flame ionization detector, and a GC-MS on a Finnigan Trace DSQ with Finnigan Trace GC Ultra System. GC Parameters: Autosampler injection volume 1.0 µl, rinses with solvent pre-run 1x, post-run 2x, rinses with sample 2x; injector temperature 240 °C; column information: Ultra 2, length: 25 m, inner diameter: 0.20 mm, film thickness: 0.11 µL, column temperature 50 °C, maximum temperature: 320 °C
Thermogravimetric analyses

The thermogravimetric analysis curves were measured on a TG 209 F3 Tarsus from Netzsch in a temperature range of 303–873 K, with a temperature gradient of 5 $K \cdot min^{-1}$, using the software 'Netzsch Measurement 5.2.1'.

Atomic absorption spectrometry

The quantification of the chromium content of the MIL-101Cr derivatives for catalysis project (chapter 3.1) was done with a Perkin Elmer AAnalyst100 instrument (flame AAS, acetylene/air as firing gas, burner head length: 10 cm). $Cr(NO_3)_3 \cdot 9\ H_2O$ was chosen as material for the preparation of the Cr(III) standards in methanol. The concentrations of the standards were 0.1 ppm and 0.5 ppm, which correspond to absorptions of 0.005 and 0.053, respectively.

8.3 Syntheses

8.3.1 Synthesis of a glucose modified terephthalic acid linker

Synthesis of compound A[180]

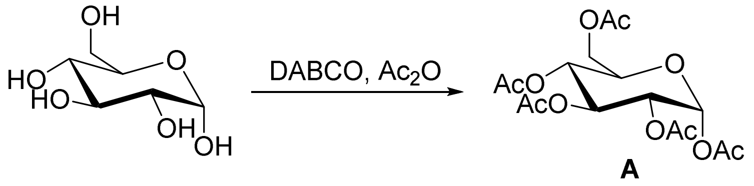

Glucose (5.0 g, 25.8 mmol) was dissolved in acetic anhydride (14.8 mL, 30.9 mmol). 1,4-Diazabicyclo[2.2.2]octane (DABCO) (2.9 g, 25.8 mmol) was added slowly under stirring. The reaction mixture was stirred for 24 h at 50 °C. The reaction progress was monitored by thin layer chromatography (TLC) (ethylacetate/hexane 3:2, $KMnO_4$ as staining reagent). After completion of the reaction the mixture was poured into ice cold water. A white solid precipitated, which was separated by filtration, washed with ethanol and dried *in vacuo*. The product was obtained in 90 % yield.

MS (ESI): *m/z* (%) = 408.3 $[M+NH_4]^+$, 413.2 $[M+Na]^+$

^{1}H-NMR (300 MHz, dmso-d_6) δ[ppm] = 6.07 (m; 1H); 5.40 (d; 1H); 4.99 (m; 2H); 4.19 (m; 2H). 4.01 (m; 1H).

Synthesis of compound B[181],[182]

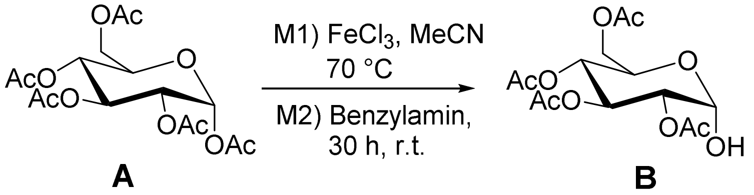

Method1: Compound A (0.4 g; 1.0 mmol) was dissolved in a mixture of acetonitrile (5 mL) and a catalytic amount of water. $FeCl_3 \cdot 6H_2O$ (0.3 g; 1.0 mmol) was added and the mixture was stirred at 50 °C for 30 min. The reaction was monitored by TLC and after completion the solvent was removed. Acetonitrile (2 mL) and saturated aqueous Na_2CO_3 (25 mL) was added. A brown solid precipitated and was separated by centrifugation. The supernatant solution was extracted with dichloromethane (DCM) (3x100 mL) and the organic phase was dried over sodium sulfate. The solvent was removed and the product was purified by column chromatography (silica, ethylacetate:n-hexane, gradient from 1:1 to 2:1). The final product was obtained as colorless oil. Yield: 28%.

Rf-Wert: 0.35

MS (ESI): *m/z* (%) = 366.2 $[M+NH_4]^+$, 371.3 $[M+Na]^+$

^{13}CNMR: (600 MHz. dmso-d_6) δ[ppm] = 170.8; 170.2; 170.1; 169.6; 90.2; 71.0; 69.3; 68.4; 67.3; 61.9; 20.8. 20.7. 20.7. 20.6.

Method 2: Compound A (3.9 g; 10.0 mmol) and N-Benzylamine (1.2 mL; 11.0 mmol) were dissolved in THF (45 mL) and stirred for 30 h at 21 °C. The solvent was removed and the product was dissolved in DCM (100 mL). The organic phase was extracted with hydrochloric acid (1.0 mol/L, 100 mL) and with water (100 mL). The crude product was purified by column chromatography (silica, ethylacetate:n-hexane, gradient from 1:1 to 2:1). The product was obtained as brown oil. Yield: 40%

Rf-Wert: 0.32

^{13}C NMR: (300 MHz. dmso-d_6) δ[ppm] = 169.0; 168.3; 167.8; 167.7; 88.2; 69.3; 68.1; 65.2; 66.7; 60.1; 18.9; 18.8; 18.8; 18.8.

Synthesis of compound C[184]

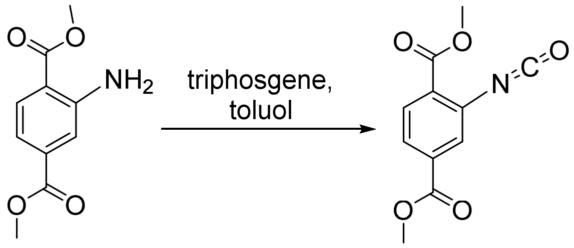

C

A solution of dimethyl-2-aminoterephthalat (99 mg; 0.47 mmol) in toluol (2 mL) was added to triphosgene (169 mg; 0.57 mmol) in toluol (2 mL). The reaction mixture was stirred at 130 °C for 2.5 h. Attention, hydrochloric acid vapor develops during the reaction, which was neutralized by passing into a sodium hydroxide solution. After reaction was completed the solvent was removed and the product was obtained as white solid. The product was stored under Argon atmosphere. Yield: 99%

^{1}H-NMR (300 MHz, dmso-d_6) δ[ppm] = 8.07 (d; 1H); 7.87 (dd; 1H); 7.77 (d; 1H); 3.98 (s; 3H); 3.94 (s; 3H)

^{13}C NMR: (300 MHz, dmso-d_6) δ[ppm] = 165.6; 168.3; 134.8; 134.5; 131.67; 127.5; 127.01; 126.0; 52.7. 52.7.

Synthesis of compound Ligand-1-protected[185]

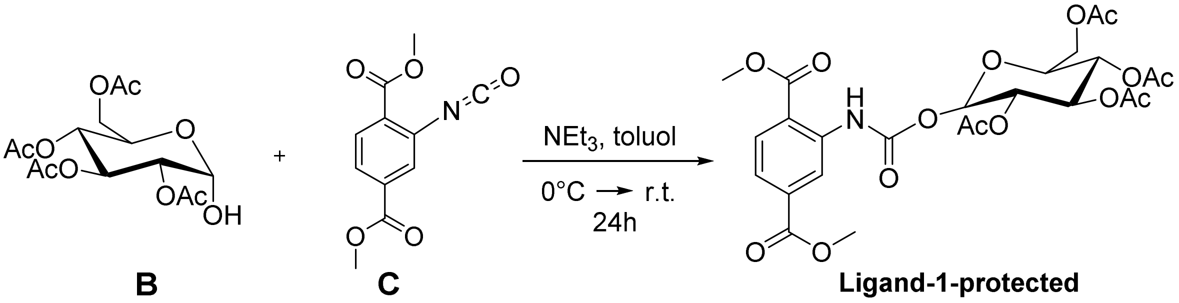

Triethylamine (47 mg; 0.47 mmol) was added to a mixture of compound B (162 mg; 0.47 mmol) in toluol (6.4 mL). Compound C (110 mg; 0.47 mmol) in toluol (3 mL) was added under inert atmosphere at 0 °C. The reaction mixture was stirred for 24 h at 21 °C. The solvent was concentrated and the product precipitated at white solid. Yield: 43 %

MS (ESI): *m/z* (%) = 601.3 $[M+NH_4]^+$, 606.3 $[M+Na]^+$, 1189.1 $[2*M+ NH_4]^+$.

^{1}H-NMR (300 MHz, dmso-d_6) δ[ppm] = 11.98 (s; 1H); 10.60 (d; 1H); 9.00 (s; 1H); 8.02 (s; 1H). 5.20 (s; 3H); 4.24 (s; 1H); 4.09 (s; 1H); 4.06 (s; 6H). 1.98 (s; 12H)

^{13}C NMR: (300 MHz, dmso-d_6) δ[ppm] = 170.6; 170.1; 169.4; 169.2; 167.6; 165.9; 151.0; 140.7; 135.5; 131.1; 123.3; 120.2; 118.6; 93.1; 73.0; 72.8; 70.3; 67.9; 61.6; 52.8; 52.6; 20.7; 20.6; 20.6; 20.6.

Synthesis of compound Ligand-2-protected

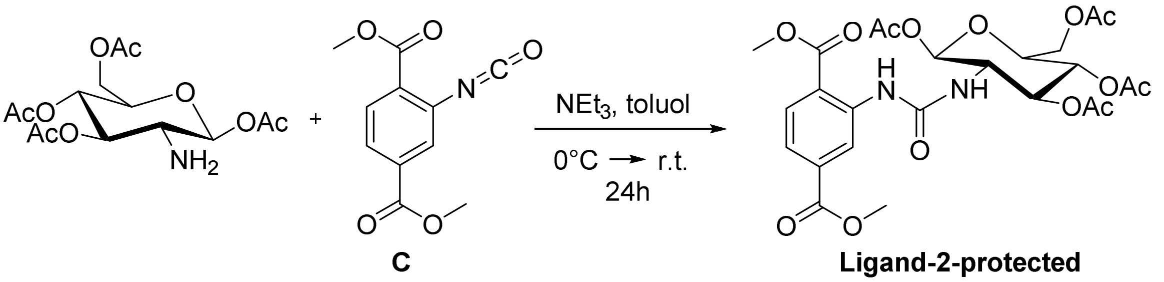

Triethylamine (0.1 mL; 0.65 mmol) was added to a mixture of 1,3,4,6-*tetra*-*O*-acetyl-2-amino-2-deoxy-β-D-glucopyranose (250 mg; 0.65 mmol) in toluol (12 mL). Compound C (153 mg; 0.65 mmol) in toluol (8 mL) was added under inert atmosphere at 0 °C. The reaction mixture was stirred for 24 h at 21 °C. The solvent was concentrated and the product precipitated at white solid.

^{1}H-NMR (300 MHz. dmso-d_6) δ[ppm] = 1.19 (t, J = 7.3 Hz, 10H), 1.93 (s, 3H), 1.97 – 2.09 (m, 8H), 3.07 (q, J = 7.6 Hz, 8H), 3.89 (d, J = 3.8 Hz, 6H), 4.04 (ddd, J = 18.9, 10.9, 3.0 Hz, 2H), 4.21 (dd, J = 12.3, 4.3 Hz, 1H), 4.93 (t, J = 9.6 Hz, 1H), 5.27 (t, J = 9.9 Hz, 1H), 5.81 (d, J = 8.8 Hz, 1H), 7.56 (dd, J = 8.3, 1.8 Hz, 1H), 7.83 (d, J = 8.8 Hz, 1H), 8.00 (d, J = 8.3 Hz, 1H), 8.95 (d, J = 1.7 Hz, 1H), 9.80 (s, 1H).

8.3.2 Synthesis of MOF@MO core-shell composites

Synthesis of MOF@MO-A

MIL-101Cr (40 mg) was suspended in isopropanol (30 mL) and stirred for 20 h at room temperature. Since MIL-101Cr is acidic itself, after stirring for 20 h the pH was controlled (calibrated pH electrode, metrohm) and set to 2 using hydrochloric acid (conc.). Cetyltrimethylammoniumbromid (CTAB) (0.09 g, 0.25 mmol) was added and resulting reaction mixture was stirred for 5 h. Zr(propoxide) (0.11 mL, 0.38 mmol) and Ti (isopropoxide) (0.17 mL, 0.38 mmol) were added to the reaction mixture followed by stirring for 30 min. and subsequent heating at 60 °C for 48 h. After heating reaction mixture was clear, no (additional) solid has formed. The metal oxide@MIL-101Cr composite (in the following **MOF@MO-A**) was separated by centrifugation and suspended in ethanol (30 mL). Then H_2O (4 mL) was added. The mixture was stirred overnight, separated and dried at 100 °C for 15 h. Yield: 40.1 mg
MOF@MO-A BET Surface area: 2036 m^2/g.

Synthesis of MOF@MO-B

MIL-101Cr (45 mg) or MIL-101Cr-SO_3H (45 mg) was suspended in isopropanol (25 mL) and stirred for 20 h at room temperature. Since MIL-101Cr is acidic itself, after stirring for 20 h the pH was controlled (calibrated pH electrode, metrohm) and set to 2 using sulfuric acid (conc.). Cetyltrimethylammoniumbromid (CTAB) (0.09 g, 0.25 mmol) was added and resulting reaction mixture was stirred for 5 h.

A precursor solution of the sixfold amount of Zr(propoxide) (0.11 mL, 0.38 mmol) and Ti (isopropoxide) (0.17 mL, 0.38 mmol) was prepared in isopropanol (12 mL) under inert atmosphere in order to facilitate addition of the compounds. To each of 6 attempts 2 mL of precursor solution was added. The reaction mixture was stirred for 1 h at room temperature. Then different amounts of H_2O were added (0.5 mL, 1.5 mL and 3 mL) to the reaction mixtures containing MIL-101Cr or MIL-101Cr-SO_3H. After short stirring, the mixture was heated at 60 °C for 48 h.

In the case of 1.5 mL and 3 mL water, after heating period a mixture of a white and green solid was observed, showing that hydrolysis occurred to a large extent and in addition to possible product also pure metal oxide was obtained. Since separation of solids was not possible, the attempts were not longer followed up. Using 0.5 mL water the reaction solution was turbid, but the green solid (**MOF@MO-B.1** derived from MIL-101Cr and **MOF@MO-B.2** derived from MIL-101Cr-SO_3H) could be separated by sedimentation. MOF@MO-B.1+2 were washed with ethanol (50 mL each) at 80 °C for 17 h. MOF@MO-B.1+2 were separated via sedimentation the turbid supernatant solution was removed and new ethanol (50 mL) was added. Finally MOF@MO-B1+2 were separated by slow centrifugation (30 min at 1000 rpm) and dried at 70 °C.

Yield [mg], BET surface area [m²/g]

MOF@MO-B.1: 61 mg, 886 m²/g

MOF@MO-B.2: 72 mg, 592 m²/g

MOF@MO-B.3-5 were synthesized as described above, but varying the amount of CTAB and using only titanium tetraisopropoxide (

Table 13:). MIL-101Cr (40 mg) and isopropanol (30 mL) were used

Table 13:Variation of stochiometric amounts for MOF@MO composites.

Material	CTAB [mmol]	$Ti(isoprop)_4$ [mmol]	Ratio CTAB:Ti	Solvent[a] [mL]
MOF@MO-B.3	0.25	0.75	1:3	30
MOF@MO-B.4	0.75	2.3	1:3	30
MOF@MO-B.5	0.75	0.75	1:1	30

Yield [mg], BET surface area [m²/g]

MOF@MO-B.3: 103 mg, 691 m²/g

MOF@MO-B.4: 263 mg, 412 m²/g

MOF@MO-B.5: 102 mg, 682 m²/g

For calcinations experiments the material (MOF@MO or metal oxide) was placed in a ceramic cup and heated to 500 °C, temperature was held for 30 min., then the sample was cooled to room temperature in air.

MOF@MO-B.3-500 °C: weighted portion: 56 mg, after calcination: 32 mg mass loss: 24 mg (43%)

BET surface area: 112 m²/g

Synthesis of Fe_3O_4@MIL-101Cr-NH_2

2-Aminoterephthalic acid (0.46 g, 2.5 mmol) and chromium nitrate nonahydrate (1.0 g, 2.5 mmol) were dissolved in H_2O (10 mL) and stirred for 2 days at room temperature. L-3,4-Dihydroxyphenylalanine functionalized Fe_3O_4 nanoparticles (55 mg) were suspended in H_2O (4 mL) and treated with ultrasound before adding to the reaction mixture. The mixture was stirred for 1 h before transfer in two Teflon autoclaves (volume 10 mL each). Heating program was as following: Heating within 2 h to 130 °C, at 130 °C for 24 h, cooling to 25 °C within 18 h. A green-brown suspension was obtained. The solid was separated by centrifugation, washed with H_2O and ethanol (150 mL each) at room temperature and subsequent in new ethanol (150 mL) at 80 °C for 2 days. After centrifugation the solid was dried at 60 °C *in vacuo*. Yield: 0.42 g

8.3.3 Syntheses of nanoMOFs using microemulsion and ultrasound

Synthesis of MIL-88AFe with a ultrasound horn

Fumaric acid (0.58 g, 5 mmol) was dissolved in H_2O and $FeCl_3$ (1.35 g, 5 mmol) was added directly before before the start of the reaction. Parameters for horn type ultrasound reactor: 30% amplitude, temperature 50 °C. The Temperature was additionally controlled by an water bath (started at r.t), because the solution heats itself due to ultrasound vibrations. After different times, usually between 30 and 90 min. reactions was stopped and the resulting orange solid was washed with ethanol (40 mL each time), separated by centrifugation and dried in air.

Formation of microemulsion

Sodium oleate (0.2 g, 0.66 mmol) was suspended in *n*-heptane (14 mL). To the milky white solution a certain amount of H_2O (here at least 0.35 mL) was added until the mixture became clear. After adding the water, the mixture was stirred for at least 20 min and treated with ultrasound (horn type reactor, 30 % amplitude, 10 min).

Synthesis of nano-MIL-88AFe Method A

Method A: First, the microemulsion was formed using sodium oleate (2.0 g, 6.6 mmol), *n*-heptane (140 mL) and H_2O (2.0 mL). The mixture was sonicated for 10 min (30% amplitude). Fumaric acid (0.06 g, 0.5 mmol) and $FeCl_3$ (0.14 g, 0.5 mmol) were dissolved separately in water (total volume of H_2O:1.5 mL, small amount of NaOH was added for better solubility of fumaric acid) and added to the microemulsion. The mixture was sonicated at 50 °C for 30 min. (30% amplitude). The reaction temperature was controlled using a water bath. After cooling down the reaction to room temperature ethanol (150 mL) was added. Still an orange solution remained. After centrifugation an orange-brown solid was obtained. The solid was washed with ethanol (3 x 40 mL), separated by centrifugation and dried in air at 70 °C.
Yield: 0.193 g
Method B: This method was adapted from W. Lin *et al.*.[265] Two microemulsion of the same composition were prepared, whereas each contains sodium oleate (1.0 g, 3.3 mmol), *n*-heptane (60 mL) and water (1.6 mg). To microemulsion A $FeCl_3$ (0.14 g, 0.5 mmol) was added and to the second one fumaric acid (0.06 g, 0.5 mmol). Both emulsions were heated to 50 °C, mixed together and directly reacted using ultrasound (30% amplitude, 50 °C) for 60 min. After reaction a clear orange solution was obtained, also after addition of ethanol no solid precipitated. Therefore, the solution was centrifugated at 24 000 rpm for 2 h at 25 °C. An orange-brown solid was obtained which was washed with ethanol (3x 10 mL) and dried in air at 70 °C.

8.3.4 Syntheses of mesoporous compounds

Synthesis of mesoporous compound 1, MC-1

Linker-1 (70 mg, 0.12 mmol) and dimethyl-2-aminoterephtalic acid (23 mg, 0.12 mmol) were added to a solution of $Cr(NO_3)_3 \cdot 9H_2O$ (96 mg, 0.24 mmol) in H2O/DMF (1:1, 4 mL). The mixture was stirred at room temperature for 10 min and was transferred into a teflon lined steel autoclave. Oven program was set as following: 5 h heating to 130 °C, 130 °C for 24 h, cooling time 15 h to room temperature.

After synthesis a brown gel like solid was obtained which was washed with H_2O (40 mL) at room temperature, separated by centrifugation and suspended in the next solvent. This procedure was repeated with DMF, THF and ethanol. Finally the solid was dried at 100 °C in air.

The synthesis was repeated with different reactants. An overview over reactions and surface area is provided in the following (Table 12).

Table 12: Overview about MO@MOF experiments.

Material	$Cr(NO_3)_3$• $9H_2O$	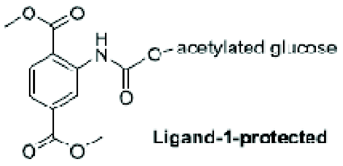 Ligand-1-protected	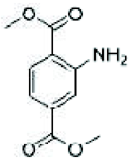	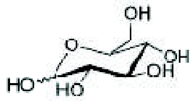	Other	Solvent	Surface area (BET), [m^2/g]	Pore volume [cc/g]	Ratio linker vs additive
MC-1	X	X	X			H_2O/DMF1:1	439	0.44	1:1:0.5
MC-2	X		X	X		H_2O/DMF 1:1	423	0.33	1:1:0.5
MC-3	X		X		glucosepenta-acetate	H_2O/DMF1:1	436	0.73	1:1:0.5
MC-4	X		X	X		H_2O/DMF1:1	372	0.35	1:1:1
MC-5	X			X	2-amino-terephtalic acid	H_2O/DMF1:1	166	0.12	1:0.5
MC-6	X			X	terephthalic acid, TMAOH	H_2O	280	0.61	1:1:0.5
MC-7	X		X	X		buffer7/ DMF 1:1	482	0.47	1:1:0.5
MC-8	X		X	X		DMF	193	0.24	1:1:0.5
MC-9	X		X			H_2O/DMF1:1	457	0.69	1:1:0
MC-10	X		X			H_2O	1947	1.60	1:1
MC-11	X		X	X		H_2O/DMF2:1	206	0.57	1:1:0.5
MC-12	X		X			H_2O/DMF2:1	407	0.82	1:1

8.3.5 Syntheses of MOF@xerogel composites

Figure 167: custom built apparatus for mixing of MOF@xerogel mixtures.

MIL-101Cr: Synthesis procedure was adapted from reference [330].

Terephthalic acid (0.66 g, 4.0 mmol) was added to an aqueous solution of TMAOH (20 mL, 0.05 mol/L) and stirred for 10 min at room temperature. $Cr(NO_3)_3 \cdot 9H_2O$ (1.6 g, 4.0 mmol) was added and the mixture was stirred again for 20 min. The suspension was transferred into a Teflon lined autoclave and was heated to 180 °C for 24 h (heating ramp 10 h; cooling ramp 18 h).

Activation procedure for MIL101Cr: The green solid was washed with H_2O. The centrifuged product was stirred in DMF overnight at room temperature, centrifuged again and then heated in new DMF for 5 h at 110 °C. After cooling to room temperature the powder was centrifuged off and resuspended in ethanol. The mixture was stirred again at room temperature overnight and then heated for 3 days at 90 °C. The last step was repeated with new ethanol, but stirring at 90 °C for 1day. Then the product was dried at 70 °C overnight and afterwards at 150 °C overnight. Yield: around 47%, BET surface area: 3050 – 3070 m^2/g.

MIL-101Cr-NH$_2$: Synthesis procedure was adapted from reference [231].

2-Aminoterephthalic acid (0.69 g, 3.8 mmol) was added to a solution of $Cr(NO_3)_3 \cdot 9H_2O$ (1.5 g, 3.8 mmol) in water (21 mL) and the mixture was stirred for 3 h. The green suspension was transferred into a Teflon lined autoclave and was heated to 130 °C for 24 h (heating ramp 2 h; cooling ramp 18 h).

Activation procedure for MIL101Cr-NH$_2$: The green solid was washed with H_2O. The centrifuged product was heated in ethanol at 90 °C for 2 days. The procedure was repeated a second time with new ethanol. The product was dried at 70 °C overnight and afterwards at

130 °C under vacuum. Yield: 15%, BET surface area: 1800 – 2463 m^2/g (dependent on batch).

MIL-101Al-NH_2: Synthesis procedure was adapted from reference [331].

In contrast to the literature procedure, the addition of $Al(Cl)_3 \cdot 6H_2O$ was slowed down.

2-aminoterephthalic acid (0.82 g, 4.5 mmol) was dissolved in DMF (180 mL) and heated to 110 °C. $Al(Cl)_3 \cdot 6H_2O$ (2.2 g, 9 mmol) was split into 8 parts and one part of aluminium salt was added every 20 min. The reaction mixture was stirred at 110 °C for 3h and heated without stirring for 16 h. The precipitated solid was separated by centrifugation and activated by washing with DMF at room temperature as well as with methanol (300 mL) at 65 °C for 15 h.

The product was dried in vacuo at 150 °C. Yield: 80%. BET surface area: 2240 m^2/g.

MIL-53Al-NH_2: Synthesis procedure was adapted from reference [332].

$AlCl_3 \cdot 6H_2O$ (0.76 g, 3.1 mmol) was dissolved in H_2O and 2-aminoterephthalic acid (0.56 g, 3.1 mmol) was separately dissolve in DMF. The two solutions were put together resulting in a mixture of H_2O and DMF (40 vol% H_2O, 30 mL). The mixture was introduced into a 100 mL Teflon-lined steel autoclave placed in an oven at 150 °C for 24 hours under static conditions. The yellow solid product was isolated by centrifugation and activated in boiling DMF (150 mL) for 5 h and 5 h in boiling ethanol (150 mL). Finally the product was dried at 70 °C in air. Yield: 91%%. BET surface area: 1043 m^2/g.

Standard procedure for the synthesis of MOF@xerogel composites

6.88 g resorcinol (62.5 mmol) was dissolved in 29.6 g of an aqueous Na_2CO_3 solution ($2.1 \cdot 10_{-3}$ mol·L_{-1}; 0.063 mmol Na_2CO_3). Then 10.7 g of formaldehyde solution (85.5 mmol; ρ = 1.06 g·mL_{-1}; 24 wt% in H_2O) was added and the solution was stirred for 1 h. The molar ratios of the starting materials are: R/F = 0.73, R/C = 1000, R/W = 0.031. The clear solution was pre-polymerized for 5 h at 343 K until it was almost solid and cooled to room temperature.

Note: The synthesis of pre-polymerized R, F polymer can be upscaled easily, when using longer pre-polymerization times, respectively. After cooling the viscous material to room temperature, it can be stored and reused for several weeks at 5 °C.

To the pre-polymerized gel (1.03 g) well ground MOF powder (amount depending on loading) and deionized water (0.6 mL) were added. The suspension was stirred for 30 min with a mechanical stirrer in a custom-made, closable glass vial, to achieve a homogenous distribution. The vial was closed and the gel was cured for 7 days at 343 K. The resulting monolith was stored in 50 mL of acetic acid (10 wt% in water) for 24 h, followed by soaking in EtOH (3 x 50 mL, min. 7 h each washing step) and drying it without cap for 3 days at 333 K.

For syringe experiments (Figure 140), MOF@xerogel composites were washed with acetic acid and ethanol using a vacuum apparatus (Figure 141).

8.3.6 Shaping approaches for MIL-101Cr and MIL-101Cr-NH_2

MIL-101Cr-NH_2 was synthesized as described above.

Synthesis of the suspension 3% in water

Sodiumdodecylsulfate (5.4 g) was in dissolved in water (30 mL) at room temperature. MIL101Cr-NH_2 (0.91 g) was added and the resulting green suspension was treated with an ultrasound horn reactor three times for 15 min. The suspension was stirred at room temperature overnight.

A stable green suspension was obtained. Without stirring no solid was observed at the bottom of the flask after 12 h. After longer time a small amount of solid was observed which was easy to remove by shaking the flask or stirring.

Since it was found, that the addition of SDS is not necessary, for all experiments following sample 1, MIL-101Cr-NH_2 was simply suspended in water or THF with the same concentration stated above.

Suspensions were send to Prof. Wim Defermé for spray-coating.

Shaping of MIL-101Cr and MIL-101Cr-NH_2 powders

The shaping of MOF powder to pellets was performed with an IR press (company RIIC) at different pressures. The sample holder displayed a diameter of 1.2 cm. The pressure was hold for 30 sec and 100 mg MOF powder was used. After each use the sample holder (metal) was cleaned with metal polish, otherwise it was not possible to remove the pellets as a whole from the sample holder. The lowest adjustable pressure was 0.5 kbar (due to readout of the device)

Material shaped into pellets:

MIL-101Cr (0.5kbar): 6.9 g

MIL-101Cr-NH_2 (0.5kbar): 5.3 g

9. References

[1] J. Gascon, A. Corma, F. Kapteijn, F. X. Llabrés i Xamena, *ACS Catal* **2014**, *4*, 361–378.

[2] G. A. Ozin, *Energy Environ. Sci.* **2015**, *8*, 1682–1684.

[3] M. B. W. McDonough, P. T. Anastas, J. B. Zimmerman, *Environ. Sci. Technol.* **2003**, *37*, 434–441.

[4] M. Aresta, A. Dibenedetto, A. Angelini, *Chem. Rev.* **2013**, *114*, 1709–1742.

[5] D. Esposito, M. Antonietti, *Chem. Soc. Rev.* **2015**, *44*, 5821–5835.

[6] A. A. Koutinas, A. Vlysidis, D. Pleissner, N. Kopsahelis, I. Lopez Garcia, I. K. Kookos, S. Papanikolaou, T. H. Kwan, C. S. K. Lin, *Chem. Soc. Rev.* **2014**, *43*, 2587–2627.

[7] I. Fechete, Y. Wang, J. C. Védrine, *Catalysis Today* **2012**, *189*, 2–27.

[8] S. Kulprathipanja (Hrsg.) *Zeolites in industrial separation and catalysis*, Wiley-VCH, Weinheim, **2010**.

[9] E.-P. Ng, S. Mintova, *Microporous and Mesoporous Materials* **2008**, *114*, 1–26.

[10] C. Janiak, J. K. Vieth, *New J. Chem.* **2010**, *34*, 2366–2388.

[11] A. Corma, H. García, Llabrés i Xamena, F X, *Chem. Rev.* **2010**, *110*, 4606–4655.

[12] A. H. Chughtai, N. Ahmad, H. A. Younus, A. Laypkov, F. Verpoort, *Chem. Soc. Rev.* **2015**, *44*, 6804–6849.

[13] J. Liu, L. Chen, H. Cui, J. Zhang, L. Zhang, C.-Y. Su, *Chem. Soc. Rev.* **2014**, *43*, 6011–6061.

[14] C. Janiak, *Dalton Trans.* **2003**, *14*, 2781–2804.

[15] J. L. Rowsell, O. M. Yaghi, *Micropor Mesopor Mater* **2004**, *73*, 3–14.

[16] O. M. Yaghi, G. Li, H. Li, *Nature* **1995**, *378*, 703–706.

[17] Batten Stuart R., Champness Neil R., Chen Xiao-Ming, Garcia-Martinez Javier, Kitagawa Susumu, öhrström Lars, O'Keeffe Michael, Paik Suh Myunghyun, Reedijk Jan **2013**, *85*, 1715–1724.

[18] S. R. Batten, N. R. Champness, X.-M. Chen, J. Garcia-Martinez, S. Kitagawa, L. Öhrström, M. O'Keeffe, M. P. Suh, J. Reedijk, *CrystEngComm* **2012**, *14*, 3001–3004.

[19] D. J. Tranchemontagne, J. L. Mendoza-Cortés, M. O'Keeffe, O. M. Yaghi, *Chem. Soc. Rev.* **2009**, *38*, 1257–1283.

[20] W. Lu, Z. Wei, Z.-Y. Gu, T.-F. Liu, J. Park, J. Park, J. Tian, M. Zhang, Q. Zhang, T. Gentle et al., *Chem. Soc. Rev.* **2014**, *43*, 5561–5593.

[21] Makoto Fujita, Yoon Jung Kwon, Satoru Washizu, Katsuyuki Ogura, *J. Am. Chem. Soc.* **1994**, *116*, 1151–1152.

[22] D. Farrusseng, S. Aguado, C. Pinel, *Angew. Chem.* **2009**, *121*, 7638–7649.

[23] J. Lee, O. K. Farha, J. Roberts, K. A. Scheidt, S. T. Nguyen, J. T. Hupp, *Chem. Soc. Rev.* **2009**, *38*, 1450–1459.

[24] A. Dhakshinamoorthy, M. Alvaro, H. Garcia, *Chem. Commun.* **2012**, *48*, 11275–11288.

[25] A. Dhakshinamoorthy, M. Opanasenko, J. Cejka, H. Garcia, *Adv. Synth. Catal.* **2013**, *355*, 247–268.

[26] A. Dhakshinamoorthy, H. Garcia, *Chem. Soc. Rev.* **2014**, *43*, 5750–5765.

[27] A. Dhakshinamoorthy, M. Opanasenko, J. Čejka, H. Garcia, *Catal. Sci. Technol.* **2013**, *3*, 2509–2540.

[28] A. Dhakshinamoorthy, M. Alvaro, H. Garcia, *Catal. Sci. Technol.* **2011**, *1*, 856–867.

[29] J.-L. Wang, C. Wang, W. Lin, *ACS Catal.* **2012**, *2*, 2630–2640.

[30] A. Dhakshinamoorthy, H. Garcia, *Chem. Soc. Rev.* **2012**, *41*, 5262–5284.

[31] A. Dhakshinamoorthy, M. Alvaro, A. Corma, H. Garcia, *Dalton Trans.* **2011**, *40*, 6344–6360.

[32] M. Opanasenko, *Catalysis Today* **2014**, *243*, 2–9.

[33] H. Furukawa, K. E. Cordova, M. O'Keeffe, O. M. Yaghi, *Science* **2013**, *341*, 1230444-1-1230444-12.

[34] A. Torres-Knoop, D. Dubbeldam, *ChemPhysChem* **2015**, *16*, 2046–2067.

[35] P. García-García, M. Müller, A. Corma, *Chem. Sci.* **2014**, *5*, 2979–3007.

[36] N. Qadir, S. A. Said, H. M. Bahaidarah, *Micropor Mesopor Mater* **2015**, *201*, 61–90.

[37] A. Dhakshinamoorthy, H. Garcia, *ChemSusChem* **2014**, *7*, 2392–2410.

[38] J. J. Low, A. I. Benin, P. Jakubczak, J. F. Abrahamian, S. A. Faheem, R. R. Willis, *J. Am. Chem. Soc.* **2009**, *131*, 15834–15842.

[39] F. Jeremias, A. Khutia, S. K. Henninger, C. Janiak, *J. Mater. Chem.* **2012**, *22*, 10148–10151.

[40] J. Ehrenmann, S. K. Henninger, C. Janiak, *Eur. J. Inorg. Chem.* **2011**, *4*, 471–474.

[41] F. Jeremias, V. Lozan, S. K. Henninger, C. Janiak, *Dalton Trans* **2013**, *42*, 15967–15973.

[42] A. Khutia, H. U. Rammelberg, T. Schmidt, S. Henninger, C. Janiak, *Chem. Mater.* **2013**, *25*, 790–798.

[43] F. Jeremias, D. Fröhlich, C. Janiak, S. K. Henninger, *New J. Chem.* **2014**, *38*, 1846–1852.

[44] N. C. Burtch, H. Jasuja, K. S. Walton, *Chem. Rev.* **2014**, *114*, 10575–10612.

[45] K. Leus, T. Bogaerts, J. de Decker, H. Depauw, K. Hendrick, H. Vrielinck, V. van Speybroeck, P. van der Voort, *Micropor Mesopor Mater* **2016**, *226*, 110–116.

[46] G. Férey, C. Serre, C. Mellot-Draznieks, F. Millange, S. Surblé, J. Dutour, I. Margiolaki, *Angew. Chem. Int. Ed.* **2004**, *43*, 6296–6301.

[47] P. Horcajada, S. Surblé, C. Serre, D.-Y. Hong, Y.-K. Seo, J.-S. Chang, J.-M. Grenèche, I. Margiolaki, G. Férey, *Chem. Commun.* **2007**, *27*, 2820–2822.

[48] C. Volkringer, D. Popov, T. Loiseau, G. Férey, M. Burghammer, C. Riekel, M. Haouas, F. Taulelle, *Chem. Mater.* **2009**, *21*, 5695–5697.

[49] T. Loiseau, C. Serre, C. Huguenard, G. Fink, F. Taulelle, M. Henry, T. Bataille, G. Férey, *Chemistry □A European Journal* **2004**, *10*, 1373–1382.

[50] C. Serre, F. Millange, S. Surblé, G. Férey, *Angew. Chem. Int. Ed.* **2004**, *43*, 6285–6289.

[51] G. Férey, *Science* **2005**, *309*, 2040–2042.

[52] S. Bhattacharjee, C. Chen, W.-S. Ahn, *RSC Adv* **2014**, *4*, 52500–52525.

[53] T. Zhao, F. Jeremias, I. Boldog, B. Nguyen, S. K. Henninger, C. Janiak, *Dalton Trans.* **2015**, *44*, 16791–16801.

[54] D.-Y. Hong, Y. K. Hwang, C. Serre, G. Férey, J.-S. Chang, *Adv. Funct. Mater.* **2009**, *19*, 1537–1552.

[55] K. K. Tanabe, S. M. Cohen, *Chem. Soc. Rev.* **2011**, *40*, 498–519.

[56] S. M. Cohen, *Chem. Rev.* **2012**, *112*, 970–1000.

[57] Q. Wang, J. Bai, Z. Lu, Y. Pan, X. You, *Chem. Commun.* **2016**, *52*, 443–452.

[58] J. D. Evans, C. J. Sumby, C. J. Doonan, *Chem. Soc. Rev.* **2014**, *43*, 5933–5951.

[59] O. Karagiaridi, W. Bury, J. E. Mondloch, J. T. Hupp, O. K. Farha, *Angew. Chem.* **2014**, *126*, 4618–4628.

[60] P. Deria, W. Bury, I. Hod, C.-W. Kung, O. Karagiaridi, J. T. Hupp, O. K. Farha, *Inorg. Chem.* **2015**, *54*, 2185–2192.

[61] C. K. Brozek, M. Dincă, *Chem. Soc. Rev.* **2014**, *43*, 5456–5467.

[62] P. Deria, J. E. Mondloch, O. Karagiaridi, W. Bury, J. T. Hupp, O. K. Farha, *Chem. Soc. Rev.* **2014**, *43*, 5896–5912.

[63] Y. Song, X. Li, L. Sun, L. Wang, *RSC Adv* **2015**, *5*, 7267–7279.

[64] A. Corma, H. García, *Chem. Rev.* **2003**, *103*, 4307–4366.

[65] P. Valvekens, F. Vermoortele, D. de Vos, *Catal. Sci. Technol.* **2013**, *3*, 1435–1445.

[66] J. Marco-Contelles, E. Pérez-Mayoral, A. Samadi, M. do Carmo Carreiras, E. Soriano, *Chem. Rev.* **2009**, *109*, 2652–2671.

[67] E. Pérez-Mayoral, J. Čejka, *ChemCatChem* **2011**, *3*, 157–159.

[68] E. Perez-Mayoral, Z. Musilova, B. Gil, B. Marszalek, M. Polozij, P. Nachtigall, J. Cejka, *Dalton Trans* **2012**, *41*, 4036–4044.

[69] M. Položij, E. Pérez-Mayoral, J. Čejka, J. Hermann, P. Nachtigall, *Catalysis Today* **2013**, *204*, 101–107.

[70] F. Vermoortele, B. Bueken, G. Le Bars, B. van de Voorde, M. Vandichel, K. Houthoofd, A. Vimont, M. Daturi, M. Waroquier, V. van Speybroeck et al., *J. Am. Chem. Soc.* **2013**, *135*, 11465–11468.

[71] A. Herbst, A. Khutia, C. Janiak, *Inorg. Chem.* **2014**, *53*, 7319–7333.

[72] J. Jiang, O. M. Yaghi, *Chem. Rev.* **2015**, *115*, 6966–6997.

[73] M. R. Avhad, J. M. Marchetti, *Renew. Sust. Energ. Rev.* **2015**, *50*, 696–718.

[74] R. Beerthuis, G. Rothenberg, R. N. Shiju, *Green Chem* **2015**, *17*, 1341–1361.

[75] C. Chatterjee, F. Pong, A. Sen, *Green Chem* **2015**, *17*, 40–71.

[76] S. Dutta, S. Pal, *Biomass Bioenerg.* **2014**, *62*, 182–197.

[77] S. González-García, B. Gullón, S. Rivas, G. Feijoo, M. T. Moreira, *Journal of Cleaner Production* **2016**, *120*, 170–180.

[78] M. Hara, K. Nakajima, K. Kamata, *Sci. Technol. of Adv. Mater.* **2016**, *16*, 34903.

[79] P. Lanzafame, G. Centi, S. Perathoner, *Chem. Soc. Rev.* **2014**, *43*, 7562–7580.

[80] J. S. Luterbacher, D. Martin Alonso, J. A. Dumesic, *Green Chem* **2014**, *16*, 4816–4838.

[81] R. A. Sheldon, *J. Mol. Catal. A* **2016**.

[82] R. Rinaldi, F. Schüth, *ChemSusChem* **2009**, *2*, 1096–1107.

[83] J. S. Kruger, V. Nikolakis, D. G. Vlachos, *Curr Opin Chem Eng.* **2012**, *1*, 312–320.

[84] C.-H. Zhou, X. Xia, C.-X. Lin, D.-S. Tong, J. Beltramini, *Chem. Soc. Rev.* **2011**, *40*, 5588–5617.

[85] D. J. Hayes, *Catalysis Today* **2009**, *145*, 138–151.

[86] S. Inkinen, M. Hakkarainen, A.-C. Albertsson, A. Södergård, *Biomacromolecules* **2011**, *12*, 523–532.

[87] J. Becker, A. Lange, J. Fabarius, C. Wittmann, *Curr. Opin. Biotechnol.* **2015**, *36*, 168–175.

[88] B. Murillo, B. Zornoza, O. de La Iglesia, C. Téllez, J. Coronas, *J. Catal.* **2016**, *334*, 60–67.

[89] B. M. Upton, A. M. Kasko, *Chem. Rev.* **2016**, *116*, 2275–2306.

[90] J. E. Holladay, J.F. White, J.J. Bozell, D. Johnson, *Pacific Northwest National Laboratory, US Department of Energy* **2007**.

[91] G. Akiyama, R. Matsuda, H. Sato, M. Takata, S. Kitagawa, *Adv. Mater.* **2011**, *23*, 3294–3297.

[92] Xiaofang Liu, Heng Zhang, Fei Chang, Shan Huang, Kaili Yang, Song Yang, *Curr. Org. Chem.* **2016**, *20*, 761–776.

[93] J. H. Cavka, S. Jakobsen, U. Olsbye, N. Guillou, C. Lamberti, S. Bordiga, K. P. Lillerud, *J. Am. Chem. Soc.* **2008**, *130*, 13850–13851.

[94] K. M. Gupta, K. Zhang, J. Jiang, *Sci. Rep.* **2015**, *5*, 12821 (1-9).

[95] G. Akiyama, R. Matsuda, H. Sato, S. Kitagawa, *Chem. Asian J.* **2014**, *9*, 2772–2777.

[96] J. Tang, X. Guo, L. Zhu, C. Hu, *ACS Catal.* **2015**, *5*, 5097–5103.

[97] J. Chen, S. Wang, J. Huang, L. Chen, L. Ma, X. Huang, *ChemSusChem* **2013**, *6*, 1545–1555.

[98] S. Wang, J. Chen, L. Chen, *Catal Lett* **2014**, *144*, 1728–1734.

[99] L. Wang, F.-S. Xiao, *Green Chem.* **2015**, *17*, 24–39.

[100] M. Moliner, Y. Roman-Leshkov, M. E. Davis, *Proc. Natl. Acad. Sci.* **2010**, *107*, 6164–6168.

[101] A. Onda, T. Ochi, K. Yanagisawa, *Green Chem.* **2008**, *10*, 1033–1037.

[102] J. Pang, A. Wang, M. Zheng, Y. Zhang, Y. Huang, X. Chen, T. Zhang, *Green Chem.* **2012**, *14*, 614–617.

[103] J. Geboers, S. van de Vyver, K. Carpentier, K. de Blochouse, P. Jacobs, B. Sels, *Chem. Commun.* **2010**, *46*, 3577–3579.

[104] Y. Zhang, V. Degirmenci, C. Li, E. J. M. Hensen, *ChemSusChem* **2011**, *4*, 59–64.

[105] M. M. Ozer, Y. Jia, Z. Zhang, Thompson, JR, H. H. Weitering, *Science* **2007**, *316*, 1594–1597.

[106] L. Bromberg, X. Su, T. A. Hatton, *Chem. Mater.* **2014**, *26*, 6257–6264.

[107] J. Chen, K. Li, L. Chen, R. Liu, X. Huang, D. Ye, *Green Chem.* **2014**, *16*, 2490–2499.

[108] Z. Hu, Y. Peng, Y. Gao, Y. Qian, S. Ying, D. Yuan, S. Horike, N. Ogiwara, R. Babarao, Y. Wang et al., *Chem. Mater.* **2016**, *28*, 2659–2667.

[109] K.-i. Shimizu, R. Uozumi, A. Satsuma, *Catal. Commun.* **2009**, *10*, 1849–1853.

[110] Z. Huang, W. Pan, H. Zhou, F. Qin, H. Xu, W. Shen, *ChemSusChem* **2013**, *6*, 1063–1069.

[111] T. Wang, M. W. Nolte, B. H. Shanks, *Green Chem.* **2014**, *16*, 548–572.

[112] G. Tsilomelekis, M. Orella, Z. Lin, Z. Cheng, W. Zheng, V. Nikolakis, D. Vlachos, *Green Chem* **2016**, *18*, 1983–1993.

[113] A. Osatiashtiani, A. F. Lee, D. R. Brown, J. A. Melero, G. Morales, K. Wilson, *Catal. Sci. Technol.* **2014**, *4*, 333–342.

[114] C. Lansalot-Matras, C. Moreau, *Catal. Commun.* **2003**, *4*, 517–520.

[115] L. Yang, G. Tsilomelekis, S. Caratzoulas, D. G. Vlachos, *ChemSusChem* **2015**, *8*, 1334–1341.

[116] R. Weingarten, A. Rodriguez-Beuerman, F. Cao, J. S. Luterbacher, D. M. Alonso, J. A. Dumesic, G. W. Huber, *ChemCatChem* **2014**, *6*, 2229–2234.

[117] R. Bermejo-Deval, M. Orazov, R. Gounder, S.-J. Hwang, M. E. Davis, *ACS Catal.* **2014**, *4*, 2288–2297.

[118] A. Herbst, C. Janiak, **2016, submitted**.

[119] R.-J. van Putten, J. C. van der Waal, E. de Jong, C. B. Rasrendra, H. J. Heeres, J. G. de Vries, *Chem. Rev.* **2013**, *113*, 1499–1597.

[120] I. Jiménez-Morales, A. Teckchandani-Ortiz, J. Santamaría-González, P. Maireles-Torres, A. Jiménez-López, *Appl. Catal. B: Environ.* **2014**, *144*, 22–28.

[121] J. Wang, J. Ren, X. Liu, J. Xi, Q. Xia, Y. Zu, G. Lu, Y. Wang, *Green Chem.* **2012**, *14*, 2506–2512.

[122] V. V. Ordomsky, J. van der Schaaf, J. C. Schouten, T. A. Nijhuis, *ChemSusChem* **2013**, *6*, 1697–1707.

[123] O. M. Yaghi, *PNAS* **2006**, *103*, 10186–10191.

[124] R. Banerjee, A. Phan, B. Wang, C. Knobler, H. Furukawa, M. O\textquoterightKeeffe, O. M. Yaghi, *Science* **2008**, *319*, 939–943.

[125] S. A. Moggach, T. D. Bennett, A. K. Cheetham, *Angew. Chem. Int. Ed.* **2009**, *48*, 7087–7089.

[126] N. Liédana, A. Galve, C. Rubio, C. Téllez, J. Coronas, *ACS Appl. Mater. & Inter.* **2012**, *4*, 5016–5021.

[127] M. S. Holm, Y. J. Pagán-Torres, S. Saravanamurugan, A. Riisager, J. A. Dumesic, E. Taarning, *Green Chem.* **2012**, *14*, 702–706.

[128] C. M. Osmundsen, M. S. Holm, S. Dahl, E. Taarning, *Proc. R. Soc. A* **2012**, *468*, 2000–2016.

[129] J. Chen, R. Liu, Y. Guo, L. Chen, H. Gao, *ACS Catal.* **2014**, *5*, 722–733.

[130] Q. Yuan, D. Zhang, L. van Haandel, F. Ye, T. Xue, E. J. Hensen, Y. Guan, *J. Mol. Chem. A: Chemical* **2015**, *406*, 58–64.

[131] R. Fang, R. Luque, Y. Li, *Green Chem* **2016**, DOI: 10.1039/C5GC03051J.

[132] G. D. Yadav, R. V. Sharma, *Appl. Catal. B: Environ.* **2014**, *147*, 293–301.

[133] A. Takagaki, M. Takahashi, S. Nishimura, K. Ebitani, *ACS Catal.* **2011**, *1*, 1562–1565.

[134] J. Kim, G. T. Neumann, N. D. McNamara, J. C. Hicks, *J. Mater. Chem. A* **2014**, *2*, 14014.

[135] J. Kim, G. T. Neumann, N. D. McNamara, J. C. Hicks, *J. Mater. Chem. A* **2014**, *2*, 14014–14027.

[136] D. Zhang, F. Ye, Y. Guan, Y. Wang, E. J. M. Hensen, *RSC Adv.* **2014**, *4*, 39558–39564.

[137] H. J. Bart, J. Reidetschlager, K. Schatka, A. Lehmann, *Ind. Eng. Chem. Res.* **1994**, *33*, 21–25.

[138] F. Cirujano, A. Corma, F. Llabrés i Xamena, *Chem. Engin. Sci.* **2015**, *124*, 52–60.

[139] D. R. Fernandes, A. S. Rocha, E. F. Mai, C. J. Mota, V. Teixeira da Silva, *Appl. Catal. A: General* **2012**, *425*, 199–204.

[140] K. Y. Nandiwale, S. K. Sonar, P. S. Niphadkar, P. N. Joshi, S. S. Deshpande, V. S. Patil, V. V. Bokade, *Applied Catalysis A: General* **2013**, *460*, 90–98.

[141] Z. Li, R. Wnetrzak, W. Kwapinski, J. J. Leahy, *ACS Appl. Mater. & Inter.* **2012**, *4*, 4499–4505.

[142] L. Valenzano, B. Civalleri, S. Chavan, S. Bordiga, M. H. Nilsen, S. Jakobsen, K. P. Lillerud, C. Lamberti, *Chem. Mater.* **2011**, *23*, 1700–1718.

[143] A. Sivasamy, K. Y. Cheah, P. Fornasiero, F. Kemausuor, S. Zinoviev, S. Miertus, *ChemSusChem* **2009**, *2*, 278–300.

[144] M. Koberg, A. Gedanken, *Energy Environ. Sci.* **2012**, *5*, 7460–7469.

[145] D. Sun, Y. Yamada, S. Sato, W. Ueda, *Appl. Catal. B: Environ.* **2016**, *193*, 75–92.

[146] C. Chizallet, *J. Am. Chem. Soc.* **2010**, *35*, 12367–12377.

[147] J. Chen, R. Liu, H. Gao, L. Chen, D. Ye, *J. Mater. Chem. A* **2014**, *2*, 7205–7213.

[148] A. Zięba, A. Pacuła, A. Drelinkiewicz, *Energy Fuels* **2010**, *24*, 634–645.

[149] V. Stavila, R. Parthasarathi, R. W. Davis, F. El Gabaly, K. L. Sale, B. A. Simmons, S. Singh, M. D. Allendorf, *ACS Catal.* **2016**, *6*, 55–59.

[150] F. Zhang, Y. Jin, Y. Fu, Y. Zhong, W. Zhu, A. A. Ibrahim, M. S. El-Shall, *J. Mater. Chem. A* **2015**, *3*, 17008–17015.

[151] F. Zhang, S. Zheng, Q. Xiao, Y. Zhong, W. Zhu, A. Lin, M. Samy El-Shall, *Green Chem* **2016**, *18*, 2900–2908.

[152] Z. Zhu, H. Tan, J. Wang, S. Yu, K. Zhou, *Green Chem.* **2014**, *16*, 2636–2643.

[153] J.-P. Lange, *Angew. Chem.* **2015**, *127*, 13382–13394.

[154] R. C. Klet, Y. Liu, T. C. Wang, J. T. Hupp, O. K. Farha, *J. Mater. Chem. A* **2016**, *4*, 1479–1485.

[155] J. Canivet, J. Bonnefoy, C. Daniel, A. Legrand, B. Coasne, D. Farrusseng, *New J. Chem.* **2014**, *38*, 3102–3111.

[156] K. Tan, N. Nijem, Y. Gao, S. Zuluaga, J. Li, T. Thonhauser, Y. J. Chabal, *CrystEngComm* **2015**, *17*, 247–260.

[157] M. Wickenheisser, A. Herbst, R. Tannert, B. Milow, C. Janiak, *Micropor Mesopor Mater* **2015**, *215*, 143–153.

[158] W. Lin, *J. of Sol. State Chem.* **2005**, *178*, 2486–2490.

[159] L. Ma, C. Abney, W. Lin, *Chem. Soc. Rev.* **2009**, *38*, 1248–1256.

[160] K. K. Bisht, B. Parmar, Y. Rachuri, A. C. Kathalikattil, E. Suresh, *CrystEngComm* **2015**, *17*, 5341–5356.

[161] M. Yoon, R. Srirambalaji, K. Kim, *Chem. Rev.* **2011**, *112*, 1196–1231.

[162] Y. Liu, W. Xuan, Y. Cui, *Adv. Mater.* **2010**, *22*, 4112–4135.

[163] C. Wang, M. Zheng, W. Lin, *J. Phys. Chem. Lett.* **2011**, *2*, 1701–1709.

[164] D. J. Lun, G. I. N. Waterhouse, S. G. Telfer, *J. Am. Chem. Soc.* **2011**, *133*, 5806–5809.

[165] J. M. Thomas, *Phys. Chem. Chem. Phys.* **2014**, *16*, 7647–7661.

[166] J. M. Thomas, R. Raja, D. W. Lewis, *Angew. Chem. Int. Ed.* **2005**, *44*, 6456–6482.

[167] N. V. Maksimchuk, O. V. Zalomaeva, I. Y. Skobelev, K. A. Kovalenko, V. P. Fedin, O. A. Kholdeeva, *Proc. R. Soc. A* **2012**, *468*, 2017–2034.

[168] D. S. Sholl, R. P. Lively, *J. Phys. Chem. Lett.* **2015**, *6*, 3437–3444.

[169] Y. Zhang, Y. Zhou, Y. Zhao, C.-j. Liu, *Catalysis Today* **2016**, *263*, 61–68.

[170] C. Copéret, A. Comas-Vives, M. P. Conley, D. P. Estes, A. Fedorov, V. Mougel, H. Nagae, F. Núñez-Zarur, P. A. Zhizhko, *Chem. Rev.* **2016**, *116*, 323–421.

[171] S. Pullen, H. Fei, A. Orthaber, S. M. Cohen, S. Ott, *J. Am. Chem. Soc.* **2013**.

[172] H. Fei, S. M. Cohen, *J. Am. Chem. Soc.* **2015**, *137*, 2191–2194.

[173] J. Canivet, D. Farrusseng, *ChemCatChem* **2011**, *3*, 823–826.

[174] E. D. Bloch, D. Britt, C. Lee, C. J. Doonan, F. J. Uribe-Romo, H. Furukawa, J. R. Long, O. M. Yaghi, *J. Am. Chem. Soc.* **2010**, *132*, 14382–14384.

[175] J. Canivet, S. Aguado, Y. Schuurman, D. Farrusseng, *J. Am. Chem. Soc.* **2013**, *135*, 4195–4198.

[176] J. M. Falkowski, T. Sawano, T. Zhang, G. Tsun, Y. Chen, J. V. Lockard, W. Lin, *J. Am. Chem. Soc.* **2014**, *136*, 5213–5216.

[177] T. Duerinck, J. Denayer, *Chem. Engin. Sci.* **2015**, *124*, 179–187.

[178] L. Nagya , A. Szorcsikb, *J.of Inorg. Biochem.* **2002**, *89*, 1–12.

[179] D. Steinborn, H. Junicke, *Chem. Rev.* **2000**, *100*, 4283–4318.

[180] R. Ch, M. Tyagi, P. R. Patil, K. Ravindranathan Kartha, *Tetrahedron Letters* **2011**, *52*, 5841–5846.

[181] G. Wei, L. Zhang, C. Cai, S. Cheng, Y. Du, *Tetrahedron Letters* **2008**, *49*, 5488–5491.

[182] T. B. Cai, D. Lu, X. Tang, Y. Zhang, M. Landerholm, P. G. Wang, *J. Org. Chem.* **2005**, *70*, 3518–3524.

[183] T. B. a. G. Hans-Joachim Knolker, *Angew. Chem. Int. Ed. Engl.* **1995**, *34*, 2497–2500.

[184] M. N. Jo, H. J. Seo, Y. Kim, S. H. Seo, H. Rhim, Y. S. Cho, J. H. Cha, H. Y. Koh, H. Choo, A. N. Pae, *Bioorganic & Medicinal Chemistry* **2007**, *15*, 365–373.

[185] W. Scheeren, R. G. G. Leenders, E. W. P. Damen, R. Ruytenbeek, *Synthesis* **1996**, 1309–1312.

[186] S. Han, Y. Wei, C. Valente, I. Lagzi, J. J. Gassensmith, A. Coskun, J. F. Stoddart, B. A. Grzybowski, *J. Am. Chem. Soc.* **2010**, *132*, 16358–16361.

[187] M. Ávalos, R. Babiano, P. Cintas, M. B. Hursthouse, J. L. Jiménez, M. E. Light, J. C. Palacios, E. M. S. Pérez, *Eur. J. Org. Chem.* **2006**, *3*, 657–671.

[188] J. Shen, T. Ikai, Y. Okamoto, *J. Chrom. A* **2014**, *1363*, 51–61.

[189] Z. R. Herm, B. M. Wiers, J. A. Mason, J. M. van Baten, M. R. Hudson, P. Zajdel, C. M. Brown, N. Masciocchi, R. Krishna, J. R. Long, *Science* **2013**, *340*, 960–964.

[190] M. Maes, L. Alaerts, F. Vermoortele, R. Ameloot, S. Couck, V. Finsy, J. F. M. Denayer, D. E. de Vos, *J. Am. Chem. Soc.* **2010**, *132*, 2284–2292.

[191] B. van de Voorde, B. Bueken, J. Denayer, D. de Vos, *Chem. Soc. Rev.* **2014**, *43*, 5766–5788.

[192] X. Bao, L. J. Broadbelt, R. Q. Snurr, *Micropor Mesopor Mater* **2012**, *157*, 118–123.

[193] X. Zhang, Q. Han, M. Ding, *RSC Adv* **2015**, *5*, 1043–1050.

[194] X. Shen, J. L. Shamshina, P. Berton, G. Gurau, R. D. Rogers, *Green Chem* **2016**, *18*, 53–75.

[195] X. Zeng, C. A. S. Andrade, M. D. L. Oliveira, X.-L. Sun, *Anal Bioanal Chem* **2012**, *402*, 3161–3176.

[196] B. Li, M. Chrzanowski, Y. Zhang, S. Ma, *Coord. Chem. Rev.* **2016**, *307*, 106–129.

[197] R. Haldar, T. K. Maji, *CrystEngComm* **2013**, *15*, 9276–9295.

[198] Z. Yin, Y.-L. Zhou, M.-H. Zeng, M. Kurmoo, *Dalton Trans* **2015**, *44*, 5258–5275.

[199] A. D. Burrows, *CrystEngComm* **2011**, *13*, 3623–3642.

[200] P. Hu, J. V. Morabito, C.-K. Tsung, *ACS Catal.* **2014**, *4*, 4409–4419.

[201] C. Rösler, R. A. Fischer, *CrystEngComm* **2014**, *17*, 199–217.

[202] P. Falcaro, R. Ricco, A. Yazdi, I. Imaz, S. Furukawa, D. Maspoch, R. Ameloot, J. D. Evans, C. J. Doonan, *Coord. Chem. Rev.* **2016**, *307*, 237–254.

[203] M. Zhao, K. Deng, L. He, Y. Liu, G. Li, H. Zhao, Z. Tang, *J. Am. Chem. Soc.* **2014**, *136*, 1738–1741.

[204] a) T. Fukushima, S. Horike, H. Kobayashi, M. Tsujimoto, S. Isoda, M. L. Foo, Y. Kubota, M. Takata, S. Kitagawa, *J. Am. Chem. Soc.* **2012**, *134*, 13341–13347; b) S. Furukawa, K. Hirai, K. Nakagawa, Y. Takashima, R. Matsuda, T. Tsuruoka, M. Kondo, R. Haruki, D. Tanaka, H. Sakamoto et al., *Angew. Chem. Int. Ed.* **2009**, *48*, 1766–1770; c) S. Furukawa, K. Hirai, Y. Takashima, K. Nakagawa, M. Kondo, T. Tsuruoka, O. Sakata, S. Kitagawa, *Chem. Commun.* **2009**, 5097–5099.

[205] a) K. Hirai, S. Furukawa, M. Kondo, H. Uehara, O. Sakata, S. Kitagawa, *Angewandte Chemie International Edition* **2011**, *50*, 8057–8061; b) T. Li, J. E. Sullivan, N. L. Rosi, *J. Am. Chem. Soc.* **2013**, *135*, 9984–9987; c) P. A. Szilagyi, M. Lutz, J. Gascon, J. Juan Alcaniz, H. Geerlings, B. Dam, J. van Esch, F. Kapteijn, R. van de Krol, *CrystEngComm* **2013**, *15*, 6003–6008.

[206] J. Ren, N. M. Musyoka, H. W. Langmi, B. C. North, M. Mathe, X. Kang, *International Journal of Hydrogen Energy* **2014**, *39*, 14912–14917.

[207] K. Koh, A. G. Wong-Foy, A. J. Matzger, *Chem. Commun.* **2009**, *41*, 6162–6164.

[208] J. Son, H. J. Lee, M. Oh, *Chemistry □A European Journal* **2013**, *19*, 6546–6550.

[209] K. A. McDonald, J. I. Feldblyum, K. Koh, A. G. Wong-Foy, A. J. Matzger, *Chem. Commun.* **2015**, *51*, 11994–11996.

[210] C. Jo, H. J. Lee, M. Oh, *Adv. Mater.* **2011**, *23*, 1716–1719.

[211] Z. Li, H. C. Zeng, *J. Am. Chem. Soc.* **2014**, *136*, 5631–5639.

[212] Z.-Q. Li, A. Wang, C.-Y. Guo, Y.-F. Tai, L.-G. Qiu, *Dalton Trans.* **2013**, *42*, 13948–13954.

[213] V. Pascanu, A. Bermejo Gómez, C. Ayats, A. E. Platero-Prats, F. Carson, J. Su, Q. Yao, M. À. Pericàs, X. Zou, B. Martín-Matute, *ACS Catal.* **2014**, *5*, 472–479.

[214] A. Ahmed, M. Forster, R. Clowes, D. Bradshaw, P. Myers, H. Zhang, *J. Mater. Chem. A* **2013**, *1*, 3276–3286.

[215] N. Zhang, B. Zhu, F. Peng, X. Yu, Y. Jia, J. Wang, L. Kong, Z. Jin, T. Luo, J. Liu, *Chem. Commun.* **2014**, *50*, 7686–7689.

[216] S. Sorribas, B. Zornoza, P. Serra-Crespo, J. Gascon, F. Kapteijn, C. Téllez, J. Coronas, *Micropor Mesopor Mater* **2016**, *225*, 116–121.

[217] G. Zhu, R. Graver, L. Emdadi, B. Liu, K. Y. Choi, D. Liu, *RSC Adv.* **2014**, *4*, 30673–30676.

[218] M. Raynal, P. Ballester, A. Vidal-Ferran, P. W. N. M. van Leeuwen, *Chem. Soc. Rev.* **2014**, *43*, 1734–1787.

[219] Z.-Y. Gu, J. Park, A. Raiff, Z. Wei, H.-C. Zhou, *ChemCatChem* **2014**, *6*, 67–75.

[220] M. Zhao, S. Ou, C.-D. Wu, *Accounts Chem. Res.* **2014**, *47*, 1199–1207.

[221] L.-H. Chen, S.-T. Xu, X.-Y. Li, G. Tian, Y. Li, J. C. Rooke, G.-S. Zhu, S.-L. Qiu, Y.-X. Wei, X.-Y. Yang et al., *J. Colloid Interface Sci.* **2012**, *377*, 368–374.

[222] X.-Y. Li, L.-H. Chen, Y. Li, J. C. Rooke, Z. Deng, Z.-Y. Hu, J. Liu, A. Krief, X.-Y. Yang, B.-L. Su, *Micropor Mesopor Mater* **2012**, *152*, 110–121.

[223] M.-H. Sun, L.-H. Chen, X.-Y. Li, Y. Yang, Y.-T. Ouyang, W. Geng, Y. Li, X.-Y. Yang, B.-L. Su, *Micropor Mesopor Mater* **2013**, *182*, 122–135.

[224] Z.-Y. Yuan, T.-Z. R. A. Vantomme, B.-L. Su, *Chem. Mater.* **2004**, *16*, 5096–5106.

[225] F. Wu, J. Bai, J. Feng, S. Xiong, *Nanoscale* **2015**, *7*, 17211–17230.

[226] K. E. deKrafft, C. Wang, W. Lin, *Adv. Mater.* **2012**, *24*, 2014–2018.

[227] Y. Gu, Y.-n. Wu, J. Shen, Z. Li, S. Chen, H. Lu, F. Li, *Chem. Eur. J.* **2015**, *21*, 17485–17490.

[228] K. Bahranowski, W. Włodarczyk, E. Wisła-Walsh, A. Gaweł, J. Matusik, A. Klimek, B. Gil, A. Michalik-Zym, R. Dula, R. P. Socha et al., *Micropor Mesopor Mater* **2015**, *202*, 155–164.

[229] G. Akiyama, R. Matsuda, H. Sato, A. Hori, M. Takata, S. Kitagawa, *Micropor Mesopor Mater* **2012**, *157*, 89–93.

[230] R. Ricco, L. Malfatti, M. Takahashi, A. J. Hill, P. Falcaro, *J. Mater. Chem. A* **2013**, *1*, 13033–13045.

[231] D. Jiang, L. L. Keenan, A. D. Burrows, K. J. Edler, *Chem. Commun.* **2012**, *48*, 12053–12055.

[232] X. Chen, N. Ding, H. Zang, H. Yeung, R.-S. Zhao, C. Cheng, J. Liu, T.-W. D. Chan, *J. Chrom. A* **2013**, *1304*, 241–245.

[233] Y. Liu, Z. Tang, *Adv. Mater.* **2013**, *25*, 5819–5825.

[234] F. Ke, L. Wang, J. Zhu, *Nanoscale* **2015**, *7*, 1201–1208.

[235] L. Lux, K. Williams, S. Ma, *CrystEngComm* **2015**, *17*, 10–22.

[236] H. B. Tanh Jeazet, C. Staudt, C. Janiak, *Dalton Trans* **2012**, *41*, 14003–14027.

[237] E. M. Dias, C. Petit, *J. Mater. Chem. A* **2015**, *3*, 22484–22506.

[238] Z. Hasan, S. H. Jhung, *Journal of Hazardous Materials* **2015**, *283*, 329–339.

[239] P. Kumar, K.-H. Kim, E. E. Kwon, J. E. Szulejko, *J. Mater. Chem. A* **2016**, *4*, 345–361.

[240] Y. Cui, S. Teo, W. Leong, C. Chai, *IJMS* **2014**, *15*, 9255–9284.

[241] R. F. M. Elshaarawy, F. H. A. Mustafa, A. Herbst, A. E. M. Farag, C. Janiak, *RSC Adv* **2016**, *6*, 20901–20915.

[242] Z. Zhang, J. MacMullen, H. N. Dhakal, J. Radulovic, C. Herodotou, M. Totomis, N. Bennett, *Building and Environment* **2013**, *59*, 47–55.

[243] C. Janiak, *Topics in Organometallic Chemistry* **2015**, *51*, 17–53.

[244] A. Carne, C. Carbonell, I. Imaz, D. Maspoch, *Chem. Soc. Rev.* **2011**, *40*, 291–305.

[245] N. Stock, S. Biswas, *Chem. Rev.* **2012**, *112*, 933–969.

[246] N. A. Khan, S. H. Jhung, *Coord. Chem. Rev.* **2015**, *285*, 11–23.

[247] J. Della Rocca, D. Liu, W. Lin, *Acc. Chem. Res.* **2011**, *44*, 957–968.

[248] E. A. Flügel, A. Ranft, F. Haase, B. V. Lotsch, *J. Mater. Chem.* **2012**, *22*, 10119–10133.

[249] M. Giménez-Marqués, T. Hidalgo, C. Serre, P. Horcajada, *Coord. Chem. Rev.* **2016**, *307*, 342–360.

[250] H. Xu, B. W. Zeiger, K. S. Suslick, *Chem. Soc. Rev.* **2013**, *42*, 2555–2567.

[251] P. Silva, S. M. F. Vilela, J. P. C. Tomé, F. A. Almeida Paz, *Chem. Soc. Rev.* **2015**, *44*, 6774–6803.

[252] W.-J. Son, J. Kim, J. Kim, W.-S. Ahn, *Chem. Commun.* **2008**, *47*, 6336–6338.

[253] B. Seoane, J. M. Zamaro, C. Tellez, J. Coronas, *CrystEngComm* **2012**, *14*, 3103–3107.

[254] E. Haque, N. A. Khan, J. H. Park, S. H. Jhung, *Chem. Eur. J.* **2009**, *16*, 1046–1052.

[255] Jeff Gordon, Hossein Kazemian, Sohrab Rohani, *Micropor Mesopor Mater* **2012**, *162*, 36–43.

[256] T. Chalati, P. Horcajada, R. Gref, P. Couvreur, C. Serre, *J. Mater. Chem.* **2011**, *21*, 2220–2227.

[257] A. Schaate, P. Roy, A. Godt, J. Lippke, F. Waltz, M. Wiebcke, P. Behrens, *Chem. Eur. J.* **2011**, *17*, 6643–6651.

[258] J. M. Chin, E. Y. Chen, A. G. Menon, H. Y. Tan, A. T. S. Hor, M. K. Schreyer, J. Xu, *CrystEngComm* **2013**, *15*, 654–657.

[259] Q. Liu, L.-N. Jin, W.-Y. Sun, *CrystEngComm* **2013**, *15*, 8250–8254.

[260] D. Jiang, A. D. Burrows, K. J. Edler, *CrystEngComm* **2011**, *13*, 6916–6919.

[261] A. Ranft, S. Betzler, F. Haase, B. Lotsch, *CrystEngComm* **2013**, *15*, 9296–9300.

[262] M.-H. Pham, G.-T. Vuong, A.-T. Vu, T.-O. Do, *Langmuir* **2011**, *27*, 15261–15267.

[263] V. Uskoković, M. Drofenik, *Adv. Colloid Interface Sci.* **2007**, *133*, 23–34.

[264] M. A. Malik, M. Y. Wani, M. A. Hashim, *Arabian Journal of Chemistry* **2012**, *5*, 397–417.

[265] W. J. Rieter, K. M. L. Taylor, H. An, W. Lin, W. Lin, *J. Am. Chem. Soc.* **2006**, *128*, 9024–9025.

[266] K. M. L. Taylor, A. Jin, W. Lin, *Angew. Chem. Int. Ed.* **2008**, *47*, 7722–7725.

[267] K. M. L. Taylor, W. J. Rieter, W. Lin, *J. Am. Chem. Soc.* **2008**, *130*, 14358–14359.

[268] D. Tanaka, A. Henke, K. Albrecht, M. Moeller, K. Nakagawa, S. Kitagawa, J. Groll, *Nature Chem* **2010**, *2*, 410–416.

[269] Z.-Q. Li, L.-G. Qiu, T. Xu, Y. Wu, W. Wang, Z.-Y. Wu, X. Jiang, *Mater. Lett.* **2009**, *63*, 78–80.

[270] C. Mellot-Draznieks, C. Serre, S. Surblé, N. Audebrand, G. Férey, *J. Am. Chem. Soc.* **2005**, *127*, 16273–16278.

[271] W. Wang, Y. Yang, H. Zhao, Q. Guo, W. Lu, Y. Lu, *J. Radioanal. Nucl. Chem.* **2012**, *292*, 1093–1098.

[272] J. Borné, T. Nylander, A. Khan, *Langmuir* **2001**, *17*, 7742–7751.

[273] C.-B. Xia, Y.-Z. Yang, X.-M. Xin, S.-X. Wang, *J. Radioanal. Nucl. Chem.* **2008**, *275*, 535–540.

[274] Klaus Rottländer, *Dissertation*, Universität zu Köln, Köln, **2007**.

[275] J. Xu, A. Yin, J. Zhao, D. Li, W. Hou, *J. Phys. Chem. B* **2012**, *117*, 450–456.

[276] C. Goddeeris, F. Cuppo, H. Reynaers, W.G. Bouwman, G. Van den Mooter, *Int. J. Pharm.* **2006**, *312*, 187–195.

[277] M. S. Bakshi, *Cryst. Growth Des* **2016**, *16*, 1104–1133.

[278] X.-Y. Yang, A. Léonard, A. Lemaire, G. Tian, B.-L. Su, *Chem. Commun.* **2011**, 2763–2786.

[279] D. Bradshaw, S. El-Hankari, L. Lupica-Spagnolo, *Chem. Soc. Rev.* **2014**, *43*, 5431–5443.

[280] W. Xuan, C. Zhu, Y. Liu, Y. Cui, *Chem. Soc. Rev.* **2012**, *41*, 1677–1695.

[281] M. Thommes, K. Kaneko, A. V. Neimark, J. P. Olivier, F. Rodriguez-Reinoso, J. Rouquerol, K. S. Sing, *Pure Appl.Chem.* **2015**, *87*, 1051–1069.

[282] S. Furukawa, J. Reboul, S. Diring, K. Sumida, S. Kitagawa, *Chem. Soc. Rev.* **2014**, *43*, 5700–5734.

[283] L.-G. Qiu, T. Xu, Z.-Q. Li, W. Wang, Y. Wu, X. Jiang, X.-Y. Tian, L.-D. Zhang, *Angew. Chem. Int. Ed.* **2008**, *47*, 9487–9491.

[284] S. Cao, G. Gody, W. Zhao, S. Perrier, X. Peng, C. Ducati, D. Zhao, T. Cheetham, *Chem. Sci.* **2013**, *4*, 3573–3577.

[285] V. Choudhary, S. H. Mushrif, C. Ho, A. Anderko, V. Nikolakis, N. S. Marinkovic, A. I. Frenkel, S. I. Sandler, D. G. Vlachos, *J. Am. Chem. Soc.* **2013**, *135*, 3997–4006.

[286] X. Liu, Z.-Q. Shen, H.-H. Xiong, Y. Chen, X.-N. Wang, H.-Q. Li, Y.-T. Li, K.-H. Cui, Y.-Q. Tian, *Micropor Mesopor Mater* **2015**, *204*, 25–33.

[287] Z.-Y. Gu, C.-X. Yang, N. Chang, X.-P. Yan, *Acc. Chem. Res.* **2012**, *45*, 734–745.

[288] B. Zornoza, C. Tellez, J. Coronas, J. Gascon, F. Kapteijn, *Micropor Mesopor Mater* **2013**, *166*, 67–78.

[289] E. Adatoz, A. K. Avci, S. Keskin, *Sep. Purif. Technol.* **2015**, *152*, 207–237.

[290] C.-L. Lin, S. Lirio, Y.-T. Chen, C.-H. Lin, H.-Y. Huang, *Chem. Eur. J.* **2014**, *20*, 3317–3321.

[291] D. Ge, H. K. Lee, *J. Chrom. A* **2012**, *1257*, 19–24.

[292] P. Marchetti, M. F. Jimenez Solomon, G. Szekely, A. G. Livingston, *Chem. Rev.* **2014**, *114*, 10735–10806.

[293] E. M. Dias, C. Petit, *J. Mater. Chem. A* **2015**, *3*, 22484–22506.

[294] T. Nema, E. C. Chan, P. C. Ho, *J. Pharm. Biomed. Anal.* **2014**, *87*, 130–141.

[295] Y.-Y. Fu, C.-X. Yang, X.-P. Yan, *Chem. Commun.* **2013**, *49*, 7162–7164.

[296] H.-Y. Huang, C.-L. Lin, C.-Y. Wu, Y.-J. Cheng, C.-H. Lin, *Anal. Chim. Acta* **2013**, *779*, 96–103.

[297] S. Yang, F. Ye, Q. Lv, C. Zhang, S. Shen, S. Zhao, *J. Chrom. A* **2014**, *1360*, 143–149.

[298] D. Qian, C. Lei, G.-P. Hao, W.-C. Li, A.-H. Lu, *ACS Appl. Mater. Interfaces* **2012**, *4*, 6125–6132.

[299] M. Wickenheisser, C. Janiak, *Micropor Mesopor Mater* **2015**, *204*, 242–250.

[300] M. Savonnet, D. Bazer-Bachi, N. Bats, J. Perez-Pellitero, E. Jeanneau, V. Lecocq, C. Pinel, D. Farrusseng, *J. Am. Chem. Soc.* **2010**, *132*, 4518–4519.

[301] H. Saleem, U. Rafique, R. P. Davies, *Micropor Mesopor Mater* **2016**, *221*, 238–244.

[302] K. K. Tanabe, S. M. Cohen, *Angew. Chem. Int. Ed.* **2009**, *48*, 7424–7427.

[303] S.-S. Liu, C.-X. Yang, S.-W. Wang, X.-P. Yan, *Analyst* **2012**, *137*, 816–818.

[304] A. Khutia, C. Janiak, *Dalton Trans* **2014**, *43*, 1338–1347.

[305] R. Krishna, *RSC Adv* **2015**, *5*, 52269–52295.

[306] J. Ren, N. M. Musyoka, H. W. Langmi, A. Swartbooi, B. C. North, M. Mathe, *Int. J. Hydrogen Energy* **2015**, *40*, 4617–4622.

[307] K. Gilissen, J. Stryckers, P. Verstappen, J. Drijkoningen, G. H. Heintges, L. Lutsen, J. Manca, W. Maes, W. Deferme, *Organic Electronics* **2015**, *20*, 31–35.

[308] A. Bétard, R. A. Fischer, *Chem. Rev.* **2011**, *112*, 1055–1083.

[309] D. Bradshaw, A. Garai, J. Huo, *Chem. Soc. Rev.* **2012**, *41*, 2344–2381.

[310] L. Heinke, M. Tu, S. Wannapaiboon, R. A. Fischer, C. Wöll, *Micropor Mesopor Mater* **2015**, *216*, 200–215.

[311] J.-L. Zhuang, D. Ar, X.-J. Yu, J.-X. Liu, A. Terfort, *Adv. Mater.* **2013**, *25*, 4631–4635.

[312] F. Jeremias, D. Fröhlich, C. Janiak, S. K. Henninger, *RSC Adv.* **2014**, *4*, 24073.

[313] H. Kummer, G. Füldner, S. K. Henninger, *Appl. Therm. Eng.* **2015**, *85*, 1–8.

[314] Beatriz Seoane, Sara Sorribas, Álvaro Mayoral, Carlos Téllez, Joaquín Coronas, *Micropor Mesopor Mater* **2015**, *203*, 17–23.

[315] B. Ding, J. Cai, J. Huang, L. Zhang, Y. Chen, X. Shi, Y. Du, S. Kuga, *J. Mater. Chem.* **2012**, *22*, 5801–5809.

[316] I. Karadagli, B. Schulz, M. Schestakow, B. Milow, T. Gries, L. Ratke, *J. Supercrit. Fluids* **2015**, *106*, 105–114.

[317] J. Jiang, F. Gándara, Y.-B. Zhang, K. Na, O. M. Yaghi, W. G. Klemperer, *J. Am. Chem. Soc.* **2014**, *136*, 12844–12847.

[318] A. Dhakshinamoorthy, A. M. Asiri, H. Garcia, *Chem. Commun.* **2014**, *50*, 12800–12814.

[319] Y. J. Colón, R. Q. Snurr, *Chem. Soc. Rev.* **2014**, *43*, 5735–5749.

[320] Y. G. Chung, J. Camp, M. Haranczyk, B. J. Sikora, W. Bury, V. Krungleviciute, T. Yildirim, O. K. Farha, D. S. Sholl, R. Q. Snurr, *Chem. Mater.* **2014**, *26*, 6185–6192.

[321] S. A. Burgess, A. Kassie, S. A. Baranowski, K. J. Fritzsching, K. Schmidt-Rohr, C. M. Brown, C. R. Wade, *J. Am. Chem. Soc.* **2016**, *138*, 1780–1783.

[322] Y. Chen, S. Ma, *Dalton Trans.* **2016**.

[323] M. D. Allendorf, V. Stavila, *CrystEngComm* **2015**, *17*, 229–246.

[324] G. Yang, Y. Ding, *Bioorg. Med. Chem.* **2014**, *22*, 5604–5612.

[325] A. Barrozo, F. Duarte, P. Bauer, A. T. Carvalho, S. C. Kamerlin, *J. Am. Chem. Soc.* **2015**, *137*, 9061–9076.

[326] B. Manna, S. Singh, A. Karmakar, A. V. Desai, S. K. Ghosh, *Inorg. Chem.* **2015**, *54*, 110–116.

[327] B. Xiao, M. Zheng, X. Li, J. Pang, R. Sun, H. Wang, X. Pang, A. Wang, X. Wang, T. Zhang, *Green Chem* **2016**, *18*, 2175–2184.

[328] Z. Zhang, K. Deng, *ACS Catal.* **2015**, *5*, 6529–6544.

[329] S. H. Madani, A. Badalyan, M. J. Biggs, P. Pendleton, *Micropor Mesopor Mater* **2015**, *214*, 210–216.

[330] J. Yang, Q. Zhao, J. Li, J. Dong, *Micropor Mesopor Mater* **2010**, *130*, 174–179.

[331] M. Hartmann, M. Fischer, *Micropor Mesopor Mater* **2012**, *164*, 38–43.

[332] X. Cheng, A. Zhang, K. Hou, M. Liu, Y. Wang, C. Song, G. Zhang, X. Guo, *Dalton Trans* **2013**, *42*, 13698–13705.